DE-FC21-93MC30256--99
(5879)

The Extraction of Bitumen From Western Oil Sands
Volume II

Final Report
November 26, 1997

By
Alex G. Oblad; Donald A. Dahlstrom
Milind D. Deo; John V. Fletcher
Francis V. Hanson; Jan D. Miller
J.D. Seader

Work Performed Under Contract No.: DE-FC21-93MC30256

For
U.S. Department of Energy
Office of Fossil Energy
Federal Energy Technology Center
P.O. Box 880
Morgantown, West Virginia 26507-0880

By
University of Utah
Department of Chemical and Fuels Engineering
Department of Metallurgical Engineering
Salt Lake City, Utah 84112

Disclaimer

TWO-STAGE THERMAL RECOVERY OF BITUMEN USING HEAT PIPES

Principal Investigator:	J.D. Seader
Graduate Student:	Charles J. Coronella
Graduate Student:	Atul S. Bhadkamkar
Graduate Student:	Kiran R. Khot

INTRODUCTION

In these days of plentiful fuel supplies, synthetic fuels are not in demand; but with the current rate of consumption of oil the importance of synthetic fuels will only increase. The United States currently imports 50% of its transportation fuel and such a dependence could be potentially dangerous, as was evidenced by the 1973 Arab oil embargo. Hence it is important to develop technologies that will make it economically feasible to utilize reserves to produce synthetic fuels. Natural bitumen, which includes materials commonly termed as tar sands, oil sands, or natural asphalt, is a significant potential source of synthetic fuel and this work deals with optimizing the operation of a thermally-coupled fluidized-bed tar sands extraction process.

Tar Sand Resources

The demonstrated resources of natural bitumen amount to about 2500 billion barrels (181). Of these resources, about 90% is found in North America, mainly in Alberta, Canada; 4% in South America, 2% in Russia; 1% in Europe; and small amounts elsewhere. Figure 139 shows this distribution on a world map. In the United States the resource in place is estimated to total about 42 billion barrels half of which is in Utah

(52, 182-184). Ritzma and Campbell conducted one of the most detailed studies on Utah tar sands (185). Table 50 shows the aerial extent, gross oil in place, and other important reservoir properties of these deposits. The estimates of Table 50 have not changed during the last decade, except for the Sunnyside deposit, which, due to drilling and characterization, has been reported to contain 6.1 billion/bbls (186).

Bitumen Recovery Methods

Bitumen recovery processes can be generally classified into two types - in-situ and ex-situ methods. The selection of a bitumen recovery process is dependent on the nature of the bitumen, the properties of the sand substrate, and the geological and topographical setting of the deposit (51). Ex-situ methods are possible if mining of the deposit is economically feasible, which is the case if the ratio of the depth of the overburden layer to the depth of the bitumen-impregnated layer is less than or equal to unity.

The in-situ processes include:

1. Thermal processes:

   a) Cyclic Steaming,

   b) Steam Flooding,

   c) Hot Water Flooding,

   d) In-situ Combustion and

2. Solvent processes.

All these processes involve introduction of some type of fluid or energy into the tar sand reservoir to reduce the viscosity and mobilize the bitumen to a production well

(187). The temperature of the reservoir can be increased by injection of steam followed by in-situ combustion or by other heating processes such as radio frequency radiation. The advantages of these methods are that no mining is necessary and more total resource can be recovered as compared to the ex-situ methods. Steamflooding accounts for three-quarters of all Enhanced Oil Recovery (EOR) production. Its success is attributed to the low cost of steam. In-situ combustion processes have numerous operational problems such as channeling, corrosion, and pumping problems. However they are used where steamflooding is not applicable, for example in thin or deep formations containing medium gravity oil (188).

The ex-situ methods include:

1. Thermal,
2. Water-Assisted,
3. Solvent,
4. Combination of Water-Assisted and Solvent.

Thermal methods include heating the tar sand to pyrolyze the nonvolatile molecules and vaporize the volatile compounds. There is a loss of bitumen to gases and coke, but this method is still desirable because the product is a synthetic oil ready to be upgraded to a refinery feedstock. The water-assisted process depends upon the intense mechanical shear forces to detach the bitumen from the sand particles. Chemical forces are the primary separation mechanism in solvent extraction processes. Bitumen-solvent separation, solvent recovery and tailings disposal determine the economics of this process.

One of the ex-situ methods of extracting bitumen is by pyrolysis of tar sands in fluidized-bed reactors. An energy-efficient process using two thermally coupled fluidized beds has been developed, over the last several years, by researchers in the Chemical Engineering Department at the University of Utah and is described by a patent and several dissertations and theses (115-117, 189). A schematic diagram of the process is presented in Figure 140. Crushed tar sand is fed to the first reactor, which operates at 450 to 500°C and is fluidized by an inert gas such as nitrogen, by recycled pyrolysis gas, or by steam. The bitumen pyrolyzes and cracks to lighter products that are carried out with the fluidizing gas to a product recovery system where the condensable oils are separated from the light gases. Part of the bitumen undergoes condensation reactions to form a carbonaceous residue, called coke, which remains on the sand. The coked sand is then passed into a second reactor, fluidized by air and operating at 550 to 600°C, where the coke undergoes a first-stage combustion. Vertically mounted heat pipes, extending into both the beds, transfer the heat evolved during combustion to the endothermic pyrolysis reactor. Sand from the combustion bed is then transferred to a third bed, fluidized or moving, where the remaining coke is combusted. The hot spent sand is then passed through a heat recovery system.

The fraction of the original bitumen that is converted to condensable oils is called the oil yield, and has been found to vary from 50 to 80% depending on the operating conditions and the nature of the tar sand deposit. The operating conditions that primarily influence the oil yield are the pyrolysis bed temperature and the average residence time of the solids in the reactor. Different researchers, working with

different tar sands, have arrived at different conclusions regarding the optimum operating conditions to maximize the oil yield. Dorius (51), working with the PR Spring tar sand deposit, found an optimum pyrolysis temperature of 525°C whereas Venkatesan (50) found that for Sunnyside tar sand feed the optimal value was about 450°C. Wang (114) found that the oil yield and the optimum temperature increased with decreasing residence time over the range of 16 to 30 minutes. Clearly, much more experimental data is required of various tar sands to reach any definite conclusion about the optimum operating conditions.

An alternative approach to the determination of optimal operating conditions is mathematical modeling and computer simulation of the operation of the coupled fluidized bed process. Such a model must incorporate fluidization hydrodynamics, heat and mass transfer, mass and energy balances, as well as the reaction kinetics and stoichiometry of the pyrolysis and combustion reactions. An accurate model may then be used to develop an optimum commercial design, cost estimate, and financial analysis of the process to produce an upgraded refinery feedstock from tar sands.

Research Objectives

The objectives of the research during this reporting period were as follows:

1. Completion of the mathematical model for the coupled fluidized beds by adding: (a) a submodel for the transfer of heat across the heat pipes, (b) an expression for the heat of pyrolysis, and (c) a correlation for the transfer of heat to and from the fluidized beds and the heat pipes. The model could then be used to solve the energy balance equations

for the reactor system, while accounting for heat input from an external energy source or removal of excess heat from the system. Runs could then be conducted with the model to predict yields of oil and determine optimal operating conditions for the reactors.

2. Experimental verification of the mathematical model. The model incorporates mass transport, heat transport, hydrodynamic phenomena, and a novel pyrolysis network, developed by Coronella (1994). The model predicts the light gas, coke, oil yields, and oil density for a wide range of operating conditions. In this model it is found that oil field depends primarily on two operating parameters, the pyrolysis bed temperature and the average solids residence time. The reaction network in this model determines the product yield and distribution; which can also be found experimentally, from the material balance and simulated distillation runs. The model assumes certain physical characteristics associated with the pseudo components in the reaction network, which can be used to compare the results of the simulated distillation runs. The rate constants and the reaction mechanism can then be modified so that the model approaches the observed results. Experiments can also be used to justify or modify certain terms in the energy balance used in the model. Finally, the experimental data points obtained for the oil yield, gas yield and oil density as a function of the pyrolysis temperature and pyrolysis residence time can be compared with the results obtained from the model.

3. Analysis of products from experimental runs. The liquid product analysis makes it possible to determine the attractiveness of the synthetic oil as a refinery feedstock. The liquid analysis includes the following properties: (a) specific gravity, (b) viscosity, (c) pour point, (d) Conradson carbon residue, (d) ash content, (e) simulated distillation and (f) sulfur content.

4. Determination of process control methods. Possible control objectives included the following:

(a) Maximize the oil yield. It might be desirable to maximize the total amount of oil produced or it might be desirable to maximize the amount of heavy or light oil or a certain distribution of the heavy, medium and light oils.

(b) Minimize or produce a desired amount of light gases.

(c) Minimize the amount of heat used by making efficient use of heat pipes.

(d) Minimize production by maximizing feed rate, or minimizing residence time

(e) Minimize the amount of coke produced.

All these objectives can be incorporated into a cost function. This cost function is then minimized, by an optimal control strategy using variational calculus, giving the optimal path to be taken by the control variables.

REVIEW OF PREVIOUS MODELING WORK

In spite of being one of the most researched areas of chemical engineering, the various phenomena that take place in fluidized beds are not completely understood. Most researchers would agree that there is no universally applicable model for the various types of fluidization. Models for a gas-solid fluidized bed, which is the most common type of fluidization, range from the simple 1-D models, where the properties are assumed to vary only in the axial direction, to the more realistic, but highly complicated and computationally intensive, 3-D models, where properties are assumed to vary in all directions. The choice of model is dictated by the level of accuracy desired and the limitations of the computer available.

In this study, a simple 1-D, two-phase model was selected for the reactors. A brief overview of the model, the hydrodynamics, the mass transfer and the reaction kinetics is presented below. Detailed description of the derivation and solution of the fluidized-bed model is available elsewhere (118,190,191).

Fluidized bed model

The two-phase bubbling-bed model of Grace was adopted to model the fluidization hydrodynamics and the mass balances of the gas phase species. The model, shown schematically in Figure 141, assumes that: 1) the bed operates in the bubbling regime; 2) the bed is made of two phases, a bubble phase containing very few solids and a dense phase containing most of the solids; 3) the dense phase has a constant void fraction corresponding to minimum fluidization (e_{mf}); 4) the solids are well mixed in the bed; 5) the gas flows in plug flow through the bubble phase while being exchanged continuously with the dense phase; 6) the bed operates isothermally, and 7) properties vary only in the axial direction. In addition, bubble growth in the bed is accounted for by Stubington's modified model (192) of Darton et al. (193):

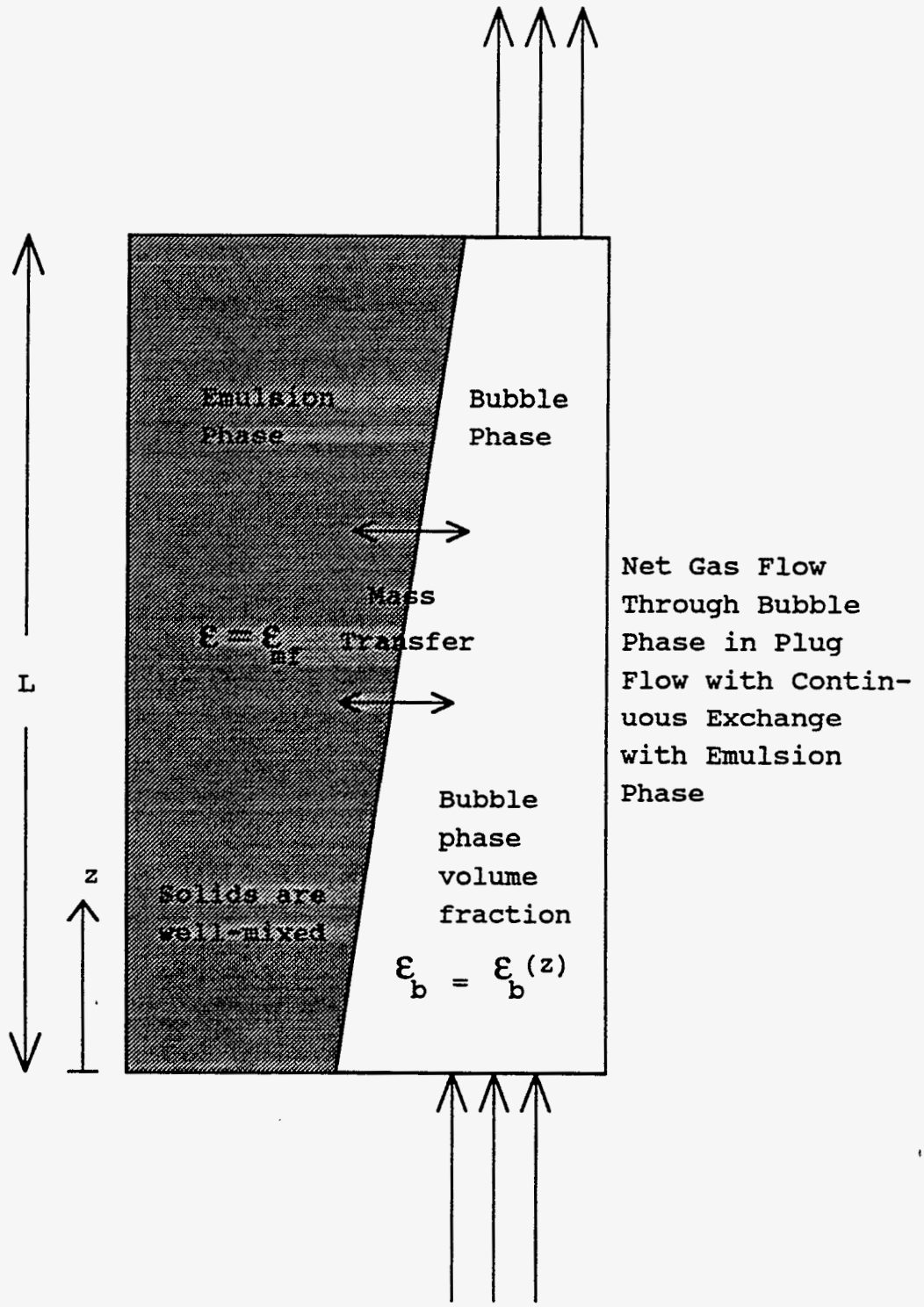

Figure 141. Schematic diagram of Grace's two-phase model for bubbling fluidized beds.

$$d_b = 0.43(u - u_{mf})^{0.4}(z + 0.4\sqrt{A_0})^{0.8} g^{-0.2} \qquad (38)$$

With the assumptions stated above, a mass balance for a species in the bubble phase gives

$$-\frac{d(uC_b)}{dz} + k_q a_b \varepsilon_b (C_d - C_b) + r_b \varepsilon_b = 0 \qquad (39)$$

and in the dense phase

$$k_q a_b \varepsilon_b (C_b - C_d) + r_d (1 - \varepsilon_b) = 0 \qquad (40)$$

where C_b and C_d are the bubble-phase and dense-phase gaseous concentrations, respectively, on a mass or molar basis. In Equation (39), the first term represents convection, the second represents mass transfer between the bubble and dense phases, and the last term represents chemical reaction.

In Equations (39) and (40), the specific mass transfer area of the bubble, a_b, is equal to $6/d_b$, while the interphase mass transfer coefficient, k_q, is evaluated by the following correlation by Grace (194):

$$k_q = \frac{u_{mf}}{3} + \sqrt{\frac{4 D_i \varepsilon_{mf} u_b}{\pi d_b}} \qquad (41)$$

The model assumes that the solid particles in the reactor are well-mixed and therefore the particles leaving the reactor may be assumed to have a residence time distribution (RTD)(195) given by

$$E(t) = \frac{1}{\bar{t}} \exp\left(\frac{-t}{\bar{t}}\right) \qquad (42)$$

Hydrodynamics

The various hydrodynamic parameters required in the model have been derived by Coronella (190) from the two-phase theory of fluidization. These are:

$$L = L_{mf}/(1-\bar{\varepsilon}b) \tag{43}$$

$$L_{mf} = \frac{4\,W\,\bar{t}}{\pi\,(1-\varepsilon_{mf})\,D_B^2} \tag{44}$$

$$\bar{\varepsilon}b = \frac{1}{L}\int_0^L \varepsilon_b(z)\,dz \tag{45}$$

$$\varepsilon_b = \frac{\varepsilon-\varepsilon_{mf}}{1-\varepsilon_{mf}} \tag{46}$$

$$\varepsilon = \frac{u_b\varepsilon_{mf}+u-u_{mf}}{u_b+u-u_{mf}} \tag{47}$$

$$u_b = 0.711\sqrt{g\,d_b} \tag{48}$$

The value of the minimum fluidization velocity, u_{mf}, is derived from the following equation valid at low Reynolds number:

$$Re_{mf} \equiv \frac{\bar{d}p\,u_{mf}\,\rho_g}{\mu_g} = \frac{Ar\,\phi_s^2\,\varepsilon_{mf}^3}{150\,(1-\varepsilon_{mf})} \tag{49}$$

where the Archimedes number is given by

$$Ar \equiv \frac{g \bar{d}_p^3 \rho_g (\rho_s - \rho_g)}{\mu_g^2} \qquad (50)$$

Pyrolysis reaction network and kinetics

Bitumen is made up of a large number of chemical compounds including cross-linked hydrocarbon chains attached to aromatic groups. During pyrolysis, these compounds undergo volatilization and cracking to form lighter products, including light hydrocarbon gases. Since the number of cracking reactions taking place is very large, bitumen pyrolysis is modeled by limiting the number of compounds and the number of reactions to a small finite number.

Coronella (118) proposed a novel reaction network for the pyrolysis of tar-sand bitumen, using pseudo-reactants and products to replace the actual chemical species. The fundamental physical properties assigned to these pseudo-components are listed in Table 51. Bitumen is said to be comprised of a light fraction, which undergoes volatilization, and a heavy fraction that cracks to lighter products. The products of pyrolysis are light gases, condensable oils, and a solid carbonaceous residue called coke. Physical properties of ethylene are used to characterize the light gas product, although it consists of all volatile compounds up through nC_5. The liquid product is divided into light oil, middle oil, and heavy oil, as suggested by Phillips et al. (196), and the boiling ranges, densities, etc., of these fractions correspond approximately to those of the products of crude distillation. Any unreacted bitumen and products residing on the sand, leaving the reactor, are included in the coke since these cannot be recovered as products.

The pseudo-components described above have been incorporated into the following network of first-order reactions to model the pyrolysis reactions.

Table 51

Physical characteristics of pseudo-components

Pseudo-Component	Boiling Range (°C)	Molecular Weight	Density (°API)	Phase in Reactor
Heavy Bitumen	> 550			Solid
Light Bitumen	≤ 550			Solid
Heavy Oil	420 - 550	400	9	Vapor
Middle Oil	180 - 420	240	19	Vapor
Light Oil	20 - 180	160	70	Vapor
Light Gas	≤ 20	28		Vapor

Solid phase reactions:

$$\text{Heavy Bitumen} \xrightarrow{k_1} s_1 \text{ Light Bitumen} + s_2 \text{ Coke} \quad (51)$$

$$\text{Light Bitumen} \xrightarrow{k_2} s_3 \text{ Heavy Oil} + s_4 \text{ Middle Oil} + s_5 \text{ Light Oil} + s_6 \text{ Light Gas} \quad (52)$$

$$\text{Heavy Bitumen} \xrightarrow{k_3} s_7 \text{ Coke} + s_8 \text{ Light Gas} \quad (53)$$

Gas phase reactions:

$$\text{Heavy Oil} \xrightarrow{k_4} s_9 \text{ Middle Oil} + s_{10} \text{ Light Oil} + s_{11} \text{ Light Gas} \quad (54)$$

$$\text{Middle Oil} \xrightarrow{k_5} s_{12} \text{ Light Oil} + s_{13} \text{ Light Gas} \quad (55)$$

The kinetic parameters for the above reactions, which were assigned on the basis of kinetic studies of Lin et al. (197) and Phillips et al. (196), are listed in Table 52. Stoichiometric constants in the above reactions refer to weight fractions. Their values, listed in Table 53, have been assigned with some knowledge of the reactions, although the exact values are somewhat arbitrary.

Kinetics of combustion

The process of coke combustion consists of five steps: 1) diffusion of oxygen to the particle surface from the bulk gas stream, 2) adsorption of oxygen on the surface, 3) chemical reaction of coke and oxygen, 4) desorption of the products, and 5) transport of products to the bulk gas stream. It has been found that for small particles, burning at low temperatures (less than 1200 K), the rate-limiting step is the chemical reaction (198).

Coke consists of predominantly carbon and small amounts of hydrogen, nitrogen, and in some cases sulfur. For the purposes of modeling the combustion of

Table 52

First-order kinetic rate constants

	Pre-exponential Factor (s^{-1})	Activation Energy (kJ/gmol)	Temperature Range (^{o}C)	Reference
k_1	6.5×10^{6}	121.1	100 - 500	197
k_2	1.7×10^{5}	82.97	100 - 500	197
k_3	6.78×10^{9}	176.7	360 - 420	196[1)]
k_4	1.05×10^{15}	230.0	360 - 420	196
k_5	1.05×10^{15}	230.0	360 - 420	196

1) Derived from reference 196

Table 53

Stoichiometric constants

Stoichiometric constant	Value (weight fraction)
s_1	0.80
s_2	0.20
s_3	0.70
s_4	0.20
s_5	0.07
s_6	0.03
s_7	0.20
s_8	0.80
s_9	0.70
s_{10}	0.20
s_{11}	0.10
s_{12}	0.60
s_{13}	0.40

coke, any reactions involving nitrogen and sulfur have been neglected. The primary combustion reactions are thus as follows:

$$C(s) + O_2(g) \rightarrow CO_2(g) \quad (56)$$

$$C(s) + 0.5\ O_2(g) \rightarrow CO(g) \quad (57)$$

$$CO(g) + 0.5\ O_2(g) \rightarrow CO_2(g) \quad (58)$$

$$H(s) + 0.25\ O_2(g) \rightarrow 0.5\ H_2O(g) \quad (59)$$

The combustion of coke is modeled as a surface reaction, as mentioned earlier, and is given by the rate expression

$$- r_c = k\, A_p\, p_{O_2} \quad (60)$$

where r_C is the rate of combustion of coke, A_p is the external surface area ($pf_s^2 d_p^2$) and p_{O_2} is the partial pressure of oxygen. The rate constant, k, is given by:

$$k = k_o \exp(-E/RT) \quad (61)$$

The values of k_o and E have been taken to be 8.71×10^3 gm/cm^2 atm O_2 and 35.7 kcal/mol respectively, as suggested by Field et al. (198). The relative amounts of carbon monoxide and carbon dioxide produced by the oxidation of carbon are given by the empirical correlation of Arthur (1951):

$$\frac{r_{CO}}{r_{CO_2}} = 2500 \exp\left(-\frac{6240\,K}{T}\right) \quad (62)$$

where 730 K < T < 1170 K. The oxidation of carbon monoxide to carbon dioxide is modeled by the empirical rate equation of Hottel et al. (199)

$$-r_{CO} = 12\times10^{10} \exp\left(-\frac{16000}{RT}\right) y_{O_2}^{0.3}\, y_{CO}\, y_{H_2O}^{0.5} \left(\frac{P}{RT}\right)^{1.8} \qquad (63)$$

where T is in Kelvin, P is in atmosphere, and R is equal to 82.057 ml atm/gmol K.

Additional modeling work required

The modeling work done previously has incorporated hydrodynamics, reaction kinetics, and stoichiometry and mass transfer considerations into Grace's bubbling-bed model to give independent comprehensive models for the combustion and pyrolysis reactors. For analyzing the laboratory results, the operating conditions specified in the model, such as fluidizing-gas flow rate and tar-sand feed rate, and the diameter of the reactor were taken to be the ones used by Smart (117). The default sand properties are those measured for a Whiterocks tar-sand deposit. The solutions of these models have been obtained by independently specifying the operating temperature of each of the two reactors.

The operating conditions in the pyrolysis reactor affect the yield of coke and hence the amount of coke deposited on the sand particles. This, in turn, affects the total heat evolved during the combustion of this coke. The combustion and pyrolysis reactors are thermally coupled through the heat pipes that transfer this heat to the pyrolysis reactor, thereby affecting the pyrolysis temperature. Clearly, the simulation of the whole reactor system requires the solution of the energy balance equations. This requires correlations for heat transfer between the fluidized bed and the heat pipes and

a model for heat transfer across the heat pipes. Also, any energy supplied, removed, or lost from the reactor system has to be included in the energy balance. This was accomplished in the reporting period covered by this report as presented in the next section.

ENERGY BALANCES AND COUPLING OF REACTOR MODELS

Energy balance around the pyrolysis reactor

A general energy balance around the pyrolysis reactor may be written as follows:

$$\begin{matrix}\text{Energy} \\ \text{flow in}\end{matrix} - \begin{matrix}\text{Energy} \\ \text{flow out}\end{matrix} - \begin{matrix}\text{Energy} \\ \text{consumed}\end{matrix} = \begin{matrix}\text{Energy} \\ \text{accumulated}\end{matrix} \qquad (64)$$

For steady-state operation the energy accumulation term can be set equal to zero. The various modes by which energy enters and leaves the pyrolysis reactor are shown in Figure 142. A steady-state energy balance over the pyrolysis reactor can thus be written as follows:

$$Q_{hp,p} + Q_p - \Delta H_{sand,p} - \Delta H_{gas,p} - \Delta H_{bitumen} - Q_{loss,p} = 0 \qquad (65)$$

The first term accounts for the energy supplied to the pyrolysis reactor by the heat pipes. Q_p is the energy supplied to the reactor by external means such as steam or electricity. Tar sand fed to the reactor is generally at ambient temperature because higher temperatures make it sticky and cause problems in the feeding operation. The fluidizing gas may be passed through a preheater before being introduced in the reactor. Since heat transfer within a fluidized bed is very rapid it is assumed that the temperature within the reactor is uniform and that all streams leaving the reactor are at pyrolysis temperature. The terms $\Delta H_{gas,p}$ and $\Delta H_{sand,p}$, in equation 65, account for the sensible heat required to heat the fluidizing gas and the sand portion of the tar-sand-feed, respectively, to the pyrolysis temperature, and are given by

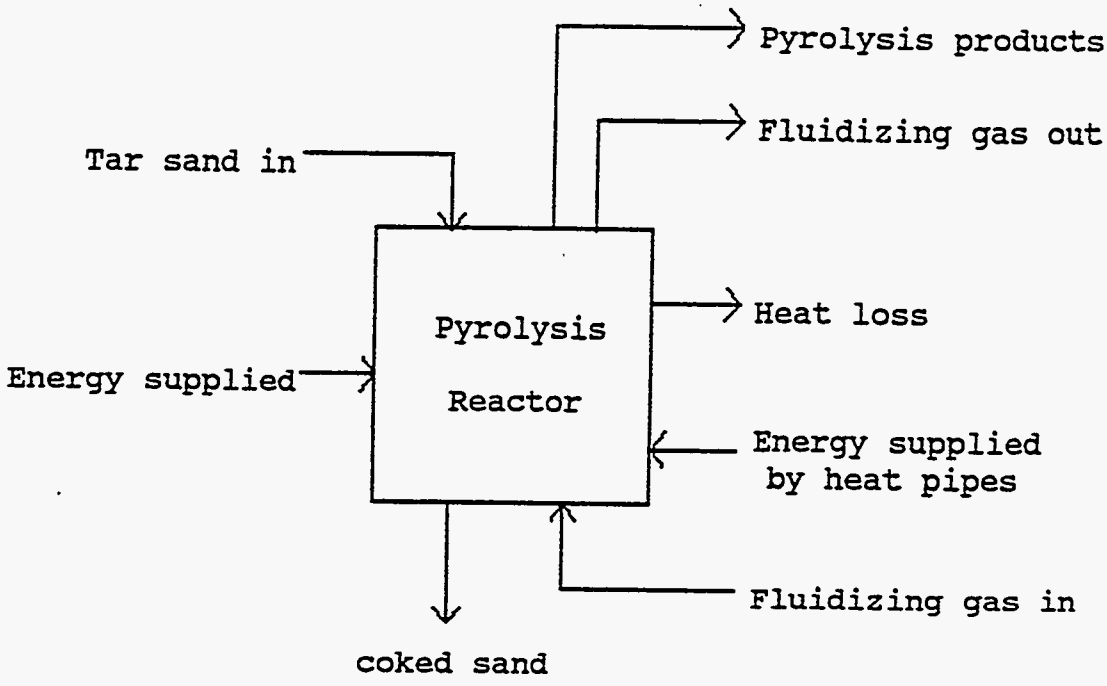

Figure 142. Energy balance around the pyrolysis reactor

$$\Delta H_{gas} = m_{gas} \int_{T_g}^{T_p} C_{p,gas}\, dT \tag{66}$$

$$\Delta H_{sand} = m_{sand} \int_{T_f}^{T_p} C_{p,sand}\, dT \tag{66}$$

It should be noted, however, that SiO_2, which is the main constituent of sand, undergoes a phase change from α-quartz to β-quartz at about 848 K (200), so the heat of this phase change must be included in equation 67 if T_p is greater than 848 K.

The term $\Delta H_{bitumen}$, in equation 65, includes the sensible heat for bitumen and the heat of the thermal pyrolysis reactions. The sensible heat component can be calculated similarly to that of sand or gas. Specific heat capacity of the bitumen is evaluated from the following generalized correlation for all petroleum-like liquids (201):

$$C_p = [0.6811 - 0.308s + (8.15 - 3.06s)\, T\times10^{-4}] \times (0.055K + 0.035) \tag{68}$$

where C_p is the heat capacity in Btu/lb^{o}F, s is the specific gravity at 60^{o}F, T is the temperature in ^{o}F, and K is the Watson characterization factor.

The second component of $\Delta H_{bitumen}$, the heat of pyrolysis reactions, ΔH_{pyr}, is evaluated by assuming that the pyrolysis process can be represented by a single reaction as follows:

$$\text{Bitumen} \rightarrow x_1 \text{ Gas} + x_2 \text{ Oil} + x_3 \text{ Coke} \tag{69}$$

where x_1, x_2, and x_3 represent the weight fractions of bitumen going to gas, oil

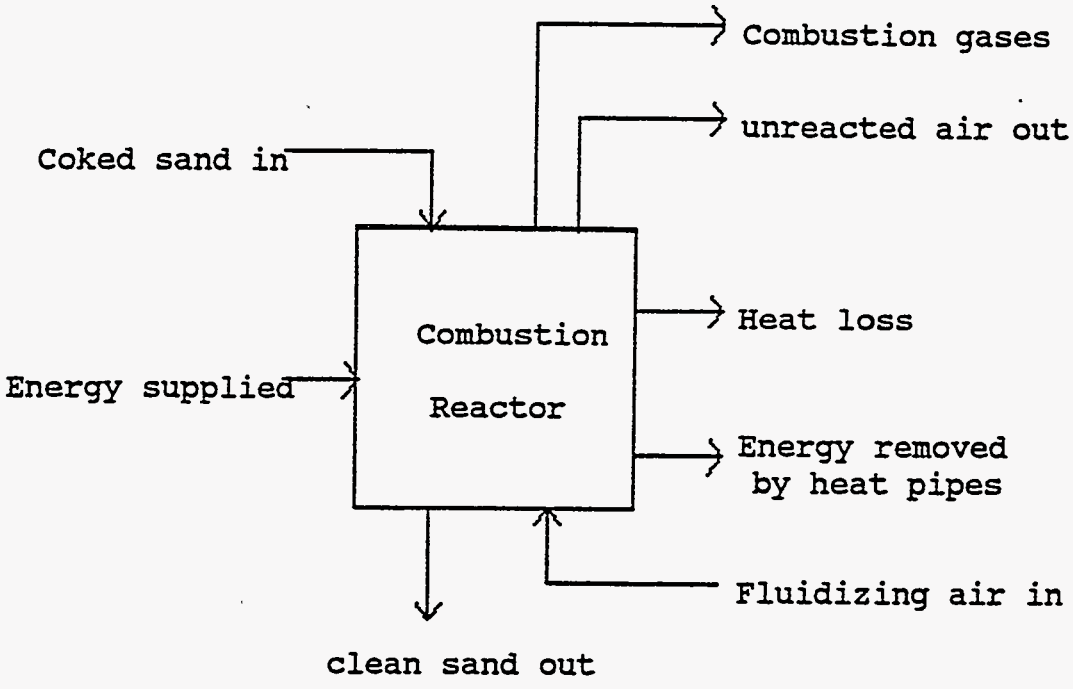

Figure 143. Energy balance around the combustion reactor.

and coke respectively. Thus

$$\Delta H_{pyr} = m_{pyr}\left(\Delta H^{\circ} + \Sigma \nu_i \int_{298}^{T_p} C_{p,i}\, dT\right) \qquad (70)$$

where m_{pyr} is the mass rate of bitumen pyrolysis, ΔH^{o} is the standard heat of pyrolysis at 25°C, and u_i represents the stoichiometric number of the species i involved in the pyrolysis reaction (equation 69).

Equation 65, also includes a term to account for heat loss from the reactor due to convection and radiation, $Q_{loss,p}$, which is evaluated as follows:

$$Q_{loss,p} = h\, A\, (T_s - T_{¥}) + e_m\, s\, A\, (T_s^4 - T_{¥}^4) \qquad (71)$$

where T_s is the absolute external surface temperature of the reactor and $T_{¥}$ is the absolute temperature of the surroundings.

Energy balance around the combustion reactor

The various modes by which energy enters and leaves the combustion reactor are shown in Figure 143. A steady state energy balance, similar to the pyrolysis reactor, can be written around the combustion bed as follows:

$$\Delta H_{coke} + Q_c - Q_{hp,c} - \Delta H_{sand,c} - \Delta H_{gas,c} - Q_{loss,c} = 0 \qquad (72)$$

The terms Q_c, $Q_{hp,c}$, $\Delta H_{sand,c}$, $\Delta H_{gas,c}$, and $Q_{loss,c}$ are analogous to those in equation 65 and can be evaluated in a similar manner. The main differences are that $Q_{hp,c}$ is the energy removed by the heat pipes, that the sand enters the reactor at the pyrolysis temperature, T_p, and that the fluidizing gas is air, instead of an inert gas like nitrogen, which reacts with the coke.

The term ΔH_{coke}, in equation 72, includes the sensible heat required to heat the coke from pyrolysis temperature, T_p, to the combustion temperature, T_c, and the exothermic heat of combustion, ΔH_{comb}. For evaluating the heat of combustion, coke entering the combustion reactor is assumed to be made up of carbon and hydrogen only and other constituents like nitrogen, sulphur, etc., if any, are neglected. Coke thus reacts with oxygen from air to form carbon dioxide, carbon monoxide, and water vapor according to equations 56 to 59. Thus, we have

$$\Delta H_{comb} = \Delta H_{CO} + \Delta H_{CO_2} + \Delta H_{H_2O} \tag{73}$$

$$\Delta H_{comb} = m_{CO}\left(\Delta H^0_{CO} + \Sigma \upsilon_i \int_{298}^{T_c} C_{p,i}\, dT\right) + m_{CO_2}\left(\Delta H^0_{CO_2} + \Sigma \upsilon_i \int_{298}^{T_c} C_{p,i}\, dT\right) + m_{H_2O}\left(\Delta H^0_{H_2O} + \Sigma \upsilon_i \int_{298}^{T_c} C_{p,i}\, dT\right) \tag{74}$$

In this equation, m_i is the mass rate of formation of species i from coke while ΔH^0_i is the corresponding standard heat of reaction at 25°C and can be evaluated from the standard free energies of formation at 25°C.

Heat transfer across the heat pipes

A typical heat pipe is shown in Figure 144. It is basically a sealed tube, lined along its inner surface with a porous capillary wick, and containing a suitable amount of working fluid (often under vacuum). Heat is supplied by external means to one end of the tube, causing the working fluid to vaporize. The resulting pressure difference drives the vapor to the other end where it condenses, giving off the latent heat of vaporization to a heat sink in that section of the pipe. Depletion of liquid by evaporation at the hot end develops a capillary pressure in the wick that pumps the condensed liquid back to the evaporating section for re-evaporation.

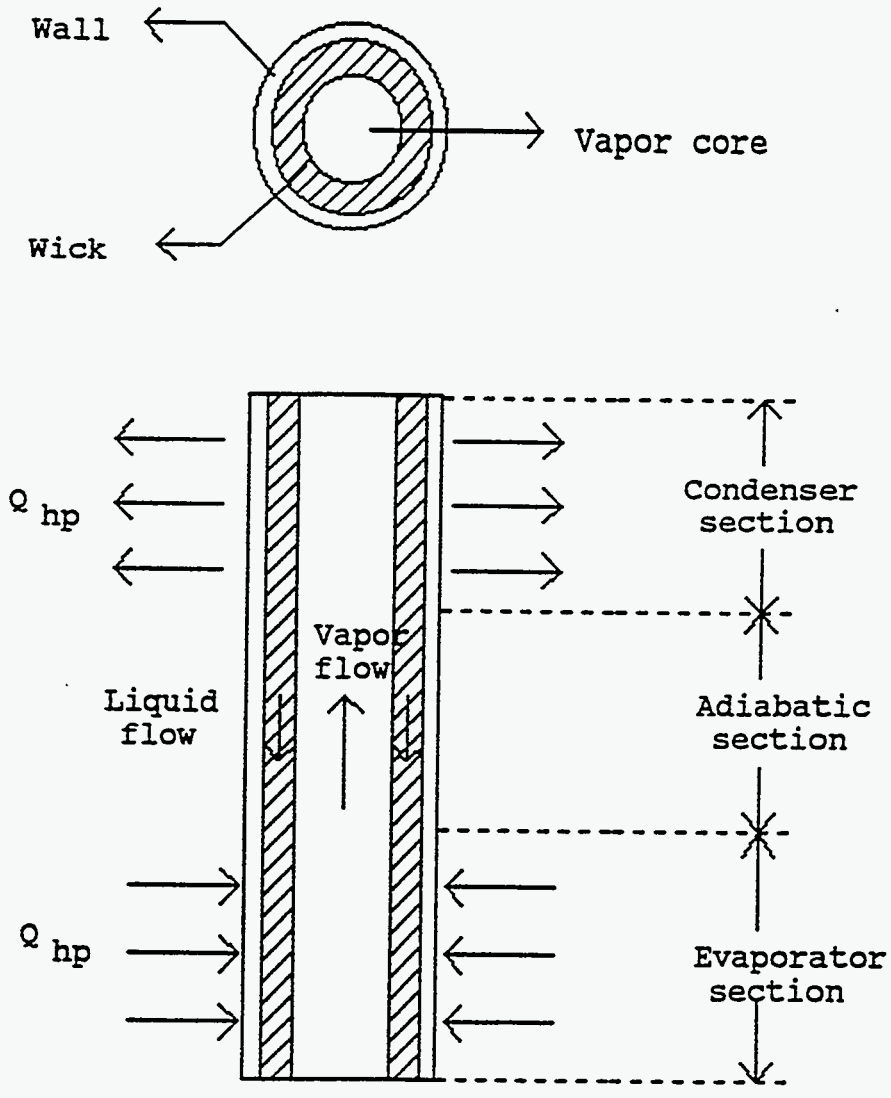

Figure 144. Components and principles of operation of a conventional heat pipe.

Since the latent heat of vaporization is generally quite large, considerable quantities of heat can be transported continuously with a very small temperature difference from end to end. Detailed descriptions of the heat pipe operation can be found in the literature (202, 203).

In the coupled fluidized-bed process developed at the University of Utah, heat pipes filled with potassium as the working fluid extend from the bottom of the combustion bed to the freeboard region (open area above the bed consisting of gas) of the pyrolysis bed. In this case, the combustion bed and the freeboard region above it serve as the heat source to vaporize the working fluid. However it has been found that heat transfer coefficients between gas-fluidized beds and vertical surfaces, such as an immersed tube, are one or two orders of magnitude larger than for gases alone. Hence the heat transferred to the heat pipes in the freeboard region may be neglected. Thus the heat supplied to the evaporating section of the heat pipes may be evaluated as follows:

$$Q_{hp,c} = h_c \, n_{hp} \, p \, d_{hp} \, L_c \, (T_c - T_{hp,c}) \qquad (75)$$

where h_c is the heat transfer coefficient from the combustion bed to the heat pipes, n_{hp} is the number of heat pipes, d_{hp} is the outside diameter of the heat pipes, L_c is the height of the combustion bed, and $T_{hp,c}$ is the external surface temperature of the heat pipe in the combustion bed.

The pyrolysis bed and the freeboard region above it serve as the heat sink. Neglecting the heat transferred to the freeboard region, we get

$$Q_{hp,p} = h_p \, n_{hp} \, p \, d_{hp} \, L_p \, (T_{hp,p} - T_p) \qquad (76)$$

It is assumed here that the heat pipes extend through the entire length, L_p, of the pyrolysis bed. If the heat pipes do not extend to the entire bed height, L_p in equation 76 should be replaced by the height to which they actually extend into the bed. In addition it is also assumed that the section between the combustion and pyrolysis reactors is adiabatic and hence there is negligible heat loss. Therefore an energy balance around the heat pipes can be written as follows:

$$Q_{hp,c} - Q_{hp,p} = 0 \tag{77}$$

Thus all the energy supplied to the heat pipes by the combustion bed is assumed to be transferred to the pyrolysis bed. The path of heat flow across the heat pipes consists of the following three steps: 1) heat conduction across the pipe wall and the liquid-saturated wick in the combustion section followed by evaporation at the liquid-vapor interface in that section, 2) axial convective transport of the latent heat by vapor from the evaporator to the condenser section, 3) condensation of vapor at the liquid-vapor interface in the condenser section of the heat pipe, and subsequent heat conduction across the liquid-saturated wick and pipe wall in that section. The temperature drop across the heat pipe wall and in the liquid-saturated wick can be derived by using Fourier's law of conduction. Thus the temperature drop across the heat pipe wall in the evaporator section is given by

$$T_{hp,c} - T_{pw,e} = Q_{hp} \frac{\ln(r_o/r_i)}{2\pi L_e k_p} \tag{78}$$

where $T_{pw,e}$ is the temperature at the pipe wall-wick interface in the evaporating section, r_o and r_i are the outside and inside diameters of the heat pipe respectively, L_e is the length of the evaporator section and k_p is the thermal conductivity of the heat pipe material. As discussed earlier, L_e is taken as the length of heat pipe

immersed in the combustion bed and does not include the length of the freeboard region. Similarly, the temperature drop across the liquid-saturated wick is treated as an effective conduction problem and is given by

$$T_{pw,e} - T_{wv,e} = Q_{hp} \frac{\ln(r_i / r_v)}{2\pi L_e k_{e,e}} \tag{79}$$

where $T_{wv,e}$ is the temperature at the interface of the wick and the vapor core in the evaporator section, r_v is the radius of the vapor core, and $k_{e,e}$ is the equivalent thermal conductivity of the wick in the evaporator region. Chi (202) recommends the following expression for the equivalent thermal conductivity of wrapped screen wicks:

$$k_e = k_l \frac{(k_l + k_w) - (1-\varepsilon_w)(k_l - k_w)}{(k_l + k_w) + (1-\varepsilon_w)(k_l - k_w)} \tag{80}$$

where e_w is the void fraction of the wick, and k_l and k_w are the thermal conductivities of the liquid and the wick, respectively. The temperature difference across the vapor-liquid interface at the wick surface is generally small and is neglected. The temperature drop along the vapor column is related to the vapor pressure by the Clausius-Clapeyron equation and is given by

$$T_{v,e} - T_{v,c} = \frac{T_v (P_{v,e} - P_{v,c})}{\rho_v \lambda} \tag{81}$$

where r_v is the density of the vapor and l is the latent heat of vaporization. The temperature drops across the saturated wick and the heat pipe wall in the condenser section are calculated similar to those in the evaporator section and are given by the following:

$$T_{wv,c} - T_{pw,c} = Q_{hp} \frac{\ln(r_i/r_v)}{2\pi L_c k_{e,c}} \tag{82}$$

$$T_{pw,c} - T_{hp,p} = Q_{hp} \frac{\ln(r_o/r_i)}{2\pi L_c k_c} \tag{83}$$

Adding equations 78, 79, 81, 82, 83, we get the overall temperature drop across the heat pipe:

$$T_{hp,c} - T_{hp,p} = Q_{hp}\left[\frac{\ln(r_o/r_i)}{2\pi L_e k_p} + \frac{\ln(r_i/r_v)}{2\pi L_e k_{e,e}} + \frac{T_v(P_{v,e} - P_{v,c})}{\rho_v \lambda} + \frac{\ln(r_i/r_v)}{2\pi L_c k_{e,c}} + \frac{\ln(r_o/r_i)}{2\pi L_c k_c}\right] \tag{84}$$

Generally, when working in the operating range of the working fluid and below flow saturation limits, the temperature gradient along the vapor core is small and the corresponding term in equation 84 can be neglected.

Heat transfer from heat pipes to fluidized bed

In order to solve the energy balance equations, the heat transfer coefficient between the heat pipes and pyrolysis bed, h_p,and the combustion bed, h_c, need to be evaluated. Fluidized-bed heat transfer is a very complex phenomenon as it is influenced by a variety of factors like gas properties, solids properties, fluidizing gas velocity, orientation and geometry of tube bundles, and temperature. Thus, correlations for heat transfer coefficients are numerous and quite often limited to a specific range of operating conditions. Saxena (204) has published a complete review of available experimental and theoretical information concerning bed to surface heat transfer coefficients and has classified particles into four groups based

on hydrodynamic and heat transfer considerations (205). Bubbling beds of sand fluidized by nitrogen or air falls into their Group I powders characterized by

$$3.55 \text{ £ Ar £ } 21700 \quad . \tag{85}$$

$$1.5\left[\frac{\mu_g^2}{\rho_g g(\rho_s - \rho_g)}\right]^{1/3} \leq d_p \leq 27.9\left[\frac{\mu_g^2}{\rho_g g(\rho_s - \rho_g)}\right]^{1/3} \tag{86}$$

where Ar is the Archimedes number given by

$$Ar = \frac{d_p^3 g \rho_g (\rho_s - \rho_g)}{\mu_g^2} \tag{87}$$

Physically, for such powders, the fluid flow around the particles is laminar and minimum fluidization voidage, e_{mf}, remains constant with changing Re_{mf} and Ar.

For Group I powders, there have been only limited efforts to find correlations for heat transfer coefficients to an immersed vertical tube. While none of these are capable of representing the experimental data corresponding to a wide range of operating conditions with sufficient accuracy, Saxena recommends the following correlation developed by Wender and Cooper (206):

$$h = 3.5\times10^{-4} C_R \frac{k_g}{d_p}(1-\varepsilon)\left(\frac{k_g}{C_{p,g}\rho_g}\right)^{-0.43} Re^{0.23}\left(\frac{C_{p,s}}{C_{p,g}}\right)^{0.8}\left(\frac{\rho_s}{\rho_g}\right)^{0.66} \tag{88}$$

where (k_g / $C_{p,g}$ r_g) is a dimensional term having units of m^2/s. Although this correlation has been found to be the best for predicting h to an axially placed tube, there is some disagreement over C_R, a correction factor proposed by Vreedenberg

(207) for nonaxial tube location. In the actual process, although the heat pipes are located nonaxially, they tend to compartmentalize the fluidized bed into smaller units and hence the correction factor, C_R, is ignored.

Considering the limited accuracy of the empirical correlations, theoretical models were evaluated to derive an expression for the heat transfer coefficient. The most successful type of model used is the packet model of Mickley and Fairbanks (208) where the heat transfer surface is assumed to be bathed alternately by emulsion packets and gas bubbles. Heat transfer occurs due to particle convection, gas convection, and radiation between the heat transfer surface and the emulsion or bubbles. Thus the total heat flux from the bed to an immersed surface is given by

$$q = (q_{pc,d} + q_{gc,d} + q_{r,d})(1 - e_b) + (q_{gc,b} + q_{r,b})e_b \qquad (89)$$

where e_b is the bubble phase fraction at the surface. It has been found that heat transfer due to radiation is negligible below 900°C (Molerus, 209), and hence the radiation terms, $q_{r,d}$ and $q_{r,b}$, may be neglected. Also for group I particles heat transfer by gas convection is small and consequently equation 89 reduces to

$$q = q_{pc,d}\,(1 - e_b) \qquad (90)$$

Kunii and Levenspiel (135) proposed a modified packet model for the heat transfer coefficient, which reduces to the following equation for group I particles at low temperatures:

$$h = 1.13\left[\frac{k_e^o\,\rho_s\left(1-\varepsilon_{mf}\right)C_{p,s}}{\tau}\right]^{1/2}\left(1-\varepsilon_b\right) \qquad (91)$$

where k_e^o is the effective thermal conductivity of a fixed bed given by

$$k_e^o = \varepsilon_{mf}\, k_g + (1-\varepsilon_{mf})k_s\left[\frac{1}{\phi_b(k_s/k_g)+2/3}\right] \tag{92}$$

The mean contact time, t, of the emulsion with the surface and the bubble phase fraction at the surface, e_b, are evaluated by the following formulas proposed by Thring (1977):

$$\tau = 8.932\left[\frac{gd_p}{u_{mf}^2(u/u_{mf}-1)^2}\right]^{0.0756}\left(\frac{d_p}{0.025}\right)^{0.5} \tag{93}$$

$$\varepsilon_b = 0.08553\left[\frac{u_{mf}^2(u/u_{mf}-1)^2}{gd_p}\right]^{0.1948} \tag{94}$$

The Kunii-Levenspiel model accounts for the effect of thermal conductivity of solids and gas, the specific heat capacity, density, and mean diameter of solids, as well as the effect of the superficial velocity. However there is no term in the model that suggests the dependence of the heat transfer coefficient on the void fraction of the bed, e, which changes with the size, location and orientation of the immersed tubes. On the other hand the Wender-Cooper correlation accounts for the effect of gas properties, solids properties, superficial velocity and also bed voidage. Thus, a qualitative comparison suggests that the latter may be more suitable.

The heat transfer coefficients predicted by the two methods were further compared with experimental data of Gelperin and Einstein (211) and Verma and Saxena (212), on heat transfer to immersed vertical tubes in beds of Group I particles. The results are shown in Figure 145. The Kunii-Levenspiel model is found to over predict the data by 30% on an average with maximum deviation of about 40%. Wender and Cooper's correlation (205), on the other hand, predicts more conservative and accurate values, the average and maximum deviation being 10% and 30% respectively. In light of these observations, the latter correlation is

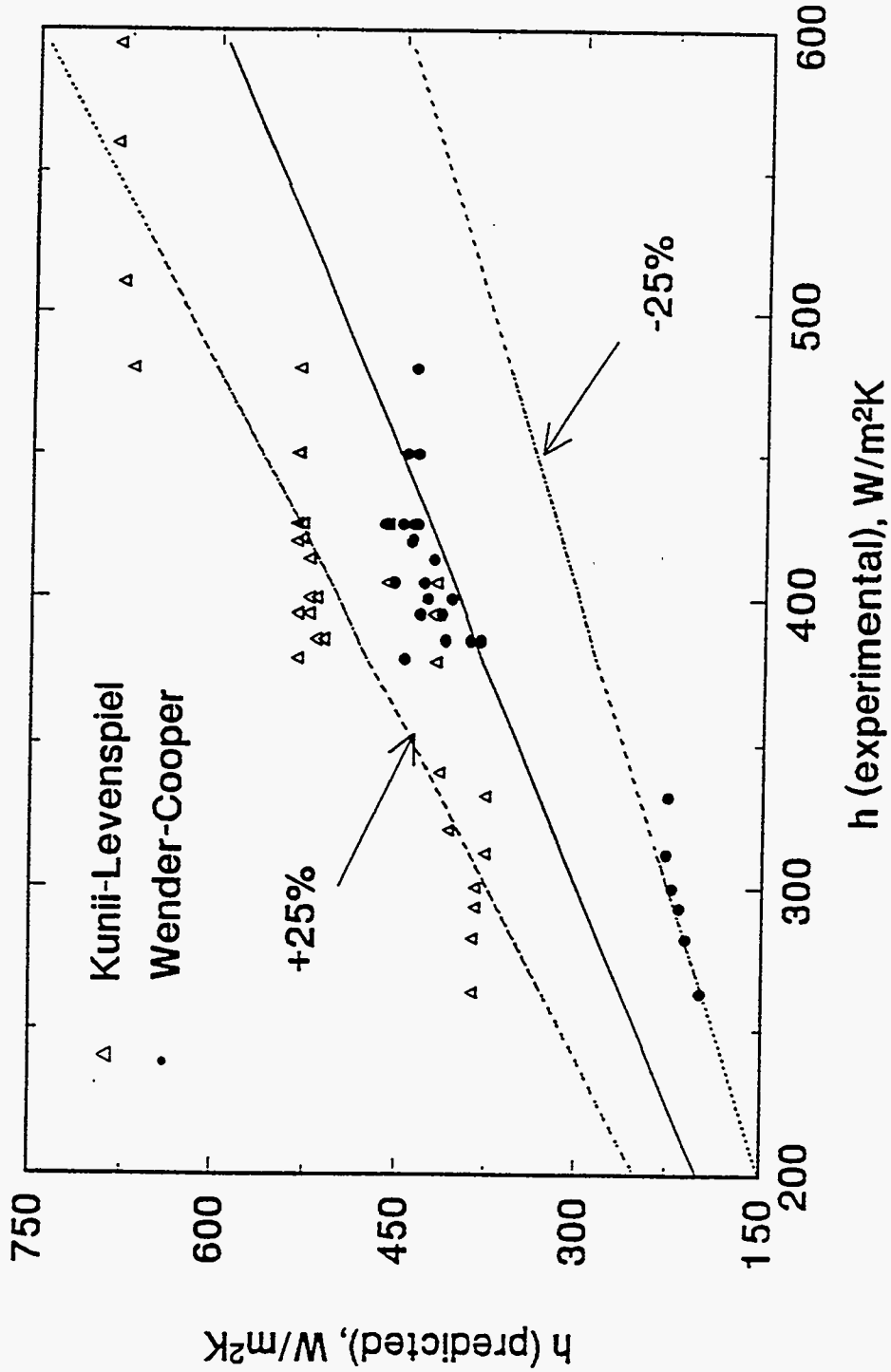

Figure 145. Comparison of heat transfer correlations with experimental data.

chosen for predicting the heat transfer coefficients between the fluidized beds and the heat pipes in the coupled reactor system. The predicted values were found to be in the range of 500-650 W/(m^2 K) depending on the fluidizing gas used and its flow rate.

Thermal coupling of models and solution of the energy balance equations

The coupling of the models involves solving the equations 65, 72, 75, 76, 77, and 84. Equations 65 and 72 are nonlinear in temperature because of the nonlinear dependence of specific heat capacities on temperature. Equations 75, 76, 77, and 84, on the other hand, are linear algebraic equations. A degrees of freedom analysis of the system of six equations gives 10 variables, viz. T_p, T_c, $Q_{ext,p}$, $Q_{ext,c}$, $Q_{loss,p}$, $Q_{loss,c}$, $Q_{hp,p}$, $Q_{hp,c}$, $T_{hp,p}$, and $T_{hp,p}$. Therefore the solution of the system of equations requires four variables to be independently specified.

The heat losses from the reactors, $Q_{loss,p}$ and $Q_{loss,c}$, can be specified by using equation 71 to evaluate them. The possible choices for the other two are T_p, T_c, $Q_{ext,p}$, or $Q_{ext,c}$. The pyrolysis model and the combustion model require the specification of the operating temperatures, T_p and T_c. Thus by not specifying T_p and T_c, an iterative procedure is required, where at first T_p is assumed and the pyrolysis model is solved. Then the combustion model is solved by assuming T_c followed by solution of the coupling and energy balance equations, which give new values of T_p and T_c. The procedure may be repeated until convergence is attained. On the other hand, by specifying T_p and T_c,

the need for an iterative procedure is eliminated. This choice of variables is logical considering the fact that in a large-scale plant, the operating temperatures would be maintained at a given set point and controlled by supplying or removing heat from the reactors. Hence T_p and T_c are chosen as the variables to be specified.

The variables in the coupling and energy balance equations are thus $Q_{ext,p}$, $Q_{ext,c}$, Q_{hp}, $T_{hp,p}$, and $T_{hp,c}$. By fixing T_p and T_c, the energy balance equations, 65 and 72, are reduced to linear form and now we have a system of simple linear algebraic equations to be solved. This can be done by using any suitable technique such as the Gaussian Elimination method.

Thus the solution procedure for the entire coupled model consists of three steps: 1) specify pyrolysis temperature and solve the pyrolysis model, which gives the yields of oil, gas, and coke from bitumen pyrolysis, 2) specify combustion temperature and solve the combustion model, which gives the conversion of coke, and 3) solve the coupling and energy balance equations, which gives the quantity of heat that has to be supplied to or removed from the reactors to maintain the optimum temperatures.

MODEL STUDIES TO OPTIMIZE PROCESS

A model of this type can be used to optimize the operation of the coupled fluidized-bed process. An objective function to be optimized could be oil yield, or operating and annualized capital costs, or the overall plant profitability. Coronella (118) has presented the results of optimizing the pyrolysis operating conditions, of which temperature is the most important. Oil yield was found to be a maximum at about 475°C and a solids residence time of 20 minutes, as shown in Figure 146. The other operating parameters do not directly influence the oil yield and hence the optimum values for these are taken as those which minimize the energy requirement of the process. Figure 147 shows the effect of combustion temperature on the conversion of coke and the energy input required for the process. The operating temperature is dictated by environmental concerns for disposal of the spent sand. However, the higher the combustion temperature, the higher is the energy requirement for heating the fluidizing air. An optimum temperature of 600°C is indicated. At higher temperatures, there is no significant improvement in the conversion of coke, while the energy required increases very rapidly.

The effect of flow rate of pyrolysis fluidizing gas on the heat pipe load and the heat requirement of the process is shown in Figure 148. Increased gas flow rate increases the bed height thereby increasing heat transfer between the bed and heat pipes. The gas flow rate has almost no effect on oil yields as long as the pyrolysis reactor is well fluidized in the bubbling regime. Thus, low flow rates would be desirable since higher flow rates only increase the energy requirement of the process.

On the other hand, in the combustion reactor, low flow rates of fluidizing air are not desirable, as shown by Figure 149, since oxygen becomes the limiting reactant. Only part of the coke gets combusted and less energy is available for

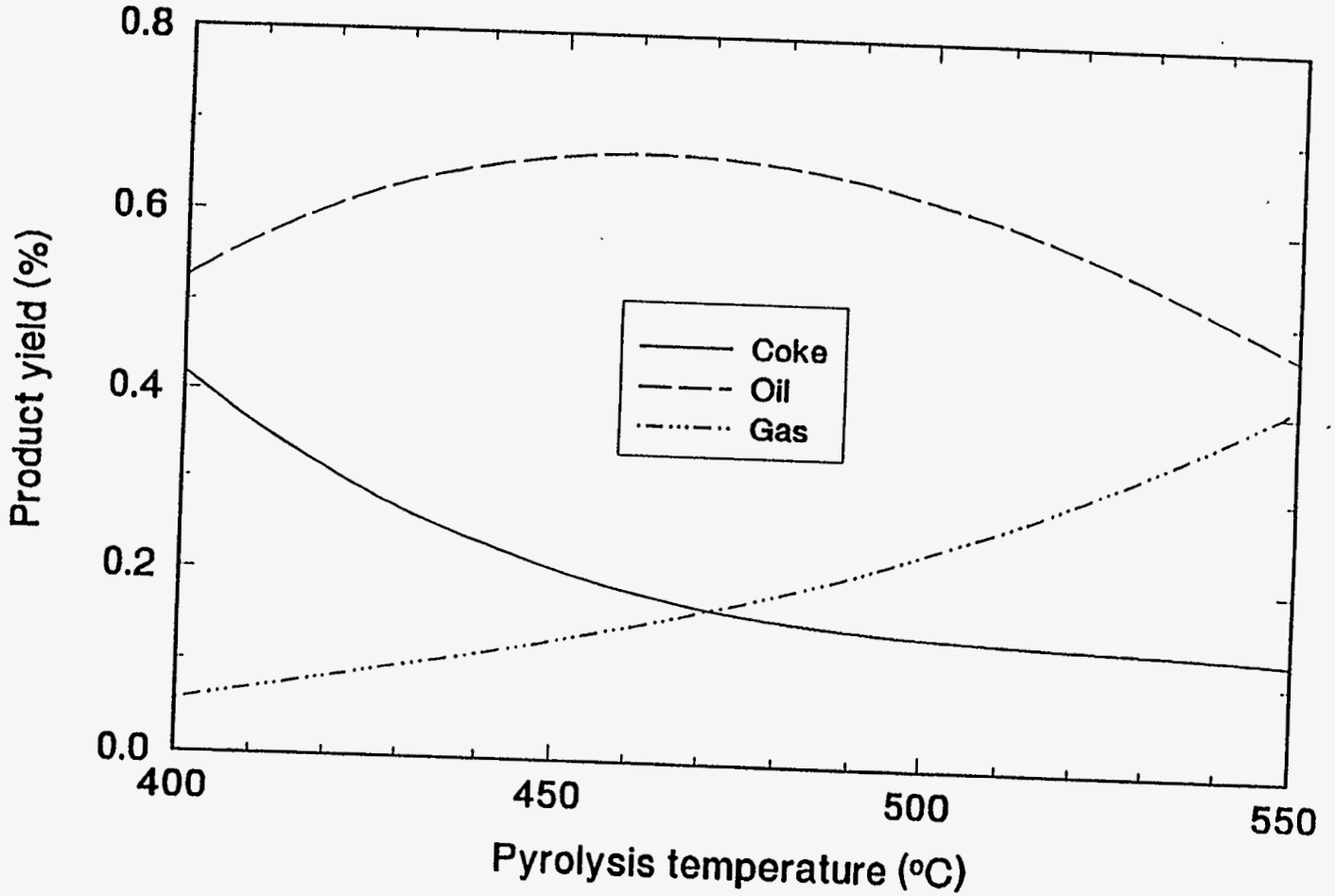

Figure 146. Effect of pyrolysis temperature on predicted oil yields.

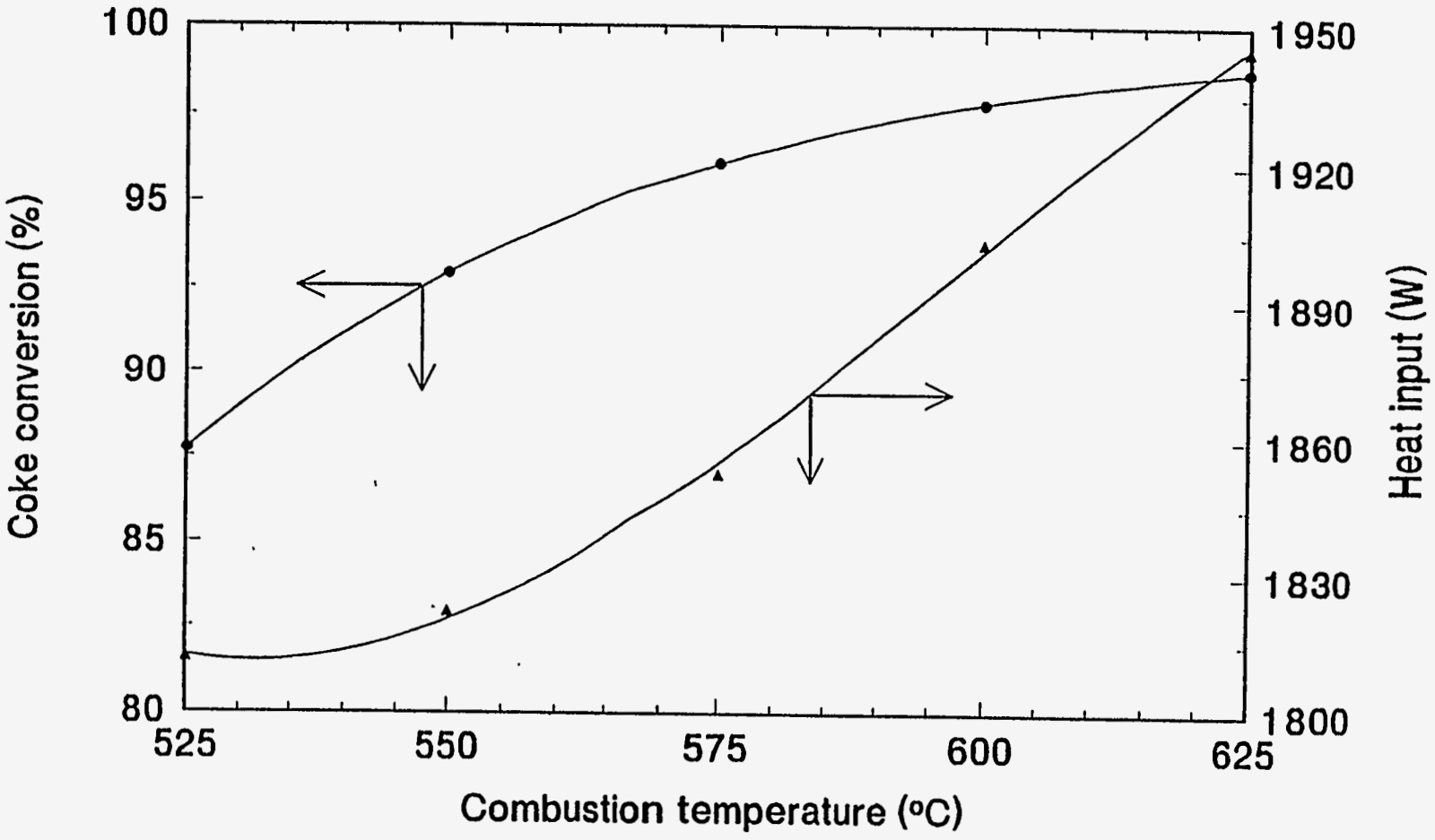

Figure 147. Effect of combustion temperature on predicted conversion of coke.

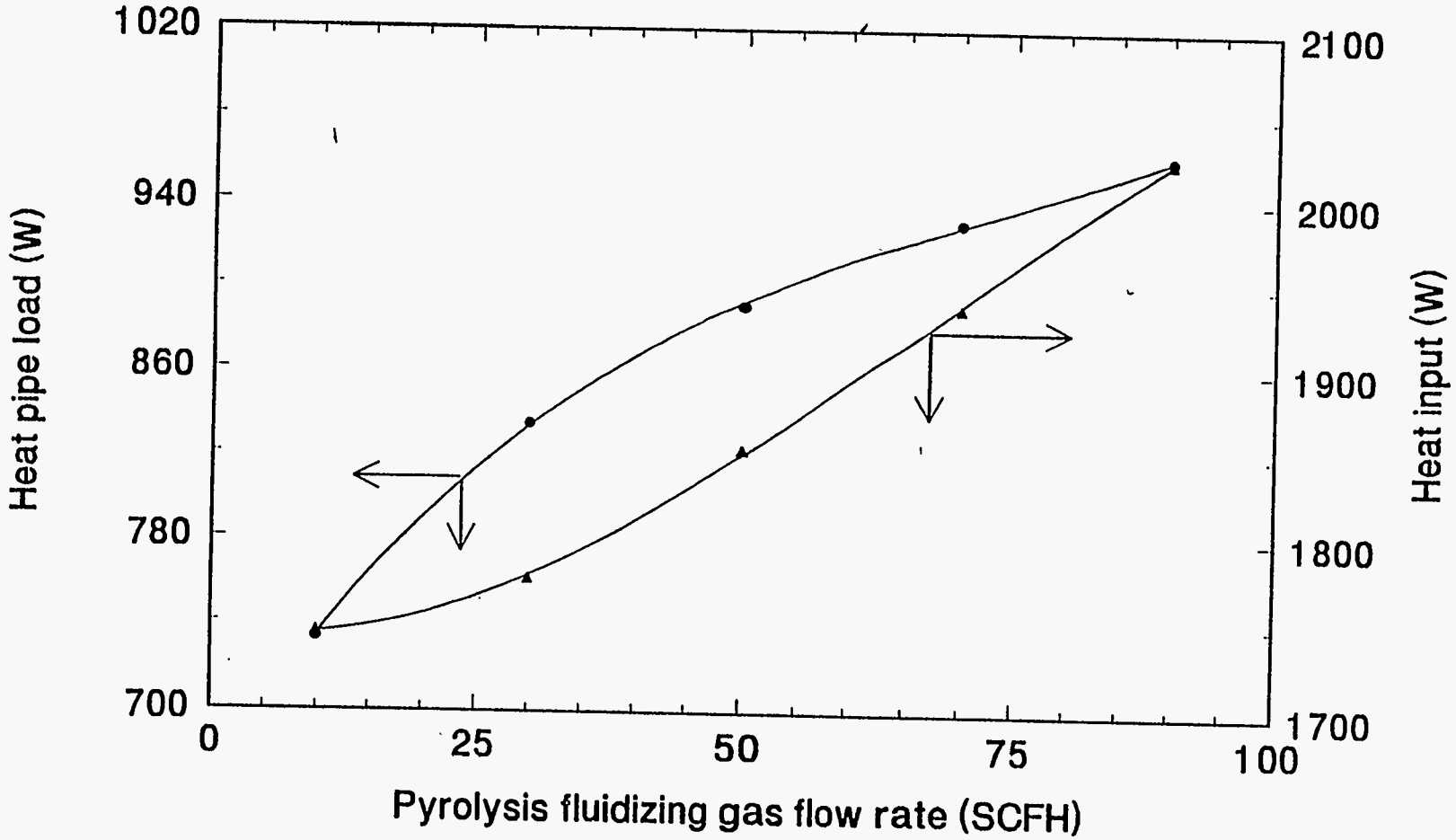

Figure 148. Effect of pyrolysis fluidizing gas flow rate on heat pipe load and energy requirement.

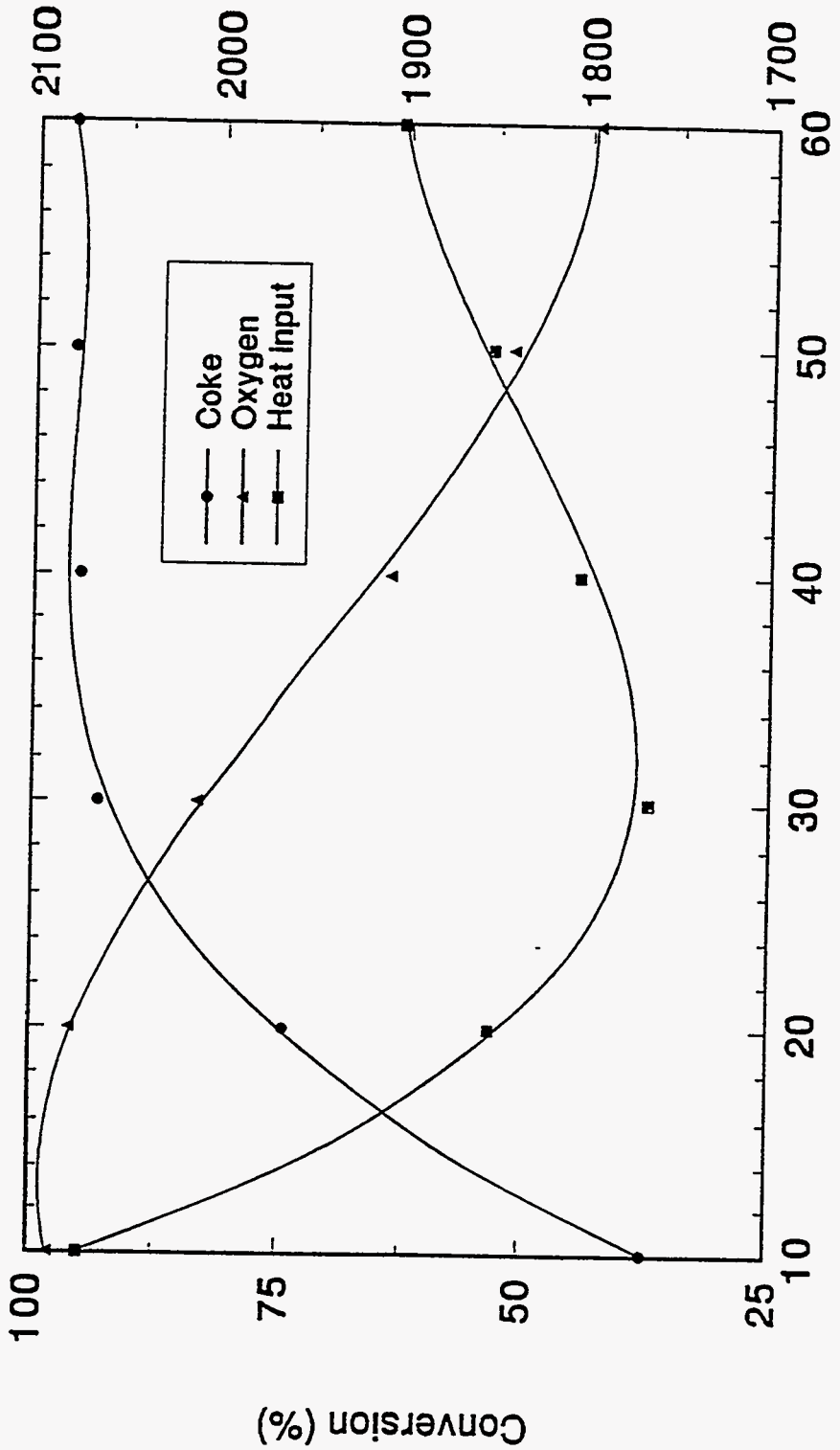

Figure 149. Effect of combustion fluidizing air flow rate on conversion of coke

pyrolysis resulting in higher external energy input. Thus, an air flow rate of about 35 scfh, for the laboratory unit, appears to be the best. The effect of flow rate of fluidizing air on the heat pipe load is shown in Figure 150. Again, higher flow rates increase the bed height and the heat transfer area causing the heat pipe load to increase.

Figures 151 and 152 show the effect of solids residence time in the combustion bed on energy balance. Residence time has the same effect as increasing the gas flow rate, since a higher residence time means a higher bed holdup and a deeper bed. A higher residence time is desirable since it allows more time for the coke to react and, thus, increases the energy available from combustion.

The preceding results are for an inlet temperature of 25°C for both fluidizing gases, which corresponds to the laboratory conditions. However, in a commercial plant the fluidizing gases can be preheated by utilizing the energy available from the spent sand leaving the reactor, pyrolysis product gases or combustion flue gases, thereby reducing the overall energy requirement significantly. However, preheating of the tar sand feed is not advisable because it makes the tar sand sticky and difficult to feed. Also, the heat loss from the reactors is significant in a lab-scale system, but may be negligible in a commercial unit with a large diameter reactor.

A model is only as good as its submodels, which, here, include fluidization hydrodynamics, pyrolysis and combustion reaction kinetics and stoichiometry, heat transfer, mass transfer, and material and energy balances. The fluidization hydrodynamics is modeled by the well-established two-phase bubbling model. The kinetics of combustion has been widely researched and is well established. Models for heat transfer and energy balances also conform to standard practice. However, the reaction network used to model the complex bitumen pyrolysis is oversimplified and relatively unproven and most importantly, the results predicted by this

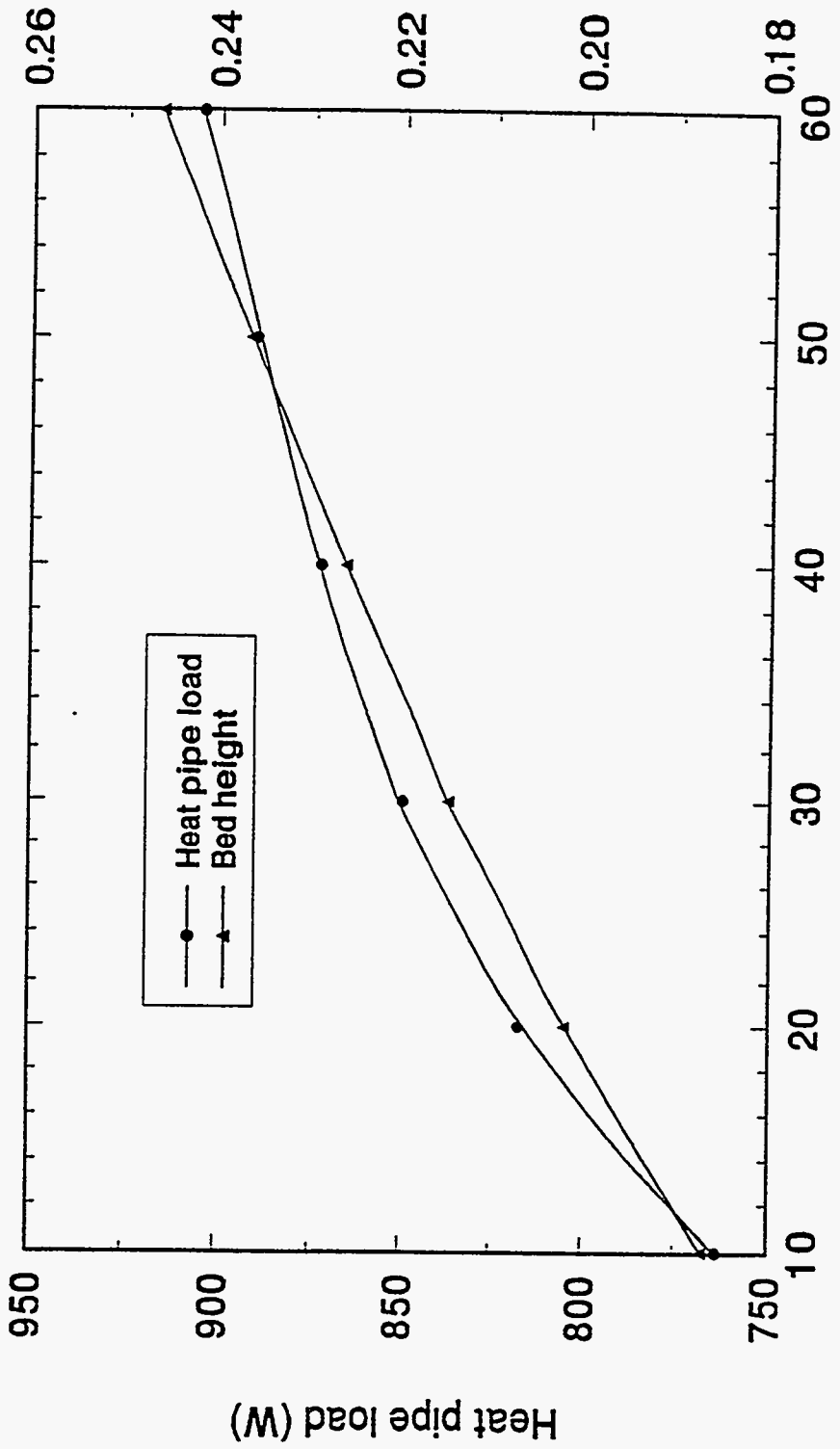

Figure 150. Effect of combustion fluidizing air flow rate on bed height and heat pipe load.

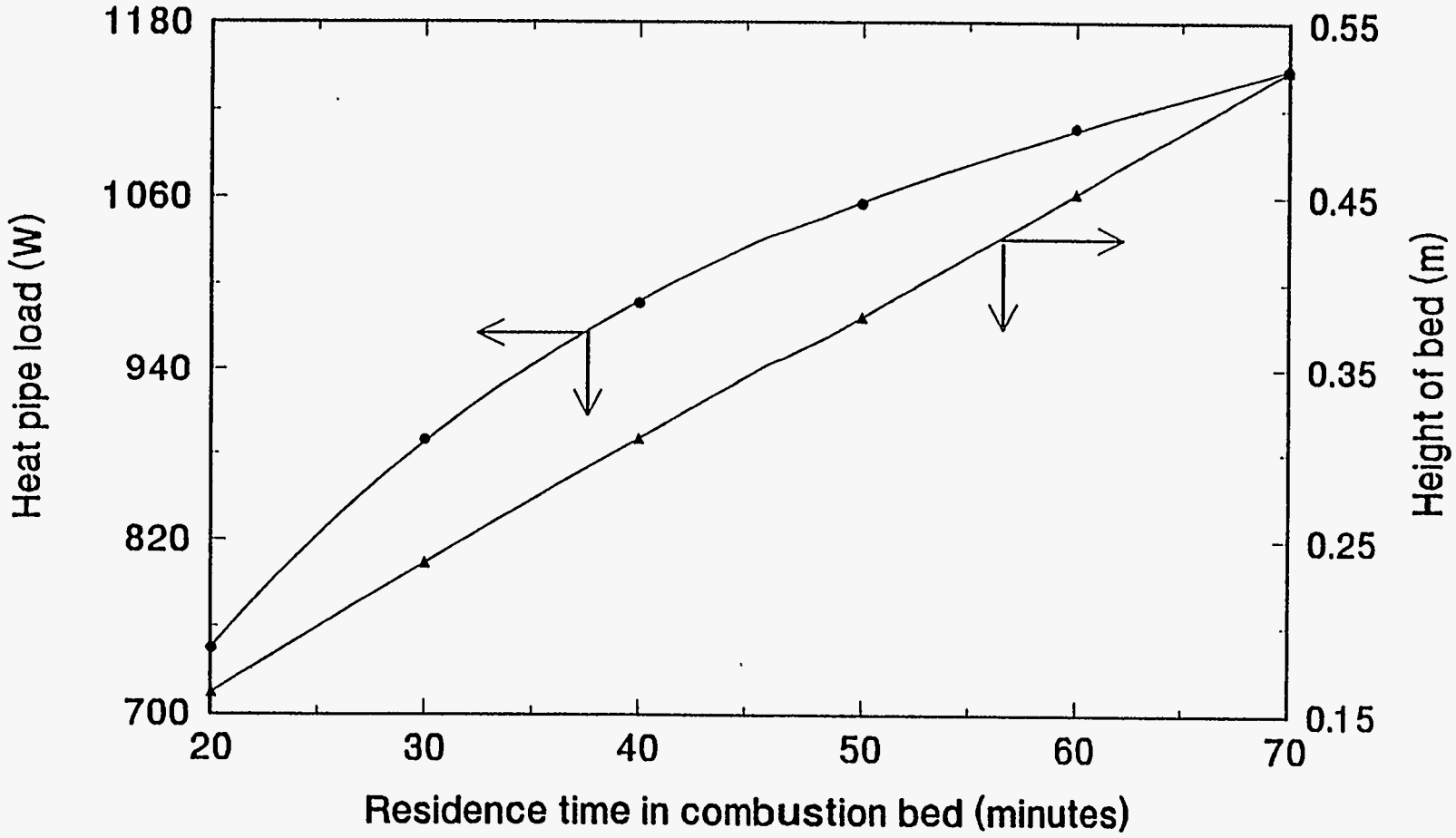

Figure 151. Effect of solids residence time on combustion bed height and heat pipe load.

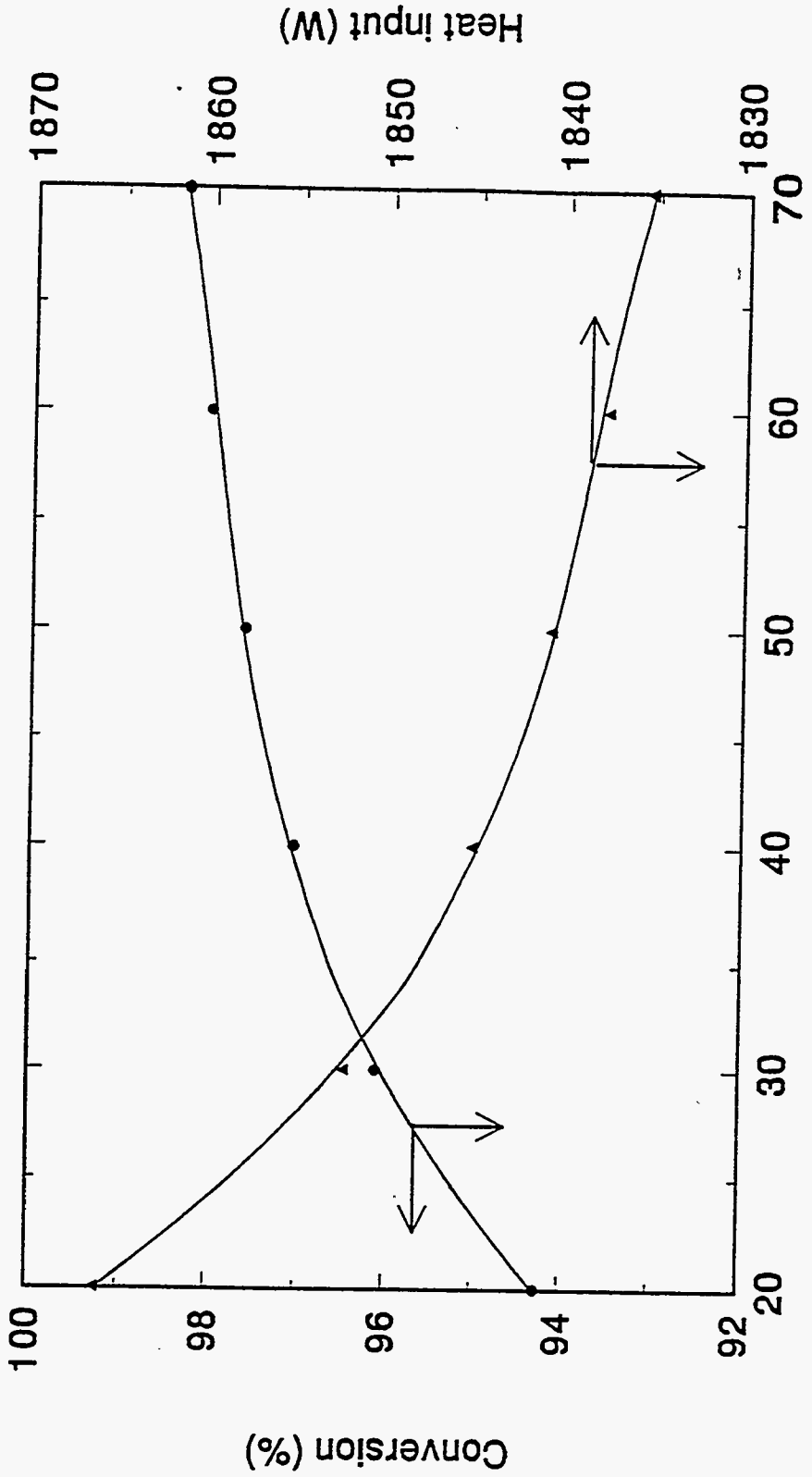

Figure 152. Effect of solids residence time on coke conversion and energy requirement.

submodel affect those of the combustion and energy balance models. For example, the amount of coke predicted determines the extent of combustion of coke and the energy generated during combustion.

The pyrolysis model is compared to values obtained by Bhadkamkar (213) in experiments with Whiterocks tar sand. The results are listed in Table 54. The experimental yields have been normalized to 100% for comparison. Base case values of the data were used for the simulation except those for the operating conditions. The results are plotted in Figure 153 and show fairly good agreement between predicted and experimental results.

However, it is well known that the characteristics of the different tar sand bitumens affect the product distribution. The compounds present in tar sand bitumens can be classified into three types based on solubility, viz. asphaltenes, resins, and oils (65). Asphaltenes have high molecular weights and very low H/C ratios of 1.03 to 1.20 indicating a highly aromatic structure. Heteroatom (N, S, or O) content is generally highest in asphaltenes compared to the other fractions. Asphaltenes are believed to be made of a highly condensed aromatic structure with the number of rings as high as sixteen with substituted alkyl side chains. Metallic impurities in bitumen are also known to be concentrated in the asphaltenes compared to the other fractions.

Resins have higher H/C ratios varying from 1.4 to 1.7, indicating lesser aromatic character. The quantity of heteroatoms is also lower, with metallic compounds present in negligible amounts. Structurally, resins are believed to consist of aromatic and naphthenic rings with long paraffinic side chains. Oils have a much higher H/C ratio compared to the other fractions indicating predominance of paraffinic and naphthenic compounds over aromatics. Heteroatoms and metal impurities are absent or present in very small amounts. Structurally, oils are

Table 54

Comparison of model with experiments

Temperature	Experimental Yields			Model Predictions		
(°C)	Oil	Gas	Coke	Oil	Gas	Coke
463	58.9	25.9	15.2	67.8	15.7	16.5
478	66.3	20.5	13.2	66.6	18.8	14.6
483	71.0	17.7	11.3	65.8	19.7	14.5
495	54.9	32.6	12.5	62.9	23.1	14.0
520	52.0	30.7	17.3	57.1	29.6	13.3

Residence time of solids : 27 min

Experimental yields are normalized to 100%

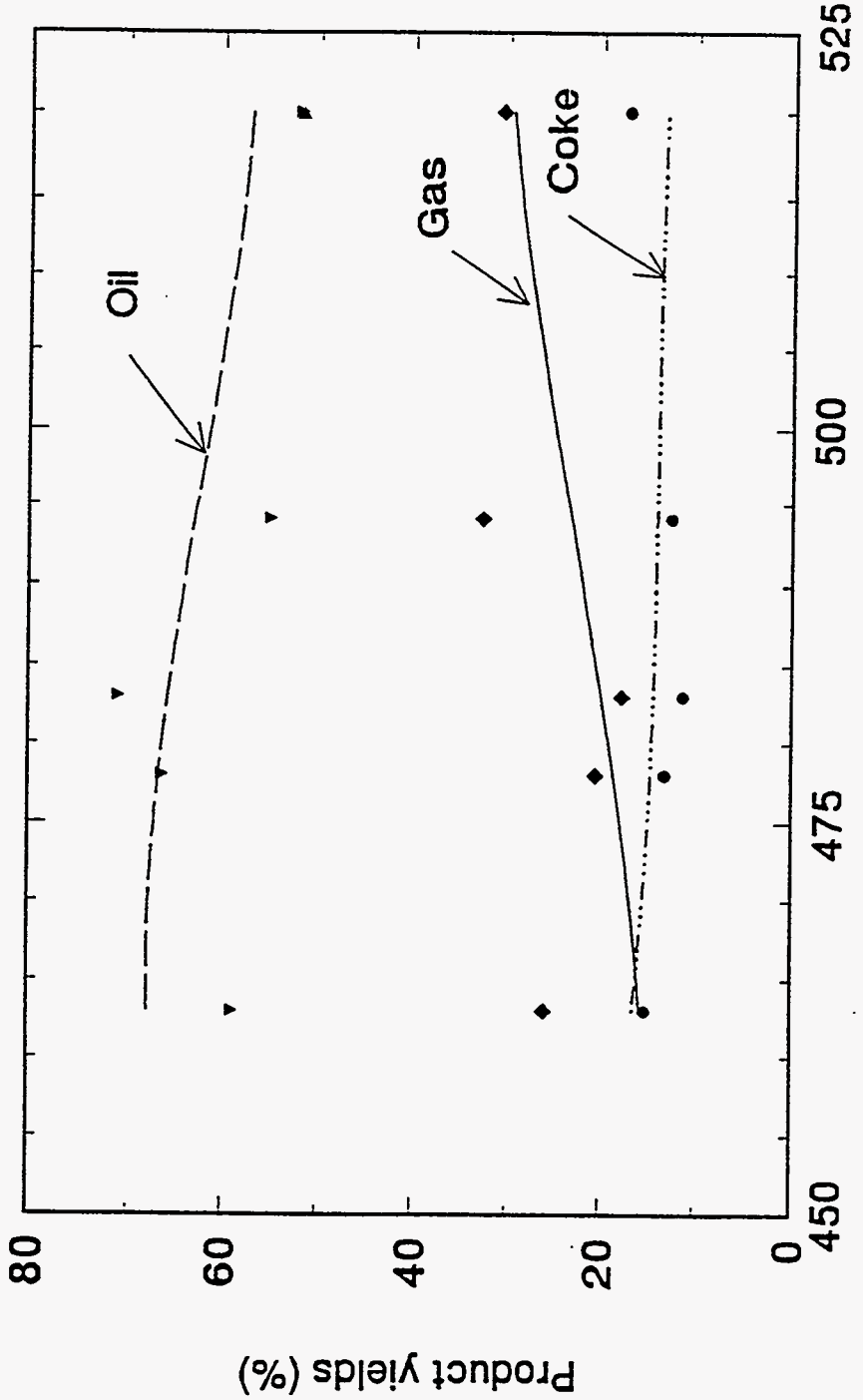

Figure 153. Comparison of model to experiments.

believed to be composed of naphthenic rings with one or more side chains of varying length.

Thus, a higher fraction of asphaltenes tends to give more coke as observed by Bunger (214). Alkyl side chains substituted on aromatic and naphthenic rings tend to break off during pyrolysis. Thus, smaller side chains give higher gas yields. On the other hand, oils and

resins pyrolyze mainly to liquid products with very little coke formation. However, present knowledge of the chemistry of bitumen constituents is limited, and although the relative amounts of the various fractions can be obtained, this alone is not adequate to predict pyrolysis behavior with certainty. More subtle factors such as degree and type of alkyl substitution, type of ring condensation and presence of coke precursors may shed more light on the chemistry of pyrolysis of bitumens

Tar sands from different sources have been found to contain varying quantities of bitumen ranging from 5% to as high as 16%. This is accounted for in the model by x_{BO}, the initial bitumen weight fraction in the tar sand. The other parameter that distinguishes between tar sands is the fraction of "heavy bitumen". This is taken as the fraction of nondistillables in the bitumen. Thus, this parameter characterizes the bitumen in terms of boiling point. Whereas the light bitumen fraction is said to volatilize (equation 52), the heavy bitumen fraction reacts through a high-temperature pathway comprised of the two cracking reactions (equations 51 and 53). Thus, a lower fraction of heavy bitumen means that a lesser fraction of bitumen will crack to coke and gas, and more bitumen will be volatilized, giving higher liquid yields at lower temperatures. The relative amounts of asphaltenes, resins, and oils in the non-volatile fraction of bitumen may also be used as a basis for assigning different numerical values to the stoichiometric constants s_1, s_2, s_7, and s_8 for different tar sands. Thus, higher values of s_2 and s_7 could possibly be used for bitumens with a higher fraction of asphaltenes, whereas presence of a

number of alkyl side chains would possibly increase the value of s_g. However, without substantial information about the bitumen structure, exact correlations for the stoichiometric coefficients cannot be obtained.

As mentioned earlier, the pyrolysis-reaction network is critical for the overall accuracy of the model. Hence a discussion of the activation energies assigned to the pyrolysis reactions is given below. The gas phase reactions involve cracking of the oil vapor, which consists mainly of paraffinic, olefinic, and naphthenic compounds, to lighter products of a similar nature. The activation energies for thermal cracking of n-paraffins heavier than hexane are in the range of 230-275 kJ/mole while those of corresponding olefins and naphthenes are about 20-40 kJ/mole lower (215). The value assigned to the activation energy for the gas phase reactions (equations 54 and 55), 230 kJ/mole, compares well with these experimental data.

Hydrocarbon cracking reactions proceed by a free-radical mechanism involving scission of the C-C bond β to the radical site and internal hydrogen transfer to form isomeric free radicals. For example,

<u>β scission</u>:

$$R\text{-}(CH_2)_n\text{-}CH_2\text{-}CH_2\text{-}CH_2. \rightarrow R\text{-}(CH_2)_n\text{-}CH_2. + CH_2{=}CH_2$$

<u>Hydrogen transfer</u>:

$$R\text{-}\underset{\displaystyle H}{\underset{|}{CH}}\text{-}(CH_2)_n\text{-}CH_2. \rightarrow R\text{-}CH.\text{-}(CH_2)_n\text{-}CH_3$$

Hydrogen transfer can take place between C-atoms separated by five other atoms. Thus, heavier compounds with longer chain lengths have a greater tendency to form

isomeric radicals and, therefore, are easier to crack. Thus, relatively low activation energy values for cracking of heavy bitumen seem reasonable. Also, the so-called volatilization reaction takes place at lower temperatures and, hence, the value for the activation energy is much lower.

Increased secondary cracking gives a lighter product (i.e., higher API gravity), but does not significantly change the oil yield and does not affect the coke yield. Thus, pyrolysis product distribution is influenced by the solid-phase cracking and volatilization, whereas the gas-phase secondary cracking reactions mainly affect the quality of the liquid product. Hence, the sensitivity of oil yield was investigated by arbitrarily varying the activation energy values for the solid-phase reactions.

Figure 154 shows the effect of varying the activation energy of the volatilization reaction. Although lower values of activation energy have no effect, higher values drastically reduce the oil yield. This happens because the volatilization reaction becomes the rate-controlling step in the pyrolysis process, and although the bitumen gets cracked, it is unable to be vaporized at the same rate. Since vaporization is a physical process, it should take place more easily than cracking. Hence, a higher value for the activation energy is not justified.

Figures 155 and 156 show the effect of changing the activation energies for the cracking reactions involving heavy bitumen. The oil yield is found to be very sensitive to any changes in the value of either activation energy. The explanation for this effect is that the two reactions are in parallel, one going to coke and g as and the other to light bitumen, which is a precursor of oil. An expression for the rate of formation of oil relative to the heavy bitumen reacted may be derived as follows:

$$\frac{d[\text{Oil}]}{-d[\text{Heavy bitumen}]} = \frac{s_1 k_1 [\text{Heavy Bitumen}]}{(k_1 + k_3)[\text{Heavy bitumen}]}$$

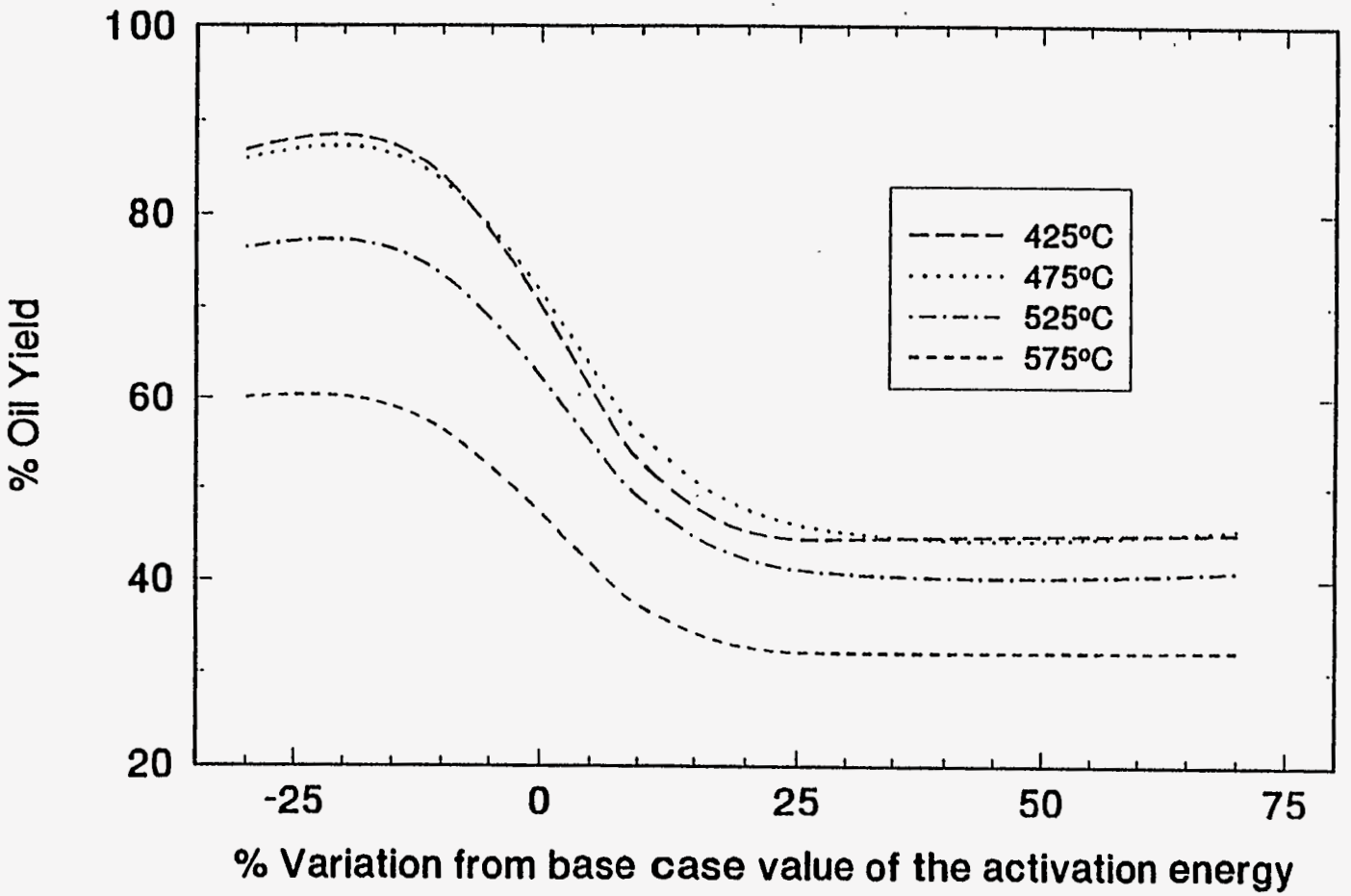

Figure 154. Sensitivity of oil yield to activation energy E_1.

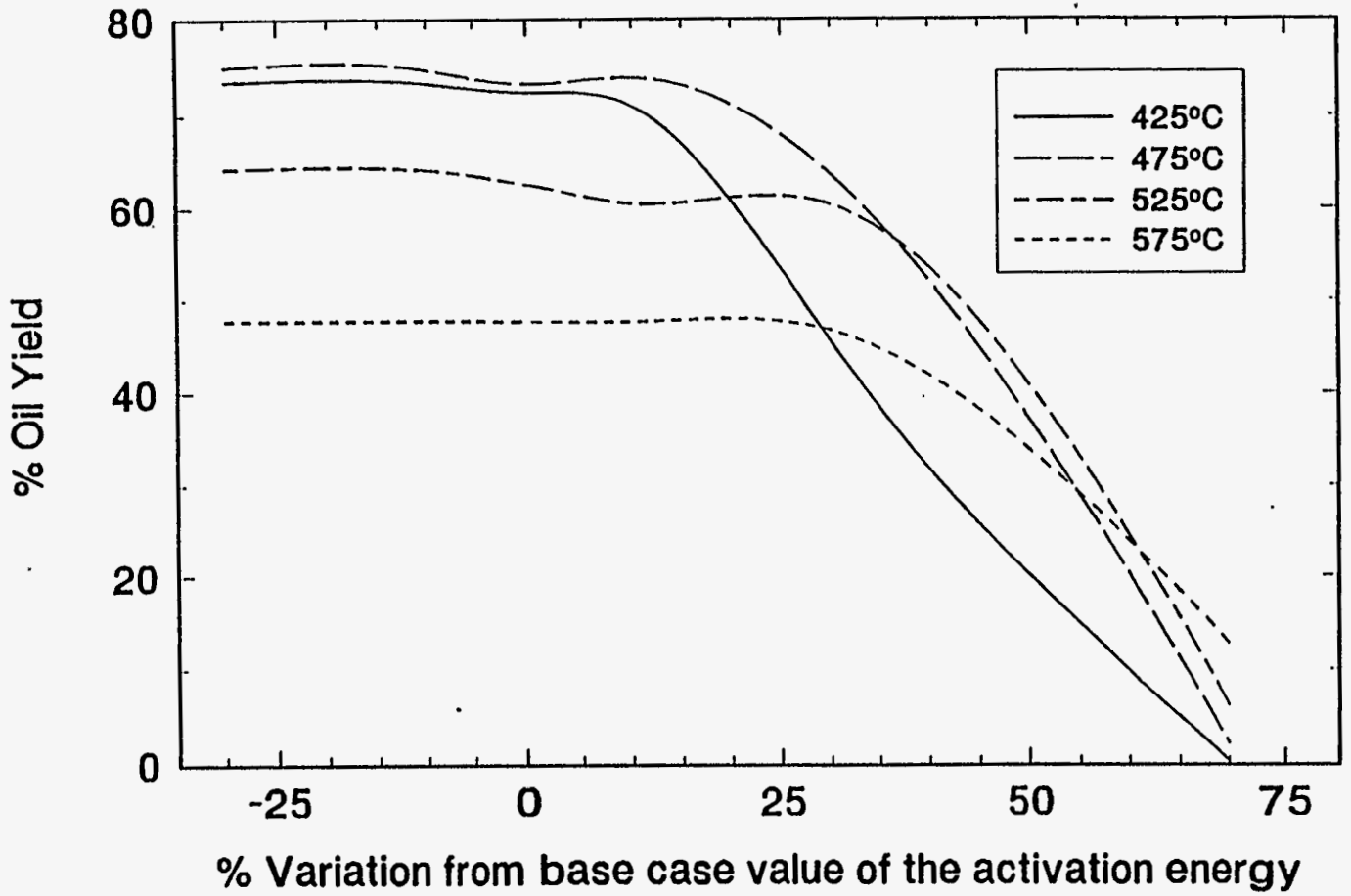

Figure 155. Sensitivity of oil yield to activation energy E_2.

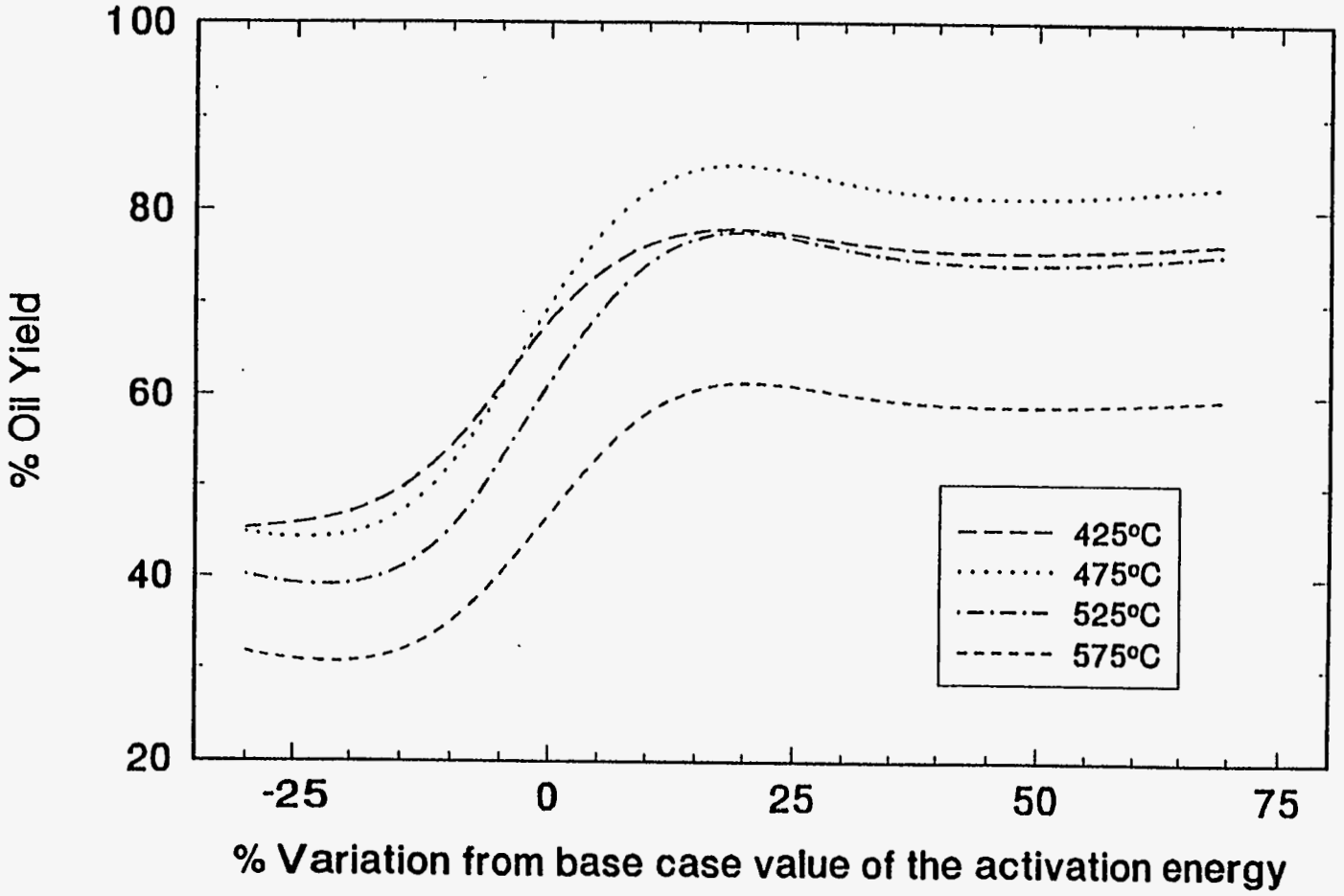

Figure 156. Sensitivity of oil yield to activation energy E_3.

$$= \frac{s_1}{1 + k_3/k_1}$$

$$= \frac{s_1}{1 + A_3/A_1 \exp[(E_1 - E_3)/RT]}$$

Thus, the fraction of oil that is formed from heavy bitumen is directly dependent on the ratio of the kinetic rate constants for the cracking reactions. Any changes in the activation energies have an exponential effect on the fraction of oil formed, as shown in Table 55.

The preceding discussion points out the pitfalls of modeling the highly complex phenomenon of the pyrolysis of tar-sand bitumen using simplified reaction networks. Any number of such models may be used to obtain a reasonable fit of the experimental data. Thus, pyrolysis models of the type used here, although developed from basic knowledge of the chemistry, are only approximations of reality, with arbitrary values assigned to the parameters.

Table 55

Sensitivity of oil yield to activation energy values

$E_3 - E_1$ (kJ/gmol)	Oil yield from heavy bitumen (%)
45.0	45.70
50.0	59.87
55.6 (base case)	70.38
60.0	74.95
65.0	77.66

Pyrolysis temperature: 475°C

REVIEW OF PREVIOUS EXPERIMENTAL WORK ON PYROLYSIS OF TAR SANDS USING FLUIDIZED BEDS

Considerable experimental work has been done at the University of Utah on the pyrolysis of tar sands using fluidized beds. Included here is a review of the experimental results obtained by Dorius (51), Venkatesan (50), Smart (117), Jayakar (116), Shun (120), Wang (114) and Fletcher (121).

Effect of Reactor Temperature on Product Yields

Dorius (51) studied the effect of temperature on PR Springs Rainbow I, PR Springs Rainbow II, and PR Spring South tar sands with a constant solids retention time of 20 minutes for the first two tar sands and 27.1 minutes for the third. For all the three types of tar sand the liquid yield first increased with temperature and then decreased. The initial increase, as explained by Dorius, was caused by the increase in the rate of cracking of the heavy components along with the increase in the rate of evaporation. The rate of cracking is more sensitive to temperature than the rate of evaporation. Hence the selectivity towards lighter products is increased with increasing temperatures, leading to a decrease in the liquid yield and an increase in the light gas yield.

The coke yield was higher at lower temperatures because of the unconverted higher molecular weight asphaltenes. As the temperature increased, the decomposition rate increased and the aliphatic side chains in the asphaltenes cracked and evaporated, thus decreasing the coke yield.

The PR Spring South tar sand gave lower liquid yields and higher coke than the other two, because the bitumen was very asphaltic in nature and had a higher Conradson Carbon Residue and lower volatility.

Venkatesan (50) obtained yields similar to those of Dorius (51) by using tar sand from the Sunnyside deposit and a retention time of 27 minutes in all his experiments. He observed a peak in the liquid yield at 723 K, and explained the lower yields at lower temperatures as being due to solvent extractable liquid or "soft" coke remaining on the sand particles with the coked bitumen resulting from incomplete pyro-distillation. Above 723 K, the rate of thermal cracking increased much more than the rate of distillation and hence caused the higher gas yields and lower liquid yields.

Fletcher (121) used Whiterocks tar sand and studied the effect of temperature while keeping the residence time in between 29 minutes and 48 minutes. He obtained much higher liquid yields and lower coke yields than previously observed. The steam used to fluidize probably suppressed coke formation.

PR Springs, Sunnyside and Whiterocks tar sand were used by Smart (117). He observed that, for a residence time of 48 minutes, the liquid yields and the gas yields increased with temperature; whereas the coke yields decreased. Incomplete bitumen pyrolysis was cited as the reason for the higher coke yields at lower temperatures; whereas the rise in the gas yield with temperature was explained by the increase in the severity of cracking.

Higher liquid yields were obtained for Asphalt Ridge than for Tar Sand Triangle feed by Jayakar (116). The trends in the yields were similar to those observed by most others.

Shun's experiments with Circle Cliffs tar sand (120) showed much lower liquid yields and higher gas yields than those observed on other tar sands by other experimenters, but the trends seen were similar. He also observed much higher CO_2 and H_2O yields. Shun (120) explained that the decrease in liquid yield with temperature was due to the secondary cracking of the bitumen-derived liquid over the catalytically active mineral Kaolinite.

Wang (114) found trends similar to those of Venkatesan (50) for his studies on the Tar Sand Triangle deposit at a residence time of 24.8 minutes; only his yields were higher, which he attributed to the fact that his study used core sand samples as opposed to Venkatesan's study which used outcrop sand samples that had undergone severe weathering over a long period of time.

Figures (157-159) show the effect of the pyrolysis temperature on the product yields.

Effect of Residence Time on Product Yields

The PR Spring Rainbow I and PR Spring South tar sands were studied by Dorius (51), for the effect of residence time on yield; while maintaining the pyrolysis temperatures at 798 K and 873 K, respectively. The liquid yields decreased with increasing residence time, but the gas yields increased and the coke yields were unaffected.

According to Dorius (51), the trend of the liquid yield can be explained by the effect of the solid-vapor contact time on the rate of the vapor-phase thermal cracking. He approximated the operation of his bed by the Kunii-Levenspiel bubbling-bed model resulting in the following expression for the conversion:

$$1-X = \exp(-H_f \, _b) \qquad (95)$$

where H_f is the effective multiphase reaction-rate coefficient and $_b$ is the vapor-solid contact time. Thus the overall conversion decreased with increase in the vapor-solid contact time.

Venkatesan carried out studies by varying the retention times from 20.4 minutes to 31.4 minutes at various temperatures. At higher sand feed rates, the velocity of the rising bubbles decreased because of an increase in the hydrostatic pressure, and this

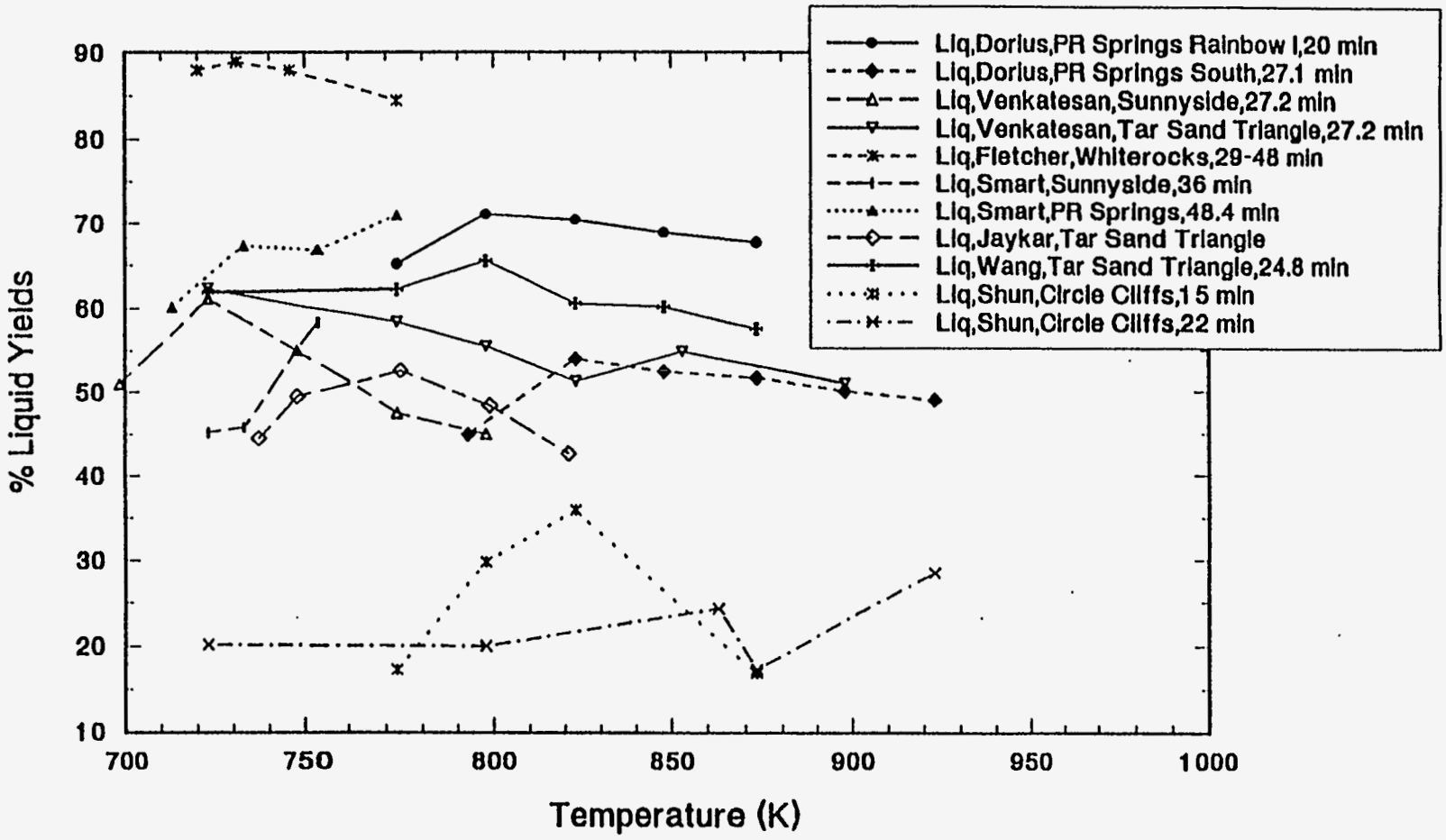

Figure 157. Effect of Temperature on the Liquid Yields

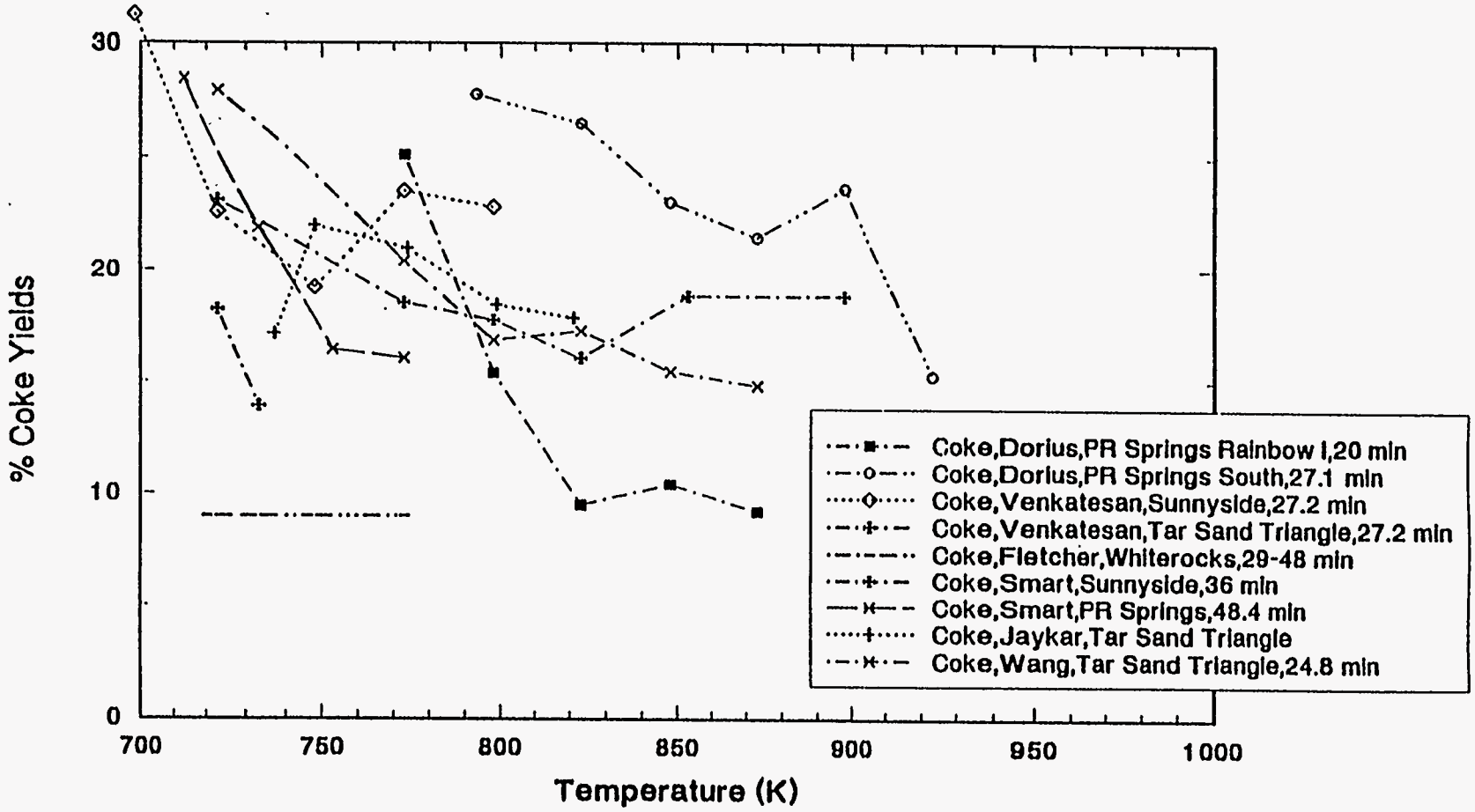

Figure 158. Effect of Temperature on the Coke Yields

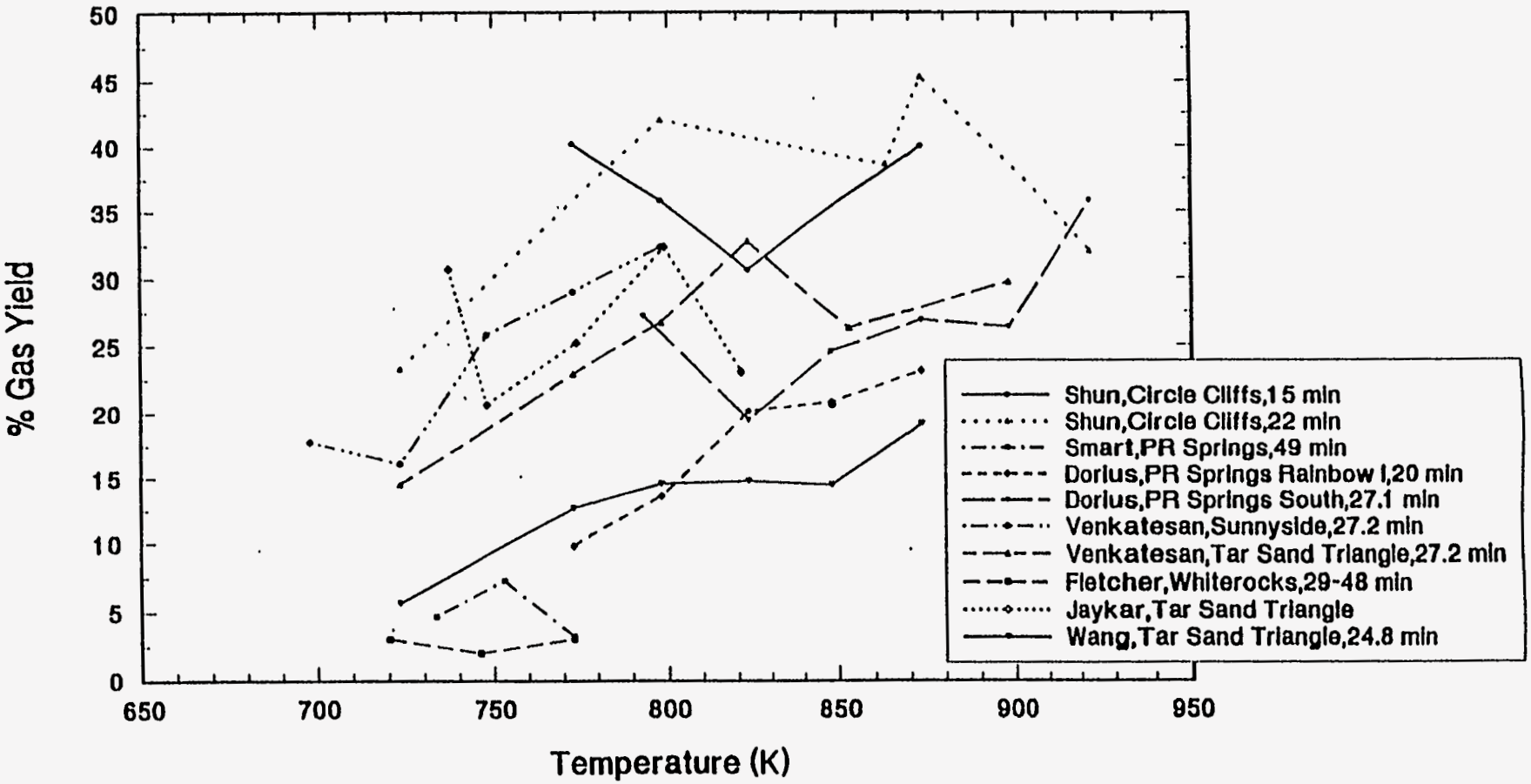

Figure 159. Effect of Temperature on the Gas Yields

resulted in slugging. Under these conditions, pyro-distillation took place mainly in the particulate phase and hence there was less secondary cracking in the vapor phase, resulting in lower gas yields and higher liquid yields. At lower sand feed rates, however, the gas bubbles moved through the reactor rapidly causing adequate solid mixing and facilitating the transfer of vapors from the particulate phase to the bubble phase. In this bubble phase, the vapors underwent further cracking; thus causing the high observed gas yields and low observed liquid yields.

Smart observed an increase in the liquid yields with increasing residence time for his studies on the PR Spring tar sand at a temperature of 773 K, a trend that was in contradiction to the ones observed by others.

Liquid product yields decreased and gas yields increased with increasing residence time in the experiments on Circle Cliffs tar sand by Shun at a temperature of 873 K. However, at temperatures above 873 K, the cracking rates were high enough that the residence time showed no effect on the yields.

Wang found that liquid yields decreased and gas yields increased with increasing residence time, from his experiments on Tar Sand Triangle at a reactor temperature of 798 K. Wang explained that the primary cracking reactions were appreciable above 773 K and occurred in the bitumen film surrounding the sand grain. Thus at lower residence times, the extent to which the liquid phase was thermally cracked was less and hence resulted in higher liquid yields.

These observations are plotted in Figures (160-162), which show the effect of the residence time on the product yields.

The Effect of Pyrolysis Temperature on the Quality
of the Products

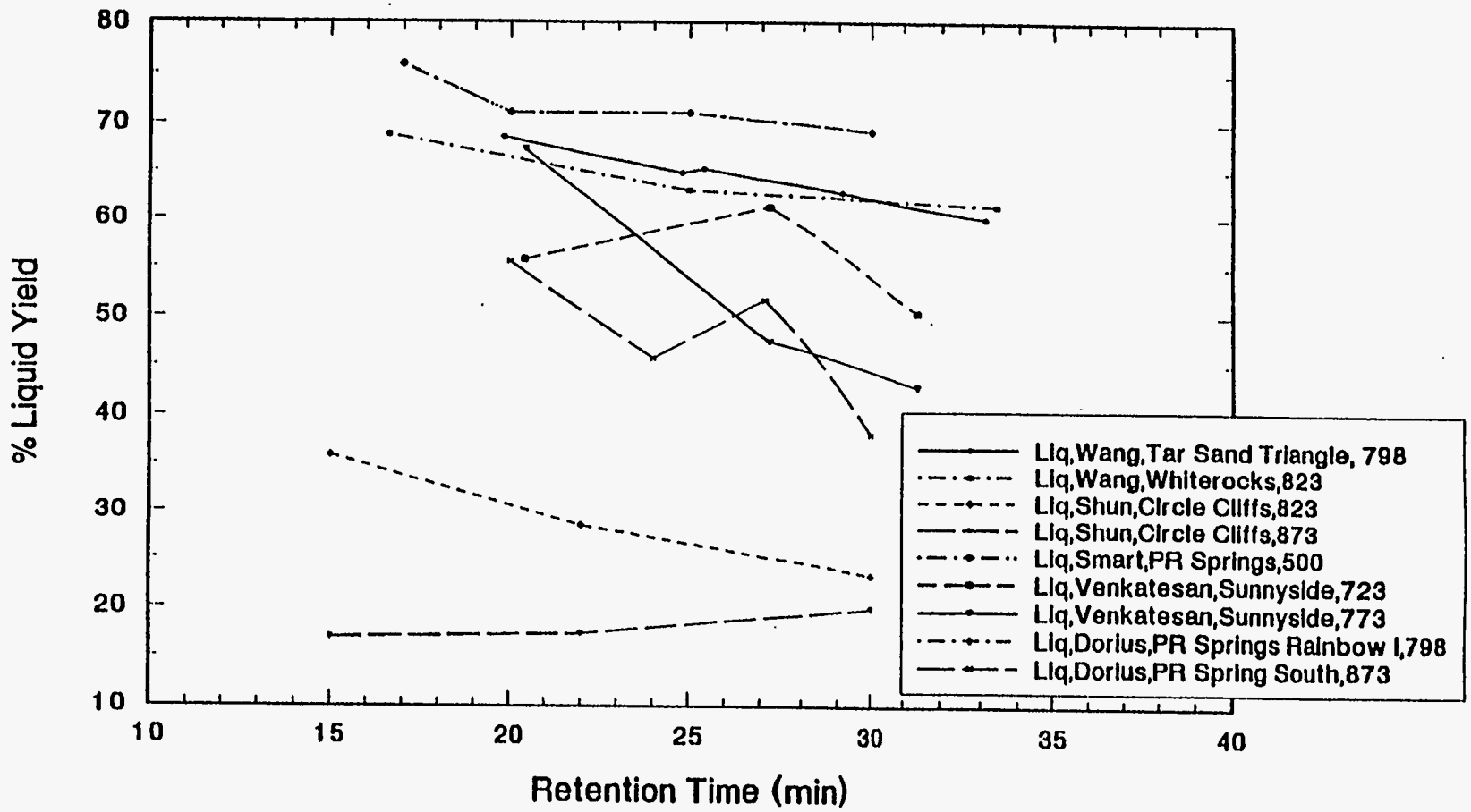

Figure 160. Effect of Residence Time on the Liquid Yields

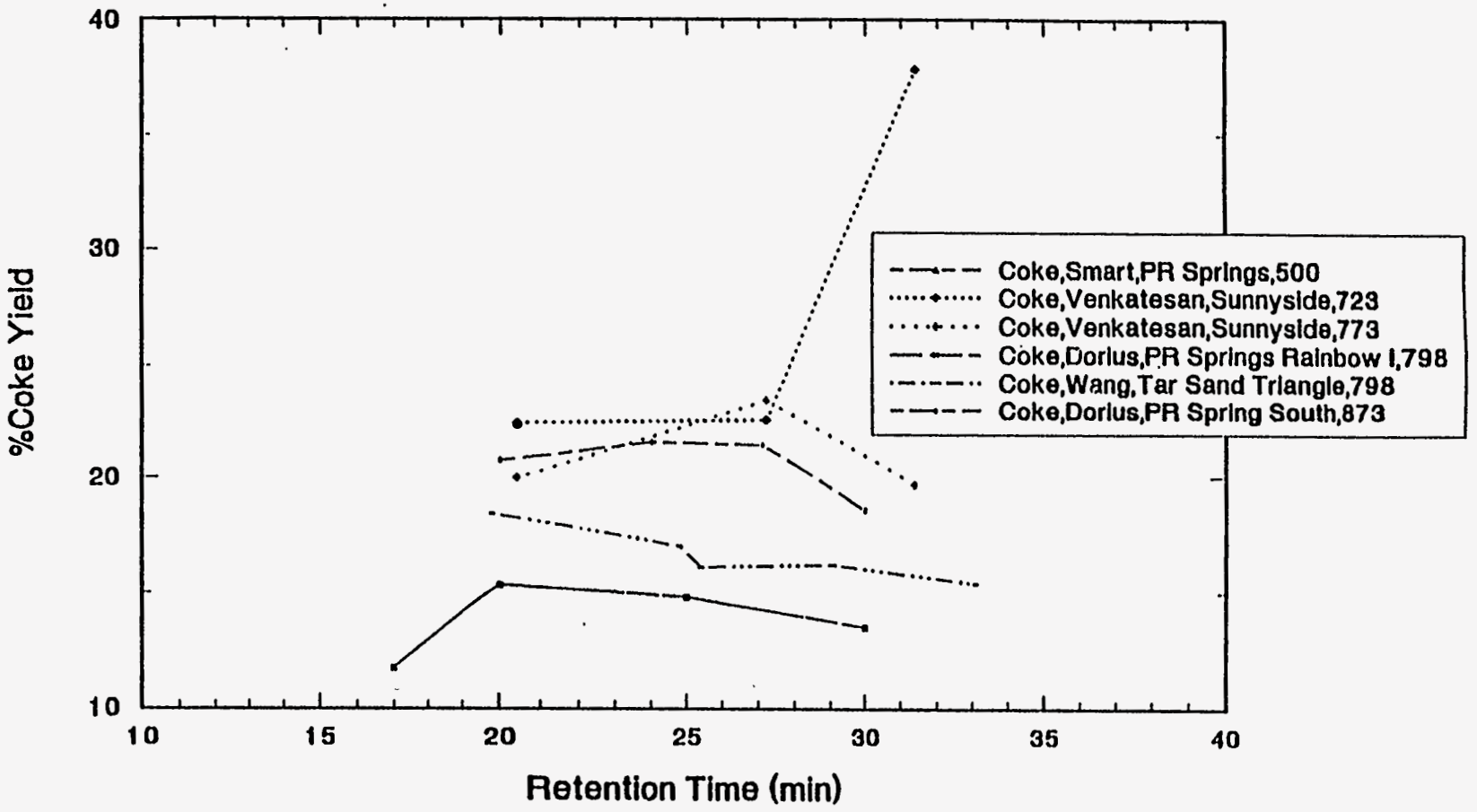

Figure 161. Effect of Residence Time on the Coke Yields

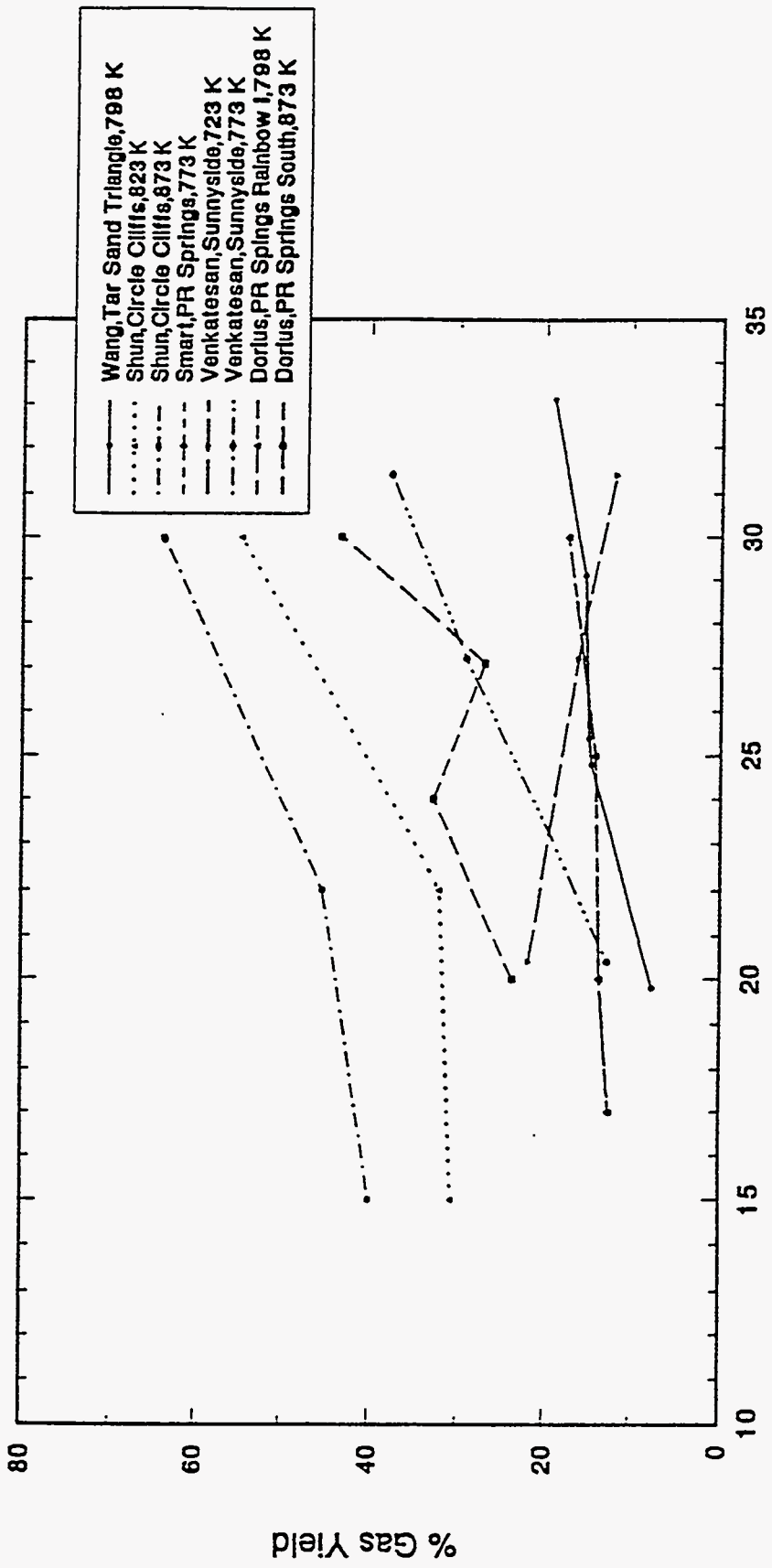

Figure 162. Effect of Residence Time on the Gas Yields

API Gravity

Dorius (51) explained the decrease in API gravity with increasing temperature for the PRS-S (PR Spring South) deposit by relating it to the severity of thermal cracking. PRS-S bitumen is asphaltic in nature and hence is composed of a large number of polynuclear aromatic structures with long alkyl side chains, which cracked as the reactor temperature was increased and led to the increase in the aromaticity of the product liquids and hence the decrease in API gravity. For PRS-RI (PR Spring Rainbow I) the amount of saturates and resins remained constant over the range of temperatures and hence the API gravity remained constant.

The studies on Sunnyside and Tar Sand Triangle by Venkatesan (50) showed a linear decrease in the API gravity with reactor temperature, which was explained by the increase in aromaticity of the liquid products. The Sunnyside synthetic liquid had a higher hydrogen content, was more saturated, and hence exhibited a higher API gravity.

Fletcher observed a slight increase in the API gravity with temperature for his Whiterocks samples.

No clear trend was seen by Smart (117). The fact that the API gravities of the products were below 20 indicated that the oil was of a naphthenic or naphthenic-aromatic base.

The API gravity decreased only slightly with temperature as reported by Wang for his studies on Tar Sand Triangle product.

All these observations are shown in Figure 163.

Oil Viscosity

Dorius (51) observed that the viscosity of the PRS-S oils was much higher than the viscosities of the PRS-RI and PRS-RII oils, and furthermore that the viscosity of the PRS-S oils increased with temperature contrary to the trend observed for the other

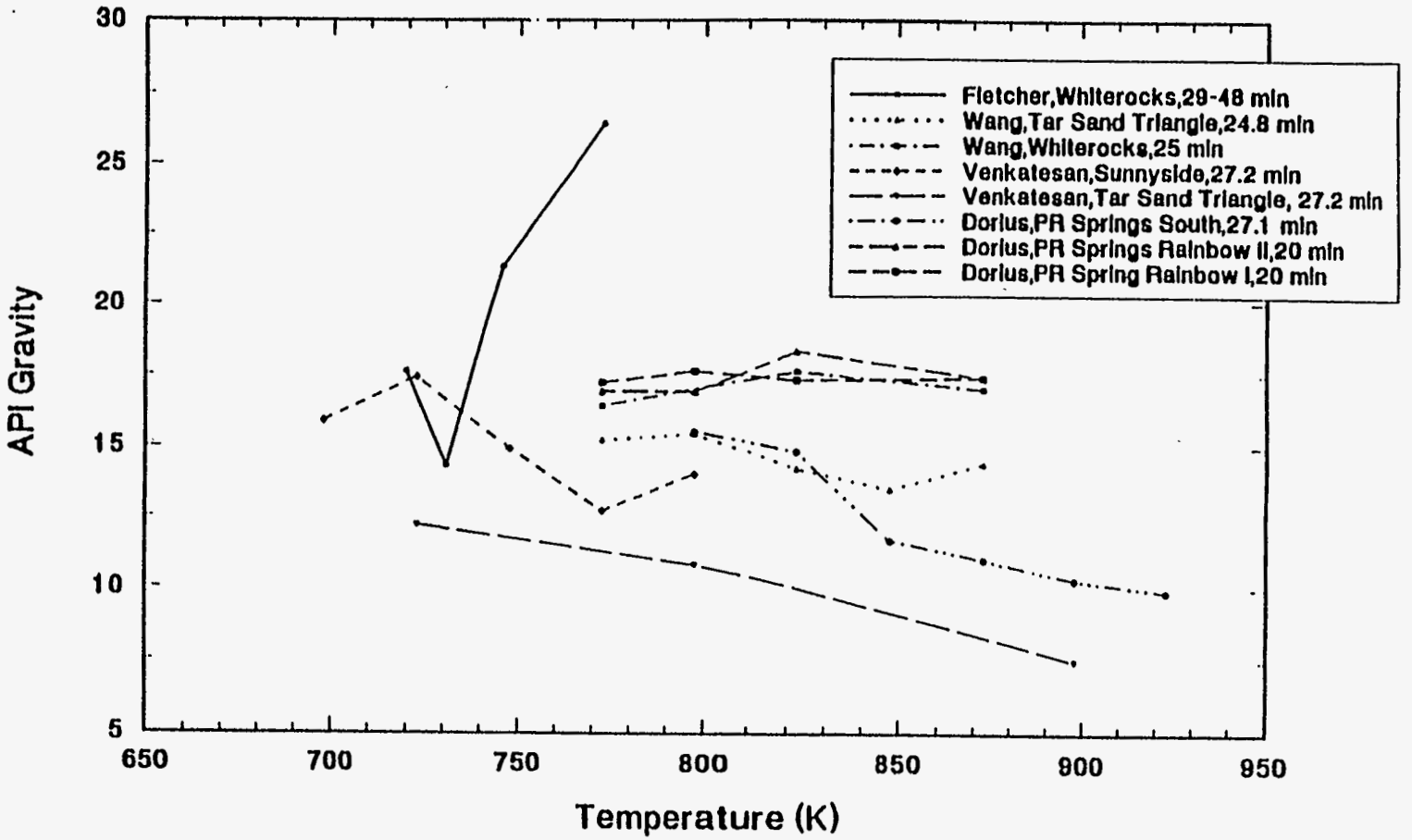

Figure 163. Effect of Temperature on API Gravity

two bitumen types. The decrease in viscosity for the PRS-RI and PRS-RII oils was attributed to the decrease in molecular weight; whereas the increase in viscosity of the PRS-S oils was explained by the formation of sticky coke precursors, during the asphaltene condensation, with increased cracking severity.

Venkatesan (50) observed no trend in viscosity for the oil from Tar Sand Triangle, which was consistent with the observation that the change in the molecular weight was also insensitive to the change in temperature. The Sunnyside liquids showed a decrease in viscosity with temperature above 723 K. Between 698 K and 723 K the viscosity increased due to an increase in the molecular weight.

The viscosity of the Whiterocks samples studied by Fletcher (121), and of the PR Springs and Sunnyside samples studied by Smart (117) decreased with increasing temperature.

According to Wang's study (114), the viscosity of the Tar Sand Triangle product liquid was relatively insensitive to the reactor temperature.

Figure 164 is a plot of the viscosity versus the pyrolysis temperature.

Conradson Carbon Residue

According to Dorius (51), the Conradson Carbon Residue of the PRS-RI and PRS-RII oil products increased with temperature because of the increase in aromatics which formed coke precursors.

Trends, similar to those of Dorius (50), were observed by Venkatesan (51) for both the Sunnyside and Tar Sand Triangle oil samples. The Conradson Carbon Residue of the Sunnyside oil samples showed a higher sensitivity with temperature than that of the Tar Sand Triangle.

No trend was observed for the Conradson Carbon Residue of the Whiterocks sample by Fletcher (121).

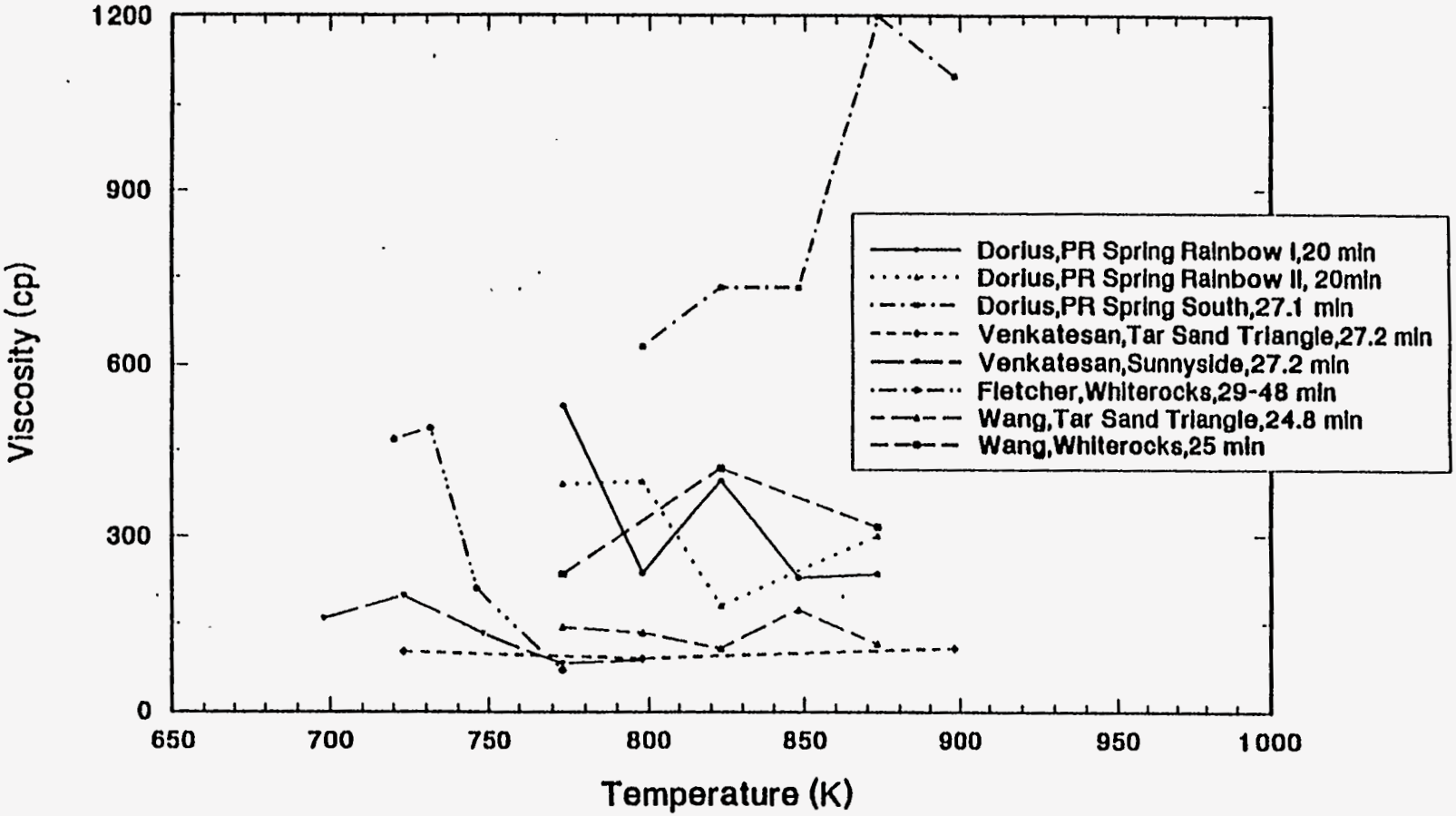

Figure 164. Effect of Temperature on Viscosity

Refer to Figure 165 to see the effect of pyrolysis temperature on the Conradson Carbon Residue, as observed by the various experimenters.

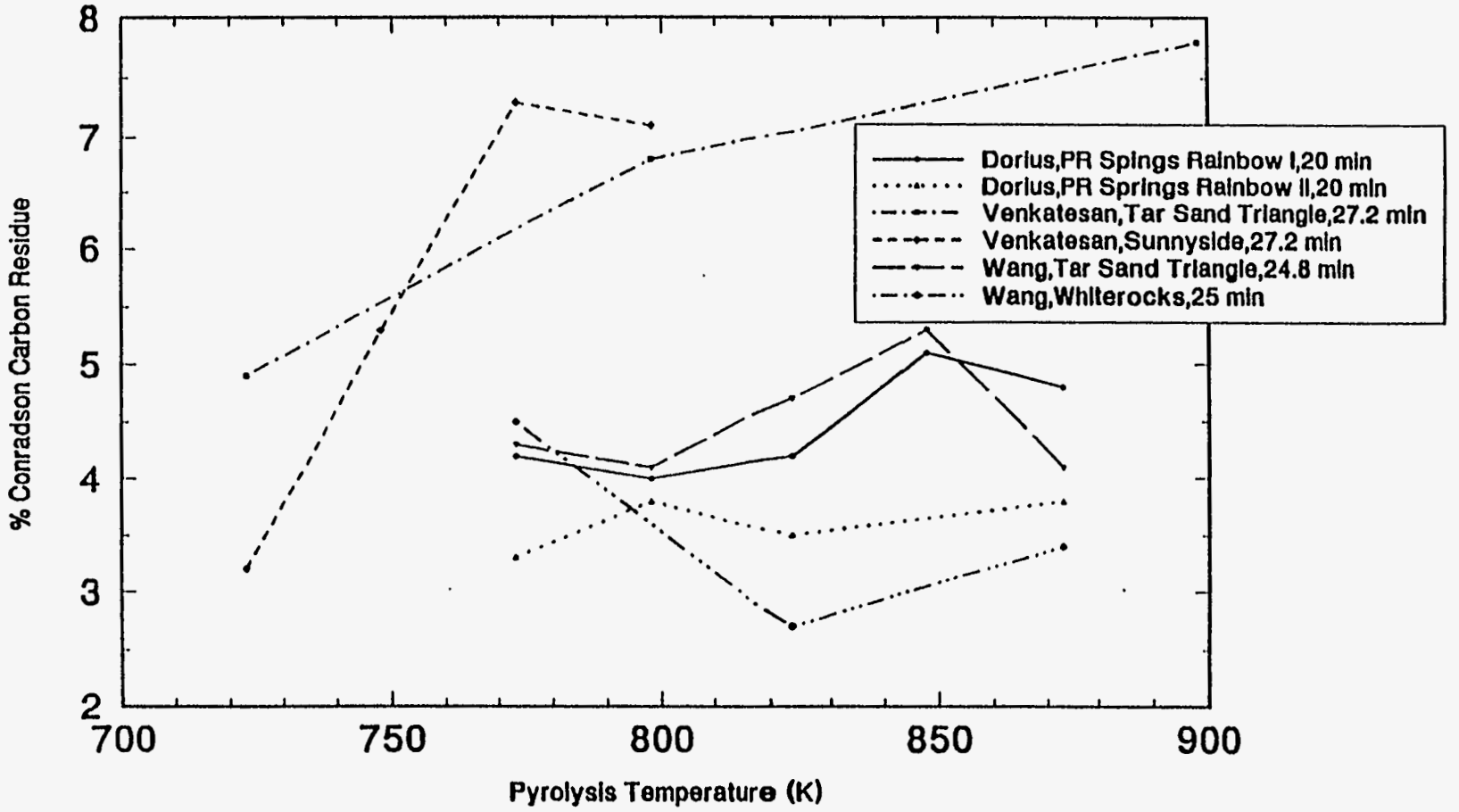

Figure 165. Effect of Temperature on Conradson Carbon Coke Value

EXPERIMENTAL APPARATUS AND PROCEDURE

In 1950 Peter and Gishler (108) proposed the first thermal fluidized bed process for extracting and upgrading tar sand bitumen. Seader and coworkers (116, 117, 189-191, 216, 217) developed an energy-efficient thermally coupled fluidized-bed reactor system for the pyrolysis of tar sand bitumen.

Fluidized Bed Reactor System

A detailed description of the apparatus is found in Smart's thesis (117). The modifications done on the control system and the data acquisition unit and the feeding system are described by Coronella (118).

A schematic of the reactors is shown in Figure 166. Figure 167 shows the schematic for the product recovery system. The tar sand is fed into the pyrolysis reactor, which is fluidized using nitrogen and typically operated between 450°C to 500° C. The bitumen on the sand particles cracks and evaporates and is carried by the fluidizing gases to a product recovery system; where it passes through water-cooled heat exchangers is condensed and collected. The coked sand from the pyrolysis reactor is passed continuously through a downcomer to the combustion reactor, typically maintained between 550°C to 600°C, where the fluidizing air burns the coke on the sand. Three heat pipes, mounted vertically and extending into both the beds, transfer the heat of combustion to the pyrolysis bed to preheat the tar sand and supply the heat of pyrolysis.

Before the current experiments were performed, a few modifications were made to the reactors to improve their operation. The vertical pipe, connecting the feeder output to the pyrolysis reactor, was replaced by a larger pipe whose internal diameter was 4 inches. This was done because the tar sand would get stuck in a smaller diameter pipe and would cause the feed auger to get twisted.

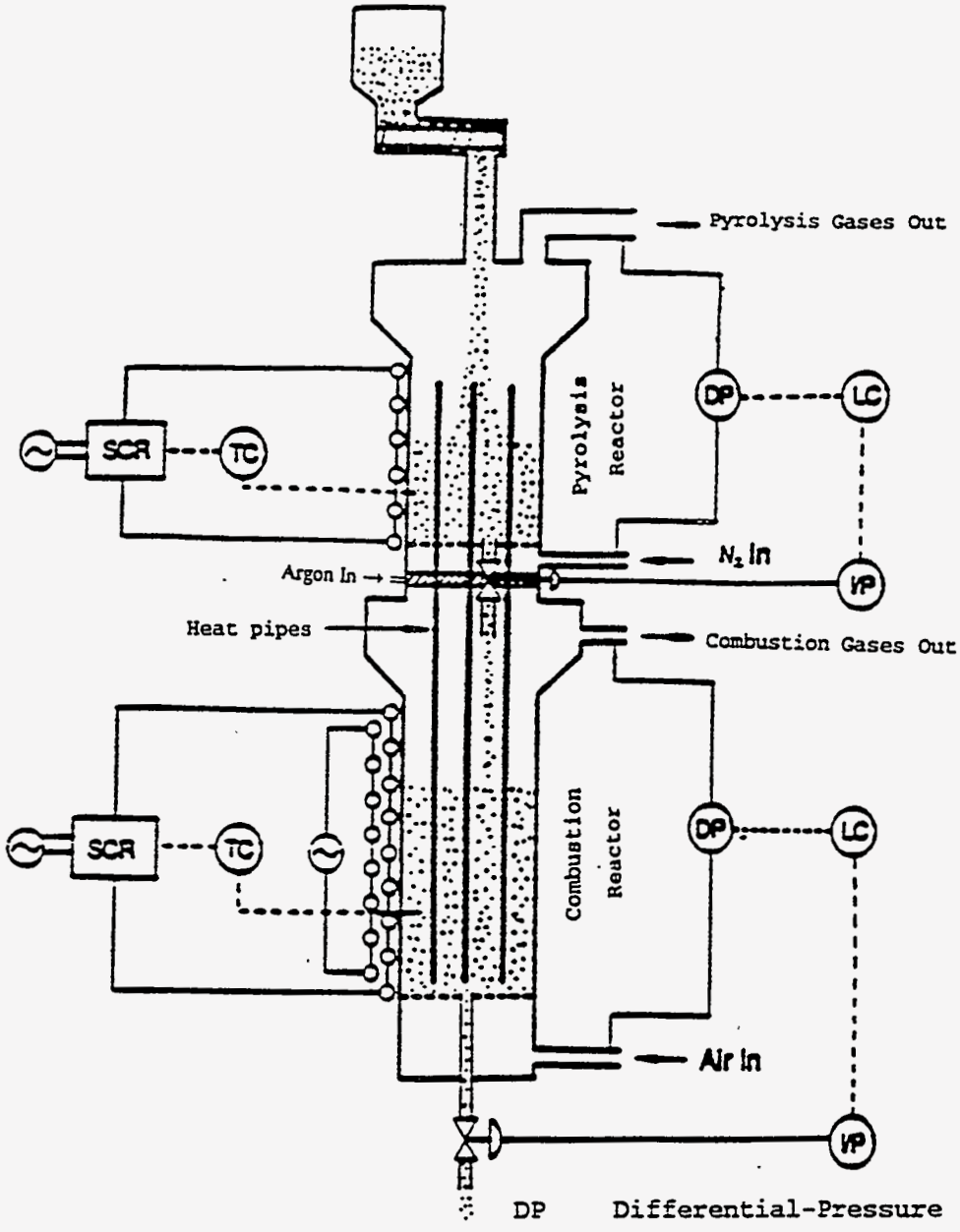

DP Differential-Pressure

I/P Electric-To-Pneumatic Converter

LC Level Controller

TC Temperature Controller

SCR Power Package

o-o-o Heating Wire

⊖ AC Source

Figure 166. Schematic Diagram of the Process

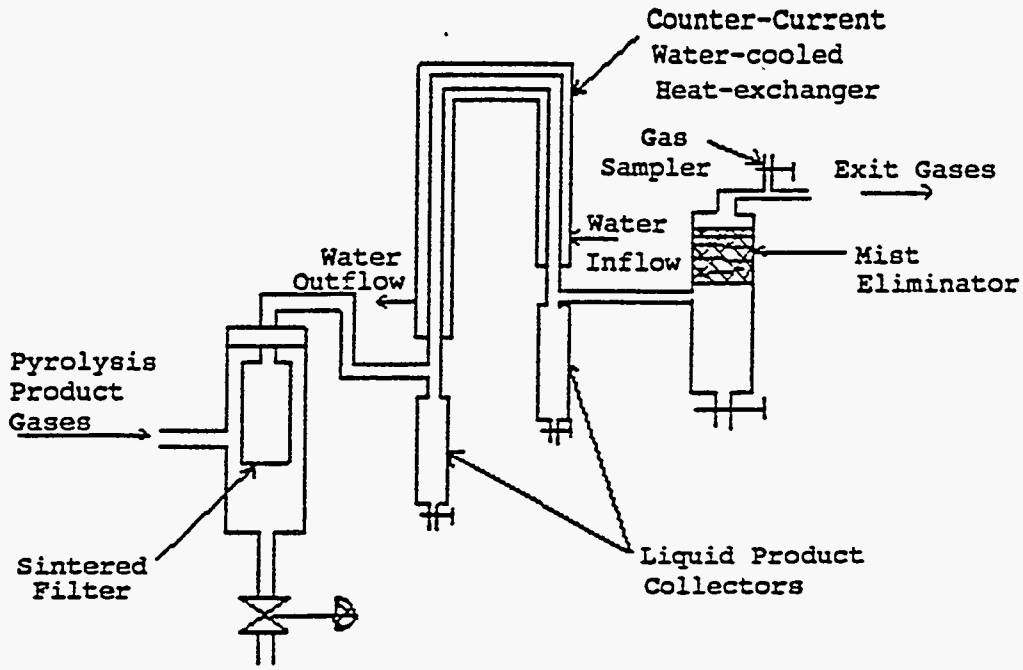

Figure 167. Schematic of the Product Recovery System

In addition, an argon seal was introduced in the downcomer, connecting the pyrolysis and combustion reactors. The purpose of the seal was to maintain the pressure in the downcomer high enough so that there was no upflow of the combustion gases to the pyrolysis reactor and no downflow of the pyrolysis gases into the combustion reactor. This pressure was usually maintained at a value of 1 psig greater than the pressure at the bottom of the pyrolysis reactor or 1 psig greater than the pressure at the top of the combustion reactor, whichever was greater.

Experimental Procedure

Before every run the following steps were completed to prepare the reactor:

(1) The sintered filter unit shown in Figure 167 was disassembled and cleaned. This was necessary because of the build-up of solid sand particles on the sintered filter.

(2) The elbow connection between the pyrolysis reactor and the filter was also cleaned because the entrained sand would collect in it.

(3) The cyclone at the exit of the combustion reactor was cleaned. The copper tubing in the combustion exit line was cleaned.

(4) A bucket of Whiterocks tar sand, weighing approximately 6.8 kg, was crushed in a grinding machine. Clean sand was then added to the tar sand such that the final ratio of the tar sand to the clean sand was 86:14. The clean sand reduced the agglomeration of the tar sand and improved its fluidizing properties.

(5) The feeder was emptied of all the tar sand left in it from the previous run. The left over tar sand was then weighed and this weight was later used in the material balance calculations for the previous run. The expansion unit had to be disconnected to empty the feeder.

(6) The oil from the two product collectors was drained out over a period of 2 days. The collectors were then disconnected from the reactor system and weighed; and then cleaned with acetone and weighed again; after which they were reconnected.

(7) The oil in the tubing leading from the collector to the mist eliminator was drained out. The oil collected in the mist eliminator vessel was also drained out. The material of the mist eliminator was checked once in every four to five runs. Since there was not much accumulation of oil on the mist eliminator material, the entire material was changed only twice during the course of all the runs.

(8) Once in every few runs, the graphite packing material in the control valve was checked. This packing prevented the gases from leaking during the operation of the valve. The packing was replaced once every three to five runs.

(9) The sampler from which the pyrolysis sand samples were obtained would get plugged with the pyrolysed tar sand after almost every run. This problem was usually solved by pushing a wire through the sampler. But in the case of severe caking, the sampler was first wetted with acetone by using a pippete and then a long syringe needle was pushed into the sampler, thus clearing it.

(10) The flange connecting the exit of the pyrolysis reactor to the filter unit was tightened after cleaning the gaskets and the surface of the flanges. The other end of the filter unit was connected to one end of the water-cooled condensers.

(11) The water-cooled condensers were cleaned with acetone, once in every four or five runs, to remove the oil lining the inner walls and improve the heat transfer.

(12) Two layers of ceramic wool insulation were wrapped around the filter unit; and the top surface of the pyrolysis reactor was also covered with insulation.

(13) The electrical connections to the filter were tightened and all other electrical connections were checked to ensure that they were properly connected.

(14) It was made sure, that there was one full N_2 cylinder and an Ar cylinder with a minimum pressure of 800 psi, prior to each run.

The following procedure was implemented to start up and run the reactor.

(1) The heating of the filter was started about 8 hours prior to starting the run by keeping the variac setting of the filter at about 40% of its maximum value. This was

necessary because the filter heated up more slowly compared to the rest of the reactor and needed to be at about 350°C during the course of the run.

(2) Eight kilograms of coked sand were weighed in a bucket. A PC-based data acquisition system was used. A Quickbasic program named "level" was used to control the sand content of the two reactors. The "level" program was started on the computer and air flowrates to the pyrolysis and combustion reactors were started and maintained at about 40 SCFH. The setpoints for the pyrolysis and combustion reactors were 5 lb and 8 lb respectively. The coked sand was poured slowly from the top of the reactor. Quite often the downcomer would get plugged with the sand, and then the air purge would be used to dislodge the sand. This procedure was stopped when there was about 5 lb in the pyrolysis reactor and 8 lb in the combustion reactor.

(3) The expansion unit was then reconnected by tightening the flange connection.

(4) The electrical heating was started and carried out in steps. The pyrolysis and combustion temperature setpoints were kept at 200°C initially and then slowly increased to the desired values. The variac settings for heating the combustion reactor and the exit of the pyrolysis reactor were kept at about 40% of the maximum. The wattmeter reading for the combustion heating was noted.

(5) The "level" program recorded the pressure drop across the pyrolysis and combustion reactors and the temperatures in both the reactors, every 6 seconds. The pressure drop readings, which were continuously displayed on the screen, gave a good indication of the amount of sand in the reactors and also if the the bed was properly fluidized.

(6) The "level" program also calculated the amount of electricity supplied to the pyrolysis and combustion reactors by measuring the amount of time that the temperature controller remained on.

(7) The water flow to the condensers was started.

(8) When the reactor temperatures had reached the desired values, a measured amount of tar sand was put into the feeder. Vacuum grease was applied on the gaskets lining the lid of the feeder and then the lid was clamped onto the feeder.

(9) If the filter had been cleaned properly and heated to about 300°C for about 3 hours prior to the run, then the pressure at the bottom of the pyrolysis reactor read about 3 psig.

(10) The air flow to the pyrolysis reactor was changed to a N_2 flow of about 60 SCFH and the N_2 purge flow to the top of the reactor was adjusted to about 1 SCFH. This purge flow minimized any flow of the pyrolysis product gases to the feeder.

(11) The Ar flow was started and maintained at a pressure of about 1 psi greater than the pressure at the bottom of the pyrolysis reactor. The pressure at the top of the combustion reactor was usually lower than that at the bottom of the pyrolysis reactor; hence the Ar flow was used to prevent any downflow of the pyrolysis products.

(12) The feeder setting was set to the appropriate value and the feeder was started. After about 5 minutes when the temperature in the pyrolysis reactor dropped, the time was noted as the time at which the feed was actually started.

(13) Before the start of the run, the temperature of the reactor was kept about 10°C greater than desired, because once the feed was introduced the cold feed caused the temperature to drop. If the temperature dropped below the desired value, the feed was turned off for a few seconds. This was done only during the initial few minutes of the run until the temperature stabilized.

(14) During the course of the run, a constant watch was kept on: the bed levels displayed on the screen, the Ar pressure, the pressure at the bottom of the pyrolysis reactor, and the temperature of the pyrolysis reactor.

(15) While the reactor was operating stably, two to three gas samples were collected.

(16) A normal run lasted for about 1 to 1.5 hour. At the end of the run, the tap on the pyrolysis sand sampler was opened and a wire was pushed into the sampler to get the

pyrolysis sand flowing. Once a suitable amount of coked sand was collected, the tap on the sampler was closed.

(17) At the end of the run, the feeder was stopped and the control valve at the pyrolysis exit was manually closed.

(18) The electrical heating was turned off.

(19) All the gas flows were turned off.

(20) The pyrolysis gases were immediately analyzed using a gas chromatography instrument.

(21) The "level" program was terminated and the data files collected were saved.

(22) The next day, after the reactor had cooled down, the sand from the combustion and pyrolysis reactors was emptied.

(23) The oil from the collectors was collected in bottles that were previously weighed.

Material Balance

The purpose of the material balance was to find out what fractions of the bitumen fed were converted to liquid, gas, and coke. A poor material balance is indicative of an unstable operation of the reactor or errors in method of analysis of the products. Most of the material balances obtained were above 90% and hence were considered reliable.

The feeder was filled with a weighed amount of tar sand before a run. After the run, the feeder was emptied of all the tar sand, and this tar sand was then weighed. The difference in the two weighings was the amount of tar sand fed during the entire run. This value divided by the time interval of the run was the average feed rate. The sand coming out of the combustion bed was collected and the sand left in the combustion and pyrolysis reactors after the run was also collected. This value when corrected for its coke content should equal the total clean sand fed to the reactor. The total clean sand fed was also calculated by correcting the total amount of tar sand fed

from the feeder for its bitumen content. The two values usually agreed to within 10%. The average sand holdup in the bed was calculated from the collected data, and this when divided by the average feed rate gave the average residence time of the reactor. The average pyrolysis and combustion reactor temperatures were also calculated from the data.

The bitumen content of the feed was obtained by burning small weighed samples in a muffle furnace for 16 to 20 hours at 798 K, since carbonate decomposition does not occur below 923 K. The weight loss was attributed to the bitumen content. From the bitumen content and the total feed, the total bitumen fed is obtained.

Besides the pyrolysis sand sampler, the coked sand samples were also obtained from the sand left in the pyrolysis and combustion reactors after the run. The coke content of all these samples was obtained by burning small weighed samples in a muffle furnace for 16 to 20 hours at 798 K. The coke content on the sand obtained from the pyrolysis sampler was, usually, slightly higher than the coke content on the sand in the pyrolysis reactor. An average value was taken.

The total amount of liquid was obtained by emptying both the oil collectors and the mist eliminator. The empty oil collectors were weighed to make sure that there was no significant oil left inside them. Any oil left inside the tubing, connecting the exit gases to the mist eliminator, was collected and weighed. If the filter was not heated to a high enough temperature, some oil would collect inside the sintered filter. The filter was then held turned upside down in a vise over a period of a couple of days and all the oil was drained out and weighed. During normal runs, a sand layer collected on the outside walls of the filter, in the bottom of the filter unit and in the exit pipe connecting the pyrolysis reactor to the filter unit. This sand was collected, weighed and then weighed samples of it were burned in a muffle furnace for 16 to 20 hours at 798 K. The weight loss was taken as the oil on the sand, after it was corrected for the coke content on the sand. The coke content on the sand was assumed to be the same as that

on the sand in the pyrolysis reactor. This weight loss was then added to the total oil yield.

The gas analysis was done on a Hewlett Packard Model 5890 II gas chromatograph with thermal conductivity and flame ionization detectors. The response factors were calculated from calibration experiments.

Energy Balance

The electrical heat input to the pyrolysis and combustion reactors was measured using the data acquisition system. Temperature sensitive stickers from Omega were used to find the temperature at the surface of the insulation, and this was used to estimate the heat loss from the system. The coke content of the sand entering and exiting the combustion bed was found as mentioned above. The heat of combustion was estimated from the amount of coke burned in the reactor. All other terms in the energy balance were calculated.

Product Quality Analysis

Standard ASTM procedures were followed in determining the various properties. The ASTM 1747 method was used for viscosity determination, ASTM D 70 for specific gravity, ASTM D 189 for Conradson Carbon Residue, and ASTM D 97 for pour point. Simulated distillation was performed on a Hewlett Packard 5890 Series II gas chromatograph with a FID detector and a Supleco 5 meter capillary column (Cat. No. 2-5337). The column was heated from 35°C to 380°C at rate of 12°C/minute and kept at 380°C for 8.75 minutes. The helium flowrate used was 20 ml/minute.

DISCUSSION OF EXPERIMENTAL RESULTS

The driving force for the conversion of bitumen in tar sands to lighter products is thermal activation. At the pyrolysis temperature, the C-C, C-H, and C-heteroatom bonds are broken resulting in reactive free radicals. These radicals can either continue to crack by b scission to give oil and light gas as products, or can condense to low H/C carbonaceous material referred to as coke. Thus the time and temperature of the reaction dictate the severity of the reaction and thus determine the final distribution of the products (218).

This was confirmed by the mathematical model developed by Coronella (118), which showed that the pyrolysis temperature and the residence time of the solids in the pyrolysis reactor determined the yield and distribution of the products. The same conclusion was reached by various experimenters as discussed below. In this research, a number of experiments were carried out at different pyrolysis temperatures and residence times to find the optimal pyrolysis temperature and residence time. A summary of the results is shown in Table 56.

Effect of Pyrolysis Temperature on the Product Yields

A number of experiments were carried out at various pyrolysis temperatures using Whiterocks tar sand with a bitumen saturation of about 7%. The stability of the operation during the run and the material balance obtained for the run were the criterion used in determining the quality of the run. The results from five good-quality runs are presented in Figure 168.

The pyrolysis temperature was varied in the range from 463°C to 520°C at a residence time of about 27 minutes. The highest liquid yield, which was 65.1%, was obtained at a temperature of 478°C. The liquid yield, at first, increased with temperature and then decreased. Figure 169 shows another run at a pyrolysis

Table 56 Summary of the Results from the Runs

Run No:	12	13	14	15	16	17	18	19
Date of Run	4-22-94	6-7-94	6-17-94	6-29-94	7-14-94	8-11-94	8-21-94	9-1-94
Duration of Run (min)	64	129	73	82	53	68	62	103
Pyrolysis Temp. (° C)	478	493	463	474	461	479	472	520
Pyrolysis Residence Time (min)	31	27	27	22	12	16	16	21
Feed Rate (kg/hr)	4.72	4.70	4.13	6.32	11.17	8.79	7.65	5.34
Wt % Bitumen in Feed	6.84	6.74	6.37	6.64	6.82	8.94	6.7	6.7
Pyrolysis Bed Holdup (lb)	4.9	4.61	4.11	5.17	5.03	5.21	4.62	4.07
Pressure at the top of the Pyrolysis Bed (psig)	3.0	2.5	3.0	2.5	3.0	2.5	2.5	2.5
N_2 Flowrate to Pyrolysis (SCFH)	50	30	30	30	50	60	60	60
Combustion Temp. (°C)	576	565	548	573	572	556	551	560
Combustion Residence Time (min)	48.3	53.4	64.9	35.1	20.7	26.9	31.7	45.9
Combustion Bed Holdup (lb)	7.8	8.6	9.2	7.6	7.9	7.9	8.3	8.4
Pressure at the top of the Combustion Bed (psig)	0.3	0.3	0.3	0.3	0.3	0.3	0.3	0.3
Air Flowrate to Combustion (SCFH)	40	40	40	40	40	40	40	40
Wt % Coke Left on the Pyrolysis sand	1.06	1.0	0.9	0.58	1.59	1.48	1.13	1.13
Wt % Coke Left on the Combustion sand	0.59	0.08	0.16	0.19	0.97	0.61	0.49	0.49
Wt % Gas Yield	21.2	33.1	26.3	18.4	10.0	14.8	19.9	30.4
Wt % Liquid Yield	65.1	50.0	56.3	72.4	74.6	71.9	63.0	52.5
Wt % Coke Yield	13.6	16.7	17.4	9.2	15.2	13.2	17.0	17.0
Wt % C_5-C_6 Yield of Total Yield	17.9	15.4	13.2	14.3	49.4	41.4	17.0	17.9
% Material Balance	107.4	88.8	89.5	90.2	111.2	115.7	93.4	93.2

Average barometric pressure = 12.5 psia

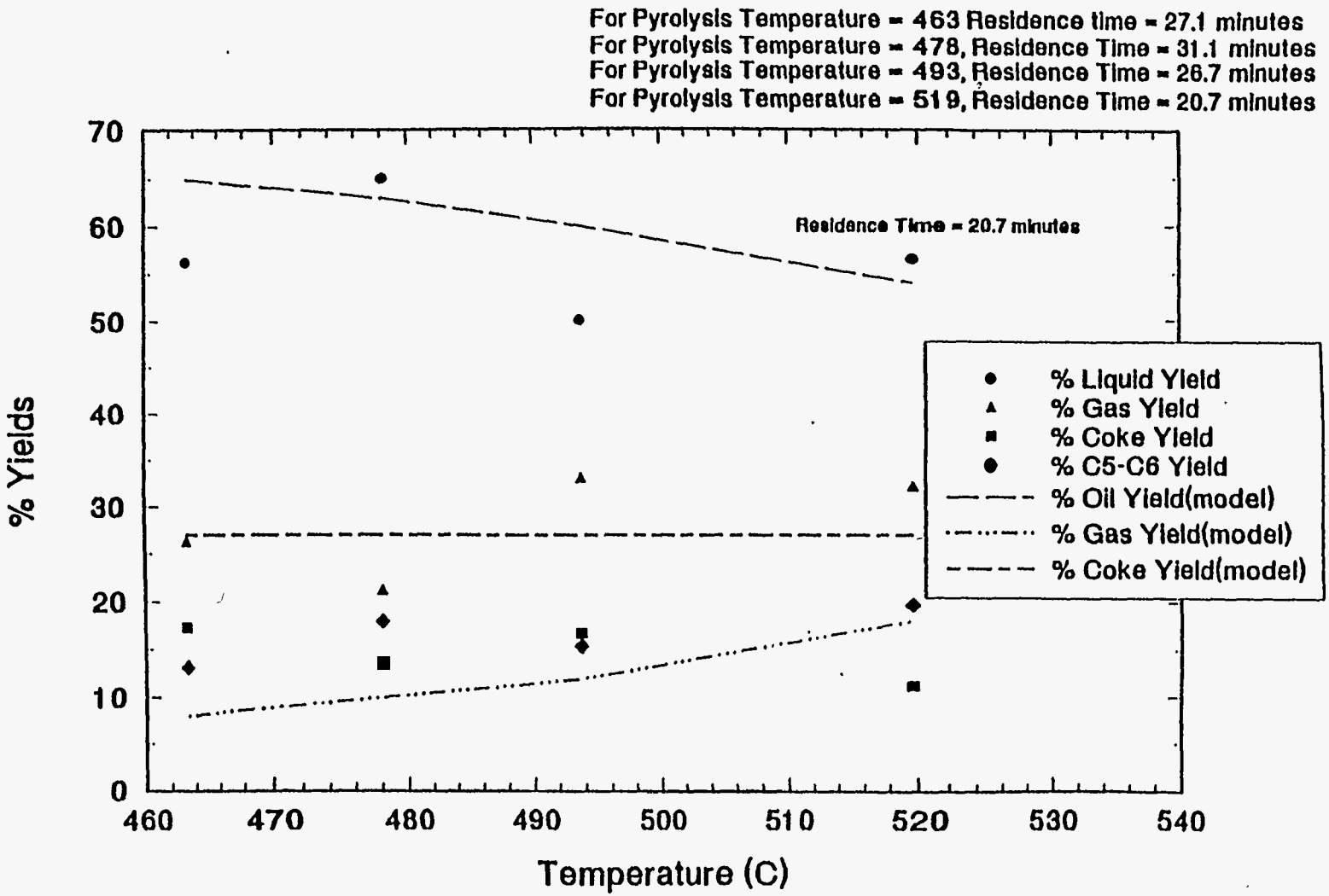

Figure 168. Effect of Pyrolysis Temperature on Yields

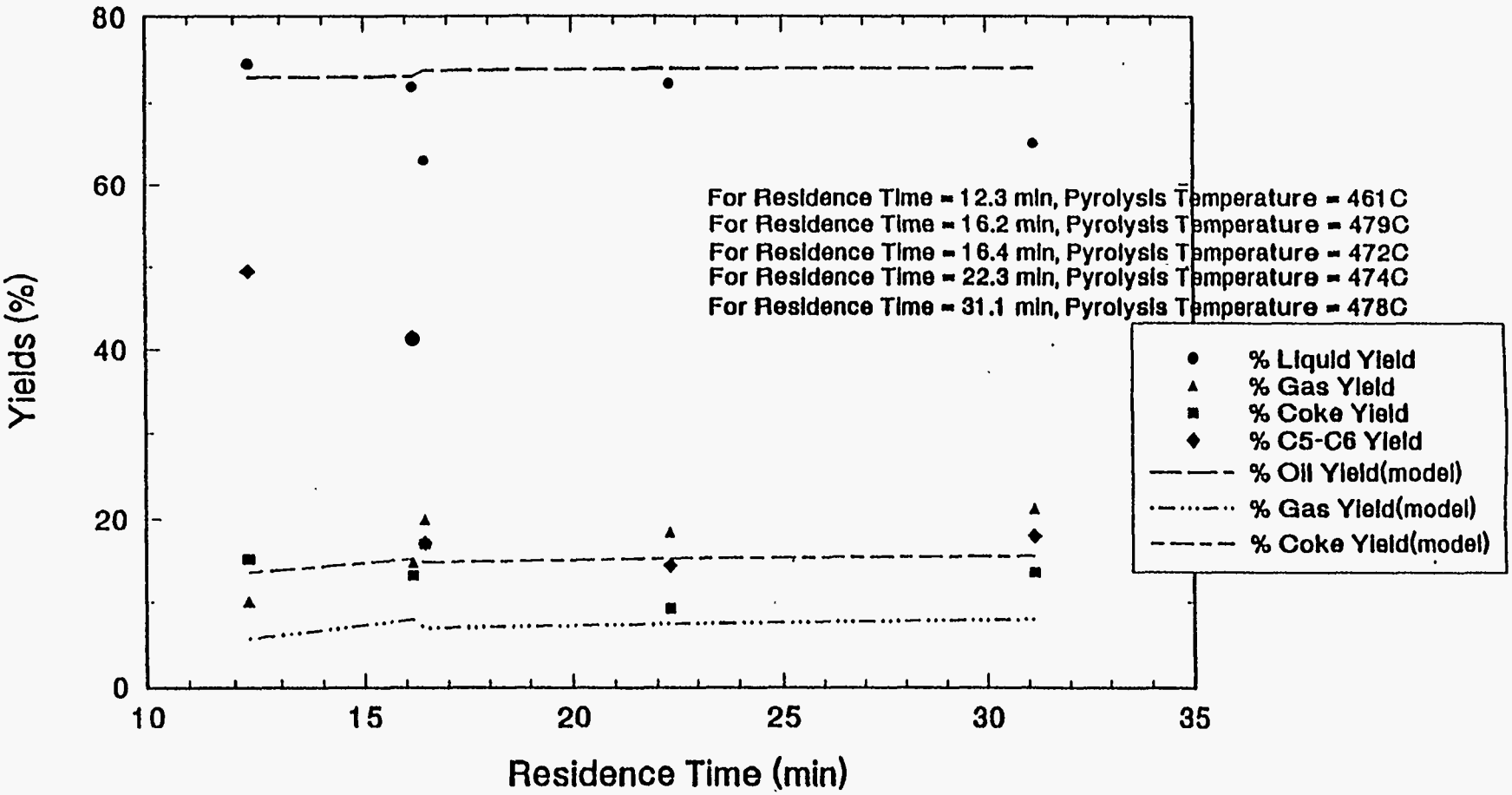

Figure 169. Effect of Residence Time on Yields

temperature of 472°C and a residence time of 16.44 minutes with a liquid yield of 63%, which is higher than the liquid yield of 56% observed at a temperature of 463°C. Thus there are sufficient data to justify the statement that at lower temperatures the liquid yield increased with temperature. The gas yield increased with increasing temperature. The gas yield at the pyrolysis temperature of 520°C is slightly lower than the yield at 494°C, and the liquid yield at the temperature of 520°C is slightly higher than the yield at 494°C. This can be explained by the fact that the run at 520°C was at a much lower residence time of 20.7 minutes as compared to the run at 494°C, which was at a residence time of 26.7 minutes. The amount of "unreacted bitumen + coke" remained almost constant for all the temperatures. These trends are similar to those observed by most experimenters.

The liquid yields obtained from the model, shown by continuous lines in Figure 168, are in reasonably good agreement with the experimental data points. The model also shows an increase in the liquid yield with temperature at lower temperatures; however, it predicts a maximum liquid yield at a temperature of 460°C, which is much lower than the experimentally observed peak. The model also predicts a constant value for the amount of "unreacted bitumen + coke" at all temperatures, but this value is much higher than the experimentally observed values. Also, the model predicts much smaller quantities of C_1-C_4 light gases.

The observed yields can be explained by considering the reaction mechanism used in the mathematical model. The model assumes that the bitumen consists of two fractions, namely, the heavy bitumen and the light bitumen (118). The heavy bitumen undergoes a cracking reaction and the lighter bitumen undergoes distillation as shown in Equations 96 and 97.

$$\text{Heavy Bitumen} \xrightarrow{k1} s_C \text{ Light Bitumen} + s_D \text{ Coke} \quad (96)$$

$$\text{Light Bitumen} \xrightarrow{k2} s_E \text{ Heavy Oil} + s_F \text{ Middle Oil} + s_G \text{ Light Oil} + s_H \text{ Light Gas} \quad (97)$$

The significant quantities of the light gas formed by the pyrolysis of asphaltenes are accounted by the reaction:

$$\text{Heavy Bitumen} \xrightarrow{k1} s_A \text{ Coke} + s_B \text{ Light Gas} \quad (98)$$

The gas-phase cracking reactions are:

$$\text{Heavy Oil} \xrightarrow{k5} s_I \text{ Middle Oil} + s_J \text{ Light Oil} + s_K \text{ Light Gas} \quad (99)$$

$$\text{Middle Oil} \xrightarrow{k6} s_L \text{ Light Oil} + s_M \text{ Light Gas} \quad (100)$$

Thus, at higher pyrolysis temperatures, the cracking severity is increased due to greater thermal activation and hence the ease of formation of radicals. The product selectivity is shifted towards the lighter products and hence the liquid yields are decreased and the gas yields increased. At lower temperatures, however, cracking is not severe and some of the bitumen remains unreacted. Thus, with increasing temperatures, more of the bitumen is cracked giving more light bitumen and this increases the liquid yield at lower temperatures. At lower temperatures, there is more unreacted bitumen and less coke formation, but the opposite is true at higher temperatures; which explains the reason why the amount of "unreacted bitumen + coke" remains constant at all temperatures.

Compared to resins and asphaltenes, oils are much more paraffinic and their H/C atomic ratios are much higher. Oils may be composed of a naphthene ring with one of more side chains of varying length.

The pyrolysis behavior of various hydrocarbons varies (219). N-paraffins pyrolyze to form olefins by dehydrogenation. The olefin yields from pyrolysis of i-paraffins is less than from n-paraffins, but i-paraffins undergo more chain scission to give methane and hydrogen. Olefins undergo chain scission to give lower molecular weight olefins and dehydrogenate to form alkynes. Naphthenes dehydrogenate to yield aromatics, whose ring structure is not easy to rupture. The alkyl side chains of the aromatic rings undergo chain scission of the C-C bond, while the rings condense to give polynuclear aromatics, which later form coke. The pyrolysis of a complex mixture of hydrocarbons, such as bitumen, is extremely complex because the large number of free radicals formed during pyrolysis can react with one another in a number of ways and can promote and inhibit certain cracking reactions. The reaction mechanism used in the mathematical model, though a very simplified representation of the actual pyrolysis process, gives the general picture of the type of reactions occurring and also gives a good explanation of the yields obtained.

Effect of the Solids Retention Time on the Product Yields

The effect of the solids retention time on the product yields was studied, using the same Whiterocks tar sand, by varying the residence time of the solids from about 12 minutes to 31 minutes, while keeping the pyrolysis temperature at about 470°C. The yields are shown in Figure 169.

As seen from the figure, the yields predicted by the model are in close agreement with the experimental data. The liquid yield appeared to be constant for the different residence times. The gas yield showed a slight increase with residence time and the "unreacted bitumen + coke" yield remained constant.

However, a very striking trend is noticed in the formation of C_5-C_6 gases, which is not a product that is predicted by the model of Coronella. At low residence times, more than 40% of the total product formed was in the form of C_5-C_6 gases. At a residence time of about 16 minutes, there was a sharp decrease in the amount of C_5-C_6 gases produced; and with further increase in the residence time the C_5-C_6 gas yield remained almost constant. The model only predicts total gas yields, and certain modifications in the reaction mechanism would be necessary to approach the observed results.

Any trends that could have been observed in the liquid yields are masked by the large amounts of C_5-C_6 gases formed, since the error in the measurement of the C_5-C_6 gases is sufficient to offset any trends in the liquid yields.

As mentioned earlier, pyrolysis is a very complex process with a number of reactions occurring simultaneously. Hence a number of reaction mechanisms are possible. One such mechanism is described here (220). In pyrolysis every compound can undergo, both concurrently and consecutively, many reactions. The concept of primary and secondary reactions has been widely accepted by many researchers. Primary reactions are reactions occurring first, whereas secondary reactions are the subsequent reactions of products formed in the primary reaction.

Whiterocks tar sand consists of 18.5% saturates, 5.5% mono-nuclear and di-nuclear aromatics, 11.3% polynuclear aromatics, 18.4% resins, and 46.5% asphaltenes (82). Primary reactions, which are reactions with faster kinetics, occur predominantly at residence times lower than 16 minutes. The paraffins and cycloparaffins crack by the free-radical mechanism which involves: (1) Initiation, where free radicals are created by thermal activation. (2) Propagation, where products are formed from reactants without any change in the radical concentration. (3) Termination, where the radicals combine to form stable products. The products formed are lighter olefins and paraffins (215). As described above, the aromatics with alkyl groups mainly undergo

the chain scission of the C-C bond and dehydrogenation in the alkyl side chain, without the rupture of the refractory aromatic ring. Whiterocks tar sand has a large percentage of asphaltenes, which have a number of aromatic rings and, thus, the dealkylation of the alkylsubstituted aromatic rings produces the large amount of C_5 - C_6 gases observed at residence times that are less than 16 minutes. The olefins crack by mechanisms similar to paraffin cracking to yield lower olefins.

The secondary reactions are the reactions with slower kinetics and occur predominantly for residence times greater than 16 minutes. The polycluster compounds in the asphaltene fraction are cleaved to give monocluster compounds and the aromatic rings are alkylated with lower olefins in the presence of the solid acids in the inorganic part of the tar sand. The paraffins and olefins crack further to give lower paraffins and olefins. The last two reactions explain the reduction in the amount of C_5's and C_6's and the increase in the liquid oil yield observed at larger residence times.

The primary and secondary reactions occur simultaneously at all times. The primary reactions occur predominantly for residence times less than 16 minutes and the secondary reactions occur predominantly for residence times greater than 16 minutes. In the pyrolysis of bitumen the predominant mechanism is a free-radical chain, and the radical intermediates formed by one compound can interact with those produced by another or with the reactant itself. The replacement of a rate-determining step can change the kinetics and, thus, the selectivities can change because the distribution of the intermediates is altered. The cracking of a refractory compound is accelerated by the presence of reactive compounds, whereas the cracking of a reactive compound is inhibited by the presence of refractory compounds. As residence time was increased, more of the unreacted bitumen cracked, leading to an increase in the amount of primary products, which were more reactive. This induced the cracking of the refractory compounds present; for example the cleavage of the polycluster compounds. This cleavage resulted in an increase in the number of sites that could be alkylated and, thus,

led to an increase in the alkylation of the aromatic rings. This explains the reduction in C_5 - C_6 compounds observed with an increase in the residence time.

Three product liquids were analyzed to obtain the ratio of asphaltene to maltene. Asphaltenes was the fraction insoluble in n-pentane, and maltenes was the fraction that was soluble. It is indeed observed, as seen in Table 57, that for the run at lower residence time the asphaltene fraction is significantly higher.

The Effect of Pyrolysis Temperature on the Quality of the Product Liquids

The effect of temperature on the API gravity of the product liquid is shown in Figure 170. The API gravity for lower temperatures increased with temperature and then decreased with increasing temperature. The initial sharp increase in the API gravity can be attributed to the increase in the cracking of the large asphaltene molecules. At these low temperatures the cracking reactions are just beginning to occur. As temperature is increased the cracking severity is increased, and the light paraffins and olefins crack further to give larger amounts of light gases. The olefins also undergo the Diels-Alder reaction to give cycloolefins, and the naphthenes dehydrogenate to give aromatics. Higher temperatures also favor the condensation of the aromatic rings to give polyaromatics. All these reactions lead to an increase in the aromaticity and hence in an increase in the specific gravity (decrease in API gravity). The API gravity at the temperature of 520° C in Figure 170 is probably higher than it should be, because the run was carried at a lower residence time of 20 minutes as compared to the other runs at 27 minutes.

The effect of temperature on the viscosity of the liquid products is shown in Figure 171. The initial sharp decrease in the viscosity is caused by the increase in the cracking of the larger asphaltene molecules. The viscosity increases with temperature, at higher temperatures, because of the increase in aromaticity and in the amount of sticky coke precursors, as explained earlier.

Table 57

Weight Fraction of Asphaltenes in the Product Liquid

Run Number	Residence Time (minutes)	Pyrolysis Temperature (°C)	% C_5-C_6 Yield of Total Product	Weight Fraction of Asphaltenes
14	27	463	13	0.072
17	16.1	479	41	0.122
18	16.4	472	17	0.058

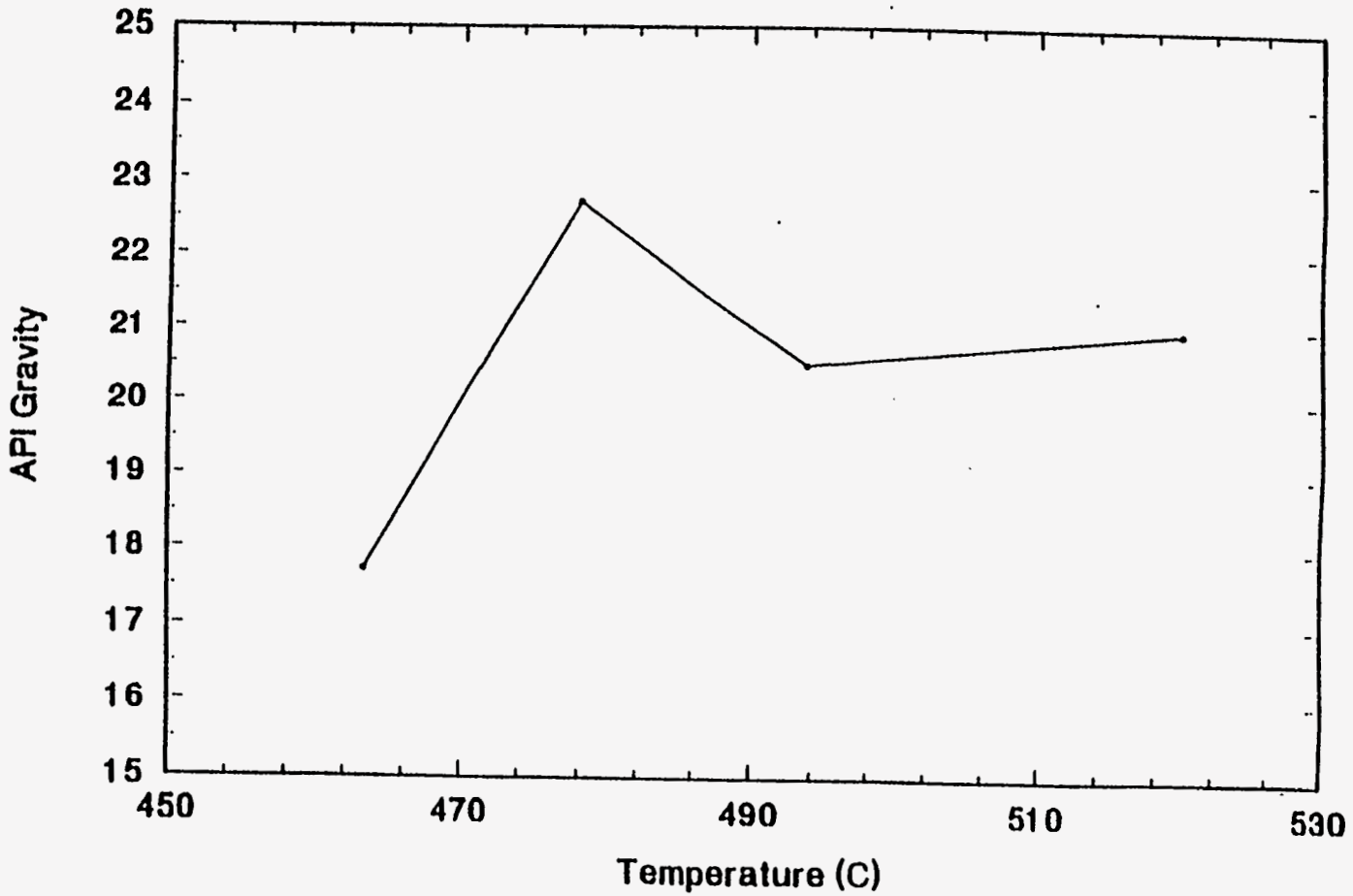

Figure 170. Effect of Temperature on the API Gravity

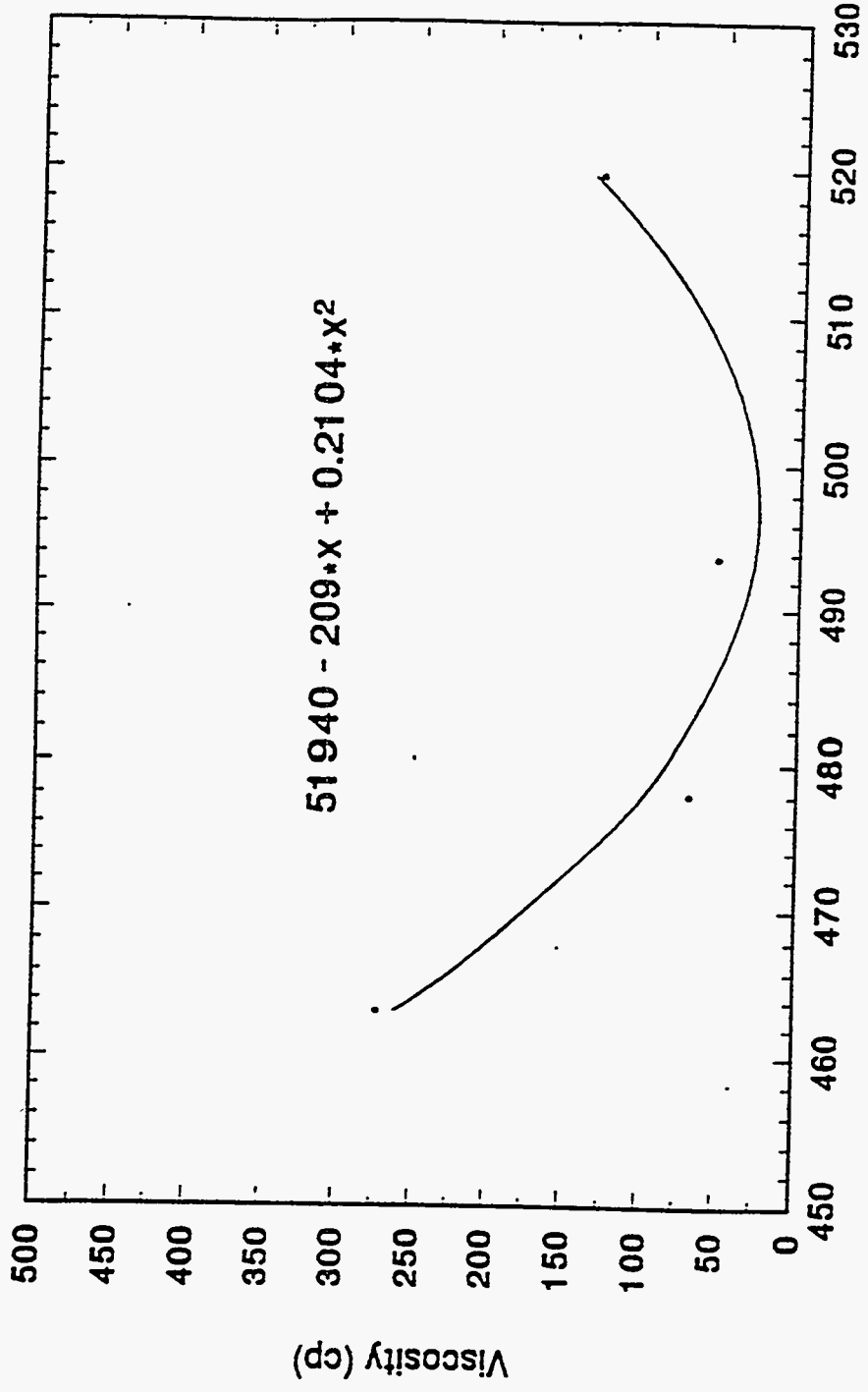

Figure 171. Effect of Temperature on Viscosity

The effect of temperature on the Conradson Carbon Residue of the liquid products is shown in Figure 172. A correlation exists between the H/C ratio and the Conradson Carbon Residue (CCR) value as follows (221):

$$H/C = 1.71 - 0.0115*CCR \qquad (101)$$

This equation holds within two limits; at H/C values ³ 1.71, CCR = 0; at H/C values £ 0.5, CCR = 100. This correlation was based on 114 data points from 15 crude oils. At lower temperatures, because of the increase in the cracking of the larger asphaltene molecules, there is an increase in the H/C ratio, which explains the decrease in the Conradson Carbon Residue value. With further increase in temperature, the aromaticity increases and the H/C ratio decreases and thus the observed increase in the Conradson Carbon Residue value.

The effect of temperature on the pour point of the liquid products is shown in Figure 173. The product liquids are chilled without disturbance at a standard rate (ASTM D-97). As cooling is continued, the oil becomes more and more viscous and the flow becomes slower and slower. The pour point is the lowest temperature at which the oil flows. As seen in Figure 173 the pour point increases with increase in aromaticity at higher temperatures. The initial decrease in pour point is only slight.

Figure 174 shows the effect of pyrolysis temperature on the simulated distillation cuts. As the temperature increases, there is an increase in the proportion of lighter fractions, namely, gasoline and middle distillate and a decrease in the proportion of the heavier fractions, namely, gas oil and residue. The data point at a pyrolysis temperature of 520° C was obtained at a residence time of 20.7 minutes and, hence, the proportion of the lighter fractions is probably less than it would be for the same pyrolysis temperature but for a residence time of 27 minutes. All the other runs were carried out at residence times close to 27 minutes.

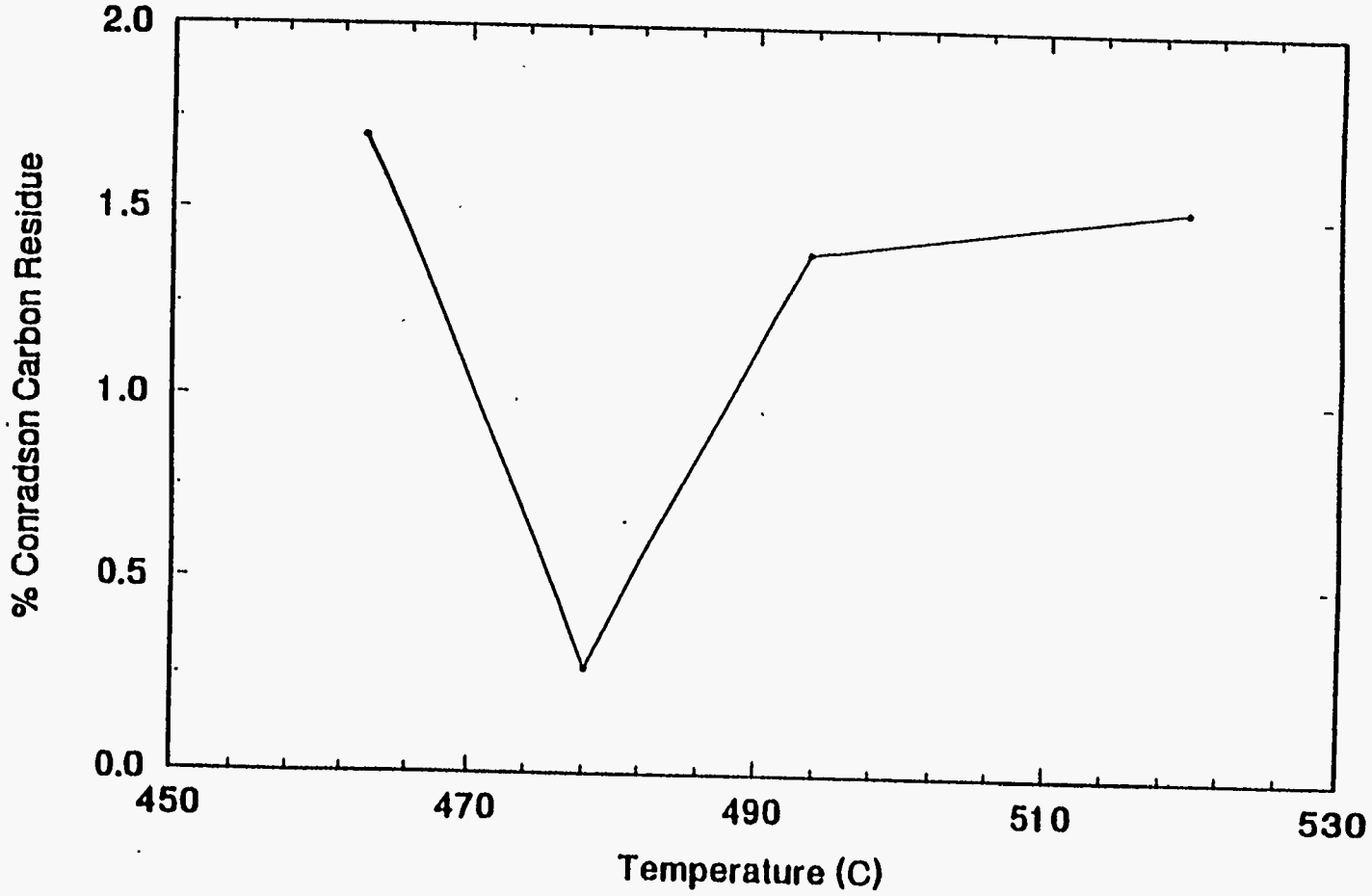

Figure 172. Effect of Temperature on Conradson Carbon Residue

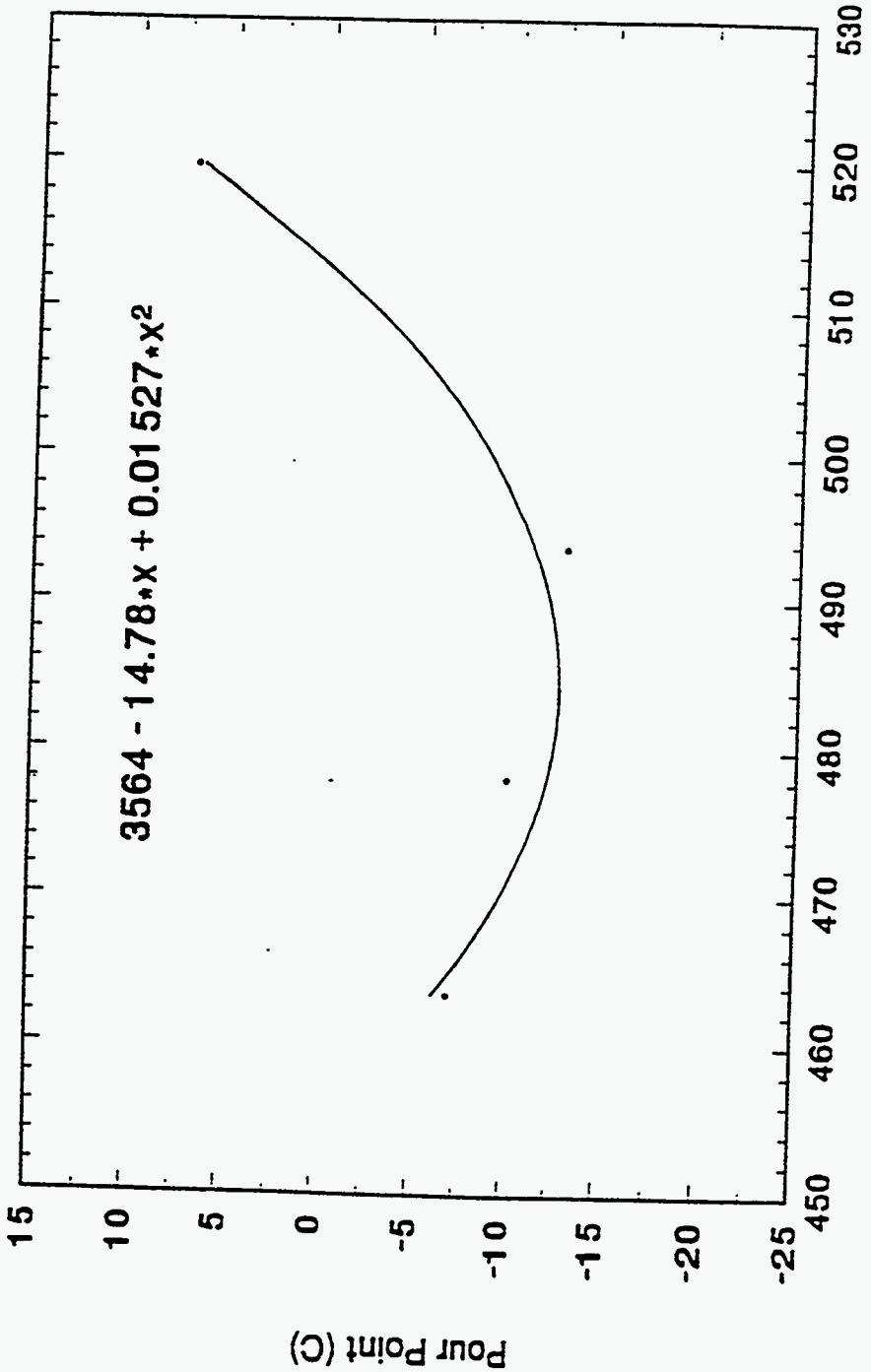

Figure 173. Effect of Temperature on the Pour Point

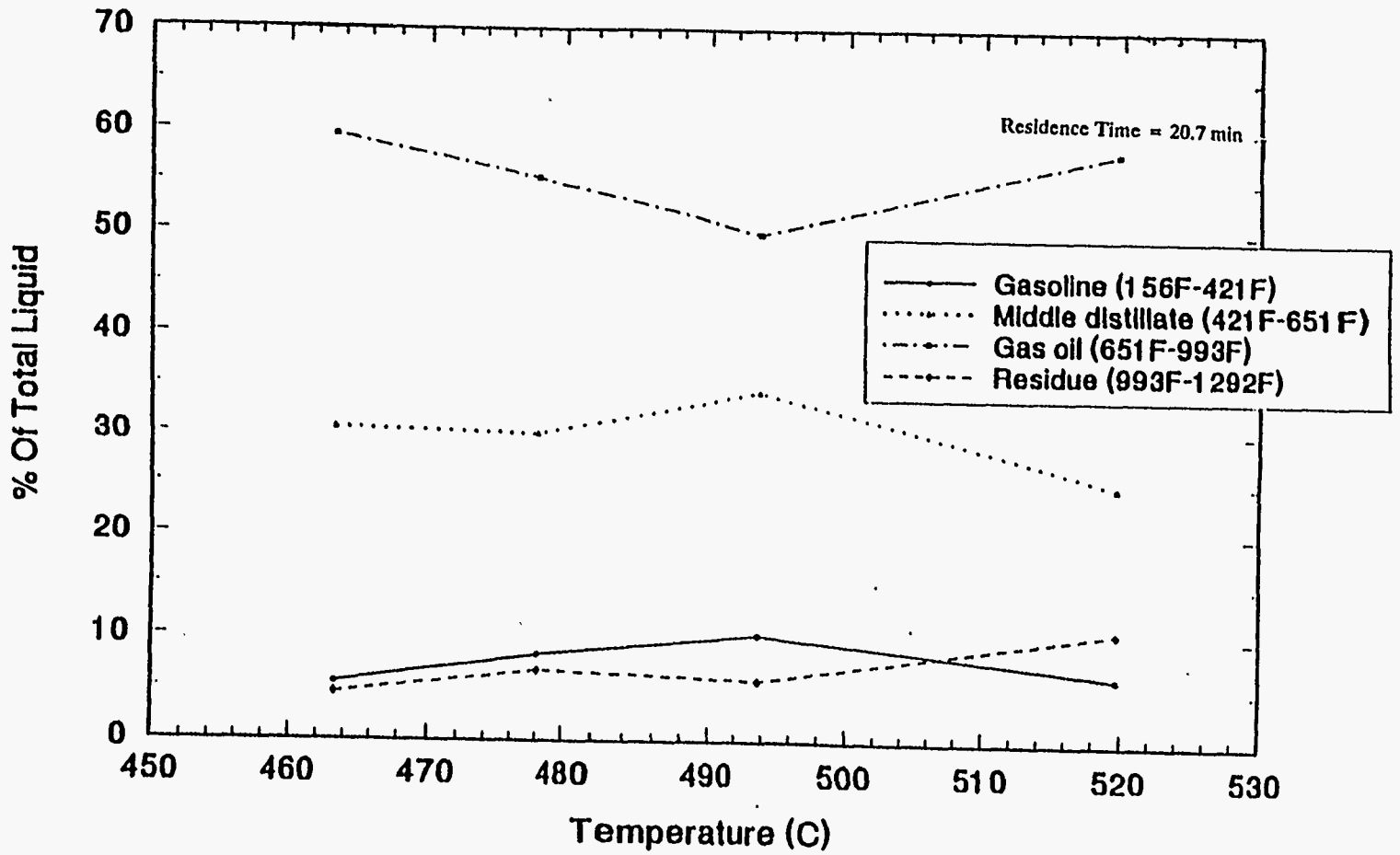

Figure 174. Effect of Temperature on the Simulated Distillation Cuts

The Effect of Residence Time on the Quality of the Product Liquids

The effect of residence time on the API gravity of the product liquid is shown in Figure 175, where it is seen that the specific gravity is high at lower residence times and decreases with increase in residence time. The specific gravity at the residence time of 16.4 minutes is higher than that at a residence time of 16.2 minutes, because the pyrolysis temperatures for the two runs are 472°C and 479°C, and as seen in Figure 170, the specific gravity at lower temperatures is higher. The product liquids at the low residence times of 12.3 minutes and 16.2 minutes do not include the large amounts of C_5 and C_6 compounds formed at these low residence times because these compounds did not condense appreciably. Thus, a large amount of the olefins and paraffins formed during the dealkylation of the alkylsubstituted aromatic rings escape, leaving behind the aromatic ring structures of the asphaltene molecules, resulting in the higher specific gravities and viscosities observed at the lower residence times.

The effect of residence time on the viscosity of the product liquid is shown in Figure 176. As pointed out in the previous discussion, the viscosity at the lower residence times is higher than that at higher residence times. The product liquid from the run at a residence time of 16.4 minutes and pyrolysis temperature of 472°C had the highest observed viscosity of 473 cp. For this run, the amount of C_5 and C_6 gases formed were much less compared to the runs carried at lower residence times. Hence it may be assumed that there was some cleavage of the polycluster compounds and the C_5 and C_6 compounds were consumed in the alkylation of the aromatic rings. However, it is possible that a large number of polycluster groups were not cleaved, and hence the viscosity and Conradson Carbon Residue of the product liquid was high.

The effect of residence time on the Conradson Carbon Residue of the product liquid is shown in Figure 177. For the reason explained above, the Conradson Carbon Residue of the product liquid, for the run at residence time of 16.4 minutes, is high.

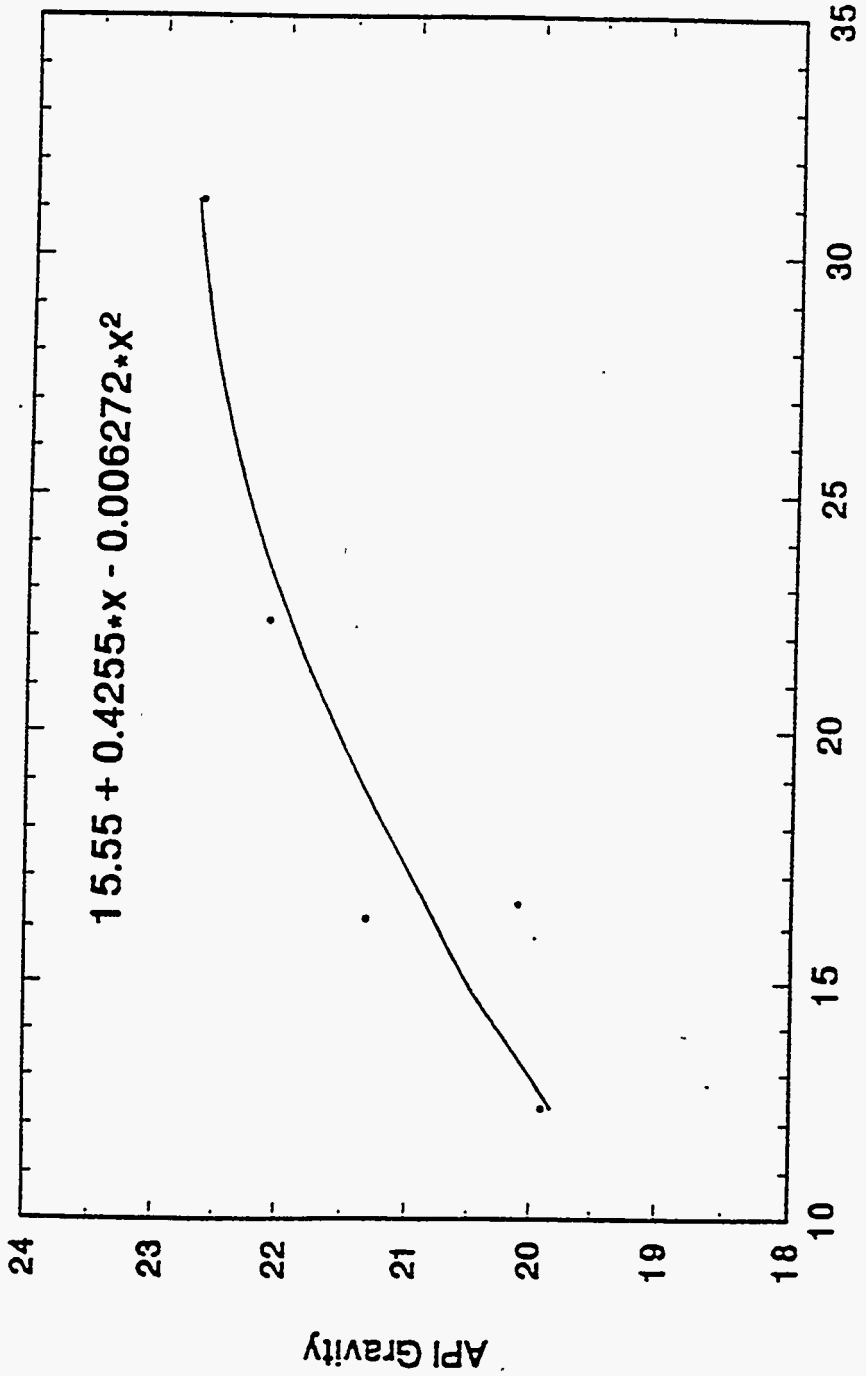

Figure 175. Effect of Residence Time on API Gravity

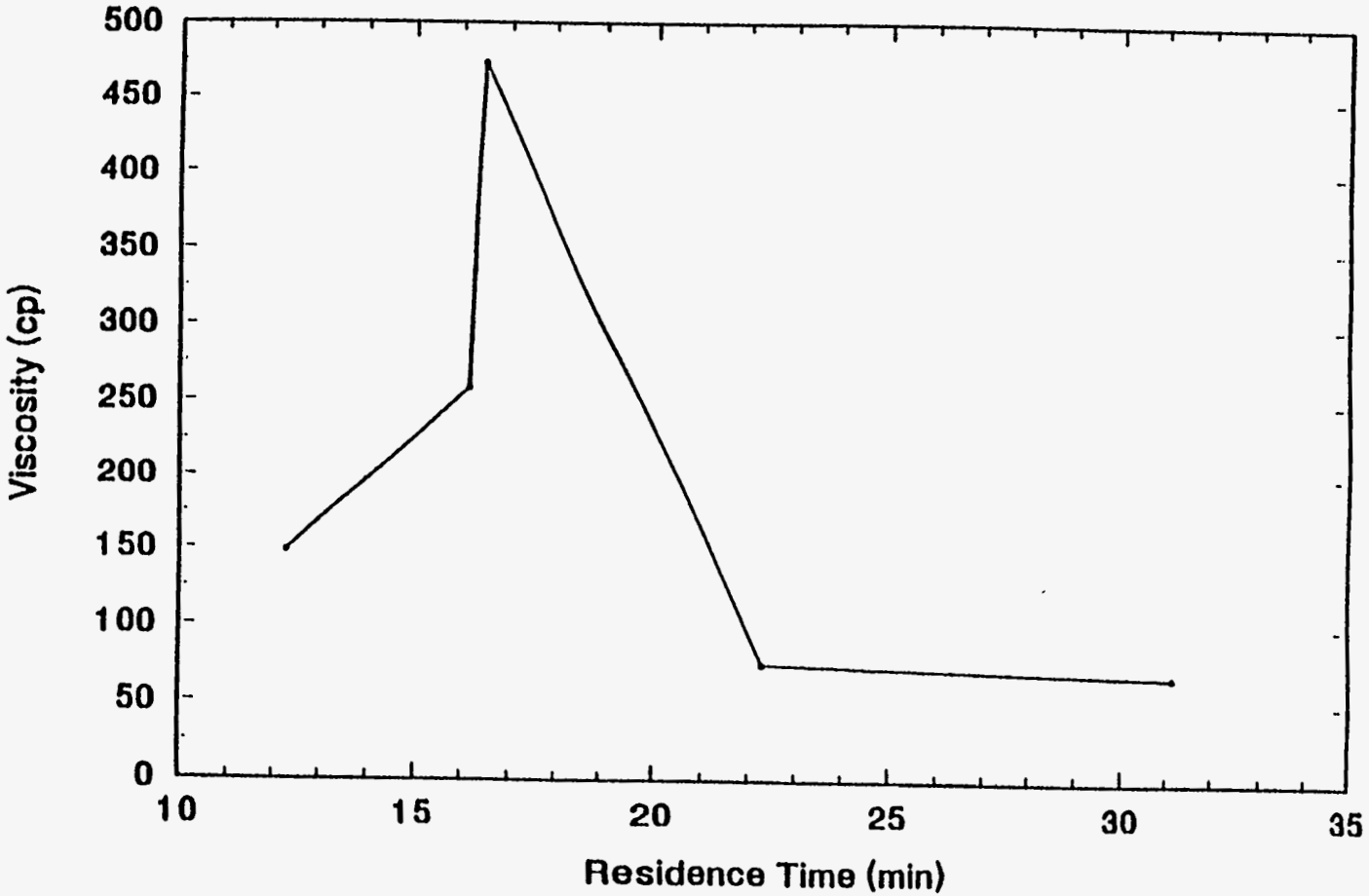

Figure 176. Effect of Residence Time on Viscosity

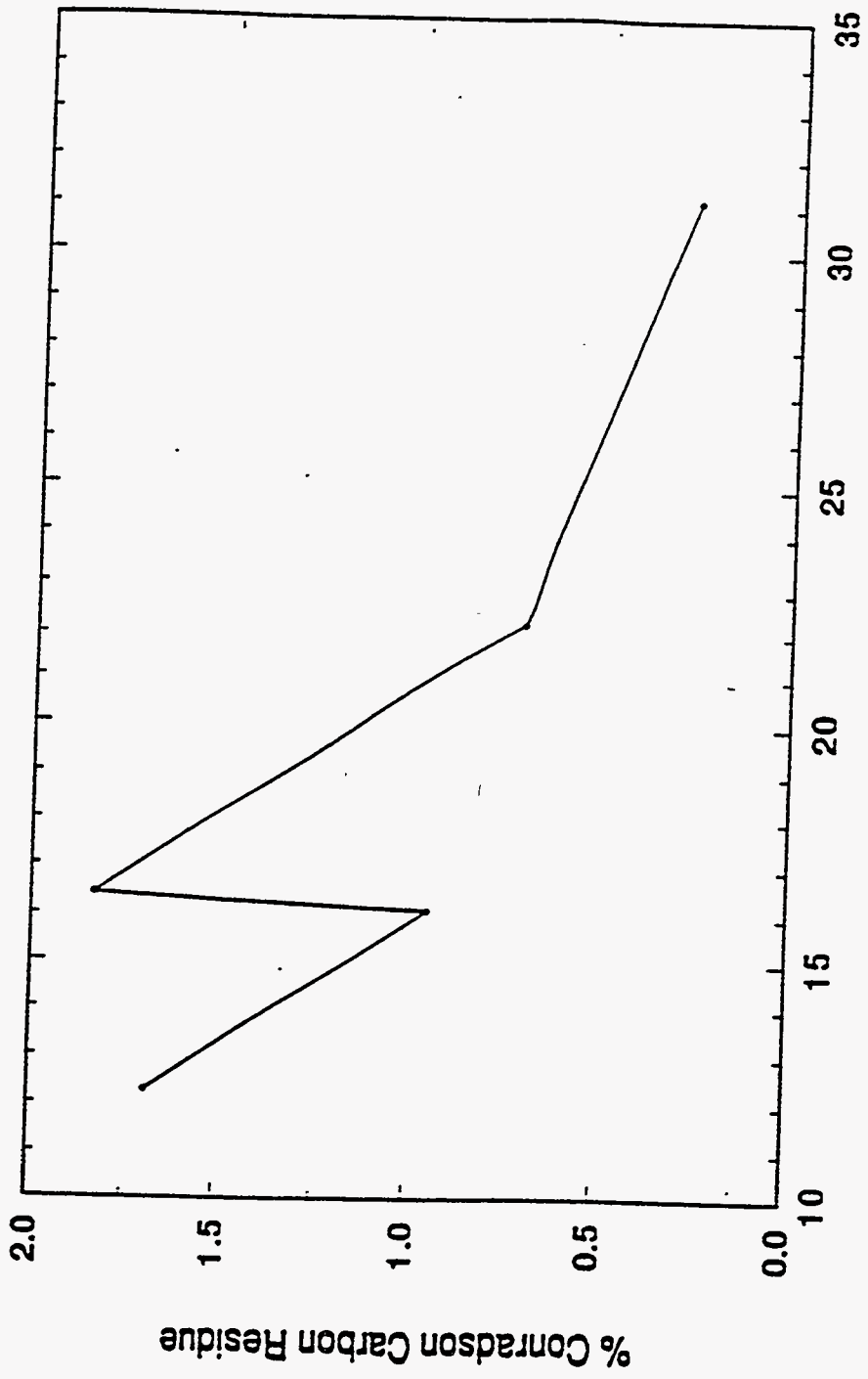

Figure 177. Effect of Residence Time on Conradson Carbon Residue

For higher residence times the cleaving of the polycluster compounds and the alkylation of the aromatic rings increases the H/C ratio of the product liquid and decreases the Conradson Carbon Residue. The low value of the Conradson Carbon Residue for the run at a residence time of 16.2 minutes cannot be explained.

The effect of residence time on the pour point of the product liquid is shown in Figure 178. The more viscous product liquids from the runs at lower residence times have a higher pour point. The high pour point of 3 °C for the run at a residence time of 22.3 minutes cannot be explained.

Figure 179 shows the effect of residence time on the simulated distillation cuts. At small residence times, the product liquid has a higher proportion of the lighter fractions, namely, gasoline and middle distillate. The lighter fractions get consumed in the alkylation reactions.

Energy Balance for the Reactor System

A few results of the energy balance carried out on the laboratory thermally coupled fluidized-bed reactor system are presented in this section. These calculations showed that a large amount of heat was lost from the reactor surfaces. The largest amount of heat loss occurred from the surface of the pipe that connected the feeder to the top of the pyrolysis reactor.

The details of the energy balance calculations can be found in the M.S. thesis by Khot (222). The only differences in the results presented here are: (1) some of the temperatures involved in the energy balance were measured experimentally and (2) the electric heating of the two beds was measured using the data acquisition system. The temperature on the surface of the insulation was measured using liquid crystal indicators and this was used in the calculation of the heat loss as described by Khot (222).

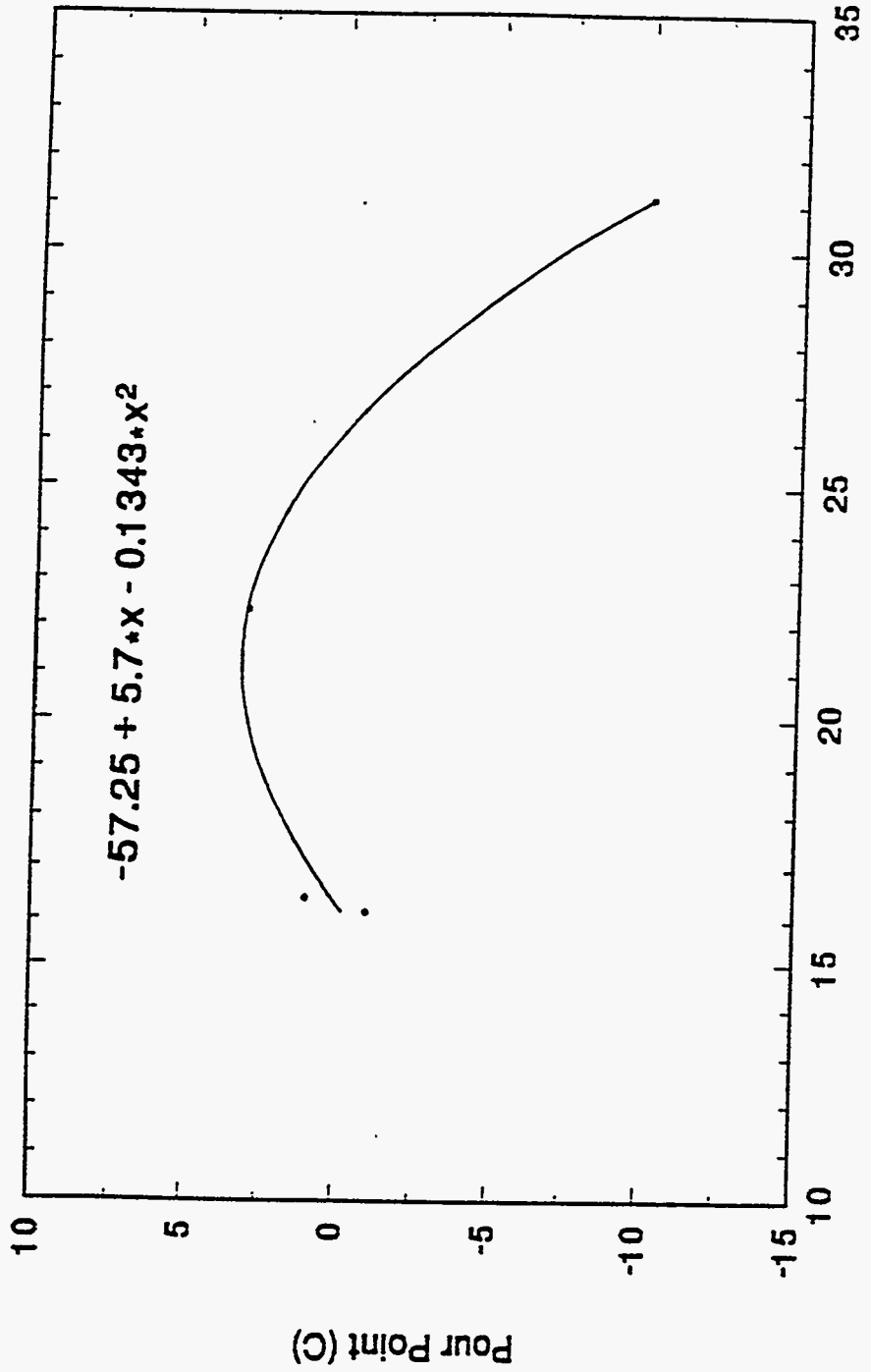

Figure 178. Effect of Residence Time on Pour Point

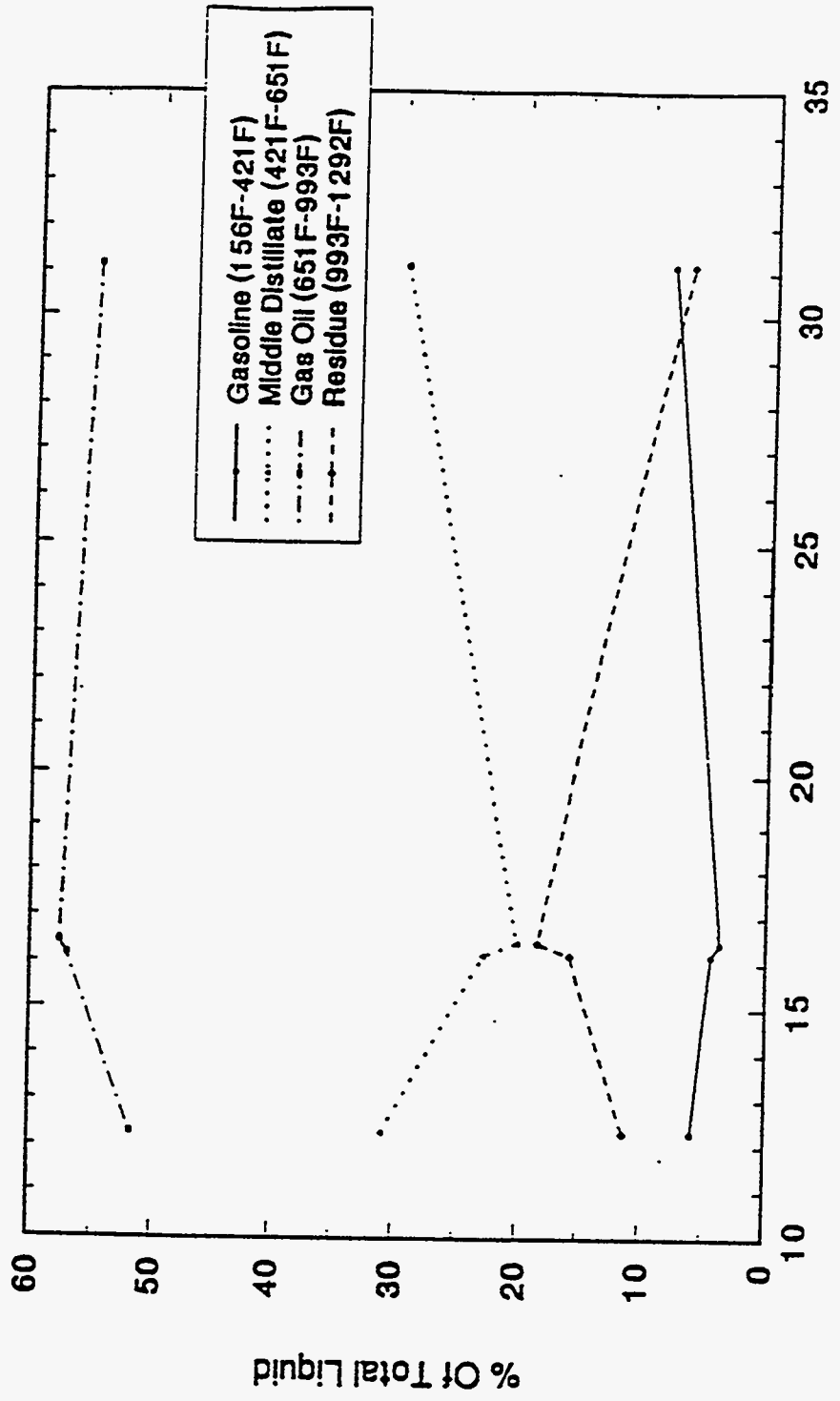

Figure 179. Effect of Residence Time on Simulated Distillation Cuts

A 43-inch long steel pipe connected the feeder to the top of the pyrolysis reactor. The temperature at the bottom of this pipe was assumed to be the same as the pyrolysis temperature, and a steady-state energy balance for the pipe was written as:

Heat lost by radiation + Heat lost by convection + Heat conducted upward through the pipe = 0

(102)

Starting from the temperature at the bottom of the pipe, the heat loss by radiation and convection was calculated for the bottom two-inch length of pipe. Using this, the heat conducted upward through the pipe was calculated and the temperature gradient for the bottom two-inch length was obtained. This was used to calculate the temperature of the pipe at two inches from the bottom. This procedure was repeated and the total heat loss was calculated by adding all the heat lost by radiation and convection and the heat conducted out by the pipe at its top end. The results from the energy balance calculations for three different runs are shown in Table 58. The heat transferred to the pyrolysis reactor from the heat pipes and the heat transferred from the combustion reactor to the heat pipes are both calculated by difference. Ideally these two quantities should be equal, since conditions are assumed to be adiabatic. However, the difference could be from unaccounted heat losses, and errors, in each of the energy balance terms. Table 58 shows that the heat pipes do transfer a significant amount of energy.

Table 58

Results of Some Energy Balance Calculations

Pyrolysis reactor	Run # 12	Run # 17	Run # 19
Pyrolysis temperature	463°C	479°C	520°C
Electric heating**	$16.9*10^5$	$47.5*10^5$	$51.9*10^5$
Sensible heating of sand	$-14*10^5$	$-27*10^5$	$-20*10^5$
Sensible heating of bitumen	$-2.7*10^5$	$-6.6*10^5$	$-3.0*10^5$
Heat of pyrolysis	$-1.4*10^5$	$-3.6*10^5$	$-1.6*10^5$
Heat loss from walls	$-7.2*10^5$	$-7.2*10^5$	$-7.2*10^5$
Heat loss from vertical pipe	$-13*10^5$	$-13*10^5$	$-14*10^5$
Sensible heating of N_2	$-7.8*10^5$	$-8.1*10^5$	$-8.8*10^5$
Heat via heat pipe (by diff.)	$30.0*10^5$	$18.5*10^5$	$2.9*10^5$

Combustion reactor	Run # 12	Run # 17	Run # 19
Combustion temperature	575°C	556°C	560°C
Electric heating	$52.9*10^5$	$54.0*10^5$	$47.7*10^5$
Heat of combustion	$8.6*10^5$	$22.8*10^5$	$9.5*10^5$
Sensible heating of O_2 in air	$-1.3*10^5$	$-1.2*10^5$	$-1.2*10^5$
Sensible heating of N_2 in air	$-4.5*10^5$	$-4.5*10^5$	$-4.5*10^5$
Sensible heating of sand	$-3.3*10^5$	$-4.6*10^5$	$-1.5*10^5$
Heat loss from insulation	$-7.2*10^5$	$-7.2*10^5$	$-7.2*10^5$
Heat via heat pipe (by diff)	$-45*10^5$	$-59*10^5$	$-42*10^5$

* All units of power are Joules/hr

OPTIMIZING THE OPERATION OF A THERMALLY-COUPLED FLUIDIZED-BED TAR-SANDS EXTRACTION PROCESS

Optimization of the Mathematical Model

Coronella (118) developed a complex mathematical model for the thermally coupled fluidized-bed tar-sands extraction process. This model incorporates hydrodynamics, heat and mass transfer, and detailed reaction mechanisms and kinetics. In this research, this model was optimized to obtain the optimal operating conditions for the reactor system. A heat recovery network was added to this model to efficiently recover the heat from the hot streams leaving the reactor. This entire model was also optimized.

Since the cost function in this optimization problem could vary from day to day because of the variation of the bitumen content of the mined tar sands, it would be essential to be able to convert the reactor from one set of operating conditions to a new set of conditions in an optimal manner. An optimal control strategy developed for this purpose is also presented.

Optimization Problem Description

Optimization of this process is desirable to see the effects of the changes in the operating conditions on the product yields and the process economics. Optimization of the operating conditions can also provide advantages in fluctuating situations, i.e., raw material costs, operating costs, product sales and product prices.

The inputs to the mathematical model are:

*Pyrolysis temperature

*Pyrolysis residence time

*Pyrolysis gas flowrate

*Weight fraction of heavy bitumen in bitumen

*Weight fraction of bitumen in tar sand

*Mean particle diameter and sphericity of solids

*Molecular weights of light gas, light oil, middle oil and heavy oil.

*Stoichiometric constants

*Pressures at bottom of combustion and pyrolysis beds

*Combustion bed temperature

*Combustion bed residence time

*Combustion bed gas flowrate

*Cross-sectional area of beds

*Volume fraction of bubble phase occupied by solids

*Weight fraction of hydrogen and carbon in coke entering the combustion bed

The outputs from the model are

*Gaseous concentration profiles in bubble and dense phases

*Pressure profiles

*Product yields

Pyrolysis temperature, pyrolysis sand residence time, and combustion temperature are varied to obtain optimal values of the outputs. Both the pyrolysis temperature and pyrolysis sand residence time dictate the product yields and quality. The combustion temperature affects the heat of combustion supplied to the pyrolysis reactor and also the electrical heating consumed during the process. The objective function included the value of the light oil, middle oil, and heavy oil produced during the process. The sum of all these terms were maximized. Also, the sum of the coke and gas formed during the process, and the electrical heating utilized were minimized.

A model of a heat recovery unit consisting of six heat exchangers, three steam generators, three turbines, two compressors and a separator was added to the

process to recover the heat from the outflowing hot sand and hot process gases. The flowsheet for this unit is shown in Figure 180. The heat exchanger network, in the flowsheet, was optimized using pinch-point technology calculations by a previous student. The objective is to preheat the pyrolysis and combustion fluidization gases as much as possible, while simultaneously producing as much power as possible. Again the operating parameters varied to minimize the objective function are the pyrolysis temperature and sand residence time and the combustion temperature.

Calculation of Cost Coefficients

The value of the different fractions of oil produced is determined by their API gravity. A plot of some recent price data as a function of API gravity is shown in Figure 181. From this plot and the known values of the API gravities of the light, middle and heavy oil; the relative values of the three fractions were calculated. The cost of electricity was taken as $.08/kWhr. The heat recovered is calculated in Joules/sec and this leads to a reduction in the electrical heating and hence the same cost coefficient as the cost of electricity is used.

Optimization Methodology

A nonlinear programming constraint optimization technique called the method of feasible directions was applied (223). The basic idea is to choose a starting point satisfying the constraint and then move to a better point according to the iterative scheme: $X_{i+1} = X_i + \quad S_i$ where S_i is the direction of movement and is the step length.

The usable feasible direction is taken as $S_i = -\nabla f(X_i)$. The only constraint used is that the combustion temperature should not exceed 600 °C. If the temperature reaches 600 °C, then movement into the constrained region was prevented by not

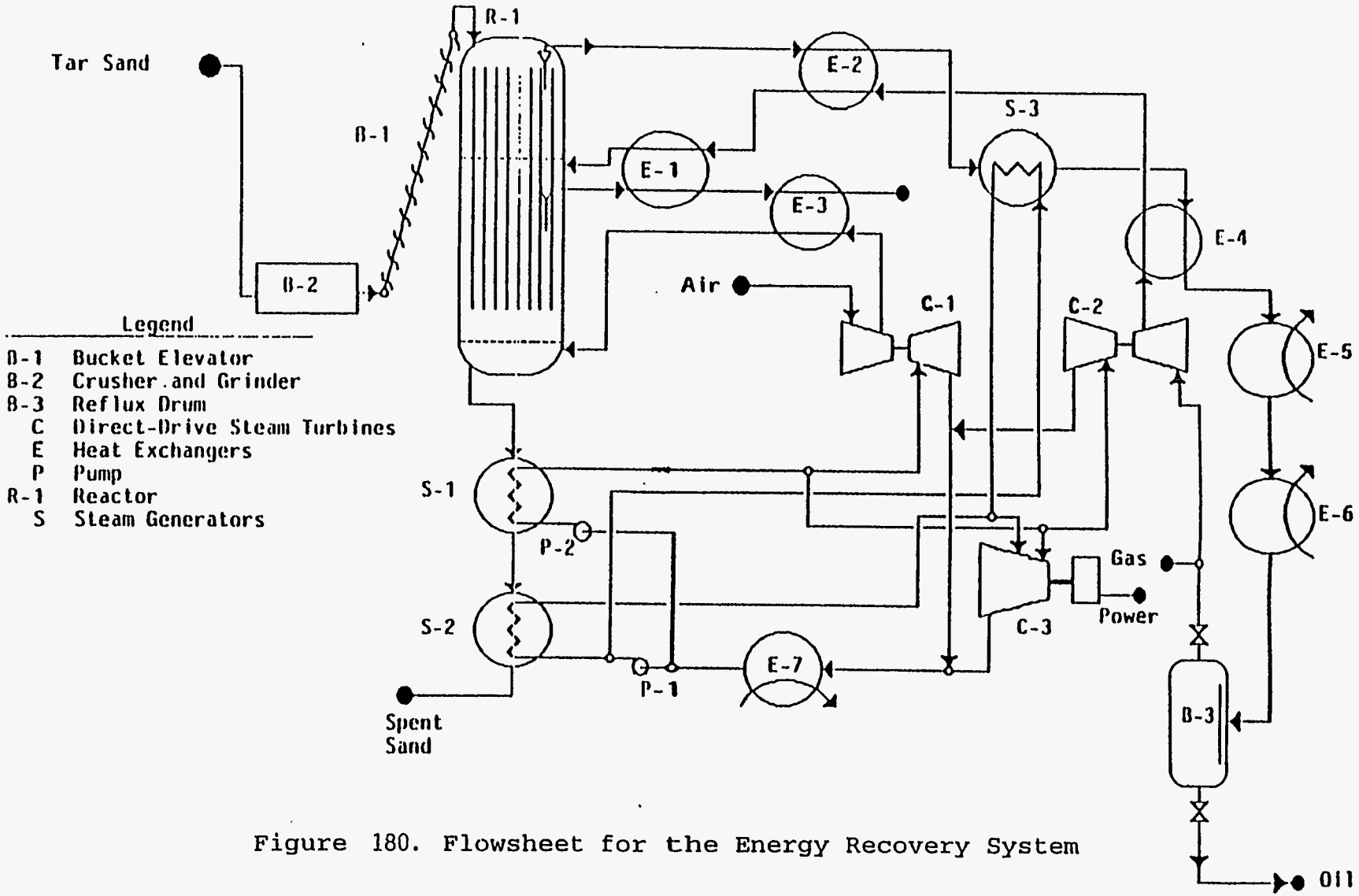

Figure 180. Flowsheet for the Energy Recovery System

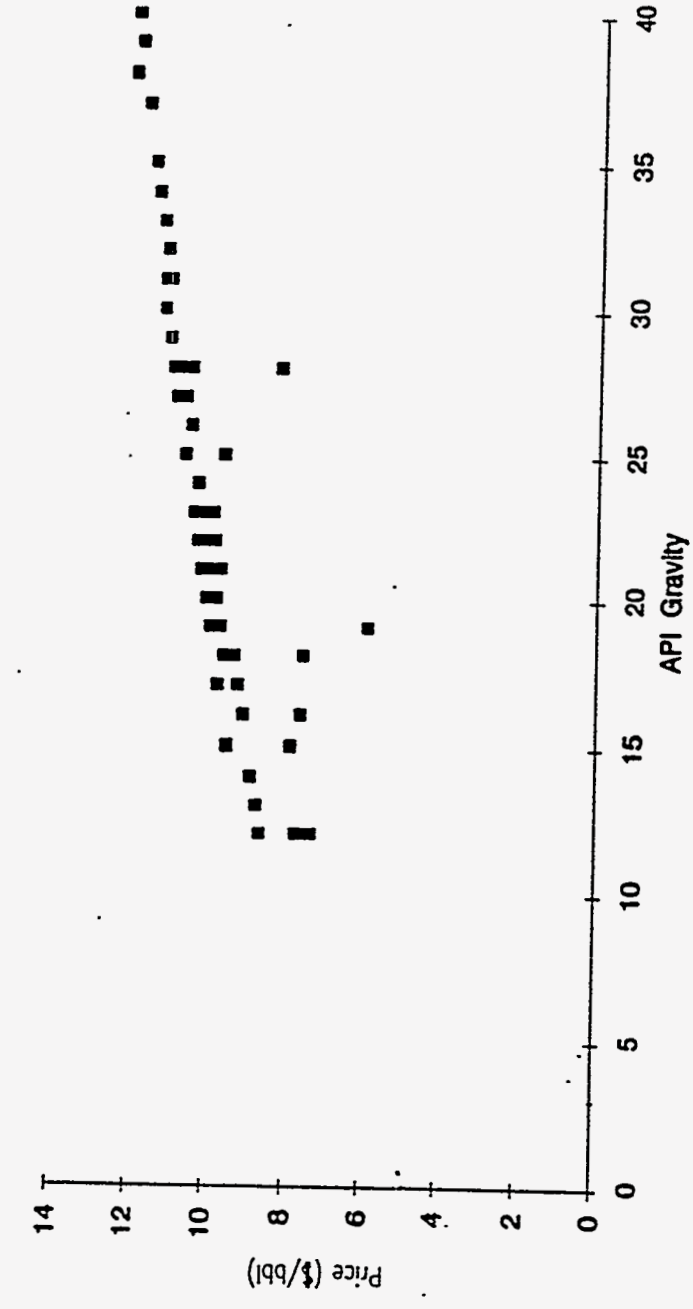

Figure 181. Plot of Price ($/bbl) vs. API Gravity

taking steps in the combustion temperature. The derivative of the objective function was calculated by numerical differentation.

A trial and error method was used to determine the step length. If the step length was too large, leading to an increase in the objective function or constraint violation, then the step length was halved. This procedure was continued until the objective funtion was reduced. The initial step length was chosen as $=-0.01 * *\frac{|f_1|}{|f'_1|}$.

As f'_1 approached zero, a finite step length was chosen.

If the variations obtained in the objective function and the operating variables were less than a certain small number, the procedure was stopped.

This algorithm was implemented using a Fortran code with a Unix operating system.

Results of Optimization

The optimization code was run both without and with the heat recovery network. The optimal operating parameters found for the two cases are as listed below.

Case 1 Optimization without Heat Recovery:

Cost function
= -0.24*(Light Oil)-0.179*(Middle Oil)-0.144*(Heavy Oil) +7.9E-9*(Pyrolysis heating) -7.9E-9*(Heat transferred by heat pipe) +7.9E-9*(Combustion heating)

Optimal Parameters

Pyrolysis temperature	449°C
Pyrolysis residence time of sand	50 min
Combustion temperature	600°C

Case 2 Optimization with Heat Recovery:

Cost function

= -0.24*(Light Oil)-0.179*(Middle Oil)-0.144*(Heavy Oil)+7.9E-9*(Pyrolysis heating)-7.9E-9*(Heat transferred by heat pipe)+7.9E-9*(Combustion heating)-7.9E-9*(Sensible heating of the fluidizing N_2 gas)-7.9E-9*(Sensible heating of the fluidizing air)-7.9E-9*(Energy generated in the turbine)

Optimal Parameters

Pyrolysis temperature	548°C
Pyrolysis residence time of sand	20.2 min
Combustion temperature	600°C

These results were obtained using different starting points. More experiments need to be carried out to see if there are multiple minimums. An upper bound of 3000 sec was used for the residence time so that the bed height obtained is within reasonable limits. An upper bound of 600°C was used for the combustion temperature to ensure the safety of the material of construction. As seen from the results for Case 1, the optimum was obtained at these constraints. According to Coronella (118), the maximum liquid yield was obtained at a temperature of 460°C and residence time of 20 minutes. Since the cost function in this study involves the yields of light, middle and heavy oil and the electrical heating of the two reactors, the optimum was expected to be different from the case that considers only the total yield of the liquid. This is indeed observed in the results. For the case with heat recovery, the cost to operate the reactor at higher temperatures is smaller as compared to the cost when the heat is not recovered. Hence the optimum shifts to a higher pyrolysis temperature and lower residence time.

Optimal Control of the Fluidized Bed System

The objective function defined in the optimization problem is constantly changing. The demand and hence the value of the light, middle, and heavy oil could change from day to day or the feed may vary in quality leading to different amounts of products formed. Hence it might be necessary to take the process from one set of operating conditions to the new set of optimum operating conditions, which are found by solving an optimization problem of a form similar to the above one. Hence an optimal control strategy was designed to achieve this.

Optimal Control Problem Description

A number of laboratory experiments were conducted on the fluidized-bed reactor system at different pyrolysis temperatures and sand residence times with the aim of finding the optimal operating conditions. Simulated distillation was carried out on the liquid products to find the relative amounts of the oil fractions formed for a given set of operating conditions. Equations were fitted to the data points obtained from the simulated distillation runs. Plots of these yields and the total liquid yield as a function of the pyrolysis temperature and sand residence time are shown in Figures 182-185. Since these yields differed substantially from the yields predicted by the model, they were chosen in preference to the model.

The mathematical model developed is a steady-state model and hence cannot predict the dynamic behavior of the process. While the experiments were conducted, all the operating parameters, including the pyrolysis and combustion temperatures, the pyrolysis and combustion residence times, and the heat inputs to the two reactors were monitered by a data acquisition system using a Quickbasic program. The process was disturbed when the feed was introduced into the pyrolysis reactor, and the dynamic data, obtained during the minutes following the introduction of the feed were fitted to a couple of unsteady-state equations representing the process.

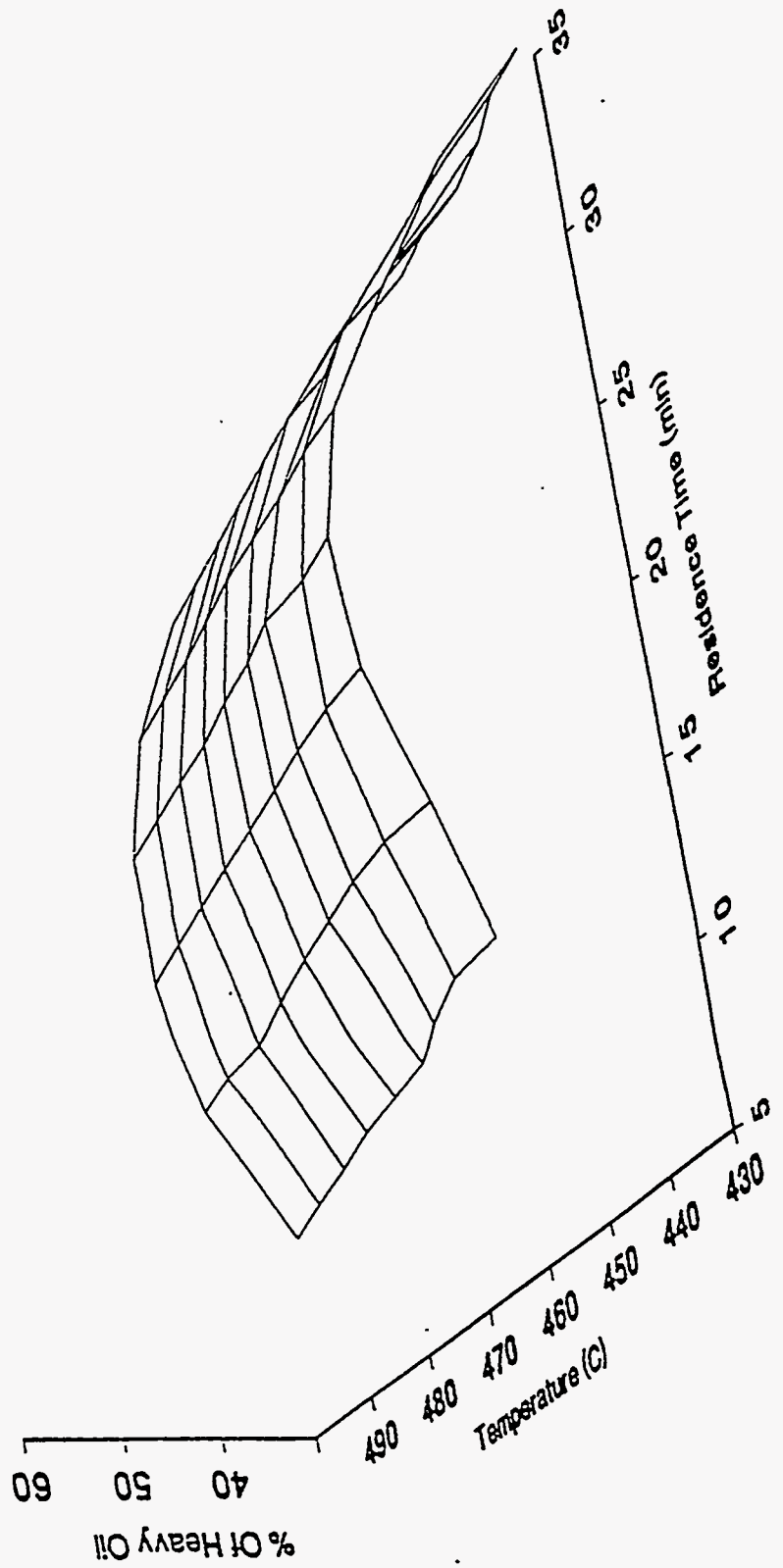

Figure 182. Percent of Heavy Oil in Liquid Product

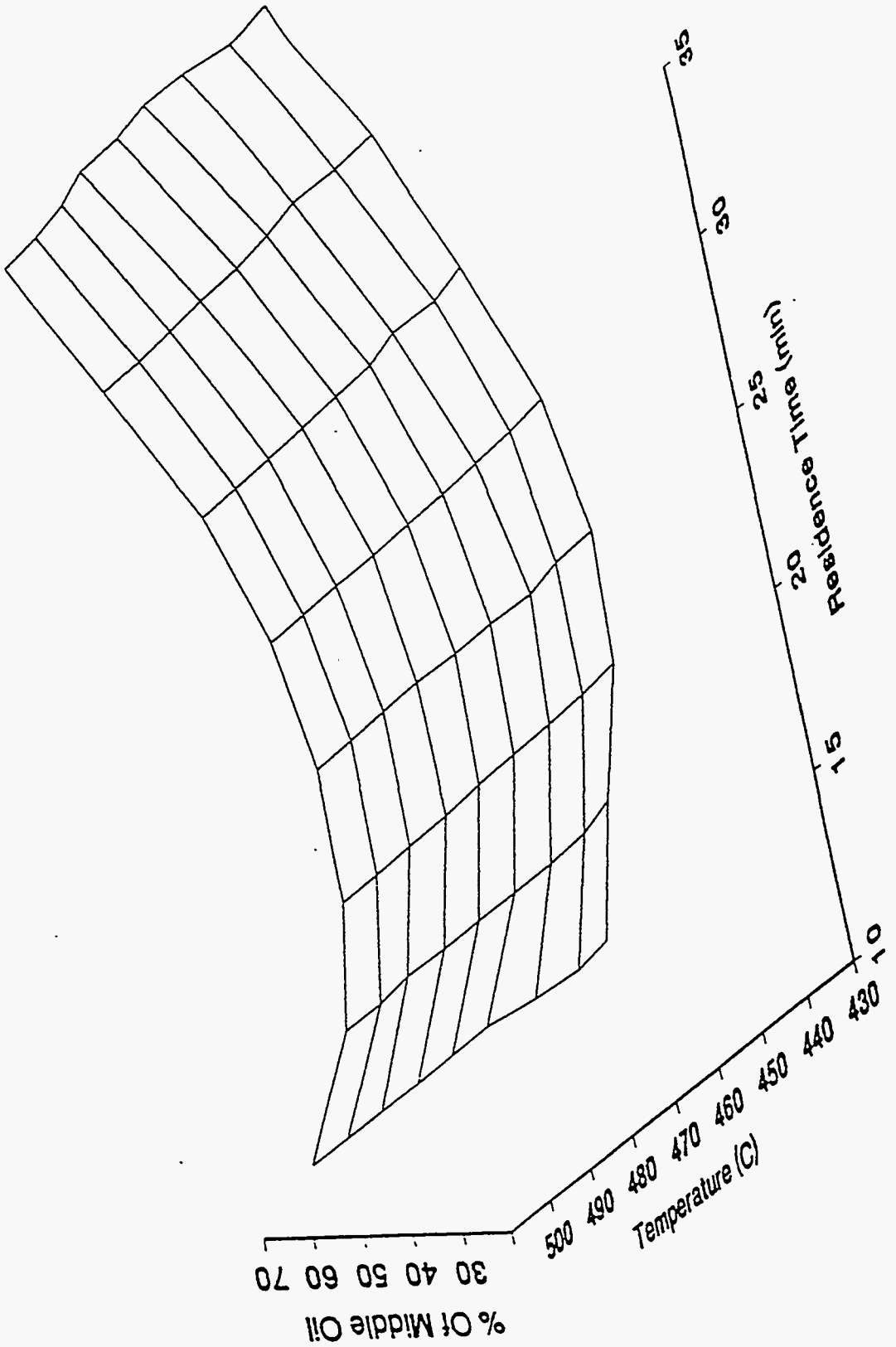

Figure 183. Percent of Middle Oil in Liquid Product

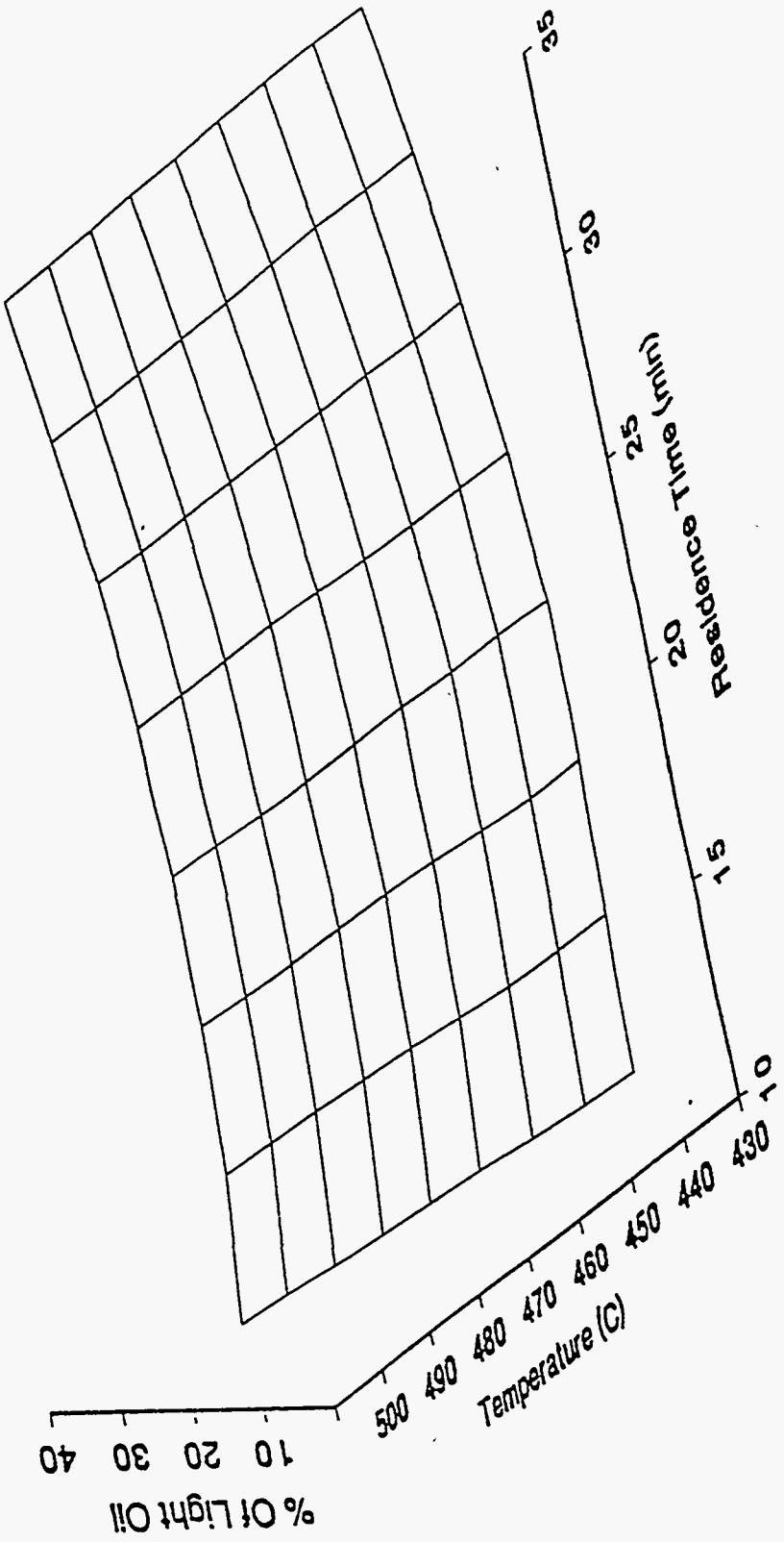

Figure 184. Percent of Light Oil in Product Liquid

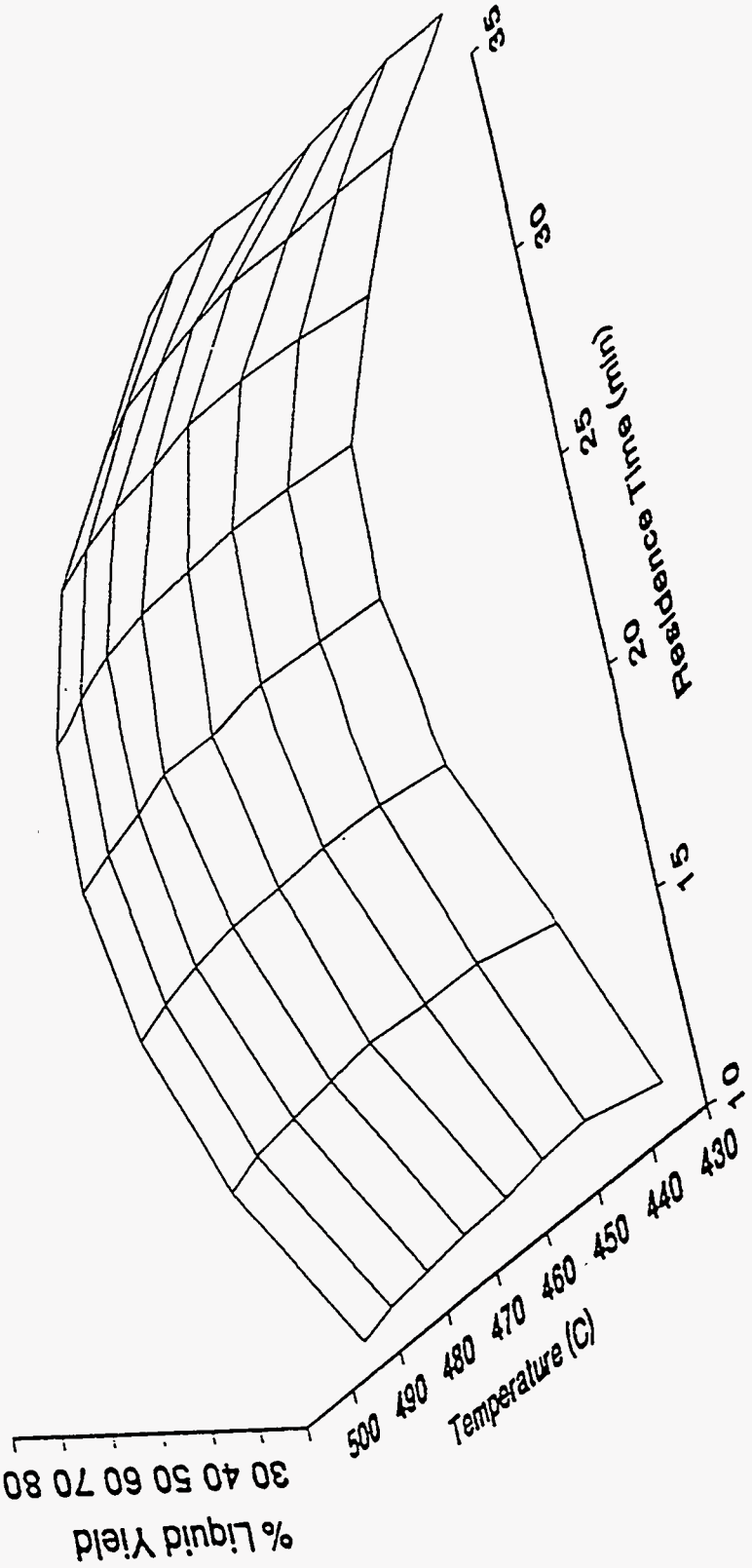

Figure 185. Percent Liquid Yield

Equations 103 to 109 represent simple energy balances written for the coupled fluidized-bed reactor system. Equations 105 to 107 represent the sensible heat requirement of the pyrolysis and combustion reactor walls, and the heat pipe walls. Since this is a small number the left-hand-sides of equations 105 to 107 were taken as zero. These equations simplify to the set of equations 108 and 109. The constants a_1, a_2, a_3, a_4, b_{11}, b_{12}, b_{13}, b_{21}, b_{22}, b_{23} were determined by fitting the experimental data by linear regression. However, since the values of the constants obtained from regression were significantly different from the values of the constants found in the literature, the literature values were used. These values were obtained by referring to Coronella (118).

$$M_{s,p}\, C_s \frac{dT_{s,p}}{dt} + C_s T_{s,p} \frac{dM_{s,p}}{dt} = h_p\, A_p\, (T_{r,p} - T_{s,p}) + h_{h,p}\, A_{h,p}\, (T_h - T_{s,p}) - W\, C_s\, (T_{s,p} - T_{s,o}) - F_{a,p}\, C_a\, (T_{a,p} - T_{a,o}) \tag{103}$$

$$M_{s,c}\, C_s \frac{dT_{s,c}}{dt} + C_s T_{s,c} \frac{dM_{c,p}}{dt} = h_c\, A_c\, (T_{r,c} - T_{s,c}) - h_{h,c}\, A_{h,c}\, (T_{s,c} - T_h) - W\, C_s\, (T_{s,c} - T_{s,p}) - F_{a,c}\, C_a\, (T_{a,c} - T_{a,o}) \tag{104}$$

$$M_{r,p}\, C_r \frac{dT_{r,p}}{dt} = Q_p - h_p\, A_p\, (T_{r,p} - T_{s,p}) \tag{105}$$

$$M_{r,c}\, C_r \frac{dT_{r,c}}{dt} = Q_c - h_c\, A_c\, (T_{r,c} - T_{s,c}) \tag{106}$$

$$M_h\, C_h \frac{dT_h}{dt} = h_{h,c}\, A_{h,c}\, (T_{s,c} - T_h) - h_{h,p}\, A_{h,p}\, (T_h - T_{s,p}) \tag{107}$$

Simplified state equations

$$a_1 \frac{dT_{s,p}}{dt} + a_3 \frac{dM_{s,p}}{dt} = b_{11}\, T_{s,p} + b_{12}\, T_{s,c} + Q_p' + b_{13} W T_{s.p} + \text{Heat Loss} \quad (108)$$

$$a_2 \frac{dT_{s,c}}{dt} + a_4 \frac{dM_{s,c}}{dt} = b_{21}\, T_{s,p} + b_{22}\, T_{s,c} + Q_c' + b_{23} W (T_{s,c} - T_{s,p}) + \text{Heat Loss} \quad (109)$$

where:

T - Temperature

Q - Rate of electrical heating

M - Mass of sand in the bed

h - heat transfer coefficient

A - Area for heat transfer

C - Specific heat

F - Fluidizing gas flowrate

W - Tar-sand feedrate

Subscripts:

c - Combustion bed

p - Pyrolysis bed

r - reactor walls

s - sand

hp- heat pipe

The objective function was the amounts of the light, middle and heavy oil produced, with the appropriate cost coefficients as determined in the optimization problem. The objective function also included the cost of electrical heating inputs to

$$J = \int_{t_o}^{tf} h(x,u,t)dt \qquad (110)$$

The initial conditions were known and the final time was fixed.

The Hamiltonian is given by:

$$H(x(t),u(t),p(t),t) = h(x(t),u(t),p(t)) + p^T(t)f + p_{n+1}[g(x,t)]^2|(-g) \qquad (111)$$

where vector 'p' is the vector of the Lagrange multipliers. The conditions for optimality are obtained as:

$$d(x_i)/dt = f_i(x,u,t) \qquad (112)$$

$$d(p_i)/dt = -\frac{\P H}{\P x_i}(x,u,p,t) \qquad (113)$$

$$H(x^*,u^*,p^*,t)£H(x^*,u,p^*,t) \qquad (114)$$

where '*' denotes the optimal solution.

In this problem the final state is unspecified, but the final time is fixed; hence the boundary conditions are:

$$x^*(t_o)=x_o \qquad (115)$$

$$p^*(t_f)=0 \qquad (116)$$

$$H(x^*(t_f),u^*(t_f),p^*(t_f),t) = 0 \qquad (117)$$

Solution of these equations gave the optimal trajectory that will take the process from one stable condition to another stable condition.

Optimal Control Algorithm

The steepest descent algorithm (223) was used to obtain the optimal solution. The steps in the algorithm are as follows:

(1) A discrete approximation to the control trajectory is initially stored. The iteration index is 0.

(2) The state equations are integrated from the initial conditions and the state trajectory is stored.

(3) Using the value of $p_i(t_f)$ and the stored state trajectory, the costate equations are integrated from t_f to t_o. $\frac{\P H}{\P u}$ is evaluated and stored.

(4) If $\left|\left|\frac{\P H}{\P u}\right|\right| \leq$ and (118)

$$\left|\left|\frac{\P H}{\P u}\right|\right|^2 \cong \int \left[\frac{\P H}{\P u}\right] \left[\frac{\P H}{\P u}\right] dt \tag{119}$$

the procedure is terminated. If the stopping criteria is not satisfied, a new control trajectory is generated by

$$u^{(i+1)}(t_k) = u^{(i)}(t_k) - \frac{\P H}{\P u}(t_k). \tag{120}$$

The step length , is chosen to decrease the objective function by a certain percent q. It is known that

$$J_a = - \left|\left|\frac{\P H}{\P u}\right|\right|^2 \leq 0 \tag{121}$$

and hence to decrease J_a by q percent, is chosen as

$$= \frac{.01*q*|J_a|}{||\frac{\P H}{\P u}||^2} \qquad (122)$$

As J_a approaches a minimum, the denominator approaches 0; and hence the value of q needs to be changed in order to prevent the step length from shooting to a large value. This algorithm was implemented using a Fortran code with a Unix operating system.

Optimal Control Results

An optimal solution was obtained starting from initial conditions of a pyrolysis temperature of 460 °C and sand residence time of 16 minutes. Figures 186 and 187 show the trajectories obtained for the temperature and residence time. Figure 186 shows a linear rise in the pyrolysis temperature. The residence time is abruptly changed from 16 minutes to 31 minutes at the end of the first minute. This can be easily accomplished in a laboratory experiment by either changing the feedrate or changing the bed holdup. The feed rate can be abruptly changed. As seen from the Figures 186 and 187, the residence time is gradually decreased with the rise in temperature, so as to optimize the production for every time interval.

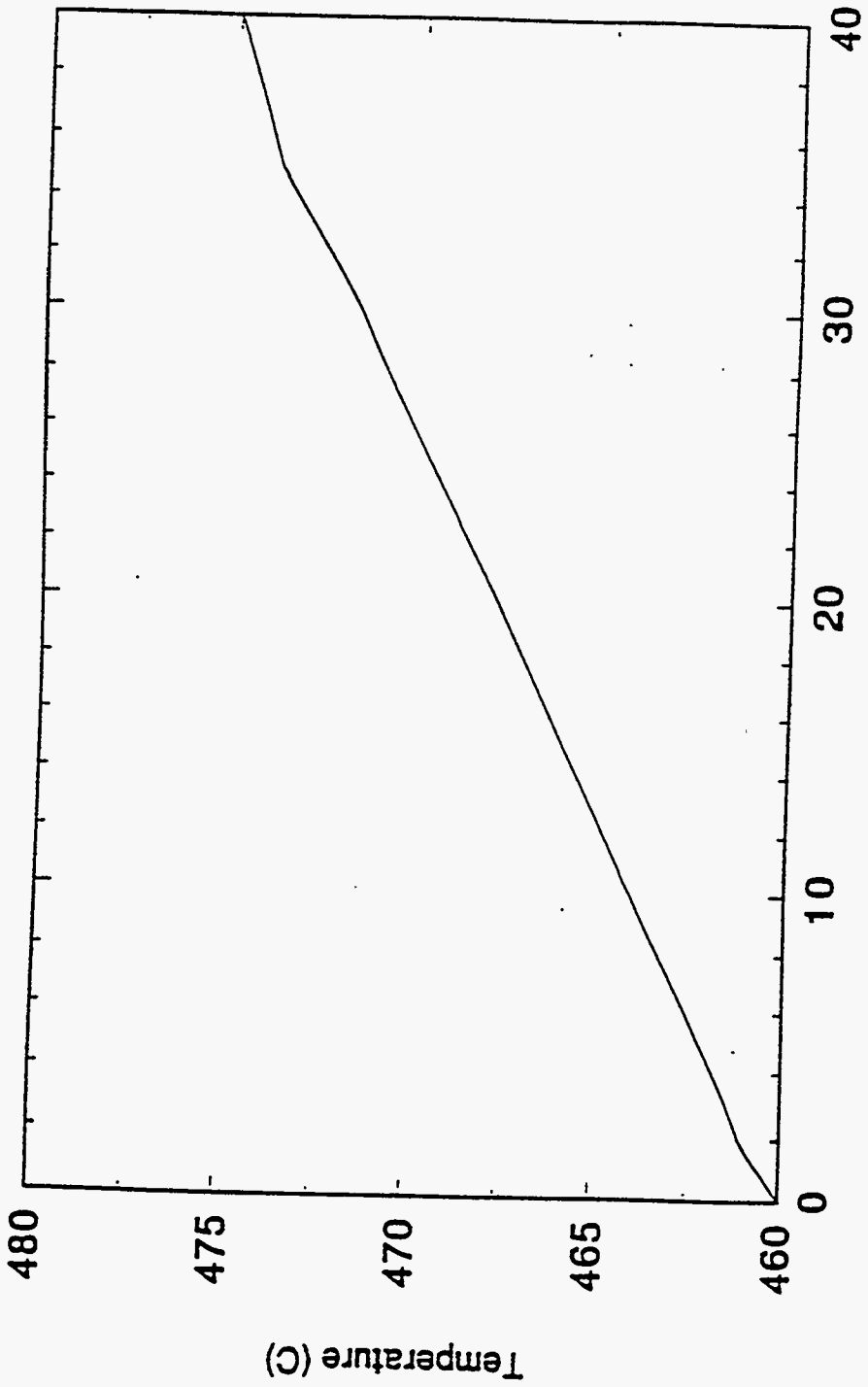

Figure 186. Trajectory of the Pyrolysis Temperature

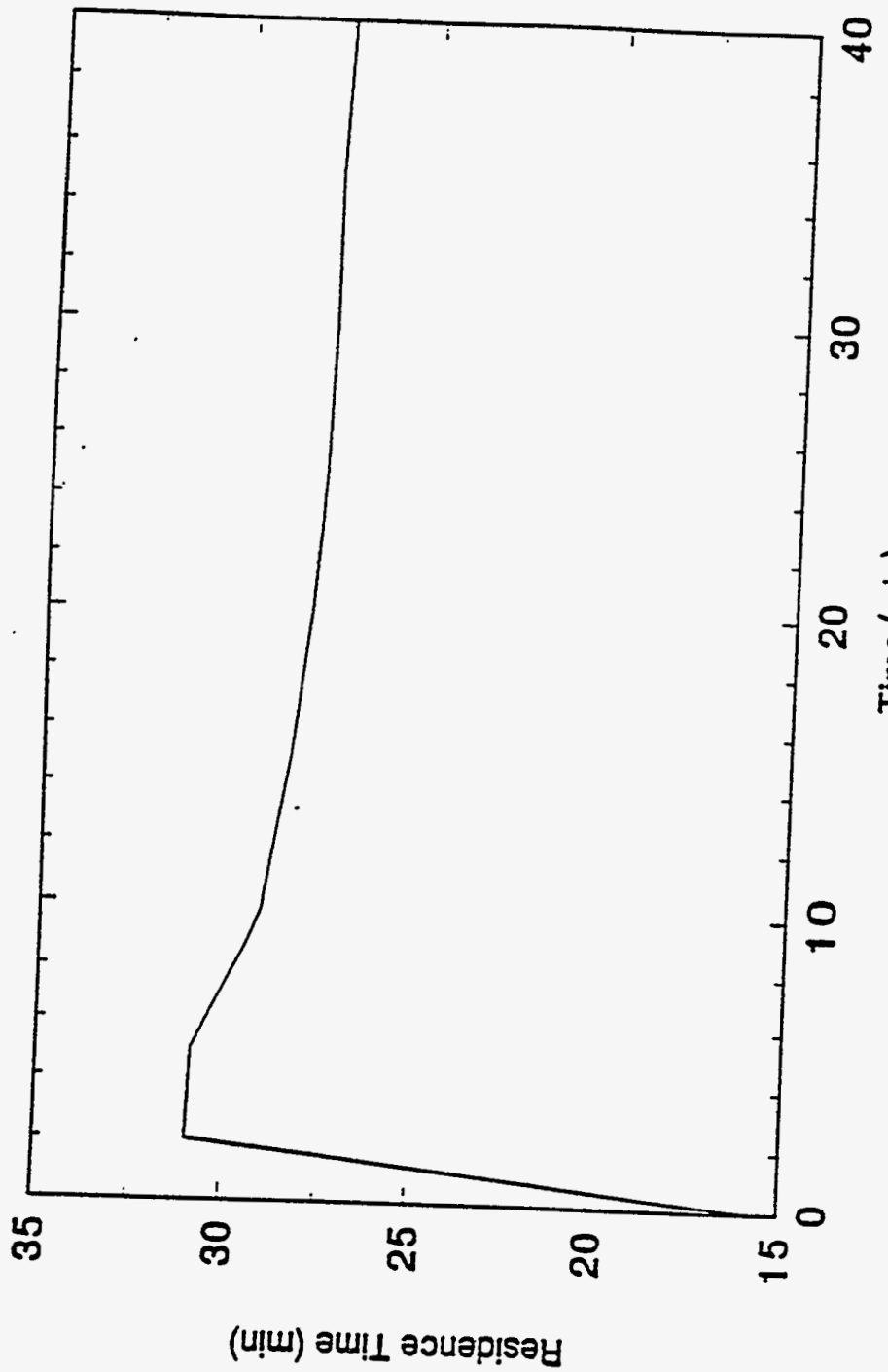

Figure 187. Trajectory of the Residence Time

SUMMARY AND CONCLUSIONS

The development of a comprehensive model for the coupled fluidized-bed process was completed during the work reported here. It incorporates models for fluidization hydrodynamics, pyrolysis and combustion kinetics, mass transfer, heat transfer, material and energy balances, and the heat pipes that couple the two fluidized beds.

The temperature of the pyrolysis reactor is found to be the most important parameter affecting the yields of bitumen and an optimum value of about 475°C is indicated. The energy requirement of the process is affected by operating temperatures, residence times of solids in the reactors, and flow rates and incoming temperatures of the fluidizing gases. Based on the results for the laboratory unit, a combustion temperature of 600°C and a combustion air flow rate of 35 scfh seem to be optimum.

The simulation results compare well with experimental results for Whiterocks tar sand. The model is also able to account for differences in the nature of bitumen from different deposits. However, an exact correlation of model parameters with bitumen properties is not possible at this time because of limited knowledge about the chemistry of the pyrolysis process. Extensive studies need to be conducted on the structure of compounds present in the bitumen so that the pyrolysis product distribution can be predicted with certainty.

The completed model, which is a steady-state model, can be used for the development of a dynamic simulation of the process that could be used to demonstrate the effect of perturbing the system through the input parameters.

In this work a number of laboratory experiments were carried out in order to verify the mathematical model developed for the process and determine the optimal

operating conditions. A product quality analysis was done to see the effect of the operating conditions on the product quality. The mathematical model was optimized to find the optimal operating parameters. An optimal control strategy was developed to minimize a selected cost function, while taking the process from one steady-state to another.

The yields obtained experimentally were very similar to those predicted by the model. The high C_5-C_6 gas yields observed at low residence times were not determined by the model. A deeper understanding of the chemistry of the bitumen and of the reaction mechanisms is required to fully understand the reason behind these high yields.

The remaining observations were in accordance with the observations of previous experimenters. A maximum liquid yield was observed at 478°C and a residence time of 27 minutes. The specific gravities of the products were in the range from 0.9 to 0.93, and the viscosities were in the range from 50 Cp to 500 Cp. The Conradson Carbon Residue values varied between 0.25% to 2.0% and the pour points were from 10°C to -15°C. The residue obtained from simulated distillation results was always less than 10%. Thus the product liquids of pyrolysis were of good quality.

An optimization code was developed to find the optimal operating pyrolysis temperature, residence time, and combustion temperature in order to minimize a selected cost function, which included the costs of light, middle and heavy oils and the costs of electric heating to the two reactors. More runs need to be made with the code, using different starting points to find if there are multiple minima. This is a time-consuming process since the code takes about one hour to converge from one starting point.

The optimal control strategy gave the optimal trajectories for the pyrolysis temperature and residence time, while minimizing a cost function that included the

yields of the light oil, middle oil and heavy oil and the electric heating to the two reactors. This strategy needs to be implemented to prove its usefulness.

In situ Technologies: Steam Assisted Gravity Drainage (SAGD)

Principal Investigator: M. D. Deo
Graduate Student: A. Hobbs

Introduction

Horizontal Wells

Geologist and petroleum engineers have long known that vertical wells are not the best means of extracting fluids from the ground. The geology of the earth is essentially that of layers stacked upon layers, much like that of an onion. In the production of an oil field, the engineer is interested in the relatively narrow band of layers that contain the oil and the layers immediately above and below. Engineers refer to this area as the pay zone. A main goal of the reservoir engineer is to maximize well bore/pay zone interface area. Vertical wells, which may be tens of thousands of feet deep, are in contact with the pay zone for only a small fraction of the well's length. This limited contact area greatly reduces the well's production capabilities, resulting in the need to drill more wells to effectively produce the field. Undoubtedly, the best method of improving the contact area between the well bore and the formation would be to drill a well that parallels the formation, in essence, an horizontal well. The idea of the horizontal well has been around for more than 50 years. Attempts at drilling horizontal wells were made as early as 1937 by the Russians (224). Table 59 gives a brief overview of how horizontal drilling has progressed in the last 50 years.

Early horizontal wells were invariably drilled from tunnels, but stating in the 1940's attempts were made to drill horizontally from already existing vertical wells. Using pre-existing wells offered several advantages, such as immediate access to the pay zone and a good knowledge of

Table 59 - Overview of the horizontal well drilling projects

Year	Field	Depth (feet)	Reservoir Contact (feet)	Comments
1937	Yarega, USSR	-	300	Mine assisted steam
1952	La Paz, Venezuela	10,000	50-100	Drilled to reduce gas coning
1967	China	3,600	1,600	Produced 5-7 times the oil as the vertical well, but collapsed after 7 days
1981	Rospo Mare, Italy	4,500	1988	Produced 15 times as much oil as the conventional well
1985	Cold Lake, Canada	3,558	3330	Cyclic Steam Stimulation
1986	Prudhoe Bay, Alaska	9,000	-	Three fold increase in production rates over conventional well

the formation dimensions. Still, the technology remained commercially unattractive. What horizontal wells were drilled were prohibitively expensive in comparison to vertical wells and exhibited structural and geomechanical problems. When performing as designed, the horizontal wells often produced 2 or 3 or even up to 15 times more oil than their vertical counterparts. Such improved rates prompted the oil industry to keep trying.

By the mid 1980's, drilling technology had reached a point where horizontal wells were beginning to be viewed as a viable recovery tool. The cost of horizontal wells still is 1.5 to 2.5 times that of a conventional well, but the increased production rate results in few wells having to be drilled so overall capitalization cost can be lower with some horizontal wells. In the past 5 years, great progress has been made in the area of short radius drilling. Previously, a horizontal well was created by slowly angling a vertically initiated well towards the horizontal. This method worked in the sense that it eventually drilled a horizontal well, but the long horizontal distances required by the minimal curvature radius often resulted in unacceptable losses of precious lease footage. Recent advances in drilling techniques have lead to short radius drilling systems. Such systems can dramatically reduce the distance required to change from a vertical system to a horizontal system. Jurgens and Bitto (225), describe one case in which 1,000 feet of horizontal displacement are desired. Using older techniques that operate with a medium radius well curvature would consume a minimum of 300 feet of lease before the well would reach the target zone. Drilling the same well with a short radius profile resulted in a loss of only 40 feet of lease. The shorter radius has the advantages of greatly enhancing the chances of placing the well within the target zone, avoiding the common problem of having to drill a long distance through a tough over layer, and simplifying the completion work.

This is not to suggest that horizontal wells are quickly becoming the industry standard. Vertical wells still constitute the vast majority of drilling projects, but horizontal wells offer an additional means to produce the field. Nor should it be inferred that all the technological problems of horizontal drilling have been solved. Completion work remains a complex job and horizontal wells remain susceptible to collapse and clogging. Additionally, remediation of horizontal wells has proven to be much more difficult than in conventional wells. Remedial stimulations to clean up perforations or near well bore damage are expensive and difficult to perform in horizontal wells. These difficulties result in wells that produce from only parts of the completed horizontal interval.

The primary advantages of horizontal wells are as follows.

1. Horizontal wells provide flexibility in selecting appropriate well configurations for a project. Various combinations of vertical and horizontal wells can be attempted for optimal process implementation.

2. Horizontal wells increase direct contact between wellbore and pay zone. The perforated interval per vertical well is limited to the pay zone thickness.

3. It is possible to drill several horizontal wells from the same location. This advantage becomes particularly important in environmentally sensitive or offshore areas where preparation of drill sites is a major expense.

4. For certain thin formations with bottom water table, horizontal wells defer and reduce water coning by providing a low-pressure area over a long distance than at a single point as with vertical wells.

5. Horizontal wells inject and/or produce fluids orthogonal to vertical wells. This provides potential of improving the sweep efficiency of a flood and therefore, the recovery efficiency.

Some of the disadvantages of horizontal wells are summarized below.

1. For a successful horizontal well project, a good geologic description of the field is necessary. In some instances, horizontal wells have been drilled outside the producing formation because of a lack of good knowledge of geology or formation dip. On the other hand, a highly characterized field may not have enough well spacing for drilling horizontal wells.

2. Horizontal well drilling costs are high. Typical drilling cost for an ultra-short turning radius horizontal well in the U.S. is about $ 25,000 to $ 30,000 per radial. The typical cost for a short-radius well at 5000 ft depth is approximately $ 120,000 to $ 200,000 for a 250 ft long horizontal well, whereas a medium radius well at the same depth costs about $ 600,000 without completion (226).

3. Sand control is a serious problem in all the horizontal well field projects. Sands that come into the well with fluids cause serious permeability reduction around the wellbore. Unlike the vertical wells, these sands cannot be removed by gravity. So, horizontal wells are to be completed with specialized liners with wire wraps or gravel packed to reduce the sand control problems. These completion techniques are complex and expensive.

Steam Assisted Gravity Drainage

Steam Assisted Gravity Drainage (SAGD) is considered by many to be one of the most promising methods for large scale in-situ bitumen production. The theory behind the process and

the development of viable SAGD models has been actively pursued by Butler (227) and others.

A major problem with conventional lateral steam flooding is the tendency for steam to override the oil zone and break through at the production well. This effect can be reduced by completing the producer near to the base of the reservoir and by removing product at a controlled rate in order to allow gravity to keep the steam zone segregated. A considerable improvement can be achieved if the reservoir dips and if the steam is injected so that it flow down dip. The concept of steam assisted gravity drainage is a natural consequence of this process. Butler and coworkers implemented the fundamental gravity drainage theory of Cardwell and Parsons in the development of a semi-analytical computer model for simulating the SAGD process for the production of tar-sand bitumen using horizontal wells (227). In this production process, two horizontal wells are placed one above the other at the base of a tar sand reservoir. The spacing between the wells averages about 20 feet. Around the tubing of the upper well, the steam penetrates the reservoir and condenses, transferring its heat to the reservoir. Any uncondensed steam or hot water is produced to the surface via the annulus.

At the end of the induction period, the viscosity of the bitumen between the upper and lower wells has been reduced sufficiently enough to allow for drainage via the lower horizontal well. At this point, a small steam chamber has developed, which encloses the both of the horizontal well. Due to the small vertical spacing between the two horizontal wells, care must be taken to maintain a negligible pressure between the two wells. If the pressure difference is too great, injected steam would bypass the reservoir and be produced by the lower well. Bypassing is a serious concern with this process.

With no pressure drop between the two wells, but with a steam pressure higher than the reservoir pressure, the steam flows up through the sand within the developing chamber and condenses when it reaches the cooler tar sand at the chamber-reservoir interface. The heat liberated from the condensation of the steam is transferred via conduction into the tar sand, reducing the viscosity of the trapped oil. With it's greatly reduced viscosity, the oil now flows toward the production well under the influence of gravity. As the heated oil is drained, it is replaced by steam, which rises into the steam chamber above and along the length of the horizontal well pair. As the entrained oil is produced the steam chamber continues to grow, with steam replacing the produced oil. Eventually, the chamber will grow large enough to reach the prevailing overburden. Although the vertical growth is now arrested, the chamber can continue to grow through lateral spreading. These phases of growth are referred to as the rising-steam chamber phase and the spreading-steam-chamber phase, respectively.

A major potential for the steam assisted gravity drainage process lies in overcoming the shortcomings of conventional steam flooding that are created by the tendency of the steam to override. With conventional wells the pressure gradients associated with radial flow to the production well make the maximum rate that is achievable without steam coning relatively low. In the steam assisted gravity drainage process, vertical wells are dispensed with in favor of the horizontal wells, and production rates of the order of 0.3 B/d per foot of horizontal well are indicated to be practical without steam coning; with long horizontal wells this provides an economic drainage rate.

Numerical Simulations of Steam Assisted Gravity Drainage

A good deal of research has gone into the development of semi-analytical models to describe the complex flow patterns of in-situ processes. While providing a solid basis from which to work, analytical models are often incapable of completely describing real, physical phenomena. One tool available to engineers to help overcome the limitations of analytical models is the computer simulator. All of the results in this report were obtained via computer simulation, specifically, the commercial reservoir simulator, *STARS*. STARS is an adaptively implicit, finite-difference computer model that can be used to simulate the fluid flow and heat transfer processes for the thermally stimulated production of oil in a reservoir. It has been developed by Computer Modeling Group (CMG) of Calgary, Alberta, Canada (228).

The purpose of numerical research was two-fold: (1) optimization of such operational parameters as injection temperature and pressure, well patterns, and the examination of the effects of pressure drop between the injecting and producing wells and (2) determination of some of the inherent limitations of the simulator, particularly with respect to grid size. Since SAGD involves vertical drainage of oil, it has been speculated in the literature that the resolution on the vertical scale need to be of an order of a meter for stable results. The simulations to test the effect of grid size on simulator predictions were run in order to verify this hypothesis.

Input Data

In order to run thermal simulators, the user must provide input data describing the reservoir, the oil, and the rock-fluid properties. The input must also include a description of the well geometry as well as initial and boundary conditions concerning the injection and production temperatures, target flow rates, and flow rate constraints. Numerical control input parameters

allow for either a fully implicit calculation sequence or internally controlled switching between explicit and implicit calculation sequences.

Grid and Reservoir Description

The STARS simulator allows for either rectangular or cylindrical coordinates. Rectangular coordinates were chosen for all simulation runs. A general grid size of 1,000 feet long by 1,000 feet wide by 100 feet thick was adopted. Initial runs, where the main objective was to determine the effect of grid size on simulation output, consisted of five 200 foot long blocks in both the *I* and *J* directions. In subsequent runs, the *J* parameter was generally set at 50 feet, but occasionally reduced to just 10 feet. The vertical dimension *K* was allowed to vary from 20 to 0.5 feet, resulting in a range of 5 to 200 grid blocks. Overall, the total number of grid blocks varied from 125 to 10,000. STARS allows for the porosity and absolute permeability to be specified for element individually. Porosity values for all runs stayed constant at 0.30%. Some runs were made with varying permeabilities, but eventually, values of 2.0 Darcy in the horizontal direction and 0.50 Darcy in the vertical direction were selected as standards.

Fluid Properties

STARS allows for any number of components and phases. In all of these simulation runs only two components, oil and water, were used. Also the number of phases present in the reservoir was limited to two. Finally, the water and oil phases were treated as homogeneous, so the number of components in water and oil were 1, resulting in 2 total components.

STARS has the capability to internally correlate viscosity data directly from temperature values, but the oil viscosity values used in these simulations were determined as a function of temperature based on the data found in Table 60. The values are calculated for field conditions.

Table 60 - Oil and water viscosities as functions of temperature

Temperature, ^{0}F	Oil Viscosity (cp)	Water viscosity (cp)
50	136053	1.2
100	14859	0.7
150	1023	0.4
200	162	0.3
250	46	0.2
300	19	0.2
350	11	0.2
400	7	0.2
450	5	0.1
500	4	0.1
550	4	0.1

Rock-Fluid Properties

A table relating typical water-oil relative permeabilities water saturation is supplied under the *rockfluid* keyword in the STARS input data file. Also given in this table are typical liquid-gas relative permeabilities.

Initial Conditions

In all simulations, the initial reservoir temperature was set at 74^{0}F. Initial reservoir pressure varied from a low of 80 psi to a high of 500 psi, with most of the simulations initially set at 250 psi or 500 psi. Values of 0.20 and 0.80 were assigned to water and oil saturation, respectively.

Well Configurations

Two types of well configurations were used in this study: a vertical steam injector coupled with a horizontal producer and a horizontal injector/producer pair. In both configurations, the injector was located 20 feet above the producer. Both configurations were utilized in three different types of well patterns. The vertical well system used only one production well, but the number of injectors varied from 1 to 3 wells.

SAGD Simulation Results

In the previous section, the general range of properties for all the simulations was described. Table 61 lists the reservoir properties common to all of the simulations. The data was originally presented by Edmunds et al. (229) at the 1988 UNITAR Conference (major differences among the individual cases include well configuration and well spacing).

Grid Block Size

The first step in the modeling process was determining appropriate grid sizes to use in the

Table 61 - Input data for most simulations

Variable	**Value**
Reservoir dimensions (feet)	
Horizontal (x and y)	1000
Vertical (pay thickness)	100
Grid dimensions (feet)	
Horizontal (x and y)	50
Vertical	variable
Permeabilities (Darcy)	
Horizontal (x and y)	2.0
Vertical	0.5
Porosity	0.3
Initial water saturation	0.2
Well radius (feet)	
Producer	0.5
Injector	0.33
Initial reservoir temperature	74 ^{0}F
Initial reservoir pressure	250 psi
Injection steam temperature	515 ^{0}F
Steam injection rate (water equivalent)	500 barrels/day
Reservoir thermal conductivity	77 Btu/ft D ^{0}F
Reservoir thermal diffusivity	0.4 ft^2/day
Pattern area (acres)	22.96

simulations. Previous studies had used grid-block sizes ranging from 2 inches (229) to 20 feet (230). Closemann and Smith (231) observed that the grid-block thickness had a strong effect on the rate of rise of the horizontal steam chamber. Using a vertical permeability of 0.5 Darcy, the rise rate was observed to level off at a value of 1.02 inches/day, for a vertical grid block thickness of 1.0 feet. Further decreases in block thickness produced no further increase in rise rate. A block thickness of 10 feet produced a rate that was 95% of the value obtained for a thickness of 1 foot.

In order to obtain an optimal block thickness for the STARS program, eight simulations were run with the only variable being the vertical block thickness. Thicknesses ranged from 2 feet to 20 feet. The criteria for comparison was the water-to-oil ratio (WOR) found in the production well. The effects of vertical block size on WOR are listed in Table 62. Also included are the times required for the simulations to run.

Table 62: Effect of grid block size (z) on WOR and CPU time

Vertical Grid Block Size (feet)	WOR	Time (hours)
20	3.199	0.2
10	3.527	0.55
6.6	3.452	0.75
5	3.421	1.05
4	3.455	2.0
2	3.455	12.2

The results parallel the findings of Closemann and Smith, in that the WOR value associated with grid size of 10 feet was within 95% of the WOR value obtained using 2.0 foot blocks. Of obvious importance is the length of time required to run the simulations. The simulation with the larger grid blocks took just over an half hour, while the second simulation required one full day In an effort to optimize numerical efficiency and to stay below the maximum number of grid blocks allowed by STARS (12,500), the 10 foot thick grid block was chosen as an acceptable value for vertical thickness.

After obtaining a suitable grid size for the vertical direction, similar test were run to find acceptable dimensions in the horizontal directions. Final simulation results indicated that the WOR was not as sensitive to horizontal grid block size as it was to vertical differences. One possible explanation is that the modeled process is inherently vertical, with gravity being one of the prime influences. Such a force, by its very nature, would be more susceptible to variations in the vertical direction as opposed to the horizontal direction. Model results showed that grid blocks up to 50 feet in length were acceptable.

One method used to maximize accuracy while minimizing computer time involved using grid blocks of various sizes. Near the well bores, blocks measuring 5 feet high by 20 feet long by 20 feet thick were employed. Further away from the well bores, the blocks measured 10 x 30 x 30 feet, and towards the boundaries grid size was increased to 20 x 50 x 50. The viability of such a configuration is effectively demonstrated in the following chapter, where the reader can see that the peripheral areas of the reservoir are essentially unaffected by the steam injection process.

A typical configuration, using the prescribed thicknesses, might consist of six blocks 5 feet thick, three blocks 10 feet thick, and two blocks 2 feet thick. Such a pattern keeps the number of vertical elements to a manageable size (11) and allows for a more flexible allocation of the

remaining horizontal grid blocks.

Permeabilities

Reservoir permeabilities play a significant role in the development of any oil field. In order to determine the magnitude of the effects of permeability, simulations were run with absolute permeabilities (Darcy) of (0.2, 0.2, 0.1), (0.7, 0.7, 0.2), (1.5, 1.5, 0.5), and (2.0, 2.0, 0.5), with respect to the x, y, and z directions. The first range of values is common for many of the Utah tar sands (232), while the last set of values is typical of Athabasca sands (233). The middle sets represents values which can be found in either Utah or Alberta sands, although the Utah sands tend to have values predominantly at the lower end of the range.

In order to determine how reservoir permeability would effect cumulative oil production and water-to-oil ratios, a number of simulations were run with the only variable being permeability. Figures 188 and 189 summarize the results of these runs. Base case physical parameters, as described above (Table 62), were used as input. Figure 188 shows the marked difference in oil production between the 0.2 Darcy sand and the 0.7 Darcy sand. The 0.5 Darcy increase in permeability resulted in a difference of over 200,000 barrels of oil produced over a seven year period. Increased permeability resulted in increased oil production in all of the simulations, but the size of the increase was not as dramatic as between the first two values. It should be noted that although the scale of the figure does not really show it, the difference in production between 0.7 Darcy sand and 2.0 Darcy sand is a not insignificant 75,000 barrels.

Figure 189 gives a comparison of the effects various permeabilities on WOR. Not unexpectedly, the tightest formation (i.e. the one with the lowest permeabilities) had the highest WOR. As can be seen from the figure, the overall WOR decreases with increasing permeabilities.

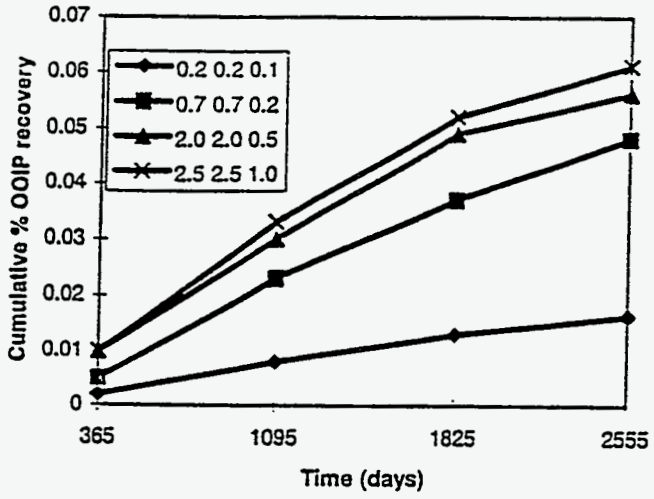

Figure 188 - Effect of reservoir permeability on cumulative oil production

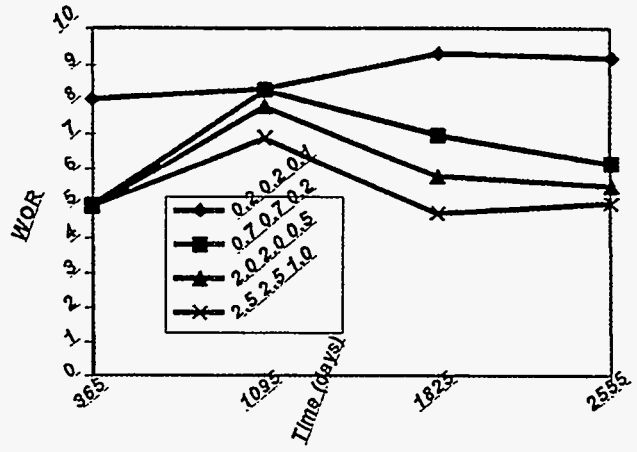

Figure 189 - Effect of reservoir permeability on cumulative oil production

An interesting note is that all four cases showed an increase of water-oil-ratio after three years with respect to first year values. This may result from a combination of depleted oil sands in the region between the well-bores and the still relatively small area of the steam chamber. After reaching a critical size, the oil/steam interface grows large enough to produce oil from the unaffected, oil-rich regions of the reservoir. The increased oil production results in a lower WOR.

Although the figures do not explicitly show it, the period of peak efficiency occurred near the seven year mark. Between years 7 and 8, overall production did not change much and daily volumes experienced severe decreases. A correspondingly large increase in WORs was observed across the board. The optimal length of operation for each of the projects was within the time range of 7 to 7.5 years.

Injection Pressure and Reservoir Pressure

Like permeabilities, another reservoir property which is beyond the control of the engineer is reservoir pressure. Having established the importance of permeabilities on recovery performance, similar steps were taken to asses the effects of reservoir pressure on production performance. The injection pressure in all the cases was set at 775 psi, which resulted from using an injection temperature of 515 ^{0}F. Figures 190 and 191 show that production values and WOR values are essentially independent of reservoir pressure.

This independent relationship appears to hold true as long as the injection pressure is substantially higher than the initial reservoir pressure. ($\Delta P > 50$ psi) One simulation, where the difference between injection and reservoir pressures was on the order of 5 psi, showed negligible production even after 5 years. Where as system with large pressure drops produced oil on the order of 100,000 barrels, the project with the smaller pressure drop produced less than

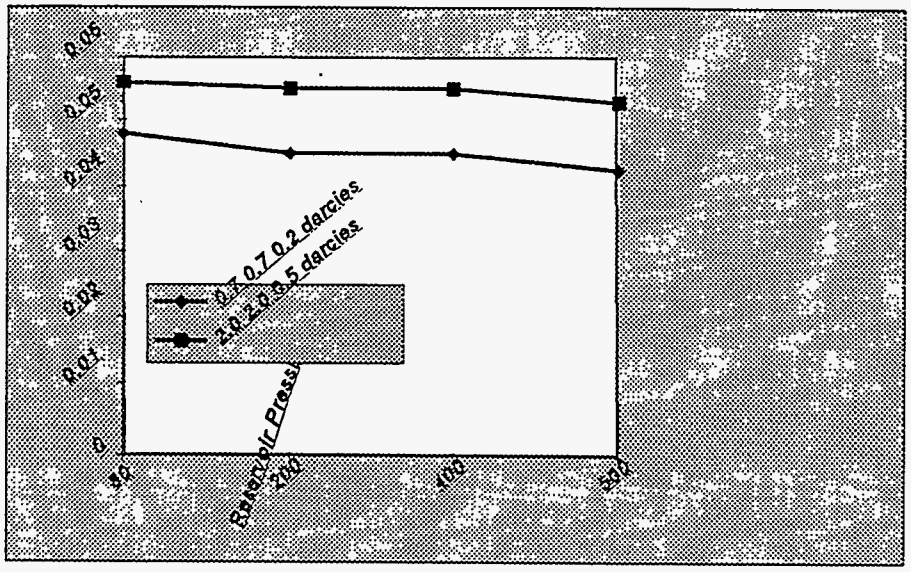

Figure 190 - Effect of reservoir permeability on WOR

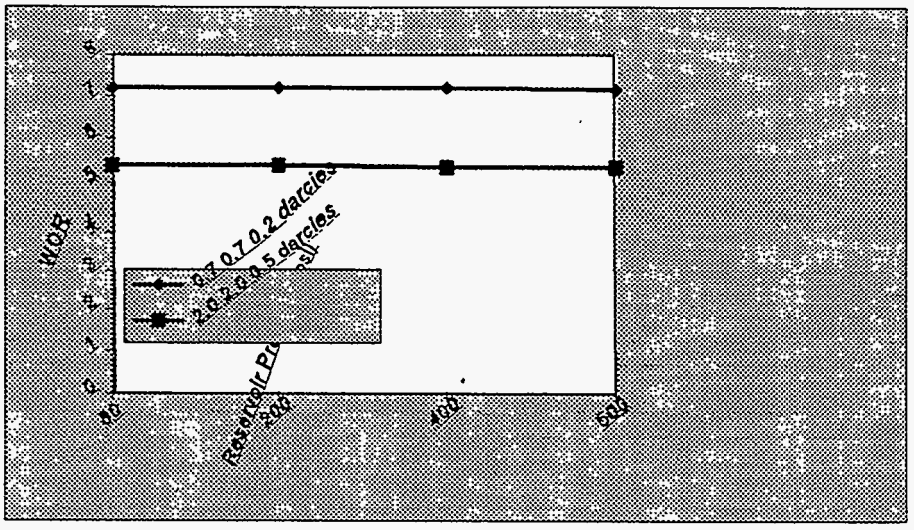

Figure 191 - Effect of reservoir pressure on cumulative oil production

1,000 barrels of oil. Additionally, the best WOR obtained in the latter case was 33.40.

Ideally this problem could be circumvented by always injecting the steam at a substantially higher pressure than the reservoir of interest. Such a solution works well with deeper, higher pressure reservoirs, although care must be taken to avoid fracturing the reservoir, but using high injection pressures in shallow reservoirs can result in the steam breaking through the overburden and short circuiting to the surface. Once break through occurs, the overall effectiveness of the process is greatly reduced, most often to the point of having to abandon the project.

Injection Pressure and Production Pressure

One factor which can be regulated within the reservoir with a high degree of control and which greatly influences recovery results is the pressure drop between the injection wells and the production wells. When there is a substantial difference between the injection and production pressures, steam does not spread through the reservoir. Instead, it drains directly to the production well. This process is referred to as "short circuiting". The main cause for short circuiting in this process was the initially low production pressure. Initially the pressure drop between injector and producer was over 400 psi Subsequent simulation runs with a continuously decreasing pressure differential, resulted in better and better recovery ratios until a leveling off effect was noted in the range of 5 to 20 psi. See Figure 192. It appears that reservoirs with relatively low pressures (80-200 psi) required pressure drops in the area of 5 psi before WORs stabilized, but reservoirs with pressures near 500 psi stabilized with pressure drops near 20 psi.

Discretized Wellbore

Several simulations were run using the STARS *discretized wellbore* option. This option results

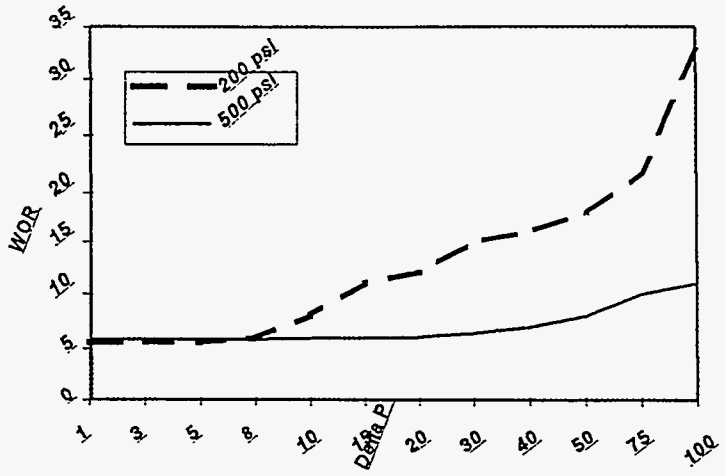

Figure 192 - Effect of injector/producer pressure drop on WOR

in the simulation carrying out a much more detailed and robust analysis of the physical processes occurring inside the wellbores, albeit at the cost of a considerably increased run time (four or more times longer). When a well is not specifically discretized, the simulator does not account for the actual physical presence of the wellbore. Instead, the simulator simply allocates a point "source'' for the injector and a point "sink'' for the producer. With the discretized wellbore option, the physical dimensions and properties associated with the wellbore are incorporated into the calculations. Comparisons made between a single injection/production pair and a discretized injection/production pair indicated no significant differences in oil production or WORs. A similar comparison between wells in a 3 well pair system produced parallel results. Discretization did not noticeably affect production performance.

The comparisons used identical reservoir sizes and identical grid block configurations, with the only difference being the inclusion of the physical presence of the wellbore in the discretized option. In both the single well pair and three well pair simulations, oil production and WORs were comparable for the two different models.

Well Pattern Effects

Initial spacing between injectors, both vertical and horizontal, was 300 feet. Subsequent simulations indicated a strong correlation between well spacing and overall oil recovery. Decreases in well spacing resulted in improved production performance. Performance reached peak efficiency with a spacing on the order of 100 feet. Further reductions in the well spacing yielded lower oil recoveries and higher WOR's. This behavior is attributed to the interaction of individual steam chambers associated with the various injectors. At a spacing of 100 feet, interaction between the steam chambers is not observed until near the 3-year mark. With smaller spacing distances,

interaction occurs sooner resulting in decreases in both reservoir sweep and production performance.

Figure 193 compares the overall performance of the two single injector/single producer systems. A comparison of WORs shows the horizontal system having a slightly better water to oil ratio than the vertical system, 5.85 to 6.55, respectively. Although the vertical injector configuration slightly outperformed the horizontal configuration, neither system was particularly effective in terms of cumulative % OOIP recovery. Seven years of production yielded only 7% of OOIP recovery for the vertical pair and just 6% for the horizontal pair.

This is not unexpected, as the reservoir is fairly large and the sweep of a one injector system is rather limited. The visualizations in next section show how much of the reservoir is completely unaffected by the injection wells. Even the three well systems leave much of the volume near the reservoir boundaries unaffected. This is the main reason why the overall recovery percentages seem so low. If the reservoir dimensions had been smaller than the arbitrarily selected volume (1000 x 1000 x 100), the recovery percentages would have been higher.

Adding a second vertical injector and an additional horizontal pair significantly increased the cumulative recovery percentages. Reducing the well spacing further improved the wells' performance.. Figure 194 describes the performance of the two-injector systems. The two horizontal pairs with 100 feet spacing system shows a three fold increase in recovery with respect to the single horizontal pair system. Accompanying the production increase was a decrease in WOR. In fact, all four 2-injector patterns had lower WORs than their 1-injector counterparts.

Figure 195 shows the recovery performances for the 3-injector systems. Again, the 100 foot spacing systems outperformed the more widely spaced configurations, although the magnitude of improvement in the vertical configurations was only 2%. Even so, in terms of actual barrels

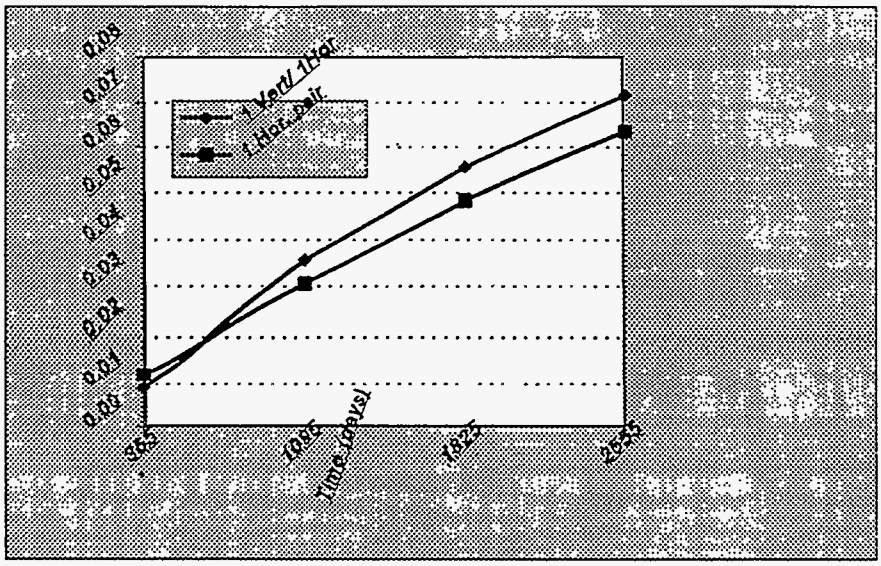

Figure 193 - Comparison of a horizontal well pair with single vertical injector/horizontal producer

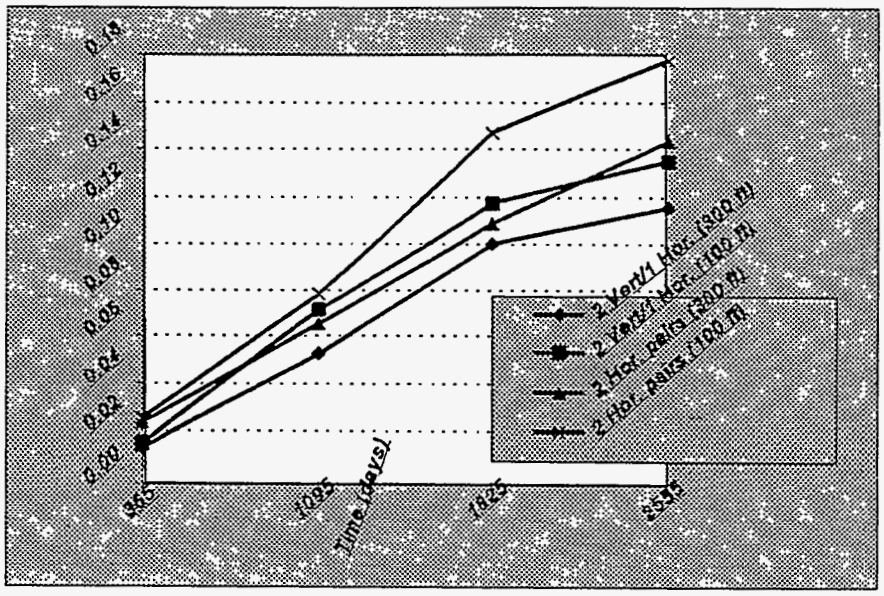

Figure 194 - Comparison of two-well patterns

produced, the closer spaced vertical pattern produced 50,000 more barrels of oil, with a corresponding lower WOR, than the vertical system with 300 foot spacing.

Further review of Figure 194 and Figure 195 demonstrates the strong trend towards increased well performance as well spacing decreases. At an initial spacing of 250 feet the 3 pair system shows no sign of interaction between the well pairs. Essentially they operate as three independent wells. Once the well spacing is reduced to 150 feet and from there to 100 feet a significant amount of constructive interaction takes place. Not only does percent OOIP recovery increase, but overall WOR decreases. In the case with 100 foot spacing, the operating WOR centered around 4.8 with production of over 740,000 barrels of oil. In earlier work, Sarkar (230) demonstrated the potential of a vertical injection/horizontal production configuration. Figure 195 supports his findings.

Visualizations of Simulation Results

The following pages contain visual representations of oil saturation and temperature profiles derived from *STARS* output files. In order to produce the visualizations several *sed* and *awk* scripts were applied to the original *STARS* output file. *Sed* and *awk* are editing tools which operate under the *Unix* operating system. Appropriately fashioned scripts can accurately cull the significant numerical data from a 5,000 line long alpha-numeric output file in a few seconds. During the paring process, the bulk of the output file was stripped away, leaving a core of oil saturation and temperature data in tabular form.

The revised output file was then processed through a third program and converted into a format compatible with *Spyglass* visualization software. During the conversion process, the files were reduced from tabular form into vertical stacks of 2-dimensional arrays. In order to maintain a

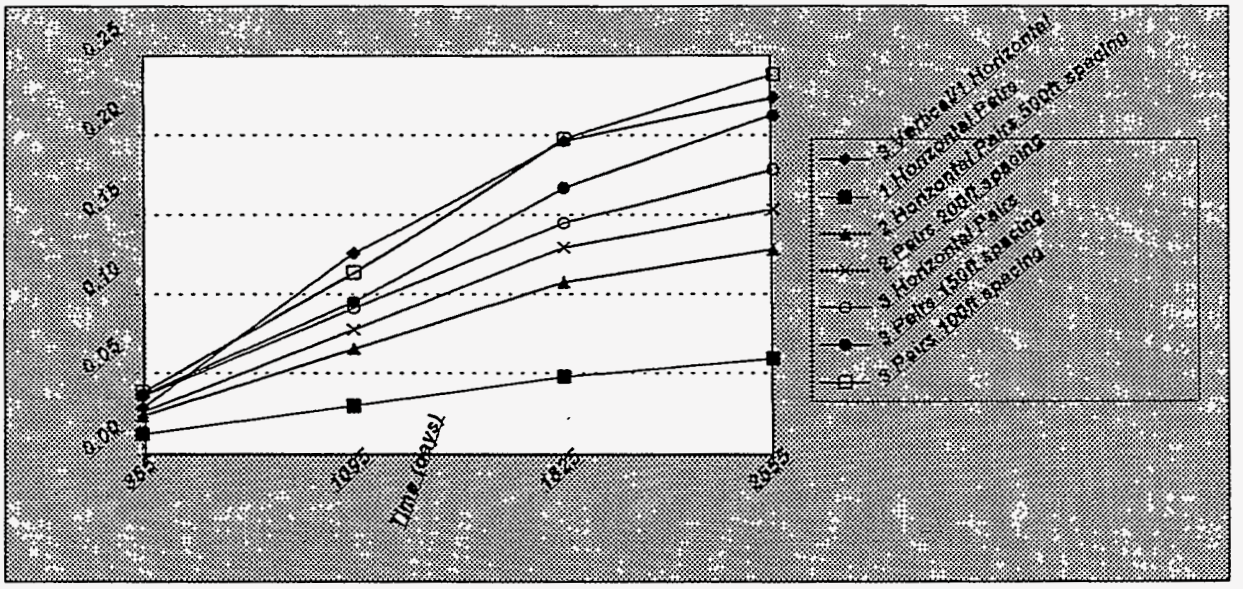

Figure 195 - Comparison of the performance of various well configurations

certain degree of consistency in the visualizations, the depths of the vertical stacks were held at a constant value of 10, although the dimensions in the x and y directions were allowed to vary depending upon how the grid systems in the original *STARS* files were defined.

Even with the help of the sed and awk scripts and the conversion program, the actual process of inputting the data into *Spyglass* proved to be quite time intensive. *Spyglass* did not allow for the inputting of 3-dimensional blocks, so each visualization required all ten vertical arrays to be processed one at a time. Once the data was input, *Spyglass* reconstructed the data into 3 dimensions.

Although time intensive, the results obtained by producing visualizations cannot be over emphasized. Trying to decipher a typical STARS output file, which is usually on the order of thousands of lines, is not a trivial matter. The following pictures present a clear, concise view of the direction of oil and temperature flow. Such views give immediate insight into the differences associated with various well configurations, operating conditions, and reservoir characteristics. Furthermore, the visualizations allow an analyst to quickly spot trends in economically important areas such as vertical and lateral spread.

Absolute Permeabilities and Permeability Ratios

Figures 196 and 197 show two related comparisons of oil saturation profiles for a horizontal injector-horizontal producer pair. Both figures were developed from data taken at the end of the fifth year of production. In both instances, the reader is looking down the axis of the production well, i.e. the producer and injector are perpendicular to the plane of the page. Note the volume of the reservoir that remains unaffected by the injection process even after five years.

The first group of three profiles indicates the differences in the flow of oil associated with actual permeability differences. All three cases exhibit increased oil saturation along the steam

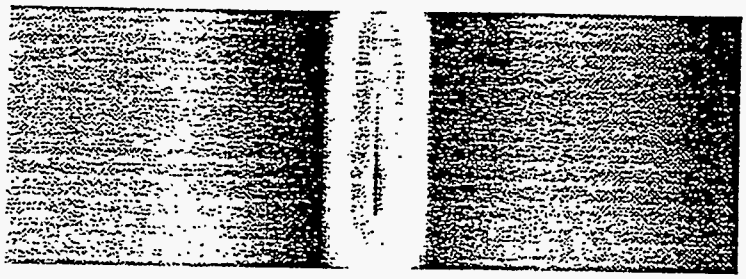

A. Permeabilities 0.2, 0.2, 0.1 in x, y, and z

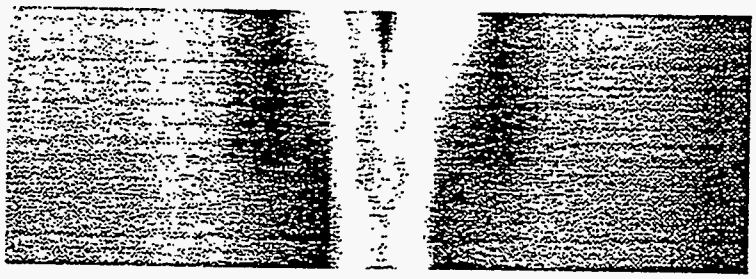

B. Permeabilites 2.0, 2.0, 0.5 in x, y, and z

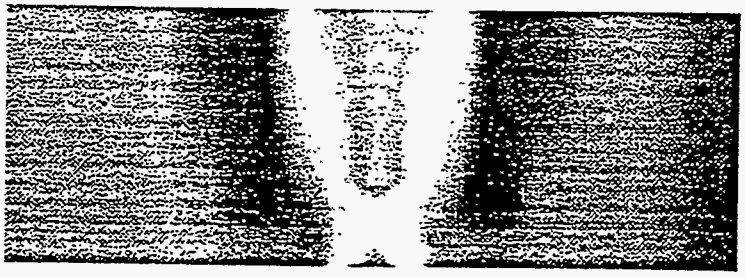

C. Permeabilities 10, 10, 1.0 in x, y, and z

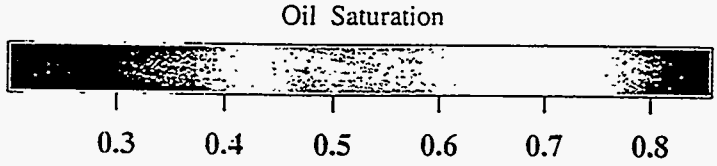

Figure 196 - **Oil saturations for reservoirs with different permeabilities: Single horizontal injector and a single horizontal producer**

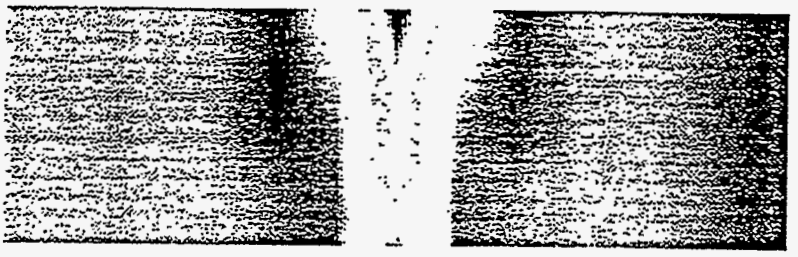

Kx/Kz permeability ratio 1.0.

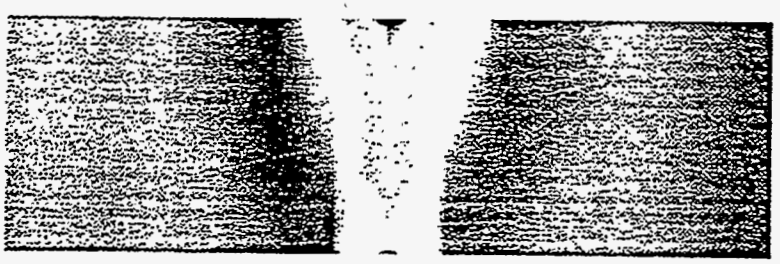

Kx/Kz permeability ratio 0.25.

Kx/Kz permeability ratio 0.10.

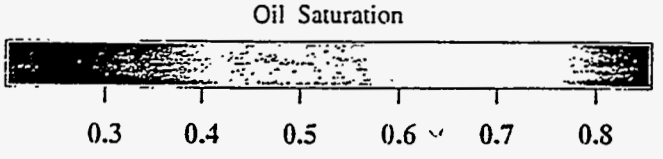

Figure 197 - **Oil saturations for reservoirs with different permeability ratios: Single horizontal injector and a single horizontal producer**

chamber/reservoir boundary. Not surprisingly, this phenomenon is most pronounced in the reservoir with the greatest permeability. The greater permeability allows for improved transport and dispersion of the steam, which in turn leads to a greater volume of the reservoir being effected by the process. The predominant color seen in the visualizations is the orange associated with the original reservoir oil saturation of 0.80, but along the steam chamber boundary, the main color is red. Red indicates an oil saturation greater than 0.80. These areas of increased oil saturation indicated the flow lines of the free flowing oil. Figure 196A, with its very low permeabilities, shows almost vertical flow lines. In this case, the steam chamber is expanding, not in the preferred horizontal direction, but in the unwanted and energy wasteful vertical direction. In a shallow reservoir, steam following this model would soon break through to the surface and effectively end the project. While a vertical trend can still be seen in Figure 196B, a marked increase in horizontal spread is observed. Again, the reservoir with the greatest permeability, Figure 196C, demonstrates the most desired characteristics.

Towards the center of each colored plate, the colors go from yellow to green to blue. Each change in color represents a decrease in oil saturation. Certain areas of the lower permeability simulations show a greater oil depletion than the corresponding areas of higher permeability simulations. This may result from the continued introduction of high temperature steam into the relatively small volume of previously drained reservoir. This could lead to short circuiting, a process where connecting channels between the injector and producer are more quickly formed, leading to a more rapid depletion process centered around the well bores. While initially appealing, this process soon leads to vertical growth and ultimately results in poorer returns than found in the high permeability models.

As can be seen in Figure 197, not only are absolute permeabilities important, but so are

permeability ratios. When the ratio of k_z to k_x or k_y is near 1.0, the steam chamber tends to be more vertical than horizontal. Whereas, when the permeability ratio tends toward 0.10 the lateral spread of the steam chamber is much more pronounced.

Time dependence of Steam Chamber Development

Figures 198 and 199 help demonstrate the significance of two major factors which effect the economic viability of any recovery project: the length of time involved before any meaningful volumes of bitumen are recovered and the importance of proper well spacing. The wells are located two hundred feet apart, with each well being 400 feet from the nearest edge of the reservoir. (The ends of the reservoir have been cropped off by 150 feet on both sides. This was done to give a more detailed view of the area near the well bores.)

Figures 198 and 199 show the oil saturation in the reservoir at 1, 3, 5, and 7 years, respectively for a 2 pair horizontal injector/horizontal producer system. One year into the project, the overall effects of steam injection are negligible. Not until the third year are significant areas of depletion noticeable. Between the fifth and seventh years, substantial volumes of bitumen are recovered and large areas of oil depletion are created. (Again, it must be stressed that the pictures shown are expanded views of the areas near the well bores and that large volumes of space near the edges of the reservoir are not affected at all during the lifetime of the project.) A minimal increase in the size of the depletion zone is noted between the 7 and 10 year mark, but the efficiency of the recovery process during this time period decreases dramatically because most of the heat injected during this time span flows to the overburden where it is quickly dissipated.

As the figures show, no real interaction between the two wells is observed, even after 5.years of operation. Essentially, the two wells act as independent systems and no signs of interference

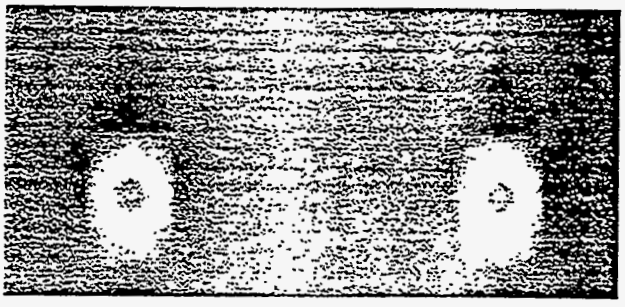

A. 365 days

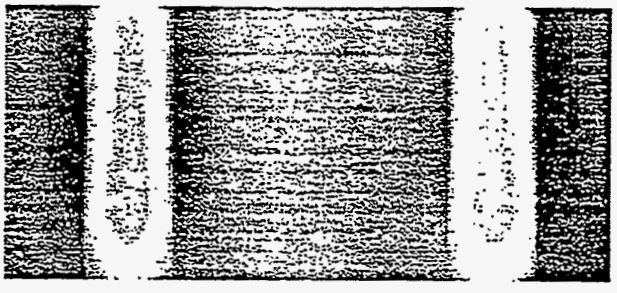

B. 1095 days

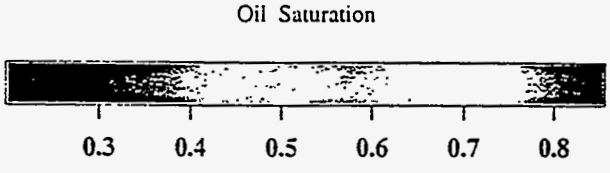

Figure 198 - **Pictures showing the evolution of the steam chamber; the wells are 400 feet apart**

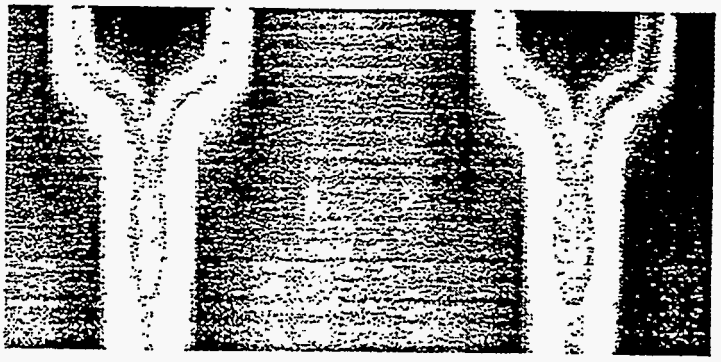

C. 1825 days

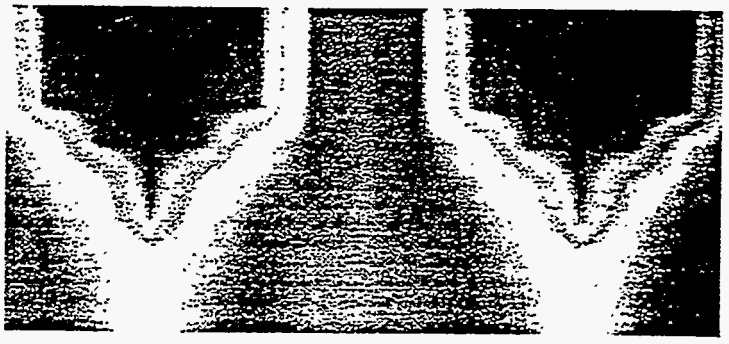

D. 2555 days

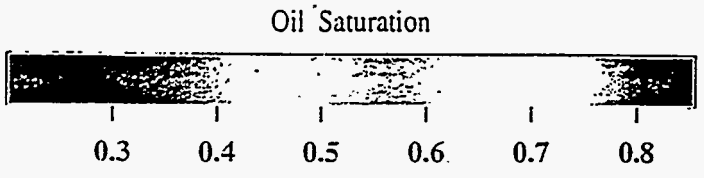

Figure 199 - **Pictures showing the evolution of the steam chamber; the wells are 400 feet apart**

(positive or negative) are noted. Findings reported in the previous chapter indicate that overlap in adjacent steam chambers results in significant gains in both productivity and process efficiency. It appears that 200 foot well spacing is still too much to efficiently produce bitumen reservoirs.

A clearer picture of the effects of well spacing appears in Figure 200. In the three horizontal pair system, there is a stark contrast in temperature profiles between the system with 200 foot spacing and the one with 100 foot spacing. Although the pattern in Figure 200A encompasses more of the total reservoir volume, the wells exhibit no signs of interacting with each other, and as was seen in Figure 200B, act as if they were isolated pairs. In Figure 200B the interaction between the three well pairs is immediately obvious. A larger, interconnected area of high, 300^{0}F steam encompasses all the wells, resulting in more efficient heat transfer to the reservoir and a corresponding decrease in viscosity and greatly enhanced oil recovery. This figure, in fact, represents the best case well pattern studied.

Reservoir Sweep and Lateral Spread

Enhancing reservoir sweep, the volume of the reservoir actually effected by the process, is one of the main objectives in any recovery project. Ultimately, the decision to go ahead with a recovery project is determined by the value of the product (i.e. volume of bitumen produced) versus the cost associated with injecting steam into the ground. With this in mind, the reservoir engineer must try to maximize the volume of reservoir bitumen that is heated, while limiting the volume of steam injected. One method of determining the process efficiency is to compare the water injected to oil produced ratios. Such analyses are presented in the previous chapter. Figures 201-203 show the lateral spread produced by one, two, and three injector systems. (In each of the figures, the reader is looking down the axis of the producing well bore). Time is 7 years.

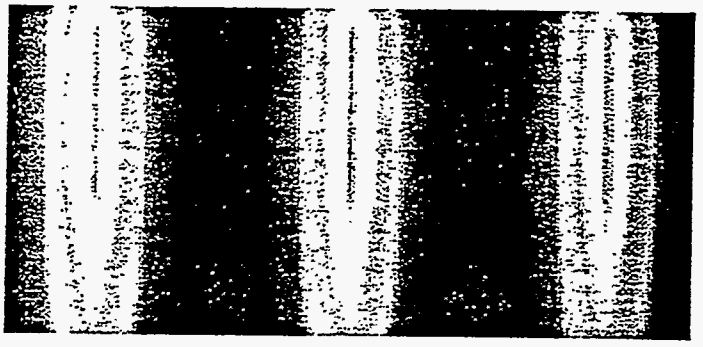

A. 200 foot spacing

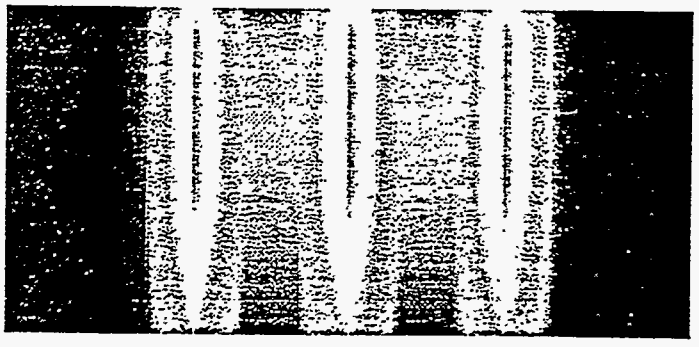

B. 100 foot spacing

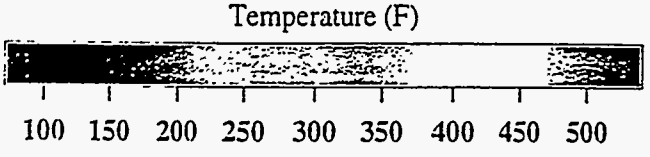

Figure 200 - **Oil saturations for two different well spacings; horizontal injector-producer configurations**

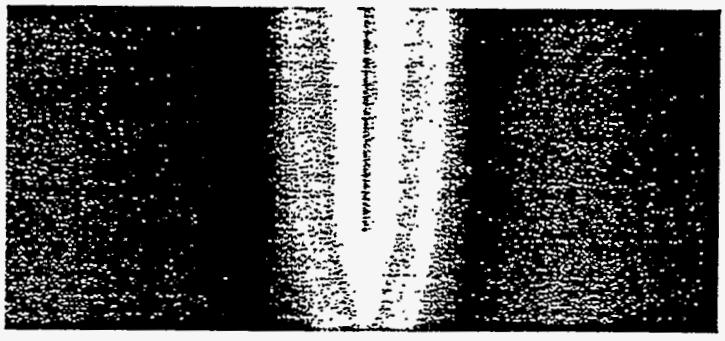

A. Horizontal injector

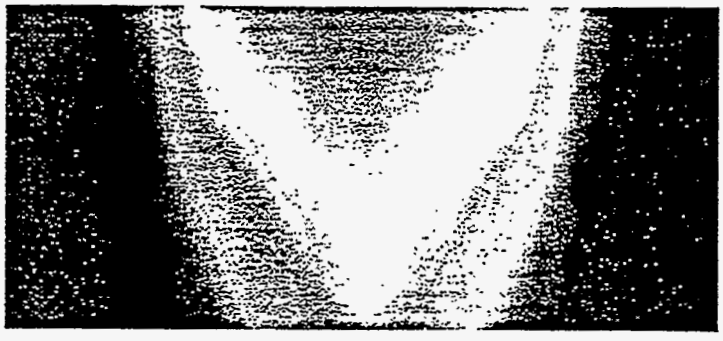

B. Vertical injector

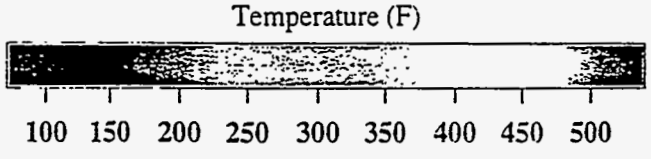

Figure 201 - Comparison of temperature profiles for the horizontal and the vertical injection configurations

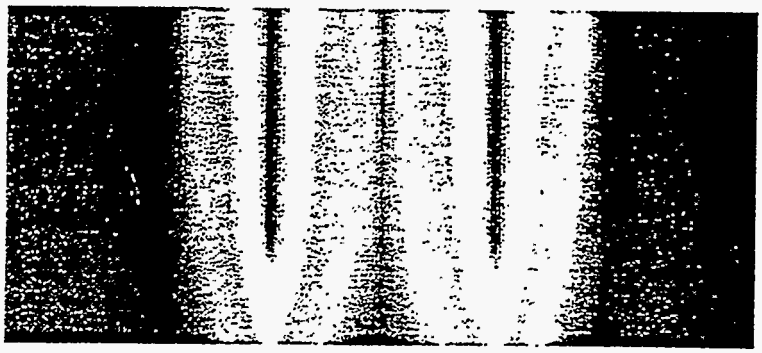

A. Two horizontal injectors

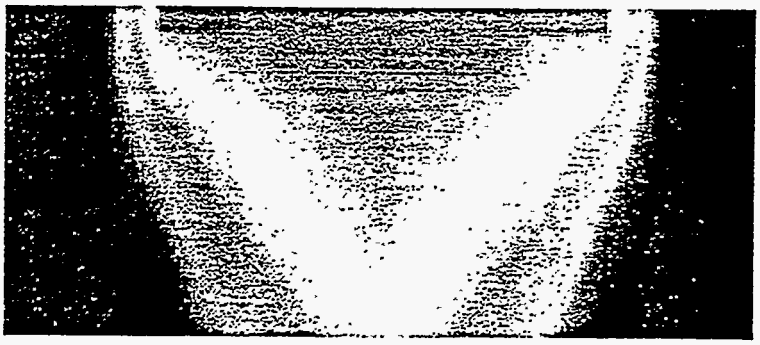

B. Two vertical injectors

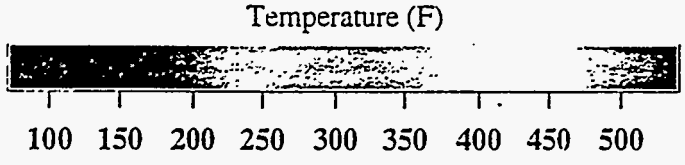

Figure 202 - Comparison of temperature profiles for two-well configurations

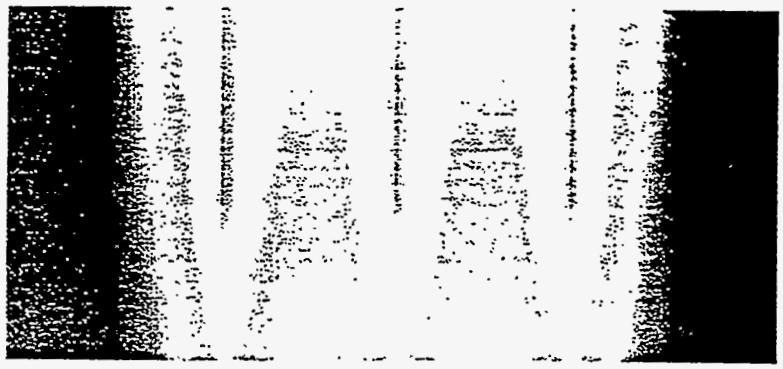

A. Three horizontal injectors

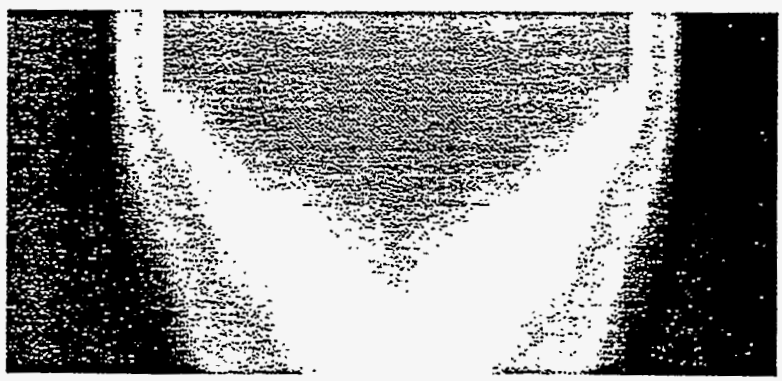

B. Three vertical injectors

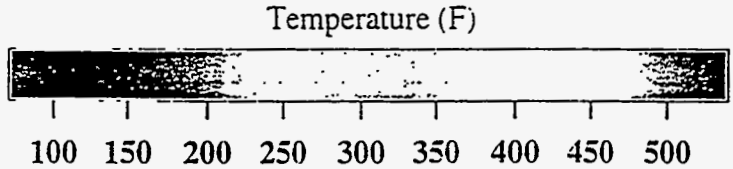

Figure 203 - Comparison of temperature profiles for three-well configurations

It must be noted that the figures were created with data taken at the center of the reservoir, which tends to maximize the vertical pattern cases. When a longitudinal view of the three injector systems is studied (Figure 204) the horizontal system seems to be the more efficient pattern. This view is not completely accurate either, since the view is directly centered over the length of the horizontal producer, which tends to exaggerate the volume effected by the horizontal injector (compare to the lateral spread in Figure 204).

The difference in lateral spread between the single vertical injector and the single horizontal injector are pronounced (Figure 201). Temperature profiles show that the area of reservoir effected in the vertical pattern is more than double the area of reservoir effected in the horizontal pattern. With the introduction of a second injector, (Figure 202), both patterns exhibit an increase in effected area, but the differences between the two is no longer double. Adding yet another injector, again increases the effected area (Figure 203) but the horizontal pattern now effects almost as much area as the vertical pattern, although the heat is not as uniformly distributed in the horizontal pattern as it is in the vertical pattern.

A more realistic view of differences found in the three injector pattern appears in Figure 205. This figure gives volumetric comparisons of the two patterns based on reservoir temperature. The figure shows the volume of the reservoir that has reached a temperature of 300^0F or more. In the three vertical injector pattern, 21.5% of the reservoir is affected by the steam injection, but this number climbs to 31.7% in the horizontal pattern.

Summary and Conclusions

Historically enhanced oil recovery (EOR) methods have depended upon creating pressure differentials within a reservoir and using these differences in pressure to drive oil from one well

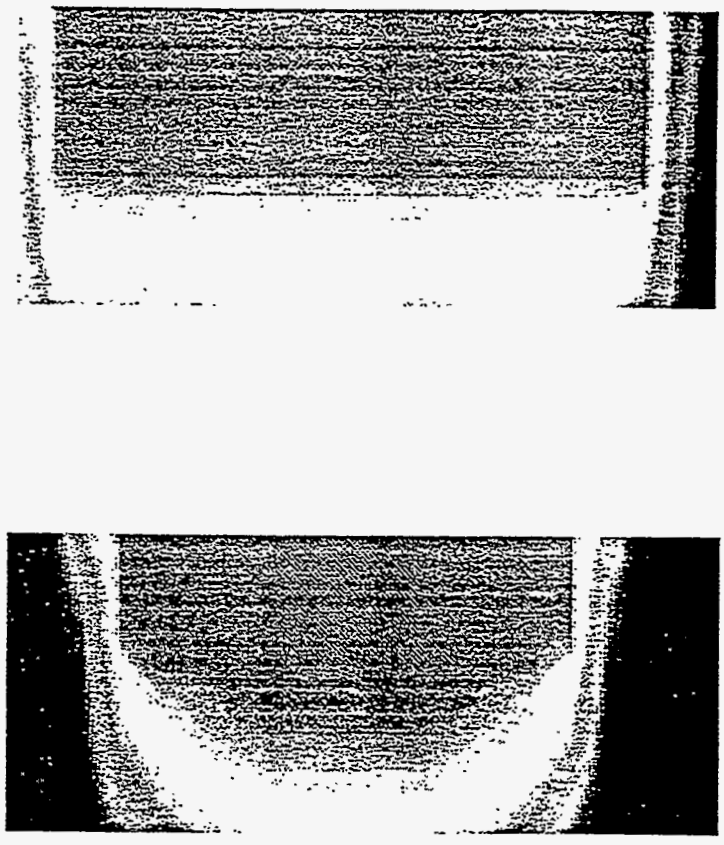

Figure 204 - A different cross-section of the temperature profiles for the three-well systems

A. Three vertical injectors

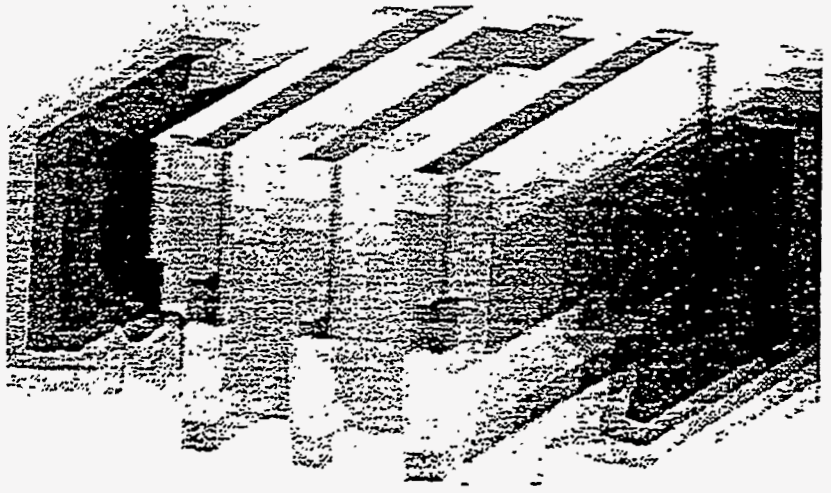

B. Three horizontal injectors

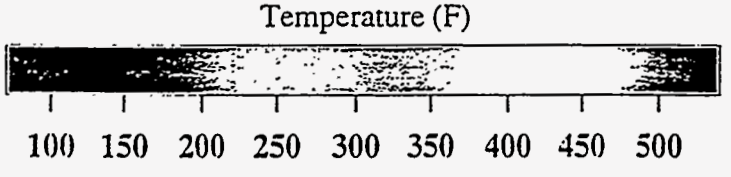

Figure 205 - A three-dimensional view of the temperatures for the three-well systems

(injector) to another well (producer). Due to the extremely high viscosities predominantly found in oil sands, traditional thermal processes do not work well. One promising new method for the recovery of oil from oil bearing sands is the steam assisted gravity drainage (SAGD) method. SAGD centers around reducing the viscosity of the entrained oil via thermal methods instead of attempting to initiate pressure driven viscous flow.

This thesis has examined the relationship between reservoir permeability, well patterns, and well spacing with regards to steam assisted gravity drainage. Additionally, numerous sensitivity studies helped determine critical simulation parameters such as grid block size and the overall number of grid blocks.

Grid size sensitivity studies revealed that using blocks of two to three meters thickness provided adequate resolution without requiring inordinate amounts of computer time. Best results were obtained by using grid blocks of various size. Regions of high activity such as near the well bore consisted of 5 foot thick grid blocks, while areas near the edge of the reservoir were adequately represented with 20 foot thick grid blocks. Length and width parameters were not found to be as critical as in the vertical dimension and were generally 2.5 times greater than the vertical thickness.

Several sensitivity comparisons were made between the source-sink model and the discretized well bore model. A discretized well bore model allocates space within the simulation to account for the actual physical presence of the well bore while the source-sink model wells to be point sources. The discretized method is much more rigorous, but also much more time intensive, than the source-sink model. Results indicated no significant differences in the output data between the two models.

Changes in reservoir pressures did not noticeably effect the amount of oil recovered as long as the pressure difference between injector and reservoir was greater than 50 psi. Smaller pressure

differences greatly reduced the recovery efficiencies. Output from the simulations indicates a strong correlation between high recovery efficiencies and high reservoir permeability. This relationship is most noticeable at lower permeability levels, where a permeability increase of just 0.1 darcies, in the vertical direction, resulted in a four-fold increase in recovery efficiency.

Simulation results have shown that high permeabilities combined with larger numbers of wells and reduced spacing between the wells resulted in the highest efficiency processes. Generally, the horizontal pairs provided a slight efficiency edge over the vertical/horizontal pairs, but the difference was not large enough to rule out vertical/horizontal pairs as the preferred economic method of developing a particular reservoir. A significant advantage of the three vertical injectors / one horizontal producer was the ratio of vertical wells to horizontal wells. Although horizontal drilling technologies have made impressive gains in the last five years, the drilling of horizontal wells is still relatively expensive and risk filled in comparison to the drilling of vertical wells. Additionally, the completion of a vertical well is routine, while the completion of a horizontal well is still more art than science.

Substantial well communication was also a significant contributor to maximizing recovery efficiencies. Well visualizations demonstrated that if the wells were too far apart and no communication was developed between them, multiple wells would essentially act as isolated systems. Data analysis showed the performance gains, based on recovery percentages of original oil in place, obtained with increasing the number of wells and decreasing the spacing between the wells. However, in the case of horizontal pairs, the desire to pack wells in closer and closer must be tempered with the observation that such wells exhibit a tendency to short-circuit under modest pressure differences if the injector and producer are too close together.

At the moment, the low permeabilities predominantly found in Utah tar sands would preclude

the implementation of a SAGD system using current technologies. Canadian reservoirs, however, seem well suited for future SAGD development. Since reservoir permeability has such a pervasive influence on recovery efficiencies and ultimately economic viability, future studies into SAGD should include simulations which incorporate the effects of both natural and man-made fractures.

Pertinent data from the massive output files were extracted using appropriate sed and awk UNIX scripts. Although all the data is contained in large two-dimensional arrays, tabular arrays do not lend themselves to easy analysis. The scripts along with additional Fortran and C programs were used in reading the data to a form suitable for visualization.

UINTA BASIN BITUMEN HYDROTREATING: CATALYTIC UPGRADING OF THE PR SPRING BITUMEN OVER A COMMERCIAL HDM CATALYST

Principal Investigator: Francis V. Hanson
Postdoctoral Fellow: D.C. Longstaff
Graduate Student: J. Kim

INTRODUCTION

Bitumen-containing oil sands have been studied in Canada and the United States as alternative fuel sources and have been commercially developed in Canada. Technical alternatives that have been suggested for upgrading bitumens and heavy oils are based on carbon rejection (coking processes) or on hydrogen addition (hydroprocessing). Coking is presently utilized to upgrade bitumen (234,235) and is based on carbon rejection as coke. Hydroprocessing may have greater potential for upgrading heavy oils than coking processes because of nearly complete utilization of the feed (236,237). Many heavy oils and bitumens contain high heteroatom (sulfur and nitrogen), asphaltene and metal concentrations (65, 238, 239). Sulfur and nitrogen compounds are removed in the form of H_2S and NH_3; respectively, however, metals are deposited on the catalyst surface. This can lead to catalyst deactivation and short catalyst cycle life. Hydrodemetallation is necessary to protect downstream hydrotreating catalysts from being poisoned via metal deposition (240). HDM catalysts with wide pore radii are required for upgrading bitumens or heavy oils prior to subsequent hydroprocessing (65, 240) because the HDM catalyst can accommodate high metal deposition without excessive deactivation.

A Mo-on-alumina catalyst was employed for HDM because the catalyst had a higher pore volume than primary hydrotreating catalysts. Several researchers have reported that metal sulfides on low-acidity supports exhibit residuum conversion activity (238, 239) in which gas oil, distillate,

naphtha, and gases are produced via mild hydrocracking.

The objectives of this study were to determine the effects of temperature, space velocity, and pressure on the extent of heteroatom and nickel removal, Conradson carbon residue (CCR) and residuum conversion and on the product distributions and yields when processing the bitumen from the PR Spring oil sands.

EXPERIMENTAL

The bitumen used in this study was obtained by reflux extraction of the PR Spring oil sands with toluene. The oil sand ore was mined, crushed and sieved to a particle size of < 0.6 cm prior to solvent extraction. The majority (85-90%) of the toluene in the bitumen-toluene solution was removed by rotary evaporation. The remaining toluene was removed by batch vacuum distillation. The physical and chemical properties of the PR Spring bitumen are presented in Table 63. The bitumen contains high levels of asphaltenes and potential coke precursors. It also contains high levels of sulfur relative to the Athabasca bitumens.

The fixed-bed reactor system was operated in the upflow mode to facilitate isothermal operation and to insure complete wetting of the catalyst (241, 242). The liquid and gas products from the reactor were separated in a high pressure vapor-liquid separator. The gaseous products were withdrawn from the separator through a back pressure regulating valve (BPRV) which also controlled the system pressure. The liquid product was removed from the separator through an Annin control valve. A schematic of the hydrotreater system is presented in Figure 206. The reactor consisted of three zones whose temperatures were independently controlled: the preheating zone, the catalyst bed and the postreaction zone. The catalyst bed was located in the central 30.5 cm of the reactor and contained 152 cm^3 of catalyst. Preheating and postreaction zones were filled with inert α-alumina spheres (0.32 cm) and supported the catalyst bed. The reactor was heated

Table 63. Physical and chemical properties of PR Spring bitumen.

API Gravity	9.2
Conradson Carbon Residue, wt%	16.0
Asphaltenes, wt%	18.1
Elemental Analysis	
C, wt%	85.9
H, wt%	10.9
N, wt%	1.06
S, wt%	0.43
Ni, ppm	72
H/C Atomic Ratio	1.51
Simulated Distillation	
Volatility, wt%	37.4
C_5 - 477 K, wt%	0.1
477 - 617 K, wt%	6.2
617 - 811 K, wt%	31.1
>811 K, wt%	62.6
IBP, K	514

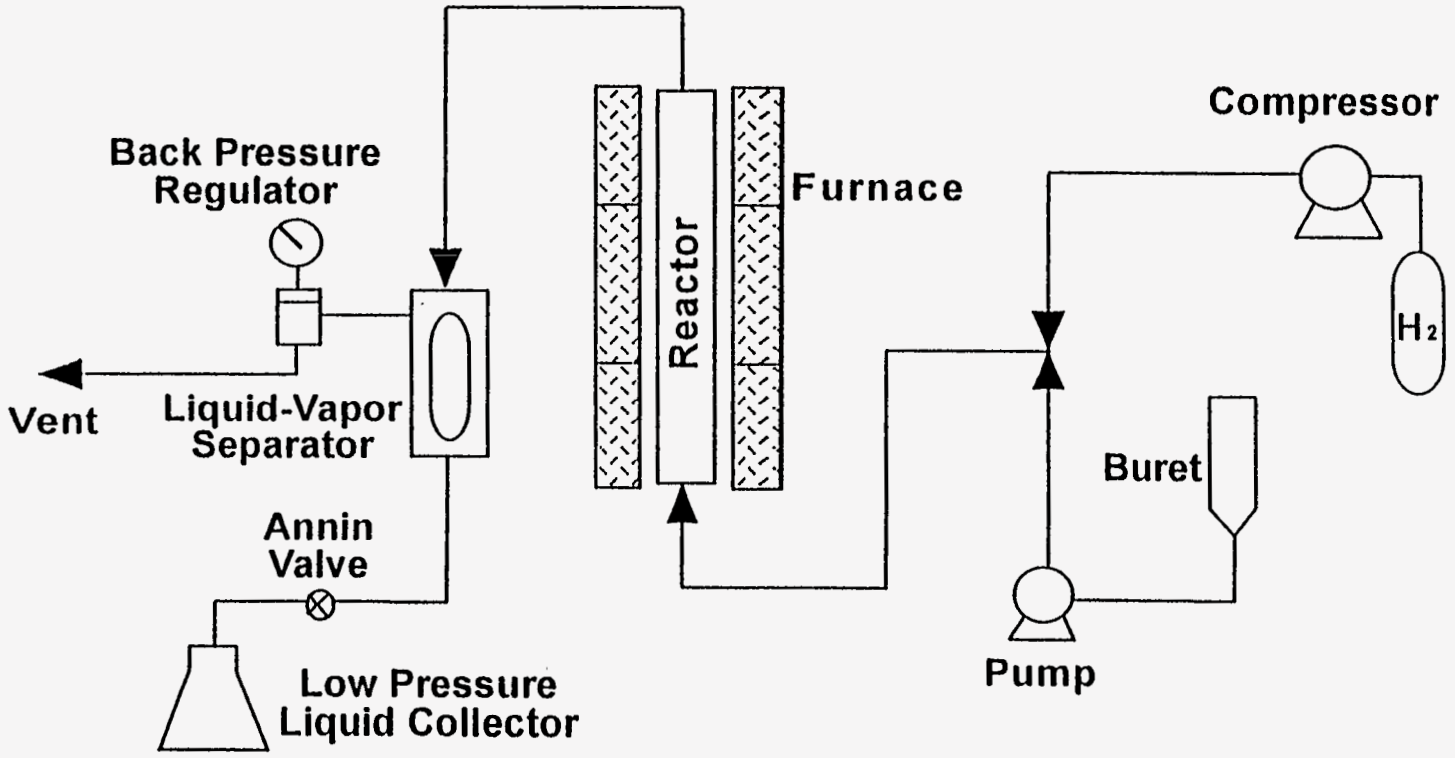

Figure 206. Schematic of the hydrotreater system.

by a three zone electrical furnace. The axial temperature profile in the catalyst zone was measured by a traveling thermocouple.

A commercial Mo/Al_2O_3 HDM catalyst in the form of 1.6 mm trilobe shaped extrudates was used in this study. The catalyst contained 6.0 wt% MoO_3 and had a surface area of 130 m^2/g and a pore volume of 0.85 cc/g. The catalyst was dried in-situ in flowing nitrogen at 700 K for one hour and was cooled to ambient temperature prior to sulfiding. The catalyst was sulfided with a 2 wt% sulfur solution of dimethyldisulfide in kerosene. The sulfiding procedure consisted of feeding the sulfiding solution and hydrogen upflow through the catalyst. The catalyst bed was heated from ambient temperature to 505 K at a rate of 27.8°C/h. The reactor temperature was held at 505 K for 2 hours to insure that the catalyst was properly sulfided. Sulfiding was completed when the reactor temperature reached 645 K. The hydrogen-to-sulfiding solution ratio was 890 m^3 (STP)/m^3. The reactor pressure and the sulfiding solution feed rate were 6.1 - 6.3 MPa and 1 LHSV; respectively.

After the catalyst had attained a stable activity, experiments were conducted by varying the reactor temperature (625 - 685 K), WHSV (0.26-1.55 h^{-1}) and reactor pressure (11.1-16.6 MPa). Experiments were performed in a cyclic mode (base case condition-operating condition-base case condition) to assess the extent of catalyst deactivation. The aging rate was estimated by monitoring the API gravity of the total liquid product produced at base case conditions with respect to time-on-stream (TOS). Base case conditions were 642 K, 0.41 h^{-1} LHSV and 13.7 MPa. The experimental apparatus and procedures have been described in detail elsewhere (243).

RESULTS AND DISCUSSION

Reactor operating variables were selected so that only one of the three process variables

was changed at a time while the remaining two were kept constant. The range of process operating conditions is summarized as a function of TOS in Table 64.

Effects of Temperature

Temperature effects were investigated by varying the temperature at fixed pressure (13.7 MPa) and space velocity (0.78 h^{-1}WHSV). The effects of temperature on nitrogen, sulfur and nickel removals, on CCR and residuum conversions and on product distributions and yields are presented in Table 65. Increasing temperature resulted in an increase in the API gravity, the H/C atomic ratio relative to the bitumen and an increase in H_2 consumption. The increase in API gravity was large compared to the increase in H/C atomic ratio over the entire range of temperatures studied.

Fractional conversions of nitrogen, sulfur, residuum, nickel and CCR with respect to temperature are presented in Figure 207. Nitrogen, sulfur and nickel removals, and CCR and residuum conversions over the HDM catalyst increased as temperature increased. The degree of sulfur removal was higher than residuum conversion and nitrogen removal. Nitrogen was the least reactive species. The fact that the extent of sulfur removal was higher than nitrogen removal is in agreement with Ho (244) who observed that sulfur compounds are easier to convert than nitrogen compounds.

The relative percent decrease in the residuum, sulfur and nitrogen contents of the total liquid products were 4, 12, and 2%; respectively, when the reaction temperature increased from 625 to 642 K. The CCR and nickel contents decreased by 6 and 7%; respectively, for the same increase in temperature. Sulfur removal was significant at lower temperatures. The residuum and nitrogen contents of the liquid product decreased by 21 and 22%; respectively, as the temperature increased from 664 to 685 K. The sulfur content decreased by 8%, the CCR content by 16% and

Table 64. Process operating conditions.

Run Number	WHSV (h^{-1})	Temperature (K)	Pressure (MPa)	Time on stream (h)
HDM-4	0.78	642	13.7	80
HDM-5	0.78	685	13.7	114
HDM-6	0.78	642	13.7	143
HDM-7	0.78	664	13.7	168
HDM-8	0.78	642	13.7	192
HDM-9	0.26	664	13.7	240
HDM-10	0.78	642	13.7	264
HDM-11	1.55	666	13.7	288
HDM-12	0.78	642	13.7	312
HDM-13	0.78	625	13.7	336
HDM-14	0.78	642	13.7	360
HDM-15	0.43	664	13.7	403
HDM-16	0.78	642	13.7	427
HDM-17	0.78	664	16.6	456
HDM-18	0.78	642	13.7	480
HDM-19	0.78	664	11.1	504
HDM-20	0.78	642	13.7	528

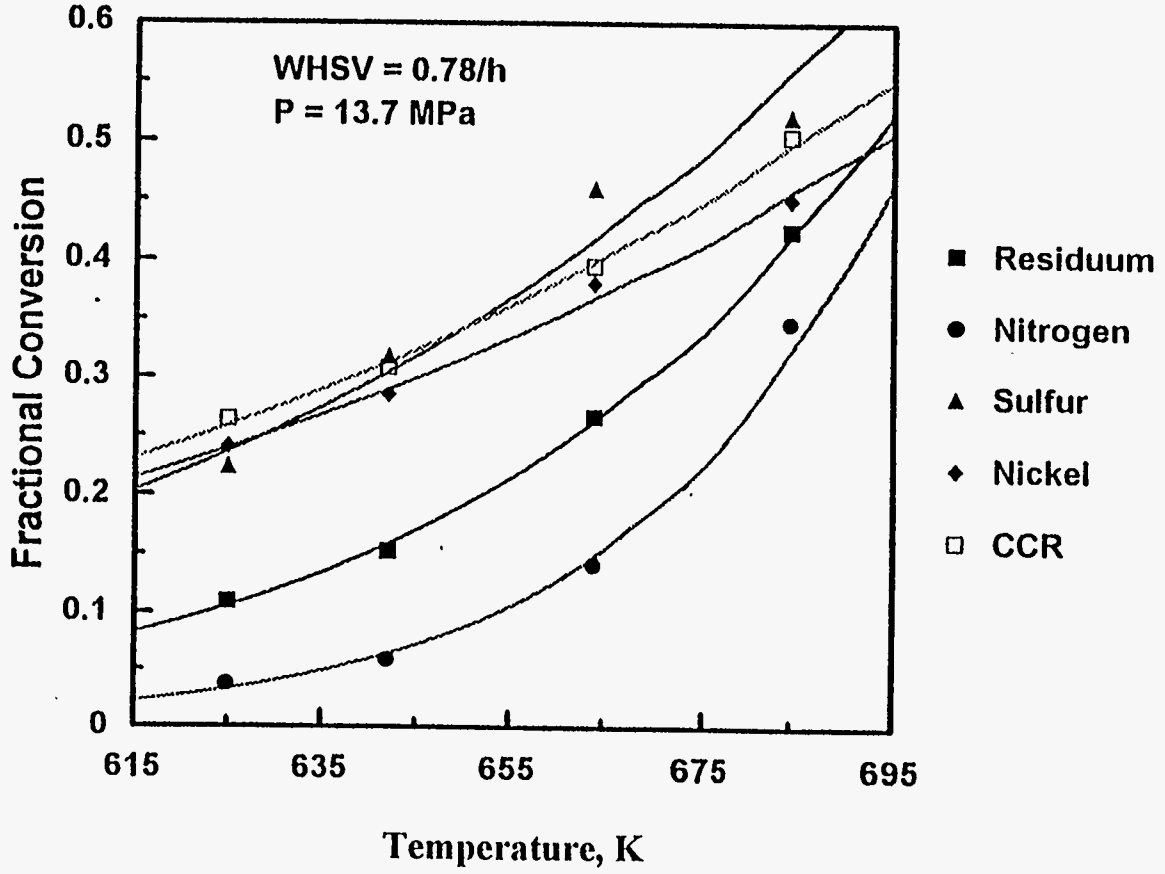

Figure 207. Fractional conversions of residuum, nitrogen, sulfur nickel and CCR vs temperature.

Table 65. Effects of temperature on product properties of the hydrotreated bitumen.

Run number	5	7	8	13
Process operating conditions				
Temperature, K	625	642	664	685
WHSV, h^{-1}	0.78	0.78	0.78	0.78
Pressure, MPa	13.7	13.7	13.7	13.7
H_2 consumption(l/l)	64	68	91	105
API gravity, °API	11.1	11.7	13.4	15.6
Specific gravity	0.992	0.988	0.977	0.962
CCR, wt%	12.0	11.3	10.0	8.4
Elemental analysis				
C, wt%	85.5	85.7	85.9	86.1
H, wt%	11.7	11.8	11.9	12.0
N, wt%	1.03	1.01	0.93	0.73
S, wt%	0.34	0.30	0.24	0.22
Nickel, ppm	56	52	46	42
H/C atomic ratio	1.63	1.64	1.65	1.66
Product yields, wt%				
C_1	0.3	0.3	0.6	0.8
C_2	0.1	0.1	0.3	0.4
C_3	0.1	0.1	0.3	0.6
i-butane	0.1	0.1	0.1	0.2
n-butane	0.1	0.1	0.2	0.6
C_5^+ liquid product	96.7	97.8	98.7	96.7
Liquid yield (vol%)	98.4	99.8	99.7	98.4
Simulated distillation of total liquid product				
Volatility, wt%	43.5	45.8	52.6	61.7
IBP, K	484	447	416	410
IBP-477 K, wt%	0.6	0.9	1.9	3.7
477-617 K, wt%	8.6	9.3	11.9	16.0
617-811 K, wt%	34.3	35.6	38.8	42.0
>811 K, wt%	56.5	54.2	47.4	38.3

the nickel content by 9% with the same increase in temperature. Nitrogen removal and CCR and residuum conversions significantly increased with increasing temperature; however, the sulfur and nickel contents of the total liquid products did not decrease significantly indicating that the unreacted sulfur and nickel species were quite refractory. Nitrogen removal may be indirectly related to thermal reactions because nitrogen contained in residuum is not catalytically converted until the residuum is cracked to lower molecular weight products via both thermal and catalytic pathways (245).

The effect of temperature on the product distributions of the liquid products are presented in Figure 208. Increased thermal cracking rates at higher temperatures resulted in higher yields of volatile products and lower yields of residuum (>811 K). However, the yields of gas oil (617-811 K), distillate (477-617 K), naphtha (IBP-477 K) and light gases (C_1-C_4) increased continuously with increasing temperature.

Effects of WHSV

The effect of weight hourly space velocity (WHSV) was investigated by varying WHSV between 0.26 - 1.55 h^{-1} at fixed temperature (664 K) and pressure (13.7 MPa). The effect of WHSV on nitrogen, sulfur and nickel removals, on CCR and residuum conversions and on product distribution and yields is presented in Table 66. The API gravity of the total liquid products increased from 12.2 °API to 16.2 °API as the WHSV decreased from 1.55 to 0.26 h^{-1}. Hydrogen consumption and the H/C atomic ratio of the total liquid products also increased as the WHSV decreased.

The fractional conversions of residuum, nitrogen, sulfur, nickel and CCR are presented in Figure 209 with respect to reciprocal WHSV. The degrees of nitrogen, sulfur and nickel removal and of CCR and residuum conversion were significant as the space velocity decreased

Table 66. Effects of WHSV on product properties of the hydrotreated bitumen.

Run number	11	7	15	9
Process operating conditions				
Temperature, K	666	664	664	664
WHSV, h^{-1}	1.55	0.78	0.43	0.26
Pressure, MPa	13.7	13.7	13.7	13.7
H_2 consumption(l/l)	35	68	109	144
API gravity, °API	12.2	13.4	14.6	16.2
Specific gravity	0.984	0.977	0.969	0.958
CCR, wt%	10.8	10.0	8.7	7.4
Elemental analysis				
C, wt%	86.1	85.9	86.1	86.7
H, wt%	11.8	11.9	12.0	12.2
N, wt%	1.00	0.93	0.81	0.68
S, wt%	0.28	0.24	0.19	0.17
Nickel, ppm	51	46	40	28
H/C atomic ratio	1.64	1.65	1.66	1.68
Product yields, wt%				
C_1	0.4	0.6	0.8	1.0
C_2	0.2	0.3	0.3	0.5
C_3	0.2	0.3	0.4	0.6
i-butane	0.1	0.1	0.2	0.3
n-butane	0.1	0.2	0.3	0.4
C_5^+ liquid product	97.3	97.8	97.1	96.7
Liquid yield (vol%)	99.1	99.8	99.0	98.7
Simulated distillation of total liquid product				
Volatility, wt%	48.6	52.6	58.3	63.4
IBP, K	424	416	415	410
IBP-477 K, wt%	1.3	1.9	2.4	3.1
477-617 K, wt%	10.6	11.9	14.4	17.7
617-811 K, wt%	36.7	38.8	41.5	42.6
>811 K, wt%	51.4	47.4	41.7	36.6

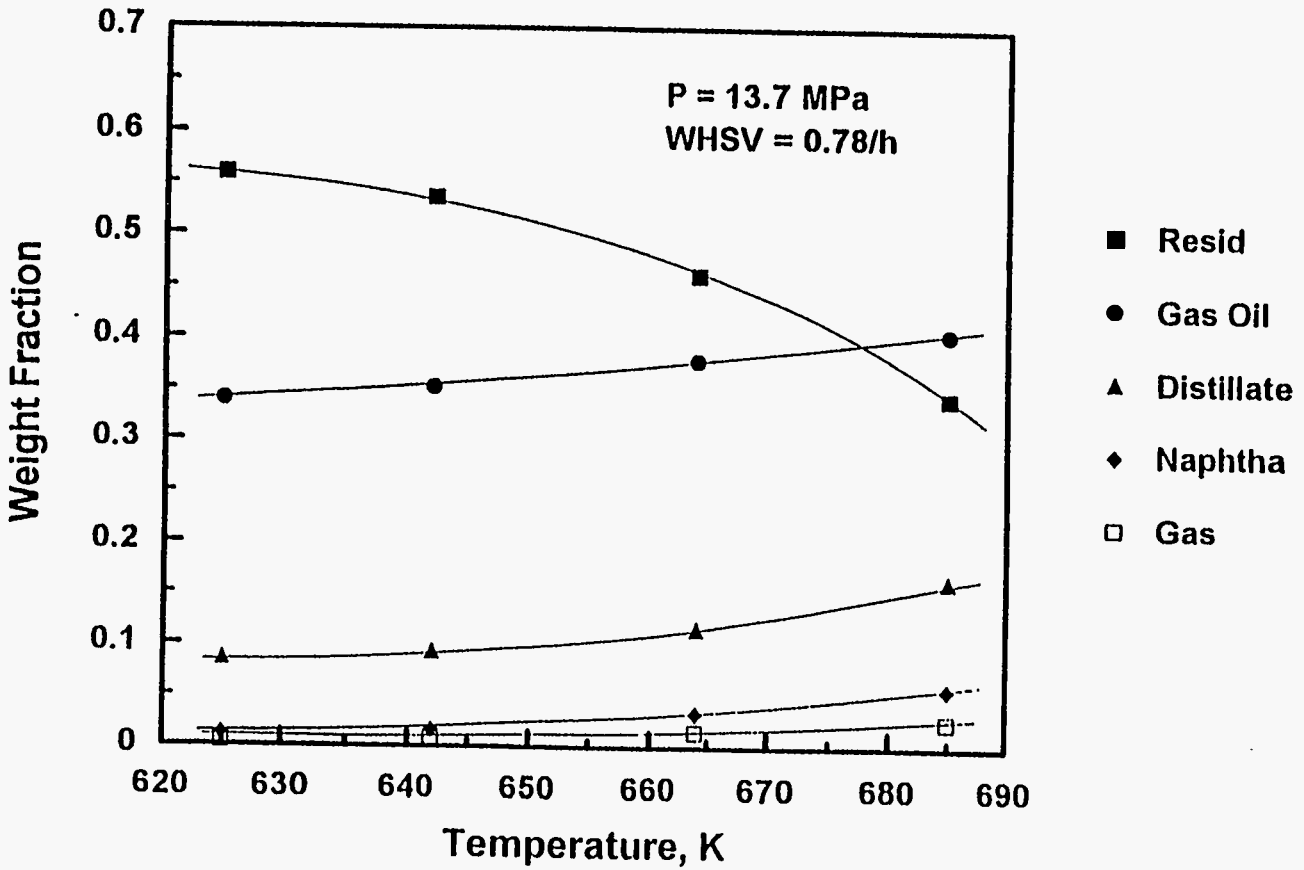

Figure 208. Effect of temperature on yields of residuum, gas oil, distillate, naphtha, and gases.

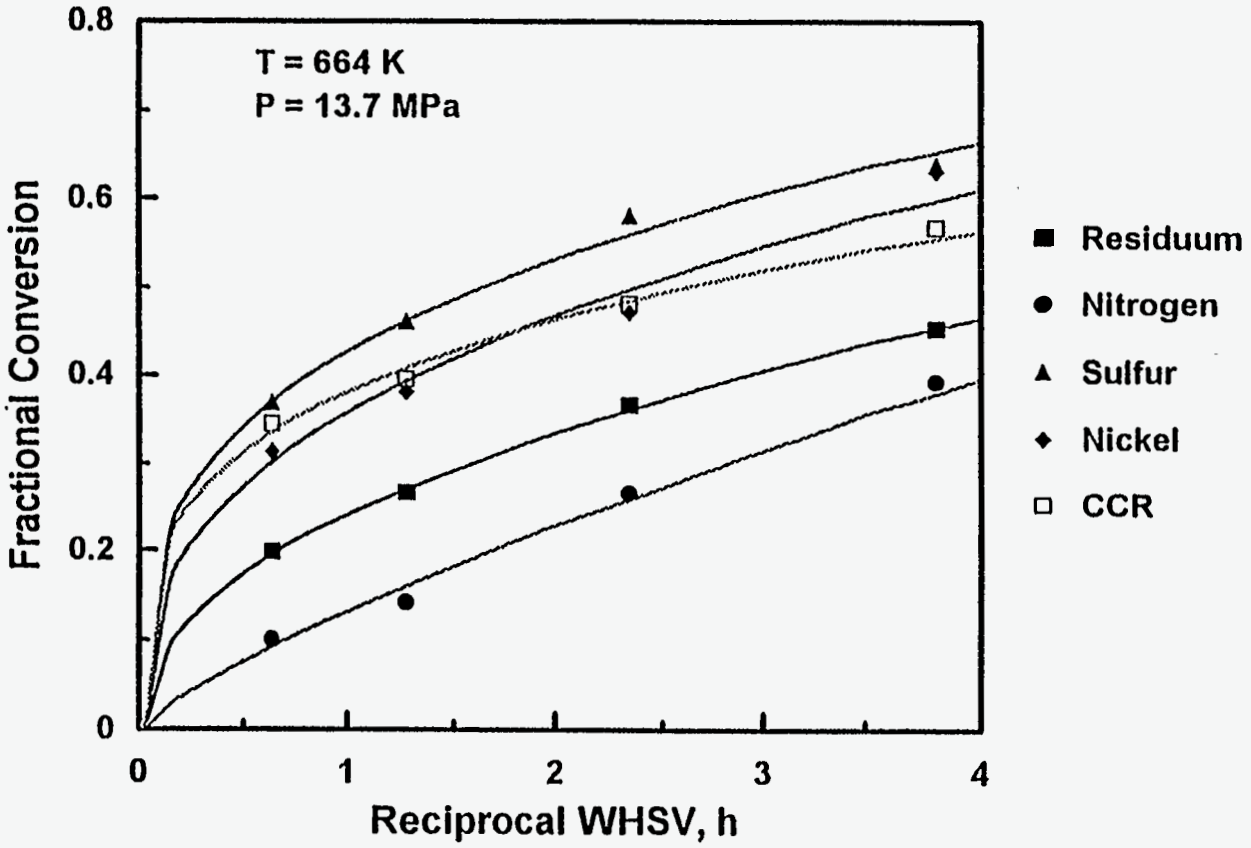

Figure 209. Fractional conversions of residuum, nitrogen and sulfur, nickel and CCR vs reciprocal WHSV.

from 1.55 to 0.26 h^{-1} WHSV. The extent of sulfur removal was greater than residuum conversion which was greater than nitrogen conversion over the entire range of reciprocal WHSV. Residuum conversion surpassed nitrogen removal in all cases over the commercial HDM catalyst. It was expected that sulfur removal would exceed nitrogen removal because sulfur compounds are known to be more reactive than nitrogen compounds (244).

At 1.55 h^{-1} WHSV, the sulfur content decreased by 33%; the residuum content decreased by 18%; the nitrogen content decreased by 6%; the CCR content decreased by 30%; and, the nickel content decreased by 26% relative to the feed. The extent of sulfur removal was highest at 1.55 h^{-1} WHSV relative to the other compounds. This suggests that a large portion of the sulfur is significantly more reactive than the residuum and/or nitrogen. It is thought that PR Spring bitumen may contain aliphatic sulfides such as have been detected in Canadian bitumens (246). The presence of aliphatic sulfides in PR Spring bitumen would explain the significant sulfur conversion which occurs at large WHSV. The nitrogen, sulfur and nickel removal increased by 19%, 34% and 25%; respectively, as the space velocity decreased from 1.55 to 0.43 h^{-1} WHSV. Both residuum and CCR conversion increased by 19% as the space velocity decreased from 1.55 to 0.43 h^{-1} WHSV. The extent of sulfur removal was higher than that of the other compounds at high space velocity. 30% nickel removal was achieved as the space velocity decreased from 0.43 to 0.26 h^{-1} WHSV. 11% sulfur and 16% nitrogen removals and 12% residuum and 15% CCR conversions were achieved as the space velocity decreased from 0.43 to 0.26 h^{-1} WHSV. The slope of sulfur removal decreased substantially with increasing reciprocal WHSV. The reduction in nitrogen content was almost linear over the entire range of reciprocal WHSV. The slope of residuum and CCR conversion also decreased with increasing reciprocal WHSV.

The effect of reciprocal WHSV on the product yields are presented in Figure 210. Yields

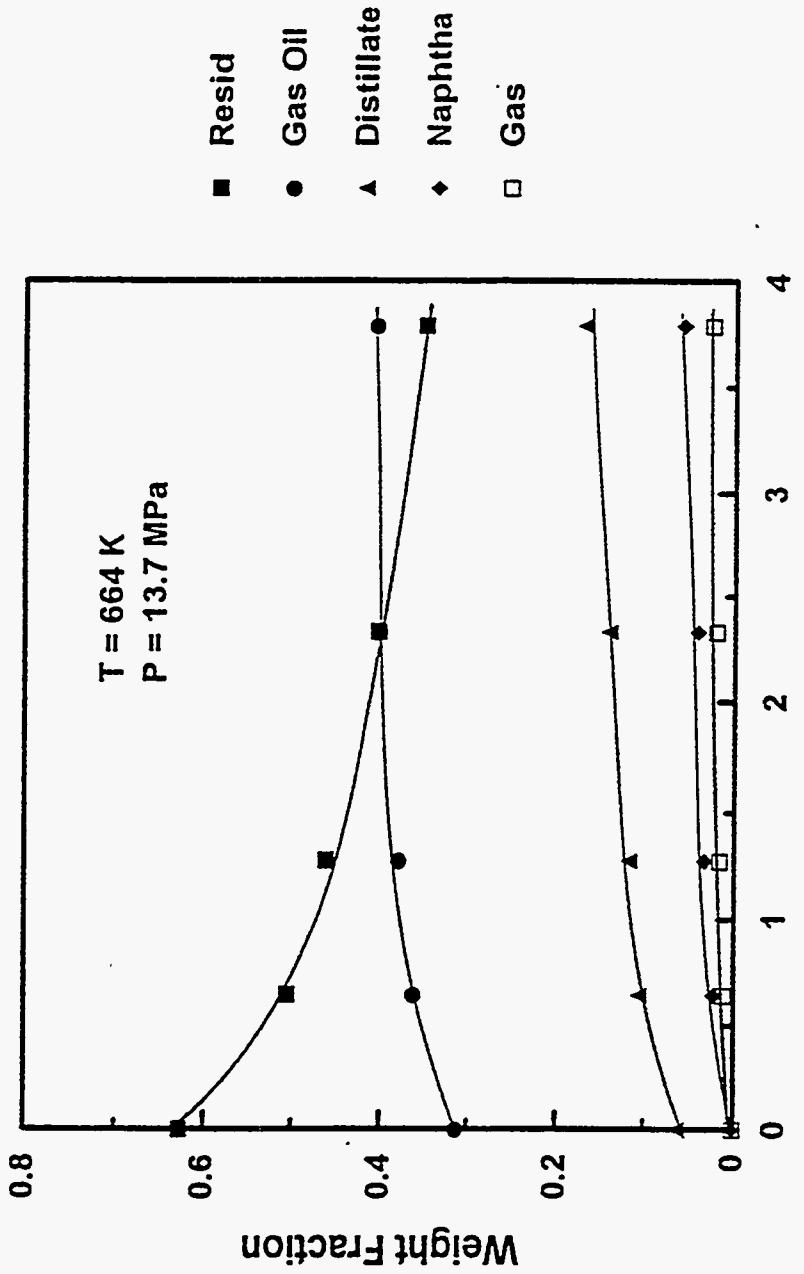

Figure 210. Effect of reciprocal WHSV on yields of residuum, gas oil, distillate, naphtha, and gases.

of the various fractions changed with varying WHSV at constant temperature and pressure. The volatile product increased at higher reciprocal WHSV because higher residuum conversion was achieved at longer contact times. The residuum fraction (> 811 K) was significantly converted with increasing residence time whereas the yields of gas oil (617-811 K), distillate (477-617 K), naphtha (IBP-477) and C_1 - C_4 gases increased monotonically. The yields of gas oil, distillate and naphtha exhibited an initial rapid increase at lower reciprocal WHSV. This is attributed to the rapid conversion of native residuum into volatile fractions.

Effects of Pressure

The effect of pressure was studied by varying pressure between 11.1 - 16.6 MPa at a fixed space velocity (0.78 h^{-1} WHSV) and reaction temperature (664 K). The product distributions and yields, nitrogen and sulfur removals and CCR and residuum conversions are reported as a function of reactor pressure in Table 67. The fractional conversions of residuum, nitrogen, sulfur and CCR are presented in Figure 211 with respect to reactor pressure. Reactor pressure exhibited little influence on the liquid product distributions and yields. Even though hydrogen consumption increased as the reactor pressure increased from 11.1 to 16.6 MPa, the API gravity increased only slightly from 9.7 to 10.2°API. The H/C atomic ratio increased from 1.62 to 1.66 because of increased hydrogenation due to the higher pressure. Nitrogen and sulfur removals and CCR and residuum conversions were only slightly enhanced with increasing reactor pressure (Figure 211). Liquid product distributions and yields are most strongly affected by thermal and catalytic cracking. The contribution of hydrogen to cracking is primarily indirect in that hydrogen suppresses coke formation and saturates the olefinic products produced in cracking reactions. The only direct contribution that hydrogen can make is to saturate aromatic rings to hydroaromatics which can then be cracked; however, this contribution is minor and will only result in minor

Table 67. Effects of reactor pressure on product properties of the hydrotreated bitumen.

Run number	19	7	17
Process operating conditions			
Temperature, K	664	664	664
WHSV, h^{-1}	0.78	0.78	0.78
Pressure, MPa	11.1	13.7	16.6
H_2 consumption(l/l)	85	91	142
API gravity, °API	13.0	13.4	13.5
Specific gravity	0.979	0.977	0.975
CCR, wt%	10.2	10.0	9.7
Elemental analysis			
C, wt%	85.8	85.9	85.9
H, wt%	11.7	11.9	12.0
N, wt%	0.90	0.93	0.88
S, wt%	0.23	0.24	0.22
H/C atomic ratio	1.63	1.65	1.66
Product yields, wt%			
C_1	0.6	0.6	0.8
C_2	0.3	0.3	0.3
C_3	0.3	0.3	0.4
i-butane	0.1	0.1	0.1
n-butane	0.2	0.2	0.2
C_5^+ liquid product	98.6	97.8	98.0
Liquid yield (vol.%)	100.0	99.8	99.3
Simulated distillation of total liquid product			
Volatility, wt%	52.0	52.6	53.9
IBP, K	418	416	417
IBP-477 K, wt%	1.6	1.9	1.6
477-617 K, wt%	11.9	11.9	12.6
617-811 K, wt%	38.5	38.8	39.7
>811 K, wt%	48.0	47.4	46.1

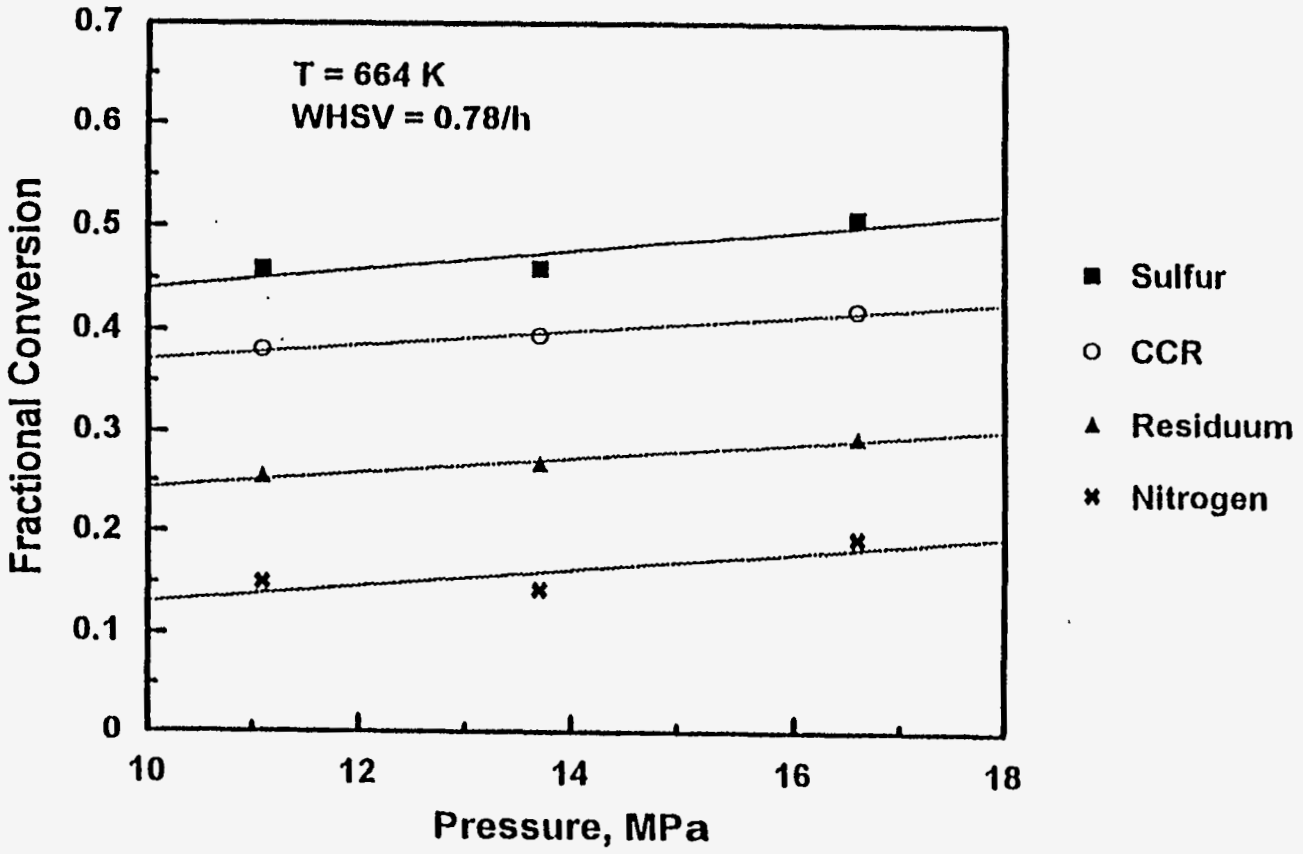

Figure 211. Fractional conversions of residuum, nitrogen, sulfur and CCR vs reactor pressure.

increases in cracking. Based on pure compound studies hydrogen pressure should be more important for heteroatom and CCR conversions than it is for residuum conversion. However, since heteroatoms and CCR in high molecular weight moieties are unreactive (247) residuum cracking may be the rate limiting step for a substantial portion of the removal of heteroatoms in PR Spring bitumen (248). In this situation, heteroatoms and CCR removal would not be substantially affected by hydrogen pressure.

SUMMARY AND CONCLUSIONS

Sulfur compounds were substantially converted with increasing temperature and contact time over the commercial HDM catalyst whereas the nitrogen removal remained low over the entire range of temperature and space velocities. Nickel removal was increased significantly with increasing contact time. Residuum conversion and nickel removal increased significantly with increasing temperature. The yield of distillate, naphtha and gas oil increased rapidly at higher temperatures because thermal cracking of residuum increased. The yield of gas oil, distillate and naphtha rapidly increased with decreasing WHSV. There was an initial rapid decrease of residuum yield at lower reciprocal WHSV. This was attributed to the conversion of residuum to volatile products. It is expected that the main reaction of residuum conversion is cracking of paraffinic side chains.

The effect of reactor pressure was minimal on nitrogen and sulfur removal and CCR and residuum conversion. The influence of reactor pressure on the product distribution and yields was also small. The catalyst deactivation was about 0.02°API/day during the hydrotreating.

UINTA BASIN BITUMEN HYDROTREATING: CATALYTIC UPGRADING OF THE PR SPRING BITUMEN OVER A COMMERCIAL HDN CATALYST

Principal Investigator: F.V. Hanson
Post Doctoral Fellow: D.C. Longstaff
Graduate Student: J. Kim

INTRODUCTION

As the worldwide supply of light crude oil decreased, more attention has been paid to the refining of heavy oils (including bitumens) and residuums into lighter and more valuable liquid products. The heavy oils and residuums contain high concentrations of sulfur, nitrogen and metals (238). Sulfur and nitrogen are sources of air pollution during combustion and play a significant role in poisoning of reforming and cracking catalysts (249). Minute amounts of metal elements can severely affect the activity of cracking catalysts (65). Therefore, the removal of heteroatoms and metals from heavy oils is an important goal in hydrotreating.

The feed oil sand used in this investigation was obtained from the PR Spring U-Tar pit deposit which is located in SE 1/4 NE 1/4, Section 5, Township 16 South, Range 24 East in eastern Utah. The oil sand ore was mined, crushed and sized to yield the desired distribution of oil sand particles (0.6 cm) for solvent extraction. The bitumen ecxtracted from the PR Spring oil sand was used in this study and has high nitrogen and low sulfur contents.

A NiMo on alumina hydrodenitrogenation catalyst was employed to hydrotreat this oil because NiMo on alumina is more effective for removing high concentrations of nitrogen than CoMo on alumina (244). Several researchers have reported that metal sulfides on low-acidity supports catalyze residuum conversion (239,250). Mild hydrocracking (MHC) is defined as the conversion of residuum from heavy oils into gas oil, distillate, naphtha, and gases and can be achieved under the process conditions utilized in this study (250).

The objective of this study was to determine the effect of process variables on heteroatom and metal removal and on Conradson carbon residue and residuum conversions. The process variables investigated were reactor temperature and space velocity at fixed reactor pressure (13.7 MPa).

EXPERIMENTAL

Feedstocks used in this study were the bitumen-derived heavy oils produced from the PR Spring oil sand by continuous reflux extraction with toluene . The toluene in the bitumen-toluene solution was removed by rotary evaporation followed by batch vacuum distillation. The physical and chemical properties of the bitumen-derived heavy oils used in this study are presented in Table 68.

The reactor system was constructed so that the hydrogen and oil were delivered to the packed constrained catalyst bed in an upflow mode to insure efficient contacting of the oil with the catalyst (241, 242). The liquid and gas products from the reactor were separated in a high pressure vapor-liquid separator. The gas product was removed from the separator through a back pressure regulating valve (BPRV) which controlled the system pressure. The liquid product was removed from the separator through a control valve (Annin valve).

The reactor had three different zones: the preheating zone, the catalyst bed zone, and the post heating zone. The catalyst zone was located in the central 30.5 cm of the reactor. 152 cm^3 of catalyst was loaded in the catalyst zone. Inert α-alumina spheres (0.32 cm) were placed in the preheating and post heating zones to support the catalyst bed, and to insure efficient distribution of the liquid and hydrogen. The preheating and the post heating zones volumes were 128.3 and 126.7 cm^3, respectively. The reactor was heated by a three zone electrical furnace. The temperatures in the catalyst zone were measured by a traveling thermocouple located within an axial thermowell (0.32 cm O.D.). The reactor operated in the upflow mode to minimize thermal gradients in the catalyst bed and to ensure complete wetting of the catalyst. A detailed schematic of the reactor system is

Table 68: Physical and chemical properties of PR Spring bitumen-derived heavy oil

API Gravity, °API	9.2
Conradson Carbon Residue, wt%	16.0
Specific Gravity	1.005
Pour Point, K	333
Asphaltenes[a], wt%	18.1
Elemental Analysis	
C, wt%	85.9
H, wt%	10.9
N, wt%	1.06
S, wt%	0.43
Ni, ppm	72
V, ppm	17
As, ppm	< 4
H/C Atomic Ratio	1.5
Simulated Distillation	
Volatility, wt%	37.4
C_5 - 477 K, wt%	0.1
477 - 617 K, wt%	6.2
617 - 811 K, wt%	31.1
>811 K, wt%	62.6
IBP, K	514

[a] Pentane-insolubles

presented in Figure 212.

A commercial $NiMo/Al_2O_3$ hydrodenitrogenation (HDN) catalyst was placed in the catalyst bed (152 cm^3) of the reactor. The HDN catalyst consisted of 1.3 mm trilobe shaped extrudates and contained 3.8 wt% NiO, and 19.5 wt% MoO_3. The catalyst had 155 m^2/g of surface area, and 0.47 cc/g of pore volume (water porosimeter).

The catalyst was dried in-situ in flowing nitrogen at 700 K for one hour and was cooled to ambient temperature prior to sulfiding. The catalyst sulfiding was conducted with a 2 wt% sulfur solution as dimethyldisulfide in kerosene. The reactor was heated to 505 K at the rate of 28 °C/h in flowing hydrogen. The hydrogen-to-liquid feed ratio was 890 m^3 (STP)/m^3. The reactor pressure and the sulfiding solution feed rate were 6.1 - 6.3 MPa and 1 h^{-1} LHSV, respectively. The reactor temperature was held at 505 K for 2 hours. The reactor was then heated to 645 K at the rate of 28 °C/h. Sulfiding was completed when the catalyst zone temperature reached 645 K.

The catalyst deactivation rate was estimated by measuring the API gravity of the total liquid product at the base case conditions which were 642 K, 0.41 h^{-1} LHSV and 13.7 MPa. After the catalyst had reached pseudo-steady activity (TOS=106 hrs), experiments were conducted by varying the reactor temperature (625 - 685 K) and LHSV (0.14 - 0.80 h^{-1}) at fixed pressure (13.7 MPa). Experiments were performed in a cyclic mode (base case condition-operating condition-base case condition) to determine the extent of catalyst deactivation that occurred during each run conducted at different operating conditions. The API gravity of the total liquid product produced at base case conditions with respect to TOS (time on stream) is presented in Figure 213.

RESULTS AND DISCUSSION

The primary process variables studied were temperature and liquid hourly space velocity (LHSV). Pressure was fixed in all experiments at 13.7 MPa. Reactor operating conditions were

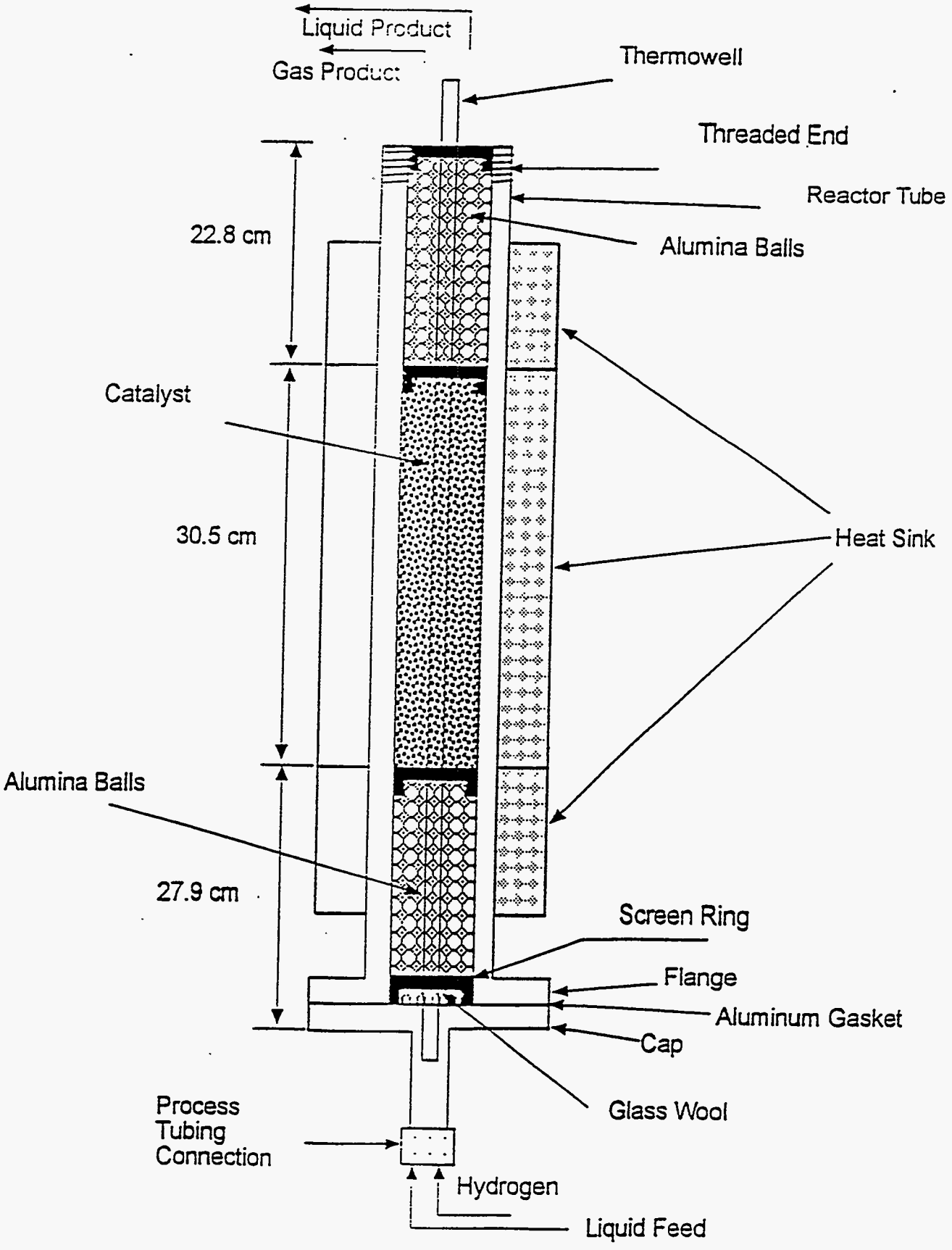

Figure 212. Schematic of Reactor.

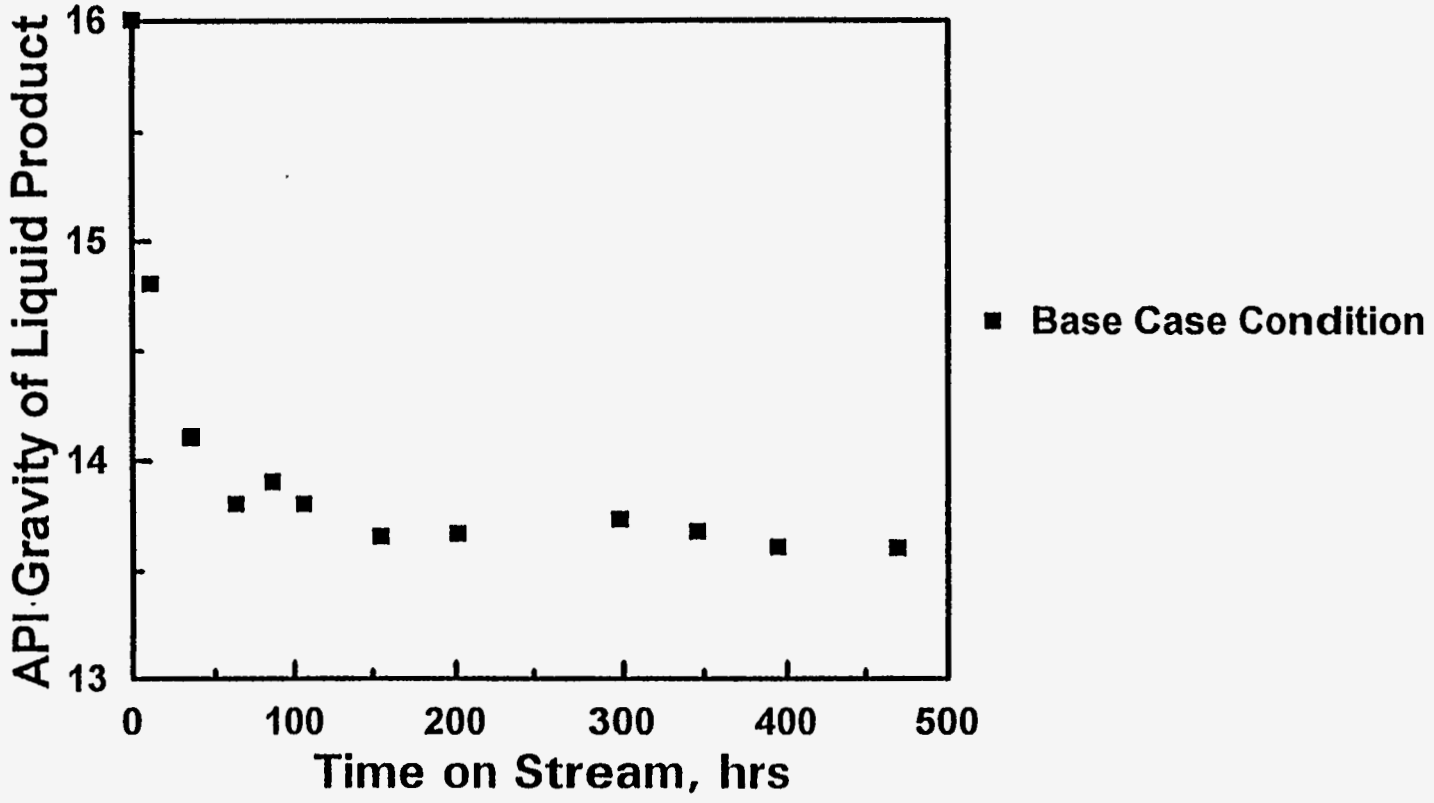

Figure 213. The API Gravity of Liquid Product with Respect to TOS.

selected so that only one of the three process variables was changed while the remaining two variables were kept constant. For example, temperature was varied while pressure and LHSV were kept constant and LHSV was varied while temperature and pressure were kept constant. The range of process operating conditions over which each variable was changed is summarized as a function of TOS (time on-stream) in Table 69.

Effect of LHSV.

Temperature and pressure were fixed at 664 K and 13.7 MPa respectively, to study the effect of LHSV. The effects of LHSV on product distribution and yields and on nitrogen, sulfur and nickel removals and on CCR and residuum conversions are presented in Table 70.

The API gravity of the total liquid products increased significantly from 13.3 °API to 25.5 °API as the residence time (reciprocal LHSV) increased. Hydrogen consumption and the H/C atomic ratio of the total liquid products also increased as the residence time increased.

The fractional conversions of residuum, nitrogen and sulfur are presented in Figure 214 with respect to reciprocal LHSV. The fractional conversions of nickel and CCR are displayed in Figure 215 as a function of reciprocal LHSV. The degree of nitrogen, sulfur and nickel removal and of CCR and residuum conversion was significant as reciprocal LHSV increased from 1.25 to 7.14 h.

It can be seen from Figure 214 that sulfur in the PR Spring heavy oil exhibited a broader range of reactivities than nitrogen. The nitrogen and sulfur lumps in the PR Spring heavy oil consist of a large number of moieties which exhibit a range of reactivities (251, 252). At short contact times, sulfur removal was greater than nitrogen removal This indicates that the most reactive portion of the sulfur lump is more reactive than the most reactive portion of the nitrogen lump. This is in agreement with Ho (244)who reported that nitrogen compounds are less reactive than sulfur compounds.

At long contact times, sulfur conversion was lower than nitrogen conversion. This indicates

Table 69: The process operating conditions employed in this study

Run Number	LHSV (h^{-1})	Temperature (K)	Pressure (MPa)	TOS[b] (h)
HDN-5	0.41	642	13.7	106
HDN-6	0.41	685	13.7	130
HDN-7	0.41	642	13.7	155
HDN-8	0.41	664	13.7	178
HDN-9	0.41	642	13.7	201
HDN-10	0.14	664	13.7	264
HDN-11	0.41	642	13.7	298
HDN-12	0.80	666	13.7	322
HDN-13	0.41	642	13.7	346
HDN-14	0.41	625	13.7	370
HDN-15	0.41	642	13.7	394
HDN-16	0.26	664	13.7	446
HDN-17	0.41	642	13.7	470

[b]Time On-Stream

Table 70: Effect of LHSV on product properties of the hydrotreated PR Spring bitumen-derived heavy oils

Run number	12	8	16	10
Process operating conditions				
Temperature, K	666	664	664	664
LHSV, h^{-1}	0.80	0.41	0.26	0.14
Residence time, h	1.25	2.44	3.85	7.14
Pressure, MPa	13.7	13.7	13.7	13.7
API gravity, °API	13.3	16.7	18.4	25.5
Specific gravity	0.977	0.955	0.944	0.901
H_2 consumption(l/l)	58	105	95	155
CCR, wt%	9.8	7.5	6.6	5.4
Elemental analysis				
C, wt%	85.9	86.0	86.2	86.5
H, wt%	11.8	12.1	12.4	12.6
N, wt%	0.64	0.46	0.34	0.18
S, wt%	0.23	0.18	0.16	0.14
Nickel, ppm	27	20	19	14
H/C atomic ratio	1.64	1.68	1.72	1.74
Product yields, wt%				
C_1	0.5	0.4	0.9	1.0
C_2	0.3	0.2	0.4	0.5
C_3	0.3	0.3	0.5	0.8
i-butane	0.1	0.1	0.2	0.3
n-butane	0.2	0.3	0.4	0.6
C_5^+ liquid product	99.0	98.6	96.1	96.8
Liquid yield (vol.%)	100.4	101.7	101.0	104.2
Simulated distillation of total liquid product				
Volatility, wt%	55.3	62.1	69.3	83.7
IBP, K	409	405	402	399
IBP-477 K, wt%	1.7	2.5	3.5	7.2
477-617 K, wt%	12.4	15.5	19.6	24.8
617-811 K, wt%	41.2	44.1	46.2	51.7
>811 K, wt%	44.7	37.9	30.7	16.3

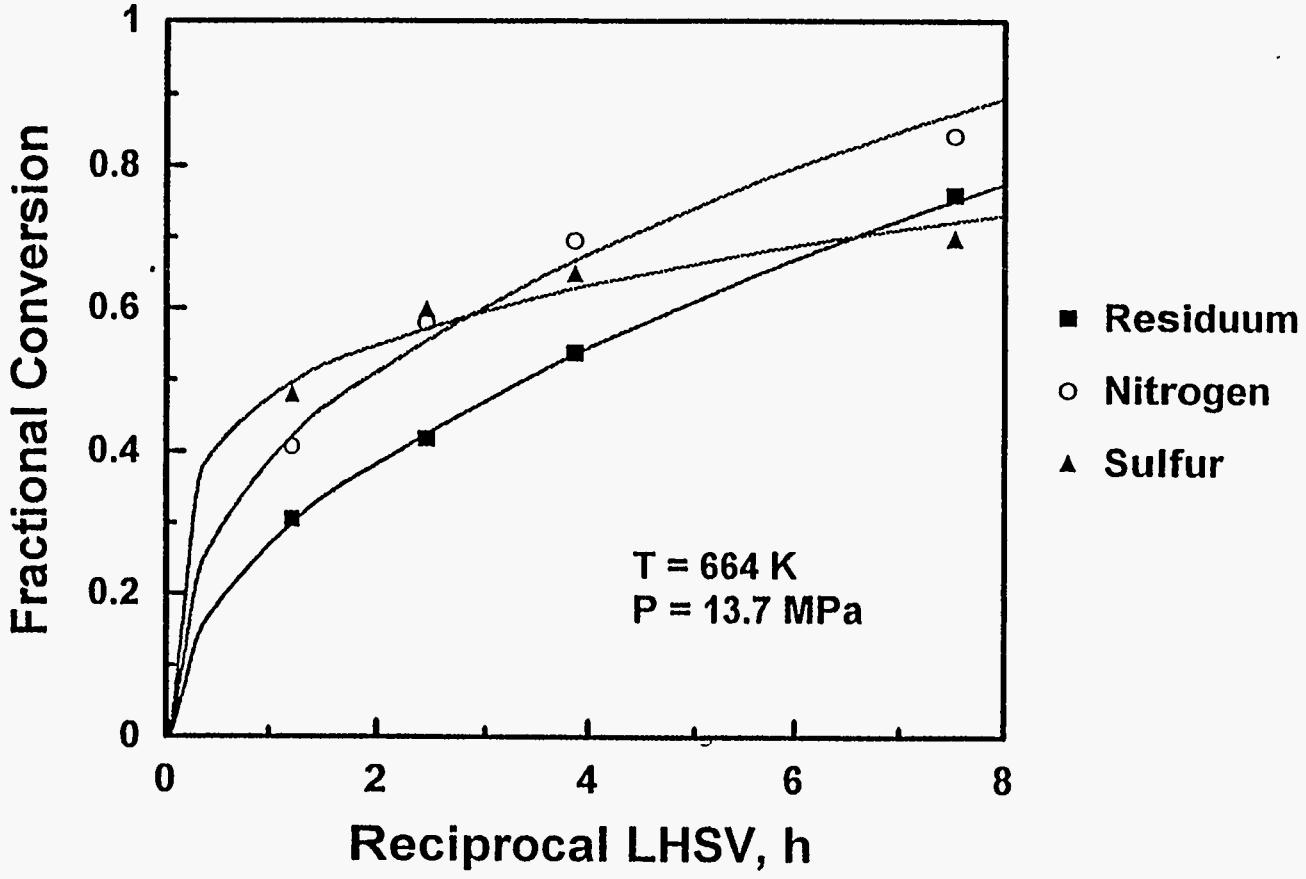

Figure 214. The Fractional Conversion of Residuum, Nitrogen and Sulfur versus Reciprocal LHSV.

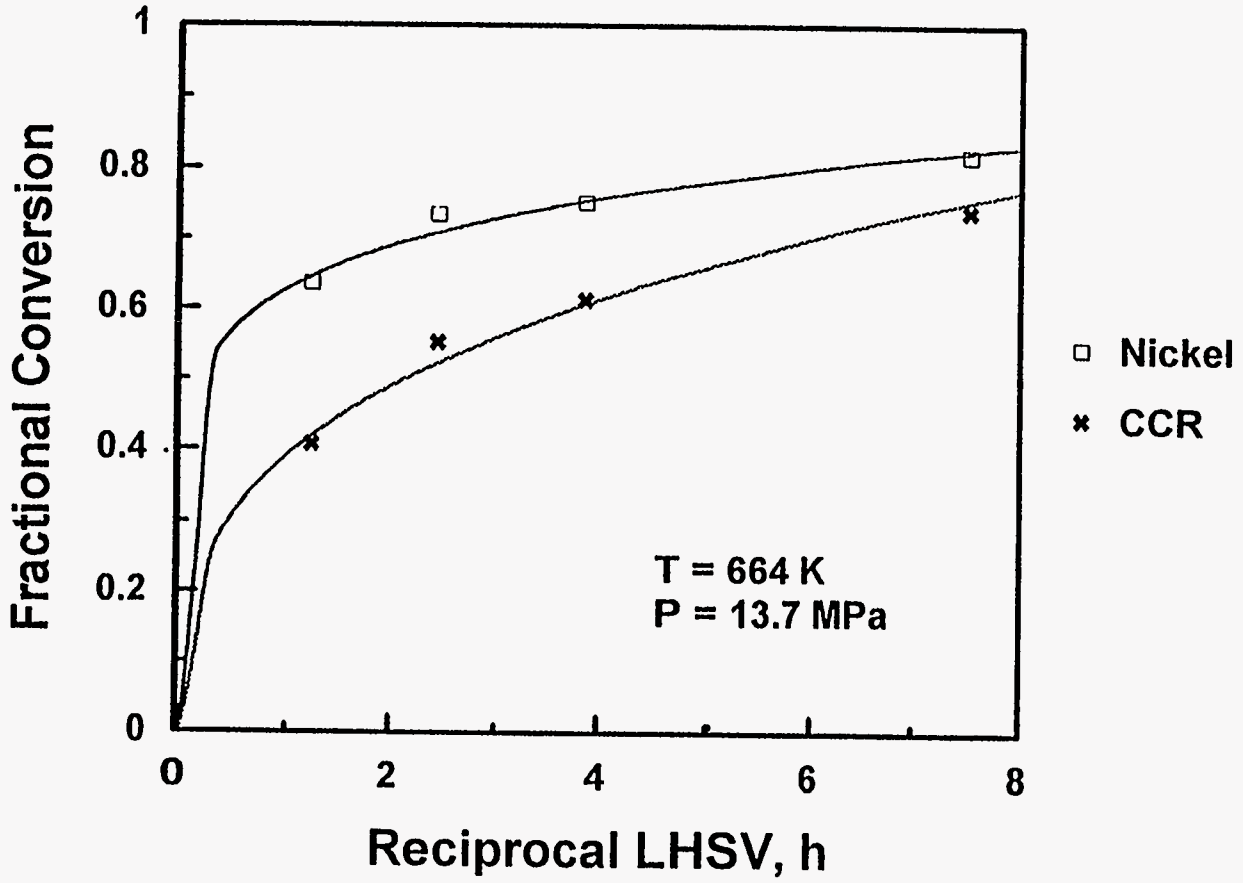

Figure 215. The Fractional Conversion of Nickel and CCR versus Reciprocal LHSV.

that the least reactive portion of the sulfur lump is even less reactive than the corresponding least reactive portion of the nitrogen lump.

Sulfur exhibits a wider range of reactivities than nitrogen, in that a certain portion of the sulfur is more reactive than the nitrogen. At the same time, some of the least reactive portion of the sulfur is less reactive than nitrogen.

The former case reflects the greater reactivity of low molecular weight sulfur compounds relative to low molecular weight nitrogen compounds. The fact that some of the sulfur is less reactive than the nitrogen suggests that sulfur may be concentrated in the higher molecular weight portions of the PR Spring heavy oil to a greater degree than nitrogen. Heteroatom reactivity is inversely proportional to the molecular weight of the oil (247, 253). Because of the relationship between molecular weight and heteroatom reactivity when sulfur is concentrated in the high molecular weight fractions to a greater degree than nitrogen, then some of the sulfur will be less reactive than the nitrogen.

63% nickel removal was achieved at 0.80 h^{-1} LHSV. Nitrogen, sulfur, CCR and residuum contents decreased by 40 %, 47 %, 39 % and 29 % at 0.80 h^{-1} LHSV; respectively, relative to the feed. The removal of nickel was greater than other components at short contact times. Apparently a significant portion of the nickel is present as reactive species which are rapidly converted at short contact times. However, the remaining nickel exhibits low reactivity because incremental increases in nickel removal were hard to achieve after the removal of the first 65-70 % of the nickel.

The simulated distillation data for the liquid products are presented in Table 70. The product yield distribution with respect to reciprocal LHSV is presented in Figure 216. The residuum fraction (> 811 K) conversion increased with increasing residence time and the yields of gas oil (617-811 K), distillate (477-617 K), naphtha (IBP-477) and C_1 - C_4 gases increased continuously. The yields of gas oil, distillate and naphtha exhibited an initial rapid increase at lower reciprocal LHSV. This is

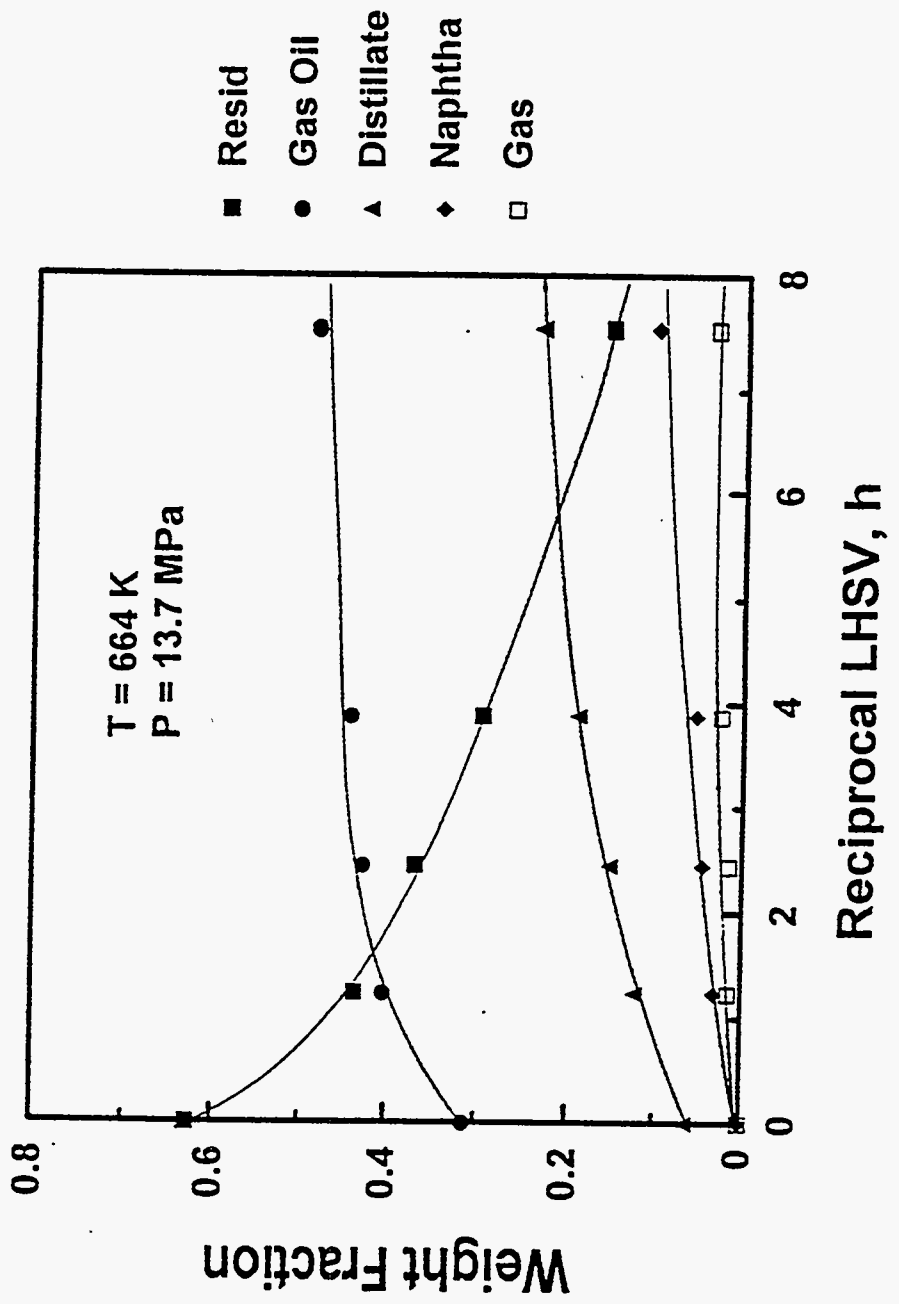

Figure 216. Effect of LHSV on Yield of Residuum, Gas Oil, Distillate, Naphtha, and Gases.

attributed to the rapid conversion of native residuum into volatile fractions. After the initial rapid increase of gas oil, a slow increase of gas oil yield was observed. This indicates that some portion of the gas oil produced from residuum conversion converted to lighter fractions at higher reciprocal LHSV (254).

Effect of Temperature

The influence of temperature was determined by varying the reactor temperature at fixed pressure (13.7 MPa) and liquid hourly space velocity (0.41 h^{-1}). The effects of temperature on product distribution and yields and on nitrogen, sulfur and nickel removals and on CCR and residuum conversions are presented in Table 71.

The increase in reaction temperature resulted in a significant increase in the API gravity of the total liquid product relative to the native bitumen. It also led to an increase in hydrogen consumption and in the H/C atomic ratio of the total liquid product.

The extents of nitrogen, sulfur and residuum removal with respect to temperature are presented in Figure 217. The fractional conversions of nickel and CCR are presented in Figure 218 with respect to temperature. Increasing temperature resulted in increased nitrogen, sulfur and nickel removals as well as increased CCR and residuum conversions over the HDN catalyst. The degree of sulfur removal was lower than residuum conversion and nitrogen removal at higher temperature. This again indicates that a certain portion of the sulfur exhibits a low reactivity. The degree of nitrogen and sulfur removal was higher than residuum conversion at low temperatures. The extent of nickel removal was greater than CCR conversion in all cases. Nickel removal was high at low temperatures and remained high throughout the temperature range.

A majority of nitrogen and sulfur moieties are distributed in the less reactive fractions such as resins and asphaltenes (239, 255, 256). Nitrogen removal was higher than residuum conversion within the entire range of temperature and indicated that the HDN catalyst exhibited more activity

Table 71: Effect of temperature on product properties of the hydrotreated PR Spring bitumen-derived heavy oils

Run number	6	8	11	14
Process operating conditions				
Temperature, K	625	642	664	685
LHSV, h^{-1}	0.41	0.41	0.41	0.41
Residence time, h	2.44	2.44	2.44	2.44
Pressure, MPa	13.7	13.7	13.7	13.7
API gravity, °API	12.4	13.7	16.7	22.1
Specific gravity	0.983	0.974	0.955	0.921
H_2 consumption(l/l)	89	94	105	121
CCR, wt%	5.3	7.5	9.5	11.0
Elemental analysis				
C, wt%	85.3	85.8	86.0	86.3
H, wt%	11.6	11.7	12.1	12.6
N, wt%	0.80	0.73	0.46	0.22
S, wt%	0.26	0.22	0.18	0.17
Nickel, ppm	29	25	20	18
H/C atomic ratio	1.74	1.68	1.63	1.63
Product yields, wt%				
C_1	0.3	0.3	0.4	1.2
C_2	0.2	0.2	0.2	0.7
C_3	0.2	0.2	0.3	1.0
i-butane	0.1	0.1	0.1	0.3
n-butane	0.1	0.1	0.3	0.8
C_5^+ liquid product	99.2	99.1	98.6	93.3
Liquid yield (vol.%)	100.5	101.0	101.7	99.6
Simulated distillation of total liquid product				
Volatility, wt%	48.0	52.8	62.1	80.9
IBP, K	470	413	405	399
IBP-477 K, wt%	0.7	1.5	2.5	8.0
477-617 K, wt%	9.1	10.7	15.5	26.5
617-811 K, wt%	38.2	40.6	44.1	46.4
>811 K, wt%	52.0	47.2	37.9	19.1

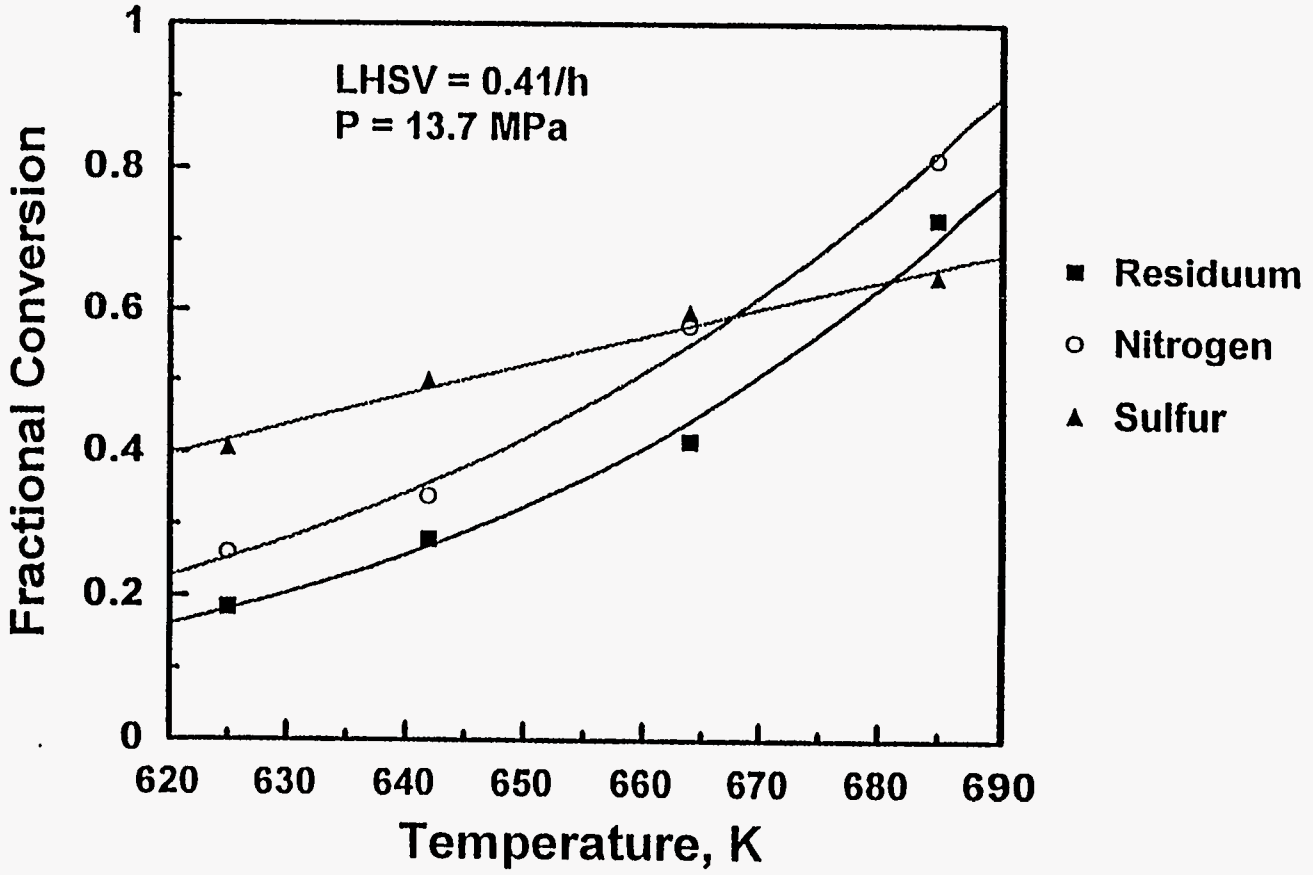

Figure 217. The Fractional Conversion of Residuum, Nitrogen and Sulfur versus Temperature.

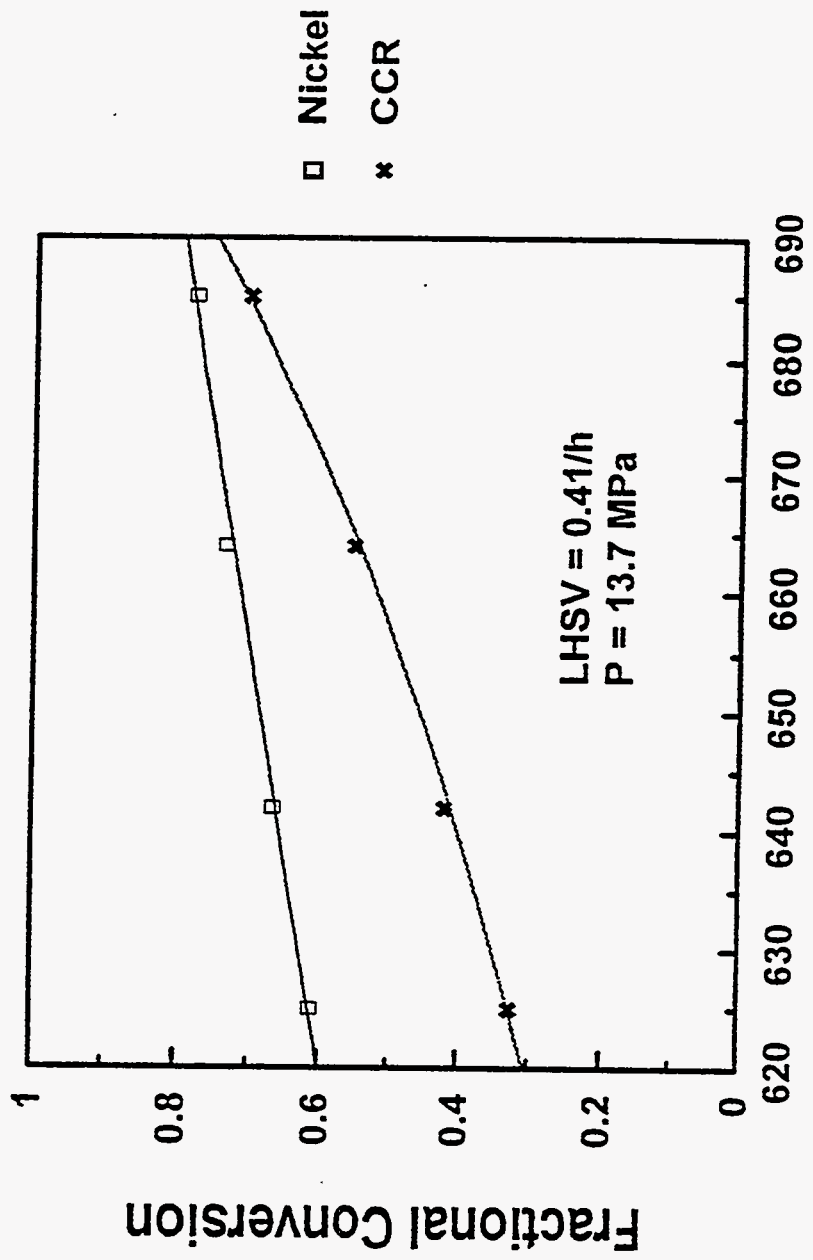

Figure 218. The Fractional Conversion of Nickel and CCR versus Temperature.

for nitrogen removal than it did for residuum conversion. Residuum conversion increased by 50% as the reaction temperature increased from 664 to 685 K. Nitrogen removal also increased by 52%. Sulfur, nickel and CCR contents decreased by 5%, 10% and 38%, respectively, over the same temperature range.

The simulated distribution data for the liquid products are presented in Table 71 with respect to temperature. The product yield distribution is presented in Figure 219 with respect to temperature. Residuum was significantly converted to volatiles at higher temperatures. The yield of distillate, naphtha and gas increased rapidly at higher temperatures. It is presumed that paraffinic side chains and paraffinic bridges exposed to acidic sites were rapidly cracked into volatile products and into lower molecular weight residuum at low temperatures. As temperature increased thermal conversion of residuum became more important (257). The yield of gas oil passed through a broad maximum at about 670 K, indicating that gas oil produced from residuum conversion underwent secondary cracking to yield lower molecular weight volatile products. This is in agreement with Mosby et al. (251) who proposed that gas oil produced from resid recracks to lighter products.

SUMMARY AND CONCLUSIONS

The degree of nitrogen removal substantially increased with increasing temperature at a fixed residence time and with increased residence time at a fixed temperature over the commercial HDN catalyst whereas sulfur removal increased uniformly. Nickel removal was high at mild conditions. Only modest increases in nickel removal were observed with increasing severity. Residuum rapidly converted into volatiles at low contact times. The degree of residuum conversion increased with increasing temperature because of increased thermal cracking of residuum. CCR was also reduced with increasing temperature and residence time.

Molecular weight reduction was significant during upgrading of bitumen-derived heavy oils.

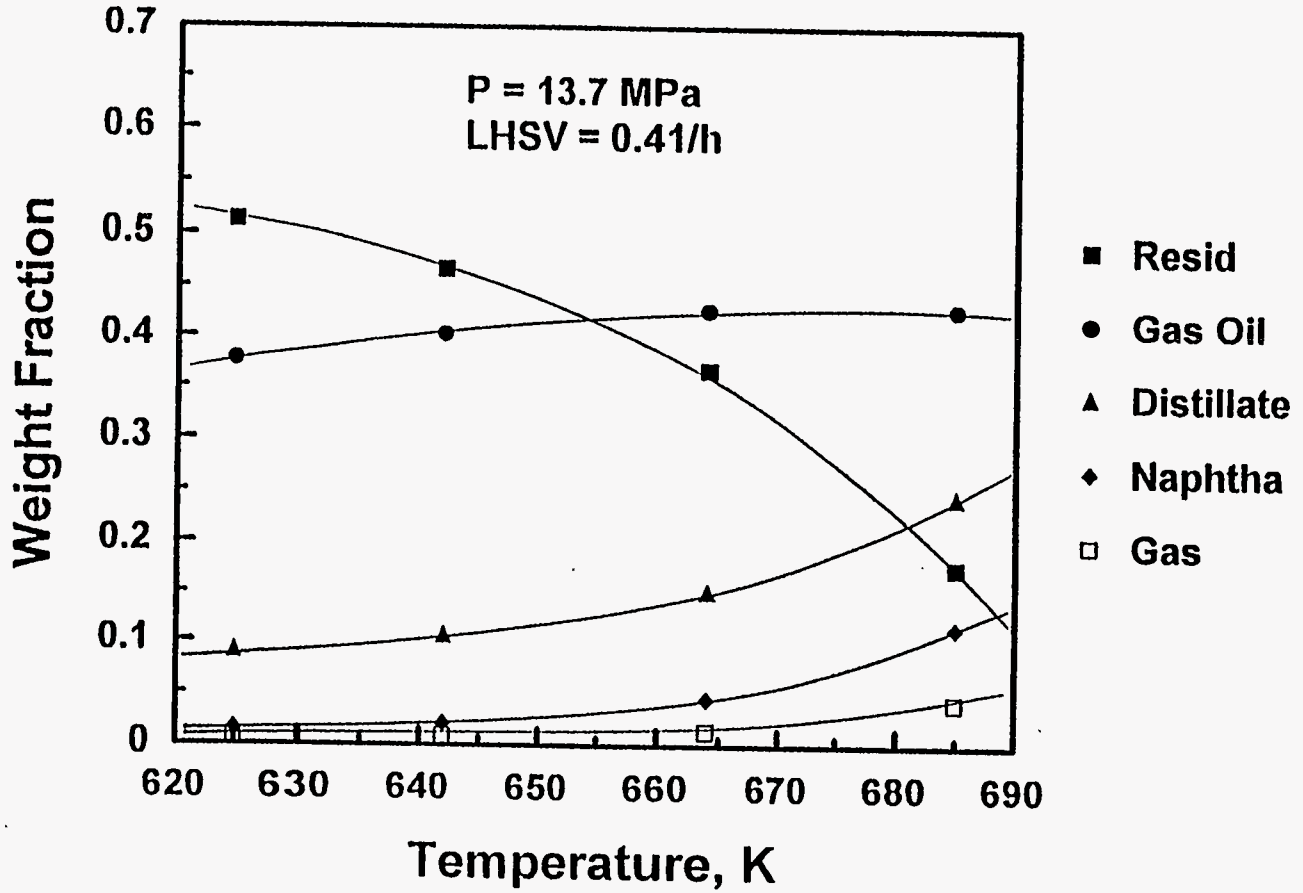

Figure 219. Effect of Temperature on Yield of Residuum, Gas Oil, Distillate, Naphtha, and Gases.

The yield of gas oil, distillate and naphtha rapidly increased at lower reciprocal LHSV. The yield of distillate, naphtha and light gases increased substantially at higher temperature because of increased thermal cracking.

UINTA BASIN BITUMEN HYDROTREATING: Thermal Conversion of PR Spring Bitumen-Derived Heavy Oil in the Presence of Na/Alumina

Principal Investigator:	Francis V. Hanson
Postdoctoral Fellow:	D.C. Longstaff
Graduate Student:	J. Kim

INTRODUCTION

Heavy oils and bitumens have low H/C atomic ratios and contain significant residuum fractions (>811 K) relative to conventional petroleum. The molecular weight and boiling range distributions of these heavy oils and bitumens must be reduced by hydrogen addition and/or carbon rejection before integration into refining feed states.

Mosby et al. (254) and Heck et al. (236) have reported that residuum conversion proceeds primarily via a thermal pathway and that catalysts used to hydrotreat heavy oils promote sulfur, nitrogen and metal removal and aromatics saturation. Several researchers (239, 258, 259) reported that light oil fractions are selectively formed during thermal cracking, even during catalytic hydroprocessing. Product distributions and yields and the chemical and physical property changes associated with the processing of the PR Spring bitumen-derived heavy oil over hydrodenitrogenation (HDN) and hydrodemetallation (HDM) catalysts have been reported (243). Reactions catalyzed by these HDN and HDM catalysts competed with noncatalytic thermal reactions which produced reactive free radicals by breaking C-C, C-H and C-heteroatom bonds (260). Thermal reactions have been reported to be more important than catalytic reactions at higher temperatures (261) due to the high activation energies for thermal cracking. However, the importance of thermal reactions can be most easily delineated in the absence of catalytic reactions.

A 2 wt% sodium-impregnated hydrodenitrogenation (HDN) catalyst support was used to investigate thermal reactions which occur during hydrotreating. The sodium-impregnated catalyst support was presumed to have little or no Brϕnsted acidity as indicated by the alpha test (262, 263) used to determine the degree of acidity. Mild hydrocracking (MHC); defined as the conversion of the residuum fraction of bitumen into distillate fractions, was achieved under the process conditions used in this study. Gas oil, distillate, naphtha, and gases were produced during mild hydrocracking of the bitumen-derived heavy oil.

The bitumen used in this investigation was extracted from the oil sands ore from the U-tar pit (SE 1/4 NE 1/4, Section 5, Township 16 South, Range 24 East) on the PR Spring oil sands deposit in the Uinta Basin of eastern Utah. The oil sand ore was mined, crushed and sieved to yield the desired distribution of sand particles ($< d_p$=0.64 cm) for solvent extraction.

The objective of this study was to determine the extent of thermal reactions in heteroatom and metal removal and Conradson carbon residue and residuum conversion as a function of process variables. The process variables investigated were reactor temperature (642-683 K) and space velocity (0.25-0.74 h^{-1}) at fixed reactor pressure (13.7 MPa).

EXPERIMENTAL

The hydrotreater feedstocks used in this study were the bitumen-derived heavy oils extracted from the PR Spring oil sands by refluxing with toluene in a Dean-Stark apparatus. The toluene/bitumen solutions were distilled in a rotary evaporator to concentrate the oil. The residual 6-8wt% toluene in the rotoevaporated solution was removed by vacuum batch distillation. Simulated distillation analyses indicated that the final heavy oil feedstock contained less than 0.1 wt% toluene. Selected physical and chemical properties of the bitumen-derived heavy oil used in this study are presented in Table 72.

Table 72
Physical and chemical properties of PR Spring Bitumen-derived heavy oil

API Gravity	9.2
Conradson Carbon Residue, wt%	16.0
Elemental Analysis	
C, wt%	85.9
H, wt%	10.9
N, wt%	1.06
S, wt%	0.43
Ni, ppm	72
H/C Atomic Ratio	1.51
Simulated Distillation	
Volatility, wt%	37.4
C_5 - 477 K, wt%	0.1
477 - 617 K, wt%	6.2
617 - 811 K, wt%	31.1
>811 K, wt%	62.6
IBP, K	514

in this study are presented in Table 72.

Thermal hydrocracking runs were conducted in a fixed-bed reactor which was operated in the upflow mode to maintain isothermal conditions and to ensure complete wetting of the catalyst support. The liquid and gas products from the reactor flowed into a high pressure vapor-liquid separator. The gas product was withdrawn from the separator through a back pressure regulating valve (BPRV) which also controlled the system pressure. The liquid product was removed from the separator through a liquid level control valve (Annin valve).

The reactor consisted of three distinct zones: the preheating zone, the catalyst bed zone, and the post heating zone. The reactor was independently heated by a three zone electrical furnace to facilitate isothermal operation of the catalyst zone. The catalyst zone consisted of 152 cm^3 of catalyst in the central 30.5 cm of the reactor. Inert α-alumina spheres (0.32 cm) were placed in the preheating and post heating zones to support the catalyst bed and to provide efficient liquid contacting with hydrogen. The temperatures in the catalyst zone were measured by a movable thermocouple in an axial thermowell. A schematic of the reactor system is presented in Figure 220.

Sodium-impregnated alumina was used to approximate the same reactor hydrodynamics as was obtained with the HDN catalyst. The alumina was impregnated with sodium to moderate its Brϕnsted acidity (264). Pines (264) has reported that alumina, containing 0.08 % K+ was significantly inhibited in its ability to skeletally isomerize cyclohexane which proceeds by a cationic mechanism (Brϕnsted acidity). Sodium-exchanged alumina is unreactive for skeletal isomerization of butenes at 811 K (265). The catalyst support consisted of 1.3 mm trilobe shaped alumina extrudates The catalyst support had a surface area of 255 m^2/g and a pore volume of 0.74 cc/g. The 2 wt% sodium-impregnated alumina was prepared by impregnating the catalyst

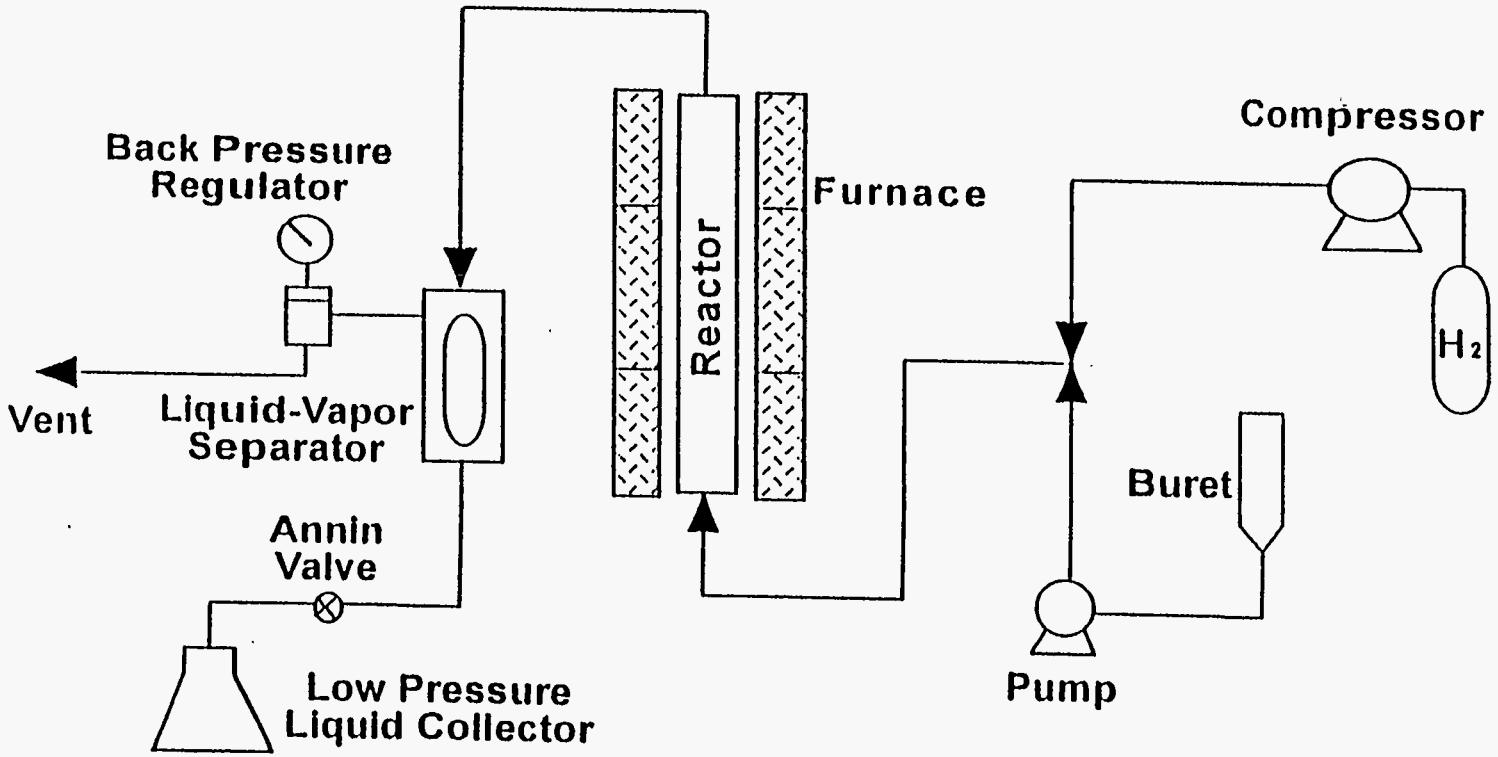

Figure 220. Schematic of the hydrotreater system.

activity was measured using the alpha test (263). The α-activity of a catalyst is a measure of its cracking activity relative to a standard silica-alumina catalyst (260, 261). The alpha numbers of the sodium-impregnated alumina catalyst support and the unimpregnated catalyst support were 0.3 and 0.8; respectively. The lower α-activity of the sodium-impregnated alumina relative to the unimpregnated alumina indicated that the sodium had been effective in eliminating the Brϕnsted acidity of the alumina.

The catalyst deactivation rate was estimated by monitoring the API gravity of the hydroprocessed liquid product with time at the base case conditions which were 642 K, 0.73 h^{-1} WHSV and 13.7 MPa. After the catalyst had reached a pseudo-steady state activity, experiments were conducted by varying the reactor temperature (642 - 683 K) and WHSV (0.25 - 0.74 h^{-1}) at fixed pressure (13.7 MPa). The experimental procedures have been described in detail elsewhere (264).

RESULTS AND DISCUSSION

Reactor operating conditions were selected so that only one of the two process variables was varied while the other variable was kept constant; i.e. temperature was varied while WHSV was kept constant and WHSV was varied while temperature was kept constant. The range of process operating conditions over which each variable was changed is summarized as a function of time-on-stream in Table 73.

Effect of WHSV

The effects of space velocity (WHSV) on nitrogen, sulfur and nickel removal and on CCR and residuum conversion were studied by varying the WHSV (0.25-0.74 h^{-1}) at a fixed temperature (664 K) and pressure (13.7 MPa) and are presented in Table 74.

The API gravity of the total liquid products increased from 11.7 EAPI to 13.7 EAPI as

Table 73
The process operating conditions employed in this study

Run Number	WHSV (h^{-1})	Temperature (K)	Pressure (MPa)	TOS[b] (h)
TH-4	0.73	642	13.7	48
TH-5	0.75	683	13.7	70
TH-6	0.73	642	13.7	93
TH-7	0.74	664	13.7	117
TH-8	0.73	642	13.7	142
TH-9	0.25	665	13.7	190
TH-10	0.73	642	13.7	250
TH-11	0.43	665	13.7	287
TH-12	0.73	664	13.7	314

[b] Time On Stream

Table 74
Effect of WHSV on product properties of the thermally cracked PR Spring bitumen-derived heavy oils

Run number	7	11	9
Process operating conditions			
Temperature, K	664	665	665
WHSV, h^{-1}	0.74	0.43	0.25
Residence time, h	2.42	4.15	7.22
Pressure, MPa	13.7	13.7	13.7
API gravity	11.7	12.3	13.7
Specific gravity	0.988	0.984	0.975
H_2 consumption(l/l)	23	45	55
CCR, wt%	11.9	11.4	10.3
Elemental analysis			
C, wt%	85.4	85.4	85.3
H, wt%	11.7	11.7	11.7
N, wt%	1.01	1.01	1.01
S, wt%	0.39	0.36	0.32
Nickel, ppm	63	53	46
H/C atomic ratio	1.64	1.64	1.64
Product yields, wt%			
C_1	0.3	0.4	0.6
C_2	0.1	0.2	0.3
C_3	0.1	0.2	0.4
$C_3^=$	0.0	0.1	0.1
i-butane	0.1	0.1	0.2
n-butane	0.1	0.1	0.3
$C_4^=$	0.1	0.1	0.2
C_5^+ liquid product	98.2	96.3	93.3
Liquid yield (vol %)	99.3	97.6	95.2
Simulated distillation of total liquid product			
Volatility, wt%	48.1	52.5	60.4
IBP, K	410	409	409
IBP-477 K, wt%	1.3	1.5	1.9
477-617 K, wt%	9.8	11.7	14.7
617-811 K, wt%	35.7	37.0	40.2
>811 K, wt%	53.2	49.8	43.2

WHSV decreased from 0.74 to 0.25 h^{-1}. This increase is low and is attributed to thermal reactions in the absence of a catalytically active species on the sodium-impregnated alumina. Higher increases in the API gravities have been observed at similar conditions in the presence of HDN catalysts [6,15]. Hydrogen consumption increased from 23 to 55 l/l as the WHSV decreased from 0.74 to 0.25 h^{-1}. This was not accompanied by an increase in the H/C ratio of the liquid product. Presumably this is due to the lack of a hydrogenation function on the sodium-impregnated alumina.

The fractional conversions of residuum, nitrogen and sulfur and of nickel and CCR are plotted with respect to reciprocal WHSV in Figures 221 and 222, respectively. The extent of nitrogen, sulfur and nickel removal and of CCR and residuum conversion increased as the WHSV decreased from 0.74 to 0.25 h^{-1}. The extent of residuum conversion over the sodium-impregnated catalyst support was greater in all cases relative to nitrogen and sulfur removal. This reflects the greater importance that thermal reaction pathways play in residuum conversion relative to heteroatom removal. The extent of nitrogen removal over the sodium-impregnated catalyst support was lower than that of all other classes of compound-types investigated (ie, sulfur, metals, CCR and residuum). CCR conversion exceeded residuum conversion and metal and heteroatom removal at all conditions. However, CCR conversion appears to have been approaching a limiting value, beyond which further CCR conversion would have been difficult to achieve.

Some researchers (236, 254, 258, 259) have reported that the presence of a catalyst does not affect residuum conversion and that residuum conversion occurs primarily via thermal reaction pathways. The fact that the sodium-impregnated catalyst support did not contain any impregnated, sulfided metals explains why residuum conversion was greater than nitrogen and sulfur removal. Sulfur removal, 26 wt%, occurred at 0.25 h^{-1} WHSV and 665 K. Khorasheh et al.(261) reported that the observed sulfur removal from bitumen-derived coker gas oil was accomplished due to

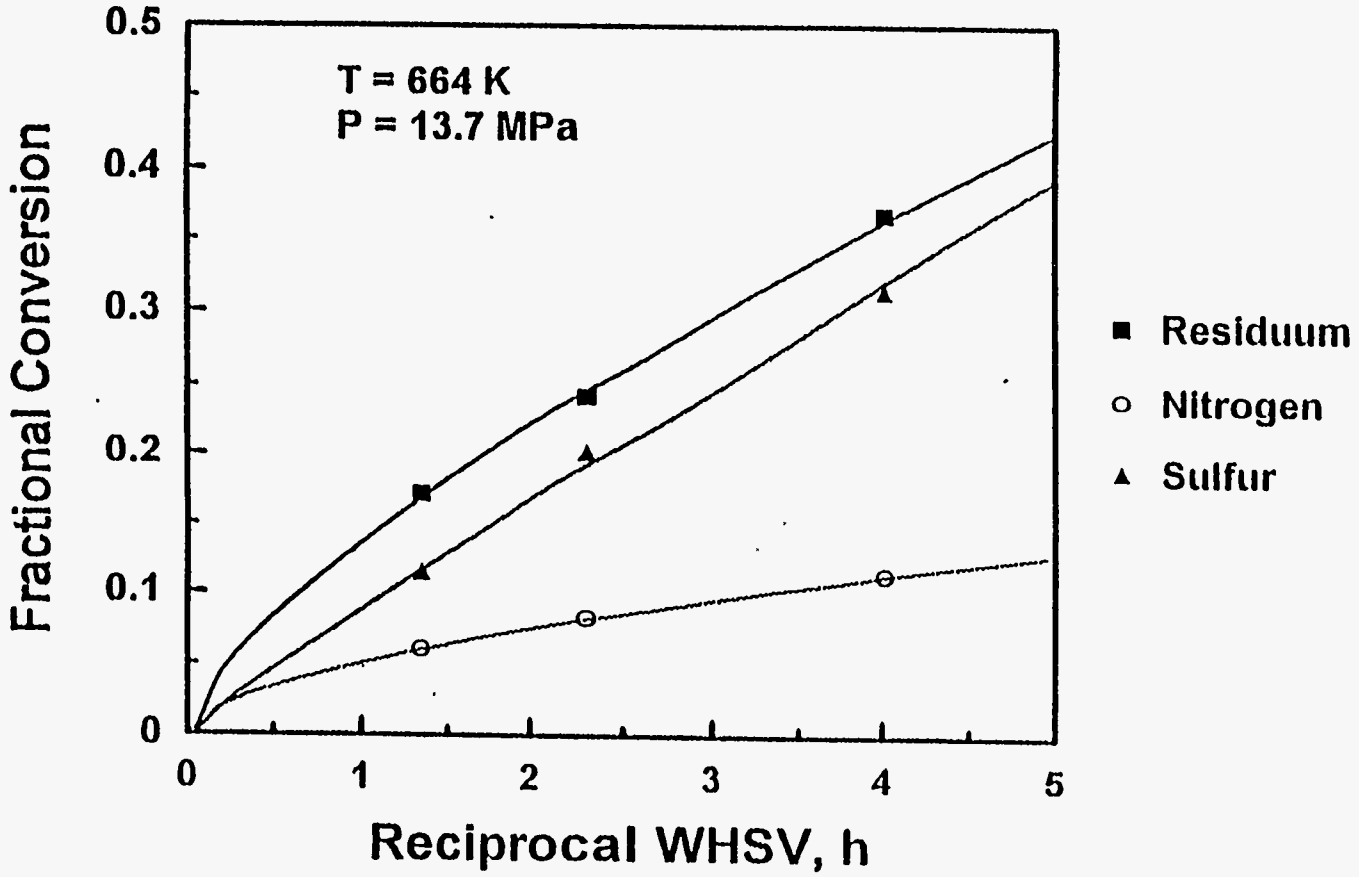

Figure 221. Fractional conversion of residuum, nitrogen and sulfur vs reciprocal WHSV.

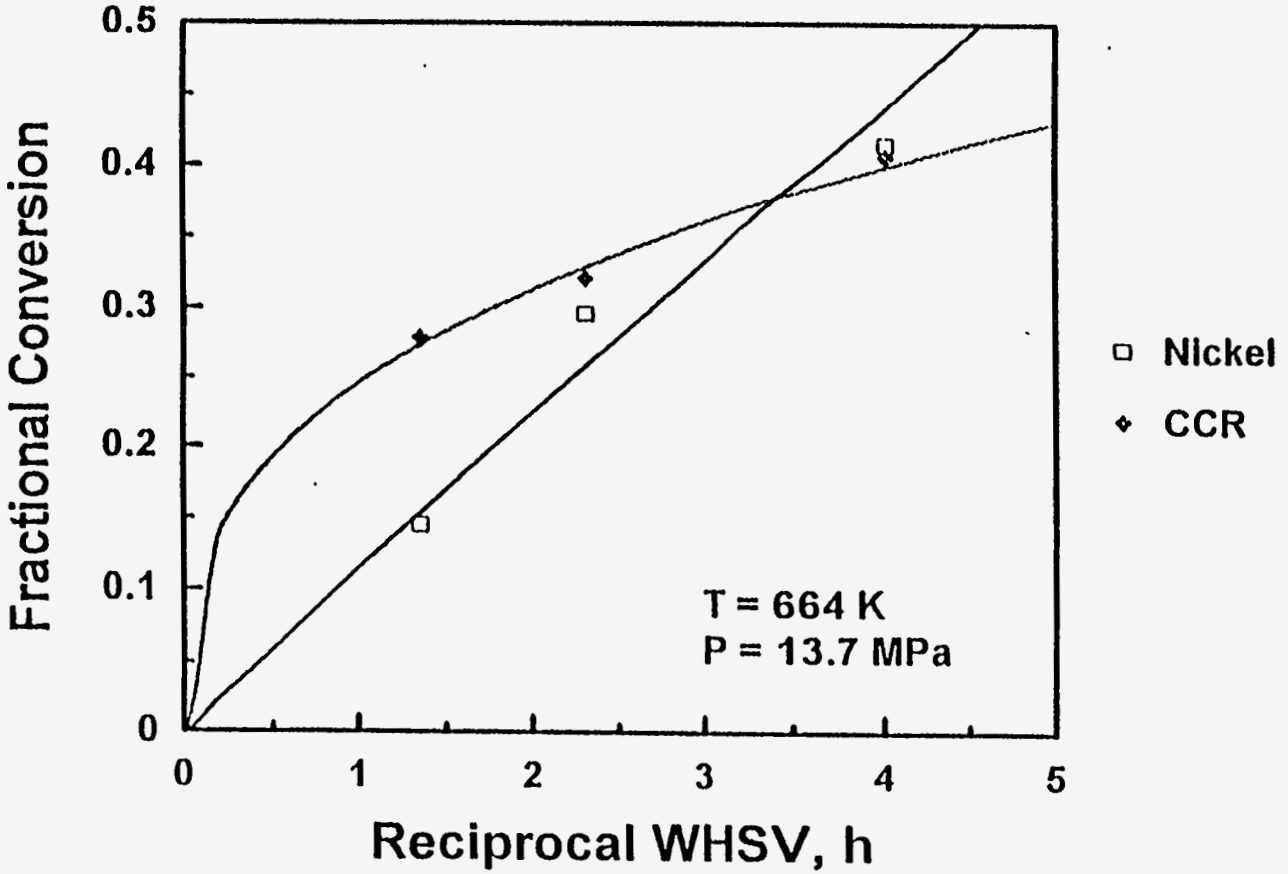

Figure 222. Fractional conversion of nickel and CCR vs reciprocal WHSV.

thermal reactions in the absence of either catalyst or catalyst support. Gray et al.(266)] also proposed that small amounts of sulfur compounds in vacuum residua may be converted by thermal reactions. Aliphatic and cyclic sulfides have been reported to be present in bitumens (267, 268) and may be present in the PR Spring bitumen-derived heavy oil. These saturated sulfides may undergo thermal C-S bond hydrogenolysis in the absence of hydrogenation and/or hydrogenolysis activity. The presence of species is inferred from the detection of saturated sulfur in Athabasca bitumens by Gray et al.(266, 267) and Asaoka, et al. (268) and the naphthenic nature of the Uinta Basin bitumens. Thus, the sulfur conversion was attributed to thermal conversion of saturated sulfur in PR Spring bitumen-derived heavy oil. Furthermore, some aromatic sulfur compounds may undergo direct C-S bond scission without aromatic ring hydrogenation (269).

The observed nitrogen conversion was unexpected because it is generally accepted that there is no aliphatic nitrogen in petroleum. Since the majority of sulfur and nitrogen in PR Spring bitumen-derived heavy oils is aromatic or bound to aromatic carbon, the absence of impregnated metal sulfides on the alumina severely limits the degree of nitrogen and sulfur removal. In contrast to nitrogen and sulfur removal it is expected that deep residuum conversion is possible by thermal reactions alone. Thermal conversion of residuum is so prominent that catalytic residuum conversion is difficult to observe even in the presence of a catalyst (236, 254). For that reason the absence of catalytically active metal sulfides affected nitrogen and sulfur removal to a greater degree than residuum conversion.

Although the sodium-impregnated alumina was not impregnated with metal components, some nickel removal (36 wt%) was detected at 0.25 h^{-1} WHSV and 665 K. This agreed with a previous report (270) that metal removal may occur under thermal hydroprocessing conditions. Takeuchi et al.(270) tested the catalytic activity of nickel and vanadium deposited on a metal-free alumina base. The activity for metal removal changed with the extent of metal deposition. The

activities of metal removal by deposited metals was small when the amount of deposited metals was small. The metal contents on the spent sodium-impregnated alumina at the conclusion of this study was not determined due to formation of carbonaceous deposits in the void spaces of the catalyst bed at the conclusion of the run. However, it can be estimated. Assuming an average metal removal of 30% and an average feed rate of 70 g/h it is presumed that 0.5g of metal would have deposited on the 80 g of sodium-impregnated alumina by the termination of this run (TOS=350h). It is presumed that the catalytic contribution of this level of nickel is insignificant compared to contributions from thermally induced reactions.

Simulated distillation data of the liquid products are presented in Table 74. The product distribution and yields with respect to reciprocal WHSV are presented in Figure 223. The residuum fraction (> 811 K) decreased with increasing residence time whereas the yields of gas oil (617-811 K), distillate (477-617 K), naphtha (IBP-477) and C_1 - C_4 gases increased continuously. It is presumed that the primary residuum conversion reaction is the cracking of paraffinic side chains which led to the reduction of the molecular weight and boiling range distributions..

Effect of Temperature

The effect of temperature on nitrogen, sulfur and nickel removal and on CCR and residuum conversion was investigated at a fixed pressure of 13.7 MPa and a WHSV of 0.74 h^{-1}. The effects of temperature on product distribution and yields, on nitrogen, sulfur and nickel removal and on CCR and residuum conversion are presented in Table 75.

The API gravity of the total liquid product increased from 10.6 to 13.0EAPI as the temperature increased from 642 to 683 K. The API gravity of the total liquid product collected during the material balance conducted at 642 K was 10.6: only 1.4EAPI above that of the feed. Increasing the temperature to 683 K yielded an oil with an API gravity of 13.0EAPI. The small

Table 75

Effect of temperature on product properties of the thermally cracked PR Spring bitumen-derived heavy oils

Run number	5	7	10
Process operating conditions			
Temperature, K	683	664	642
WHSV, h^{-1}	0.75	0.74	0.73
Residence time, h	2.40	2.42	2.46
Pressure, MPa	13.7	13.7	13.7
API gravity	13.0	11.7	10.6
Specific gravity	0.979	0.988	0.996
H_2 consumption(l/l)	56	23	12
CCR, wt%	10.4	11.9	13.2
Elemental analysis			
C, wt%	84.1	85.2	85.2
H, wt%	11.7	11.7	11.7
N, wt%	1.01	1.01	1.05
S, wt%	0.38	0.39	0.41
Nickel, ppm	62	63	66
H/C atomic ratio	1.64	1.64	1.63
Product yields, wt%			
C_1	0.5	0.3	0.1
C_2	0.2	0.1	0.0
C_3	0.3	0.1	0.0
$C_3^=$	0.1	0.0	0.0
i-butane	0.1	0.1	0.0
n-butane	0.1	0.1	0.0
$C_4^=$	0.1	0.1	0.0
C_5^+ liquid product	98.6	98.2	98.9
Liquid yield (vol %)	100	99.3	99.7
Simulated distillation of total liquid product			
Volatility, wt%	58.1	48.1	41.8
IBP, K	407	410	489
IBP-477 K, wt%	2.3	1.3	0.4
477-617 K, wt%	15.1	9.8	7.4
617-811 K, wt%	39.6	35.7	33.2
>811 K, wt%	43.0	53.2	59.0

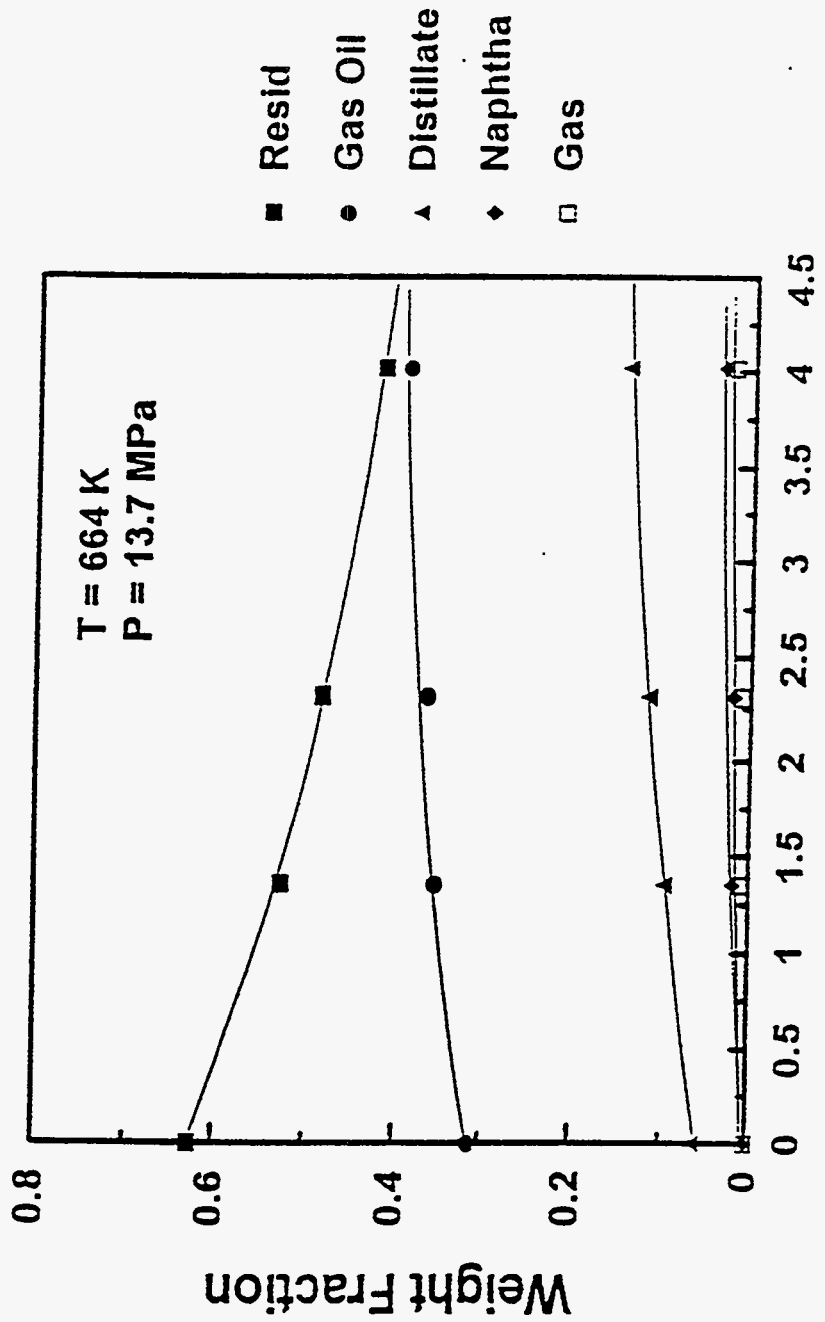

Figure 223. Effect of WHSV on yield of residuum, gas oil, distillate, naphtha and gases.

increase in the API gravity of the total liquid product relative to the PR Spring bitumen-derived heavy oil is indicative of the absence of any significant catalytic hydrogenation and cracking activity on the sodium-impregnated alumina and is attributed to thermal reactions which only become significant at higher temperatures.

The fractional conversions of nitrogen, sulfur and residuum and of nickel and CCR are presented in Figures 224 and 225; respectively, as a function of temperature. The extent of CCR conversion was greater in all cases than the extent of residuum conversion, and of sulfur, nickel and nitrogen removal. Residuum conversion was greater than nitrogen and sulfur removal as it was when WHSV was varied. Nitrogen removal was lower than the conversions of the other component-type classes.

The material in the bitumen-derived heavy oil which gives rise to CCR is thought to consist of polar, high molecular weight species which readily convert to coke during thermal processing (271). This class of components can be thought to consist of the polar, heteroatomic cores of residuum molecules which are denuded of aliphatic side chains during hydrotreating. It would be therefore expected that CCR conversion would be related to catalytic processes such as aromatic ring hydrogenation. Accordingly, in thermal processing, CCR reduction should be as difficult to achieve as nitrogen conversion. The opposite was observed in this research because in some instances, CCR conversion exceeded even residuum conversion. Thermal CCR conversion is counterintuitive because CCR is defined as the material that is not converted to volatiles in a test which strongly favors thermal conversion. Perhaps the thermal CCR conversion that was observed is related to the presence of hydrogen which stabilized free radical intermediates formed due to thermal cracking and which are precursors to carbonaceous residues. Thus, it was presumed that the observed CCR conversion was not purely thermal, but was a result of hydrothermal reactions.

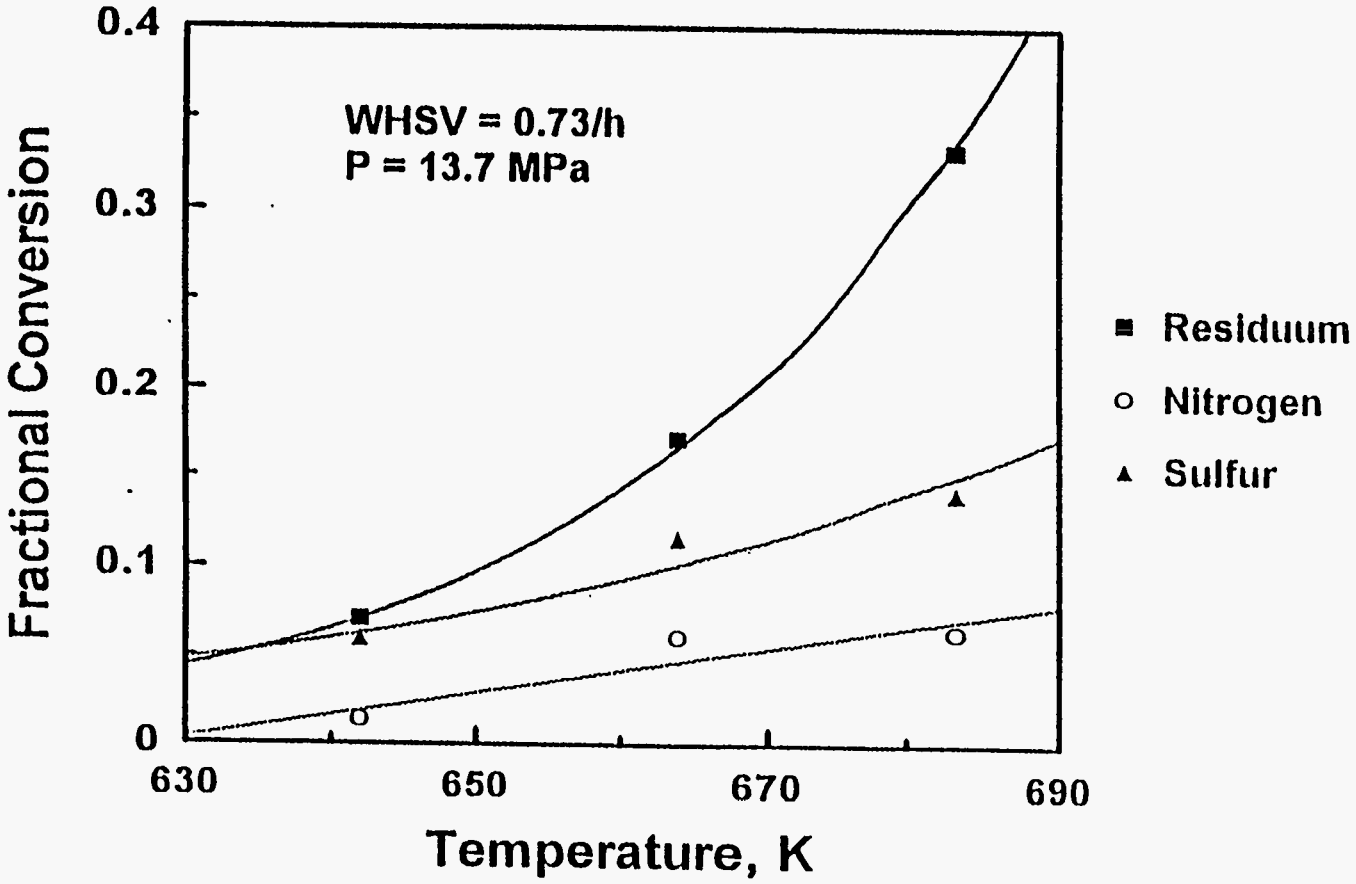

Figure 224. Fractional conversion of residuum, nitrogen and sulfur vs temperature.

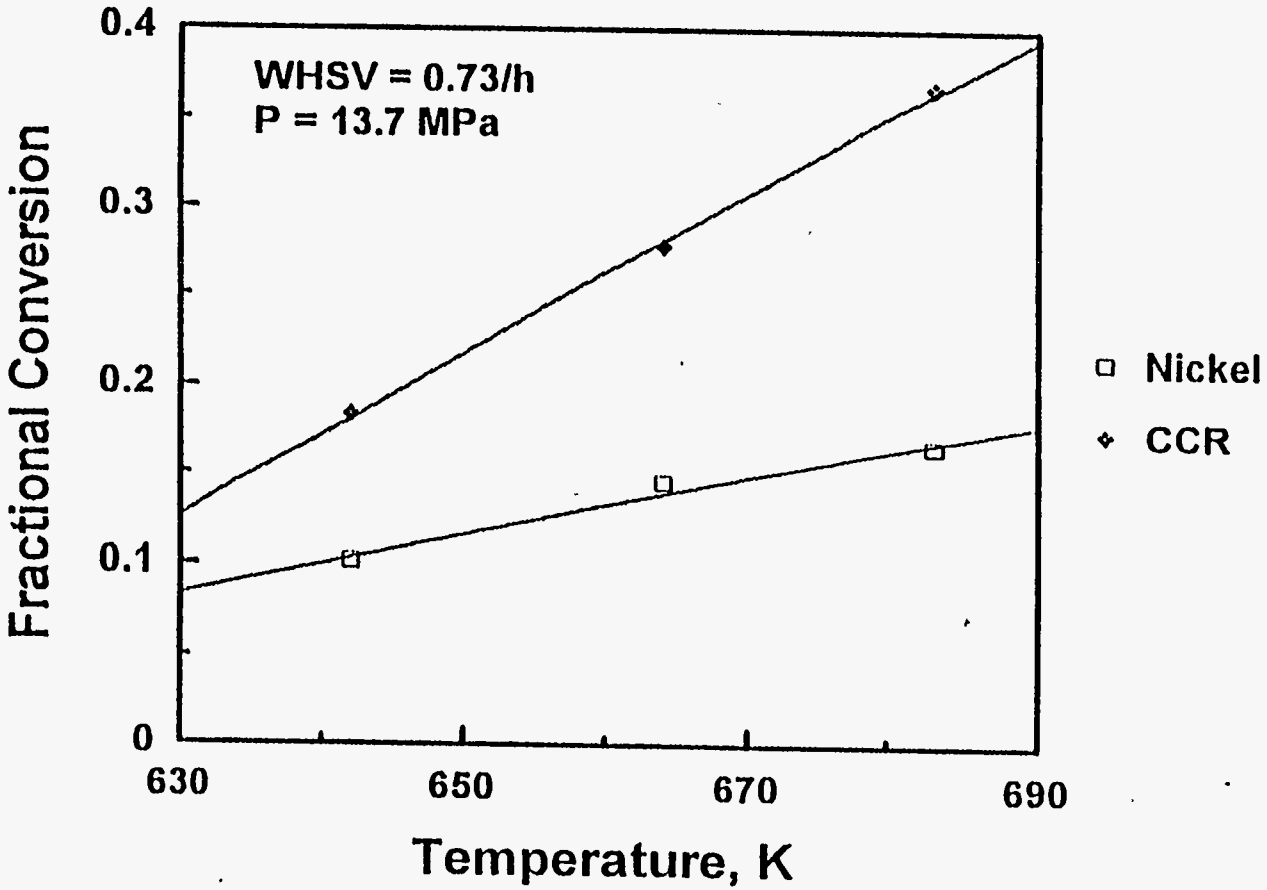

Figure 225. Fractional conversion of nickel and CCR vs temperature.

The residuum fraction of the total liquid product decreased by 19% as the reaction temperature increased from 664 to 683 K. The sulfur content decreased by 3%, nickel content decreased by 2%, the CCR content decreased by 13% and no nitrogen removal was observed when the reaction temperature increased from 664 K to 683 K. Residuum conversion was significant at higher temperatures. This is attributed to residuum being more susceptible to thermal conversion than nitrogen and sulfur removal.

Increasing contact time led to a much higher increase in CCR conversion than did increasing temperature. This is in contrast to nickel conversion which was affected equally by longer contact times and higher temperatures. This suggests that the apparent activation energy for thermal CCR conversion is low. However, the kinetic and molecular transformations of thermal and catalytic CCR conversion are not well understood. Consequently, the development of an explanation for this observation will require additional experiments. The simulated distribution data for the liquid products are presented in Table 75 and the product distributions and yields with respect to temperature are presented in Figure 226. Residuum conversion to volatiles was significant at higher temperatures. Gas oil, distillate, naphtha and gas yields increased rapidly at higher temperatures. The significant increase in residuum conversion with increasing temperature attributed to the high activation energies of thermal cracking.

SUMMARY AND CONCLUSIONS

Residuum conversion exceeded heteroatom removal over the sodium-impregnated alumina because residuum conversion involves a thermal pathway which is largely unavailable for heteroatom removal. CCR conversion was also higher than heteroatom removal indicating that CCR conversion can occur in the absence of a catalyst and is presumed to be related to thermal reactions occurring in the presence of hydrogen. The degree of conversion of CCR was

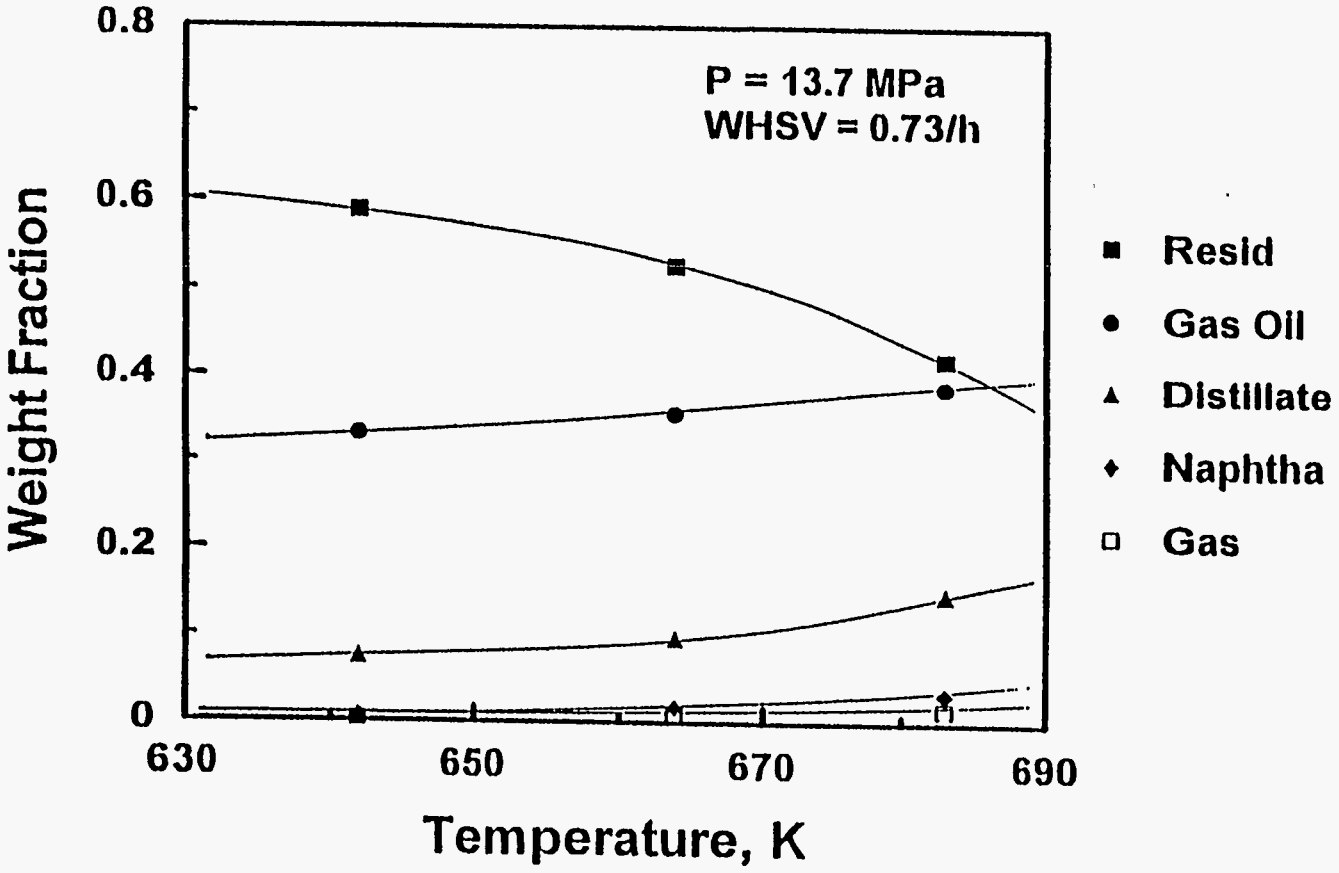

Figure 226. Effect of temperature on yield of residuum, gas oil, distillate, naphtha and gases.

substantially increased with increasing temperature and residence time. The extent of residuum conversion increased at higher temperatures because thermal cracking of residuum increased at higher temperatures.

Molecular weight reduction was observed during thermal hydrocracking of bitumen-derived heavy oils and was attributed to thermal reactions. The yield of gas oil, distillate, naphtha and light gases increased at higher temperatures due to the increase of thermal cracking of residuum at higher temperatures.

UINTA BASIN BITUMEN HYDROTREATING:
A Comparison of Catalytic and Thermal Effects during Hydrotreating of Bitumen-Derived Heavy Oils

Principal Investigator:	Francis V. Hanson
Post Doctoral Fellow:	Daniel C. Longstaff
Graduate Student:	J.-W. Kim

INTRODUCTION

The primary purpose of hydrotreating is to remove objectionable elements such as sulfur, nitrogen, oxygen and metals from the oil being hydrotreated. The catalysts used in hydrotreating also promote hydrogenation of aromatic carbon and conversion of residuum into volatile fractions. During hydrocracking the catalyst functions to supply hydrogen to oil fractions which are otherwise deficient in hydrogen (258). Catalytic reactions may compete and/or be coupled with noncatalytic thermal reactions which produce reactive free radicals by breaking C-C, C-H and C-heteroatom bonds (239, 272). Thermal reactions have higher activation energies than catalytic reactions for a given class of compounds.

Thermal reactions become more important with increasing temperature (273). Thermal and catalytic reactions occur in parallel in the conversion of asphaltenes and coal (274, 275). It has been reported that light oil fractions are formed exclusively by thermal cracking in the oil phase, even during catalytic hydroprocessing (239). Mosby et al. (254) and Heck et al. (254) have reported that residuum conversion is primarily thermal and that heavy oil hydrotreating catalysts promoted sulfur, nitrogen and metal removal, as well as, aromatics saturation. Thermal cracking converts high molecular weight species to lower molecular weight species which are accessible to the active surface of the catalyst through the pores. Therefore, thermal and catalytic reactions act sequentially via thermal scission and hydrogenation.

The oil sands used in this investigation were obtained from the U-tar pit on the PR Spring oil sands deposit. The pit is located in SE 1/4 NE 1/4, Section 5, Township 16 South, Range 24 East in eastern Utah. The bitumen-derived heavy oil from the PR Spring oil sand used as the feedstock in this study is unusual in that it exhibits a high nitrogen content (>1 wt%) and a low sulfur content (<0.5 wt%). The catalysts used in these studies were commercial alumina supported metal sulfide catalysts. The catalyst series consisted of a NiMo (HDN) catalyst, a Mo (HDM) catalyst and a 2 wt% sodium-impregnated alumina.

The objective of this study was to determine the relative magnitudes of the catalytic and thermal reactions during the upgrading of the bitumen-derived heavy oil over the HDN and HDM catalysts and the sodium-impregnated alumina. This was evaluated by investigating the role of catalyst on heteroatom and metal removal and on CCR and residuum conversion as a function of process variables. The process variables investigated were reactor temperature (625-685 K) and space velocity (0.14-0.81 h^{-1}) at a fixed reactor pressure (13.7 MPa).

EXPERIMENTAL

The feedstock used in this study was the bitumen-derived heavy oil produced from the PR Spring oil sands. The physical and chemical properties of the feedstock are presented in Table 76. Properties of the catalysts are listed in Table 77. The HDN and HDM catalysts, as well as the sodium-impregnated alumina (Na/alumina) were presulfided in the reactor with 2 wt% sulfur as dimethyldisulfide in kerosene. The Na/alumina catalyst was prepared by impregnating a high surface area alumina with 2 wt% sodium nitrate. This was done to poison the Brϕnsted acidity of the alumina. Detailed procedures for the preparation of the Na/alumina and the catalyst sulfiding procedure have been described by Kim (243).

Hydrotreating runs were conducted in a fixed-bed reactor which was operated in the upflow mode to facilitate isothermal operation and to ensure complete wetting of the catalyst bed (242). The gas and liquid products from the reactor passed into the high pressure vapor-liquid separator. The gas product was removed from the separator through a back pressure

Table76: Physical and chemical properties of PR Spring bitumen-derived heavy oil

API Gravity, API	9.2
Conradson Carbon Residue, wt%	16.0
Asphaltenes[a], wt%	18.1
Elemental Analysis	
C, wt%	85.9
H, wt%	10.9
N, wt%	1.06
S, wt%	0.43
Ni, ppm	72
H/C Atomic Ratio	1.5
Simulated Distillation	
Volatility, wt%	37.4
C5 - 477 K, wt%	0.1
477 - 617 K, wt%	6.2
617 - 811 K, wt%	31.1
>811 K, wt%	62.6
IBP, K	514

a Pentane-insolubles

Table 77: Properties of the HDN and HDM catalysts and the sodium-impregnated alumina

HDN Catalyst	
NiO, wt%	3.8
MoO_3, wt%	19.5
Al_2O_3, wt%	76.7
Pore Volume, cc/g	0.47
Surface Area, m^2/g	155
1.3 mm trilobe extrudates	
HDM Catalyst	
MoO_3, wt%	6.0
Al_2O_3, wt%	94
Pore Volume, cc/g	0.85
Surface Area, m^2/g	130
1.6 mm trilobe extrudates	
Sodium Impregnated Alumina	
Na, wt%	2.0
Al_2O_3, wt%	98
Pore Volume, cc/g	0.74
Surface Area, m^2/g	255
1.3 mm trilobe extrudates	

regulating valve (BPRV) which vented the vapor from the high pressure vapor liquid separator to ambient pressure. The system pressure was controlled by the BPRV in that excess pressure was released as vapor through the BPRV. Liquid product was continually withdrawn from the separator through an Annin valve. The reactor tube consisted of a 2.54 cm inside diameter stainless steel tube which was mounted in a three zone furnace. The temperature in each zone of the furnace was independently controlled to segregate the reactor tube into three zones: a preheating zone, a catalyst bed zone and a post-reaction zone. The central reactor zone contained 152 cm^3 of catalyst. Inert low surface area α-alumina spheres (0.32 cm) were placed in the preheating (128 cm^3) and postheating (127 cm^3) zones to support the catalyst bed and to insure efficient contacting of the liquid feed and hydrogen. Temperature profiles in the reactor were measured with a movable thermocouple in an axial thermowell which had an outside diameter of 0.32 cm.

The API gravity of the hydrotreated liquid product was known to correlate with the nitrogen content of the liquid product. Therefore, the extent of catalyst deactivation during the process variable studies was estimated by measuring the API gravity of the hydrotreated liquid product as a function of time on-stream at the base case conditions. The base case conditions were as follows: reactor pressure, 13.7 MPa; liquid hourly space velocity (LHSV), 0.41 h^{-1}; and reactor temperature 642 K. At the beginning of each experiment the freshly sulfided catalyst was contacted with oil at the base case conditions until the catalyst attained a pseudo-steady state activity.

After the catalyst had reached pseudo-steady state activity, experiments were conducted in which the reactor temperature (625-685 K) and LHSV (0.14-0.81 h^{-1}) were varied at fixed reactor pressure (13.7 MPa). The experiments were conducted in a random fashion to circumvent systematic errors. Detailed experimental procedures have been described elsewhere by Kim (243).

RESULTS AND DISCUSSION

The performance of the HDN and the HDM catalysts and of the Na/alumina support were evaluated as a function of process variables to determine the relative magnitude of catalytic and thermal effects during nitrogen, sulfur and nickel removal and during CCR and residuum conversion at comparable operating conditions.

Residuum Conversion

The effects of residence time (reciprocal LHSV), temperature and catalyst selection on residuum conversion for the bitumen-derived heavy oil are presented in Figures 227 and 228. Catalyst activity for residuum conversion was ranked as follows: HDN catalyst > HDM catalyst > Na/alumina. This ranking obtained at all temperatures and space velocities.

Pines (264) has reported that alumina, containing 0.08 % K^+ was significantly inhibited in its ability to skeletally isomerize cyclohexane which proceeds by a cationic mechanism (Brϕnsted acidity). However, up to 40% residuum conversion was observed over the Na/alumina (Figures 227 and 228). This conversion was attributed to thermal reactions because the Na/alumina catalyst contained 2 wt% sodium. The residuum conversion over the Na/alumina provides a baseline to determine the effect of catalyst on residuum conversion over the HDN and HDM catalysts.

Higher levels of residuum conversion were observed with the HDN catalyst relative to the HDM catalyst and the Na/alumina. This is due to its higher metal loading and to its higher surface acidity relative to the HDM catalyst and the Na/alumina.

It was not possible in this work to differentiate between catalytic activity originating from the metal and catalytic activity originating from the alumina surface area. In some situations, such as nitrogen conversion, catalytic activity is probably strongly determined by the metal loading. However, in residuum conversion, the surface area and acidity of the alumina support may play a role that is approximately equivalent in importance to the role of the supported metals.

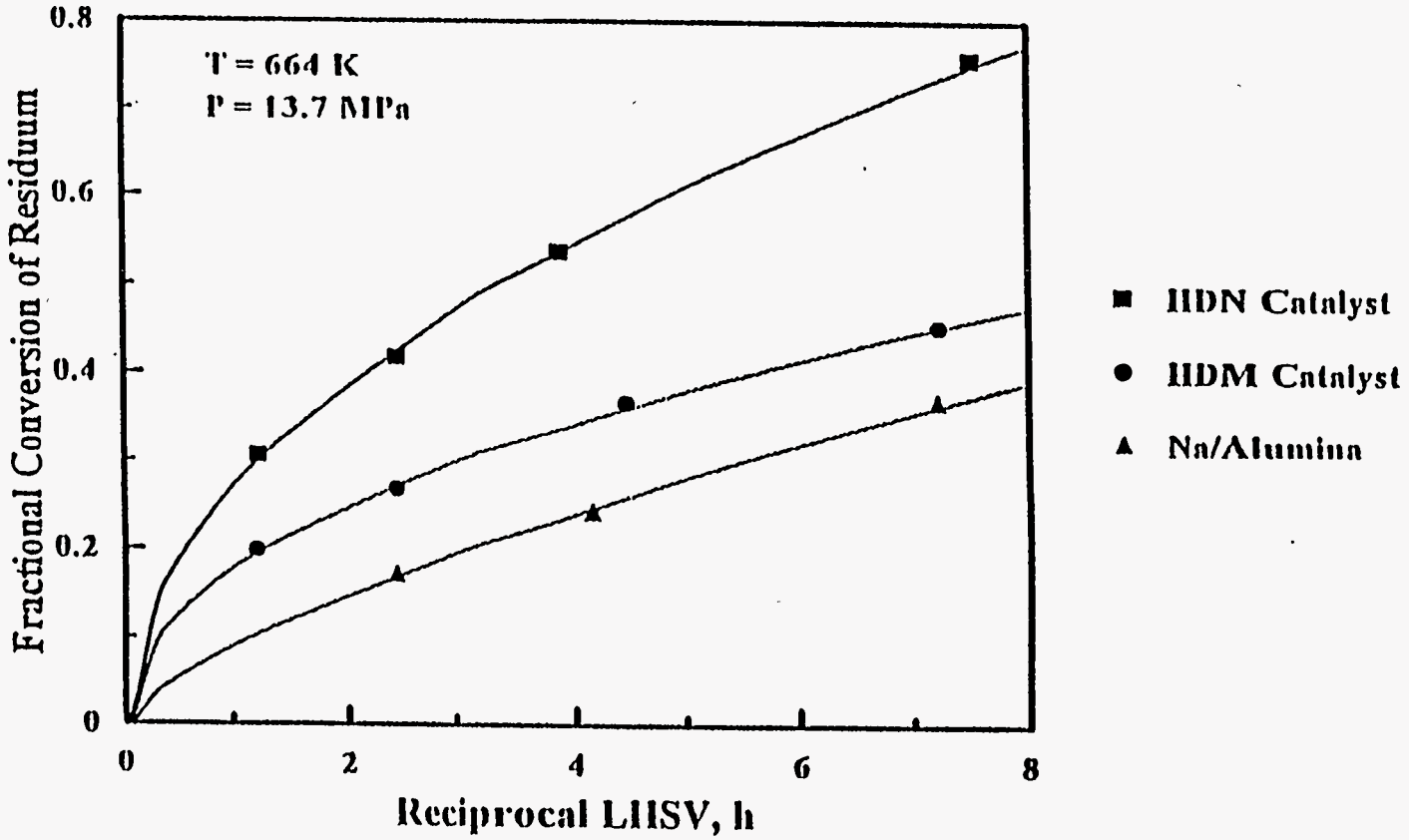

Figure 227. Effect of Residence Time and Catalyst Selection on Residuum Conversion.

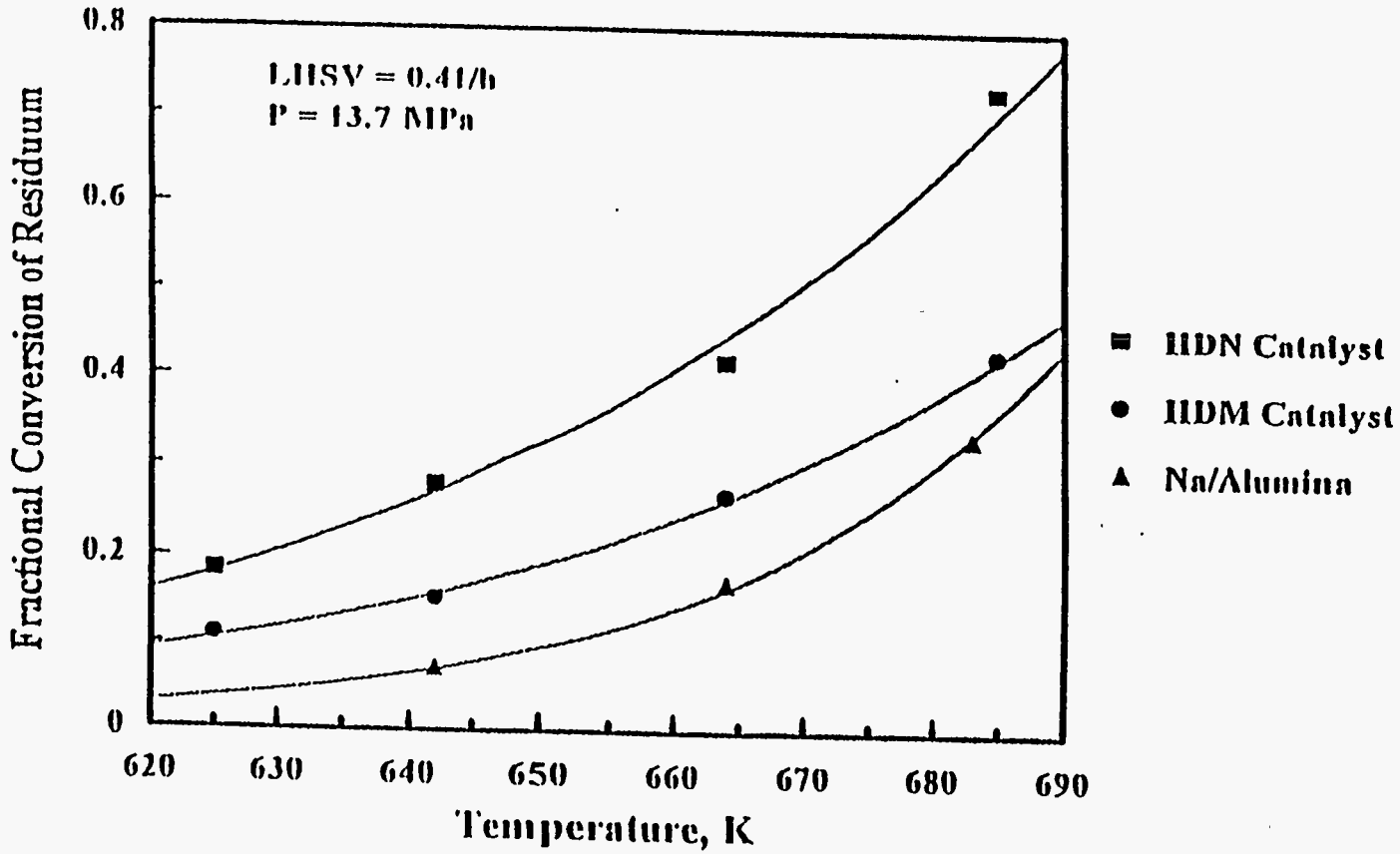

Figure 228. Effect of Catalyst Selection and Temperature on Residuum Conversion.

There is disagreement on the role of catalyst in residuum conversion. Some researchers (254, 259) have reported that catalyst does not affect residuum conversion and that residuum conversion occurs primarily by thermal reaction pathways. This conclusion was based on hydroprocessing heavy oils in stirred autoclave reactors where the catalyst-to-oil ratios were low. The opposite conclusion was reached in this work. It is clear from Figures 227 and 228 that catalyst selection played an important role in determining the extent of residuum conversion. The reason for the discrepancy between this work and that of other researchers (254, 259) may be related to the fact that catalyst densities were higher in the packed bed reactor used in this work than in stirred autoclaves used in other investigations.

In dilute catalyst systems such as stirred autoclave or ebullieted bed reactors (276), thermal conversion is emphasized relative to catalytic cracking. This is because the extent of thermal conversion is determined by the residence time of the oil in the reactor. The extent of catalytic conversion is determined by the contact time between the oil and the active catalyst surface. This is directly related to the catalyst-to-oil ratio in the reactor. Packed bed reactors with a high catalyst density will result in higher residuum conversion than stirred autoclave reactors or ebullieted bed reactors with low catalyst densities (257). In this research the catalyst density was high enough for the presence of the catalyst to noticeably increase the extent of residuum conversion relative to thermal conversion alone.

The reactor was operated in the upflow mode to ensure complete contacting of the liquid with the catalyst because of the small scale of this reactor system. This resulted in a reactor system where the oil phase was continuous and the vapor phase was discontinuous. This increased the liquid holdup of the reactor relative to industrial reactors operated in the downflow mode where liquid flows as a thin film on the outside of the catalyst particles and both liquid and vapor phases are continuous. It is expected that catalytic reactions play an even greater role in industrial downflow packed bed reactors than they did in this bench scale system that was operated in the upflow mode.

Several researchers (274, 275) have reported that a combination of catalytic and thermal reactions may be involved in residuum conversion. This is because catalysts promote hydrogenation of aromatic rings and opening of those rings occurs by either thermal reactions or reactions catalyzed by acidic sites.

Residuum cracking over the Na/alumina consisted mainly of free radical cracking reactions. It is known that free radical cracking reactions preferentially affect aliphatic side chains, aliphatic bridges and naphthenes. Gray (277) reported that paraffin groups are likely to cleave β or γ to aromatic or naphthenic rings when thermal cracking occurs at pressures of over 10 MPa. Alkyl aromatics are formed by opening of naphthenic rings during thermal conversion of residuum (252). Tsai et al. (252) performed GC/MS of bitumens, hydroprocessed bitumens and hydroprocessed liquids derived from bitumen pyrolysis. They reported that normal and methylsubstituted paraffins are absent in bitumen but are formed during bitumen hydroprocessing. Tsai et al. (252) attributed their formation to the cleavage of side chains from polycyclic clusters.

Nitrogen Removal

The effects of residence time, temperature and catalyst selection on nitrogen removal from the bitumen-derived heavy oil are presented in Figures 229 and 230. Catalyst activity for nitrogen removal was ranked as follows: HDN catalyst > HDM catalyst > Na/alumina as was anticipated. Catalyst selection played an even greater role on nitrogen conversion than it did with residuum conversion. This is because the thermal conversion pathway is largely non-existent for nitrogen conversion while it makes a significant contribution to the conversion of residuum.

The nitrogen removal that was observed with the HDN catalyst is attributed to its high metal loading relative to the HDM catalyst and the Na/alumina. Surface acidity may also have played a role because it is known that higher acidity supports can increase nitrogen conversion (278).

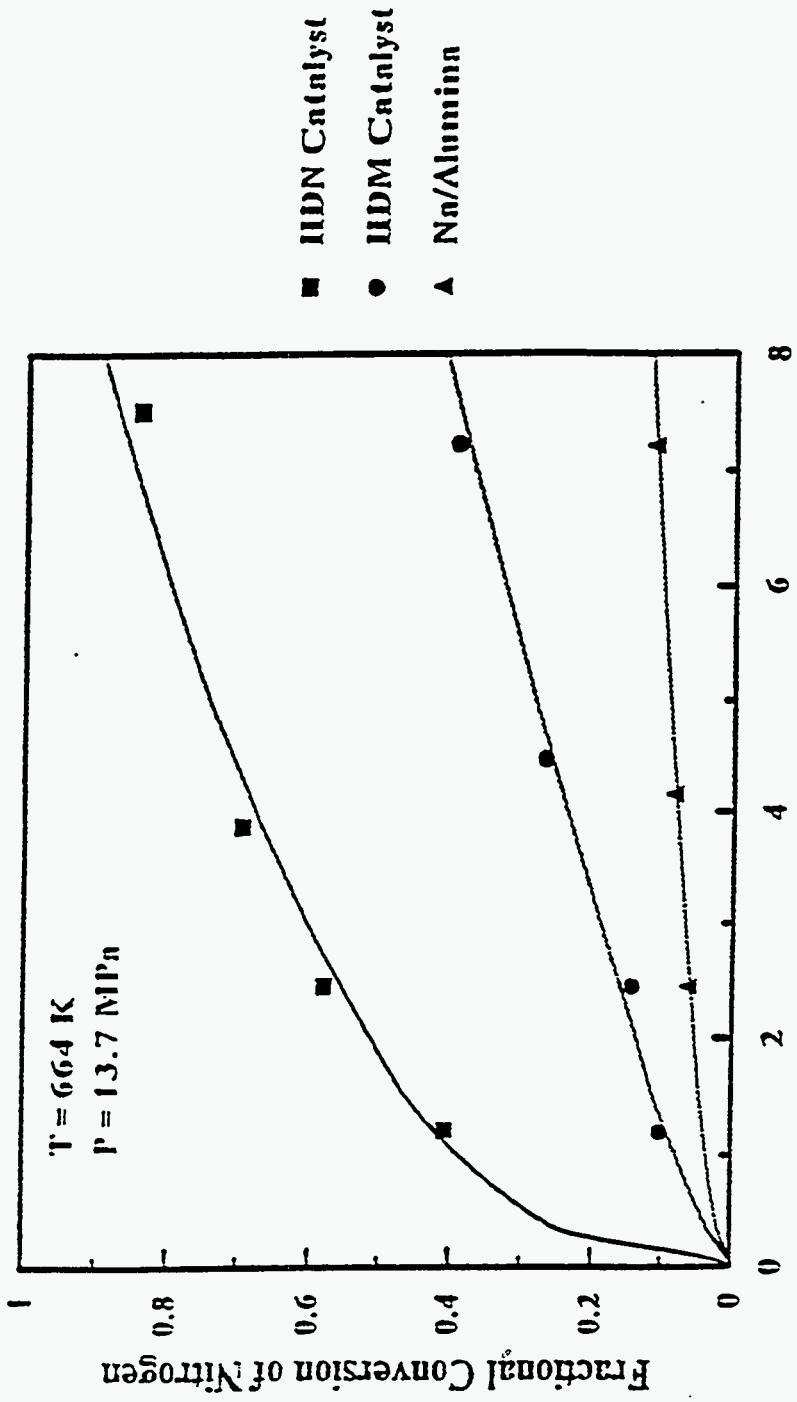

Figure 229. Effect of Residence Time and Catalyst Selection on Nitrogen Removal.

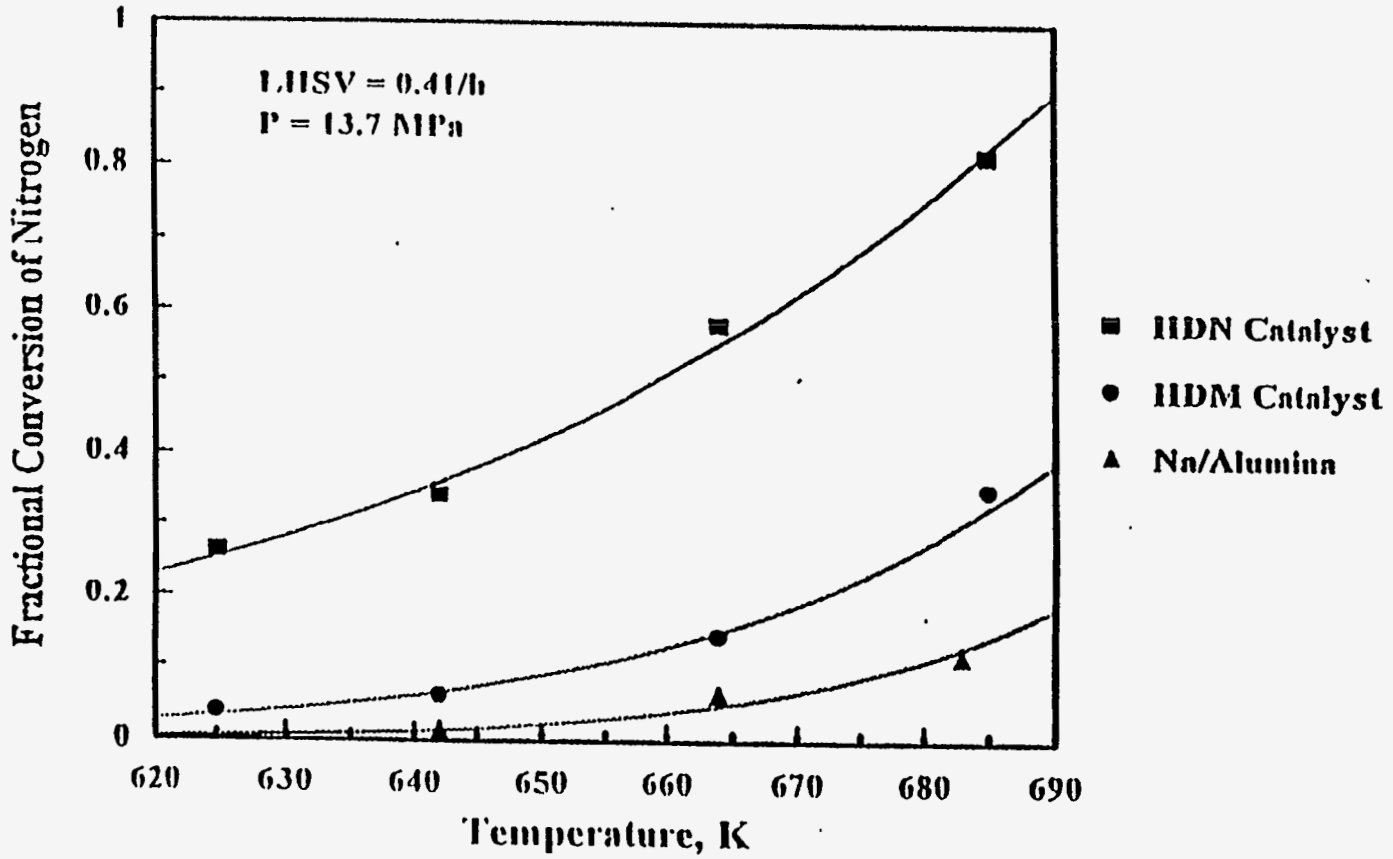

Figure 230. Effect of Temperature and Catalyst Selection on Nitrogen Removal.

Sulfur Removal

The effects of catalyst selection, residence time and temperature on sulfur removal from the bitumen-derived heavy oil are presented in Figures 231 and 232. Some sulfur removal was detected with the Na/alumina. The observed sulfur removal with the Na/alumina was presumably the result of thermal reactions involving aliphatic sulfides which have been detected in some heavy oils (266). Khorasheh et al. (261) have reported that sulfur can be removed from coker gas oil in the absence of catalyst or support. Gray et al. (266) have also proposed that small amounts of sulfur compounds in vacuum residua from different sources may be converted by thermal reactions over α-alumina. Trytten et al. (247) reported that the reactivity of sulfur compounds decreased with increasing molecular weight because of steric hindrance.

The rank of catalyst activity in sulfur removal was as follows: HDN catalyst > HDM catalyst > Na/alumina. The ranking of catalyst activity appears to be related to metal loading because both hydrogenation and hydrogenolysis pathways are catalyzed by supported metal sulfides. Catalyst acidity may play a role in that residuum conversion on the active alumina of the HDN catalyst may be a rate limiting step for the conversion of a significant portion of the sulfur (248). Gray et al. (266) reported that sulfur removal increased with increasing metal loading on the same support.

Sulfur conversion over the HDN catalyst leveled off with increasing residence time. Nitrogen conversion and the slope of the nitrogen removal increased with increasing temperature (Figure 229). The opposite trend was observed with sulfur. This is because sulfur conversion reached a point at which further conversion was limited because the remaining sulfur is considerably less reactive than the sulfur which had been converted. The presence of a significant portion of low reactivity sulfur may be related to the higher asphaltene and Conradson carbon content precursors in the PR Spring bitumen relative to other high nitrogen bitumens from the Uinta Basin.

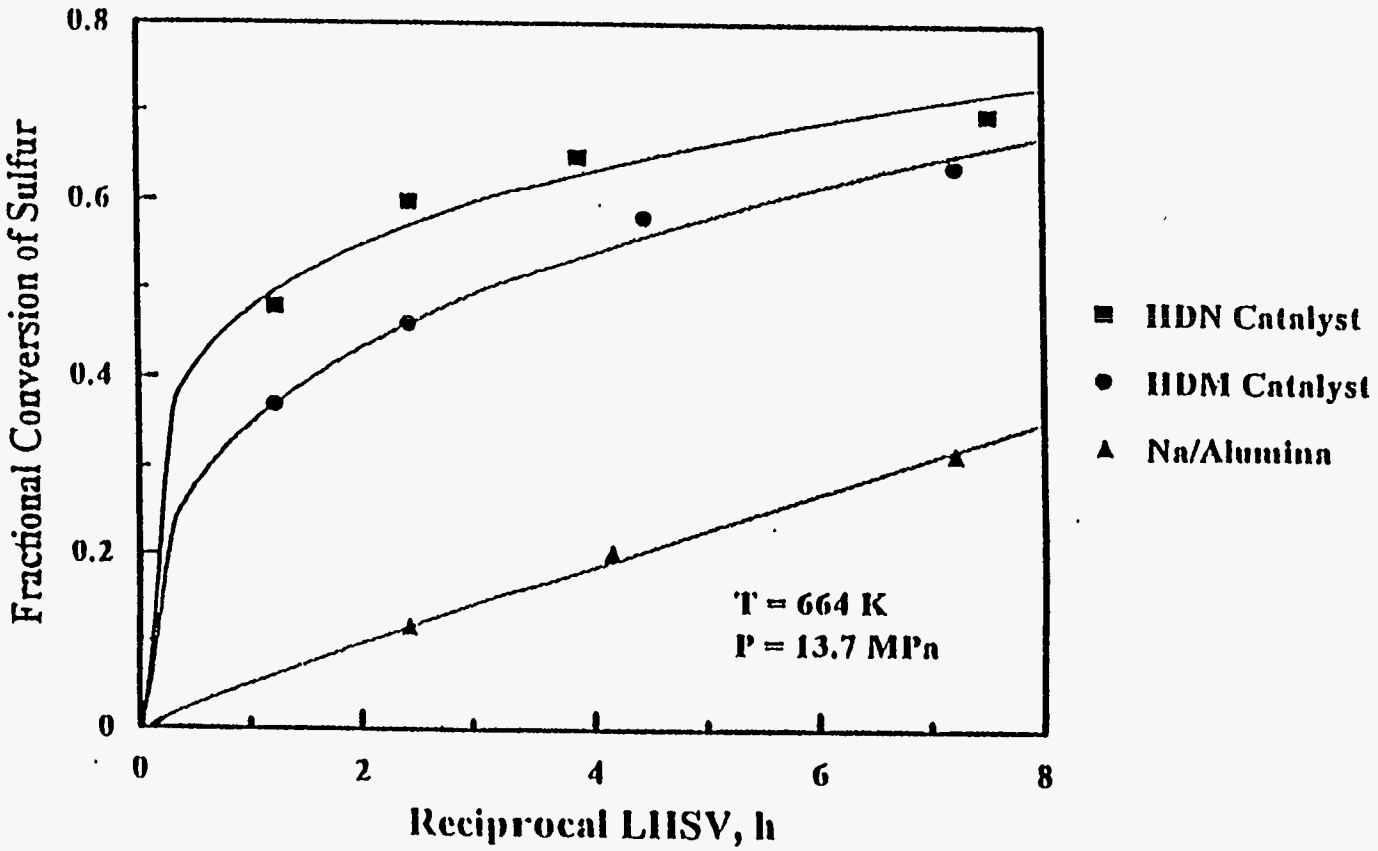

Figure 231. Effect of Residence Time and Catalyst Selection on Sulfur Removal.

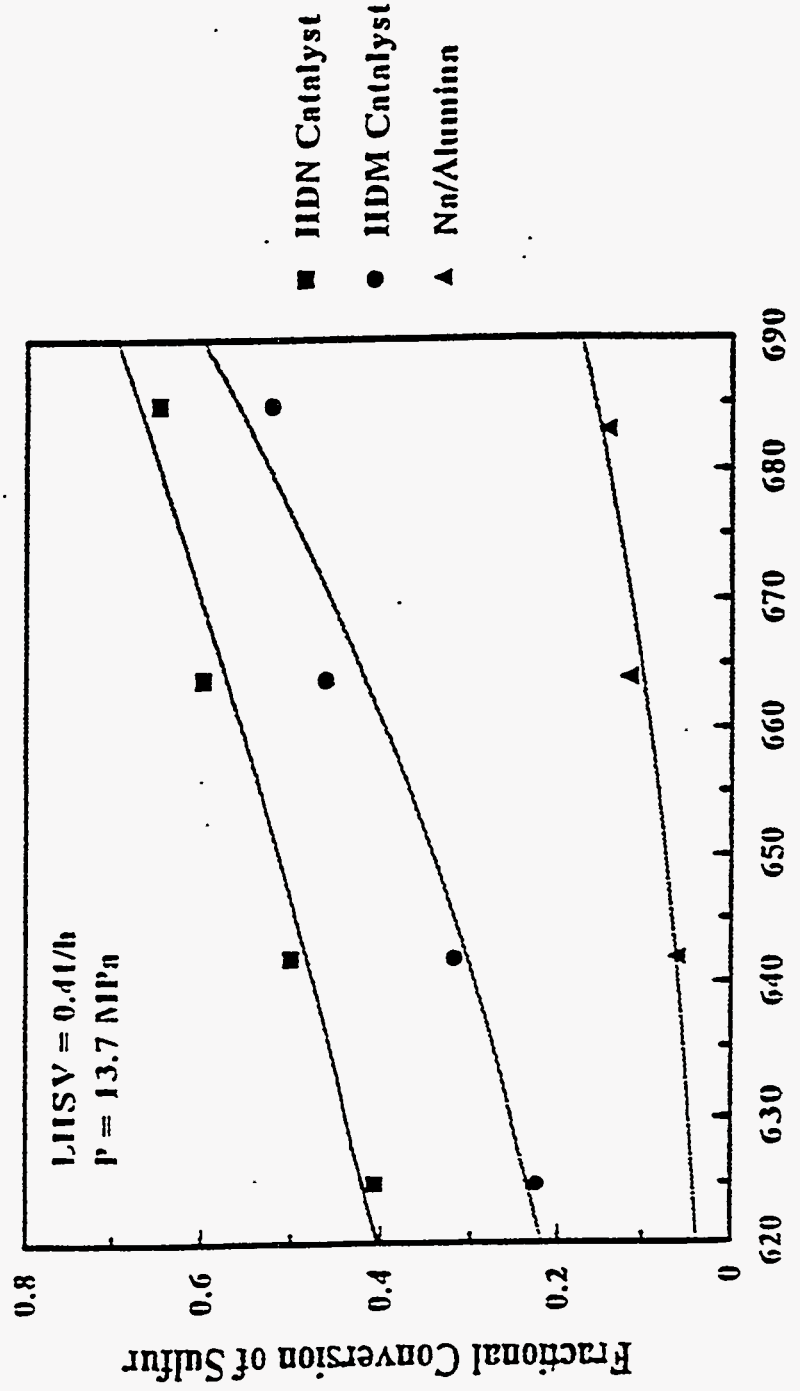

Figure 232. Effect of Temperature and Catalyst Selection on Sulfur Removal.

Nitrogen removal is plotted with respect to sulfur removal in Figure 233. The sulfur in the PR Spring bitumen-derived heavy oil exhibited a broader range of reactivities than the nitrogen. At low severities sulfur conversion exceeded nitrogen conversion. This indicates that a certain portion of the sulfur was more reactive than the nitrogen. At higher severities, nitrogen conversion exceeded sulfur conversion. This was because a significant portion of the sulfur was less reactive than the nitrogen.

Metal Removal

The effects of catalyst selection, residence time and temperature on nickel removal for the PR Spring bitumen are presented in Figures 234 and 235. Catalyst activity was again ranked according to metal content which was unexpected due to the differences in support structure.

The catalyst activity for nickel removal increased according to metal loading and surface acidity of the catalyst. Hydrogenation catalyzed by the supported metals may be linked with thermal reactions because the nickel is removed through a sequential mechanism involving hydrogenation followed by a thermal hydrogenolysis step (279-281). Some nickel removal was observed with the Na/alumina, although the Na/alumina did not contain any metals. This activity was presumed to be completely thermal.

The difference between the activity of the supported metal sulfide catalysts and the Na/alumina indicated that catalytic and thermal hydrodemetallation pathways were in operation. These different pathways may affect porphyrinic and non-porphyrinic metals to different degrees. Some researchers (279) reported that HDM of nickel etioporphyrin was negligible with alumina alone, but that some vanadyl etioporphyrin was converted with alumina. It is possible that thermal conversion is limited to non-porphyrinic metals.

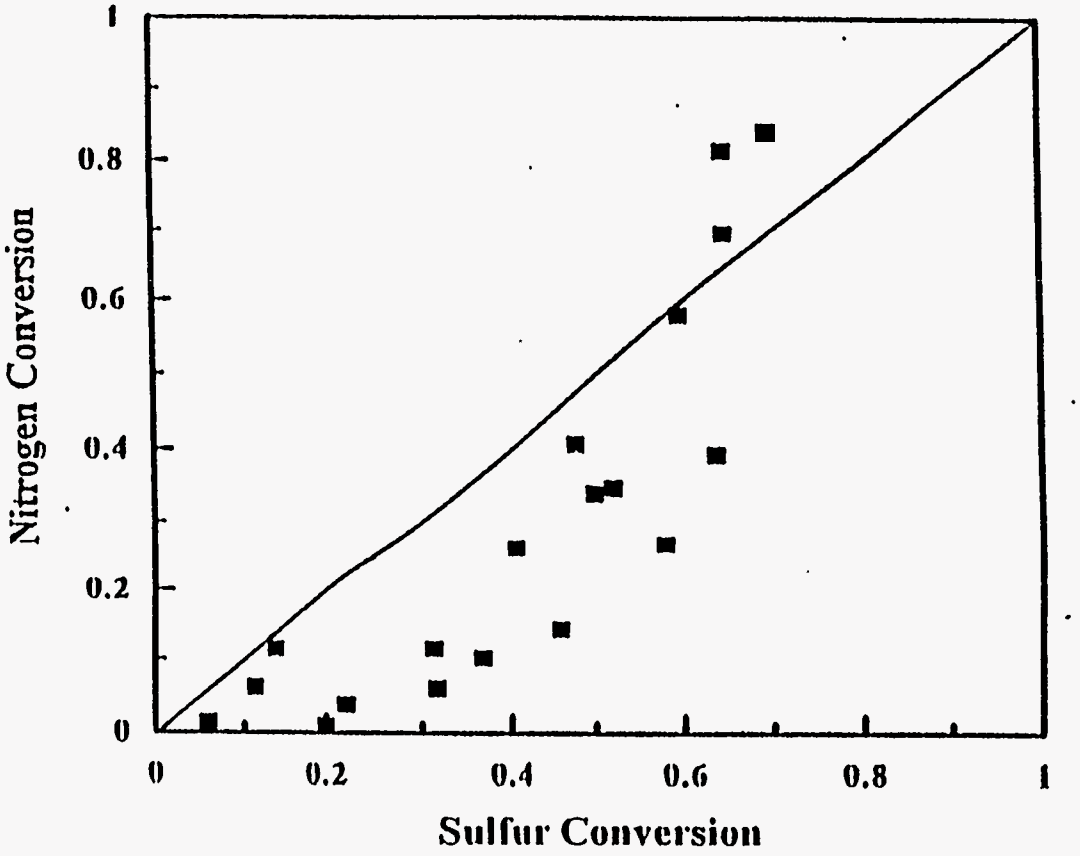

Figure 233. Nitrogen Removal With Respect To Sulfur Removal.

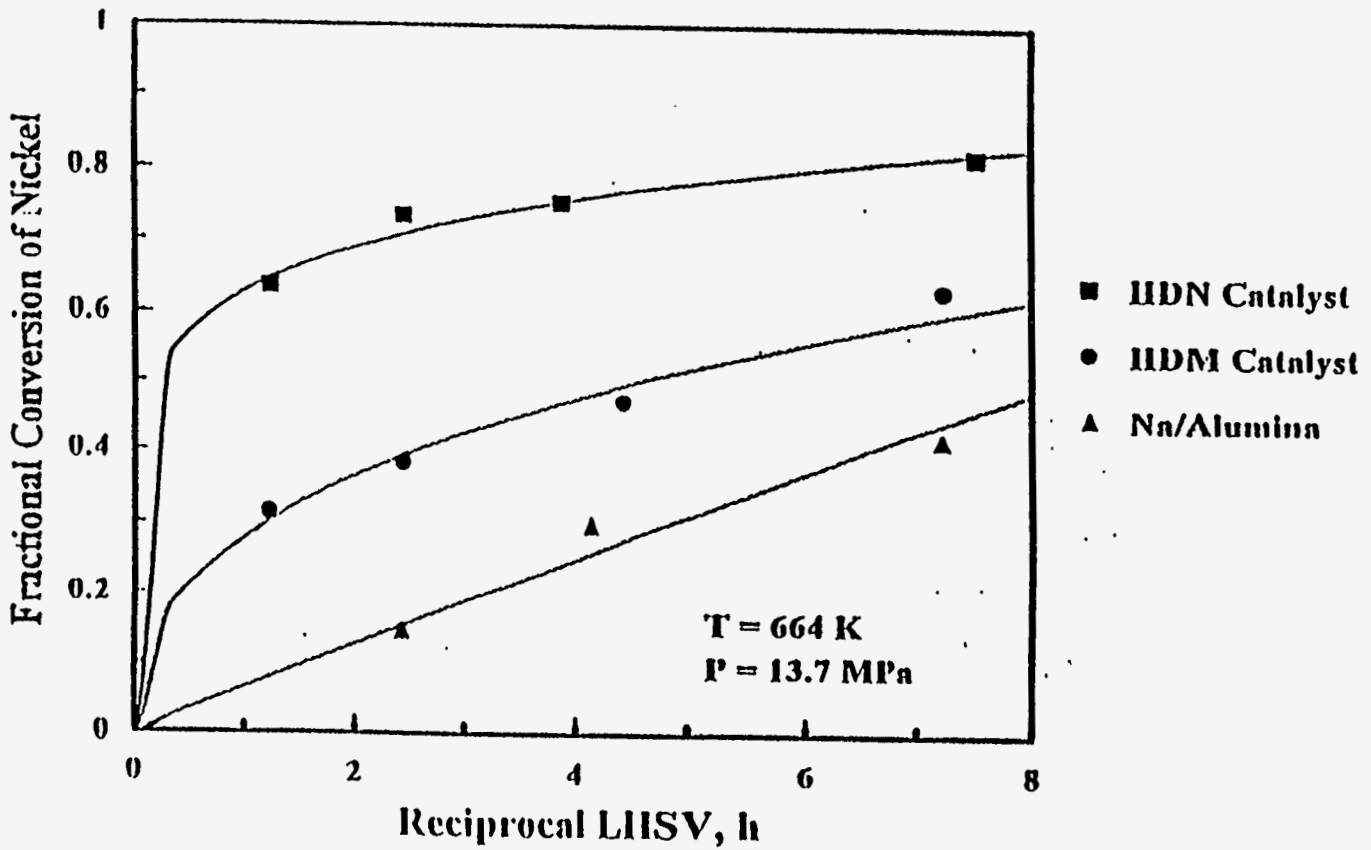

Figure 234. Effect of Residence Time and Catalyst Selection on Nickel Removal.

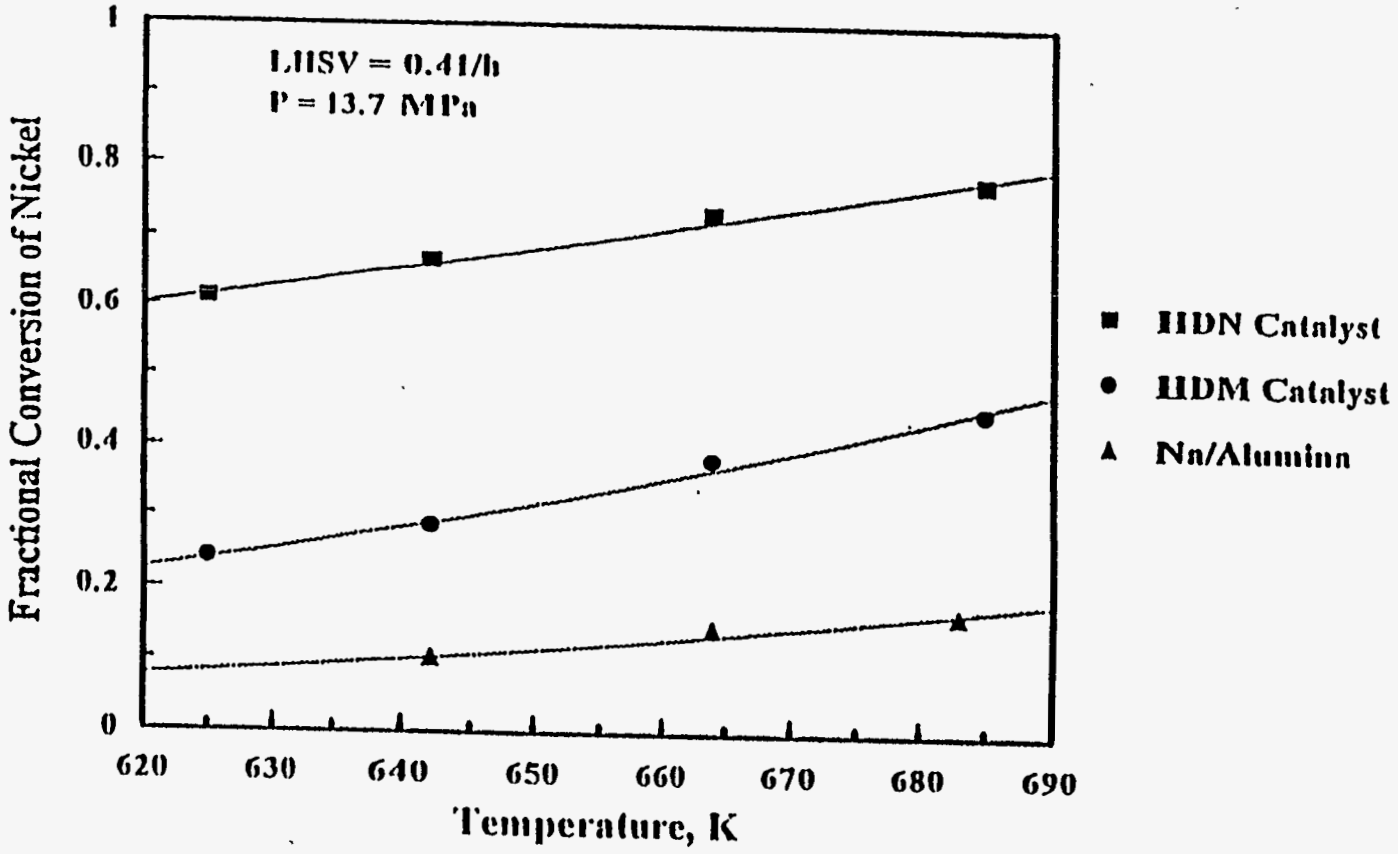

Figure 235. Effect of Temperature and Catalyst Selection on Nickel Removal.

Conradson Carbon Residue Conversion

The effects of catalyst selection, residence time and temperature on the Conradson carbon residue conversion for the bitumen-derived heavy oil are presented in Figures 236 and 237. Catalyst activity for Conradson carbon residue conversion was ranked as follows: HDN catalyst > HDM catalyst > Na/alumina. This ranking for Conradson carbon residue conversion is again due to some combination of metal loadings and surface area/acidities of the various catalysts. The suggested mechanism for Conradson carbon residue conversion consists of cracking of aliphatic side chains followed by the saturation of aromatic rings and the opening of hydroaromatic rings. Residuum conversion occurs by the same mechanism. The fact that Conradson carbon residue and residuum conversion occur in parallel is indicated by comparing the increase in Conradson carbon residue conversion with increasing temperature with the increase in resid and heteroatom conversion observed with increasing temperature. The levels of nitrogen, sulfur and metal removal obtained with the Na/HDN catalyst were much lower than the levels of Conradson carbon residue and residuum conversion. The fact that levels of Conradson carbon residue and resid conversion were similar is probably because of the significant overlap between what is considered Conradson carbon residue and residuum. This overlap also occurs between heteroatoms and residuum but to a lesser degree.

Sanford (282) observed Conradson carbon residue conversion over a deactivated catalyst and suggested that both thermal and catalytic reactions are involved in the conversion of Conradson carbon residue. Conradson carbon residue conversion does not increase as fast with increasing temperature as does residuum conversion. This indicates that one of the differences between residuum and Conradson carbon residue conversion is that a greater portion of resid conversion is thermal relative to Conradson carbon residue conversion.

High pressure hydrogen can reduce coke yields during hydrocracking by more than 50% (236, 282). Conradson carbon residue conversion is achieved by three mechanisms: 1) catalytic, 2) thermal and 3) extractive in that molecules which normally form the residue in the Conradson carbon residue test are deposited as coke in the reactor and on the catalyst.

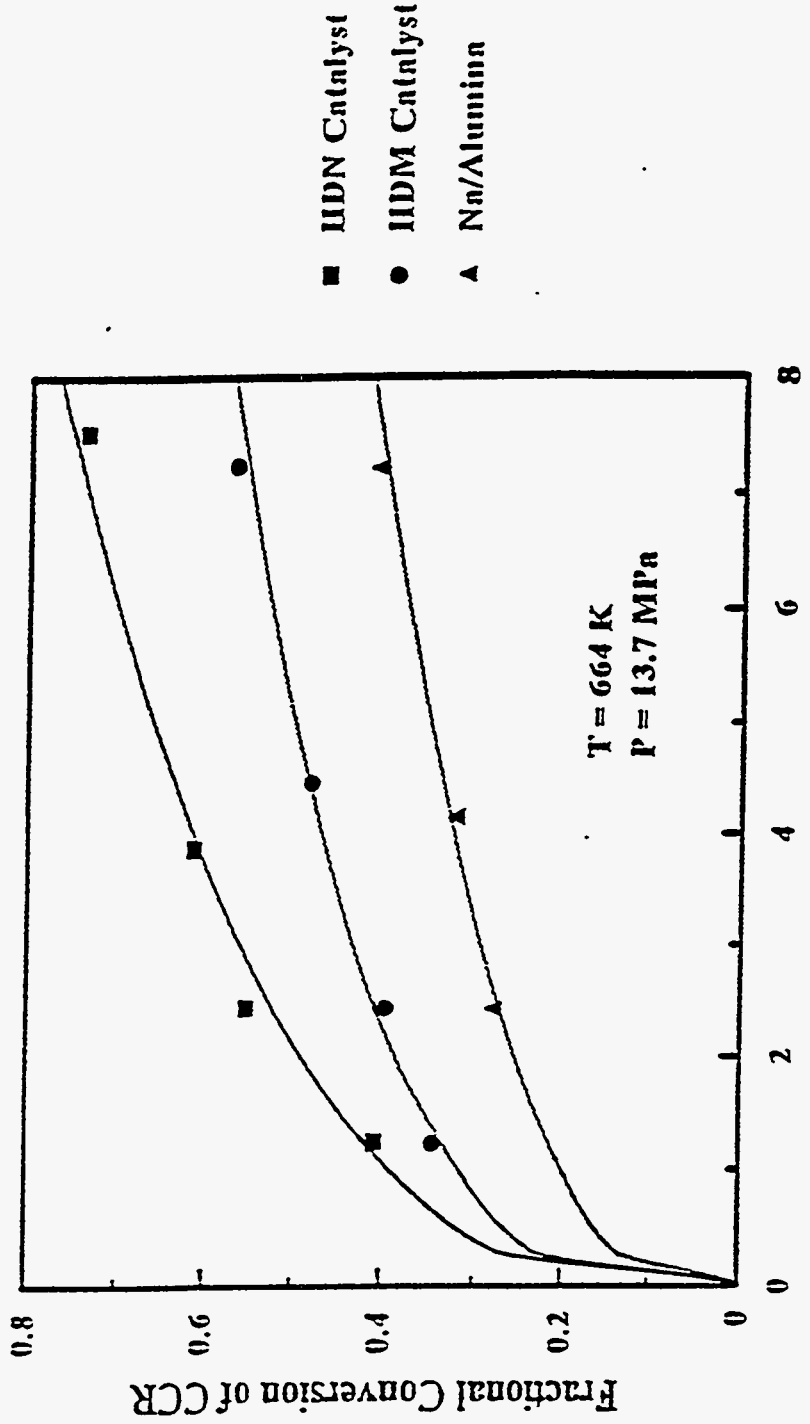

Figure 236. Effect of Residence Time and Catalyst Selection on CCR Removal.

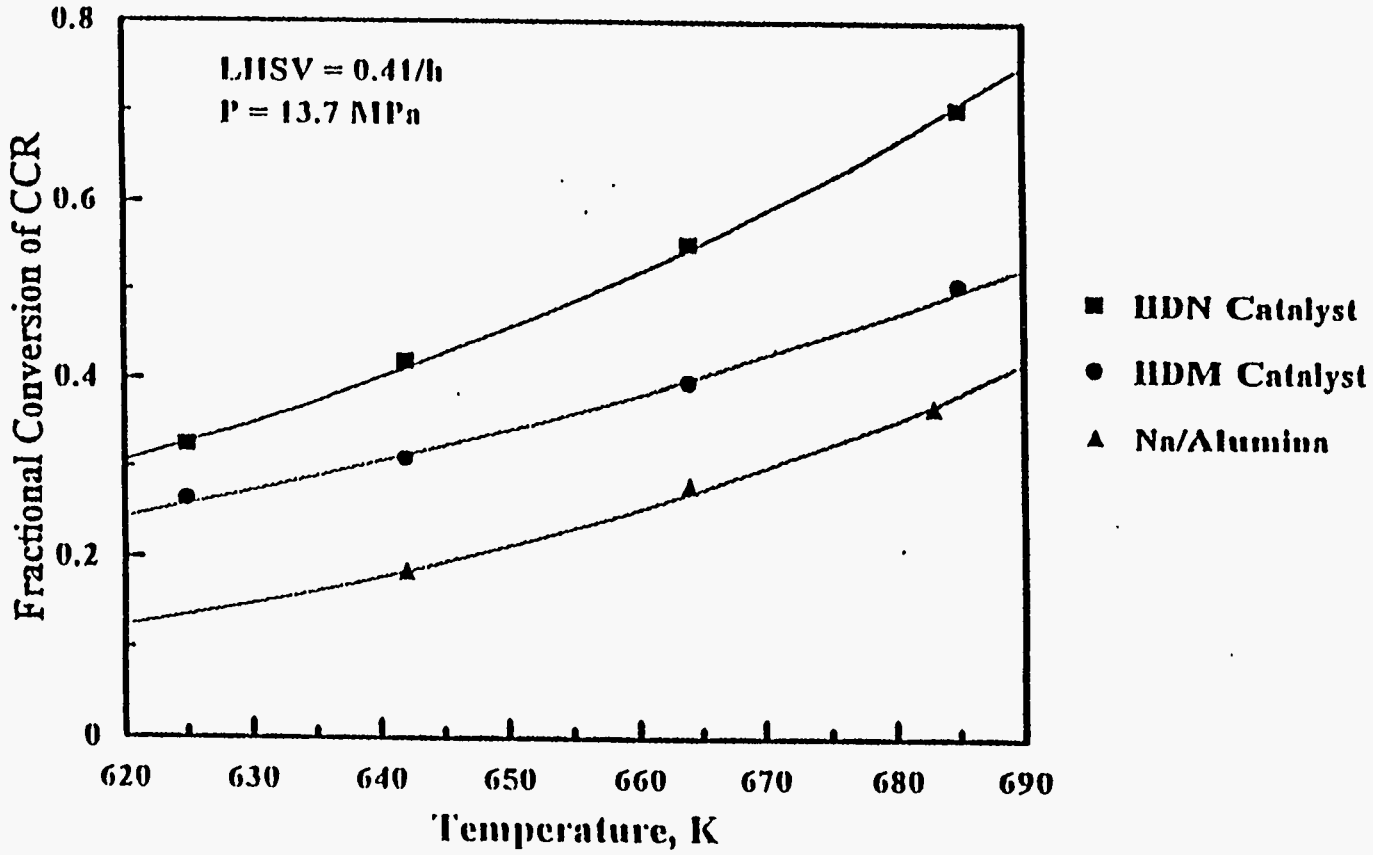

Figure 237. Effect of Temperature and Catalyst Selection on CCR Removal.

Extractive Conradson carbon residue conversion is reduced due to the presence of hydrogen because hydrogen acts to cap free radicals formed by thermal scission of carbon-carbon and carbon-heteroatom bonds.

When easy-to-break bonds are thermally broken and saturated by hydrogen these bonds are less likely to cleave during the Conradson carbon residue test and the measured Conradson carbon residue will be reduced. Catalytic Conradson carbon residue conversion is achieved by direct and indirect means in that large polar moieties are catalytically converted to lighter, less polar moieties which will volatilize in the Conradson carbon residue test rather than form coke. In addition, catalytic conversion will also indirectly reduce Conradson carbon residue by boosting the hydroaromatic content of the oil so that free radicals formed during the Conradson carbon residue test can be saturated by hydroaromatic hydrogen instead of condensing to form coke. Some Conradson carbon residue was converted over the Na/alumina, even though the Na/alumina did not contain any metal sulfides and was not acidic. Presumably this was due to hydrothermal conversion.

Heteroatom and metal removal and Conradson carbon residue and residuum conversion may be also catalyzed by metals in the feed. LePage et al. (283) reported that porphyrinic and nonporphyrinic metal complexes derived from the presence of H_2S during hydroprocessing participate in the partial hydrogenation of condensed aromatic rings and play the role of hydrogen donors. Catalytic activity which arises from deposited metal complexes may explain why Conradson carbon residue conversion occurred over the Na/alumina.

SUMMARY AND CONCLUSIONS

Heteroatom and nickel removal and CCR and residuum conversion were sensitive to catalyst selection because metal sulfides on the catalyst played a significant role in heteroatom and nickel removal, and CCR conversion. The catalyst activity for all reactions was as follows: HDN catalyst > HDM catalyst > sodium-impregnated alumina. The rank of catalyst activity is strongly dependent on the metal loading. The rank may also be dependant

to a lesser degree on the residual acidity of the catalyst support. The deactivation rates of HDN and HDM catalysts were 0.06 and 0.02°API/day, respectively.

HYDROTREATING KINETIC STUDY FOR PR SPRING BITUMEN-DERIVED HEAVY OILS OVER HDN AND HDM CATALYSTS

Principal Investigator:	Francis V. Hanson
Post Doctoral Fellow:	Daniel C. Longstaff
Graduate Student:	J.-W. Kim

INTRODUCTION

Heavy oil and bitumen hydrotreating has been extensively studied in pilot plant and bench-scale reactors (237, 247, 261, 284, 285). The objective of heavy oil hydrotreating is to achieve hydrodesulfurization (HDS), hydrodenitrogenation (HDN), hydrodemetallation (HDM) and conversion of residuum into volatile materials. Bitumen is a complex mixture which contains an abundance of aromatic, sulfur, nitrogen and metal containing moieties. Simple intrinsic kinetics cannot be applied to mixed feeds such as bitumen and heavy oils because the various components exhibit a wide range of reactivities and may even exhibit synergistic interactions.

The more reactive compounds are preferentially removed at low conversions. Increasing conversion results in a residual feed which becomes increasingly less reactive. Because of this refractory components play a significant role in the apparent kinetics at high conversion levels. These kinetics are further complicated by the presence of multiple pathways in that individual molecules can react by parallel and consecutive reactions that change the reactivity of the material being treated (286).

Commercial NiMo on alumina hydrodenitrogenation (HDN) and Mo on alumina hydrodemetallation (HDM) catalysts were employed in these hydrotreating studies. Alumina supported molybdenum HDM catalysts are necessary to protect downstream hydrotreating

catalysts from being poisoned by coke and metal deposition. This is because HDM catalysts generally contain wider pore radii and larger pore volumes relative to HDN catalysts (287).

The aim of this study was to determine which kinetic models can be used to describe the conversion or removal of the various classes of compound types which occur in the PR Spring bitumen and to also determine the kinetic parameters which apply to those compound classes: nitrogen, sulfur, nickel, CCR and residuum.

EXPERIMENTAL

The PR Spring bitumen was obtained by solvent extraction of the PR Spring oil sand. The feed oil sand used in this investigation was obtained from the U-Tar pit on the PR Spring oil sands deposit which is located in SE 1/4 NE 1/4, Section 5, Township 16 South, Range 24 East in eastern Utah. The oil sand ore was mined, crushed and sieved to pass through 0.63 mm (0.25 in) prior to solvent extraction. PR Spring bitumen was removed from the oil sand by solvent extraction with refluxing toluene. Toluene was removed from the extract solution by a combination of rotary evaporation and batch vacuum distillation. The chemical and physical properties of feedstock are presented in Table 78. PR Spring and other Uinta Basin bitumens contain low levels of vanadium and sulfur and high levels of nitrogen relative to the Athabasca bitumens. This is related to their freshwater origin.

Commercial $NiMo/Al_2O_3$ hydrodenitrogenation (HDN) and Mo/Al_2O_3 hydrodemetallation (HDM) catalysts were used in this study. The HDN catalyst consisted of 1.3 mm trilobe shaped extrudates and contained 3.8 wt% NiO, 19.5 wt% MoO_3, 155 m^2/g of surface area and 0.47 cc/g of pore volume. The HDM catalyst was a 1.6 mm trilobe shaped extrudates and contained 6.0 wt% MoO_3, had a surface area of 130 m_2/g and a pore volume of 0.85 cc/g.

The catalysts were dried in-situ in flowing nitrogen at 700 K for one hour. The reactor was then cooled to ambient temperature prior to sulfiding. Catalyst sulfiding started at ambient temperature with 2 wt% sulfur solution of dimethyldisulfide in kerosene. The

Table 78: Physical and Chemical Properties of Native PR Spring Bitumen

API Gravity	9.2
Conradson Carbon Residue, wt%	16.0
Specific Gravity	1.0
Asphaltenes[a], wt%	18.1
Elemental Analysis	
C, wt%	85.9
H, wt%	10.9
N, wt%	1.06
S, wt%	0.43
Ni, ppm	72
Simulated Distillation	
Volatility, wt%	37.4
C_5 - 477 K, wt%	0.1
477 - 617 K, wt%	6.2
617 - 811 K, wt%	31.1
>811 K, wt%	62.6
IBP, K	514

[a] Pentane-insolubles

hydrogen to liquid feed ratio was 890 $m^3(STP)/m^3$. The reactor pressure and the sulfiding solution feed rate were 6.1 - 6.3 MPa and 1 h^{-1} LHSV, respectively. The reactor was heated to 505 K at the rate of 27.8 °C/h (50 °F/h) in flowing hydrogen. The sulfiding solution was started over the catalyst and the reactor temperature was held at 505 K for 2 hours to ensure complete sulfiding. The reactor was then heated to 645 K at a rate of 27.8 °C/h. Sulfiding was completed when the reactor temperature reached 645 K.

The reactor had a 2.54 cm inside diameter and consisted of three different beds whose temperatures were independently controlled to provide a uniform temperature profile throughout the catalyst zone. The catalyst bed zone consisted of the central 30.5 cm of the reactor. 152 cm^3 of either catalyst was loaded in the catalyst zone. The preheat and the postheat zones were filled with 3.2 mm alundum (α-alumina beads) to ensure efficient contacting and distribution of hydrogen and liquid feeds. The hydrotreating experiments were conducted in a fixed-bed reactor which was operated in the upflow mode to maintain isothermal conditions and to ensure complete wetting of the catalyst.

After catalyst sulfiding was complete oil was fed over the catalyst at the base case conditions while the catalyst attained a pseudo-steady state activity. The base case conditions were a temperature of 642 K, a LHSV of 0.41 h^{-1} and a pressure of 13.7 MPa. After the catalysts had attained pseudo steady state activities process variable studies were conducted in which reactor temperature, space velocity and total reactor pressure were varied. The studies were conducted in a random, cyclic mode in which a process variable material balance was followed by a base case material balance. This method of operation permitted the determination of the extent of catalyst deactivation with time on stream. The process operating conditions are presented in Table 79. The hydrotreater system and experimental procedures have been described in detail by Kim (243).

Table 79: The Process Operating Conditions

	HDN Catalyst	HDM Catalyst
Temperature, K	625-685	625-685
LHSV, h^{-1}	0.14-0.80	0.14-0.81
Pressure, MPa	13.7	11.1-16.6

KINETIC EQUATIONS

HDN, HDS and HDM of the oil are achieved during hydrotreating. Significant molecular weight reduction may also occur depending upon the conditions (250). Under hydroprocessing conditions native residuum rapidly converts to volatile products and/or to lighter residuum (236, 288) which is termed intermediate residuum (243). The rapid conversion is thought to be due to the cracking of paraffinic side chains and aliphatic bridges from multicyclic clusters (289, 290). The products of native residuum conversion consist of volatile products ranging from light gases to gas oil (254).

The conversion or removal of residuum, sulfur, CCR and metals, can be explained as if the conversion proceeded by a combination of parallel and consecutive reaction pathways which include the intermediate residuum as presented in Equation (123):

$$A \xrightarrow{k_1} P$$
$$A \xrightarrow{k_2} A^* \xrightarrow{k_3} P \qquad (123)$$

where: A is the weight fraction of native residuum, sulfur, CCR, or metals; A* is the weight fraction of intermediates; and; P is the weight fraction of the products.

An equation which correlates residence time, τ, and conversion for this kinetic scheme was derived. It was assumed that the conversion of each pseudo component in Equation (123) obeyed first-order kinetics. The rate equations at constant hydrogen partial pressure are then:

$$\frac{dC_A}{d\tau} = -(k_1 + k_2)\, C_A \qquad (124)$$

$$\frac{dC_{A^*}}{d\tau} = k_2\, C_A - k_3\, C_{A^*} \qquad (125)$$

$$\frac{dC_p}{dt} = k_1 C_A + k_3 C_{A^*} \qquad (126)$$

where k_1, k_2 and k_3 are the apparent rate constants for each step; C_A, C_{A*} and C_p are the weight percentages of A, A* and P at τ; respectively, and τ is the reciprocal LHSV.

The solution for the native species A from Equation (124) is as follows:

$$C_A = C_{Ao} e^{-(k_1 + k_2)\tau} \qquad (127)$$

where C_{A0} is the weight fraction of the native species A in the feed.

Classification of residuum and other lumps into native and intermediate portions is based on kinetics only and is not based on the results of an analytical test. The intermediate portion of the lump, A^*, is not present in the feed.

The initial condition for A^* is therefore given by the following:

$$@\ \tau = 0: \qquad C_{A^*} = 0 \qquad (128)$$

Equation (127) for C_A (native species A) can be substituted into Equation (125). Integration of Equation (125) with the initial condition given in Equation (128) yields:

$$C_{A^*} = \frac{C_{Ao}\, k_2}{k_3 - k_1 - k_2} \left(e^{-(k_1 + k_2)\tau} - e^{-(k_3)\tau} \right) \qquad (129)$$

A new equation for fractional conversion, X_A, can be obtained by combining Equations (127) and (129):

$$(1-X_A) = e^{-(k_1 + k_2)\tau} + \frac{k_2}{k_3 - k_1 - k_2} \left(e^{-(k_1 + k_2)\tau} - e^{-(k_3)\tau} \right) \qquad (130)$$

The objective of bitumen hydrotreating is to reduce the total amount of each lump which consists of the sum of both native and intermediate portions.

Because A^*, the intermediate portion of the lump, cannot be measured there is no differentiation between A and A^* in the liquid product. The fractional conversion of the total lump is therefore defined as the conversion of both A and A^* to products:

$$X_A = 1 - \frac{C_A + C_{A^*}}{C_{Ao}} \tag{131}$$

Certain lumps, such as nitrogen, do not follow parallel-consecutive kinetics, but follow pseudo nth order kinetics instead. The parallel-consecutive kinetic model may reflect the actual conversion pathways which occur. On the other hand, pseudo nth order kinetics are purely correlative. Thus the rate of bitumen HDN can be described by a power rate law equation:

$$\frac{dC_i}{d\tau} = -k' C_i^n P_{H_2}^{\beta} \tag{132}$$

where i represents reacting component; τ is the reciprocal LHSV or WHSV; k' is the apparent rate constant; C_i is the concentration of species i; P_{H_2} is the hydrogen partial pressure; n is the pseudo reaction order and β is the reaction order with respect to hydrogen partial pressure. When the total system pressure was held constant P_{H_2} was also assumed to be constant and the pressure term was incorporated into an apparent overall rate constant. Thus equation (132) can be simplified to give:

$$\frac{dC_i}{d\tau} = -kC_i^n \tag{133}$$

where $k=k'P_{H_2}^{\beta}$. For nth-order kinetics, the solution is as follows:

$$(C_i^{1-n} - C_{i,o}^{1-n})(\frac{1}{n-1}) = k\tau \qquad \text{for } n \neq 1 \qquad (134)$$

where $C_{i,o}$ is the feed concentration; and C_i is the product concentration.

Equation (133) can be rearranged in terms of the fractional conversion of i, X_i to give:

$$\frac{1}{C_{i,o}^{n-1}} \frac{1}{n-1} [(1-X_i)^{1-n} - 1] = k\tau \qquad (135)$$

the fractional conversion of i, X_i, is defined as follows:

$$X_i = 1 - \frac{C_i}{C_{i,o}} \qquad (136)$$

the value of n is determined by non-linear regression or by plots of τ versus of f(x) where f(x) is the left hand side of Equation (132).

The solution for first order kinetics (n=1) is as follows:

$$\ln\frac{C_i}{C_{i,o}} = -k\tau \qquad \text{for } n=1 \qquad (137)$$

Equation (137) can be rearranged in terms of the fractional conversion of i, X_i:

$$-\ln(1-X_i) = k\tau \qquad (138)$$

Pseudo nth order kinetics are used when the reaction order is equal to or less than two because pseudo second order kinetics generally represent the practical limit of pseudo nth order kinetics (291). This is because the presence of unreactive components in the lumped quantity will increase the apparent reaction order up to, but not beyond, two (291).

RESULTS AND DISCUSSION

The effect of temperature, space velocity and total system pressure on the upgrading of the PR Spring bitumen was investigated over the hydrodenitrogenation (HDN) catalyst and the hydrodemetallation (HDM) catalyst. The primary process variables investigated in this research were LHSV, reactor temperature and hydrogen partial pressure. Only two process variables, LHSV and temperature, were investigated over the HDN catalyst because the HDN catalyst deactivated before the effect of pressure could be studied. The results of the HDN and HDM catalyst studies have been reported by Kim (243).

Reaction Orders

Reaction orders can be broadly defined to include both apparent reaction orders and apparent reaction pathways. This definition includes pseudo nth order kinetics and the consecutive parallel reaction model. The reaction orders are determined by varying the residence time at constant temperature and pressure.

Nitrogen Removal

Reaction order, n, was determined by fitting Equations (135) and (138) to the data for nitrogen removal over the HDN and HDM catalysts. A plot of the left hand side of Equation (135), f(x), with respect to reciprocal LHSV, τ, is presented in Figure 238 for an apparent reaction order of 1.5 which gave the best fit of the measured data over the HDN catalyst.

Nitrogen conversion over the HDM catalyst did not exhibit pseudo 1.5 order kinetics as it did with the HDN catalyst. When the negative natural log of the fraction of nitrogen remaining in the liquid product was plotted with respect to reciprocal LHSV (Figure 239) the data plotted as a straight line because nitrogen conversion was first order.

Ho and Aris (291) suggested that reaction orders greater than unity are observed when a lumped component consists of many individual components which exhibit a distribution of

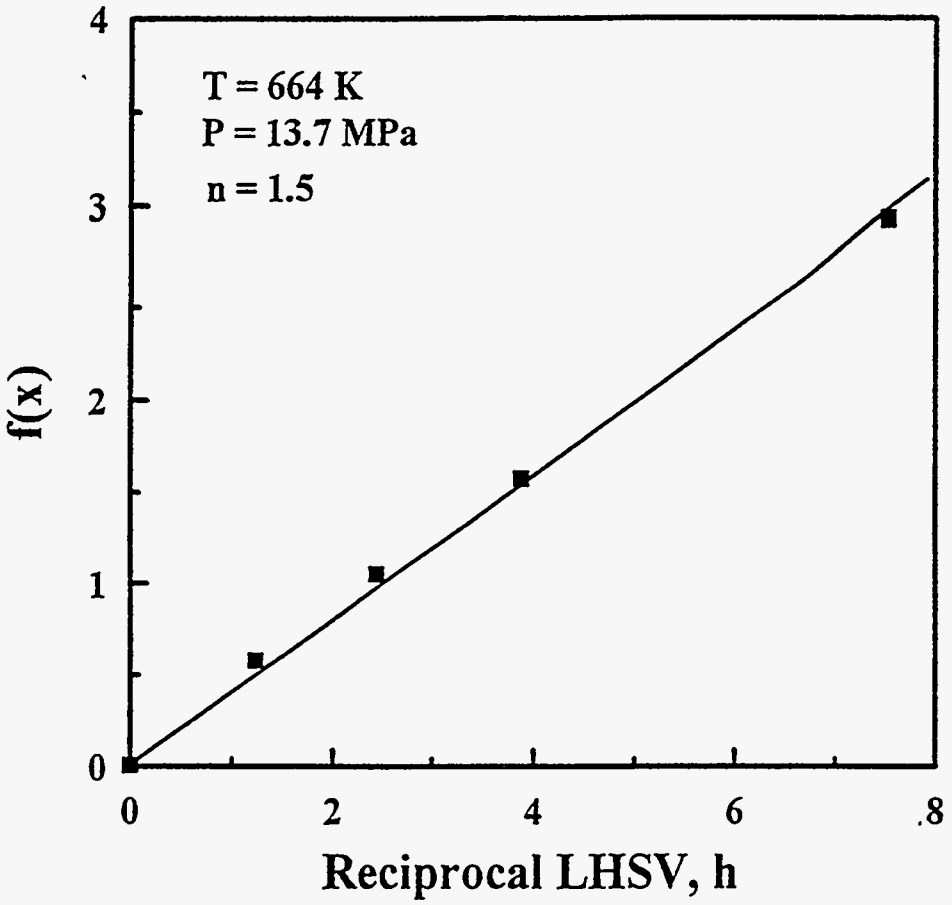

Figure 238.

Kinetic Equation Versus Reciprocal LHSV for Nitrogen Removal over HDN Catalyst

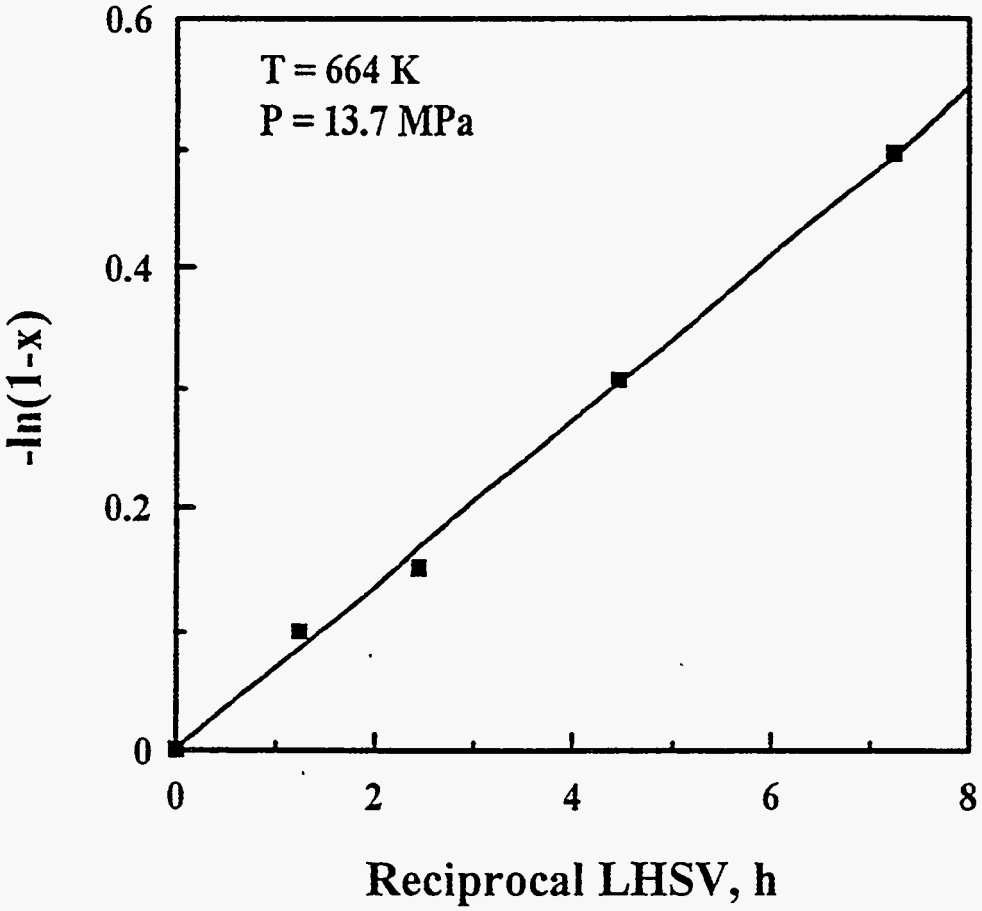

Figure 239.

-ln(1-x) Versus Reciprocal LHSV for Nitrogen Removal over HDM Catalyst

first order reactivities. Reaction order was changed with catalyst selection. This is because different catalysts related to the feed in different ways.

The effect of reducing the metal loading of the catalyst on nitrogen conversion is not simple. Increasing metal loading does not simply shift the level of conversion further along a curve based on 1.5 order kinetics. The metal loading affects different parts of the nitrogen lump in different ways and this leads to a change in the apparent reaction order.

The underlying phenomena which leads to pseudo nth order kinetics is not a distribution in first order rate constants but is a distribution in first order activation energies. The presence or absence of Ni as a promotor decreases or increases the activation energy for nitrogen conversion. If the conversion of some portion of the nitrogen lump is more amenable to promoters than other portions adding Ni as a promotor is going to expand the activation energy distribution to lower activation energies. This is going to be manifest as a wider range of reactivities and an increase in the apparent reaction order since adding a promotor will increase the reactivity of some portions of the nitrogen lump relative to other portions.

The natural log of the 1.5th reaction order rate constant for the conversion of the nitrogen plotted with respect to reciprocal temperature over the HDN catalyst is presented in Figure 240. The activation energy of nitrogen removal from bitumen changed from about 16 kcal/mol between 625 K and 645 K to around 36 kcal/mol between 650 K and 685 K. The natural log of the first order reaction rate constant for nitrogen removal over the HDM catalyst plotted with respect to inverse temperature is presented in Figure 241. The apparent activation energy for nitrogen removal over the HDM catalyst increased from 23 kcal/mol between 625 K and 645 K to around 40 kcal/mol between 650 K and 685 K.

It is generally expected that lower activation energies are exhibited in the conversion of the more highly reactive portions of a lump. The lower activation energies observed at lower temperatures are therefore related to the conversion of the more reactive portions of the nitrogen lump. The change in activation energy with temperature may indicate that nitrogen is

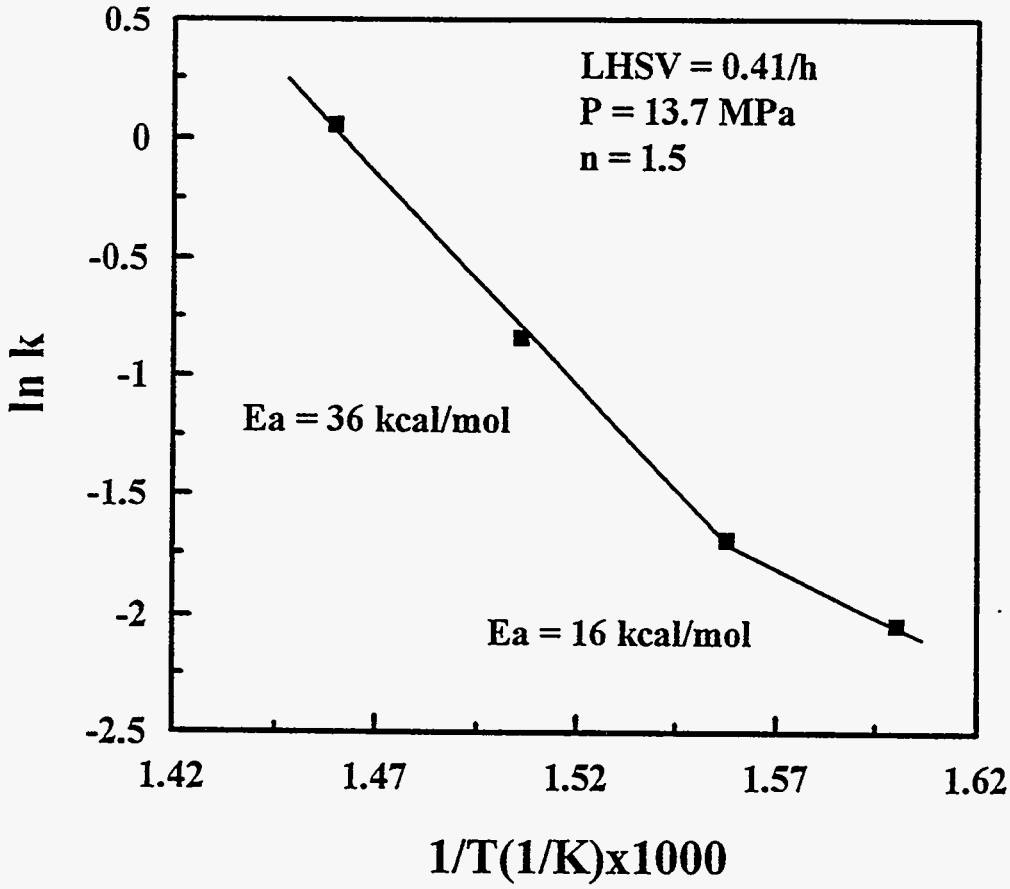

Figure 240.

In k 1.5th Order Rate Constants for Nitrogen Removal Versus Reciprocal Temperature over HDN Catalyst

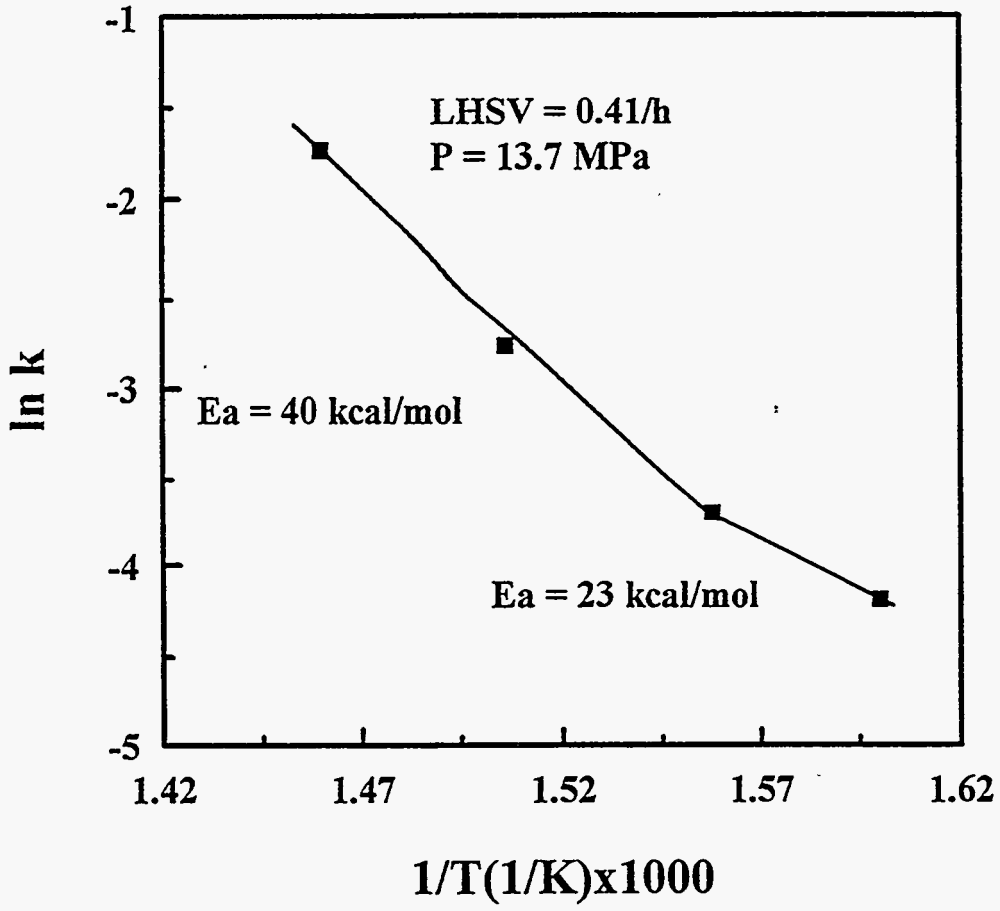

Figure 241.

In k of First Order Rate Constants for Nitrogen Removal Versus Reciprocal Temperature over HDM Catalyst

contained in several types of functional groups and that changing temperature affected conversion of different nitrogen containing functional groups differently.

Although nitrogen conversion from bitumen followed a pseudo 1.5th reaction order over the HDN catalyst, the activation energy of nitrogen removal was obtained from the first order rate constant. This was done to compare activation energies measured with the HDN catalyst with activation energies measured with the HDM catalyst.

The natural log of the first order rate constant for nitrogen removal over the HDN catalyst is plotted with respect to reciprocal temperature in Figure 242. The first order activation energy for nitrogen removal ranged from 15 kcal/mol to 29 kcal/mol as the temperature increased. Comparison of the activation energies for nitrogen removal from Figures 241 and 242 indicated that the activation energy of nitrogen removal over the HDN catalyst was lower than the activation energy of nitrogen removal over the HDM catalyst. This is attributed to the presence of the nickel promotor.

Sulfur and nickel removals and residuum and CCR conversions can be correlated with pseudo reaction orders that are greater than two. According to Ho and Aris (291) a reaction order of two means that a portion of the lump whose conversion is being modeled is essentially unreactive. Since a reaction of two is the upper limit of pseudo nth order kinetics alternatives to pseudo nth order kinetics should be sought when the pseudo reaction order exceeds two. The two parallel first order reaction model has been used in some instances (245, 292). This model may be used to explain sulfur conversion when the sulfur includes asphaltenic and nonasphaltenic sulfur (255, 293).

This model is based on the concept that the various lumps in a feed consist of a facile and a refractory portion whose reactivities differ by more than an order of magnitude (239, 254). Therefore, the relative proportion the facile and refractory portion in a lump should only depend on the feed and not on catalyst selection or on process conditions. However, it has been observed that the relative proportion of facile and refractory portions of lumps is dependant on catalyst selection and reactor temperature (243, 294) thus a parallel-consecutive

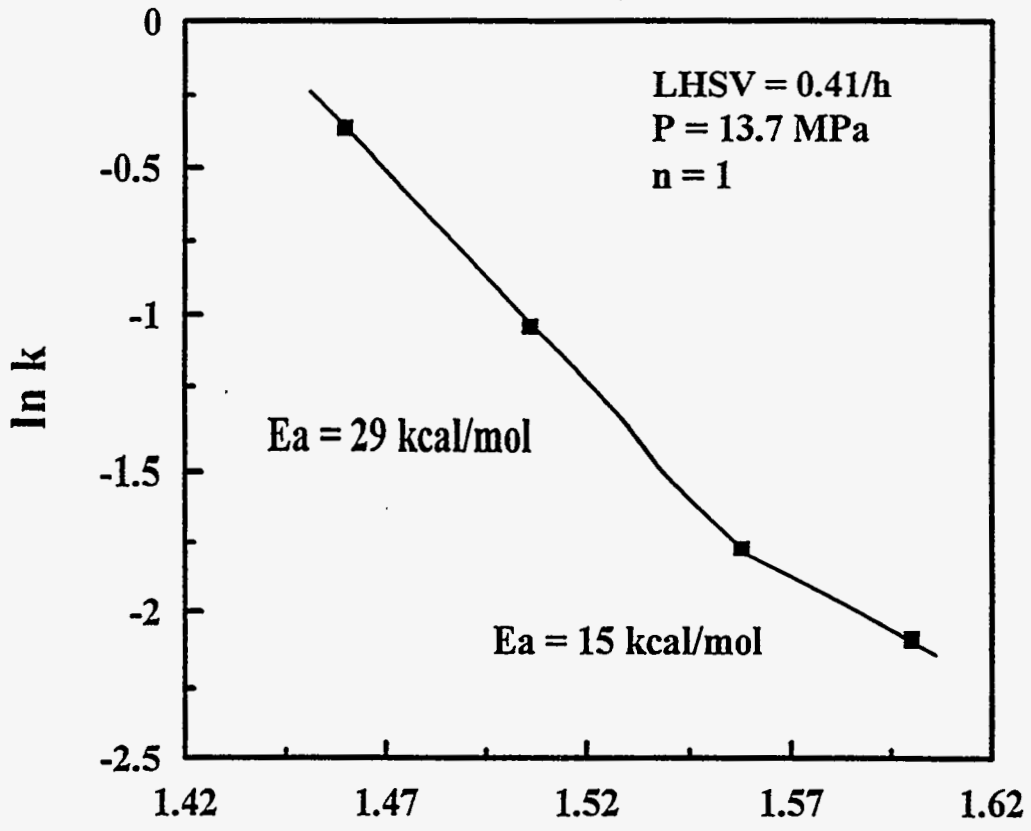

Figure 242.

In k of First Order Rate Constants for Nitrogen Removal Versus Reciprocal Temperature over HDN Catalyst

reaction model was used in place of the two parallel first order reaction model presented in Equation 123.

Residuum Conversion

First order rate constants for the parallel-consecutive reaction model were determined using nonlinear regression. The plot of the remaining fraction versus reciprocal LHSV for residuum conversion over the HDN and HDM catalysts is displayed in Figure 243. The rate constants of the parallel-consecutive reaction model for residuum conversion are presented in Table 80. In Table 80, k_1 represents the direct conversion of the native portion of the lump to products, k_2 represents the conversion of the native portion of the lump to intermediates and k_3 represents the conversion of intermediates to products.

It is clear from the relative magnitudes of k_1, k_2 and k_3 for residuum conversion that native residuum is much more reactive than intermediate residuum. Native residuum is quickly converted to intermediate residuum and to volatile products. Intermediate residuum is only slowly converted to volatile products. The low reactivity attributed to intermediate residuum agrees with the observation that product gas oil derived from residuum conversion is less reactive for cracking than native gas oil (254), i.e., intermediates are less reactive than feed moieties.

It is presumed that the conversion of native residuum consists principally of cleaving side chains from polycyclic clusters. The cleaved side chain will then be in the boiling range of volatile products. The polycyclic cluster will be classified as intermediate residuum or volatile product depending on its molecular weight and polarity (295). The feedstock did not contain any intermediate residuum. The ratio $k_1/(k_1+k_2)$ measures the fraction of residuum directly converted to products because residuum either converted directly to volatile products (k_1) or to less reactive intermediates (k_2). The fraction of the native residuum which was directly converted to products over the HDN and the HDM catalysts was about 0.15 and 0.20. This means that the majority of the residuum was only slowly converted to volatile products through intermediates.

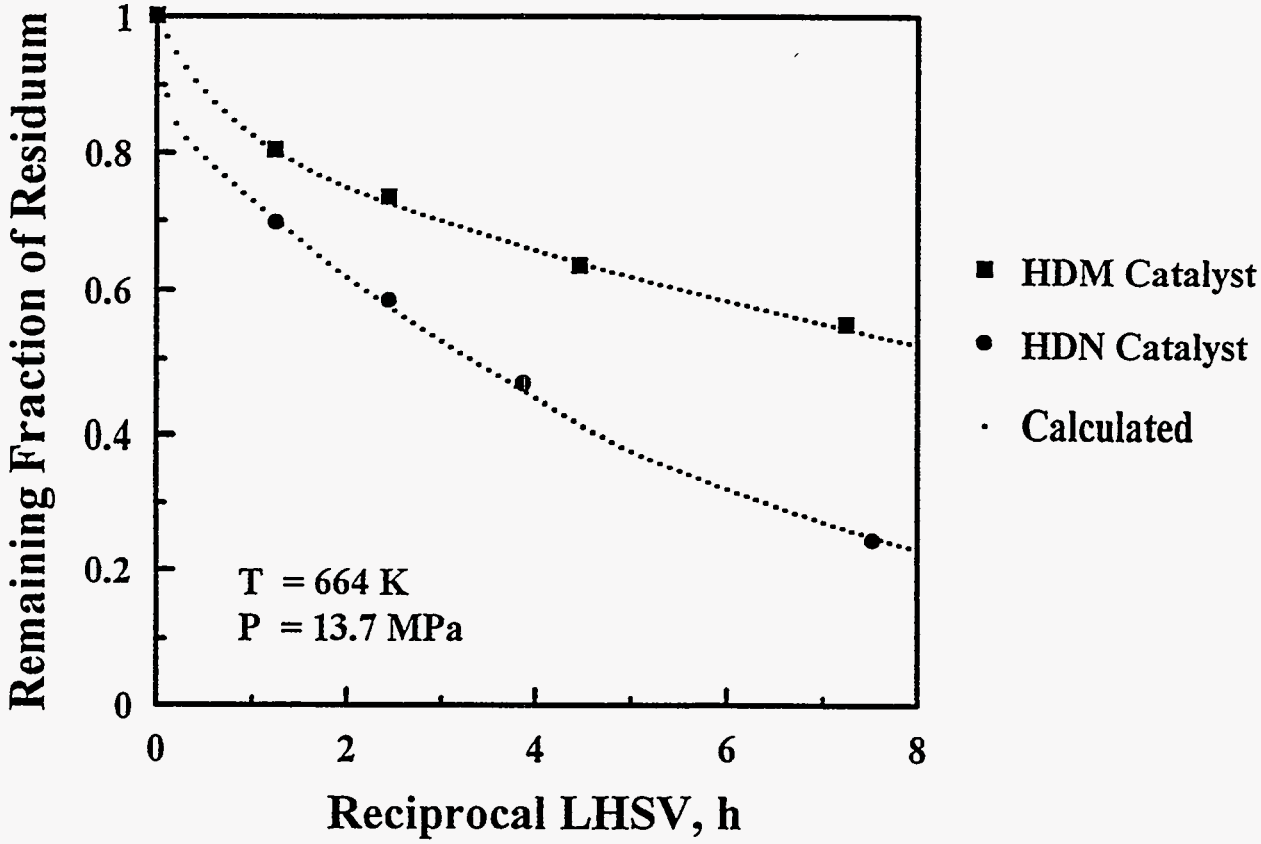

Figure 243.

Remaining Fraction of Residuum Conversion Versus Reciprocal LHSV from Parallel-Consecutive Reaction Model over HDN and HDM Catalysts

The third reaction in the parallel-consecutive reaction model gives information on the rate that intermediates are converted to products. The rate constant (k_3=0.16) for the conversion of intermediate residuum conversion over the HDN catalyst was greater than the rate constants (k_3=0.06) over the HDM catalyst, indicating that the HDN catalyst was more active for intermediate residuum conversion than the HDM catalyst. This was expected because the HDN catalyst contained a higher metal loading than the HDM catalyst.

The activation energies for residuum conversion were obtained using the parallel-consecutive model at different temperatures. Three different activation energies for residuum conversion were determined using a nonlinear regression method. The results are presented in Table 80. A plot of the natural log of the pseudo first order rate constant versus reciprocal temperature for residuum conversion over the HDN and HDM catalysts is presented in Figure 244. The rate constant in this Arrhenius plot, κ, was calculated as if residuum conversion was first order. Because this is incorrect the Arrhenius plot presented in Figure 244 is only able to give general information about apparent activation energy and temperature. The dotted lines in Figure 244 are from conversions estimated with the parallel-consecutive model and parameters reported in Table 80. The slope of the Arrhenius plot increased with increasing temperature for residuum conversion over the HDN catalyst. This indicates that residuum conversion did not become diffusion limited at higher temperatures. The slope of the Arrhenius plot remained constant for residuum conversion over the HDM catalyst.

Residuum conversion was achieved by different means on the different catalysts. There were at least three different possible pathways for residuum conversion in this system: thermal, alumina catalyzed and metal sulfide catalyzed. These three pathways are linked and all three may be combined to varying degrees in a single rate constant. Changing catalyst properties in terms of alumina surface area and/or acidity, metal loading and/or promotor concentration changes the relative rates of the three pathways. This was reflected in the apparent activation energies of the HDN and the HDM catalysts.

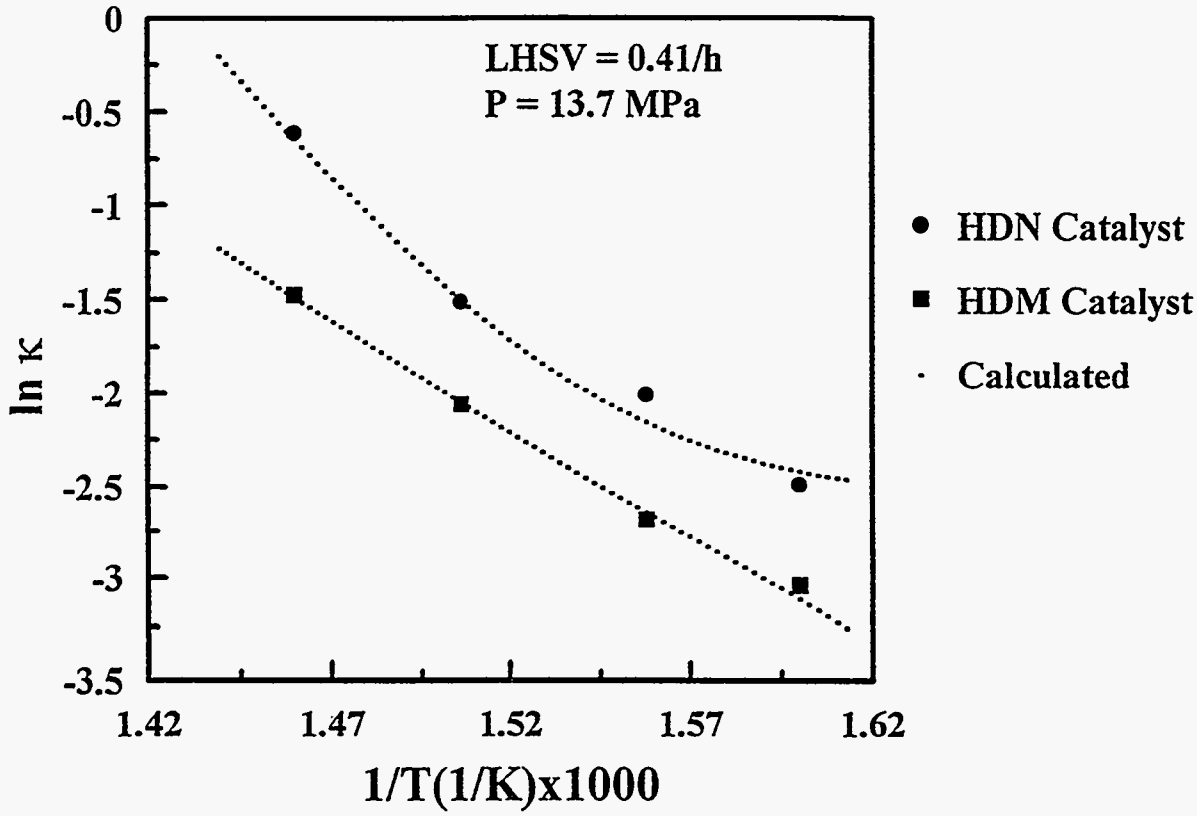

Figure 244.

In κ Versus Reciprocal Temperature for Residuum Conversion from Parallel-Consecutive Reaction Model over HDN and HDM Catalysts

Table 80: Kinetic Parameters from Parallel-Consecutive Reaction Model

	Residuum	Sulfur	Nickel	CCR
HDN Catalyst				
$k_1(h^{-1})$	1.92	0.72	1.25	0.58
$k_2(h^{-1})$	10.9	0.47	0.55	0.58
$k_3(h^{-1})$	0.16	0.04	0.07	0.10
$k_1/(k_2+k_3)$	0.15	0.61	0.69	0.50
E_1(kcal/mol)	8	21	11	21
E_2(kcal/mol)	10	17	2	21
E_3(kcal/mol)	46	2	3	43
HDM Catalyst				
$k_1(h^{-1})$	0.28	0.55	2.55	0.72
$k_2(h^{-1})$	1.13	0.74	8.79	1.45
$k_3(h^{-1})$	0.06	0.07	0.10	0.06
$k_1/(k_2+k_3)$	0.20	0.43	0.23	0.33
E_1(kcal/mol)	20	35	15	11
E_2(kcal/mol)	1	29	3	1
E_3(kcal/mol)	34	1	10	23

Residuum conversion activation energies for k_1, k_2, and k_3 over the HDN catalyst were 8 kcal/mol, 10 kcal/mol and 46 kcal/mol; respectively, and the apparent activation energies for k_1, k_2, and k_3 over the HDM catalyst were 20 kcal/mol, 1 kcal/mol and 34 kcal/mol; respectively. Because the rate constants for the conversion of the native residuum were so high kinetic parameters associated with the conversion of native residuum have wider margins of error than kinetic parameters for the conversion of intermediate residuum. The apparent activation energy for the direct conversion of native residuum over the HDM catalyst was 20 kcal/mol. The activation energy for the conversion of native residuum to intermediate residuum over the HDM catalyst was 1 kcal/mol. This difference explains why increasing temperature significantly favors conversion of the native residuum through the direct pathway. The difference between the activation energies for the direct and indirect conversion of native residuum over the HDN catalyst was smaller indicating that temperature did not significantly affect whether or not the native residuum converted by the direct or the indirect pathway.

The activation energy for intermediate residuum conversion over the HDN catalyst was 46 kcal/mol over the HDN catalyst and 34 kcal/mol for the HDM catalyst. It is expected that in the competition between thermal and catalytic contributions in a conversion mechanism for a given lump, increasing catalytic activity will result in a decrease in the activation energy for the conversion of the lump. The opposite has occurred in that the activation energy observed with the high metal loading HDN catalyst is higher than it is with the lower metal content HDM catalyst. Heavy oil conversion is extremely complicated and it is unlikely that a simple model can be developed that will reflect the actual mechanisms that are occurring. However, kinetic model development consists of presenting and verifying models. Models which are not verified by data are useful in that they may suggest new experiments or improvements in the model (296). In this process there is a continuum between a purely correlative model such as a polynomial and a very complicated model based on physical principles. The parallel-consecutive model is better at correlating data than the two parallel first order reaction model and pseudo nth order reaction model. This is because it accounts for the direct vs. indirect

conversion of native residuum with different catalysts. However, it still does not reflect the intrinsic chemistry of residuum conversion.

Sulfur Removal

Removal of heteroatoms and metal compounds may involve several intermediate steps before heteroatom and metal compounds are completely removed as NH_3, H_2S or metal sulfides (297, 298). Heteroatom and metal removal may also be sterically hindered during hydrotreating because of the complexity of bitumen (299).

The plots of the fraction remaining versus reciprocal LHSV for sulfur removal over the HDN and HDM catalysts are presented in Figure 245. The rate constants for the parallel-consecutive model for sulfur removal are presented in Table 80. The ratios $k_1/(k_1+k_2)$ for the direct sulfur removal route over the HDN and HDM catalysts were 0.61 and 0.43, respectively. The rate constant ($k_3=0.04$) for the conversion of the intermediate sulfur over the HDN catalyst was lower than that for the HDM catalyst ($k_3=0.07$). Although the data is well correlated by the parallel-consecutive model the conclusion that the HDN catalyst was less active than the HDM catalyst for intermediate sulfur conversion is implausible. It is apparent from Figure 245 that sulfur conversion is initially rapid with both catalysts and that the more active HDN catalyst reaches a kinetic barrier between about 60 and 65 % sulfur conversion. Very little additional sulfur conversion was achieved beyond this barrier. It appears that 35-40% of the sulfur in the high asphaltene PR Spring bitumen was so unreactive that further conversion was extremely slow. Sulfur conversion kinetics for other Uinta Basin bitumens that exhibit lower asphaltene contents than the PR Spring bitumen did not exhibit a kinetic barrier that was as severe as that for the higher asphaltene PR Spring bitumen (245, 294). Because the HDM catalyst was less active than the HDN catalyst sulfur conversion over the HDM catalyst did not encounter the kinetic barrier that was observed with the HDM catalyst. Thus the activity of the HDM catalyst appeared to be higher than that of the HDN catalyst for the conversion of intermediate sulfur. This higher apparent activity was related to the fact that the

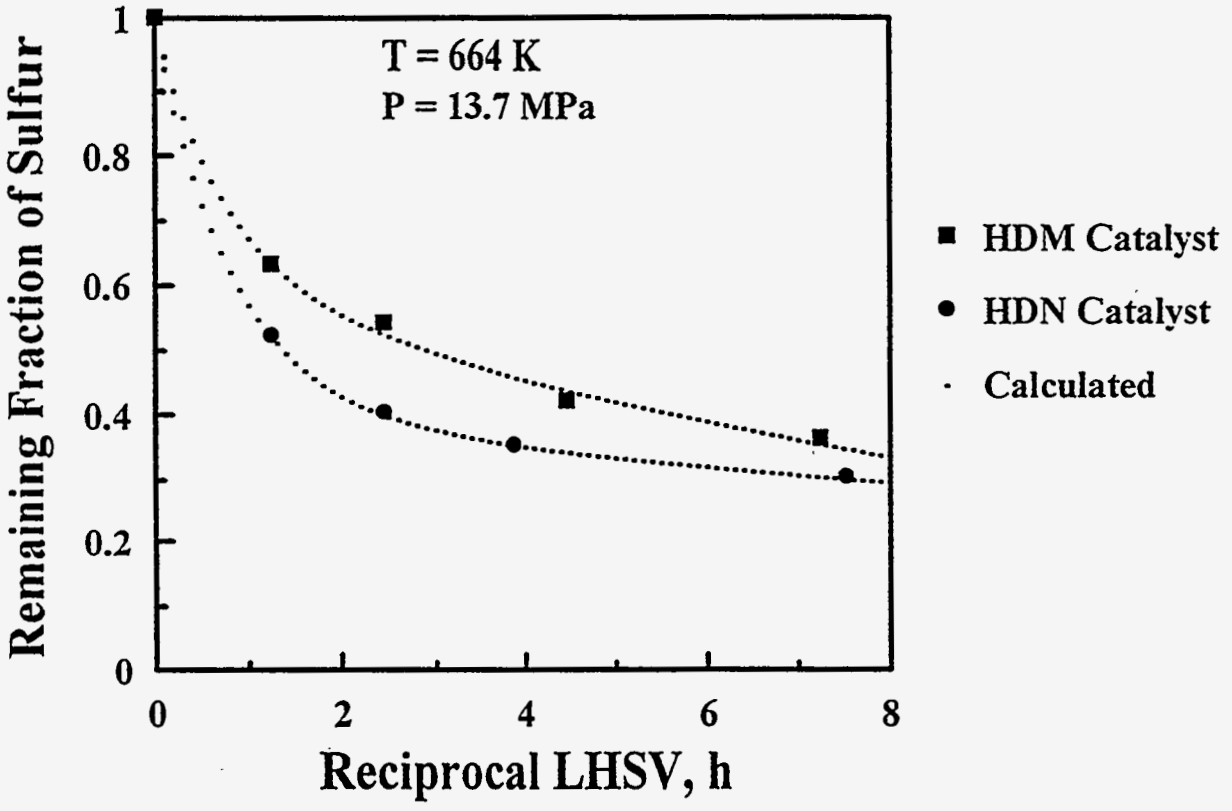

Figure 245.

Remaining Fraction of Sulfur Removal Versus Reciprocal LHSV from Parallel-Consecutive Reaction Model over HDN and HDM Catalysts

sulfur conversion over the HDM catalyst was not high enough to approach the kinetic barrier within the range of experimental conditions investigated in these studies. This observation suggests that if more data was available the parallel-consecutive model could be hybridized with the two parallel first order reaction model. The hybridized model would account for the presence of unreactive sulfur in the PR Spring bitumen feed and would also account for the conversion of the reactive sulfur through direct and indirect pathways.

A second alternative would be to consider a distributed activated energy model (300). A distributed activation model accounts for a range of first order reactivities within a lump and that the distribution of reactivities is being driven by a distribution of activation energies. At higher processing severities and/or with higher activity catalysts further conversion consists of converting less reactive portions with higher activation energies. A distribution of activation energies would therefore explain why some activation energies are higher with the HDN catalyst than with the HDM catalyst. Because the HDN catalyst cuts deeper into the sulfur lump at low severities, the sulfur that is not converted at low severities exhibits less reactivity with the HDN catalyst than with the HDM catalyst. At low conversions the portions of the lump with lower activation energies are converted first. At longer residence times and/or with higher activity catalysts further conversion consists of converting less reactive portions with higher activation energies. A distribution of activities would therefore explain why some activation energies are higher with the HDN catalyst and why the HDN catalyst appears to be less active than the HDM catalyst at longer residence times.

The plots of the natural log of the apparent first order rate constant for sulfur removal versus reciprocal temperature over the HDN and HDM catalysts are displayed in Figure 246 and the kinetic parameters of the parallel-consecutive reaction model for sulfur removal are presented in Table 80. The apparent activation energy for sulfur removal decreases with increasing temperature. If the data were truly first order the decreasing slope in the Arrhenius plot observed with increasing temperature would indicate that diffusion resistance is significant. The conclusion that diffusion resistance is significant is erroneous for the

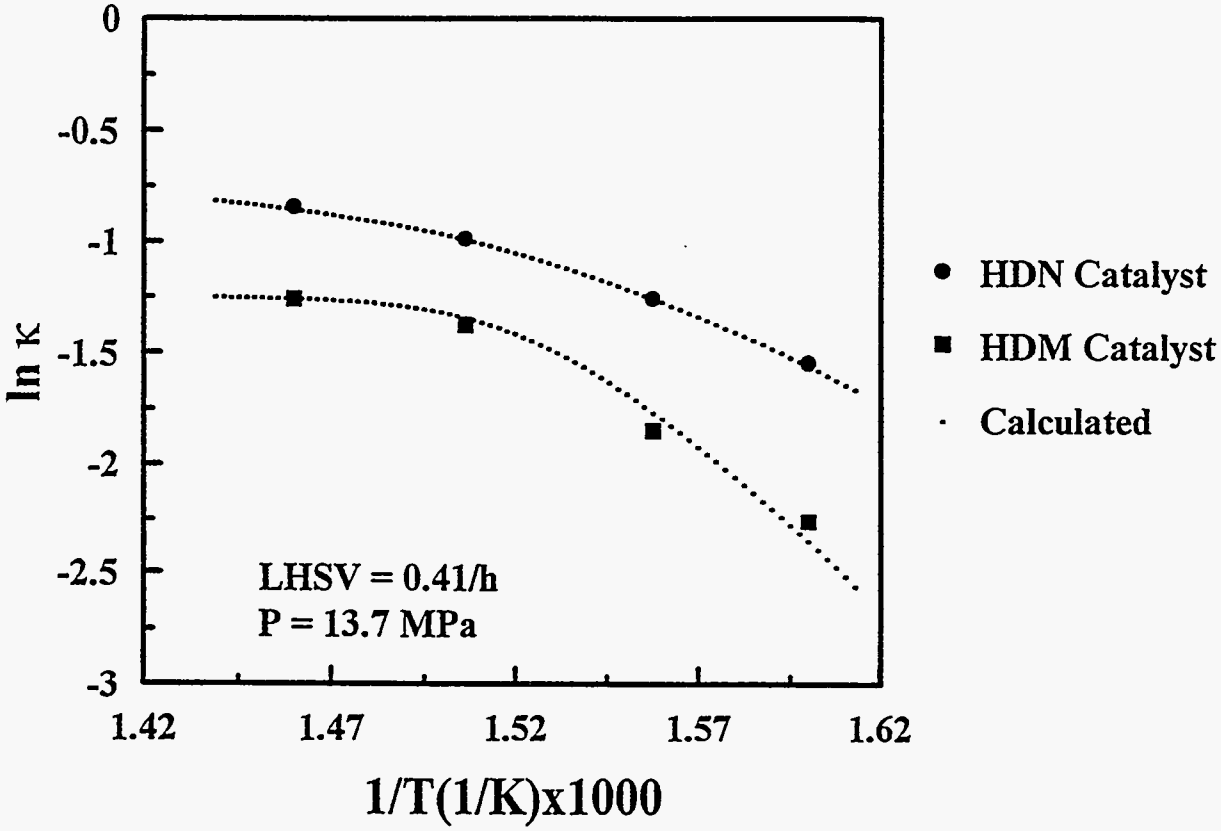

Figure 246.

In κ Versus Reciprocal Temperature for Sulfur Removal from Parallel-Consecutive Reaction Model over HDN and HDM Catalysts

following reasons. The apparent diffusion resistance is strongest with the less active HDM catalyst and it is not observed with other lumps that are at least as reactive as sulfur. The decreasing slope was an artifact because sulfur conversion kinetics were not simple first order. The decrease in slope was because the temperature was high enough for the most reactive sulfur to be conversion but yet high enough for significant conversion of the unreactive sulfur to occur. It is presumed that if process temperatures were increased to the point that the unreactive sulfur in the PR Spring bitumen became reactive the Arrhenius plot would begin to curve up with increasing temperature.

Sulfur conversion occurred by a parallel-consecutive mechanism as did residuum conversion. HDS of bitumen (267) and model compounds (261, 266) have shown that sulfur can be removed by direct hydrogenolysis of aliphatic and aromatic sulfur (301, 302). HDS can also occur through a series reaction in which heteroatomic rings are first hydrogenated. Sulfur removal then occurs through hydrogenolysis of C-S bonds (301, 303). This combination of intermediate and direct pathways may explain why HDS appeared to proceed through a parallel-consecutive mechanism. It has also been proposed that sulfur conversion in heavy oils is partly linked to residuum conversion in that sulfur contained in residuum cannot be converted until the residuum is converted to lower molecular weight products (245, 292).

Nickel Removal

It has been proposed that metals are removed by direct metal abstraction in the presence of hydrogen and hydrogen sulfide (304). Metals may also be removed in a series reaction in which metal porphyrins are first hydrogenated and then the metal is removed by hydrogenolysis (305-307). Feed metal compounds may be changed into intermediate metal species by the removal of side chains and functional groups that impart steric hinderance.

Nickel removal from the PR Spring bitumen was modeled with the parallel-consecutive model. The plots of the fraction remaining versus reciprocal LHSV for nickel removal over the HDN and HDM catalysts are presented in Figure 247. The rate constants of the parallel-

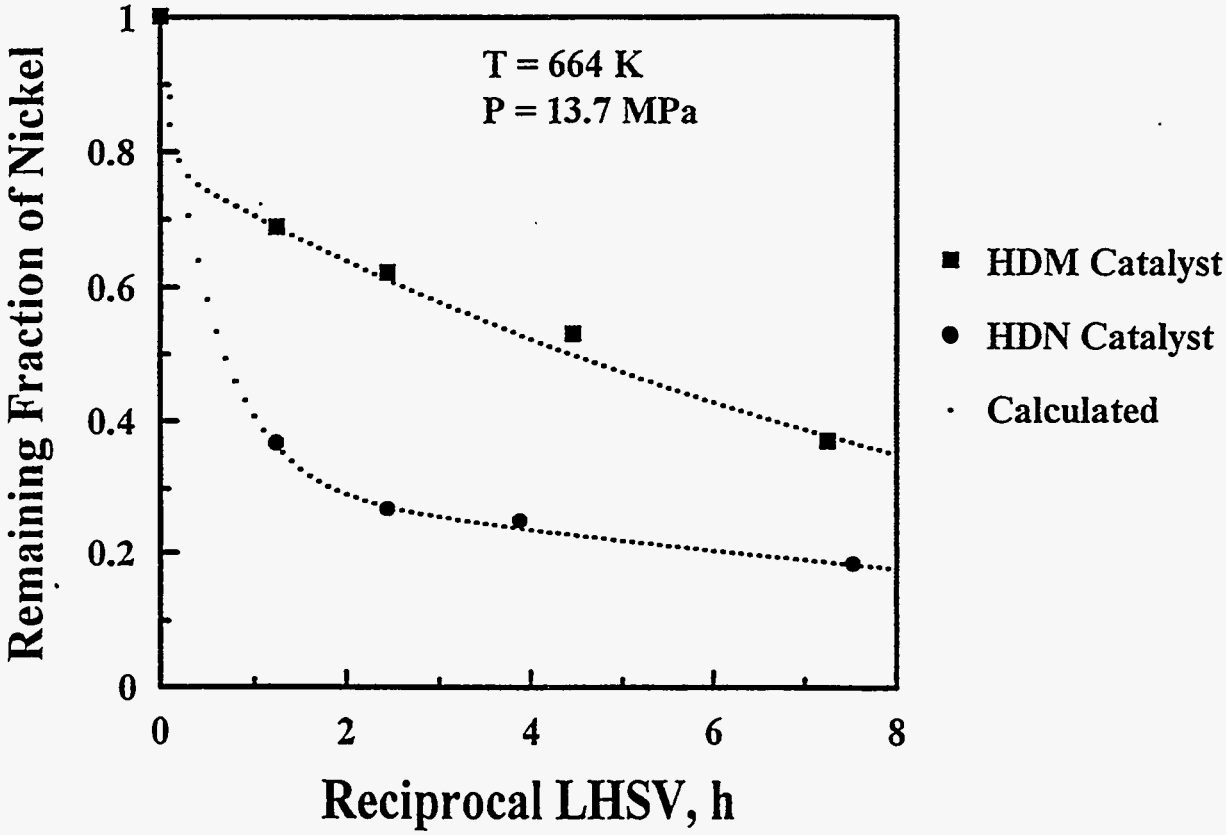

Figure 247.

Remaining Fraction of Nickel Removal Versus Reciprocal LHSV
from Parallel-Consecutive Reaction Model
over HDN and HDM Catalysts

consecutive model for nickel removal are presented in Table 80. The direct route for nickel removal was the prime conversion pathway over the HDN catalyst ($k_1/(k_1+k_2)$ = 0.69) and was significantly less important with the HDM catalyst ($k_1/(k_1+k_2)$ = 0.23). The higher activity of the HDN catalyst was manifest in favoring direct nickel removal relative to indirect removal. The rate constant (k_3=0.07) for the conversion of intermediate nickel over the HDN catalyst was lower than the HDM catalyst (k_3=0.10). This is the same phenomena that was observed with sulfur. It was concluded that the consecutive-parallel model is a correlative model and that nickel and sulfur conversion are more complicated than the mechanism that is suggested by this model.

The plots of the natural log of the apparent first order rate constant for nickel removal versus reciprocal temperature over the HDN and HDM catalysts are presented in Figure 248 and the kinetic parameters of the parallel-consecutive reaction model for nickel removal are presented in Table 80. The activation energy for the conversion of intermediate nickel was as low as 3 kcal/mol over the HDN catalyst. Generally there is an inverse relationship between activation energy and the rate constant. This is related to the compensation effect (308-310). The rate constant for intermediate nickel removal was low over the HDN catalyst. Because of compensation effect it is expected that low rate constants would be accompanied by high activation energies. The opposite was observed with intermediate nickel removal. This may be because the rate constant for intermediate nickel conversion was so low at these conditions that intermediate nickel conversion was dwarfed by feed nickel conversion when the two were lumped. It is presumed that if the temperature had been raised intermediate nickel removal would have become increasingly important relative to native nickel conversion and the apparent activation energy for intermediate nickel removal would have increased.

The rate constant for intermediate nickel removal over the HDM catalyst was higher than it was for the HDN catalyst in spite of the higher metal loading of the HDN catalyst. This suggests that some of the intermediate nickel in the model is actually refractory nickel in the feed. The same phenomena was also observed with the sulfur and suggests that a more

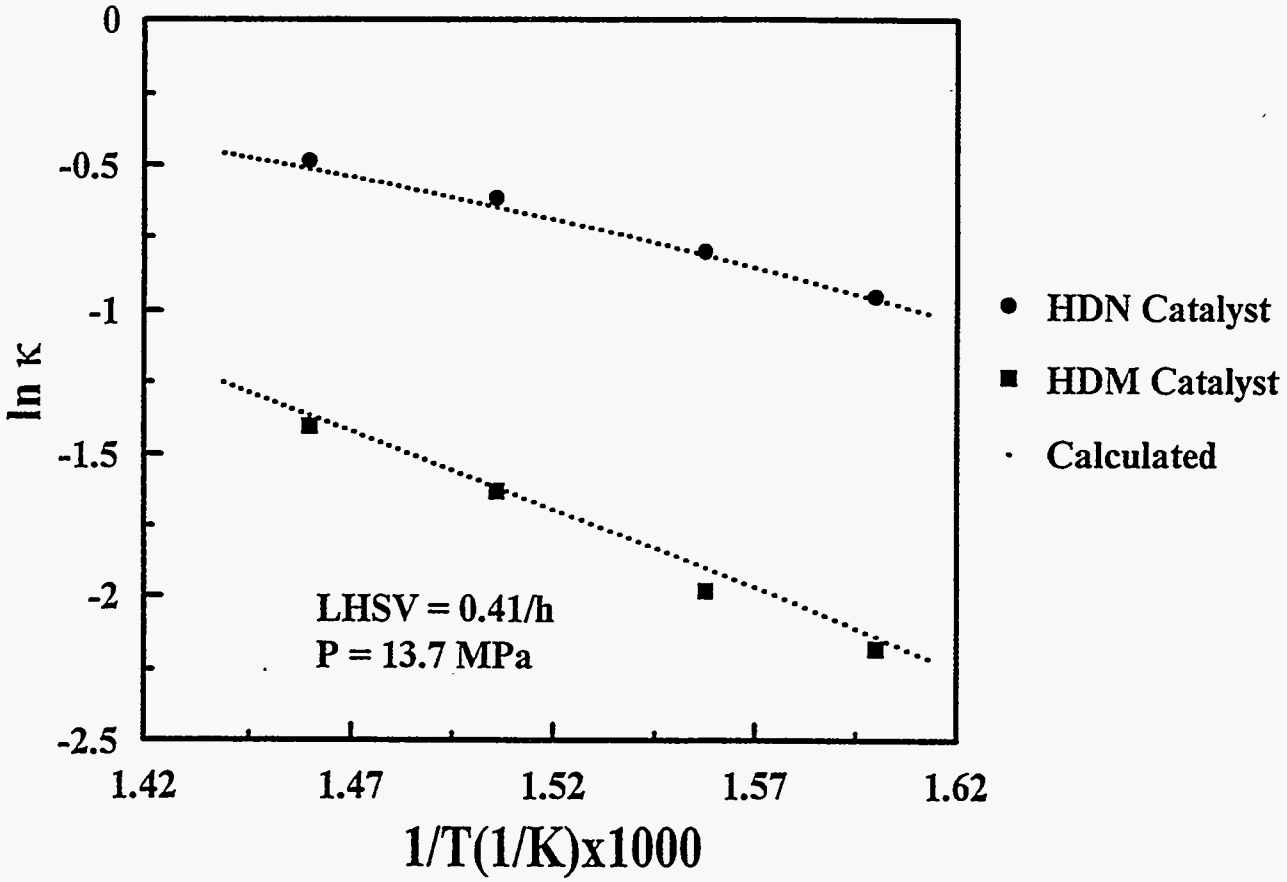

Figure 248.

In κ Versus Reciprocal Temperature for Nickel Removal from Parallel-Consecutive Reaction Model over HDN and HDM Catalysts

appropriate model would be a hybrid of the consecutive-parallel and the two parallel first order reaction model.

Because the HDN catalyst was more active than the HDM catalyst it was able to make faster progress until it encountered the kinetic barrier provided by the unreactive nickel. Further progress was extremely slow because of the low reactivity of the remaining nickel. Nickel removal with the less active HDM catalyst trails nickel removal with the HDN catalyst at all residence times. Because of this nickel removal over the HDM catalyst did not reach the kinetic barrier as quickly as the nickel removal with the HDN catalyst. Greater incremental nickel conversions were observed with the HDM catalyst at long residence times than with the HDN catalyst. This evidence incorrectly suggests that the HDM catalyst was more active for removal of intermediate nickel than the HDN catalyst.

Moieties that have been partially processed without actually being converted are less reactive (311). The lower reactivity of the intermediate nickel formed over the HDN catalyst could be because the HDN catalyst was able to produce deeper conversion of the nickel. A secondary effect of that higher activity was production of an intermediate nickel which was less reactive than the intermediate nickel formed over the HDM catalyst.

CCR Conversion

It is known that CCR is reduced by hydrogenation of aromatic rings (intermediate CCR), followed by hydrogenolysis of the rings (239). Feed CCR may also go through intermediate CCR by the removal of side chains. Some CCR moieties that are not sterically hindered may undergo direct catalytic conversion. For this reason, the apparent reaction order for CCR conversion may be higher than first order. Beaton et al. (239) proposed that the reduction of CCR did not follow a simple first order reaction, and that the reaction is coupled thermally and catalytically. The direct conversion of CCR and the consecutive reduction of CCR via an intermediate route may be illustrated by a parallel-consecutive reaction model.

The plots of the fraction remaining versus reciprocal LHSV for CCR conversion over the HDN and HDM catalysts are presented in Figure 249. The rate constants of the parallel-consecutive model for CCR conversion are presented in Table 80. The rate constant (k_3 = 0.1) for the conversion of intermediate CCR over the HDN catalyst was higher than the corresponding rate constant over the HDM catalyst (k_3 = 0.06). The direct route for CCR removal over the HDN catalyst ($k_1/(k_1+k_2)$ = 0.50) was greater than with HDM catalyst ($k_1/(k_1+k_2)$ = 0.33). The greater proportion of the CCR that was converted through the faster direct route was the result of the apparently greater activity of the HDN catalyst.

The plots of the natural log of the apparent first order rate constant for CCR conversion versus reciprocal temperature over the HDN and HDM catalysts are presented in Figure 250 and the kinetic parameters of the parallel-consecutive reaction model for CCR conversion are presented in Table 80. The activation energy for the conversion of the native CCR to intermediate CCR was 1 kcal/mol. This activation energy is unrealistic and does not agree with values of 22-26 kcal/mol that have been reported for the activation energy of CCR conversion (294). The consecutive-parallel is a good correlative model but it does not completely represent the actual mechanism which is occurring. This could also be because the range of experimental conditions was not broad enough to accurately determine the activation energy of the faster reactions.

CCR conversion appears to be similar in some respects to residuum conversion in that the HDM catalyst gave a higher activation energy for intermediate CCR conversion than the HDN catalyst. The same trend was observed with residuum conversion and was expected due to the higher catalytic activity of the HDN catalyst. This may be because the reactivities of the residuum and CCR in the PR Spring bitumen feed are more homogenous than the reactivities of the sulfur and nickel. Because of this the parallel-consecutive model is a better representation of residuum and CCR conversion than it is for sulfur and nickel removal.

Conversion of intermediate residuum consisted mainly of hydrogenation of aromatic rings, followed by C-C bond cleavage. For that reason the higher metal HDN catalyst

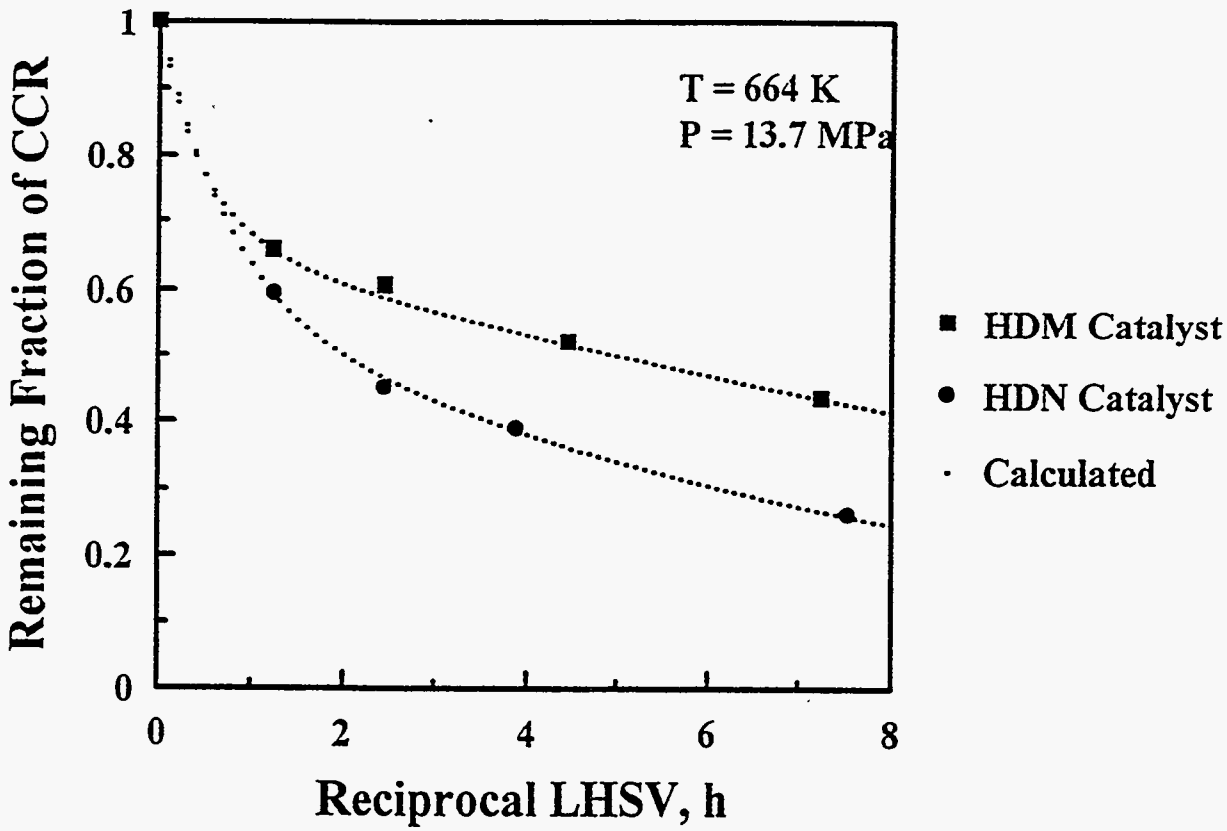

Figure 249.

Remaining Fraction of CCR Conversion Versus Reciprocal LHSV
from Parallel-Consecutive Reaction Model
over HDN and HDM Catalysts

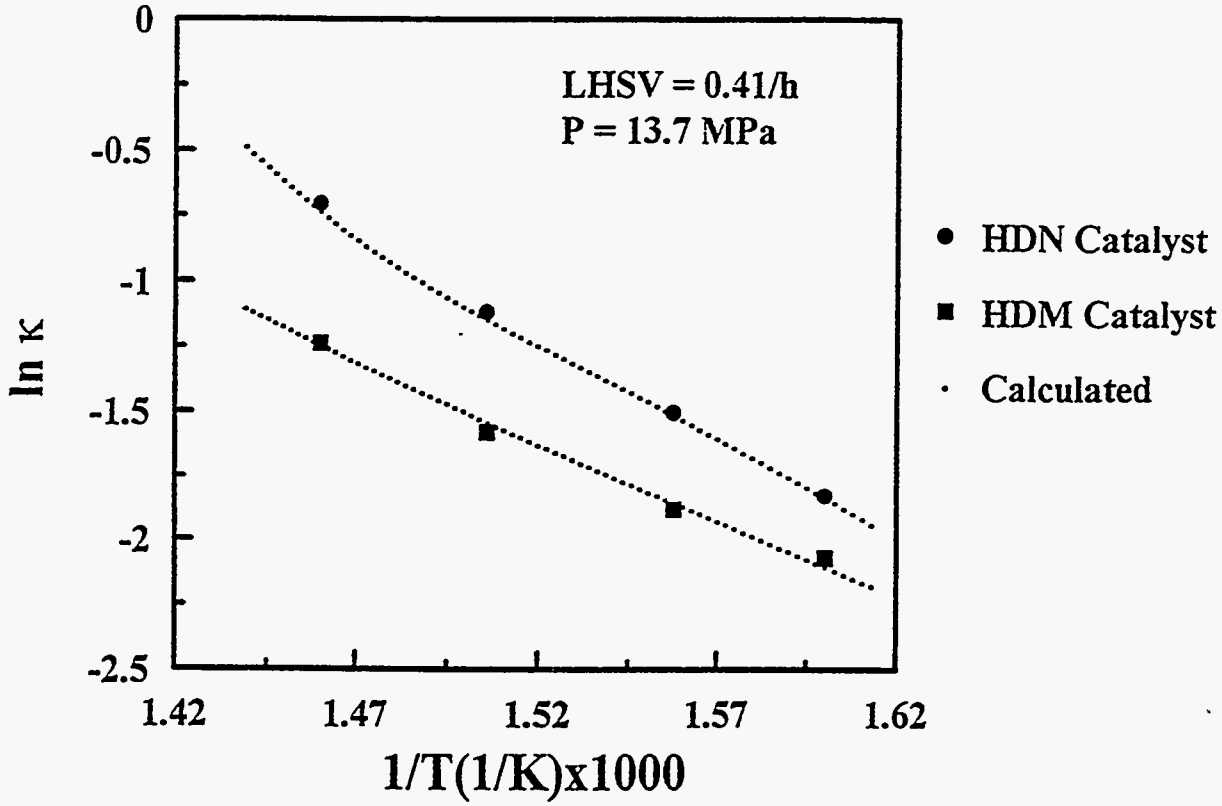

Figure 250.

In κ Versus Reciprocal Temperature for CCR Conversion from Parallel-Consecutive Reaction Model over HDN and HDM Catalysts

exhibited higher activity for intermediate residuum conversion than the lower metal content HDM catalyst.

Effect of Reactor Pressure

The effect of pressure on PR Spring heavy oil upgrading was only investigated with the HDM catalyst. When the effect of temperature and LHSV was studied over the HDM catalyst, total system pressure was kept constant so that the apparent rate constant, k_{app}, would not be affected by pressure variations. The effect of hydrogen partial pressure may be correlated by using a power term, β, on the hydrogen partial pressure in the rate expression (312, 313). Equations (124), (125), (126) and (130) may then be modified in the following manner in order to describe the dependence of conversion on hydrogen partial pressure:

$$\frac{dC_A}{dt} = -(k_1 P_{H_2}^{\beta_1} + k_2 P_{H_2}^{\beta_2}) C_A \tag{139}$$

$$\frac{dC_A^*}{dt} = k_2 P_{H_2}^{\beta_2} C_A - k_3 P_{H_2}^{\beta_3} C_A^* \tag{140}$$

$$\frac{dC_p}{dt} = k_1 P_{H_2}^{\beta_1} C_A + k_3 P_{H_2}^{\beta_3} C_A^* \tag{141}$$

$$(1-x_A) = \exp(-(k_1 P_{H_2}^{\beta_1} + k_2 P_{H_2}^{\beta_2}) t) + \frac{k_2 P_{H_2}^{\beta_2}}{k_3 P_{H_2}^{\beta_3} - k_1 P_{H_2}^{\beta_1} - k_2 P_{H_2}^{\beta_2}} [\exp(-(k_1 P_{H_2}^{\beta_1} + k_2 P_{H_2}^{\beta_2}) t) - \exp(-(k_3 P_{H_2}^{\beta_3}) t)] \tag{142}$$

$$\frac{dC_i}{d\tau} = -k C_i^n P_{H_2}^{\beta} \tag{143}$$

$$-\ln(1-x_i) = P_{H_2}^{\beta} k\tau \tag{144}$$

The partial pressure of hydrogen was determined from vapor-liquid equilibrium calculations for feed and product streams at reactor conditions. Vapor-liquid equilibrium

calculations are described in detail by Kim (243). Hydrogen partial pressures were used to estimate β for the various rate constants which appear in the pseudo nth order and in the parallel-consecutive models.

Because nickel and sulfur removal and CCR and residuum conversion over the HDM catalyst did not follow nth order kinetics, the magnitude of β was determined by nonlinear regression to calculate the parameters which appear in Equation (142). Non-linear regression was also used to correlate k_{app} and E_{app} for the various reactions in the parallel-consecutive reaction model. These values for k_{app} and E_{app} were slightly different than the original values because the addition of β terms in the regression permitted a slightly improved fit. The results of the regression analysis are presented in Table 81.

Pressure exhibited little influence on native sulfur removal, and on the conversions of native CCR and residuum. It is therefore concluded that conversion of feed moieties consisted of reactions which are not strongly dependant on hydrogen. In residuum conversion these reactions would probably consist of cleavage of alkyl side chains from polynuclear clusters. The low value of β for the conversion of feed residuum is in agreement with McColgan et al. [241] who reported that hydrogen partial pressure did not affect residuum cracking.

Pressure exhibited a significant influence on the removal of intermediate sulfur and on the conversion of intermediate CCR and intermediate residuum. This suggests that hydrogen is directly involved in the conversion of these intermediate species. Perhaps the conversion of these intermediates involves the hydrogenation of aromatic rings in polycyclic clusters.

The suggested mechanism for residuum conversion is that alkyl side chains are quickly removed from polycyclic clusters at low severities. The polycyclic clusters which remain in the gas oil or residuum boiling range depend on their molecular weight and polarity. If these clusters are in the residuum boiling range they would be classified as intermediate residuum in the consecutive-parallel reaction model. Aromatic ring hydrogenation should be important for further conversion of these polycyclic clusters which is consistent with the β of 1.3 for the conversion of intermediate residuum.

Table 81: k_{app}, E_{app} and Obtained at Different Pressures from Parallel-Consecutive Reaction Model

	Residuum	Sulfur	CCR
$k_1(h^{-1})$	0.28	0.52	0.72
$k_2(h^{-2})$	1.16	0.74	1.66
$k_3(h^{-3})$	0.002	0.002	0.006
E_1(kcal/mol)	19	38	9
E_2(kcal/mol)	1	32	1
E_3(kcal/mol)	35	1	28
β_1	0.002	0.080	0.010
β_2	0.002	0.095	0.001
β_3	1.3	1.3	1.0

Because nitrogen removal over the HDM catalyst followed first order kinetics, the magnitude of β was determined by plotting the logarithm of the first order rate constant determined for runs conducted at different pressure versus the logarithm of the hydrogen partial pressure. The slope of the plot of ln k versus ln P_{H_2} gives a value of β for nitrogen removal. A plot of the natural log of the first order rate constant for nitrogen removal versus ln P_{H_2} is presented in Figure 251. The slope was 0.7. This is consistent with the role that hydrogenation plays in the conversion of organic nitrogen.

Speight (314) found that the extent of heteroatom removal was improved by increasing hydrogen partial pressure because heteroatom removal, aromatics saturation and cracking are dependent on hydrogen pressure. Yui (312) reported that the reaction order with respect to hydrogen partial pressure varied from 1.2 to 1.8 for nitrogen removal of Athabasca bitumen-derived coker gas oil. The lower value obtained in these studies may be because these experiments were conducted in the upflow mode instead of in the downflow mode as was done by Yui (312).

SUMMARY AND CONCLUSIONS

Kinetics for conversion of CCR and residuum, as well as for removal of sulfur and metal were described by the parallel-consecutive reaction model over the HDN catalyst and the HDM catalyst. Pseudo nth order kinetics were used to correlate nitrogen removal over both catalysts. Nitrogen conversion over the nickel promoted HDN catalyst exhibited a 1.5 reaction order and was first order over the unpromoted HDM catalyst. The difference in reaction orders may be related to the nickel promotion of the HDN catalyst which creates active sites that enhance the conversion of some portions of the nitrogen lump to a greater extent than other portions. This broadened the range of the nitrogen reactivity and increased the apparent reaction order.

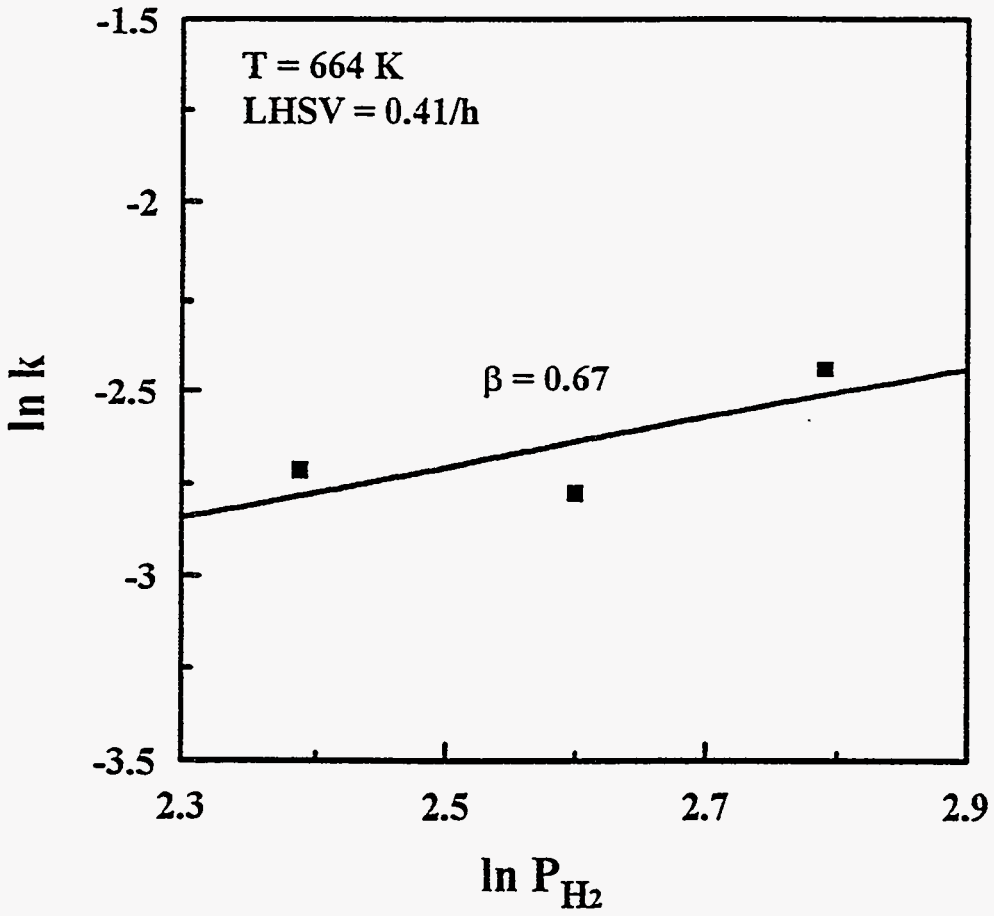

Figure 251.

In κ Versus In for Nitrogen Removal over HDM Catalyst

Pressure exhibited little influence on the conversion of feed sulfur, CCR and feed residuum conversion. However, pressure exhibited a significant influence on the conversion of intermediate sulfur, CCR and residuum over the HDM catalyst.

UINTA BASIN BITUMEN HYDROTREATING: CATALYTIC UPGRADING OF THE ASPHALT RIDGE BITUMEN

Principal Investigator: Francis V. Hanson
Postdoctoral Fellow: D.C. Longstaff
Graduate Student: T.-F. Yeh

INTRODUCTION

As the world supply of the light crude oil is preferentially depleted, bitumens, heavy oils, and petroleum residues will become more and more important to meet the demand for fuels and petrochemical feedstocks. The combination of higher fuel prices and more stringent environmental regulations has given rise to a new generation of process alternatives and focused attention on the efficient upgrading of bitumens, heavy oils and residues(315).

The depletion of conventional crude oil reserves may lead to the use of oil sands resources which are estimated at about 2.3 trillion barrels of original bitumen in-place as an alternate fossil fuel resource(181, 316). Oil sand bitumens contain high molecular weight species and more oxygen, nitrogen, and sulfur than conventional crude oils. Hence, oil sand bitumens must be upgraded before being integrated as refinery feedstocks.

Traditionally upgrading is classified according to whether carbon rejection or hydrogen addition is used to increase the hydrogen/carbon ratio. Carbon rejection is intended to remove asphaltenes and carbon residues in the form of coke by thermal cracking. Hydrogen addition is intended to increase the hydrogen/carbon ratio by hydrotreating(317, 318). The products from hydrotreating are of higher quality than those produced via the carbon rejection route(319).

The primary purpose of hydrotreating is to reduce the concentration of heteroatoms such as sulfur, nitrogen, oxygen, and metals in the total liquid product produced from the bitumen. Hydrogen addition may be conducted with or without a catalyst. Catalytic hydroprocesses are executed at moderately high temperatures (648-

693 K) and pressures (3.5-13.8 MPa) with CoMo/alumina or NiMo/alumina catalysts(320). Noncatalytic hydroprocesses are conducted at temperatures of 603-715 K and pressures of 11.8-15.2 MPa. Thus thermal reactions may occur during catalytic hydroprocesses(321).

The bitumen from the Asphalt Ridge (Utah) oil sands is higher in nitrogen and lower in sulfur content compared with the Athabasca bitumen from Canadian oil sands and residue from petroleum feedstocks(82) and has a lower metals content. These properties led to the selection of hydrodenitrogenation catalysts as potential candidates for hydrotreating the Asphalt Ridge bitumen.

Sulfur and nitrogen removals are required to minimize SO_x and NO_x production during fuel combustion. Environmental regulations will be more stringent in the future. Thus deep desulfurization and denitrogenation will be required to upgrade bitumen and heavy oils prior to integration into refinery feed slates. Metals deposition causes the deactivation of desulfurization and denitrogenation catalysts; thus metals reduction is a primary objective of preliminary upgrading. Conradson carbon residue is an important property which measures the coking tendency of a feedstock. Asphaltenes consist of highly condensed polyaromatic units bearing long aliphatic and alicyclic substitutents with heteroatoms and trace metals and cause severe disadvantages during processing such as the tendency to form coke, catalyst deactivation, and poisoning. Thus the reduction of the Conradson carbon residue and asphaltenes in a preliminary upgrading step should enhance the product yields and qualities in subsequent hydroprocessing. The residuum fraction containing asphaltenes and resins must be upgraded and converted to more valuable lighter liquids such as naphthas, distillates, and gas oils in order to gain economic advantage in processing heavy oils.

The primary objective of oil sands research and development studies is to develop processes to produce transportation fuels from oil sand bitumens. Thus this study had two goals: (1) to improve product quality through denitrogenation, desulfurization, demetallation, and saturation and (2) to convert residuum fraction to more valuable lighter liquids. The effects of process variables (temperature, pressure, and space velocity) and catalysts on sulfur, nitrogen, and nickel removal, conversion

of Conradson carbon residue, residuum, and asphaltenes, and viscosity reduction were investigated to accomplish these goals. First and second pass hydrotreating were also compared. Finally, an attempt was made to model the kinetics of the global transformation taking place.

EXPERIMENTAL APPARATUS AND PROCEDURES

Feedstock Preparation

The oil sands used in this study were mined from the Asphalt Ridge oil sands deposit in the Uinta Basin. The bitumen was obtained from the crushed, sieved oil sands by solvent extraction. The solvent was toluene. The toluene in the bitumen-toluene solutions was then removed using rotary evaporation followed by high temperature vacuum distillation.

Solvent Extraction

The bitumen-toluene solution was obtained from the oil sands by refluxing toluene in Soxhlet extractors. The extraction thimbles were filled with oil sands (800-1000 g) and were placed inside Soxhlet extractors. Approximately 2 liters of toluene and a few boiling chips to eliminate bumping were placed in the solvent reservoir. Filter papers were placed on top of the extraction thimbles to prevent fine sands from overflowing into the bitumen-toluene solutions. The extraction thimbles were also wrapped with shark skin filter papers to retain fine sands. The extractor reservoir was heated by electric heating mantles to vaporize the solvent.

During the extraction process water was evaporated from the oil sands and settled to the bottom of the trap mounted between the extractor and the water cooled condenser. The water was periodically drained off to prevent it from overflowing into the extraction thimble. The extracted bitumen-toluene solutions were therefore relatively water-free.

The color of the bitumen-toluene solutions dripping from thimbles indicated the extent of extraction. The solution turned from a dark bitumen-rich solution at the beginning of the extraction to clear toluene after 12 h. The clear toluene meant the completion of the extraction of bitumen from oil sands in the thimble. Spent sands in the thimbles were removed from the extractors, fresh toluene and boiling chips were added to the reservoirs, and fresh oil sands were placed in the thimbles inside extractors for the next extraction.

After every eight extractions, the bitumen-toluene solutions were removed from extractors and stored in 19-liter plastic containers. The bitumen-toluene solutions in the

19-liter plastic containers were allow to stand for at least four days to permit fines to settle from the solutions prior to rotary evaporation.

Rotary Evaporation

Most of the toluene was removed from the bitumen-toluene solution by rotary evaporation. A vacuum pump was connected to the evaporator in the water bath. The evaporation was carried out at a pressure of 8-14 kPa, the evaporator was rotated at 120 rpm and the water bath temperature was held at 348 K. After rotary evaporation, about 6-8 wt% solvent remained in the bitumen-rich solutions(292). This residual solvent was removed by high temperature vacuum distillation.

High Temperature Vacuum Distillation

A Podbielniak batch distillation still packed with stainless steel wire coil packing was used to remove the residual solvent. The 12-liter kettle of the still was filled with about 8 liters of the bitumen-toluene solution in each distillation. Air in the column and kettle was purged with flowing nitrogen. After purging, the system was evacuated and the kettle heater was actuated to start the vacuum distillation. During the distillation, the system was purged with nitrogen to prevent oxidation or coking of the bitumen.

The system pressure, kettle temperature and reflux temperature were monitored by a mercury manometer and J-type thermocouples, respectively. The pressure was held in the range of 5.3-10.7 kPa. The kettle temperature was kept below 600 K because the bitumen would thermally crack when the temperature reached 620-650 K.[109] The final reflux temperature was the boiling point of a 50/50 mole fraction of hexylcyclopentane and xylene mixture and was calculated based on the Antoine equation and Raoult law at a specified system pressure because the lightest materials in the bitumen were C_{11} naphthenes which have very nearly the same vapor pressure properties as hexylcyclopentane. The commercial grade of toluene used in the extraction contained impurities such as xylene.

The reflux ratios were controlled with a solenoid valve timer and changed based on a compromise between efficient separation and rapid solvent recovery. The reflux

ratio was set at 5 initially, increased to 10 near the end point of the distillation and then to 20 at the end point to give a sharp separation.

The vacuum distillation was terminated when the final reflux temperature was reached. The kettle temperature, reflux temperature and the reflux ratio versus the volume of distillated liquid collected in a graduated receiver are presented in Figure 252.

The bitumen was analyzed by simulated distillation to check residual solvent concentration. The results showed that the solvent concentration was less than the detectable limits (< 0.1 wt%). The solvent-free bitumen was collected and stored in one 23-liter and two 57-liter steel drums and blanketed with nitrogen to prevent oxidation. Because the bitumen viscosity was very high at room temperature, the bitumen in the drum was heated to 400 K with a heating tape and transferred to the liquid feed burettes in the hydrotreating system as required.

Catalyst Characterization

Three HDN catalysts were used in this study. One was provided by a commercial catalyst manufacturer, and the others were impregnated by the Engelhard Corporation using an HDN catalyst support provided by UNOCAL.

The adsorption-desorption isotherms of the fresh and spent catalyst were measured with a Micromeritics AccuSorb 2100E analyzer, using nitrogen as adsorbate at the liquid nitrogen temperature. Approximately 0.4 g of catalyst were placed in the sample flask and degassed at 493 K overnight. The surface areas, pore volumes, and pore size distributions were calculated according to the procedure provided by Micromeritics.

Hydrotreating System

The hydrotreating system used in this research consisted of five main parts: the liquid feed system, the hydrogen feed system, the reactor system, the product separation and sampling system, and the safety system. The system was designed to operate at hydrogen pressures of 20.7 MPa and 773 K and was designed for either upflow or downflow mode by placing three-way manifold valves at the inlet and outlet of the catalytic reactor.

Figure 252

Reflux and kettle temperature versus volume of distillated liquid

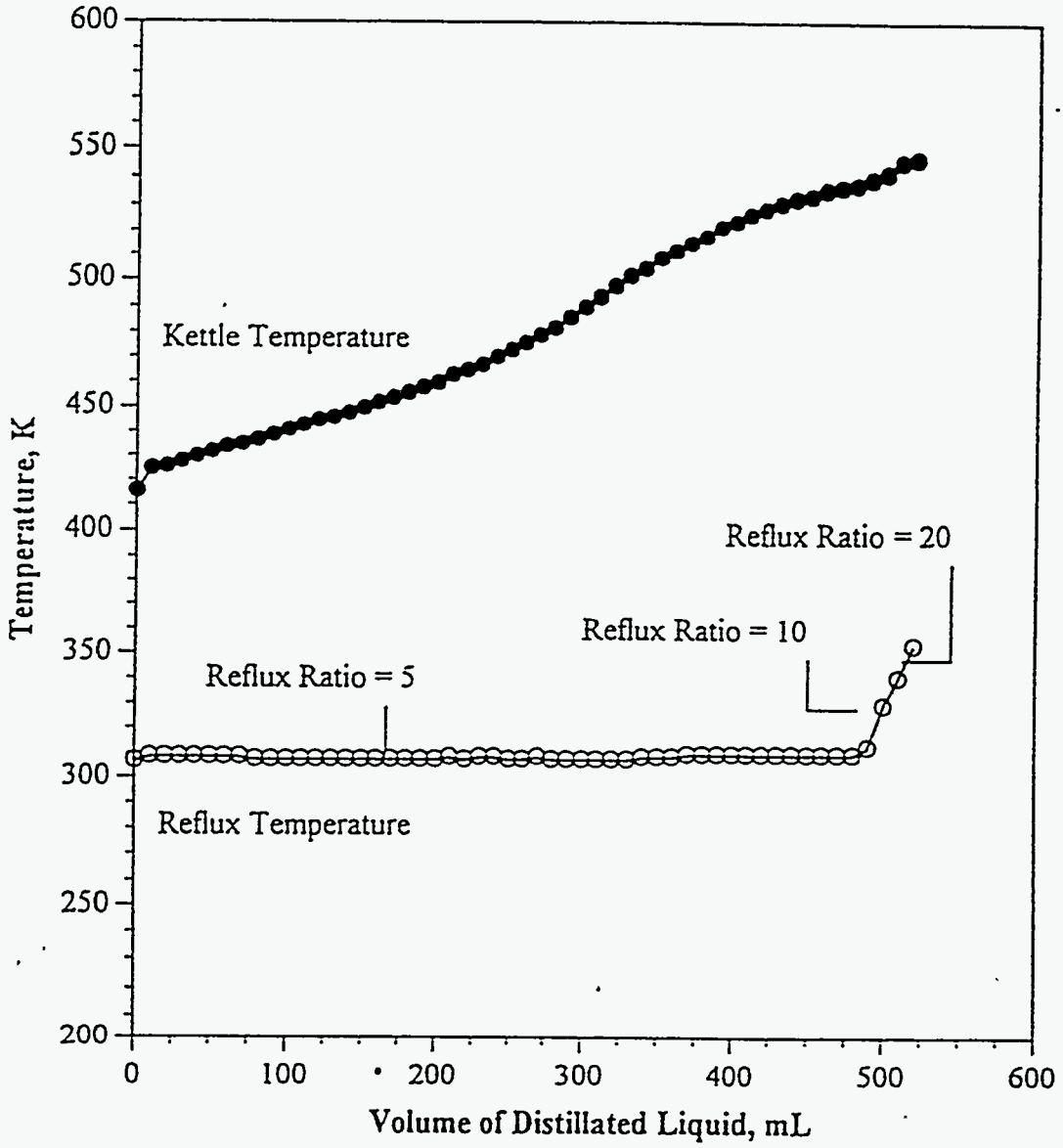
600
550
500
450
400
350
300
250
200
Temperature, K
Kettle Temperature
Reflux Ratio = 20
Reflux Ratio = 10
Reflux Ratio = 5
Reflux Temperature
0
100
200
300
400
500
600
Volume of Distillated Liquid, mL

The bitumen and hydrogen were fed to the reactor in the upflow mode in this study. The liquid and gas products were separated in the high pressure vapor-liquid separator. The gas product was removed via a back pressure regulating valve (BPRV) which also controlled the system pressure. The liquid product was withdrawn through a liquid-liquid control valve (Annin valve) and collected in a liquid receiver at ambient pressure. The schematic of the hydrotreating system is presented in Figure 253.

Liquid Feed System

Liquid was pumped from the burettes into the reactor at a controlled flow rate using a reciprocating pump which had a variable stroke length. The maximum flow rate was 1400 cm^3/h at the maximum operating discharge pressure, 34.4 MPa, of the pump and the minimum flow rate was 20 cm^3/h at the operating pressure, 13.8 MPa.

Two heat traced burettes were employed as feedstock reservoirs to supply feedstock to the reactor. The small burette with 500 cm^3 capacity was used to set or measure liquid feed flow rate accurately over short time periods. The large burette with 4000 cm^3 capacity was used to supply liquid feed during periods of steady state operation.

The temperature of the liquid in the burettes was controlled by a proportional temperature controller. Liquid density in the small burette was measured with an API hydrometer (19-31 °API). During hydrotreating of bitumen, the burettes were heated to 400 K to allow the bitumen to flow and the liquid bitumen level to be observed easily. Several drops of xylene were added to the bitumen pool in the small burette also to improve the observation of the liquid level. The vapor space in the burettes were purged with nitrogen gas to reduce oxidation of the hot bitumen.

A check valve was located between the pump and the pump outlet manifold to prevent back flow of pressurized gas into the liquid feed system. A valve connected to the discharge line of the pump was used to permit priming of the pump. A pressure relief valve was installed at the pump outlet to avoid pump damage when the pump outlet manifold was closed unintentionally or if the feed line between the pump and the pump outlet manifold was plugged.

Figure 253

Schematic of the hydrotreating system

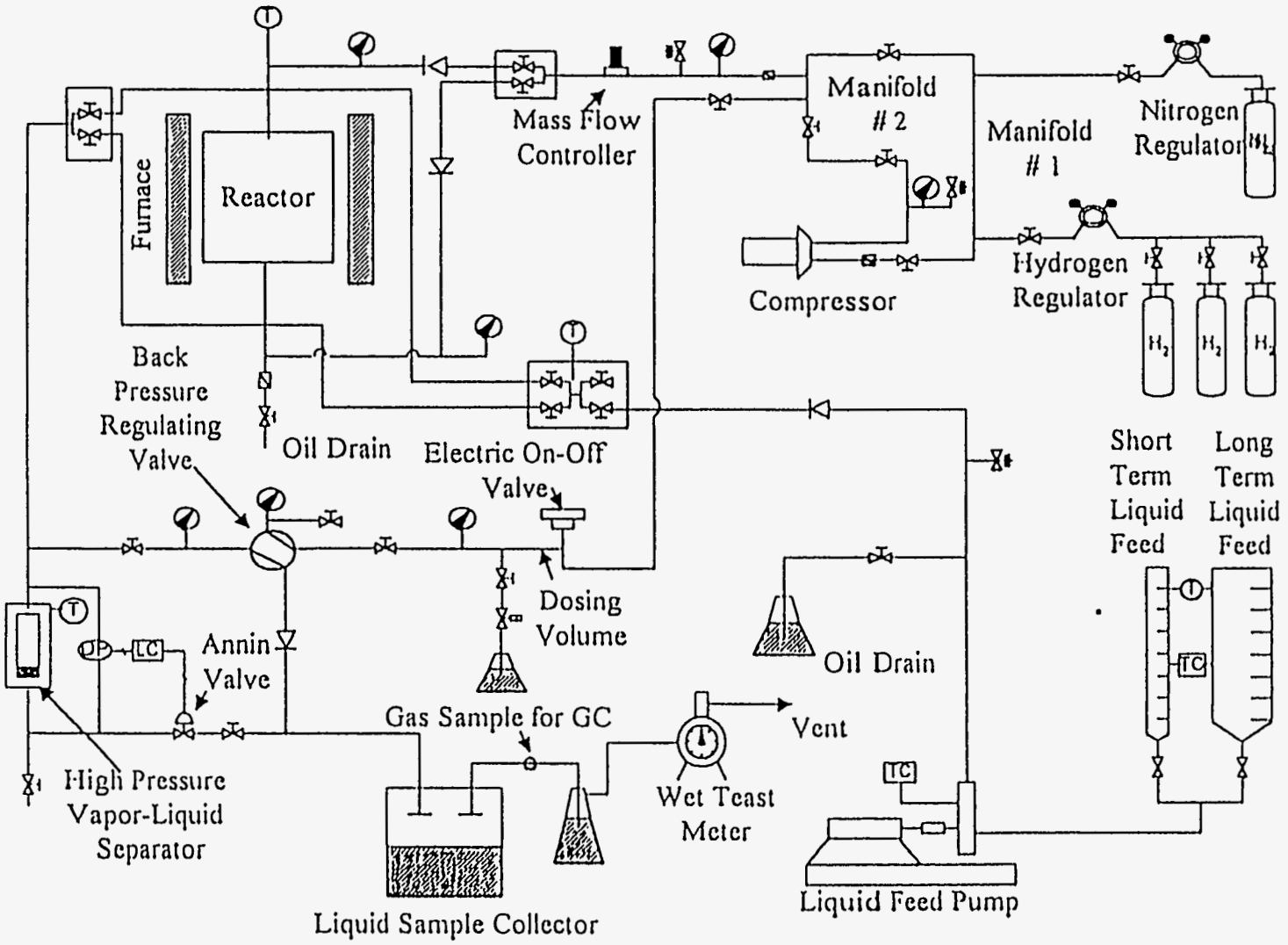
Furnace
Reactor
Mass Flow Controller
Manifold # 2
Manifold # 1
Nitrogen Regulator
Hydrogen Regulator
Compressor
Back Pressure Regulating Valve
Oil Drain
Electric On-Off Valve
Short Term Liquid Feed
Long Term Liquid Feed
Dosing Volume
Annin Valve
Oil Drain
Gas Sample for GC
Vent
High Pressure Vapor-Liquid Separator
Wet Teast Meter
Liquid Sample Collector
Liquid Feed Pump

Because the pump could process liquids with a maximum viscosity of 1500 cp, the pump head, valves and liquid transfer lines were heated to 390-400 K by heat trace tapes when pumping Asphalt Ridge bitumen. The temperature of the heat trace lines were controlled by a proportional controller.

Hydrogen Feed System

Hydrogen was supplied from three hydrogen cylinders connected in parallel through a gas manifold and compressed to the desired pressure by a compressor and then passed through a mass flow controller into the reactor.

A variable stroke length, single stage compressor (Whitey Laboratory Model LC 10) whose maximum output pressure was 20.7 MPa was used to raise the hydrogen pressure to the reactor inlet pressure. The compressor would be damaged if operated with an inlet pressure below 0.35 MPa. Owing to this limit, the compressor power supply was connected to a pressure switch designed to turn off the compressor when the compressor inlet pressure dropped below 1.38 MPa.

The compressor outlet pressure was a function of both the compressor inlet (regulator supply) pressure and the compressor stroke length. In most cases, the desired compressor outlet pressure was obtained by adjusting regulator supply pressure at fixed stroke length. Typically the compressor inlet pressure was 3.4-5.5 MPa. Therefore, the hydrogen supply gas cylinders were changed when the pressure of the hydrogen gas cylinders dropped to 5.5 MPa.

The hydrogen flow rate was controlled by a mass flow controller (Brooks model 5850 TR) which included a Dual Power Supply (Brooks model 5878) and a Readout Control Unit. The mass flow controller was placed between the compressor outlet and the reactor inlet manifold valves. Check valves were installed in the gas lines to the reactor to prevent the back flow of liquid into the mass flow controller. A pressure relief valve was located between the compressor outlet and the mass flow controller inlet to protect the controller on the occasion of system overpressurizing.

Reactor System

The reactor system included a laboratory-scale fixed-bed reactor and a furnace. The reactor was loaded with catalyst in the central section and with alumina balls in the top and bottom sections. The furnace containing three independently controlled sections was employed to heat the reactor sections. The bitumen was fed into the reactor in the upflow mode to ensure complete wetting of the catalyst and to reduce the thermal gradient across the catalyst bed. A schematic of the reactor system is presented in Figure 254.

The reactor was fabricated from seamless 316 stainless steel tubing with an inside diameter of 2.54 cm and a wall thickness of 0.95 cm. A thermowell with an outside diameter of 0.32 cm which held a movable thermocouple was installed on the centerline of the reactor. Each end of the reactor tube was threaded to a flange. Caps were fastened to the flange with bolts to seal the reactor. A 0.95 cm stainless steel tube was welded into the center of the caps to allow the introduction of the feed into and the removal of the product from the reactor.

Aluminum gaskets were used to seal the flanges and caps of the reactor because of their corrosion resistance in the presence of ammonia, hydrogen sulfide and water at pressures of 11-16 MPa, and temperatures of 620-684 K.

A three-section Lindberg furnace provided with three temperature controllers was employed to supply the heat to the reactor. The central heating section was 30.5cm long and supplied heat to the central section of the reactor containing the catalyst bed. The bottom and top sections of the furnace were 15.2 cm long and served as preheater and postheater to maintain the isothermal operation of the catalyst bed.

A three-section aluminum shield with outside diameter of 8.1 cm shrouded the reactor tube and was used as a heat sink to improve isothermal operation of the reactor. The length of each section of aluminum shield corresponded to the each section of the reactor and the furnace. The 0.32 cm fiberglass spacers were employed to restrict heat transfer between adjacent sections of the heat sink.

Figure 254

Schematic of the reactor system

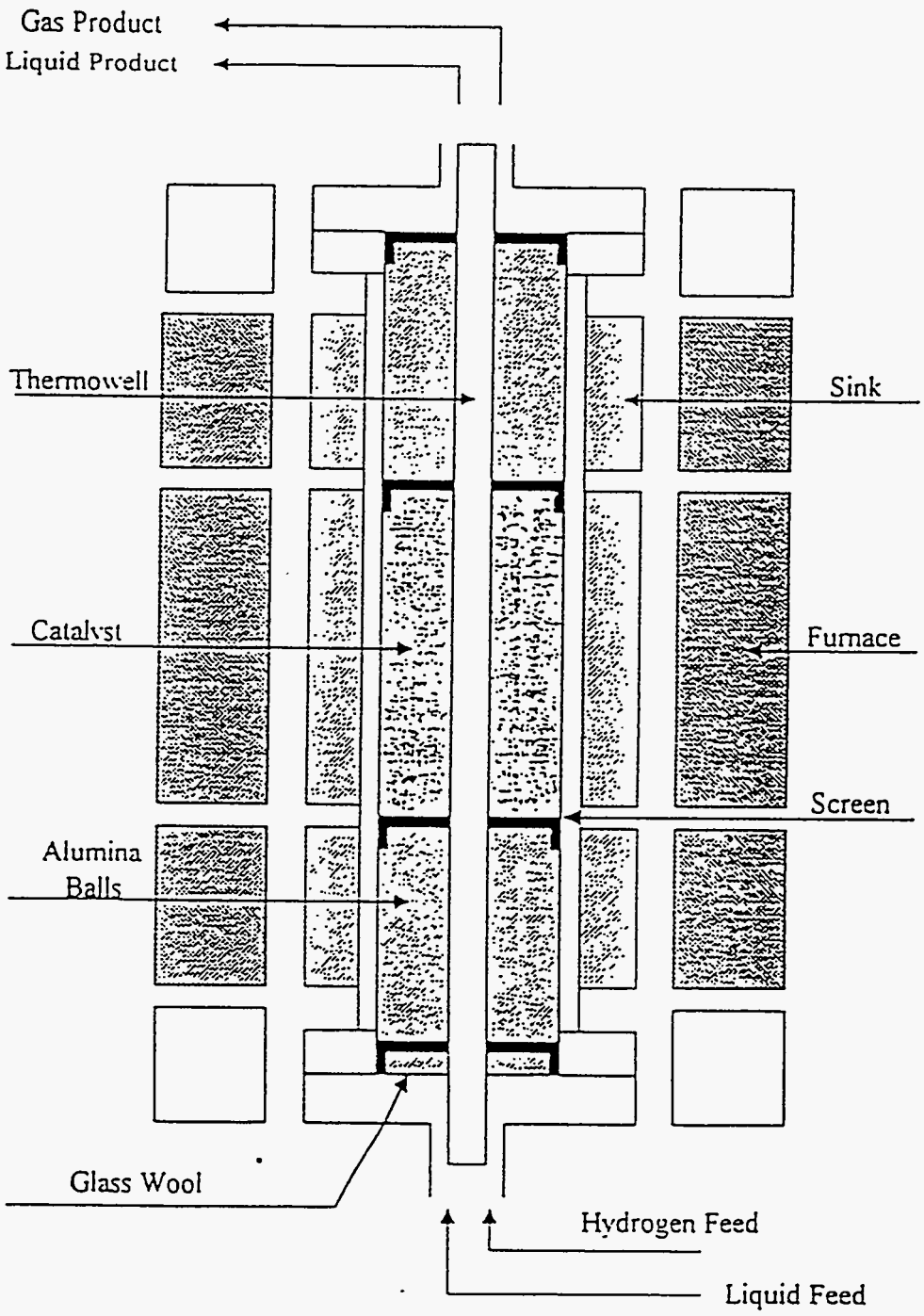
Gas Product
Liquid Product
Thermowell
Sink
Catalyst
Furnace
Screen
Alumina
Balls
Glass Wool
Hydrogen Feed
Liquid Feed

Product Separation and Sampling System

The liquid and gas products exited from the reactor and entered the high pressure vapor-liquid separator. The gas product passed through a back pressure regulating valve which decreased the gas pressure from the reactor outlet pressure to ambient pressure. The BPRV also allowed the gas to escape from the system when the system's pressure surpassed the BPRV loading pressure, thus controlling the system pressure at the desired value. The system pressure was monitored by a pressure indicator (Omega Engineering Model DP-354).

The BPRV loading pressure was regulated by a manifold located between the BPRV and the compressor outlet. A micrometering valve was employed to vent the BPRV loading pressure slowly.

The liquid product was withdrawn from the high pressure vapor-liquid separator by the liquid level control system which included a differential pressure (DP) transducer, liquid level controller, I/P converter, and an Annin valve. The DP transducer monitored the liquid level in the vapor-liquid separator and then sent a signal through liquid level controller, I/P converter, and finally to the positioner on the Annin valve. The Annin valve had a variable maximum stroke length from 0.025 to 0.38 cm. The maximum stroke length of 0.25 cm was set during the hydrotreating of bitumen.

The liquid product was collected in a 500-mL flask during mass balance periods and in a 19-liter polyethylene container during steady state or transition time periods.

Safety System

A safety alarm relay was connected to the liquid level control system and the heat trace fuse. If the liquid level in the vapor-liquid separator rose above the set point or the 4 amp heat tracing fuse burned out, the audible alarm would sound and the liquid pump would shut off. A timer connected to the liquid level alarm recorded the time when the alarm was activated.

The heat tracing lines, 25 gauge Nichrome wire coated with glass fabric insulation, were used to heat the liquid transfer lines, the valves, the vapor-liquid separator, the Annin valve, and the pump. The two heat tracing lines were powered by a 120 V power supply and connected in parallel. One line extended from the liquid feed

system to the reactor inlet and had a resistance of 60 ohms; the other line went from the reactor outlet to the product separation system and had a resistance of 70 ohms. The heat tracing controller used the temperature of the pump check valve as the reference temperature.

Experimental Procedures

Three different hydrodenitrogenation catalysts were employed to investigate the extent of heteroatom (N, S) and nickel removal, and the asphaltenes, Conradson carbon residue, and residuum conversion and to study the change of viscosity. The product distribution and yields were also determined.

The effects of process variable, that is, temperature, pressure, and liquid hourly space velocity, were studied after the activity of the catalyst reached an a stationary state.

The hydrotreated products produced under the base case condition and the highest severity condition with the A-HDN catalyst were used as feedstocks for the second pass studies at the same conditions.

Before each experiment, the reactor was cleaned to remove the solid particles on the reactor wall. The pressure indicator and wet test meter were also calibrated.

Catalyst Calcination

The catalyst adsorbed moisture during storage. Water vapor may damage the catalyst during sulfiding(305). The following calcination procedure was provided by manufacture: (1) place the catalyst in a thin layer in a container suitable to be put into a muffle furnace, (2) start with the muffle furnace at room temperature and pressure, (3) increase muffle furnace temperature to 644 K at 56-83 K/h and hold the catalyst at 644 K for 1 h, and (4) cool the catalyst to room temperature in a desiccator that does not contain any desiccant.

Catalyst Loading

The reactor system had three sections in which temperature was controlled independently. Preheating and postheating sections were filled with inert low surface area symbol 224 \f "MS LineDraw" \s 12α}-alumina balls to support the catalyst bed and

to supply space for uniform distribution of hydrogen in the liquid. The catalyst was loaded in the central reactor section with volume of 152 cm^3. The reactor was tapped frequently during the loading of the symbol 224 \f "MS LineDraw" \s 12α}-alumina balls and catalysts to ensure the proper packing density.

Each section of the reactor was separated by a screen with a 0.32 cm hole drilled through the centerline of the screen to fit the thermowell. A thermowell with 0.32 cm outside diameter was located on the centerline of the reactor before the reactor was loaded and then passed through the screen of each section.

Pressure Test

After the reactor was loaded and connected to the hydrotreating system, the system pressure test was conducted with nitrogen at 6.9 and 13.8 MPa to detect major leaks using soap bubbles. Any detected leaks were eliminated.

The BPRV and the system pressure was increased from atmospheric pressure to 6.9 MPa. The system was isolated into four sections: the line from compressor outlet to the inlet of the reactor, the reactor, the line from the outlet of the reactor to the vapor-liquid separator, and line from the vapor-liquid separator to the BPRV. The system was monitored over 16 h. If there was no pressure loss, the system pressure was increased rom 6.9 MPa to 13.8 MPa. The system was also isolated into four sections and the pressure were monitored overnight.

Mass Flow Controller Calibration

The mass flow controller was calibrated with a wet test meter. The system was operated at 13.7 MPa and room temperature. During calibration, the hydrogen flow rate in the absence of chemical reaction was measured with a test wet meter at different mass flow controller set points. The calibration curve for the mass flow controller is presented in Figure 255.

Catalyst Presulfiding

The hydrotreating catalysts are produced and supplied in the oxide form; however, the metal sulfide form of the hydrotreating catalysts are more active than the

Figure 255

Mass flow controller calibration curve

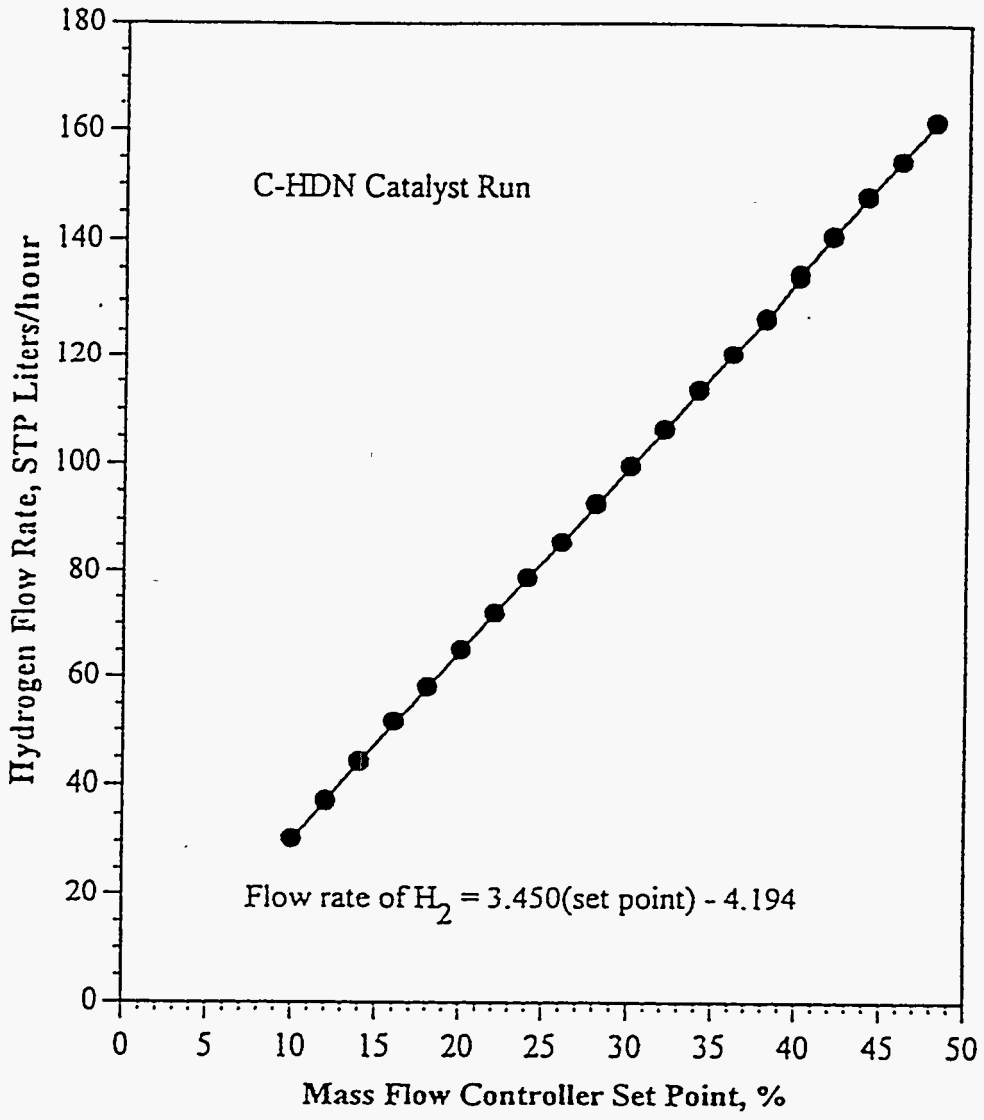
C-HDN Catalyst Run
Flow rate of H_2 = 3.450(set point) - 4.194
Hydrogen Flow Rate, STP Liters/hour
Mass Flow Controller Set Point, %
0
20
40
60
80
100
120
140
160
180
0
5
10
15
20
25
30
35
40
45
50

metal oxide form. The catalyst presulfiding process, therefore, was conducted in-situ before contact with liquid feed and hydrogen. After presulfiding, the active component of the metal in the catalyst changed from a metal oxide to a metal sulfide.

The presulfiding solution was 2 wt% sulfur as dimethyldisulfide in kerosene and was conducted in upflow mode through the reactor at a feed rate of 1 LHSV. The hydrogen to liquid ratio was 890 $m^3(STP)/m^3$. The reactor pressure was held between 6.1-6.3 MPa.

The reactor was heated from ambient temperature to 505 K at a heating rate of 28 K/h. When the reactor temperature reached 500-510 K, the exchange of oxygen and sulfur increased dramatically. The reactor temperature was kept at about 505 K for at least 4 h depending upon the metal contents of the catalyst to ensure complete sulfiding.

After the holding time, the liquid feed pump was shut off and the hydrogen flow was reversed to remove the liquid in the reactor. The reactor temperature was decreased to 490-500 K and the hydrogen flow rate was then lowered to the set point of the mass flow controller at 2 to maintain hydrogen pressure overnight.

The sulfiding process was resumed with hydrogen and the sulfiding solution at the previous flow conditions. The reactor temperature was heated to 644 K at a heating rate 28 K/h. At 644 K the liquid feed pump was shut off, the hydrogen flow was reversed to flush the sulfiding solution out of the reactor, and the reactor temperature was lowered to 615 K under hydrogen flow rate with the set point of the mass flow controller at 2.

Reactor Startup and Experimental Strategy

The bitumen and hydrogen entered the reactor in the upflow mode for all experiments. Initially, the catalyst was deactivated until the activity of the catalyst reached a stable state at the base case conditions. After the initial catalyst deactivation, the experiments were executed in a cyclic mode. During the experiment, a mass balance and temperature measurement were conducted, and gas samples and the liquid product were collected.

Initial Catalyst Deactivation

The bitumen and hydrogen were fed to the reactor at the base case conditions: 642 K, 0.48 h^{-1} LHSV, and 13.7 MPa, to monitor catalyst deactivation for three different HDN catalysts. In all experiments, the hydrogen-to-liquid ratio was fixed at 890 $m^3(STP)/m^3$.

The time that the hydroprocessed liquid product entered the vapor-liquid separator was taken as zero time on-stream (TOS), which served as the basis to estimate the catalyst deactivation rate. The catalyst deactivation was determined by monitoring the API gravity of the hydroprocessed liquid product which decreased with TOS as the catalyst equilibrated. The API gravity of the liquid product was calculated with Equation 145:

$$°API = 141.5 / (\text{Specific gravity}) - 131.5 \qquad (145)$$

The specific gravity was measured with a pyconometer according to Syncrude Analytical Methods-Method 5.5(322).

The API gravity of the hydrotreated liquid product indicated that the catalyst had attained a stationary or stable state after about 144 h on-stream. The initial catalyst deactivation reflected by the API gravity of the total liquid product as a function of TOS is presented in Figure 256.

Process Variables Study

The studies were conducted in a cyclic mode: base case condition-desired operating conditions-base case condition. The base case condition was employed to monitor the extent of deactivation that occurred at the desired operating conditions. The process variables studied were temperature (620-684 K), space velocity (LHSV 0.2-0.9 h^{-1}), and pressure (11.0-15.3 MPa). Two of the variables were kept constant while the other was varied to determine independently the effect of each process variable.

Figure 256

API gravity versus time on stream during the initial catalyst deactivation

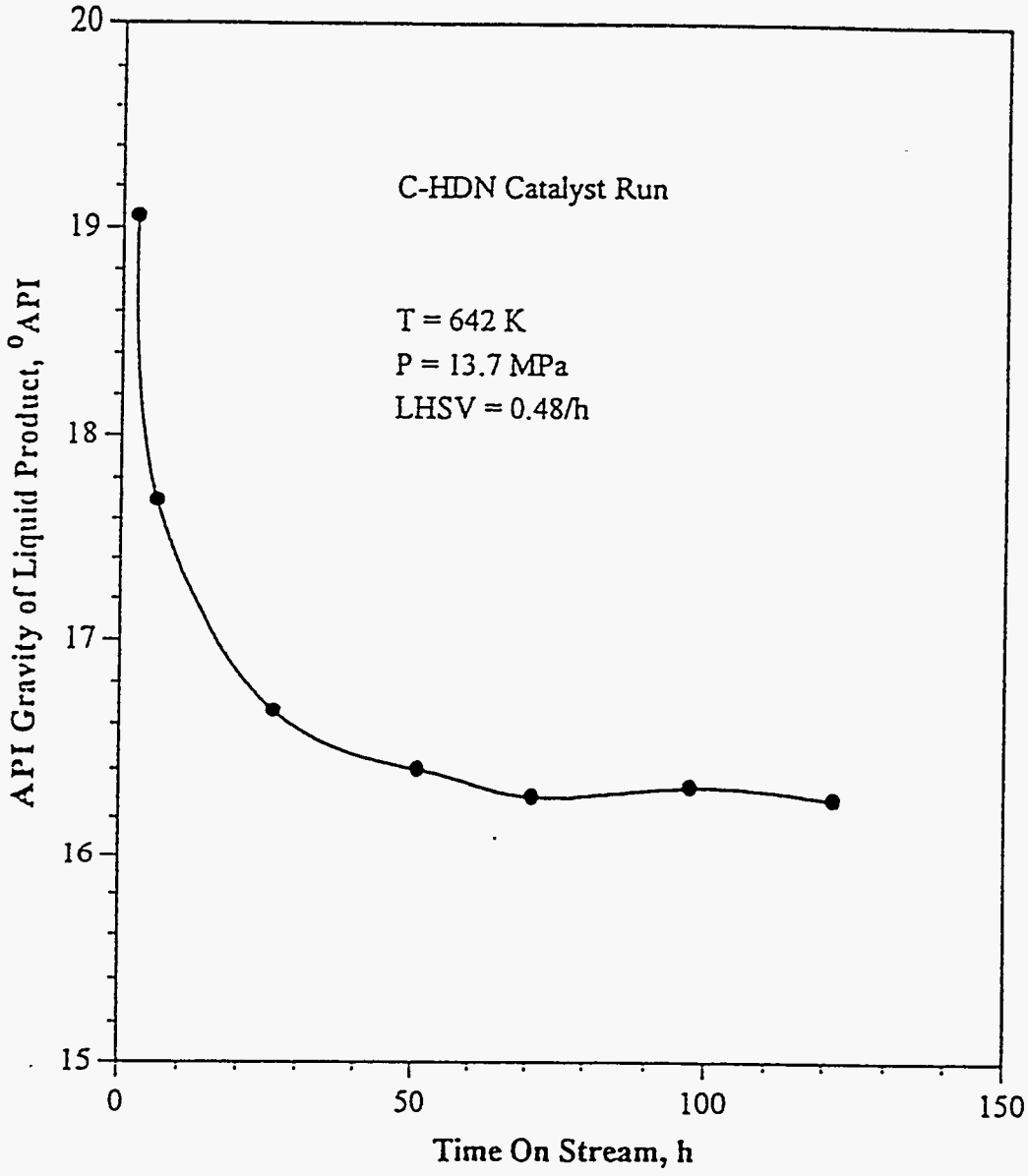
C-HDN Catalyst Run
T = 642 K
P = 13.7 MPa
LHSV = 0.48/h
API Gravity of Liquid Product, °API
Time On Stream, h
20
19
18
17
16
15
0
50
100
150

Mass Balance

Mass balances were conducted to monitor the liquid and hydrogen feed to the reactor system during discrete time periods and to collect the representative gas and liquid samples for subsequent analysis.

Mass balances were employed after the system had attained a stable state at each new set of operating conditions. It required from 9 to 36 h to allow the system to attain a steady state when the LHSV was changed from 0.9 to 0.2 h^{-1}.

During the mass balance, the liquid product was collected in the 500-mL flask at ambient pressure; the gas product stream passing through the flask was sampled for gas chromatographic analysis. The gas sample was collected at 76 K in a container immersed in a liquid nitrogen bath; and then the gas flow rate was measured with a wet test meter.

The liquid and condensed gas products were weighed at the end of each mass balance. The mass balances were in the range of 97-102 wt% for each of the three runs. The gas product sampled was analyzed with a Hewlett Packard (HP) gas chromatograph before the next mass balance to determine the relative amounts of hydrocarbon gases. The hydrogen consumption was calculated by difference between the hydrogen flowing into the reactor system and the gas product exiting the hydrotreating system.

Temperature Measurement

The axial temperature profiles of the catalyst bed along the center line of the reactor were measured with a movable J-type thermocouple. Temperature profiles were metered from 33.0 cm to 63.5 cm above the bottom of the thermowell in 2.5 cm intervals. The average temperature was calculated in two ways: the kinetic and arithmetic average temperature.

The kinetic average temperature was calculated from Equation 146:

$$T_k = \frac{-\frac{Ea}{R}}{\ln\left[\frac{1}{L}\int_0^L \exp\left[-\frac{Ea}{RT(l)}\right] dl\right]} \qquad (146)$$

where, T_k is the kinetic average temperature (K), Ea is the activation energy (kcal/mol), R is the gas constant (1.987 kcal/mol), L is the total length of the catalyst bed (cm), T(l) is the axial temperature profile along the catalyst bed. The value of the Ea, 25.5 kcal/mol, obtained from the previous study(292) was used in this calculation.

The arithmetic average temperature, T_a, was calculated based on the weighted average method. The difference between T_k and T_a was in the range of 0.02-0.3 K indicating that the reactor operation was near isothermal. A typical temperature profile with position metered from the bottom of the thermowell is displayed in Figure 257.

System Shutdown

The system shutdown procedures were conducted to clean the residual oil from the reactor and liquid transfer lines. At the completion of each run, the bitumen was withdrawn from the two burettes and the system pressure was lowered to 5.9 MPa. Kerosene was pumped into the system to flush the bitumen and hydrotreated bitumen from the hydrotreating system. The reactor temperature was gradually decreased and then held at 500 K until the liquid product and the bitumen were flushed by monitoring the color change of the liquid leaving the reactor.

The reactor temperature and system pressure were decreased to 400 K and 1.4 MPa, respectively. The heat tracing was turned off and then hexane was pumped into the system to flush the kerosene until the liquid was colorless. The reactor and transfer lines were dried with flowing nitrogen at ambient pressure and then cooled to ambient temperature. The reactor was disconnected from the system and then the spent catalyst and alumina balls were removed from the reactor. The reactor was finally cleaned with toluene.

Liquid Products Analysis

The liquid products were analyzed for elemental analysis, simulated distillation, asphaltenes, viscosity, and Conradson carbon residue.

Figure 257

Temperature profile with position metered from the bottom of thermowell

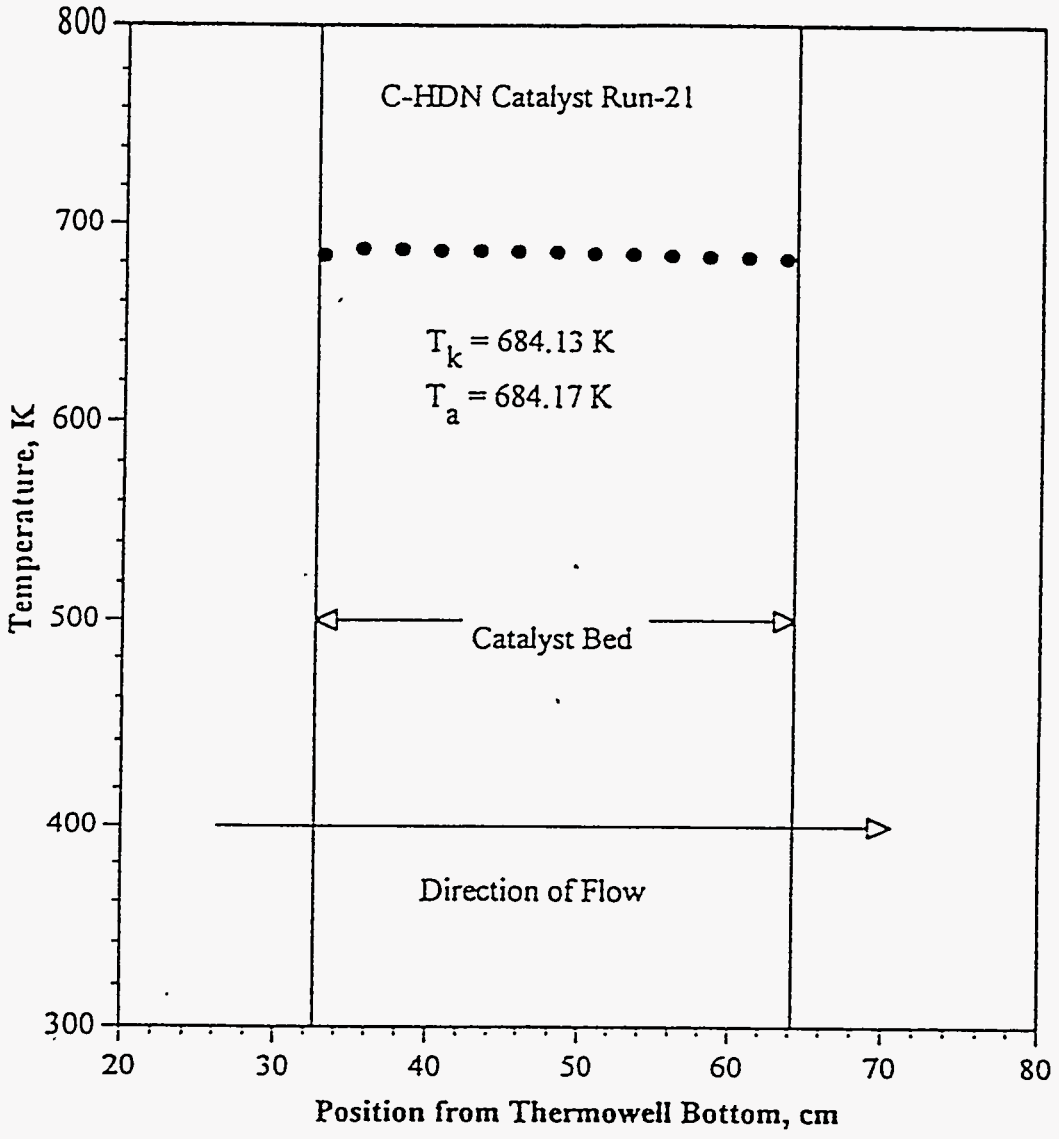
C-HDN Catalyst Run-21
T_k = 684.13 K
T_a = 684.17 K
Catalyst Bed
Direction of Flow
Temperature, K
800
700
600
500
400
300
20
30
40
50
60
70
80
Position from Thermowell Bottom, cm

Elemental Analysis

The liquid product samples were flushed with flowing helium to remove dissolved hydrogen sulfide and ammonia and then sent to Galbraith Laboratory, Inc. to be analyzed for carbon, hydrogen, nitrogen, sulfur, and nickel concentrations.

The test tube fitted with a side arm was filled with the liquid product, about 25 g, and placed in a 250-mL Erlenmeyer flask containing 175 mL of water. The flask was heated with a hot plate until water boiled, and then the helium was bubbled through the liquid product at 50 cm^3/min for 4 h. The light liquid ends were recovered from the helium in another test tube immersed in a water-ice bath and then were mixed with the purged liquid product.

The liquid samples were analyzed for carbon, hydrogen, and nitrogen with a Leco CHN 800 determinator and measured for sulfur by using Leco 432DR sulfur analyzer. The Inductively Coupled Plasma Emission Spectroscopy was employed to determine the nickel concentration.

Simulated Distillation

The boiling point distribution of the liquid products was determined by simulated distillation using a HP 5890 series II gas chromatograph with an integrator (HP 3396 series II) and a controller (HP 7673). A fused silica capillary column which was 5 m long, 0.53 mm internal diameter, with a 0.1 symbol 109 \f "Symbol" \s 12μm bonded phase film (Supelco Petrocol EX2887) was connected from injector to detector on the gas chromatography.

A temperature program was employed for the blank, the boiling point calibration samples, the liquid product samples, and the liquid product samples plus internal standard mixture. The initial oven temperature was set at 308 K and then the oven temperature was kept at 308 K for 4.5 min. The oven was then heated to 653 K at the rate of 12 K/min and held at 653 K for 8.75 min. Helium was used as the carrier gas, hydrogen was used as the fuel gas, and air was employed to aid the combustion of hydrogen. The initial pressure was 11.7 kPa.

The samples were diluted with carbon disulfide in a 1 ml vial. The samples were mixed the internal standard mixture in the weight ratio of about 10:1. The internal

standard mixture contained C_{14}-C_{17} paraffins. The calibration curve was obtained from running the boiling point calibration samples which were supplied by Hewlett Packard and Supelco.

The simulated distillation data (naphtha, middle distillate, gas oil and residuum weight fraction) were calculated from the boiling point distribution by using a modified ASTM D5307 method. .

Asphaltenes Analysis

Asphaltenes are a class of compounds defined by solubility and has been restricted to n-pentane or n-heptane insoluble materials that dissolve in benzene.

The procedure for fractionation consisted of the following steps: (1) samples (bitumen and hydroprocessed liquid products) were weighed in a tarred 250-mL Erlenmeyer flask to which toluene was added in the ratio of 1 mL per gram of samples and heated on the water bath to obtain a homogeneous mixture; (2) the mixture was cooled, followed by gradual addition of n-pentane in a ratio of 40-to-1 volumes of pentane-to-toluene with constant mixing; (3) the resulting mixture was completely shaken and placed in the dark for overnight; (4) the insoluble solids (asphaltenes) were separated from the mixture by filtration using a fritted glass funnel; and (5) the solids were washed completely with n-pentane until the washings were colorless, dried in the oven at 383 K for 2 h, and then weighed.

Viscosity Measurement

The viscosities of samples were measured by using a Brookfield viscometer (model DV-II) with a Brookfield refrigerated bath/circulator (model TC-500) and a Brookfield temperature controller (model HT-105). The viscosity measurements were made at several shear rates and temperatures with a cone/plate viscometer.

Conradson Carbon Residue Measurement

Carbon residues were measured according to Syncrude Analytical Methods-Method 5.4(323). The amount of Conradson carbon residue is intended to provide some indication of relative coke-forming properties.

RESULTS AND DISCUSSION

The objective of catalytic upgrading bitumens to fuels is to reduce the heteroatomic and metal contents and to decrease the molecular weight distribution simultaneously. Nitrogen removal is particularly important because basic nitrogen compounds can poison strongly acidic catalysts used in hydrocracking. The primary hydrotreating/upgrading process variables are temperature, pressure, and space velocity. The effect of process variables on the extent of nitrogen, sulfur, and nickel removal; CCR, residuum and asphaltenes conversion; and viscosity reduction were investigated. The influence of process variables on the product distributions and yields was also investigated. Process kinetic models were determined from experimental data.

Properties of Asphalt Ridge Bitumen

The bitumen used in this study was obtained from the Asphalt Ridge oil sand deposits in the Uinta Basin of Utah after solvent extraction, rotary evaporation, and high temperature vacuum distillation. Physical and chemical properties of the Asphalt Ridge bitumen are presented in Table 82. The nitrogen content is more than twice the sulfur content in this bitumen. Hydrodenitrogenation catalysts were chosen for use in this investigation due to the high nitrogen content.

The logarithmic plot of shear stress versus shear rate (Figure 258) is linear with a slope of unity, and there is the linear relationship between shear stress and shear rate which passed through the origin. The viscosity of the bitumen is not function of the shear rate at 343 K. These results suggest that the Asphalt Ridge bitumen is a Newtonian fluid. The viscosity of Asphalt Ridge bitumen was measured in the temperature range 333-353 K. A linear relationship was observed (Figure 259) for the logarithm of the viscosity versus reciprocal temperature.

Properties of HDN Catalysts

Bitumens contain high concentrations of heteratomic species such as nitrogen, sulfur, and metals which must be removed prior to conventional processing. Therefore,

Table 82

Physical and Chemical Properties of the Asphalt Ridge Bitumen

Gravity, °API	11.4
Conradson Carbon Residue, wt%	11.0
Pour Point, K	312
Viscosity, cp	
@ 333 K	37590
@ 343 K	11750
@ 348 K	8227
@ 353 K	5583
Asphaltenes[a], wt %	10.1
Simulated Distillation	
Volatility, wt%	45.2
Naphtha (IBP - 477 K), wt%	0.5
Distillate (477 K - 617 K), wt%	10.2
Gas Oil (617 K - 811 K), wt%	34.5
Residuum (> 811 K), wt%	54.8
Elemental Analysis	
C, wt%	84.9
H, wt%	11.2
N, wt%	0.97
S, wt%	0.42
Ni, ppm	86
V, ppm	3
As, ppm	2
H / C Atomic Ratio	1.58
Molecular Weight, g / mol	621

[a] Insoluble in n-Pentane

Figure 258

Shear diagram for Asphalt Ridge bitumen at 343 K

in logarithm and linear plot

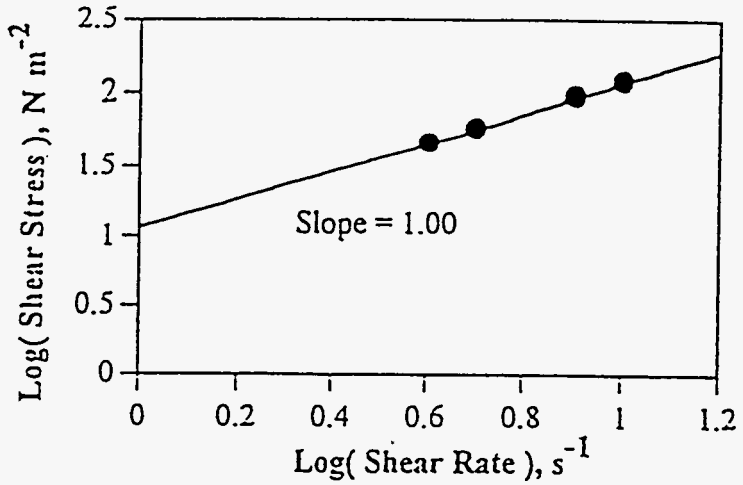
Log(Shear Stress), N m-2
2.5
2
1.5
1
0.5
0
Slope = 1.00
0
0.2
0.4
0.6
0.8
1
1.2
Log(Shear Rate), s-1

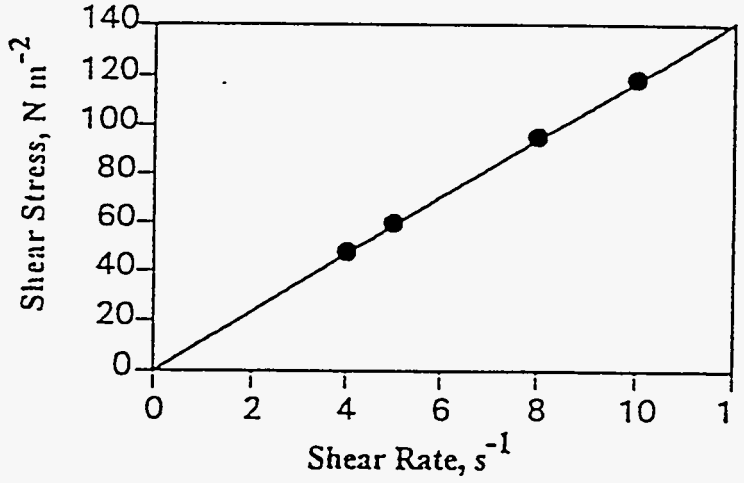
Shear Stress, N m-2
140
120
100
80
60
40
20
0
0
2
4
6
8
10
1
Shear Rate, s-1

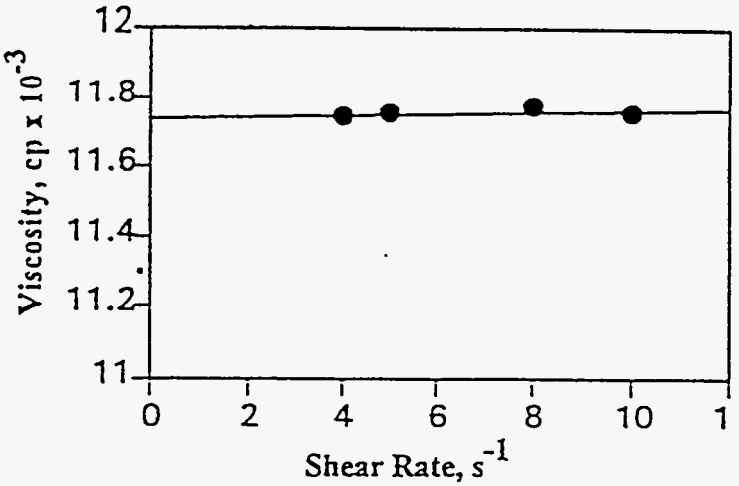
Viscosity, cp x 10-3
12
11.8
11.6
11.4
11.2
11
0
2
4
6
8
10
1
Shear Rate, s-1

Figure 259

The viscosity of Asphalt Ridge bitumen as a function of temperature

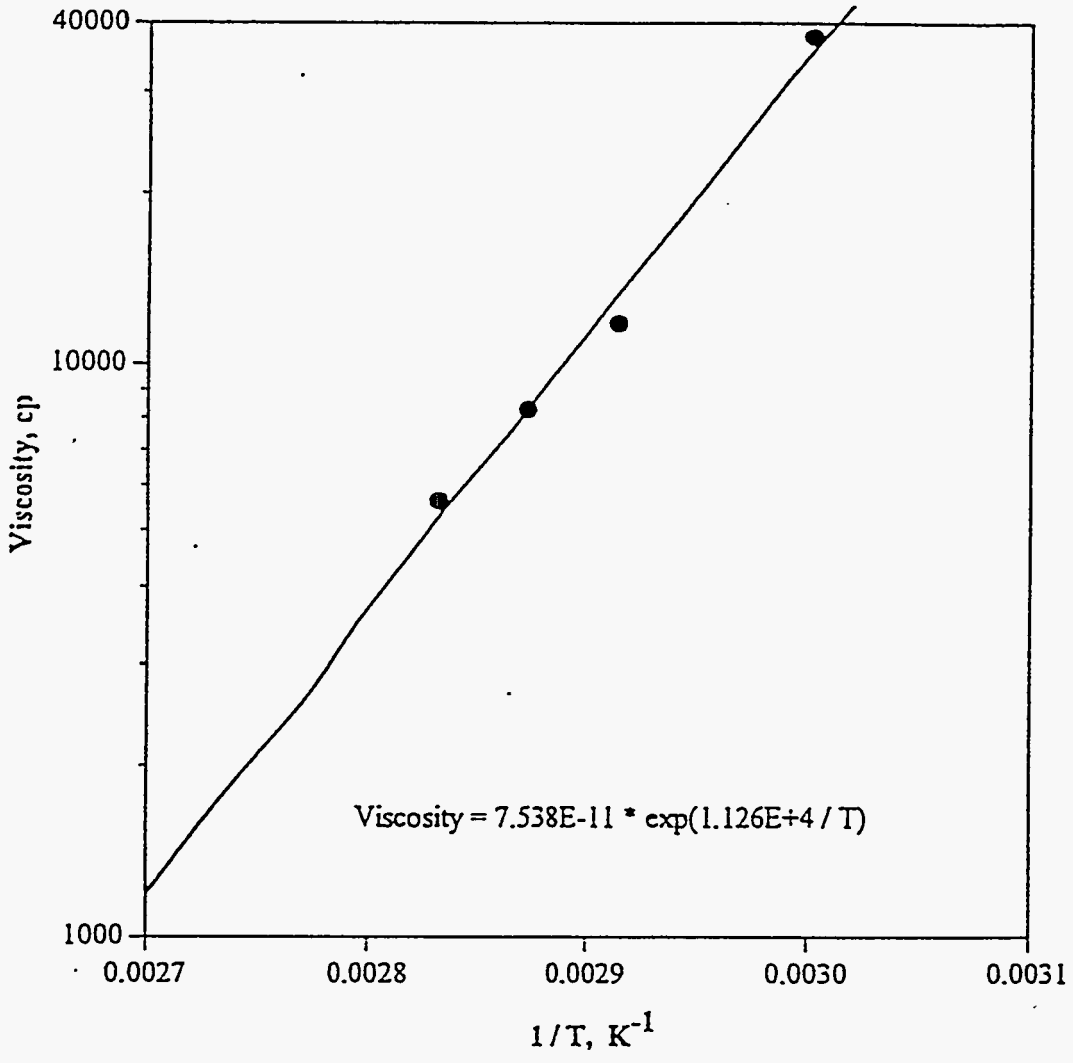
40000
10000
1000
Viscosity, cp
Viscosity = 7.538E-11 * exp(1.126E+4 / T)
0.0027
0.0028
0.0029
0.0030
0.0031
1 / T, K-1

the primary objective of this hydrotreating study was heteratom removal, especially nitrogen removal.

In hydrotreating catalysts, the most common combinations of active elements are CoMo, NiMo, and NiW. In general, NiMo catalysts are more active for both nitrogen removal and the hydrogenation of aromatics, which gives rise to higher hydrogen consumption(283, 324). Three different NiMo catalysts were used in this research. The catalyst properties are outlined in Table 83.

B-HDN catalyst was obtained from a commercial catalyst manufacturer and A- and C-HDN catalysts were impregnated with the active elements by the Engelhard Corporation using the HDN catalyst alumina support provided by UNOCAL. B- and C-HDN catalysts have similar chemical composition but different physical properties. A-HDN catalyst has lower a metals content and higher surface area than B- and C-HDN catalysts. A- and C-HDN catalyst surface areas and pore volumes were determined with a BET apparatus using nitrogen as the adsorbate at liquid nitrogen temperature.

Adsorption-desorption isotherms for the fresh HDN catalysts and extracted spent catalysts are shown in Figures 260 and 261. Comparison of the isotherms of fresh and extracted spent catalyst A-HDN in Figure 260 indicated that the size and shape of the hysteresis loops are little different, indicating pore mouth restriction by coke. C-HDN catalyst also exhibits the same trends (Figure 261).

Pore size distributions were determined employing the desorption loop of the adsorption-desorption isotherms. Pore size distributions for the fresh A- and C-HDN catalysts are compared in Figure 262. The pore size distributions were unimodal and the A- and C- HDN catalyst have similar narrow pore size distributions. Pore size distributions of the fresh and extracted HDN spent catalysts are shown in Figures 263 and 264. A slight shift to smaller pore radii was observed for each of the extracted spent catalysts.

Physical properties of the fresh catalysts and the extracted spent catalysts are compared in Table 84. The pore volumes and surface areas of the HDN catalysts exhibited loss caused by coke and metals deposition. A- and C-HDN catalysts exhibited the same losses, about one third, because the TOS for both catalysts processing the same feedstock were almost the same, 626 and 650 h, respectively. Koyama et al.[207] measured

Table 83

Chemical Composition and Physical Properties of HDN Catalysts

	A-HDN	B-HDN	C-HDN
NiO, wt%	3.52	3.8	3.75
MoO_3, wt%	12.14	19.5	19.64
Pore Volume, mL/g	0.47	0.47	0.37
Surface Area, m^2/g	215	155	175
Mean Pore Diameter[a], nm	8.7		8.5
Shape	0.125 cm quadralobe extrudates	0.125 cm trilobe extrudates	0.125 cm quadralobe extrudates
Pore Size Distribution	unimodal		unimodal

[a] Calculated by Mean Pore Radius = 2*(Pore Volume)/ Surface Area

Figure 260

Adsorption-desorption isotherm of A-HDN catalyst

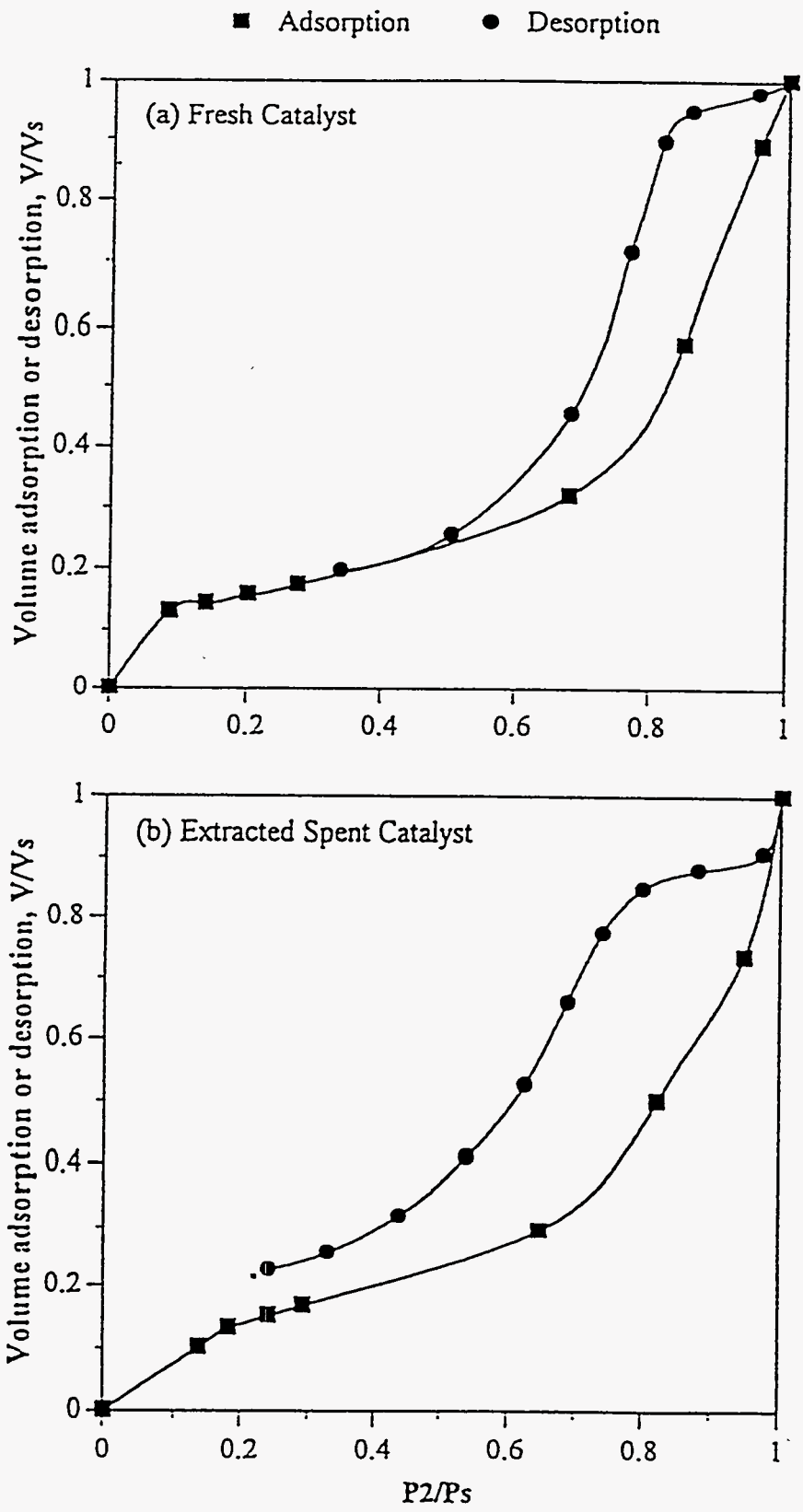
Adsorption
Desorption
(a) Fresh Catalyst
Volume adsorption or desorption, V/Vs
0
0.2
0.4
0.6
0.8
1
(b) Extracted Spent Catalyst
P2/Ps

Figure 261

Adsorption-desorption isotherm of C-HDN catalyst

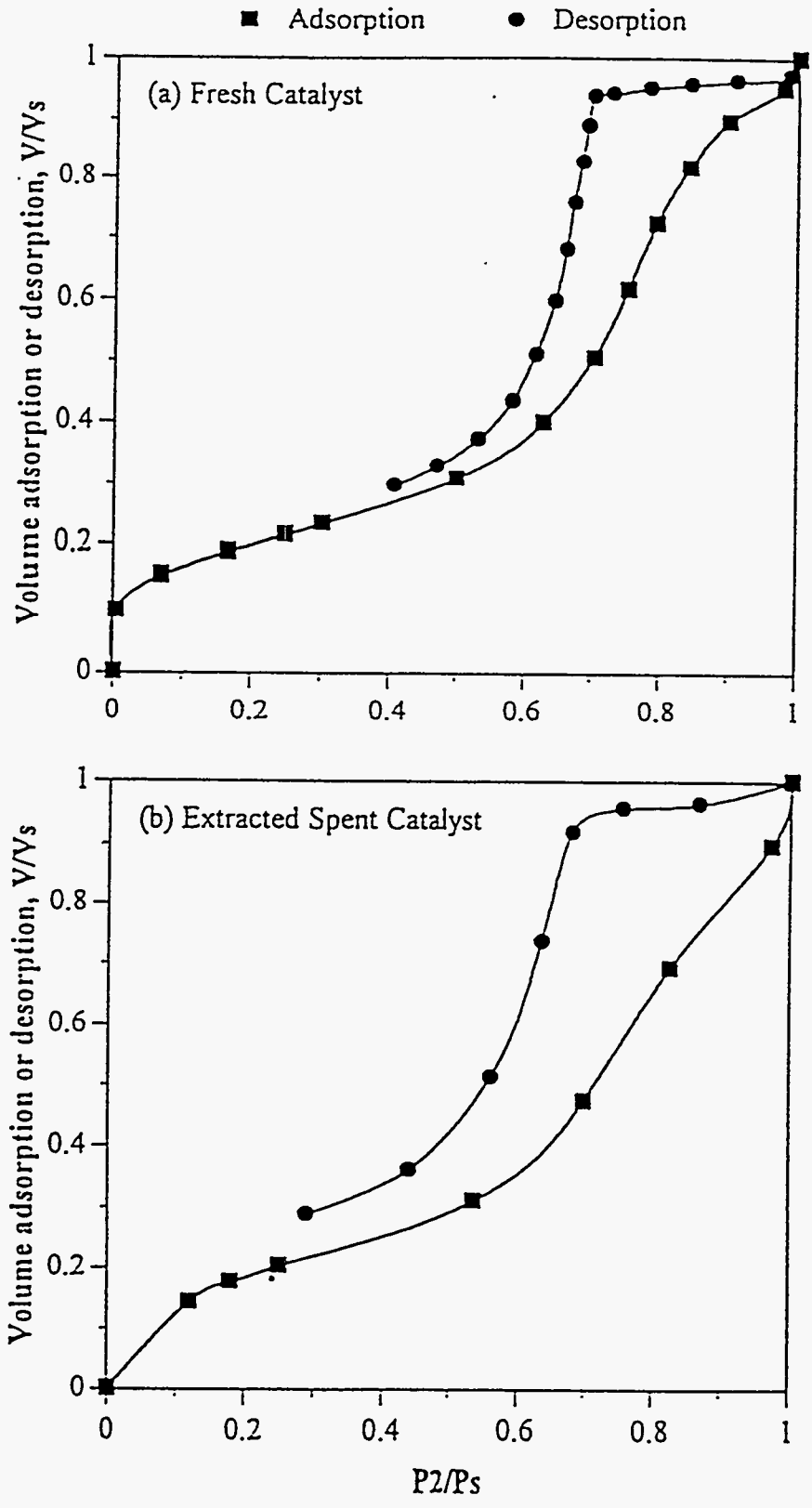
Adsorption
Desorption
(a) Fresh Catalyst
(b) Extracted Spent Catalyst
Volume adsorption or desorption, V/Vs
P2/Ps
0
0.2
0.4
0.6
0.8
1

Figure 262

Pore size distribution of fresh HDN catalysts

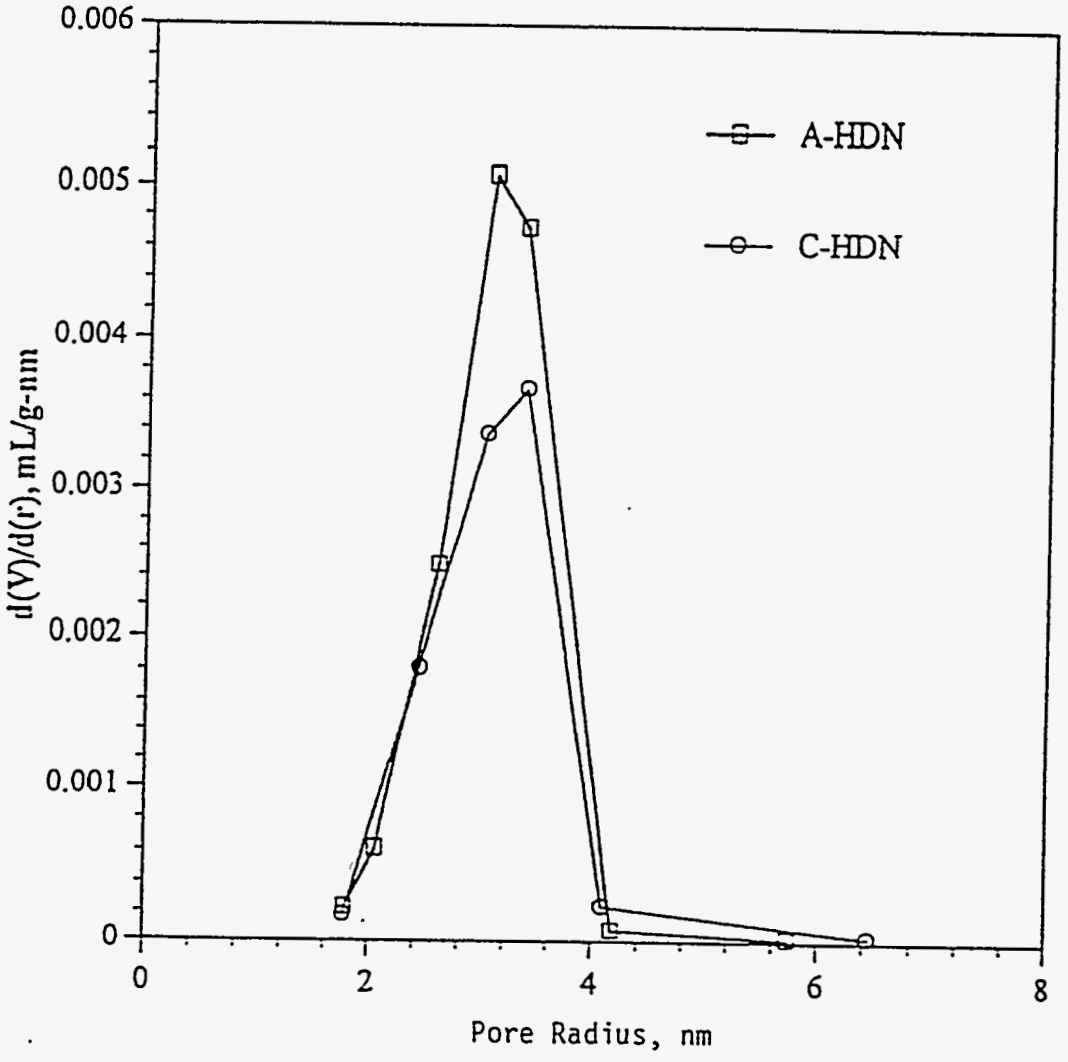
0.006
0.005
0.004
0.003
0.002
0.001
0
d(V)/d(r), mL/g-nm
0
2
4
6
8
Pore Radius, nm
A-HDN
C-HDN

Figure 263

Comparison with pore size distribution of fresh and extracted

spent A-HDN catalysts

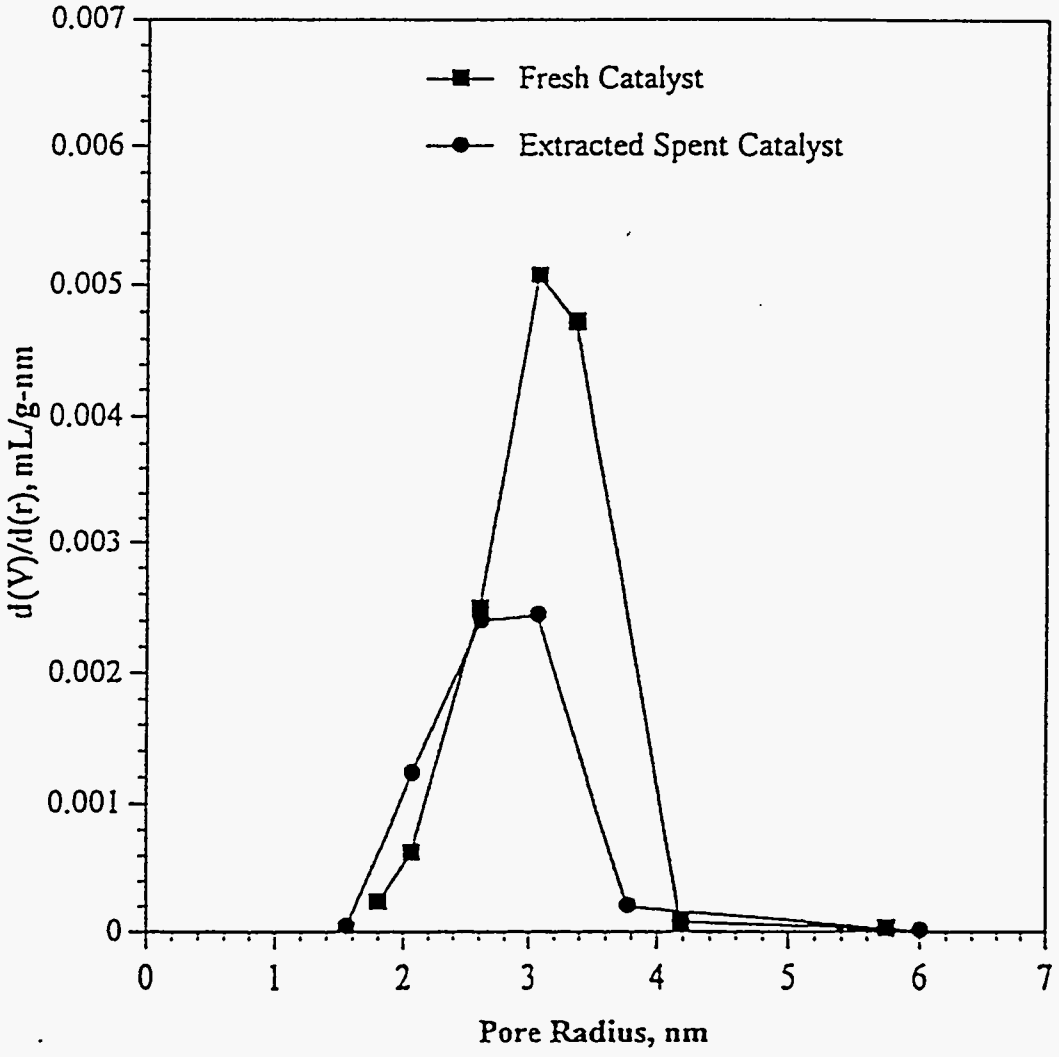
Fresh Catalyst
Extracted Spent Catalyst
d(V)/d(r), mL/g-nm
0.007
0.006
0.005
0.004
0.003
0.002
0.001
0
0
1
2
3
4
5
6
7
Pore Radius, nm

Figure 264

Comparison with pore size distribution of fresh and extracted

spent C-HDN catalysts

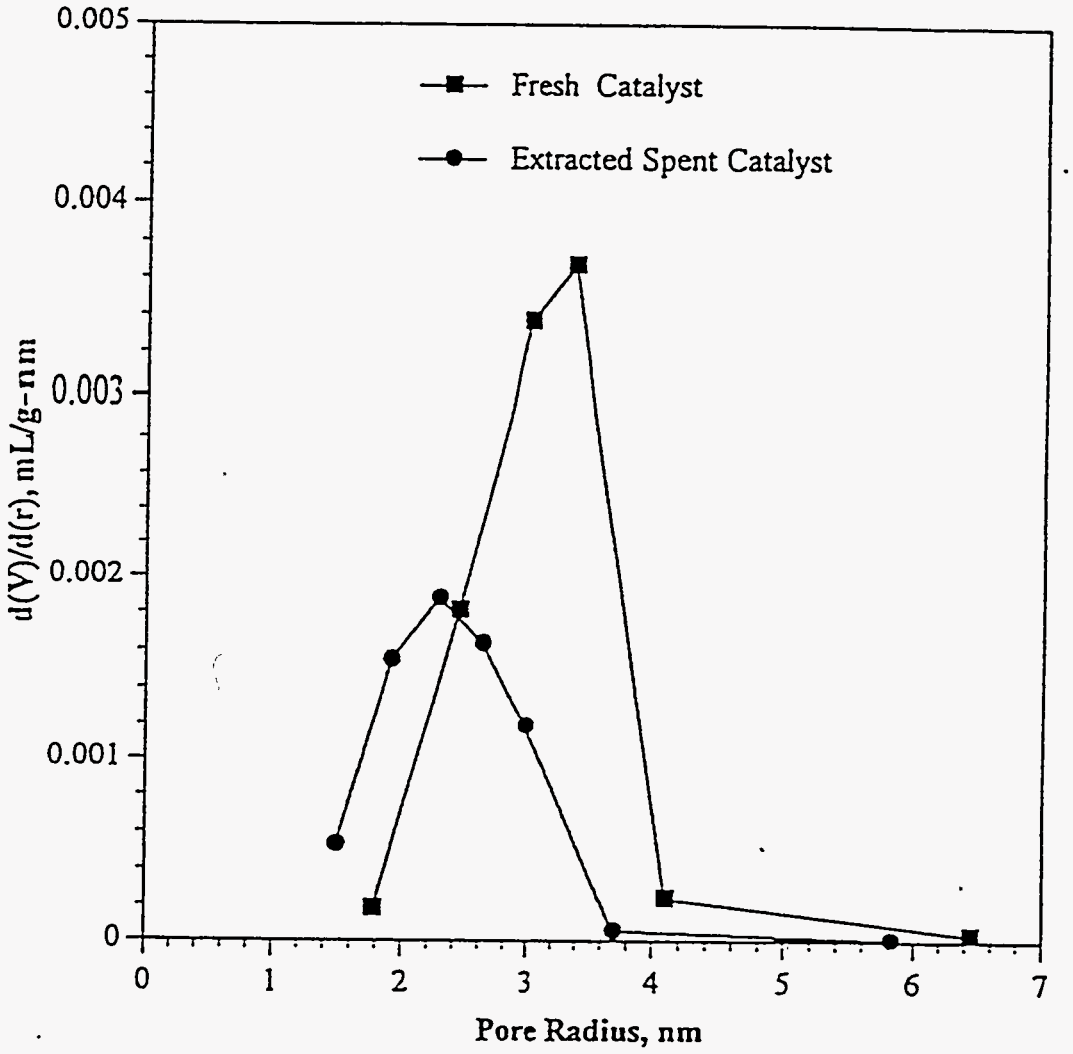
0.005
0.004
0.003
0.002
0.001
0
d(V)/d(r), mL/g-nm
Fresh Catalyst
Extracted Spent Catalyst
0
1
2
3
4
5
6
7
Pore Radius, nm

Table 84

Comparison with Physical Properties of Fresh and Spent HDN Catalysts

	A-HDN		B-HDN		C-HDN	
	Fresh	Spent	Fresh	Spent	Fresh	Spent
Pore Volume, mL/g	0.47	0.29	0.47	0.24	0.37	0.25
Surface Area, m^2 / g	215	144	155	98	175	117
Mean Pore Diameter, nm	8.7	8.1			8.5	8.5

the pore volumes and surface areas of the commercial NiMo catalyst using in vacuum residue HDS unit after 2 weeks (336 h). The losses calculated from their measured pore volume and surface area data were 30% and 10%, respectively. Chu et al.(325) reported that the coke generated from bitumen contributed significant surface area loss to the coked catalyst. Thus, the results of this study are consistent with the literature.

Reaction Conditions

When the catalyst activity had stabilized, process data were obtained which related reactor operating conditions to bitumen upgrading. The effect of temperature, pressure and liquid (or weight) hourly space velocity on sulfur, nitrogen, and nickel removal and on asphaltenes, Conradson carbon residue, and residuum conversion were determined under stable catalyst activity in this research.

Reactor operating conditions were varied such that only one of the three process variables was changed at a time and the other two variables were kept constant in successive runs. For example, LHSV was varied while the temperature and pressure were kept constant. The process operating strategies are displayed in Figures 265 and 266 for all the conditions employed in the three runs. Additionally, temperatures of 650 and 658 K were used to study the temperature effect in detail in Run Y; second pass hydrotreating was employed in Run F to obtain higher conversion of the product. The process operating conditions studied in Run Y, T, and F are listed in Tables 85-87, respectively.

The base case conditions were a temperature of 642 K, a pressure of 13.7 MPa, and a LHSV of 0.48 h^{-1}. The base case experiments were used to determine the extent of catalyst deactivation which was estimated by the change of the API gravity of the total liquid product. The process variable study was conducted in a cyclic mode, that is, base case condition-process variable experiment(s)-base case condition.

Presentation of Results

Heteroatom Removal

The conditions employed to upgrade the bitumen, as well as API gravity and the results of the elemental analyses (C, H, N, S and Ni) for the total liquid products

Figure 265

Experimental conditions as a function of temperature and LHSV

at constant pressure

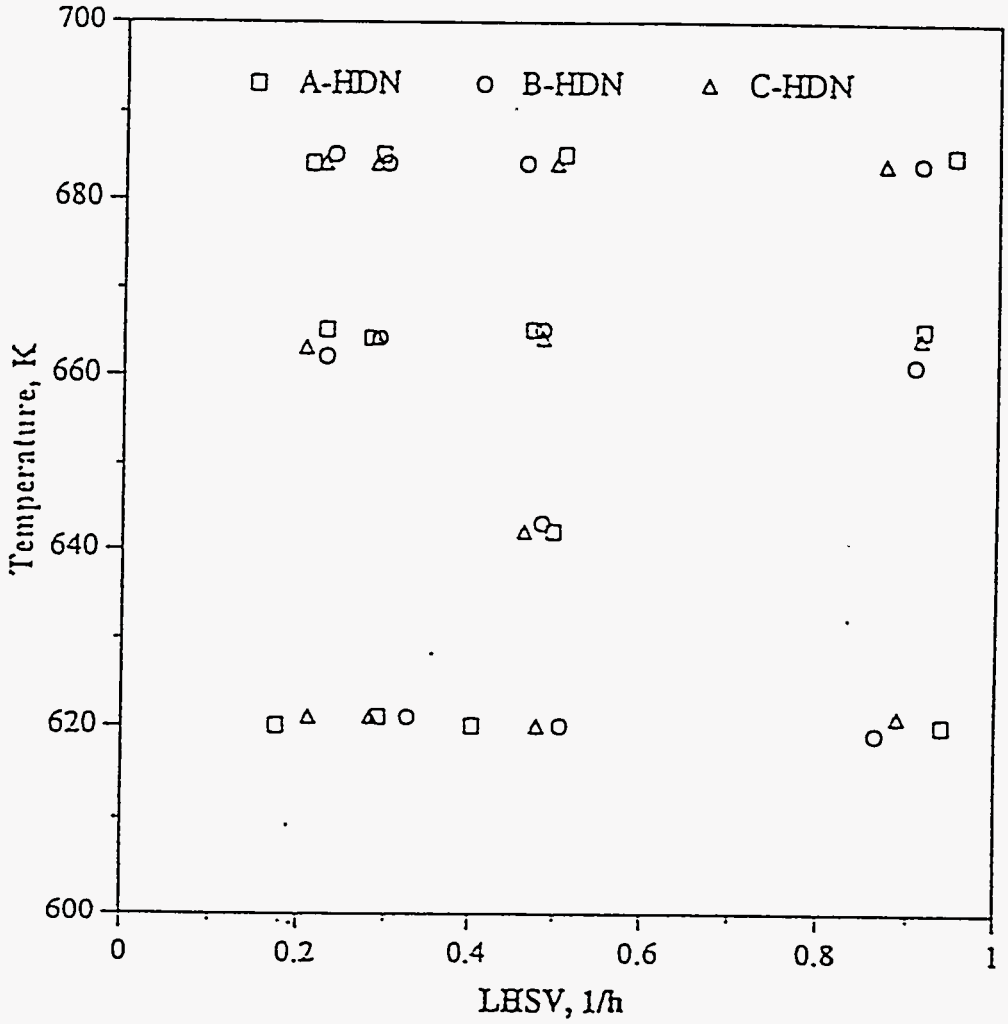
A-HDN
B-HDN
C-HDN
Temperature, K
700
680
660
640
620
600
0
0.2
0.4
0.6
0.8
1
LHSV, 1/h

Figure 266

Experimental conditions as a function of temperature and pressure

at constant LHSV

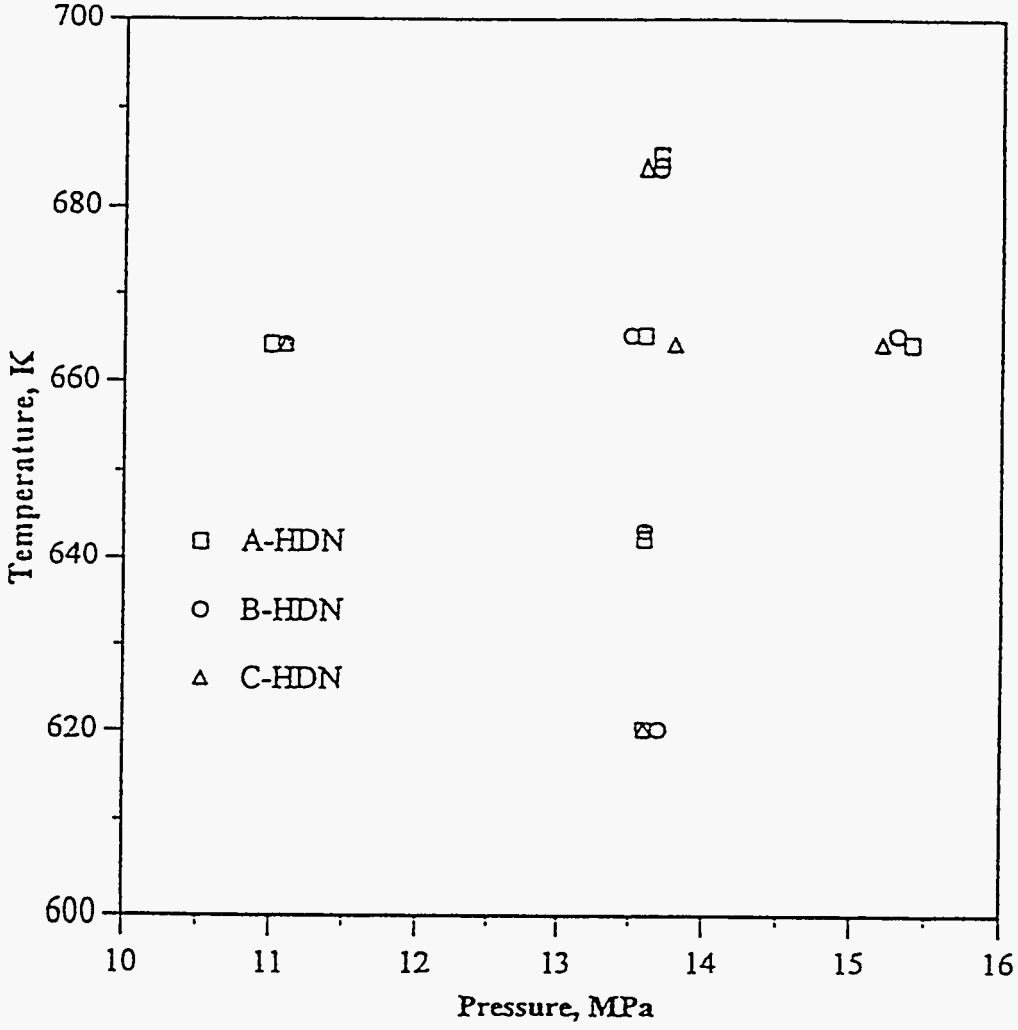
700
680
660
640
620
600
Temperature, K
10
11
12
13
14
15
16
Pressure, MPa
A-HDN
B-HDN
C-HDN

Table 85

Process Operating Conditions Studied in B-HDN Catalyst (Y Series)

Run Number	Temperature K	Pressure MPa	LHSV(WHSV) h^{-1}	Time on Stream h
Y-31	620	13.7	0.33 (0.39)	700
Y-24	620	13.7	0.51 (0.61)	531
Y-33	619	13.6	0.86 (1.04)	746
Y-16	643	13.6	0.48 (0.58)	316
Y-19	650	13.6	0.49 (0.59)	388
Y-15	658	13.7	0.49 (0.60)	292
Y-21	662	13.7	0.19 (0.23)	461
Y-26	664	13.6	0.29 (0.35)	579
Y-13	665	13.5	0.48 (0.58)	244
Y-30	660	13.6	0.90 (1.09)	673
Y-17	664	11.1	0.52 (0.62)	340
Y-23	665	15.3	0.46 (0.55)	507
Y-28	685	13.5	0.24 (0.28)	629
Y-34	684	13.6	0.30 (0.36)	773
Y-11	684	13.7	0.46 (0.55)	193
Y-37	684	13.6	0.91 (1.10)	830

Table 86

Process Operating Conditions Studied in C-HDN Catalyst (T Series)

Run Number	Temperature K	Pressure MPa	LHSV(WHSV) h^{-1}	Time on Stream · h
T-8	620	13.6	0.21 (0.26)	143
T-14	620	13.7	0.28 (0.34)	287
T-20	620	13.6	0.48 (0.58)	456
T-11	620	13.6	0.89 (1.07)	214
T-10	643	13.6	0.46 (0.56)	192
T-12	663	13.7	0.20 (0.25)	244
T-18	665	13.5	0.29 (0.37)	384
T-15	664	13.8	0.48 (0.58)	314
T-9	664	13.7	0.91 (1.10)	165
T-26	664	11.1	0.44 (0.53)	575
T-24	664	15.2	0.45 (0.54)	526
T-27	684	13.8	0.23 (0.27)	623
T-21	684	13.7	0.28 (0.34)	456
T-23	684	13.6	0.50 (0.60)	502
T-17	684	13.8	0.87 (1.05)	360

Table 87

Process Operating Conditions Studied in A-HDN Catalyst (F Series)

Run Number	Temperature K	Pressure MPa	LHSV(WHSV) h^{-1}	Time on Stream h
First Pass				
F-10	620	13.6	0.18 (0.25)	172
F-16	621	13.5	0.29 (0.42)	286
F-13	620	13.6	0.40 (0.58)	214
F-19	620	13.6	0.94 (1.35)	320
F-15	642	13.6	0.43 (0.62)	262
F-14	665	13.6	0.23 (0.33)	239
F-11	664	13.6	0.28 (0.40)	191
F-20	665	13.6	0.47 (0.68)	334
F-17	665	13.6	0.91 (1.31)	298
F-22	664	11.0	0.45 (0.64)	382
F-25	664	15.4	0.53 (0.76)	426
F-27	684	13.6	0.21 (0.30)	464
F-21	685	13.7	0.29 (0.42)	362
F-26	685	13.7	0.51 (0.73)	439
F-24	685	13.6	0.95 (1.36)	414
Second Pass				
F-29	641	13.6	0.57 (0.80)	587
F-30	684	13.5	0.20 (0.26)	631

produced over the HDN catalysts, are presented in Tables 88-90, respectively. The significant removal of nitrogen, sulfur, and nickel were accomplished with each of the three HDN catalysts. The molar ratios of hydrogen to carbon (H/C), an indication of heating value and combustion properties, of the liquid products were also improved. The atomic H/C ratios of liquid products were 1.7-1.8 at higher temperatures and close to that of light crudes, 1.8(315).

Although the primary purpose of hydrotreating the bitumens was to decrease their heteroatom contents, API gravity was employed as the primary on-line indicator of process performance. Figures 267 and 268 shows that the API gravity correlates with sulfur and nitrogen contents in the total liquid products for the three HDN catalysts, thus confirming the validity of the API gravity as an on-line monitor of catalyst performance.

The results of run number Y-28, Y-34, and Y-11 are compared in Table 88. The reported API gravity and elemental analysis data for Y-34 appeared out of line and indicated that the catalyst activity had decreased steeply. The reason may be that the API gravity of base case condition Y-32 and Y-36 drop significantly, from 15.6 to 15.1. Therefore, the data of Y-34 and Y-37 must be corrected in the evaluation of catalyst performance.

Tables 88-90 show that nitrogen, sulfur, and nickel removal increased strongly as residence time (reciprocal WHSV) and temperature increased for the Asphalt Ridge bitumen over the three HDN catalysts. However, the effect of pressure on nitrogen and sulfur removal was not significant.

Under the highest severity condition in the first pass hydrotreating study, sulfur contents in the liquid products meet the environmental product specification of unleaded gasoline in US, max. 0.04 wt% (expected future, to 2000 year)(325). After second pass hydrotreating, the sulfur concentration, 0.0023 wt%, in the liquid product meet the severe restrictions of unleaded gasoline in California, max. 0.003 wt% (expected future, to 2000 year)(325). The nitrogen concentration dropped also to 500 ppm which better than the requirement for catalytic cracking, 1500 ppm(326).

Table 88

Elemental Analyses of the Total Liquid Products Produced over the B-HDN Catalyst

Run No.	T K	P MPa	WHSV h^{-1}	Gravity °API	C wt%	H wt%	N wt%	S ppm	Ni ppm	H/C Ratio
Feed: Asphalt Ridge Bitumen				11.44	84.93	11.21	0.97	4200	86	1.58
Y-31	620	13.7	0.39	14.37	85.99	11.53	0.81	1300	36	1.61
Y-24	620	13.7	0.61	14.59	85.65	11.43	0.87	1500	28	1.60
Y-33	619	13.6	1.04	14.84	85.75	11.71	0.93	2000	49	1.64
Y-16	643	13.6	0.58	15.86	85.98	12.08	0.73	890	33	1.69
Y-19	650	13.6	0.59	16.56	86.05	11.90	0.60	830	31	1.66
Y-15	658	13.7	0.60	17.14	86.68	12.36	0.52	690	24	1.71
Y-21	662	13.7	0.23	27.07	86.84	12.77	0.28	201	18	1.76
Y-26	664	13.6	0.35	24.06	87.09	12.40	0.37	200	38	1.71
Y-13	665	13.5	0.58	19.08	85.80	11.94	0.54	570	24	1.67
Y-30	660	13.6	1.09	16.75	86.76	12.02	0.83	1100	42	1.66
Y-17	664	11.1	0.62	18.04	86.25	12.15	0.70	620	28	1.69
Y-23	665	15.3	0.55	18.80	87.11	12.15	0.43	580	23	1.67
Y-28	685	13.5	0.28	28.34	86.80	12.71	0.13	152	8	1.76
Y-34	684	13.6	0.36	24.96	87.08	12.81	0.32	195	20	1.77
Y-11	684	13.7	0.55	25.58	86.02	12.13	0.29	165	18	1.69
Y-37	684	13.6	1.10	17.66	86.09	11.89	0.69	910	33	1.66

Table 89

Elemental Analyses of the Total Liquid Products Produced over the C-HDN Catalyst

Run No.	T K	P MPa	WHSV h^{-1}	Gravity °API	C wt%	H wt%	N wt%	S ppm	Ni ppm	H/C Ratio
Feed: Asphalt Ridge Bitumen				11.44	84.93	11.21	0.97	4200		1.58
T-8	620	13.6	0.26	15.98	85.95	12.01	0.76	1000		1.68
T-14	620	13.7	0.34	15.48	86.66	12.17	0.77	1190		1.69
T-20	620	13.6	0.58	15.01	86.48	11.91	0.91	1410		1.65
T-11	620	13.6	1.07	15.23	85.87	11.94	0.94	1720	47	1.67
T-10	643	13.6	0.56	16.24	86.03	11.95	0.71	1000		1.67
T-12	663	13.7	0.25	22.78	85.84	12.58	0.31	410		1.76
T-18	665	13.5	0.37	20.69	86.55	12.51	0.46	550	31	1.73
T-15	664	13.8	0.58	18.45	86.01	12.25	0.54	800	34	1.71
T-9	664	13.7	1.10	16.81	86.29	12.38	0.69	950		1.72
T-26	664	11.1	0.53	17.79	86.72	12.33	0.68	1210		1.71
T-24	664	15.2	0.54	18.03	86.50	12.60	0.67	1000		1.75
T-27	684	13.8	0.27	27.34	87.55	13.21	0.29	240	25	1.81
T-21	684	13.7	0.34	25.37	87.21	12.93	0.30	300		1.78
T-23	684	13.6	0.60	21.45	87.09	12.61	0.51	600		1.74
T-17	684	13.8	1.05	19.45	86.75	12.38	0.56	790		1.71

Table 90

Elemental Analyses of the Total Liquid Products Produced over the A-HDN Catalyst

Run No.	T K	P MPa	WHSV h^{-1}	Gravity °API	C wt%	H wt%	N wt%	S ppm	Ni ppm	H/C Ratio
First Pass										
Feed: Asphalt Ridge Bitumen				11.44	84.93	11.21	0.97	4200		1.58
F-10	620	13.6	0.25	16.13	86.81	12.46	0.66	721		1.72
F-16	621	13.5	0.42	15.19	86.80	12.34	0.78	930		1.71
F-13	620	13.6	0.58	14.72	86.32	11.72	0.91	1080		1.63
F-19	620	13.6	1.35	13.61	86.75	12.07	0.93	1400	33	1.67
F-15	642	13.6	0.62	15.97	86.21	12.15	0.73	769		1.69
F-14	665	13.6	0.33	21.89	87.16	12.93	0.29	293		1.78
F-11	664	13.6	0.40	20.71	86.71	12.56	0.34	328	22	1.74
F-20	665	13.6	0.68	18.86	86.47	12.32	0.45	478	25	1.71
F-17	665	13.6	1.31	16.85	86.46	12.17	0.68	737		1.69
F-22	664	11.0	0.64	17.57	86.50	12.16	0.62	599		1.69
F-25	664	15.4	0.76	17.97	86.38	12.23	0.54	609		1.70
F-27	684	13.6	0.30	27.38	86.56	12.59	0.12	182	14	1.75
F-21	685	13.7	0.42	25.78	86.72	12.75	0.22	192		1.76
F-26	685	13.7	0.73	22.13	86.72	12.54	0.38	305		1.74
F-24	685	13.6	1.36	19.11	86.44	12.25	0.55	536		1.70
Second Pass										
Feed : Hydrotreated Bitumen[1]				15.96	86.14	11.64	0.67	736		1.62
F-29	641	13.6	0.80	16.94	86.46	12.08	0.62	589		1.68
Feed : Hydrotreated Bitumen[2]				27.27	85.83	12.67	0.13	54		1.77
F-30	684	13.5	0.26	31.68	87.18	13.07	0.05	23		1.80

[1] Composite Sample Prepared at Base Case Condition

[2] Composite Sample Prepared at 684 K, 13.7 MPa, and LHSV 0.2 h^{-1}

Figure 267

The correlation of API gravity versus sulfur content in the total liquid products produced over the three HDN catalysts

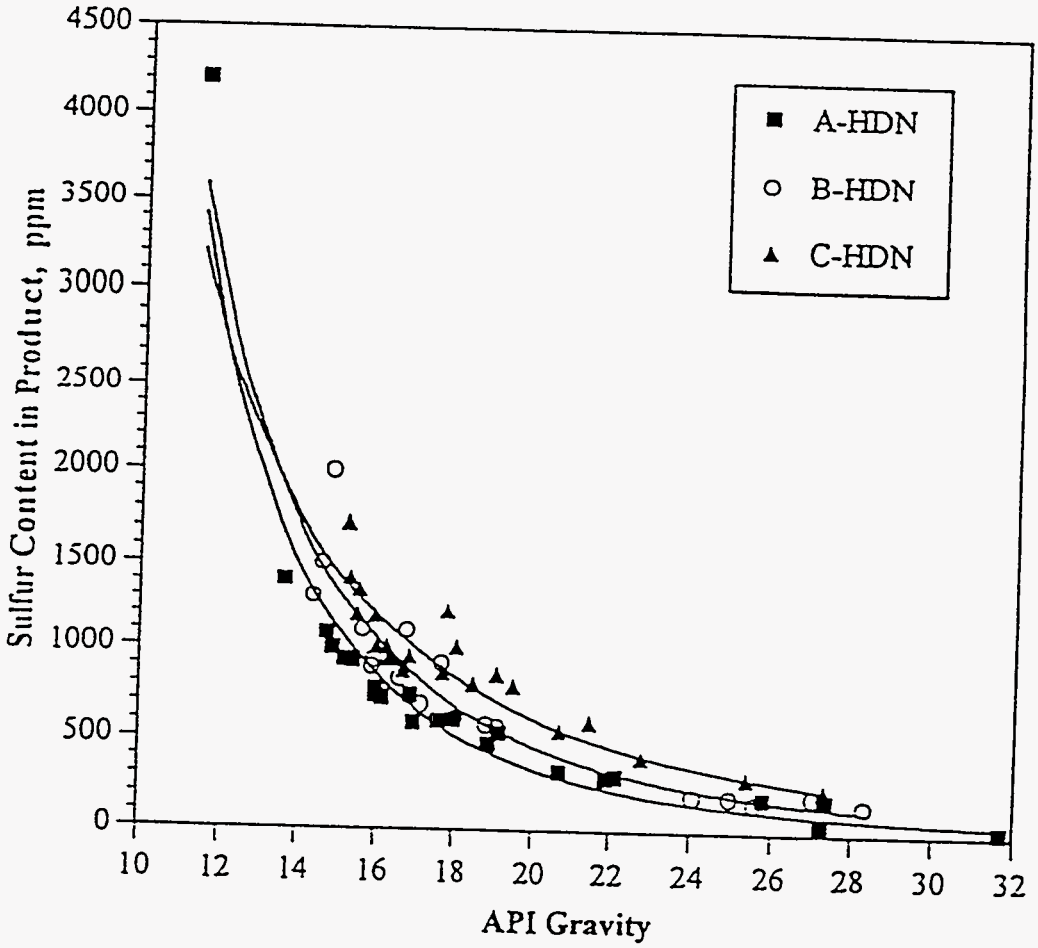
4500
4000
3500
3000
2500
2000
1500
1000
500
0
Sulfur Content in Product, ppm
10
12
14
16
18
20
22
24
26
28
30
32
API Gravity
A-HDN
B-HDN
C-HDN

Figure 268

The correlation of API gravity versus nitrogen content in the total liquid products produced over the three HDN catalysts

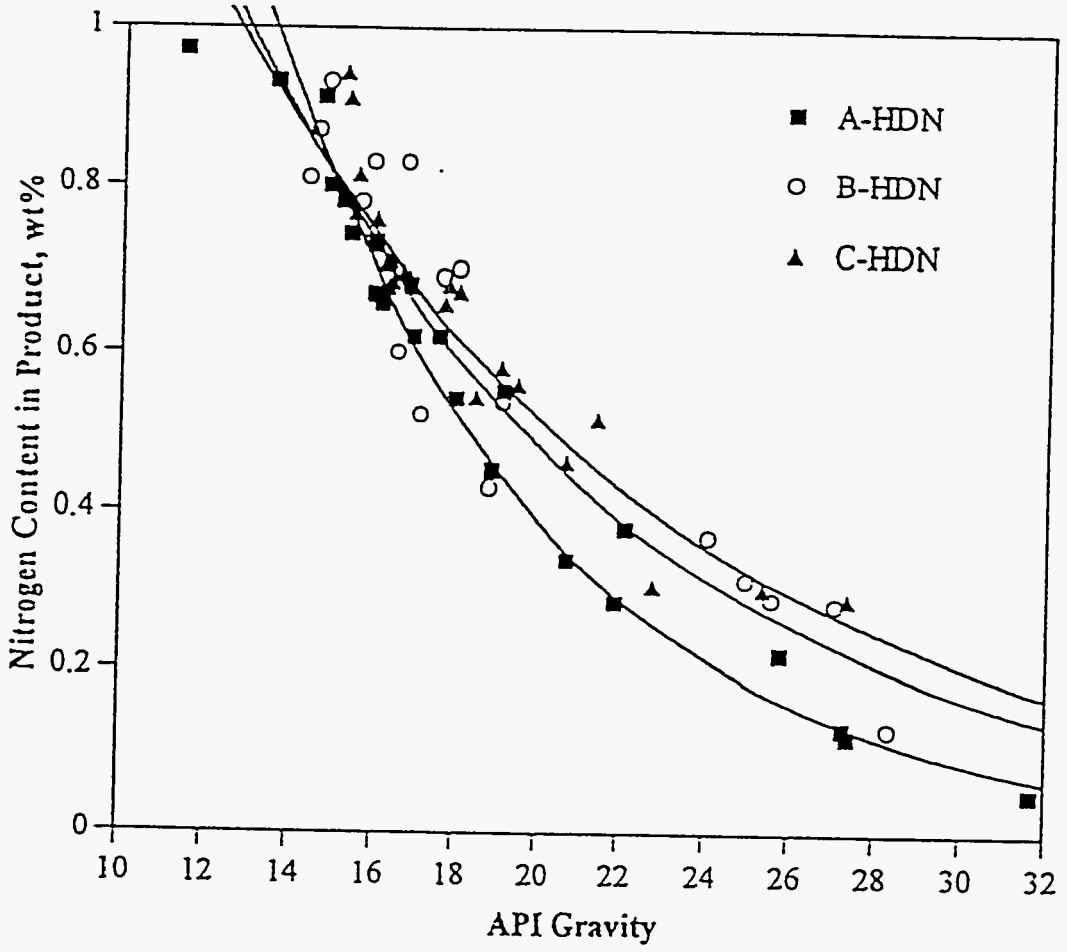
A-HDN
B-HDN
C-HDN
Nitrogen Content in Product, wt%
API Gravity
0
0.2
0.4
0.6
0.8
1
10
12
14
16
18
20
22
24
26
28
30
32

CCR and Asphaltenes Conversion

Tables 91-93 show, respectively, that CCR and asphaltene conversions and liquid yields are correlated to the operating conditions at which the total liquid products were produced over the HDN catalysts. Significant conversions of asphaltenes and CCR were obtained for all three catalysts.

The conversion of CCR increased significantly with increasing residence time (reciprocal WHSV) and temperature for the bitumen over all three HDN catalysts. The asphaltenes conversion increased as temperature increased. The conversion of asphaltenes increased with increasing residence time at higher temperature (664 and 684 K) but exhibited the opposite trend at lower temperature, 620 K, for each catalyst. As pressure increased, the conversion of CCR and asphaltenes increased, however, not significantly like in the case of the residence time and temperature.

Table 93 also presents a comparison between first and second pass hydrotreating at two operating conditions. Under the highest severity condition, the conversion of CCR and asphaltenes was over 90% after second pass hydrotreating.

Viscosity

The viscosities of liquid products produced over the HDN catalysts correlated with the operating conditions and are presented in Tables 94-96. As the temperature and residence time increased, the viscosity of the liquid product decreased significantly. With increasing pressure, the viscosities of the liquid products produced over the A- and C-HDN catalysts increased slightly, whereas the viscosity of the liquid product produced over the B-HDN catalyst decreased slightly. For the same operating conditions, the viscosity of liquid product was a function of the reactor temperature.

The viscosities of liquid products after second pass hydrotreating, compared to the liquid product produced during first pass hydrotreating and the bitumen, are also presented in Table 96. At the highest severity, the viscosity was 23.9 cp at 283.2 K, a reduction of three to four orders of magnitude.

Table 91

Selected Properties of Liquid Products Produced over the B-HDN Catalyst

Run No.	T K	P MPa	WHSV h^{-1}	Gravity °API	CCR wt%	Asphaltenes wt%	Liquid Yield wt%
Feed: Asphalt Ridge Bitumen				11.44	11.0	10.1	
Y-31	620	13.7	0.39	14.37	8.47	7.18	99.0
Y-24	620	13.7	0.61	14.59	8.75	7.15	99.0
Y-33	619	13.6	1.04	14.84	9.46	7.13	99.7
Y-16	643	13.6	0.58	15.86	7.57	6.73	98.6
Y-19	650	13.6	0.59	16.56	7.32	7.73	98.5
Y-15	658	13.7	0.60	17.14	6.58	6.88	97.7
Y-21	662	13.7	0.23	27.07	4.11	5.50	97.6
Y-26	664	13.6	0.35	24.06	5.00	6.22	97.4
Y-13	665	13.5	0.58	19.08	6.09	6.93	97.4
Y-30	660	13.6	1.09	16.75	8.30	7.21	98.2
Y-17	664	11.1	0.62	18.04	6.45	7.25	98.0
Y-23	665	15.3	0.55	18.80	6.02	6.88	97.7
Y-28	685	13.5	0.28	28.34	1.38	1.05	96.0
Y-34	684	13.6	0.36	24.96	4.19	6.13	94.9
Y-11	684	13.7	0.55	25.58	3.92	5.41	97.9
Y-37	684	13.6	1.10	17.66	7.72	8.13	97.7

Table 92

Selected Properties of Liquid Products Produced over the C-HDN Catalyst

Run No.	T K	P MPa	WHSV h^{-1}	Gravity °API	CCR wt%	Asphaltenes wt%	Liquid Yield wt%
Feed: Asphalt Ridge Bitumen				11.44	11.0	10.1	
T-8	620	13.6	0.26	15.98	7.39	7.30	98.9
T-14	620	13.7	0.34	15.48	7.89	7.03	98.3
T-20	620	13.6	0.58	15.01	8.78	6.78	98.3
T-11	620	13.6	1.07	15.23	8.71	6.61	98.5
T-10	643	13.6	0.56	16.24	7.30	6.65	99.2
T-12	663	13.7	0.25	22.78	4.43	5.88	96.5
T-18	665	13.5	0.37	20.69	5.87	6.34	97.5
T-15	664	13.8	0.58	18.45	6.81	6.50	97.2
T-9	664	13.7	1.10	16.81	7.58	8.00	98.5
T-26	664	11.1	0.53	17.79	7.83	7.42	97.2
T-24	664	15.2	0.54	18.03	7.47	7.30	97.7
T-27	684	13.8	0.27	27.34	3.34	5.58	93.8
T-21	684	13.7	0.34	25.37	4.05	6.42	93.4
T-23	684	13.6	0.60	21.45	6.07	7.28	95.1
T-17	684	13.8	1.05	19.45	6.75	7.26	96.3

Table 93

Selected Properties of Liquid Products Produced over the A-HDN Catalyst

Run No.	T K	P MPa	WHSV h^{-1}	Gravity °API	CCR wt%	Asphaltenes wt%	Liquid Yield wt%
First Pass							
Feed: Asphalt Ridge Bitumen				11.44	11.0	10.1	
F-10	620	13.6	0.25	16.13	6.99	7.56	98.4
F-16	621	13.5	0.42	15.19	7.76	7.40	99.1
F-13	620	13.6	0.58	14.72	8.10	7.62	99.2
F-19	620	13.6	1.35	13.61	8.77	6.73	99.2
F-15	642	13.6	0.62	15.97	7.27	7.82	98.3
F-14	665	13.6	0.33	21.89	3.80	5.44	96.5
F-11	664	13.6	0.40	20.71	4.31	5.88	96.5
F-20	665	13.6	0.68	18.86	5.59	6.60	96.9
F-17	665	13.6	1.31	16.85	6.95	7.31	98.3
F-22	664	11.0	0.64	17.57	6.57	7.23	97.6
F-25	664	15.4	0.76	17.97	6.24	7.22	97.4
F-27	684	13.6	0.30	27.38	1.11	1.42	91.3
F-21	685	13.7	0.42	25.78	2.38	2.75	93.8
F-26	685	13.7	0.73	22.13	4.76	6.74	94.4
F-24	685	13.6	1.36	19.11	6.24	7.73	96.1
Second Pass							
Feed : Hydrotreated Bitumen[1]				15.96	6.71	6.92	
F-29	641	13.6	0.80	16.94	6.46	6.80	99.2
Feed : Hydrotreated Bitumen[2]				27.27	1.16	1.45	
F-30	684	13.5	0.26	31.68	0.55	0.79	94.7

[1] Composite Sample Prepared at Base Case Condition

[2] Composite Sample Prepared at 684 K, 13.7 MPa, and LHSV 0.2 h^{-1}

Table 94

The Viscosity of Liquid Products Produced over the B-HDN Catalyst

Run No.	T K	P MPa	WHSV hr^{-1}	Viscosity cp						
				Temperature, K						
				333.2	343.2	348.2	353.2			
Feed: Asphalt Ridge Bitumen				37590	11750	8227	5583			
				313.2	323.2	333.2	338.2			
Y-31	620	13.7	0.39	43670	13600	4818	3187			
Y-24	620	13.7	0.61	60670	17380	6272	3896			
Y-33	619	13.6	1.04	120800	33380	11000	6639			
				298.2	303.2	308.2	313.2			
Y-19	650	13.6	0.59	35630	19140	10990	6519			
Y-15	658	13.7	0.60	11800	6673	4213	2611			
Y-17	664	11.1	0.62	5708	3306	2078	1350			
Y-23	665	15.3	0.55	4326	2675	1637	1078			
				283.2	288.2	293.2	298.2	303.2	308.2	313.2
Y-21	662	13.7	0.23	3794	1996	1224	784			
Y-26	664	13.6	0.35	5977	3262	1921	1255			
Y-13	665	13.5	0.58		12300	7220	4121	2563		
Y-30.	660	13.6	1.09				65790	34380	18830	10660
				283.2		288.2	293.2		298.2	
Y-28	685	13.5	0.28	48.6		36.5	28.7		22.7	
Y-34	684	13.6	0.36	211.7		160.3	113.6		83.1	
Y-11	684	13.7	0.55	588.8		367.6	249.7		175.8	
Y-37	684	13.6	1.10	18320		9568	5477		3258	

Table 95

The Viscosity of Liquid Products Produced over the C-HDN Catalyst

Run No.	T K	P MPa	WHSV h^{-1}	Viscosity cp				
				Temperature, K				
				333.2	343.2	348.2	353.2	
Feed: Asphalt Ridge Bitumen				37590	11750	8227	5583	
				283.2	293.2	313.2	333.2	353.2
T-8	620	13.6	0.26			17590	2403	544.4
T-14	620	13.7	0.34			32050	3729	775.7
T-20	620	13.6	0.58			59810	6408	1240
T-11	620	13.6	1.07			78130	7966	1474
T-12	663	13.7	0.25		768.0	184.8	63.5	
T-18	665	13.5	0.37		2112	394.8	117.2	
T-15	664	13.8	0.58		9996	1312	307.7	
T-9	664	13.7	1.10		41310	4152	762.0	
T-26	664	11.1	0.53		12850	1583	369.7	
T-24	664	15.2	0.54		15525	1868	427.0	
T-27	684	13.8	0.27	78.8	46.7	20.1		
T-21	684	13.7	0.34	136.3	75.0	28.7		
T-23	684	13.6	0.60	981.3	426.1	115.2		
T-17	684	13.8	1.05	5494	1986	412.3		

Table 96

The Viscosity of Liquid Products Produced over the A-HDN Catalyst

Run No.	T K	P MPa	WHSV h^{-1}	Viscosity cp				
				Temperature, K				
First Pass								
				333.2	343.2	348.2	353.2	
Feed: Asphalt Ridge Bitumen				37590	11750	8227	5583	
				283.2	293.2	313.2	333.2	353.2
F-10	620	13.6	0.25			15480	2181	486.4
F-16	621	13.5	0.42			28020	3396	720.2
F-13	620	13.6	0.58			39160	4439	926.7
F-19	620	13.6	1.35			74365	7684	1467
F-14	665	13.6	0.33		801.8	188.4	62.5	
F-11	664	13.6	0.40		1483	307.7	93.8	
F-20	665	13.6	0.68		5964	922.6	231.4	
F-17	665	13.6	1.31		36090	3729	707.4	
F-22	664	11.0	0.64		10340	1420	320	
F-25	664	15.4	0.76		12070	1607	356.4	
F-27	684	13.6	0.30	48.2	27.5	12.0		
F-21	685	13.7	0.42	99.5	52.8	20.7		
F-26	685	13.7	0.73	888.5	362.1	98.8		
F-24	685	13.6	1.36	7306	2250	433.1		
Second Pass								
Feed : Hydrotreated Bitumen[1]					102900	8274	1295	
F-29	641	13.6	0.80		45920	4564	825.3	
Feed : Hydrotreated Bitumen[2]				50.4	29.4	13.6		
F-30	684	13.5	0.26	23.9	13.6	6.18		

[1] Composite Sample Prepared at Base Case Condition

[2] Composite Sample Prepared at 684 K, 13.7 MPa, and LHSV 0.2 h^{-1}

Product Distribution

The product distributions and yields for each of the HDN catalysts are presented in Tables 97-102. The C_1-C_4 yields are presented in Tables 97-99. The product distributions consisted of light hydrocarbon gases (C_1-C_4), naphtha (C_5-478 K), middle distillate (478-616 K), gas oil (616-811 K), and residuum (>811 K) for each HDN catalyst are presented in Tables 100-102. The hydrogen consumptions reported as a function of operating conditions for each of the HDN catalysts are also presented in Tables 97-99.

The individual components (C_1, C_2, C_3, iC_4, and nC_4) and total C_1-C_4 weight contents of light hydrocarbon gases increased significantly with increasing temperature. In general, the yields also increased as residence time increased. However, the distributions of light hydrocarbon gases were not significantly influenced by pressure. The effects of process variables on the hydrogen consumption exhibited the same trends observed for light hydrocarbon gases.

Molecular weight reduction of the bitumen increased with increasing residence time and temperature over the three catalysts, however it was not significantly influenced by pressure.

Process Kinetic Models for Bitumen Hydrotreating

Bitumen is a complex mixture containing a very large number of components that cannot be resolved and identified. The conversion of individual organic sulfur, nitrogen, and residuum moieties, and carbon residues in the bitumen cannot be represented by simple intrinsic kinetics. However, the apparent kinetic models for the removal of these compounds can be expressed by treating the total organic sulfur, nitrogen, residuum moieties, and carbon residues in the bitumen as individual, composite lumps of sulfur, nitrogen, residuum, and carbon residue as a first approximation.

The kinetic models may be divided into three general categories: models assuming a single reaction, a limited number of reactions in parallel, and an infinite number of reactions in parallel.

Table 97

Product Distributions and Yields of Hydrocarbon Gases Produced over the B-HDN Catalyst

Run No.	T K	P MPa	WHSV h^{-1}	C_1 wt%	C_2 wt%	C_3 wt%	iC_4 wt%	nC_4 wt%	C_1-C_4 wt%	H_2 Consumption liter / liter
Feed: Asphalt Ridge Bitumen										
Y-31	620	13.7	0.39	0.32	0.09	0.09	0.02	0.01	0.53	69
Y-24	620	13.7	0.61	0.27	0.12	0.13	0.05	0.06	0.63	30
Y-33	619	13.6	1.04	0.03		0.01		0.01	0.05	15
Y-16	643	13.6	0.58	0.39	0.11	0.14	0.07	0.09	0.80	67
Y-19	650	13.6	0.59	0.39	0.15	0.17	0.05	0.07	0.83	59
Y-15	658	13.7	0.60	0.27	0.30	0.58	0.20	0.15	1.53	104
Y-21	662	13.7	0.23	0.46	0.22	0.32	0.12	0.23	1.35	194
Y-26	664	13.6	0.35	0.63	0.28	0.37	0.13	0.20	1.61	194
Y-13	665	13.5	0.58	0.69	0.32	0.38	0.28	0.18	1.85	147
Y-30	660	13.6	1.09	0.71	0.26	0.31	0.02	0.03	1.33	32
Y-17	664	11.1	0.62	0.49	0.24	0.31	0.20	0.12	1.36	94
Y-23	665	15.3	0.55	0.54	0.26	0.33	0.13	0.20	1.46	108
Y-28	685	13.5	0.28	0.98	0.50	0.68	0.25	0.39	2.80	238
Y-34	684	13.6	0.36	1.40	0.71	0.98	0.34	0.52	3.95	232
Y-11	684	13.7	0.55	0.34	0.16	0.23	0.10	0.16	0.99	146
Y-37	684	13.6	1.10	0.63	0.29	0.41	0.16	0.24	1.73	78

Table 98

Product Distributions and Yields of Hydrocarbon Gases Produced over the C-HDN Catalyst

Run No.	T K	P MPa	WHSV h^{-1}	C_1 wt%	C_2 wt%	C_3 wt%	iC_4 wt%	nC_4 wt%	C_1-C_4 wt%	H_2 Consumption liter / liter
Feed: Asphalt Ridge Bitumen										
T-8	620	13.6	0.26	0.60	0.17	0.05	0.20	0.10	1.12	168
T-14	620	13.7	0.34	0.89	0.25	0.37	0.07	0.12	1.70	84
T-20	620	13.6	0.58	0.87	0.20	0.53		0.06	1.66	78
T-11	620	13.6	1.07	0.85	0.19	0.50			1.54	55
T-10	643	13.6	0.56	0.18	0.05	0.05	0.02	0.04	0.34	96
T-12	663	13.7	0.25	2.00	0.72	0.11	0.23	0.44	3.50	317
T-18	665	13.5	0.37	1.38	0.47	0.14	0.17	0.32	2.48	173
T-15	664	13.8	0.58	1.42	0.49	0.21	0.15	0.29	2.56	135
T-9	664	13.7	1.10	0.85	0.29	0.08	0.10	0.10	1.47	99
T-26	664	11.1	0.53	1.66	0.43	0.17	0.19	0.34	2.79	118
T-24	664	15.2	0.54	1.20	0.44	0.15	0.18	0.33	2.30	139
T-27	684	13.8	0.27	3.08	1.23	0.14	0.61	1.17	5.62	234
T-21	684	13.7	0.34	3:29	1.35	0.33	0.56	1.10	6.63	217
T-23	684	13.6	0.60	2.48	1.00	0.15	0.46	0.84	4.93	167
T-17	684	13.8	1.05	2.23	0.59	0.20	0.25	0.45	3.72	123

Table 99

Product Distributions and Yields of Hydrocarbon Gases Produced over the A-HDN Catalyst

Run No.	T K	P MPa	WHSV h^{-1}	C_1 wt%	C_2 wt%	C_3 wt%	iC_4 wt%	nC_4 wt%	C_1-C_4 wt%	H_2 Consumption liter / liter
First Pass										
Feed: Asphalt Ridge Bitumen										
F-10	620	13.6	0.25	1.06	0.23	0.22		0.07	1.58	110
F-16	621	13.5	0.42	0.64	0.13	0.10			0.87	101
F-13	620	13.6	0.58	0.55	0.10	0.13		0.02	0.80	128
F-19	620	13.6	1.35	0.60	0.07	0.13			0.80	84
F-15	642	13.6	0.62	1.15	0.25	0.23	0.01	0.09	1.73	87
F-14	665	13.6	0.33	2.03	0.55	0.50	0.13	0.25	3.46	242
F-11	664	13.6	0.40	1.93	0.51	0.62	0.19	0.24	3.49	144
F-20	665	13.6	0.68	1.85	0.47	0.43	0.10	0.21	3.06	118
F-17	665	13.6	1.31	1.04	0.26	0.27	0.04	0.10	1.71	84
F-22	664	11.0	0.64	1.27	0.32	0.48	0.15	0.15	2.38	101
F-25	664	15.4	0.76	1.32	0.32	0.65	0.14	0.15	2.58	124
F-27	684	13.6	0.30	4.69	1.39	1.38	0.39	0.81	8.66	154
F-21	685	13.7	0.42	3.41	0.97	0.94	0.31	0.52	6.15	201
F-26	685	13.7	0.73	3.20	0.87	0.84	0.23	0.45	5.59	149
F-24	685	13.6	1.36	2.36	0.61	0.56	0.14	0.27	3.94	121
Second Pass										
Feed: Hydrotreated Bitumen[1]				1.15	0.25	0.23	0.01	0.09	1.73	87
F-29	641	13.6	0.80	0.53	0.17	0.11			0.81	13
Feed: Hydrotreated Bitumen[2]				4.69	1.39	1.38	0.39	0.81	8.66	154
F-30	684	13.5	0.26	2.41	0.91	0.97	0.39	0.62	5.30	30

[1] Composite Sample Prepared at Base Case Condition

[2] Composite Sample Prepared at 684 K, 13.7 MPa, and LHSV 0.2 h^{-1}

Table 100

Product Distributions and Yields Produced over the B-HDN Catalyst

Run No.	T K	P MPa	WHSV h^{-1}	C_1-C_4 wt%	C_5–478 K wt%	478-616 K wt%	616-811K wt%	>811 K wt%
Feed: Asphalt Ridge Bitumen					0.5	10.2	34.5	54.8
Y-31	620	13.7	0.39	0.5	2.3	10.7	41.5	45.0
Y-24	620	13.7	0.61	0.6	2.7	10.3	40.8	45.5
Y-33	619	13.6	1.04	0.1	2.3	9.9	40.7	47.0
Y-16	643	13.6	0.58	0.8	3.1	11.7	42.0	42.2
Y-19	650	13.6	0.59	0.8	3.4	12.3	42.3	41.1
Y-15	658	13.7	0.60	1.5	3.9	13.1	43.3	38.1
Y-21	662	13.7	0.23	1.4	6.5	17.6	47.1	27.4
Y-26	664	13.6	0.35	1.6	5.5	16.6	45.1	31.3
Y-13	665	13.5	0.58	1.9	4.6	14.3	43.1	36.1
Y-30	660	13.6	1.09	1.3	2.7	11.9	40.4	43.7
Y-17	664	11.1	0.62	1.4	4.4	14.2	44.1	35.9
Y-23	665	15.3	0.55	1.5	4.4	14.9	44.8	34.4
Y-28	685	13.5	0.28	2.8	10.5	24.8	39.0	22.9
Y-34	684	13.6	0.36	4.0	9.7	22.1	41.0	23.2
Y-11	684	13.7	0.55	1.0	8.2	20.7	45.3	24.8
Y-37	684	13.6	1.10	1.7	9.7	24.2	33.9	30.4

Table 101

Product Distributions and Yields Produced over the C-HDN Catalyst

Run No.	T K	P MPa	WHSV h^{-1}	C_1-C_4 wt%	C_5-478 K wt%	478-616 K wt%	616-811 K wt%	>811 K wt%
Feed: Asphalt Ridge Bitumen					0.5	10.2	34.5	54.8
T-8	620	13.6	0.26	1.1	2.7	11.7	43.2	41.4
T-14	620	13.7	0.34	1.7	2.4	10.8	40.7	44.4
T-20	620	13.6	0.58	1.7	2.3	10.1	37.9	48.0
T-11	620	13.6	1.07	1.5	2.1	9.6	37.3	49.5
T-10	643	13.6	0.56	0.3	3.1	12.6	43.2	40.6
T-12	663	13.7	0.25	3.5	6.4	18.9	46.3	25.0
T-18	665	13.5	0.37	2.5	5.4	16.7	42.1	33.3
T-15	664	13.8	0.58	2.6	4.5	14.3	41.0	37.6
T-9	664	13.7	1.10	1.5	3.4	13.2	42.6	39.3
T-26	664	11.1	0.53	2.8	4.8	14.9	39.3	38.3
T-24	664	15.2	0.54	2.3	4.5	18.5	47.4	27.2
T-27	684	13.8	0.27	5.6	12.6	27.2	36.3	17.8
T-21	684	13.7	0.34	6.6	10.4	23.0	34.6	25.6
T-23	684	13.6	0.60	4.9	8.3	19.5	36.5	30.8
T-17	684	13.8	1.05	3.7	5.9	16.6	38.4	35.5

Table 102

Product Distributions and Yields Produced over the A-HDN Catalyst

Run No.	T K	P MPa	WHSV h^{-1}	C_1-C_4 wt%	C_5-478 K wt%	478-616 K wt%	616-811 K wt%	>811 K wt%
First Pass								
Feed: Asphalt Ridge Bitumen					0.5	10.2	34.5	54.8
F-10	620	13.6	0.25	1.6	2.3	12.7	45.9	37.6
F-16	621	13.5	0.42	0.9	2.1	11.8	44.4	40.7
F-13	620	13.6	0.58	0.8	2.1	11.7	43.8	41.5
F-19	620	13.6	1.35	0.8	1.9	10.6	41.4	45.3
F-15	642	13.6	0.62	1.7	2.5	12.9	45.9	37.0
F-14	665	13.6	0.33	3.5	5.1	20.1	51.3	20.2
F-11	664	13.6	0.40	3.5	4.6	18.3	50.5	23.2
F-20	665	13.6	0.68	3.1	4.0	16.7	48.4	27.9
F-17	665	13.6	1.31	1.7	3.2	14.9	47.0	33.1
F-22	664	11.0	0.64	2.4	3.6	15.8	46.5	31.7
F-25	664	15.4	0.76	2.6	4.1	17.0	52.2	24.1
F-27	684	13.6	0.30	8.7	9.4	29.0	42.8	10.2
F-21	685	13.7	0.42	6.2	8.4	26.0	46.2	13.4
F-26	685	13.7	0.73	5.6	6.3	22.2	47.6	18.2
F-24	685	13.6	1.36	3.9	4.7	18.2	46.7	26.5
Second Pass								
Feed: Hydrotreated Bitumen[1]				1.7	2.5	12.9	45.9	37.0
F-29	641	13.6	0.80	0.8	2.6	14.9	50.0	31.7
Feed: Hydrotreated Bitumen[2]				8.7	9.4	29.0	42.8	10.2
F-30	684	13.5	0.26	5.3	12.0	35.7	37.4	9.5

[1] Composite Sample Prepared at Base Case Condition

[2] Composite Sample Prepared at 684 K, 13.7 MPa, and LHSV 0.2 h^{-1}

Single First-Order Reaction

Assuming a single first-order reaction is approximate, the conversion rate of the lumped species is assumed to follow Equation 147 at constant hydrogen partial pressure, 13.7 MPa.

$$r_i = -\frac{dC_i}{d\tau} = k' P_{H_2}^{\beta} C_i = kC_i \qquad (147)$$

where i represents the individual, composite lumped species such as sulfur, nitrogen, etc.; r_i is the conversion rate; C_i is the concentration of the lumped species i; τ is the reciprocal WHSV (or LHSV); k' is first-order rate constant; P_{H_2} is hydrogen partial pressure; β is the reaction order with respect to hydrogen partial pressure; and k is the apparent first-order rate constant. τ is used in this equation instead of the real time, t, because this equation was derived for a plug flow reactor.

If it is assumed that there is no density change during the reaction, the fractional conversion, x_i, is defined by the following equation:

$$x_i = 1 - C_i / C_{io} \qquad (148)$$

where C_{io} is the initial concentration of lumped species i. Equation 148 can be rearranged as

$$C_i = C_{io}(1-x_i) \qquad (149)$$

Substituting the Equation 149 into the Equation 147 and integrating gives the following equation:

$$-\ln(1-x_i) = k\tau \qquad (150)$$

Equation 150 indicates that if the reaction follows a simple first-order reaction, the plot of the $-\ln(1-x_i)$ versus reciprocal WHSV, τ, will be a straight line through the origin and the slope of that line will be equal to k.

The negative natural logarithms of the fraction remaining of the lumped species, such as sulfur, nitrogen, residuum, and CCR, as a function of reciprocal WHSV over the A-HDN catalyst at constant pressure are plotted in Figures 269 and 270. These figures indicate that the kinetic equations of the lumped species at three temperatures do not follow the single first-order reaction except that for CCR conversion at 684 K. Equivalent plots are shown in Appendix B for the lumped species conversions over the B- and C-HDN catalysts at three temperatures and constant pressure. In each case, it was concluded that the data do not obey simple first order kinetics.

Thus it was concluded that the simple first-order reaction model for the individual, composite lumped reactants is inadequate for the description of bitumen hydrotreating process kinetics.

Two Parallel First-Order Reactions

The two parallel first-order reactions model assumed that the each species, i.e., nitrogen, sulfur, residuum, and carbon residue, consists of facile and refractory fractions which differ in reactivity and convert by first-order reactions in parallel. The proposed reaction scheme is described by the following equation:

$$\begin{aligned} R_f &= \gamma R \xrightarrow{k_f} P \\ R_r &= (1-\gamma) R \xrightarrow{k_r} P \end{aligned} \qquad (151)$$

where R_f and R_r represent the facile and refractory fractions of the lumped species R, such as sulfur, nitrogen, residuum, and CCR; γ is the initial weight fraction of the facile components in the lumped species; k_f and k_r are apparent first-order rate constant for the conversion of facile and refractory fractions, respectively; P represents the products. After deriving the appropriate rate expressions based on Equation 151 and integrating (detailed procedures are found in Reference 292), the rate expression, expressed in terms of fractional conversion, x_R, of the lumped species R is

$$(1- x_R) = \gamma \exp(-k_f \tau) + (1-\gamma)\exp(-k_r \tau) \qquad (152)$$

Figure 269

Plot of -ln(l-x) versus reciprocal WHSV for (a) sulfur (b)nitrogen conversion over the A-HDN catalyst at constant pressure (13.7 MPa)

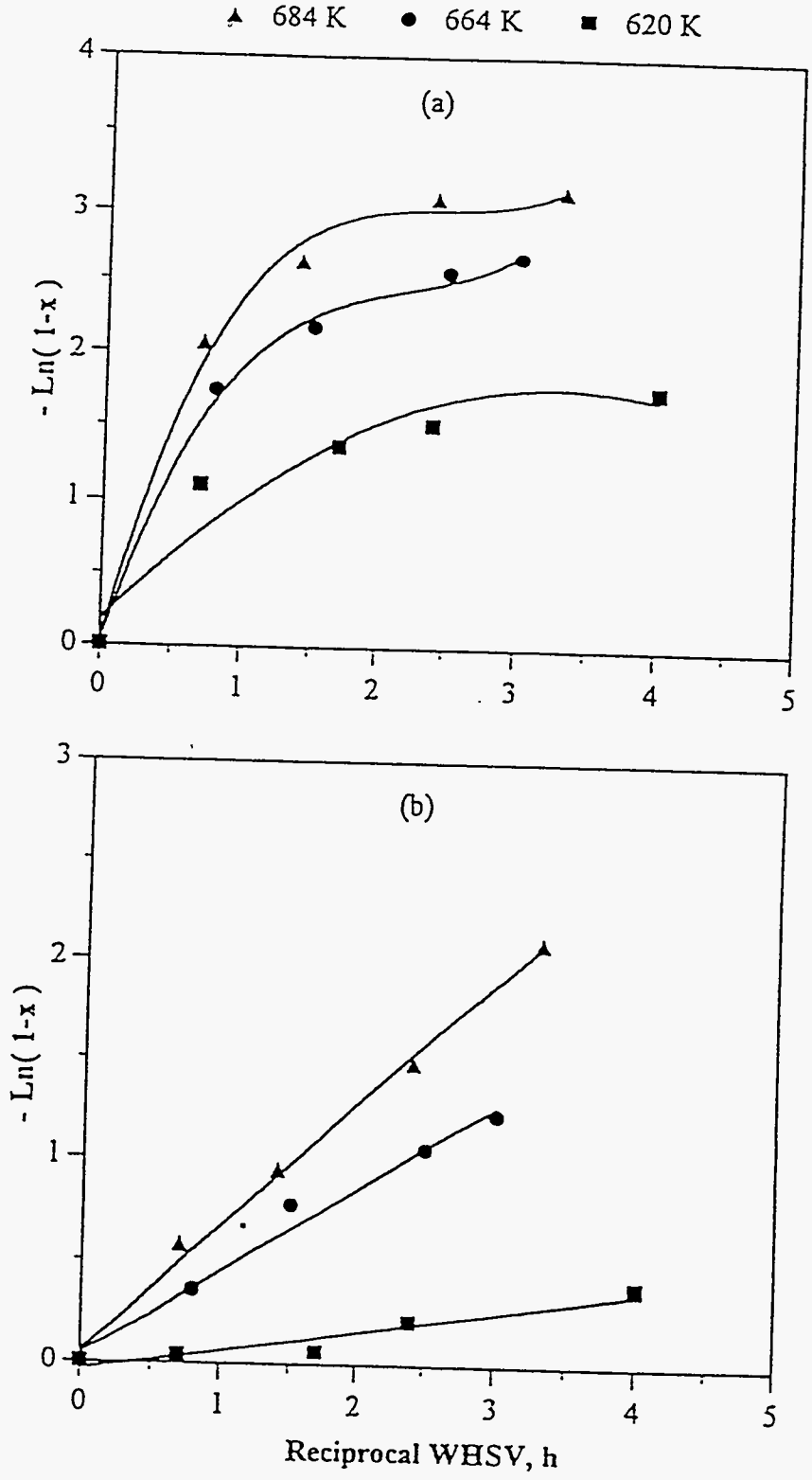
684 K
664 K
620 K
(a)
- Ln(1-x)
(b)
- Ln(1-x)
Reciprocal WHSV, h

Figure 270

Plot of -ln(l-x) versus reciprocal WHSV for (a) residuum (b) CCR conversion over the A-HDN catalyst at constant pressure (13.7 MPa)

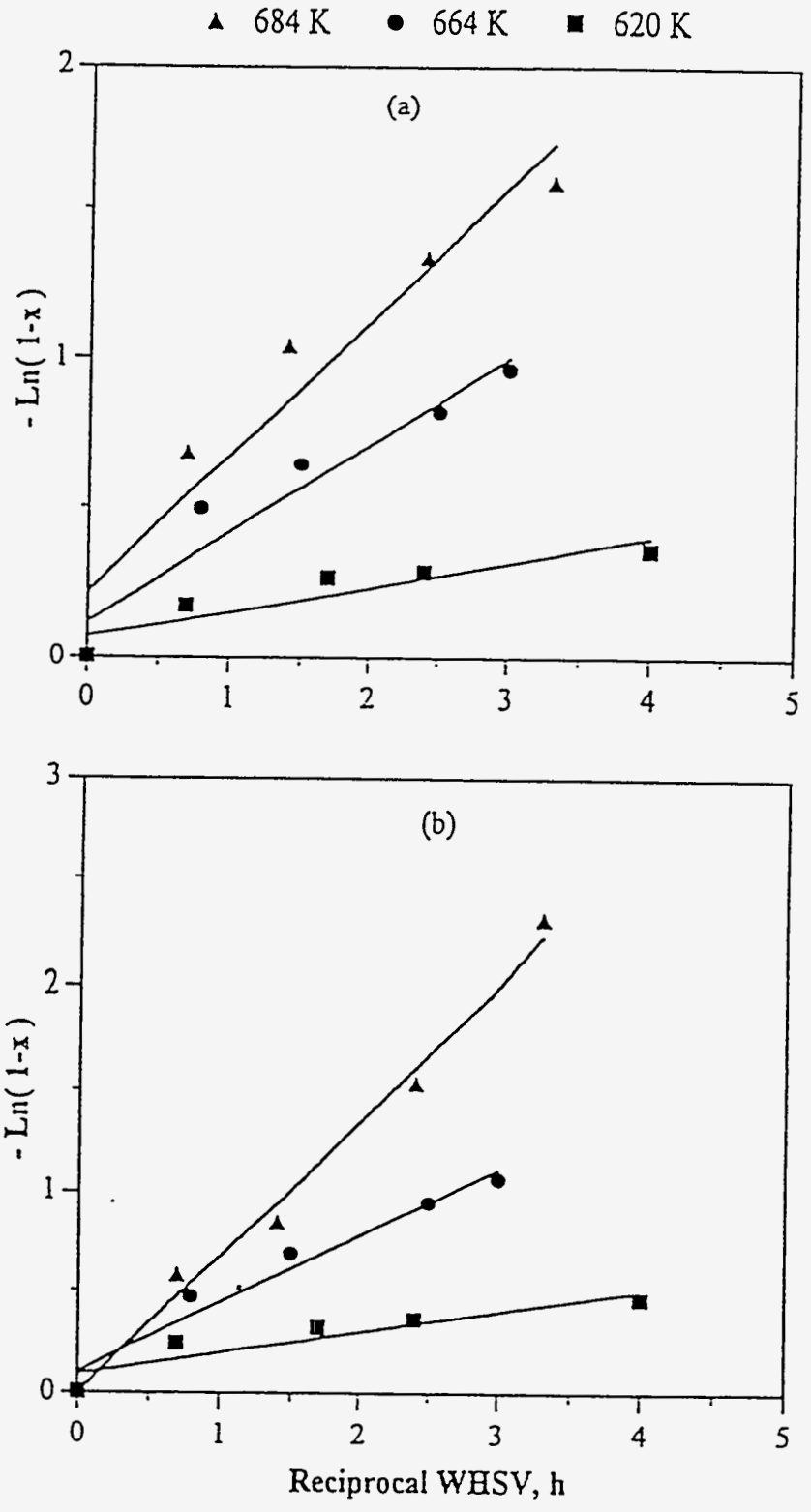
684 K
664 K
620 K
(a)
- Ln(1-x)
(b)
- Ln(1-x)
Reciprocal WHSV, h

The initial weight fraction of the facile components and the apparent first-order rate constants of the facile and refractory fractions can be estimated using nonlinear regression methods. The initial weight fraction, γ, of the facile components can be determined from the plot of $\ln(1-x_R)$ versus reciprocal WHSV, τ, which should give a straight line with a y-axis intercept of $1-\gamma$ if the model is appropriate.

The plot of $\ln(1-x_R)$ versus τ for the lumped species, such as sulfur, nitrogen, residuum, and CCR, over the A-HDN catalyst at constant pressure are presented in Figures 271 and 272. These figures indicate that different facile fractions were obtained at different temperatures for each of the lumped species. Thus the relative facile fraction of the lumped species changed with reaction temperature. Thus, the two parallel first order reactions model suggested that the relative proportion of the facile and refractory fraction is a function of the feedstock(292). Equivalent plots are shown in Appendix C for the lumped species conversions over the B- and C-HDN catalysts at three temperatures and a constant pressure. These plots also indicated that the facile fractions for the three temperatures for each lumped species were different.

The facile fractions of sulfur over the three catalysts at different temperatures and constant pressure are presented in Figure 273. Different facile fractions for sulfur were obtained over the different catalysts at each temperature. This implies that the relative facile fraction of the sulfur changed with the catalyst. Similar results were observed for the nitrogen, residuum, and CCR .

Comparison with the experimental data in this investigation, the two parallel first-order reactions model was capable of correlating kinetic data over a single catalyst at a specific temperature and pressure; however, it was deemed unrealistic because the relative facile fractions for the sulfur, nitrogen, residuum, and carbon residue were functions of feedstock, catalyst, and temperature at constant pressure which is contrary to intuition.

nth-Order Power Rate Law

For the nth-order power rate law, the reaction of lumped species, i, is assumed to occur through a number of independent nth-order reactions in parallel. The reaction rate of the lumped species, i, is given by

Figure 271

Facile fraction of lumped (a) sulfur (b) nitrogen from two parallel first-order reactions model over the A-HDN catalyst at constant pressure (13.7 MPa)

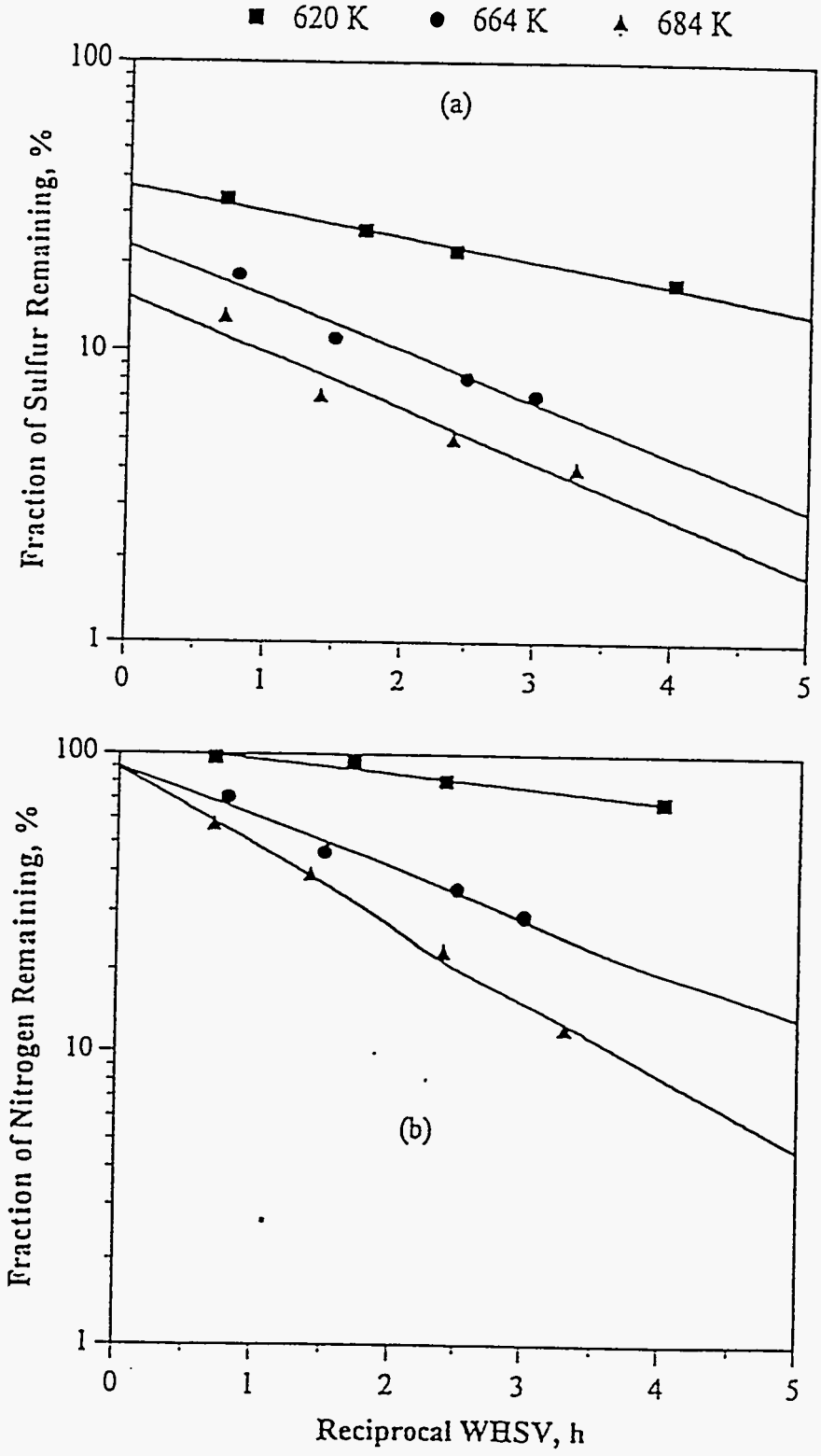
620 K
664 K
684 K
(a)
Fraction of Sulfur Remaining, %
100
10
1
0
1
2
3
4
5
(b)
Fraction of Nitrogen Remaining, %
Reciprocal WHSV, h

Figure 272

Facile fraction of lumped (a) residuum (b) CCR from two parallel first-order reactions model over the A-HDN catalyst at constant pressure (13.7 MPa)

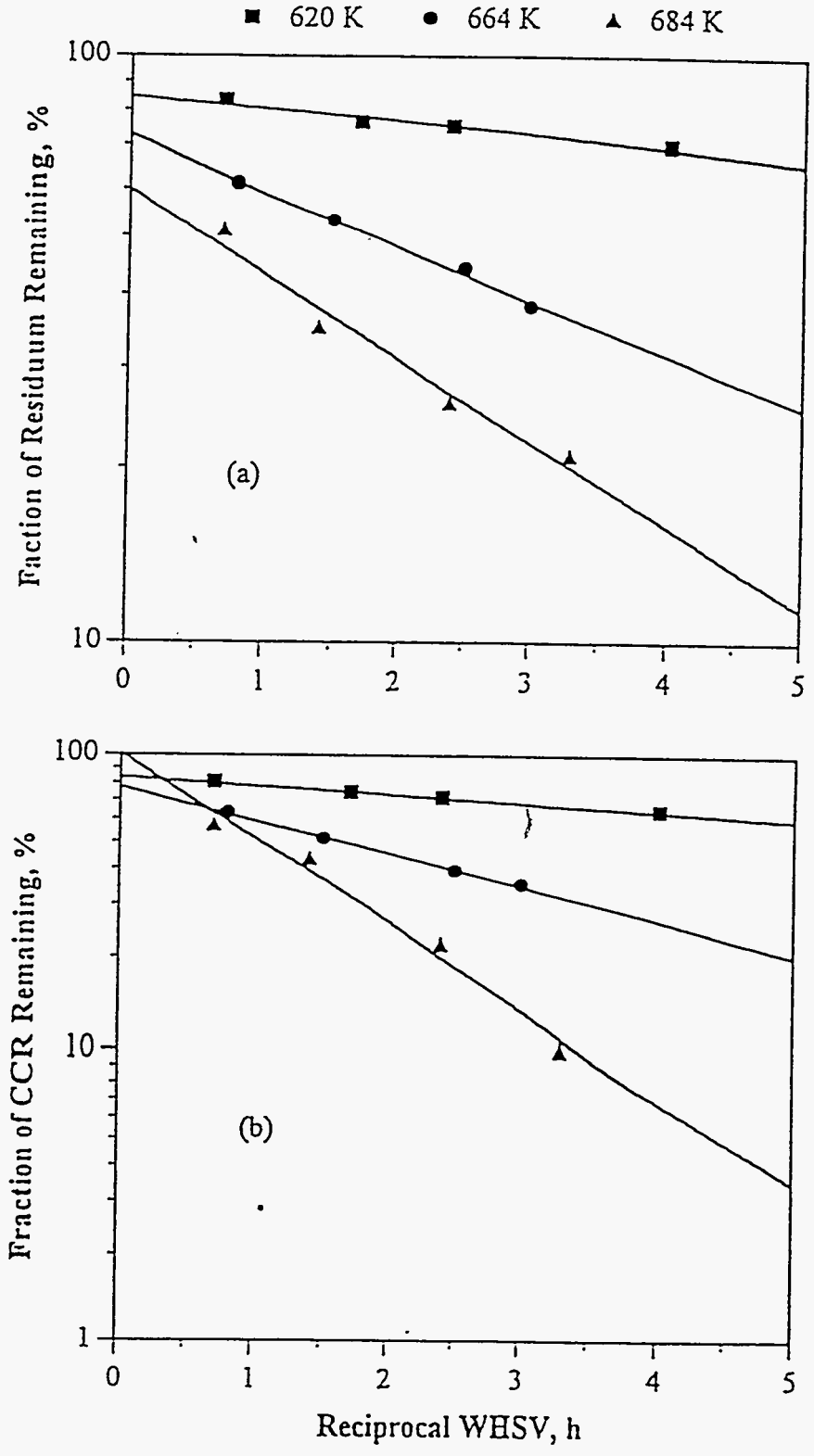
620 K
664 K
684 K
100
10
Fraction of Residuum Remaining, %
(a)
0
1
2
3
4
5
100
10
1
Fraction of CCR Remaining, %
(b)
0
1
2
3
4
5
Reciprocal WHSV, h

Figure 273

Facile fraction for sulfur for the two parallel first-order reactions model over the three HDN catalysts at constant pressure (13.7 MPa)

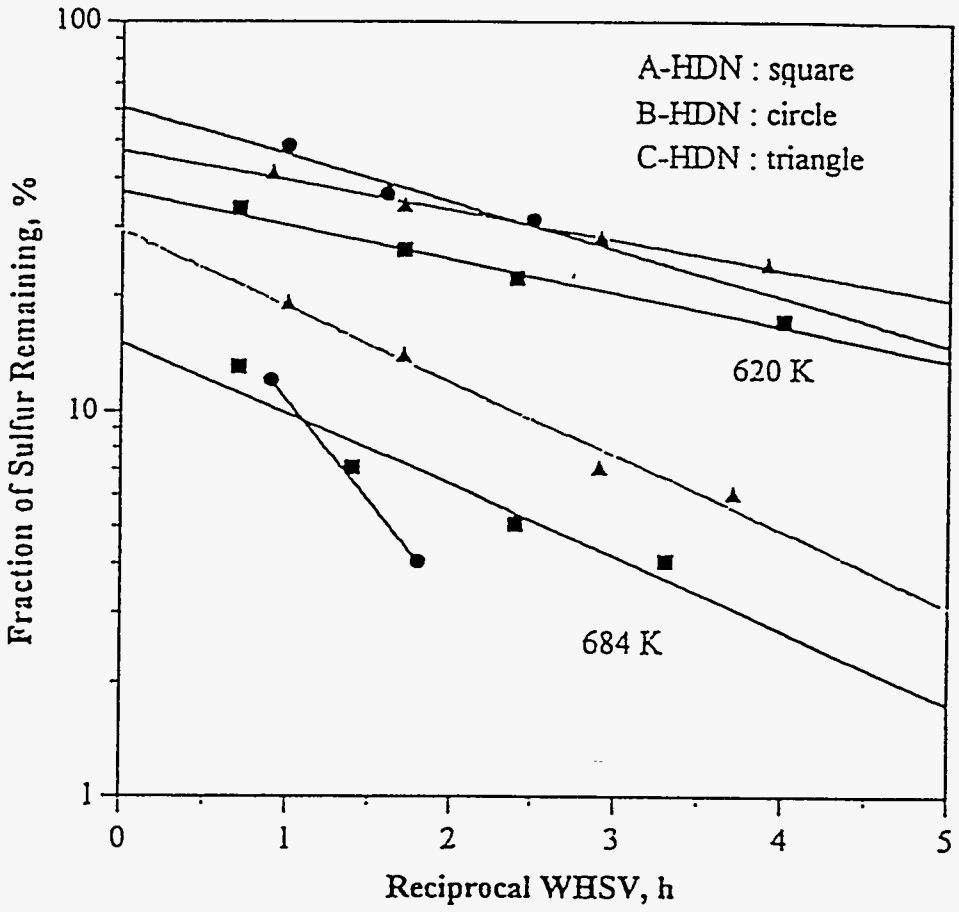
100
10
1
A-HDN : square
B-HDN : circle
C-HDN : triangle
620 K
684 K
Fraction of Sulfur Remaining, %
0
1
2
3
4
5
Reciprocal WHSV, h

$$r_i = -\frac{dC_i}{d\tau} = k' P_{H_2}^{\beta} C_i^n = kC_i^n \qquad (153)$$

where k', β, and k are constants; n is the reaction order; and $n \geq 0$ and $n \neq 1$. If the hydrogen partial pressure and apparent rate constant, k, are constants, the Equation (153) can be integrated and rearranged as follows:

$$C_i = (C_{io}^{(1-n)} + (n-1)k\tau)^{\frac{1}{1-n}} \qquad (154)$$

where C_i is the concentration of the lumped species i in the products, C_{io} is the initial concentration of lumped species in the feed.

The reaction order (n) and apparent rate constant (k) can be estimated from the subroutine AMOEBA derived from the downhill simplex method in multidimensions(315).

nth Reaction Order for Each Temperature

The simulated effective kinetic parameters for the three HDN catalysts runs under constant pressure and different temperatures are presented in Table 103. The comparisons between calculated data from the nth-order power rate law with each temperature-reaction order pair and experimental data are plotted in Figures 274 and 275 for the A-HDN catalyst run. Similar plots are presented in Appendix E for the B- and C-HDN catalyst runs. These figures indicate that the power rate law with reaction order, n, at each temperature gave the best fit to the experimental data except for nitrogen removal at 620 K.

Table 103 presents evidence that the reaction orders (n) for the HDS and HDN reactions and the residuum and CCR conversions change with reaction temperature. However, it was observed that the reaction orders for nitrogen removal were negative at the lowest temperature (620 K) for the three HDN catalysts. These are not reasonable because the reaction order should always be ≥ 0. At the

Table 103

Apparent Kinetic Parameters from nth Power Rate Law
at Constant Pressure (13.7 MPa)

	620 K		664 K		684 K	
	n	k /h	n	k /h	n	k /h
A-HDN						
Sulfur	3.6	78.5	2.4	33.6	2.2	33.8
Nitrogen	-2.3	0.494E-1	1.5	0.573	1.3	0.815
Residuum	9.6	0.769E-15	3.5	0.499E-4	2.3	0.998E-2
CCR	7.7	0.749E-7	2.5	0.219E-1	1.1	0.557
B-HDN						
Sulfur	2.8	7.93	1.6	4.47	1.8	12.7
Nitrogen	-3.4	0.430E-1	1.6	0.462	1.4	0.901
Residuum	23.0	0.657E-38	3.5	0.160E-4	9.9	0.167E-13
CCR	7.6	0.424E-7	2.7	0.995E-2	1.1	0.489
C-HDN						
Sulfur	3.7	38.6	2.9	43.6	2.1	12.1
Nitrogen	-1.5	0.464E-1	1.8	0.425	2.1	0.715
Residuum	2.0	0.149E-2	3.4	0.245E-4	2.2	0.308E-2
CCR	4.0	0.132E-3	3.0	0.439E-2	2.0	0.560E-1

n : Reaction Order
k : Apparent Rate Constant

Figure 274

Comparison with nth power rate law (three reaction orders)

and experimental data for (a) sulfur (b) nitrogen over the A-HDN catalyst

at constant pressure (13.7 MPa)

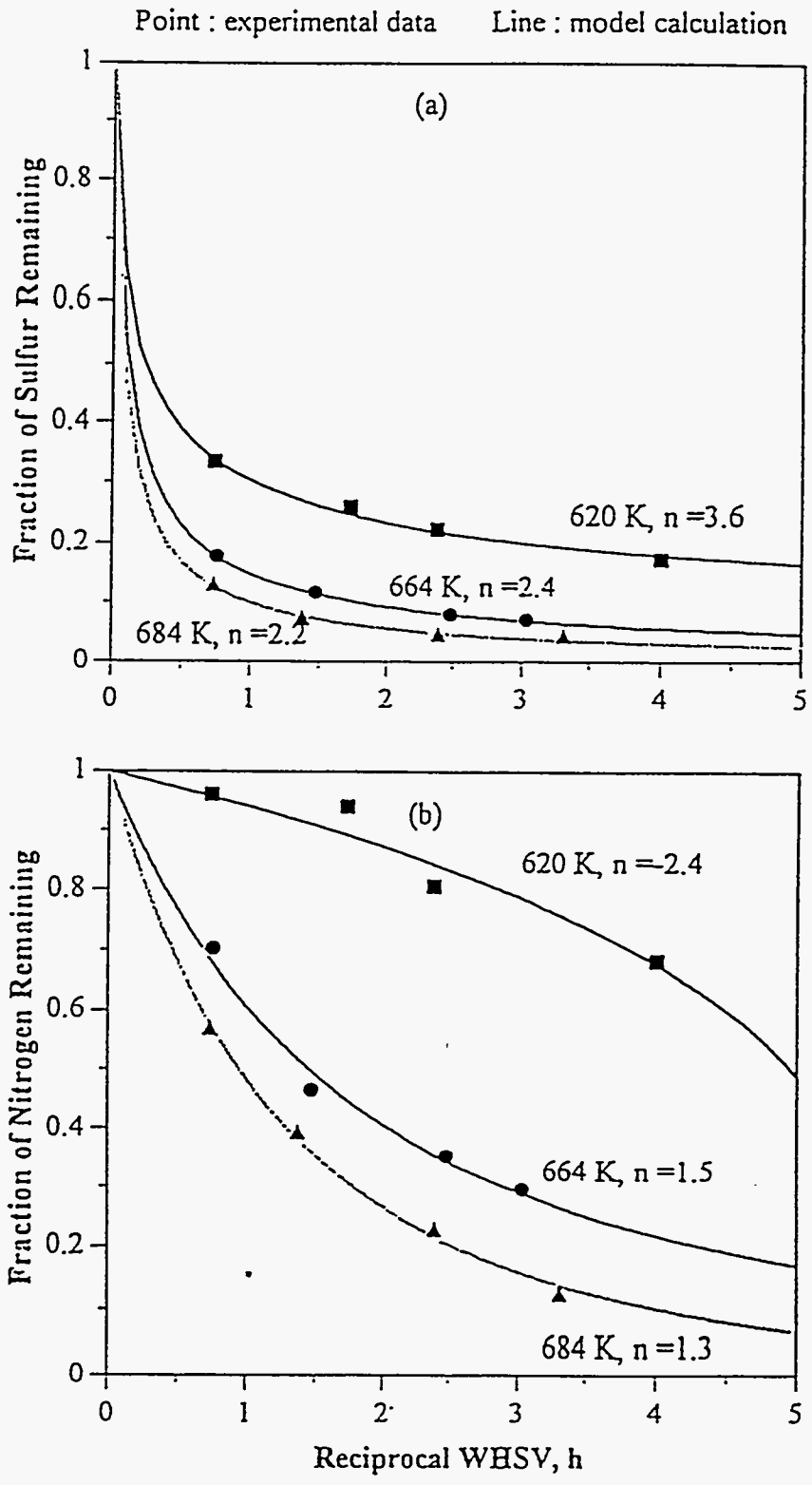
Point : experimental data
Line : model calculation
(a)
Fraction of Sulfur Remaining
620 K, n =3.6
664 K, n =2.4
684 K, n =2.2
(b)
Fraction of Nitrogen Remaining
620 K, n =2.4
664 K, n =1.5
684 K, n =1.3
Reciprocal WHSV, h

Figure 275

Comparison with nth power rate law (three reaction orders)

and experimental data for (a) residuum (b) CCR over the A-HDN catalyst

at constant pressure (13.7 MPa)

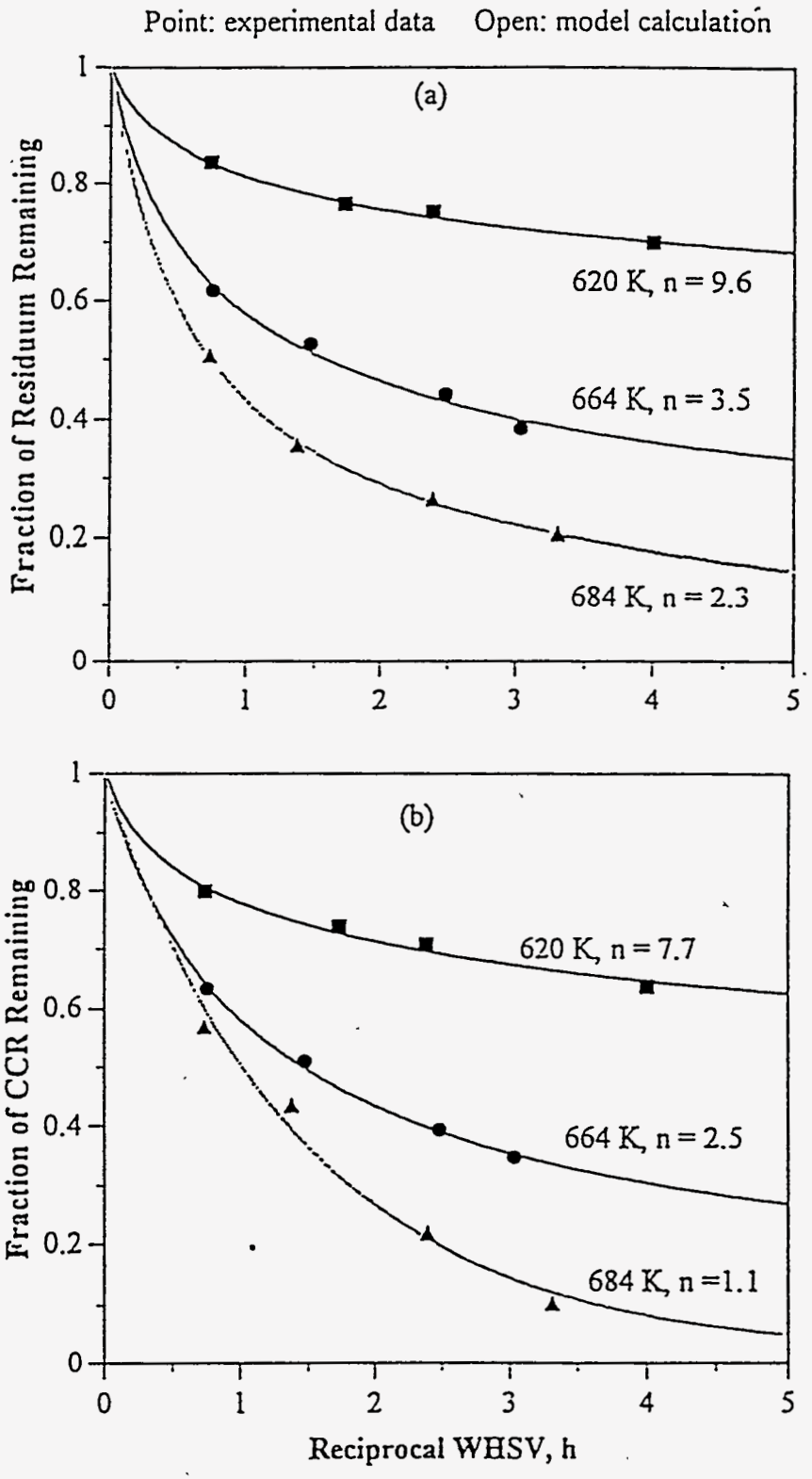
Point: experimental data Open: model calculation
(a)
Fraction of Residuum Remaining
620 K, n = 9.6
664 K, n = 3.5
684 K, n = 2.3
(b)
Fraction of CCR Remaining
620 K, n = 7.7
664 K, n = 2.5
684 K, n =1.1
Reciprocal WHSV, h

lower temperature (620 K), the nitrogen removal is small at lower residence time (less than 2 h) and then increases steeply for residence times greater than 2 h, as shown in Figures 276. Thus, in this case, the simulation produced unreasonable results. The same figures also indicate that the trend for the fraction of nitrogen remaining at 620 K is not correct compared with the trends at 664 K and 684 K reaching an apparent equilibrium level when the residence time increases to infinity.

Different reaction orders were obtained for each lumped species, such as nitrogen, over different catalysts for the same reaction conditions. These results (Table 103) indicate that the reaction order was also function of the catalyst. The reaction orders for the lumped species over the three HDN catalysts and at three different temperature are in the range of 1.6 to 3.7 for sulfur, 1.3 to 2.1 for nitrogen except at 620 K, 2.0 to 23 for residuum, and 1.1 to 7.7 for CCR. The reaction orders greater than unity indicates that lumped sulfur, nitrogen, residuum, and CCR exhibit a wide range of reactivities(256).

Yui(312) found that n = 1.5 for HDS, and n = 1.0 for HDN for hydrotreating an Athabasca bitumen-derived coker gas oil. Longstaff(292) reported that n = 1.5 for HDS and HDN for hydrotreating of Whiterocks bitumen-derived liquid, and n = 0.5 for HDN when hydrotreating the Whiterocks bitumen. Kim(243) reported n = 1.5 for HDN when hydrotreating the PR Spring bitumen.

Similar reaction orders, n = 1.5 and n = 1.6, for HDN were obtained when hydrotreating of the PR Spring and Asphalt Ridge bitumens, respectively, employing the same catalyst (B-HDN) and the same temperature (664 K) and pressure(13.7 MPa), but different LHSV (0.41 and 0.48 h^{-1}, respectively). This would appear to indicate that these two bitumens have similar distributions of nitrogen compounds.

Although Ho and Aris(291) showed that the reaction order up to second-order kinetics would arise if a fraction of the feed was essentially unreactive or if the reaction rate-concentration distribution followed a gamma distribution, they selected the gamma distribution based on its common occurrence and not from experimental data. Many authors have shown that an overall reaction order higher than two is plausible using the continuum theory of lumping(326-334).

Ozaki et al.(335) have reported reaction orders ranging from 1.4 to 5.4 for hydrodesulfurization of residual oils under certain conditions. Ho and White(336) have

also reported a reaction order of 2.5 for HDS of light catalytic cycle oil at 603 K and 2.31 MPa calculated from their asymptotic lumped kinetic model. Reaction orders, between 1.6 and 3.7, for sulfur were obtained in this study.

Asymptotic Lumped Kinetic Model

This model proposes that the kinetics of a continuum of reactions, regardless of their kinetics, are of the power rate law form at long contact times or at low space velocities(336). Assuming plug flow, one can show for a Langmuir-Hinshelwood reaction mixture that as t become sufficiently large, the fractional lumped species remaining (1-x) is given by a very simple equation(336), that is,

$$(1-x) \approx \frac{h}{t^z}$$
$$\ln(1-x) \approx \ln(h) - z\ln(t) \qquad (155)$$

where h and z are determined by the reactivity-concentration spectrum of the feed near reactivity k=0. Equation 155 implies the following lumped rate expression:

$$\frac{d(1-x)}{dt} \approx -zh^{\frac{-1}{z}}(1-x)^{1-1/z} \qquad (156)$$

where 1+1/z is the reaction order. According to Equation 155, the plot of ln(1-x) versus ln(t) should be a straight line with a slope equal to -z. The reaction order n = 1+1/z is then calculated.

The logarithmic plots of lumped species remaining versus reciprocal LHSV for sulfur, nitrogen, residuum, and CCR over the A-HDN catalyst under constant hydrogen pressure are presented in Figures 276 and 277. The corresponding slopes are also shown in the same figures. The equivalent plots are presented in Appendix F for the B- and C-HDN catalyst runs.

The reaction orders calculated from the asymptotic lumped kinetic model are compared to the reaction orders obtained from the nth power rate law in Table 104. The reaction orders obtained from the two models are almost the same for sulfur conversion. However, the reaction orders do not appear to correlate for the two models for nitrogen,

Figure 276

Logarithmic plot of fraction remaining versus reciprocal LHSV for (a) sulfur (b) nitrogen over the A-HDN catalyst at constant pressure (13.7 MPa)

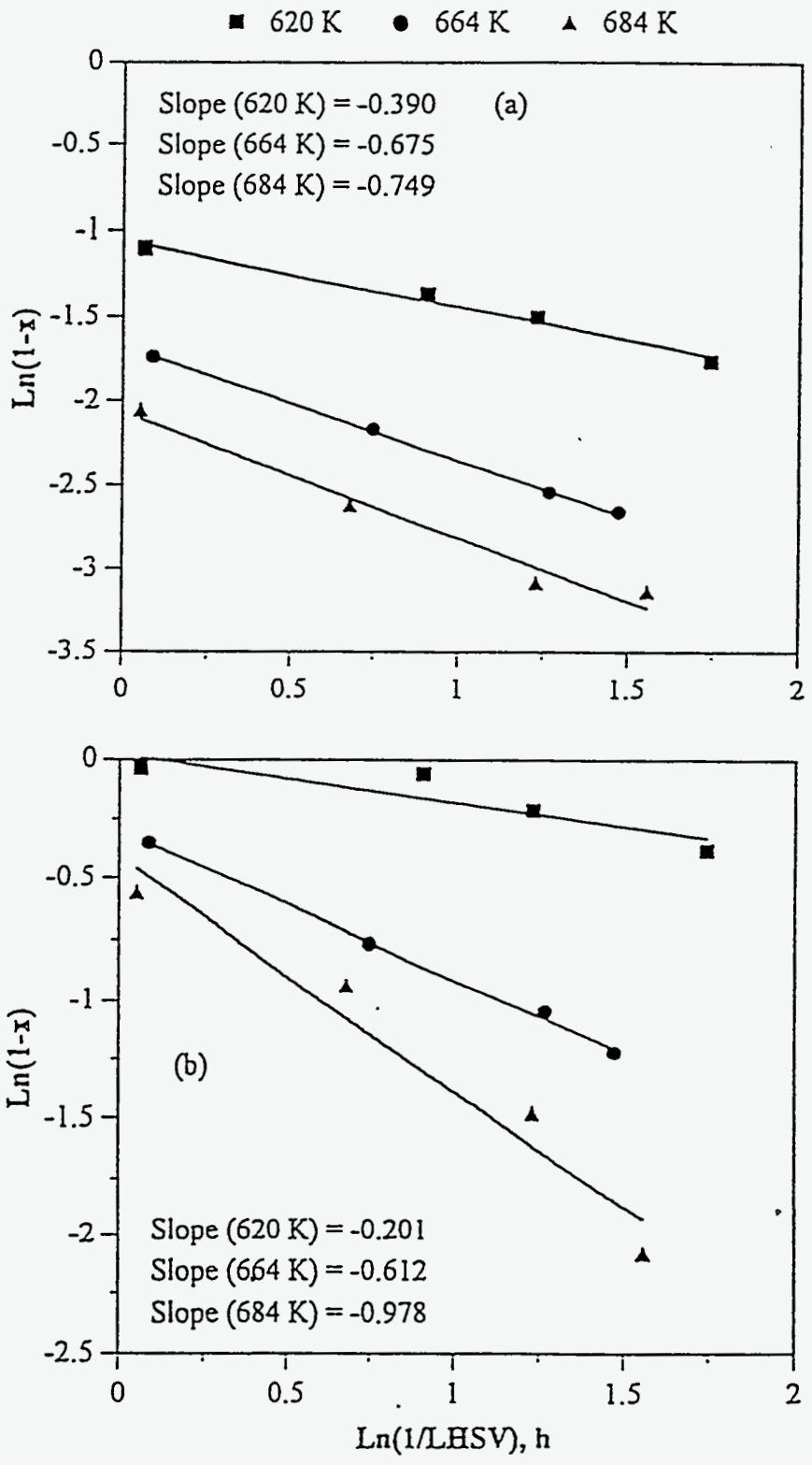
620 K
664 K
684 K
Slope (620 K) = -0.390
Slope (664 K) = -0.675
Slope (684 K) = -0.749
(a)
Ln(1-x)
0
-0.5
-1
-1.5
-2
-2.5
-3
-3.5
0
0.5
1
1.5
2
(b)
Slope (620 K) = -0.201
Slope (664 K) = -0.612
Slope (684 K) = -0.978
Ln(1/LHSV), h

Figure 277

Logarithmic plot of fraction remaining versus reciprocal LHSV for (a) residuum (b) CCR over the A-HDN catalyst at constant pressure (13.7 MPa)

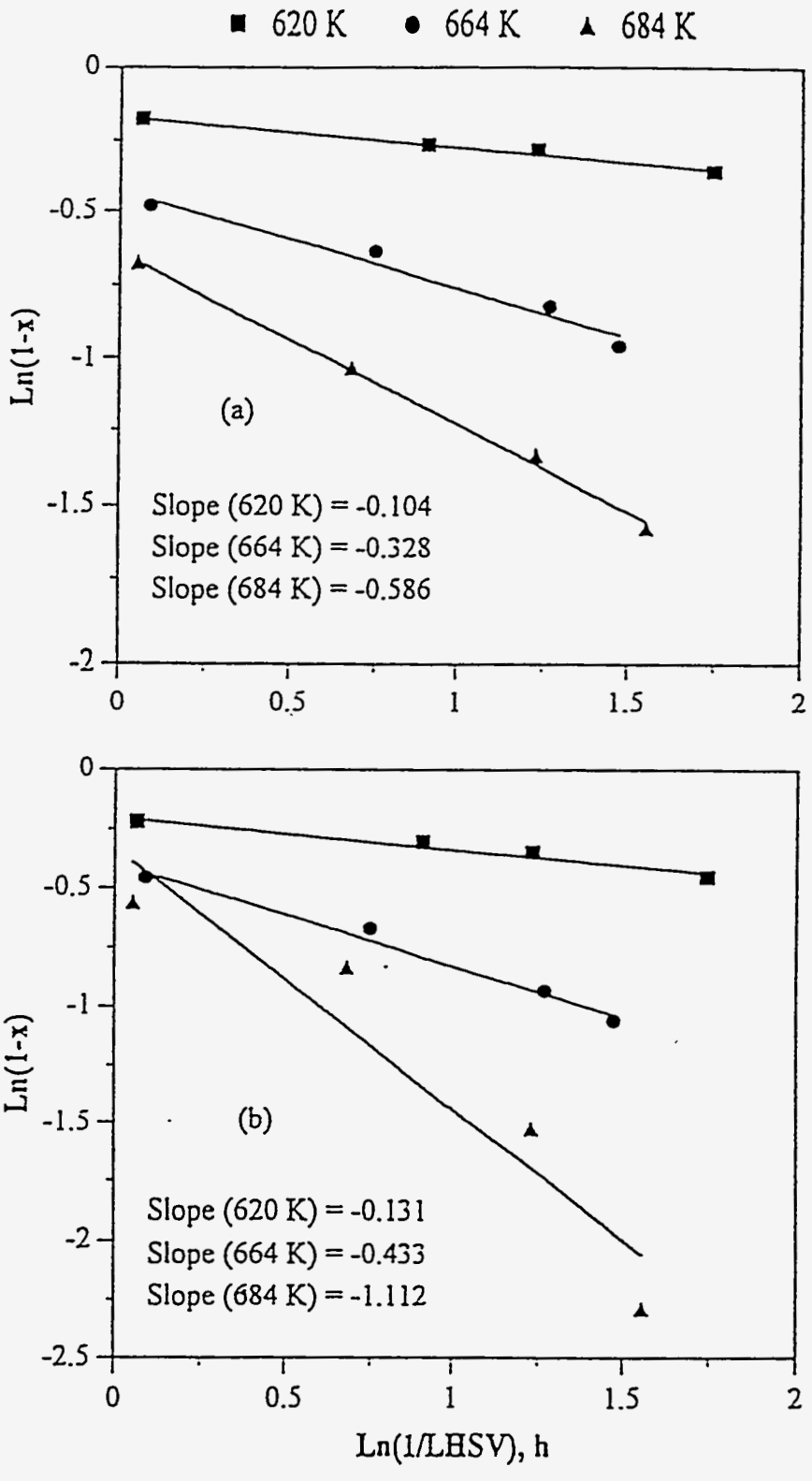
620 K
664 K
684 K
Ln(1-x)
(a)
Slope (620 K) = -0.104
Slope (664 K) = -0.328
Slope (684 K) = -0.586
(b)
Slope (620 K) = -0.131
Slope (664 K) = -0.433
Slope (684 K) = -1.112
Ln(1/LHSV), h

Table 104

Comparison with nth Power Rate Law (NPRL) and Asymptotic Lumped Kinetic Model (ALKM) for Reaction Orders

	620 K			664 K			684 K		
	NPRL	ALKM		NPRL	ALKM		NPRL	ALKM	
	n	n	R^2	n	n	R^2	n	n	R^2
A-HDN									
Sulfur	3.6	3.6	0.982	2.4	2.5	0.999	2.2	2.3	0.970
Nitrogen	-2.3	6.0	0.800	1.5	2.6	0.996	1.3	2.0	0.946
Residuum	9.6	10.7	0.986	3.5	4.0	0.964	2.3	2.7	0.997
CCR	7.7	8.6	0.956	2.5	3.3	0.984	1.1	1.9	0.902
B-HDN									
Sulfur	2.8	3.2	0.981	1.6	1.9	0.923	1.8	2.1	0.831
Nitrogen	-3.4	8.1	0.994	1.6	2.7	0.969	1.4	2.0	0.901
Residuum	23.0	23.6	1.000	3.5	4.9	0.994	9.9	10.0	0.988
CCR	7.6	9.7	0.967	2.7	3.6	0.996	1.1	1.9	0.948
C-HDN									
Sulfur	3.7	3.7	0.983	2.9	2.8	0.941	2.1	2.1	0.965
Nitrogen	-1.5	6.9	0.898	1.8	3.0	0.905	2.1	2.9	0.905
Residuum	2.0	9.1	0.899	3.4	4.8	0.758	2.2	3.4	0.827
CCR	4.0	6.8	0.981	3.0	4.0	0.875	2.0	2.9	0.931

n : Reaction Order

residuum, and CCR conversion in higher temperature. However, the agreement is much better at the higher temperature whereas at low temperature, 620 K, the nitrogen order was negative for the nth power rate law and positive for the symptotic lumped kinetic model. Furthermore, the reaction orders for residuum and CCR conversions are unrealistic for both models in the sense of interpreting the overall kinetics of the reactions.

An Overall nth Reaction Order

An overall nth reaction order was assumed for each lumped species during hydrotreating of bitumen over the HDN catalysts to compare the effect of process variables, such as catalysts and reaction conditions. The reaction rates of lumped species are described by Equation 153.

The FORTRAN programs were used to estimate the overall reaction order and apparent rate constant for each temperature over the three HDN catalysts at constant pressure. The results are listed in Table 105. The overall reaction orders over the A-, B-, and C-HDN catalysts are 3.1, 2.0, and 3.1 for HDS, 1.3, 1.5, and 1.9 for HDN, 2.9, 5.7, and 2.6 for residuum conversion, 1.6, 1.6, and 2.4 for CCR conversion, respectively. The overall activation energies (E) and pre-exponential factors (k_o), also presented in Table 105, were calculated from the slopes and y-axis intercepts of plots of ln(k) versus 1/T. The apparent rate constants k (and k_o) include the hydrogen pressure (MPa) terms from the rate expression since P^{β} was assumed to be constant. Direct comparison is not possible because the units of k are different for HDS, HDN, residuum, and CCR conversions. The overall activation energies of the lumped species are in the range of 27-34 kcal/mol for sulfur, 30-34 kcal/mol for nitrogen, 25-40 kcal/mol for residuum, and 20-24 kcal/mol for CCR. For hydrotreating of Athabasca bitumen-derived coker gas oil, the overall activation energy was 33 kcal/mol for HDS and 22 kcal/mol for HDN(312).

With the overall reaction orders and their apparent rate constants in Table 105, the plots of fraction of lumped species remaining versus reciprocal WHSV over the three HDN catalysts are presented in Figures 278-283. Compared to the experimental data, overall nth power rate law fits were satisfactory.

Table 105

Apparent Kinetic Parameters from Overall nth Power Rate Law
at Constant Pressure (13.7 MPa)

Catalyst	n	k, 620 K /h	k, 664 K /h	k, 684 K /h	E kcal/mol	k_o /h
A-HDN						
Sulfur	3.1	32.416	189.02	450.44	34.3	3.9E13
Nitrogen	1.3	0.0883	0.5291	0.8357	30.3	4.3E9
Residuum	2.9	8.652E-5	4.642E-4	1.179E-3	33.8	6.9E7
CCR	1.6	0.0370	0.1258	0.2185	23.3	5.9E7
B-HDN						
Sulfur	2.0	2.4233	8.7412	19.975	27.0	8.0E9
Nitrogen	1.5	0.0700	0.4292	0.9525	34.3	8.3E10
Residuum	5.7	1.219E-9	5.795E-9	3.072E-8	40.0	1.3E5
CCR	1.6	0.0333	0.0942	0.2216	23.9	8.5E6
C-HDN						
Sulfur	3.1	14.670	63.382	120.33	27.6	7.9E10
Nitrogen	1.9	0.0718	0.4520	0.6603	30.2	3.2E9
Residuum	2.6	1.456E-4	5.491R-4	9.305E-4	24.5	6.2E4
CCR	2.4	5.081E-3	1.471E-2	2.437E-2	20.5	8.3E4

n : Overall Reaction Order
k : Apparent Rate Constant
E : Overall Activation Energy

Figure 278

Comparison with nth power rate law and experimental data for

(a) sulfur (b) nitrogen conversion over the A-HDN catalyst

at constant pressure

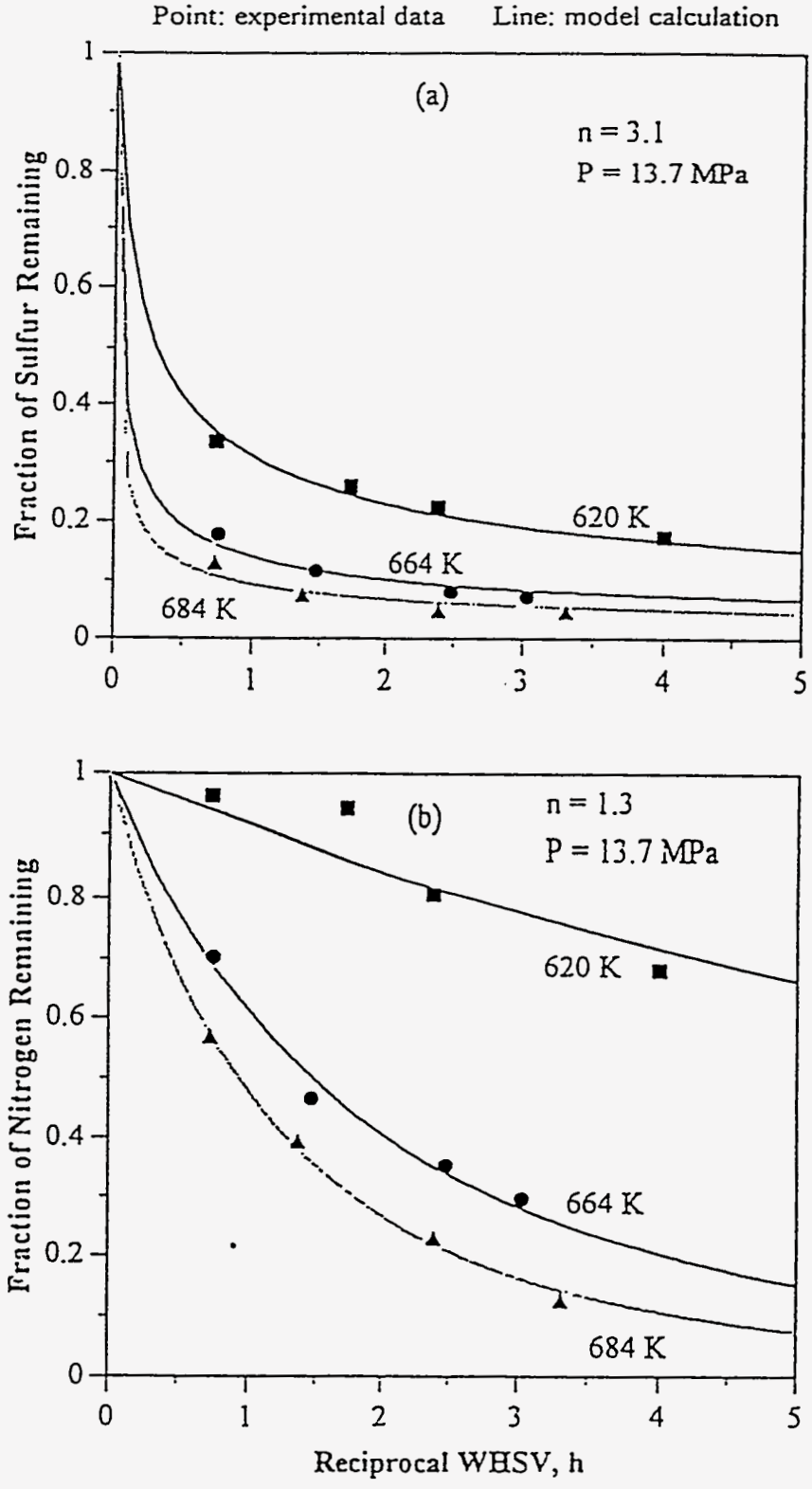
Point: experimental data
Line: model calculation
(a)
n = 3.1
P = 13.7 MPa
620 K
664 K
684 K
Fraction of Sulfur Remaining
(b)
n = 1.3
P = 13.7 MPa
620 K
664 K
684 K
Fraction of Nitrogen Remaining
Reciprocal WHSV, h

Figure 279

Comparison with nth power rate law and experimental data for

(a) residuum (b) CCR conversion over the A-HDN catalyst

at constant pressure

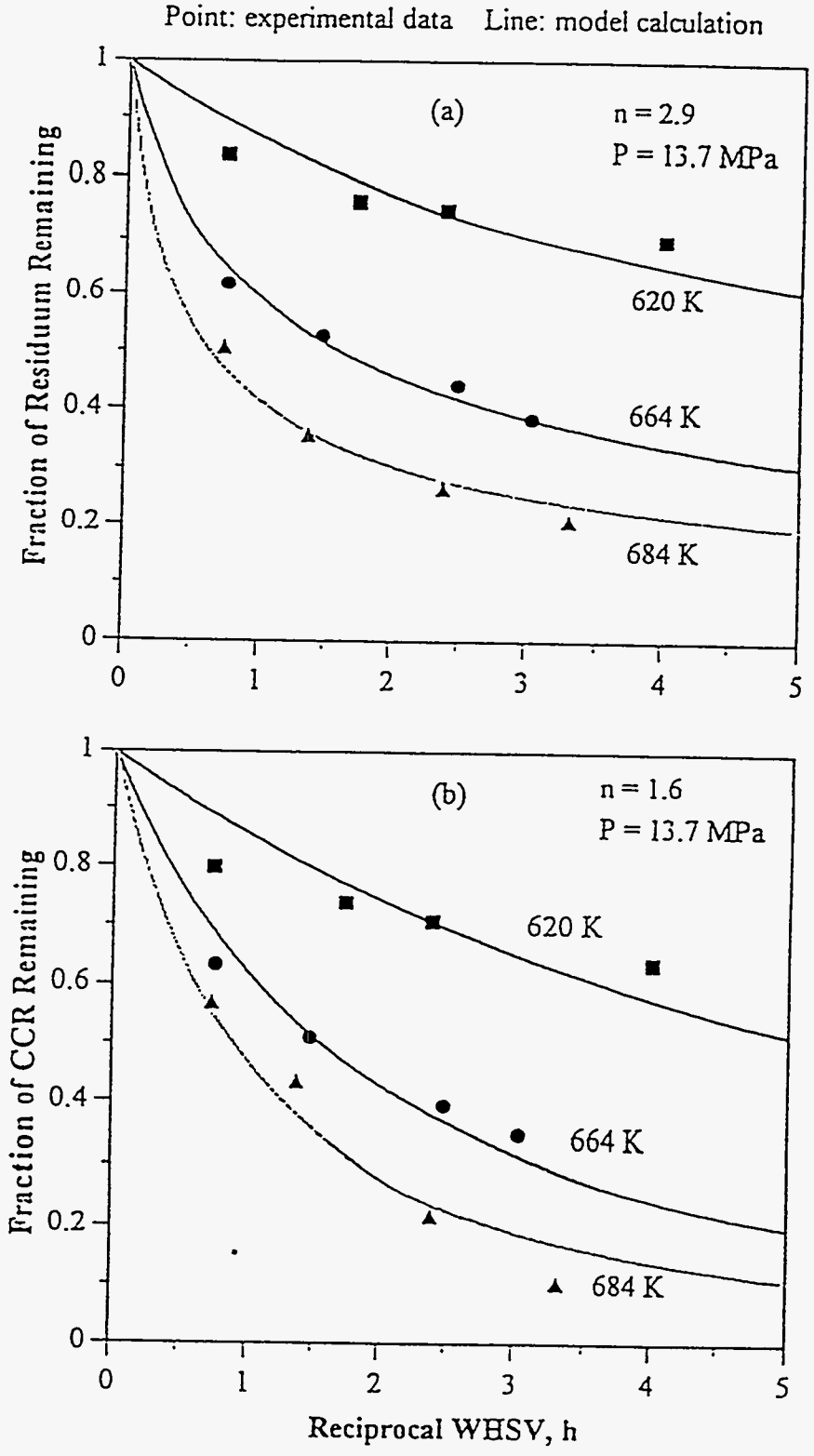
Point: experimental data Line: model calculation
(a)
n = 2.9
P = 13.7 MPa
620 K
664 K
684 K
Fraction of Residuum Remaining
(b)
n = 1.6
P = 13.7 MPa
620 K
664 K
684 K
Fraction of CCR Remaining
Reciprocal WHSV, h

Figure 280

Comparison with nth power rate law and experimental data for

(a) sulfur (b) nitrogen conversion over the B-HDN catalyst

at constant pressure

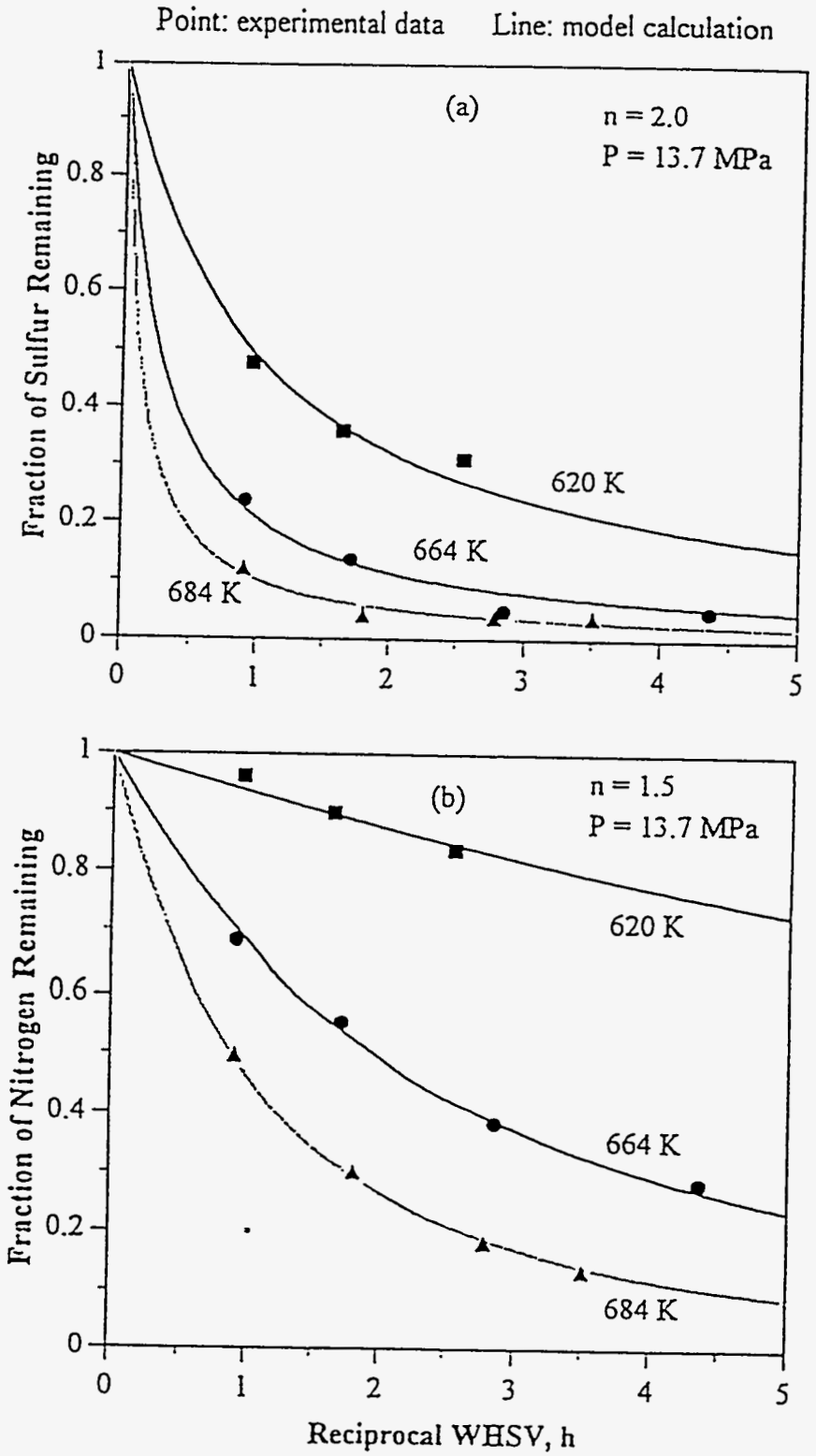
Point: experimental data
Line: model calculation
(a)
n = 2.0
P = 13.7 MPa
620 K
664 K
684 K
Fraction of Sulfur Remaining
(b)
n = 1.5
P = 13.7 MPa
620 K
664 K
684 K
Fraction of Nitrogen Remaining
Reciprocal WHSV, h

Figure 281

Comparison with nth power rate law and experimental data for

(a) residuum (b) CCR conversion over the B-HDN catalyst

at constant pressure

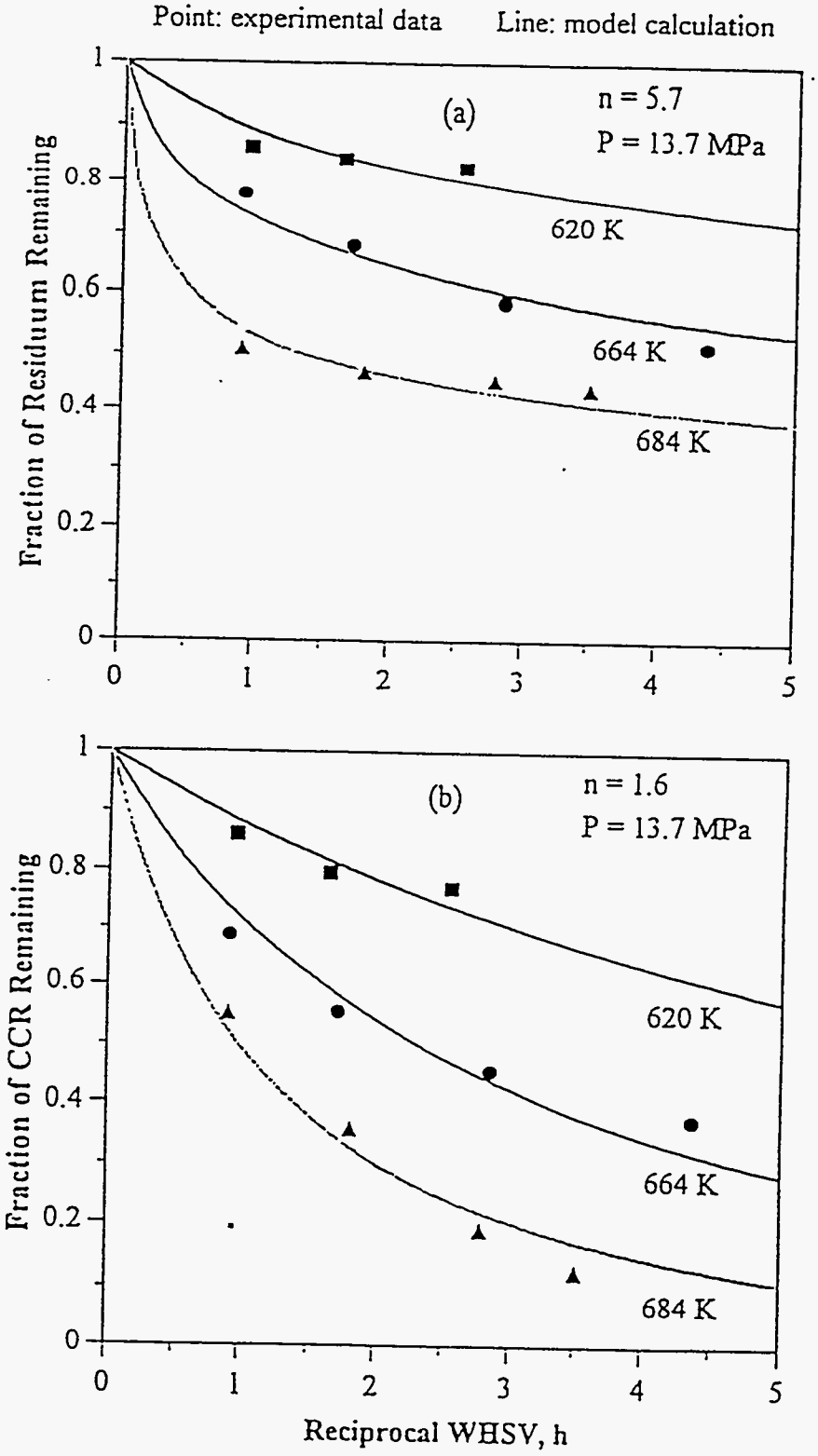
Point: experimental data
Line: model calculation
(a)
n = 5.7
P = 13.7 MPa
620 K
664 K
684 K
Fraction of Residuum Remaining
(b)
n = 1.6
P = 13.7 MPa
620 K
664 K
684 K
Fraction of CCR Remaining
Reciprocal WHSV, h

Figure 282

Comparison with nth power rate law and experimental data for

(a) sulfur (b) nitrogen conversion over the C-HDN catalyst

at constant pressure

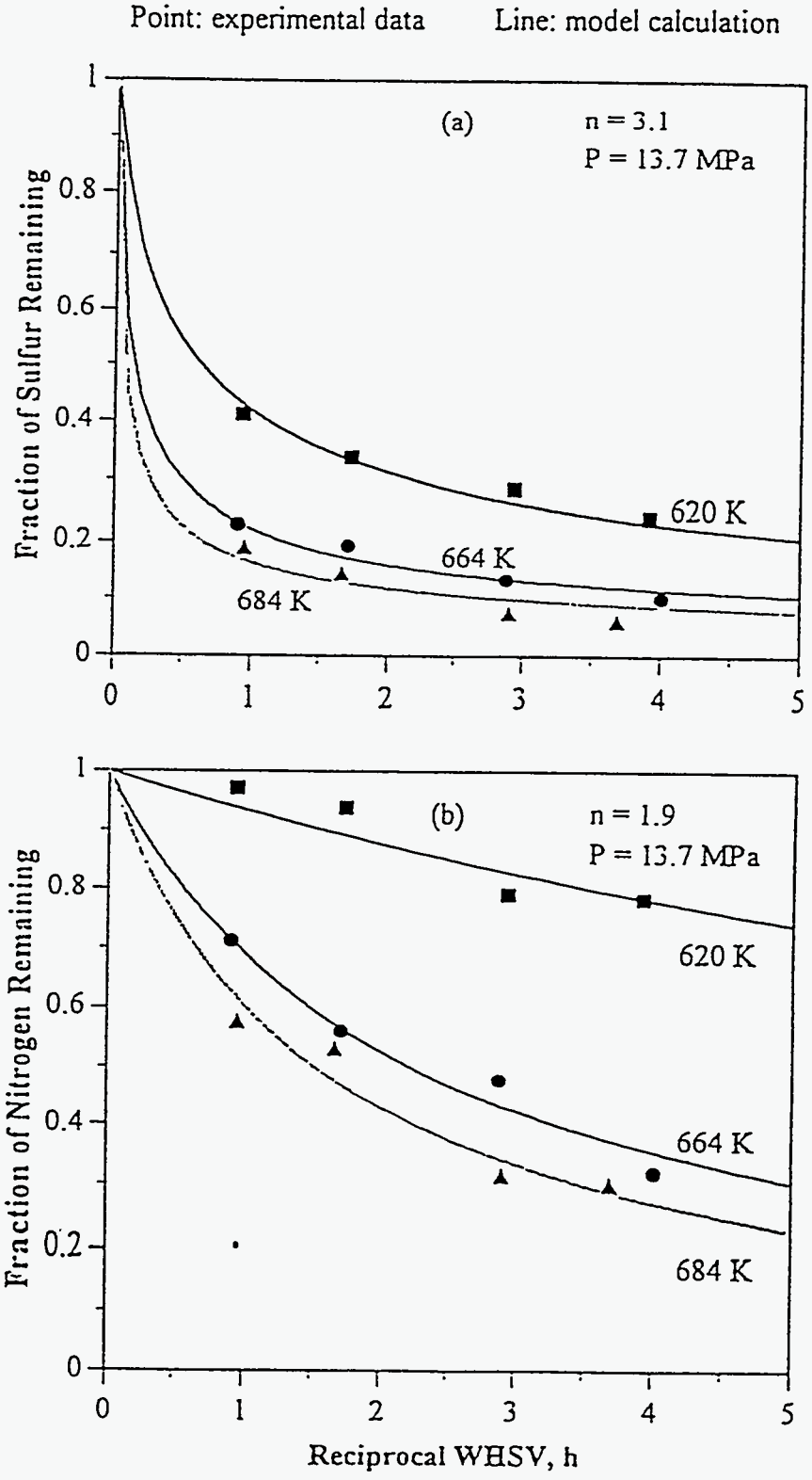
Point: experimental data
Line: model calculation
(a)
n = 3.1
P = 13.7 MPa
620 K
664 K
684 K
Fraction of Sulfur Remaining
(b)
n = 1.9
P = 13.7 MPa
620 K
664 K
684 K
Fraction of Nitrogen Remaining
Reciprocal WHSV, h

Figure 283

Comparison with nth power rate law and experimental data for

(a) residuum (b) CCR conversion over the C-HDN catalyst

at constant pressure

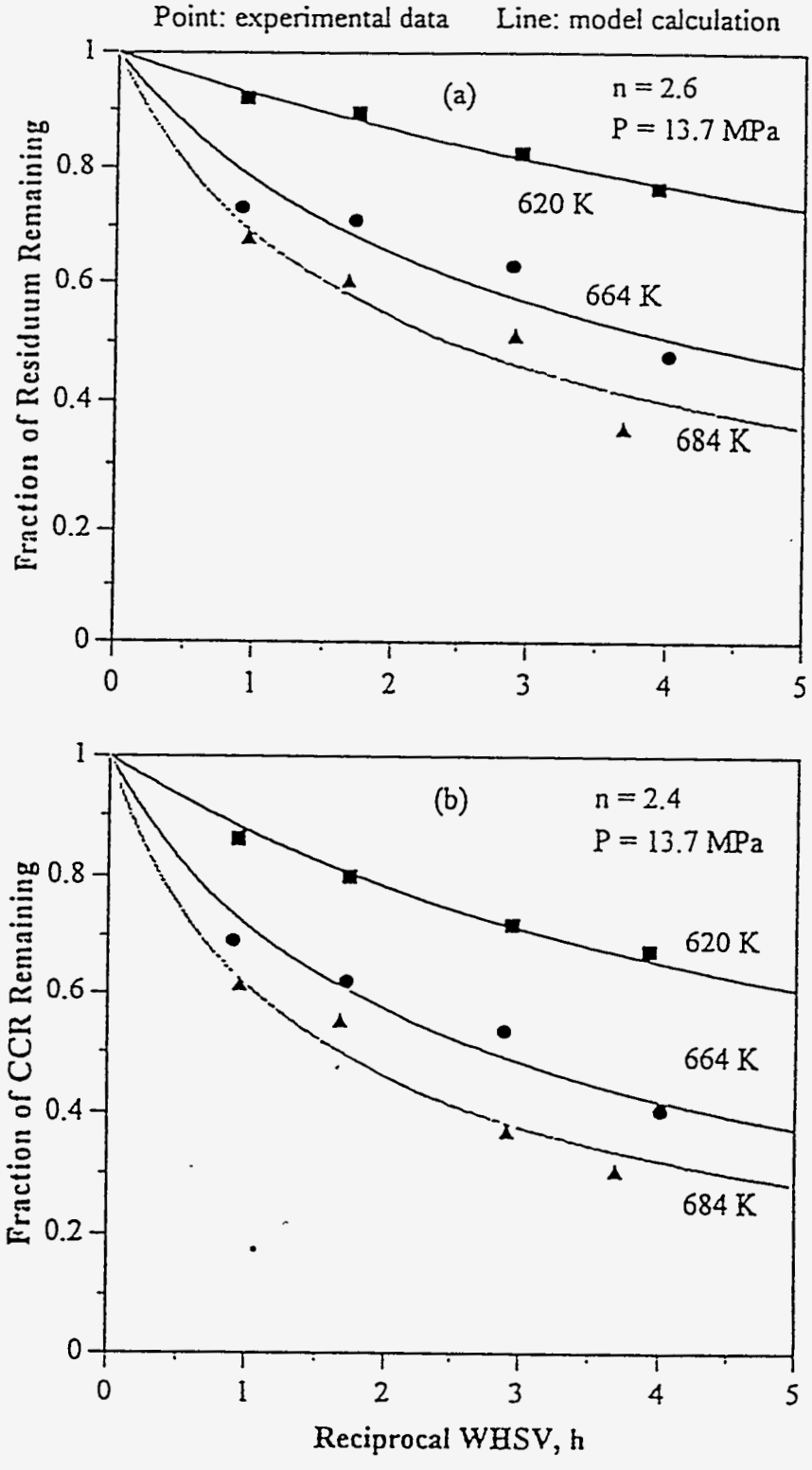
Point: experimental data
Line: model calculation
(a)
n = 2.6
P = 13.7 MPa
620 K
664 K
684 K
Fraction of Residuum Remaining
(b)
n = 2.4
P = 13.7 MPa
620 K
664 K
684 K
Fraction of CCR Remaining
Reciprocal WHSV, h

In general, the power rate law form is a convenient expression, even through the actual kinetics for mixtures might be substantially different. It is also useful for interpolation, but it cannot be employed to extrapolate reactor performance unless the overall rate equation is exactly that of a power rate law form.

Distributed Activation Energy Model

Complex reactions for coal, oil shale, and biomass pyrolysis and petroleum formation can often be accurately described by distribution activation energy model(300, 337-339). This model assumed that the complex reactions consisted of a set of irreversible, parallel first-order reactions that have different activation energies and a constant preexponential factor(338, 340). The preexponential factor is assumed to be a constant in general for all reactions to avoid the complexity of the analysis(338, 340). The reaction rate, therefore, can be expressed by Equation 147. After integrating and rearranging in terms of fractional conversion, x_i, of each lumped species, Equation 147 becomes

$$1 - x_i = \exp(-\int_0^\tau k d\tau) = \exp(-k_o \int_0^\tau \exp(\frac{-E}{RT}) d\tau) = \exp(-k_o \tau \exp(\frac{-E}{RT})) \qquad (157)$$

where k is the apparent rate constant, τ is the residence time (reciprocal WHSV), k_o is the pre-exponential factor, E is the activation energy, R is the gas constant, and T is the absolute temperature. Assuming the number of reactions is large enough to permit E to be expressed as a continuous distribution function f(E) and integrating over all energies, Equation 157 becomes

$$1 - x_i = \int_0^\infty \exp(-k_o \tau \exp(\frac{-E}{RT})) f(E) dE \qquad (158)$$

where the distribution curve f(E) is defined to satisfy

$$\int_0^\infty f(E) dE = 1 \qquad (159)$$

The focus of the analysis is the estimation of k_o and f(E). The exponential, gamma, and normal (Gaussian) distributions were used in this study to represent f(E).

Exponential Distribution

The exponential distribution f(E) is given by

$$f(E) = \frac{1}{\lambda}\exp(\frac{-(E - E_o}{\lambda}) \tag{160}$$

where λ is an empirical constant, E is the activation energy, and E_o is the mean activation energy. Substituting the Equation 160 into Equation 158, Equation 161 is obtained.

$$1 - x_i = \int_0^\infty \exp(-k_o \tau \exp(\frac{-E}{RT}))\frac{1}{\lambda}\exp(\frac{-(E - E_o)}{\lambda})dE \tag{161}$$

A new variable $y = (E - Eo)/\lambda$ is defined and substituted into Equation 161 to obtain

$$1 - x_i = \int_0^\infty \exp(-k_o \tau \exp(\frac{-(\lambda y + E_o)}{RT}))\exp(-y)dy \tag{162}$$

The first exponential term on the right side in Equation 162 is a function of the variable y which can be expressed as Equation 163:

$$f(y) = \exp(-k_o \tau \exp(\frac{-(\lambda y + E_o)}{RT})) \tag{163}$$

and then Equation 162 is rewritten as follows:

$$1 - x_i = \int_0^\infty f(y)\exp(-y)dy = \sum_{i=1}^{n} w_i f(y_i) \tag{164}$$

The integral term on the right side in Equation 164 is a Laguerre integral. The integration can be accomplished by employing the Table of zeros and weight factors for the first

fifteen Laguerre polynomials.[235] For small values of n, the value of E_o changed significantly; however, the value of E_o changed relatively little in the range from n =8 to n = 12. Thus, n=10 was selected in this study.

Apparent kinetic parameters obtained from the nonlinear regression method are presented in Table 106. Employing these parameters, the plots of the fraction of lumped species remaining versus reciprocal WHSV are presented in Figure 284. Compared with the experimental data, the exponential-DAEM is reasonable for nitrogen removal and CCR conversion; however, the curve fits for sulfur removal and residuum conversion were not particularly good.

Gamma Distribution

The gamma distribution function f(E) is given by

$$f(E) = \frac{1}{A_o}(E - E_o)^{\alpha-1} \exp(\frac{-(E - E_o)}{\beta}) \qquad (165)$$

where α, β, and A_o are empirical constants. Substituting Equation 165 into Equation 158 and then defining a variable $y = (E - E_o)/\beta$, Equation 158 is rewritten as follows:

$$1 - x_i = \frac{\beta}{A_o}\int_0^{\infty} (\beta y)^{\alpha-1} \exp(-k_o \tau \exp(\frac{-(\beta y + E_o)}{RT})) \exp(-y) dy \qquad (166)$$

The first exponential term in Equation 166 is a function of the variable y and is expressed as

$$f(y) = (\beta y)^{\alpha-1} \exp(-k_o \tau \exp(\frac{-(\beta y + E_o)}{RT})) \qquad (167)$$

Equation 167 can be rearranged as follows :

Table 106

Apparent Kinetic Parameters from Exponential-Distributed Activation Model at Constant Pressure (13.7 MPa)

Catalyst	k_o /h	E_o kcal/mol	λ
A-HDN			
Sulfur	6.0E4	13.6	3.433
Nitrogen	3.2E8	27.0	2.129
Residuum	2.1E7	23.5	26.376
CCR	2.2E6	20.4	17.994
B-HDN			
Sulfur	2.4E5	15.9	-1.968
Nitrogen	5.7E8	27.9	3.919
Residuum	4.5E5	19.2	21.943
CCR	1.1E7	22.9	13.202
C-HDN			
Sulfur	9.1E11	34.7	1.982
Nitrogen	1.2E7	23.3	-4.996
Residuum	2.4E5	18.6	2.667
CCR	3.1E4	15.5	5.325

k_o : Pre-exponential Factor
E_o : Mean Activation Energy
λ : Constant for Exponential Distribution Function

Figure 284

Comparison with exponential-DAEM and experimental data for

(a) sulfur (b) nitrogen conversion over the A-HDN catalyst

at constant pressure

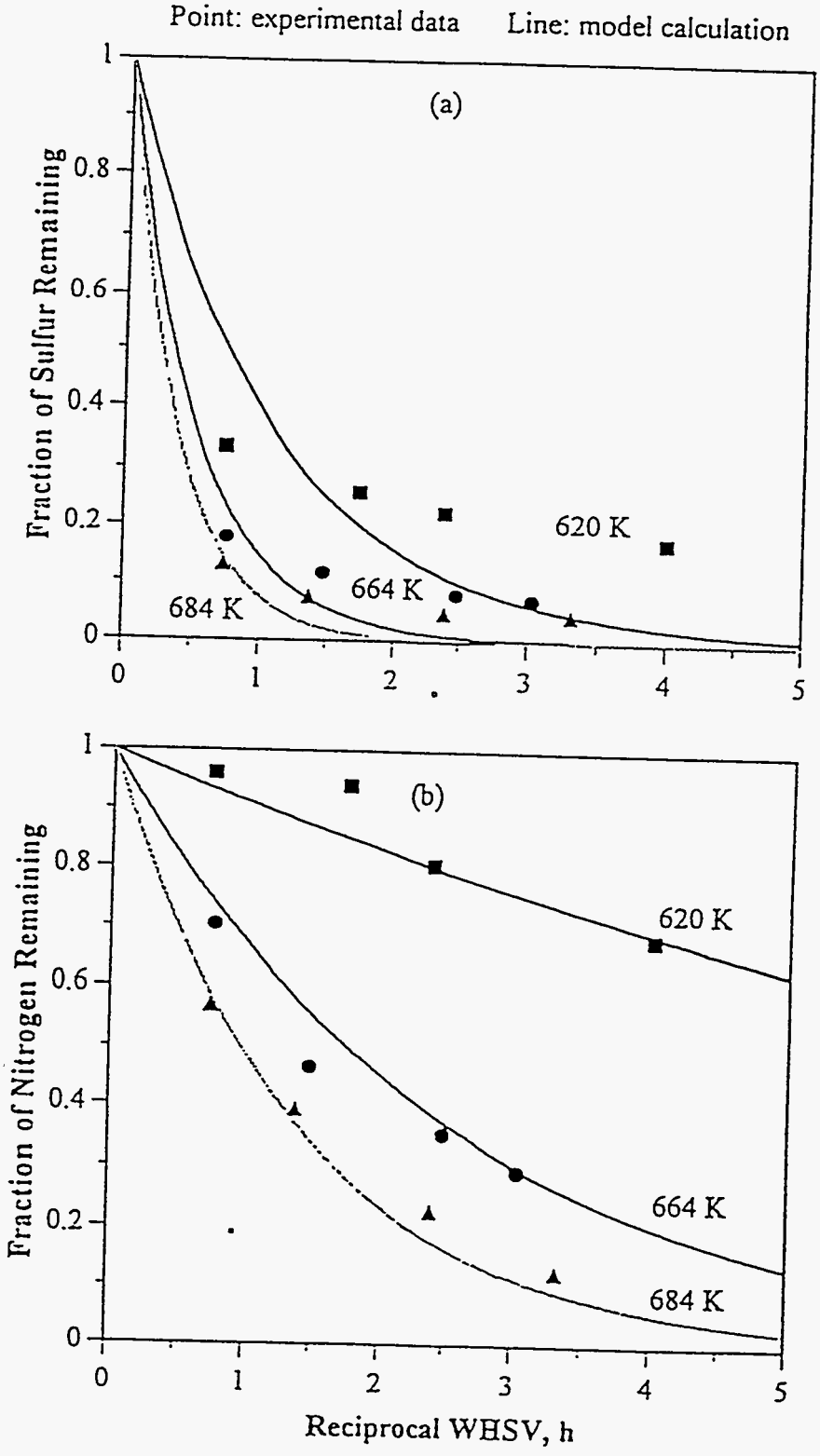
Point: experimental data
Line: model calculation
(a)
Fraction of Sulfur Remaining
620 K
664 K
684 K
(b)
Fraction of Nitrogen Remaining
620 K
664 K
684 K
Reciprocal WHSV, h

$$1 - x_i = \frac{\beta}{A_o}\int_0^\infty f(y)\exp(-y)dy = \frac{\beta}{A_o}\sum_{i=1}^{n} w_i f(y_i) \qquad (168)$$

The integral term on the right side in Equation 168 is the Laguerre integral. The calculation procedure is the same as that discussed in the previous section for the exponential distribution function.

Apparent kinetic parameters obtained using the nonlinear regression method are presented in Table 107. With these parameters, the plots of the fraction of the lumped species remaining versus reciprocal WHSV are presented in Figure 285. The fits of experimental data by the gamma distribution function-DAEM is superior for each of the lumped species to that obtained with the exponential distribution function except at lower residence times (less than 0.5 h).

Normal Distribution

The normal distribution function is given by

$$f(E) = \frac{1}{\sigma_E\sqrt{2\pi}}\exp\left(\frac{-(E-E_o)^2}{2\sigma_E}\right) \qquad (169)$$

where σ_E is the standard deviation of the activation energy distribution. Substituting Equation 169 into Equation 158 and then defining a variable y = (E-Eo)/($\sigma_E\sqrt{2}$), Equation 158 can be rewritten as follows:

$$1 - x_i = \frac{1}{\sqrt{\pi}}\int_0^\infty \exp\left(-k_o\tau\exp\left(\frac{-(E_o+\sqrt{2}\sigma_E y)}{RT}\right)\right)\exp(-y^2)dy \qquad (170)$$

The first exponential term in Equation 170 is a function of variable y and is given by

$$f(y) = \exp\left(-k_o\tau\exp\left(\frac{-(E_o+\sqrt{2}\sigma_E y)}{RT}\right)\right) \qquad (171)$$

Table 107

Apparent Kinetic Parameters from Gamma-Distributed Activation Model at Constant Pressure (13.7 MPa)

Catalyst	k_o /h	E_o kcal/mol	α	β	A_o
A-HDN					
Sulfur	6.2E5	18.0	2.650	0.686	1.404
Nitrogen	1.5E8	26.0	1.821	1.045	0.982
Residuum	5.6E10	34.5	4.754	0.563	1.354
CCR	1.7E9	26.6	5.455	0.547	2.166
B-HDN					
Sulfur	1.2E8	24.7	2.140	0.801	1.182
Nitrogen	2.9E10	30.2	1.223	1.433	1.481
Residuum	3.7E9	31.8	0.824	1.789	2.124
CCR	1.3E11	35.7	2.390	0.175	0.022
C-HDN					
Sulfur	1.2E7	22.6	0.905	0.536	1.478
Nitrogen	1.7E9	30.1	0.025	5.11E-13	1.429
Residuum	9.4E6	23.7	0.134	1.977	2.875
CCR	1.5E6	21.0	1.110	5.038	6.323

k_o : Pre-exponential Factor

E_o : Mean Activation Energy

α, β, A_o : Constants for Gamma Distribution Function

Figure 285

Comparison with gamma-DAEM and experimental data for

(a) sulfur (b) nitrogen conversion over the A-HDN catalyst

at constant pressure

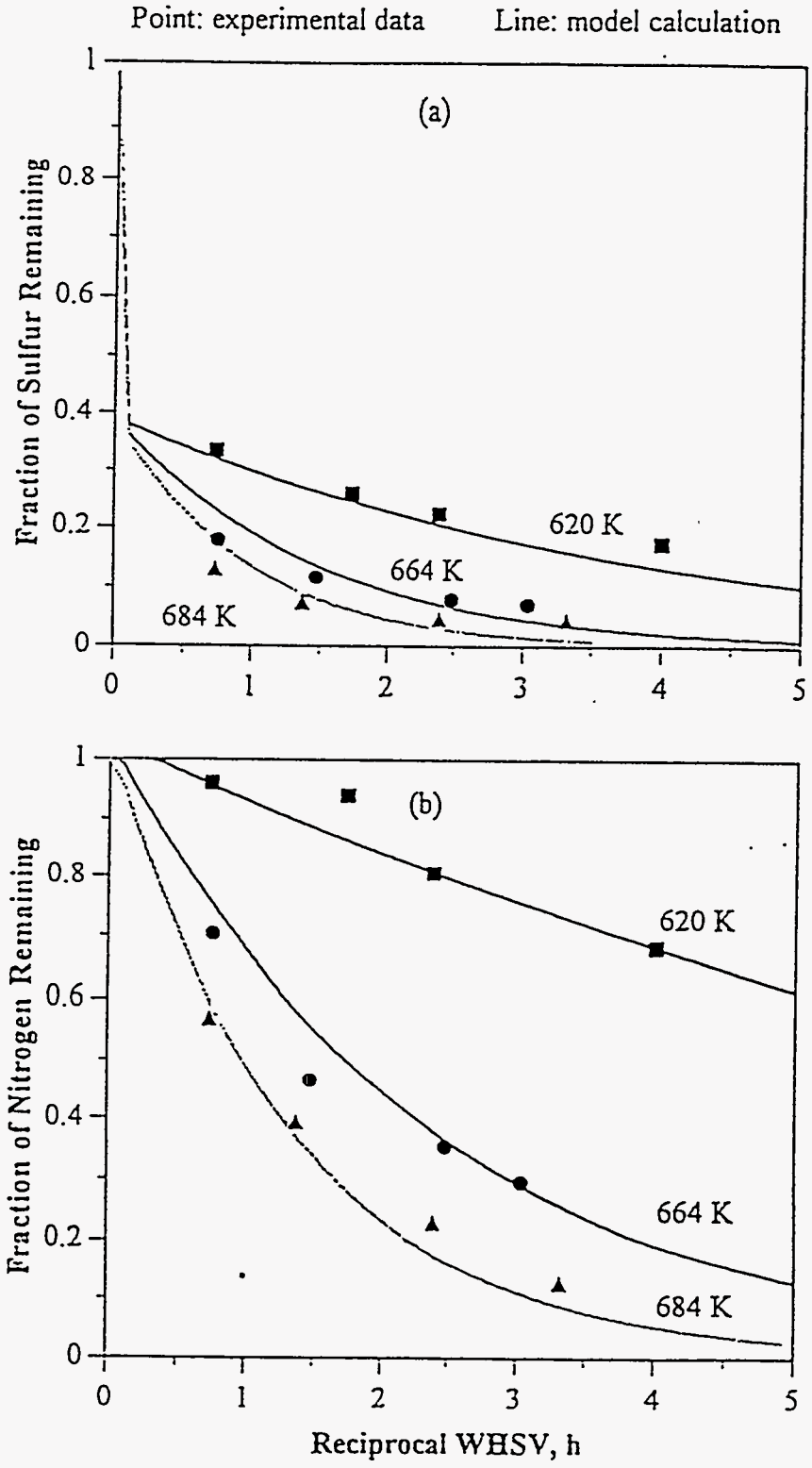
Point: experimental data
Line: model calculation
(a)
Fraction of Sulfur Remaining
620 K
664 K
684 K
(b)
Fraction of Nitrogen Remaining
620 K
664 K
684 K
Reciprocal WHSV, h

Equation 171 can be rewritten as follows:

$$1 - x_i = \frac{1}{\sqrt{\pi}} \int_0^{\infty} f(y) \exp(-y^2) dy = \frac{1}{\sqrt{\pi}} \sum_{i=1}^{n} w_i f(y_i) \qquad (172)$$

The integral term on the right-hand side of Equation 172 is the Hermite integral. The solution of this integral can be approximated by employing the Table of zeros and weight factors for the first twenty Hermite polynomials(341). The value of E_o changed relatively little in the range of n = 8 to n=12 after computer calculation for each n. Thus, n=10 was chosen in this study.

The apparent kinetic parameters computed from the nonlinear regression method are presented in Table 108. The fraction of the lumped species remaining versus reciprocal WHSV are plotted in Figures 286-291 using these parameters. The normal distribution-DAEM gave a very good fit of the experimental data for each of the lumped species over the three HDN catalysts and gave the best fit of the data of the three distributions.

Comparing the parameters of each species shown in Table 108, the mean activation energies for nitrogen conversion over the three HDN catalysts are higher than those for sulfur conversion. This result is consistent with the difficulty of removal of nitrogen compound in the feedstock relative to sulfur compounds. The standard deviations σ_E for sulfur data are higher than those for nitrogen data. This implies that the distribution of individual sulfur compounds is wider than that of individual nitrogen compounds. The preexponential factor k_o increased with increasing activation energy for the A-HDN catalyst. The trend was not obtained with the B- and C-HDN catalysts.

According to the above results, the curve fits to the experimental data for the nth power rate law and the normal distributed activation energy models were better than the other models tried. Since the best fits were obtained from models having different viewpoints, the results for the overall nth power rate law and normal distribution activation energy models are presented in Figures 292-297 and Table 109.

A comparison of the correlations of the experimental data from both models indicates the conversions of residuum and CCR over the A- and C-HDN catalysts and of

Table 108

Apparent Kinetic Parameters from Normal-Distributed Activation Model at Constant Pressure (13.7 MPa)

Catalyst	k_o /h	E_o kcal/mol	σ_E cal/mol
A-HDN			
Sulfur	1.4E9	25.2	3035
Nitrogen	1.5E9	29.1	719
Residuum	3.7E11	36.4	2370
CCR	4.7E7	24.5	1293
B-HDN			
Sulfur	1.5E9	26.4	2007
Nitrogen	1.1E11	34.9	1193
Residuum	3.2E12	40.8	3560
CCR	4.1E8	27.7	1123
C-HDN			
Sulfur	8.9E7	22.5	2984
Nitrogen	1.6E9	29.8	1391
Residuum	2.3E7	24.9	1680
CCR	5.0E4	22.4	1866

k_o : Pre-exponential Factor
E_o : Mean Activation Energy
σ_E : Standard Deviation of Activation Energy for Normal Distribution Function

Figure 286

Comparison with normal-DAEM and experimental data for

(a) sulfur (b) nitrogen conversion over the A-HDN catalyst

at constant pressure

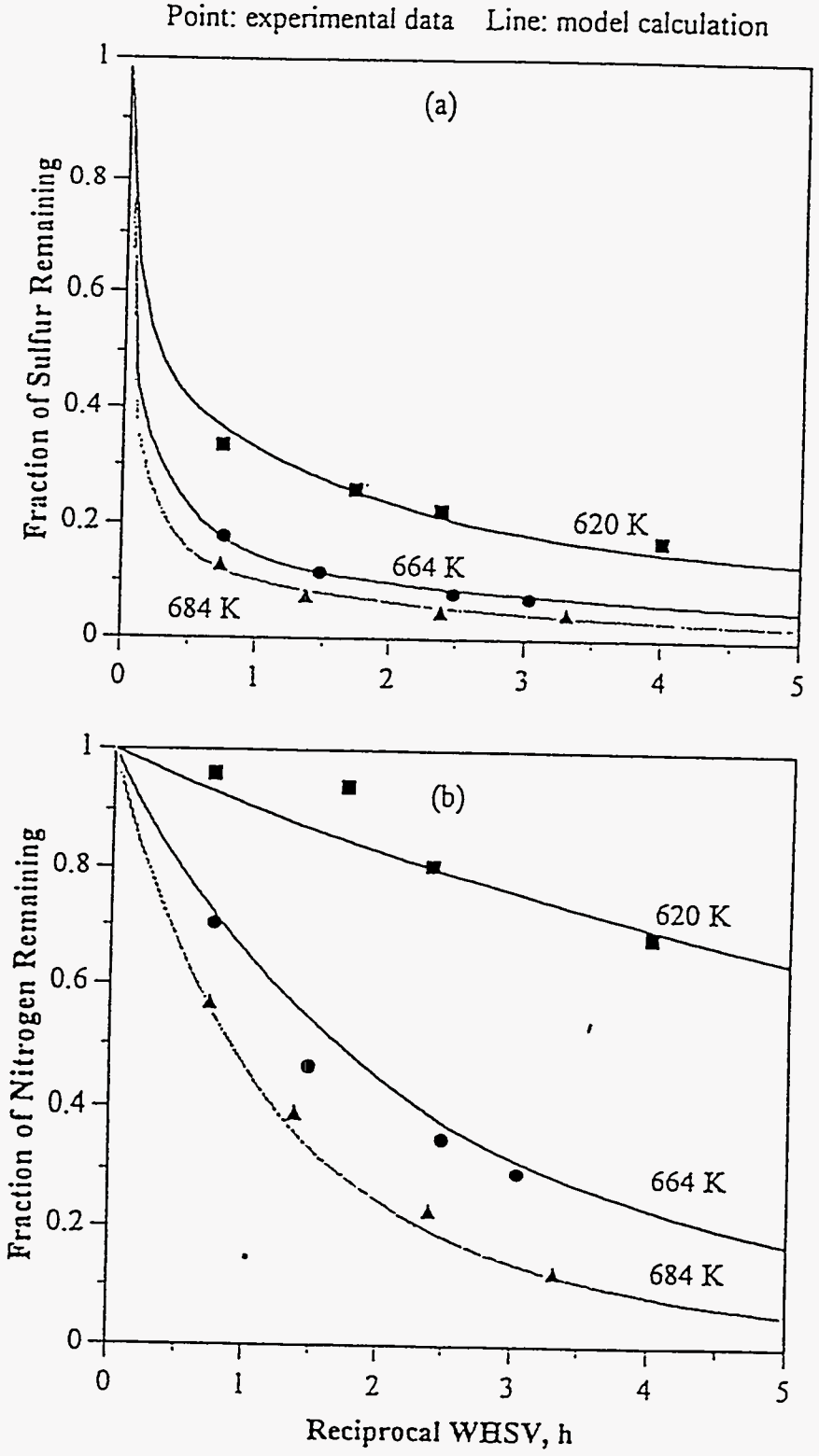
Point: experimental data Line: model calculation
(a)
Fraction of Sulfur Remaining
620 K
664 K
684 K
(b)
Fraction of Nitrogen Remaining
620 K
664 K
684 K
Reciprocal WHSV, h

Figure 287

Comparison with normal-DAEM and experimental data for

(a) residuum (b) CCR conversion over the A-HDN catalyst

at constant pressure

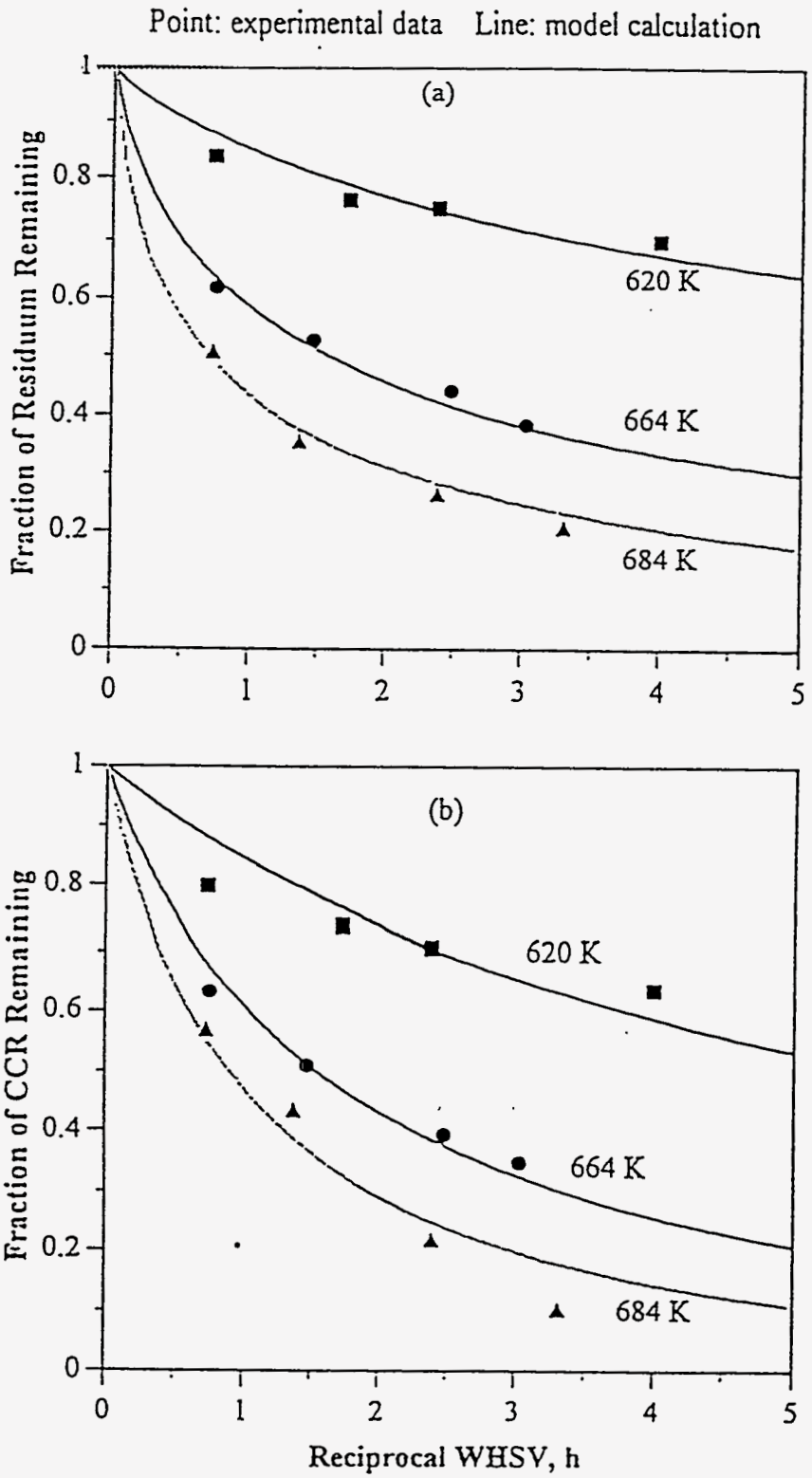
Point: experimental data Line: model calculation
(a)
Fraction of Residuum Remaining
620 K
664 K
684 K
(b)
Fraction of CCR Remaining
620 K
664 K
684 K
Reciprocal WHSV, h

Figure 288

Comparison with normal-DAEM and experimental data for

(a) sulfur (b) nitrogen conversion over B-HDN catalyst

at constant pressure

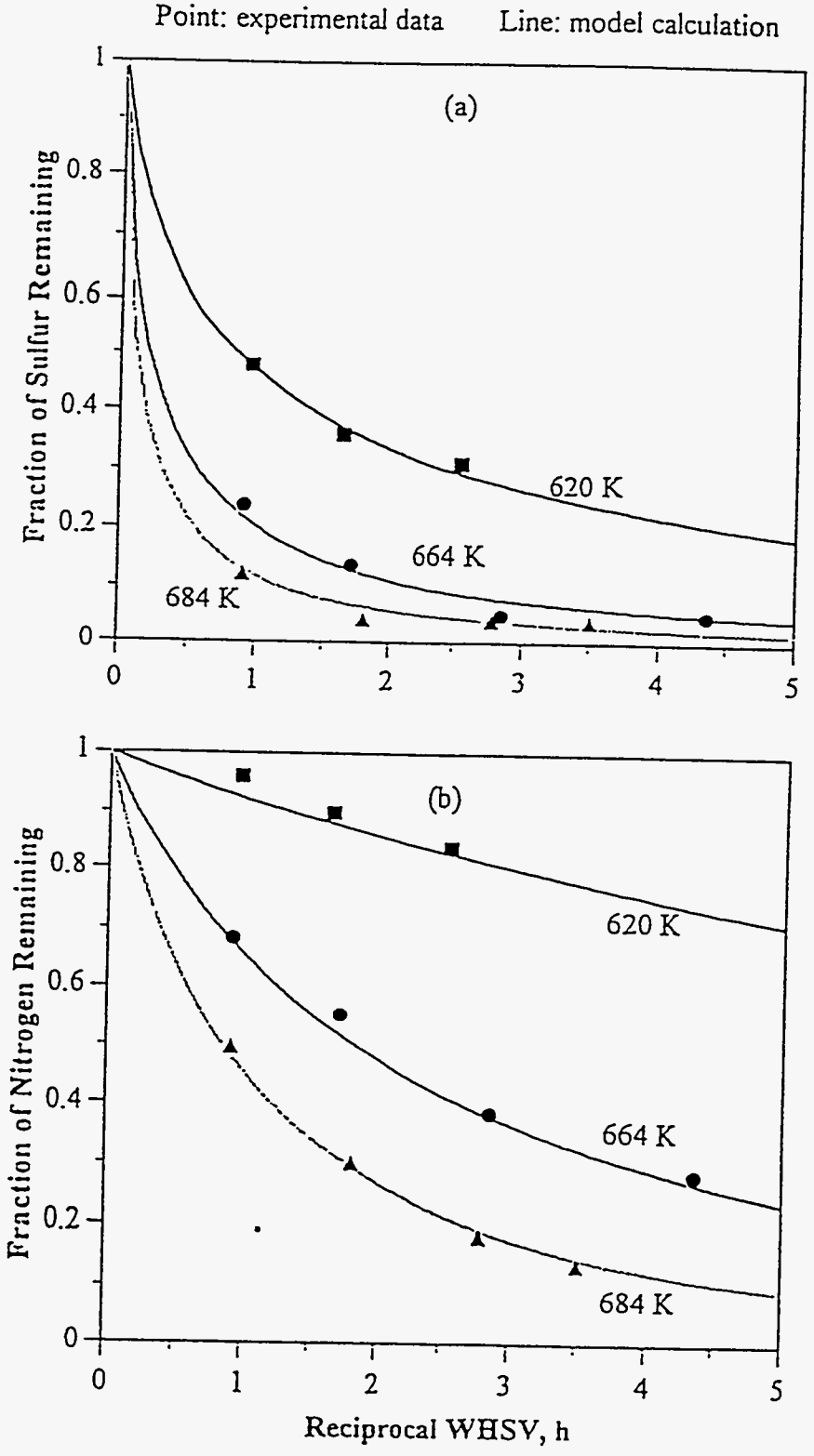
Point: experimental data
Line: model calculation
(a)
Fraction of Sulfur Remaining
620 K
664 K
684 K
(b)
Fraction of Nitrogen Remaining
620 K
664 K
684 K
Reciprocal WHSV, h

Figure 289

Comparison with normal-DAEM and experimental data for

(a) residuum (b) CCR conversion over B-HDN catalyst

at constant pressure

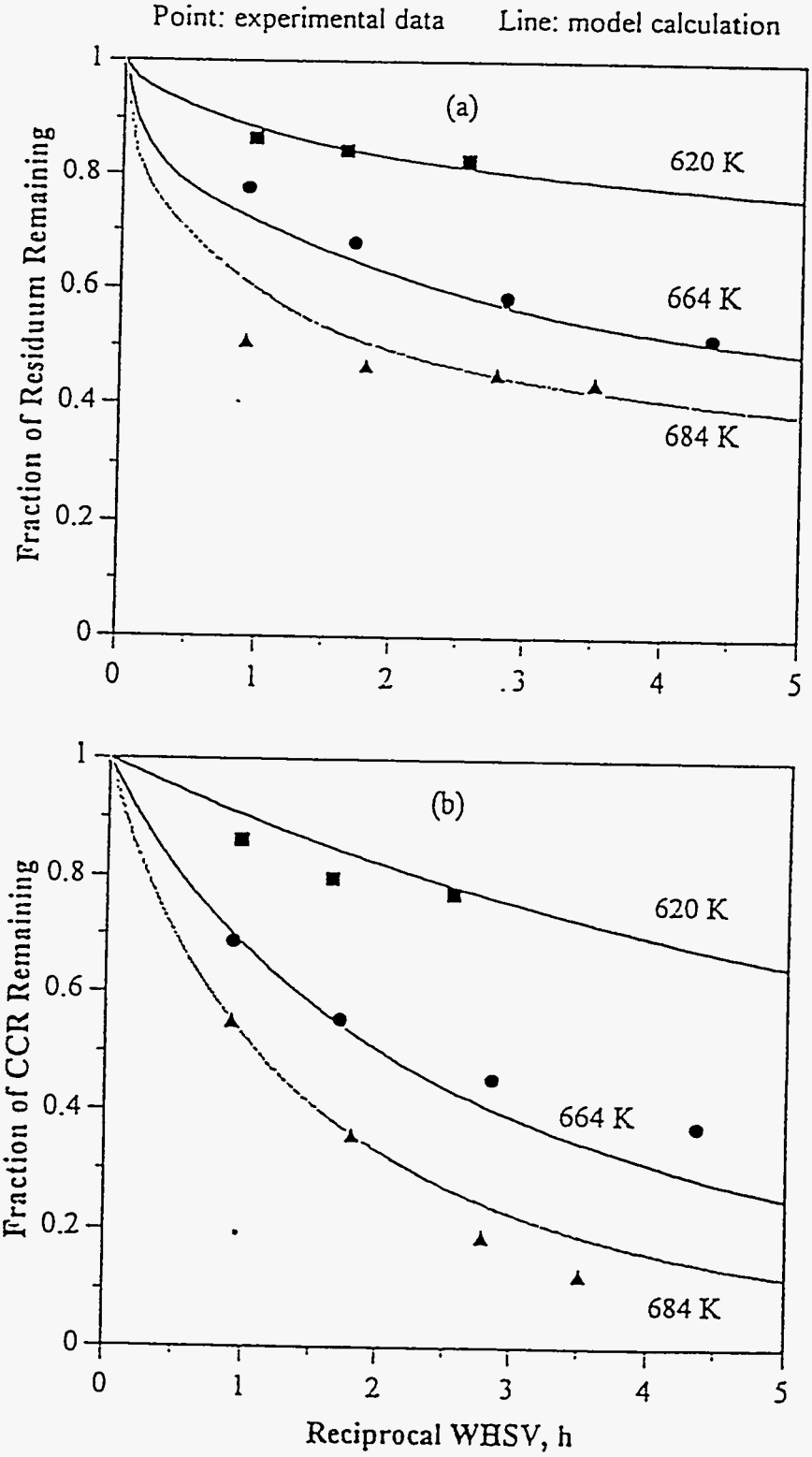
Point: experimental data
Line: model calculation
(a)
620 K
664 K
684 K
Fraction of Residuum Remaining
0
0.2
0.4
0.6
0.8
1
0
1
2
3
4
5
(b)
620 K
664 K
684 K
Fraction of CCR Remaining
Reciprocal WHSV, h

Figure 290

Comparison with normal-DAEM and experimental data for

(a) sulfur (b) nitrogen conversion over C-HDN catalyst

at constant pressure

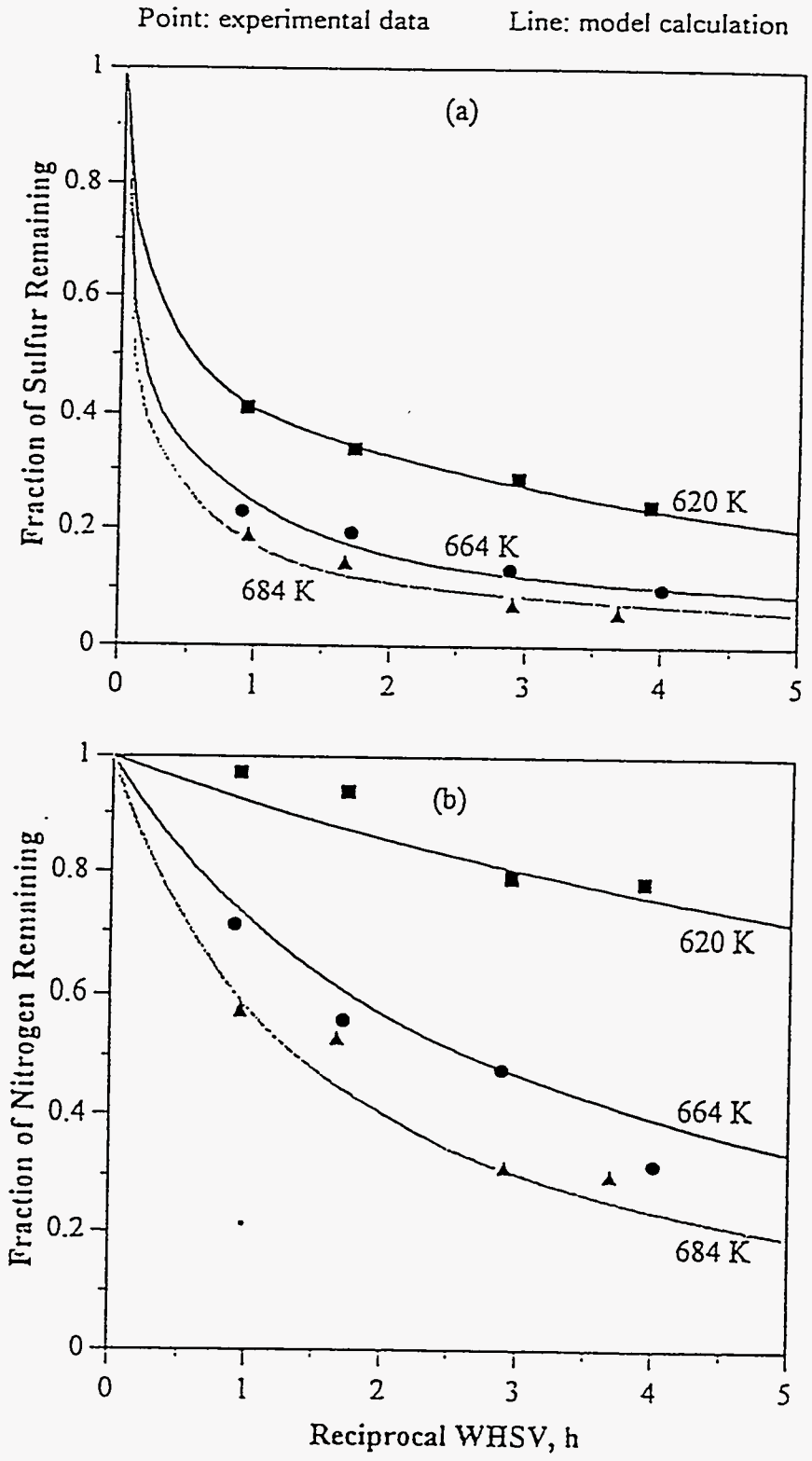
Point: experimental data
Line: model calculation
(a)
Fraction of Sulfur Remaining
620 K
664 K
684 K
(b)
Fraction of Nitrogen Remaining
620 K
664 K
684 K
Reciprocal WHSV, h

Figure 291

Comparison with normal-DAEM and experimental data for

(a) residuum (b) CCR conversion over C-HDN catalyst

at constant pressure

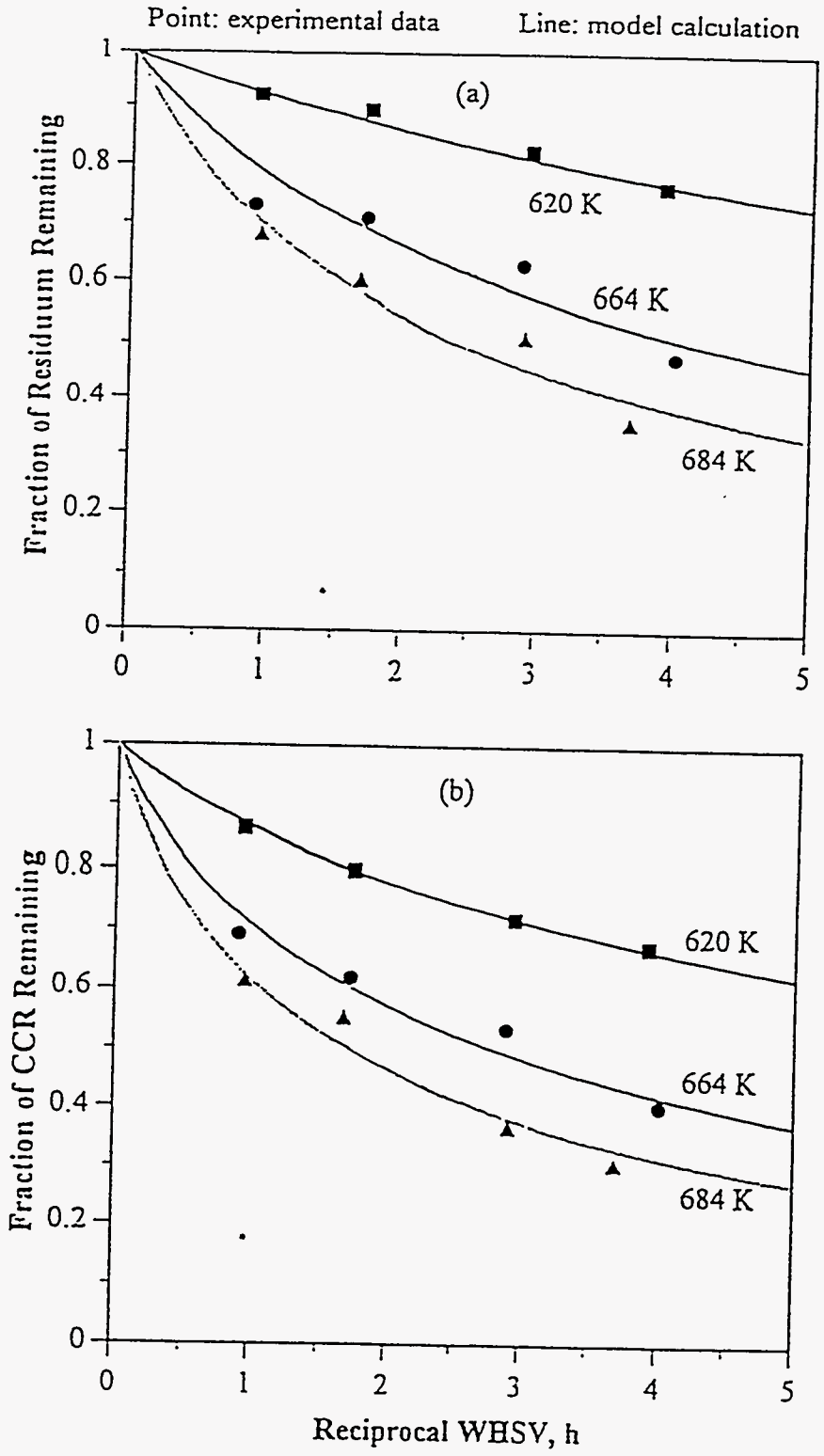
Point: experimental data
Line: model calculation
(a)
620 K
664 K
684 K
Fraction of Residuum Remaining
(b)
620 K
664 K
684 K
Fraction of CCR Remaining
Reciprocal WHSV, h

Figure 292

Comparison with experimental data from the nth power rate law and normal DAEM for (a) sulfur (b) nitrogen conversion over A-HDN catalyst at constant pressure (13.7 MPa)

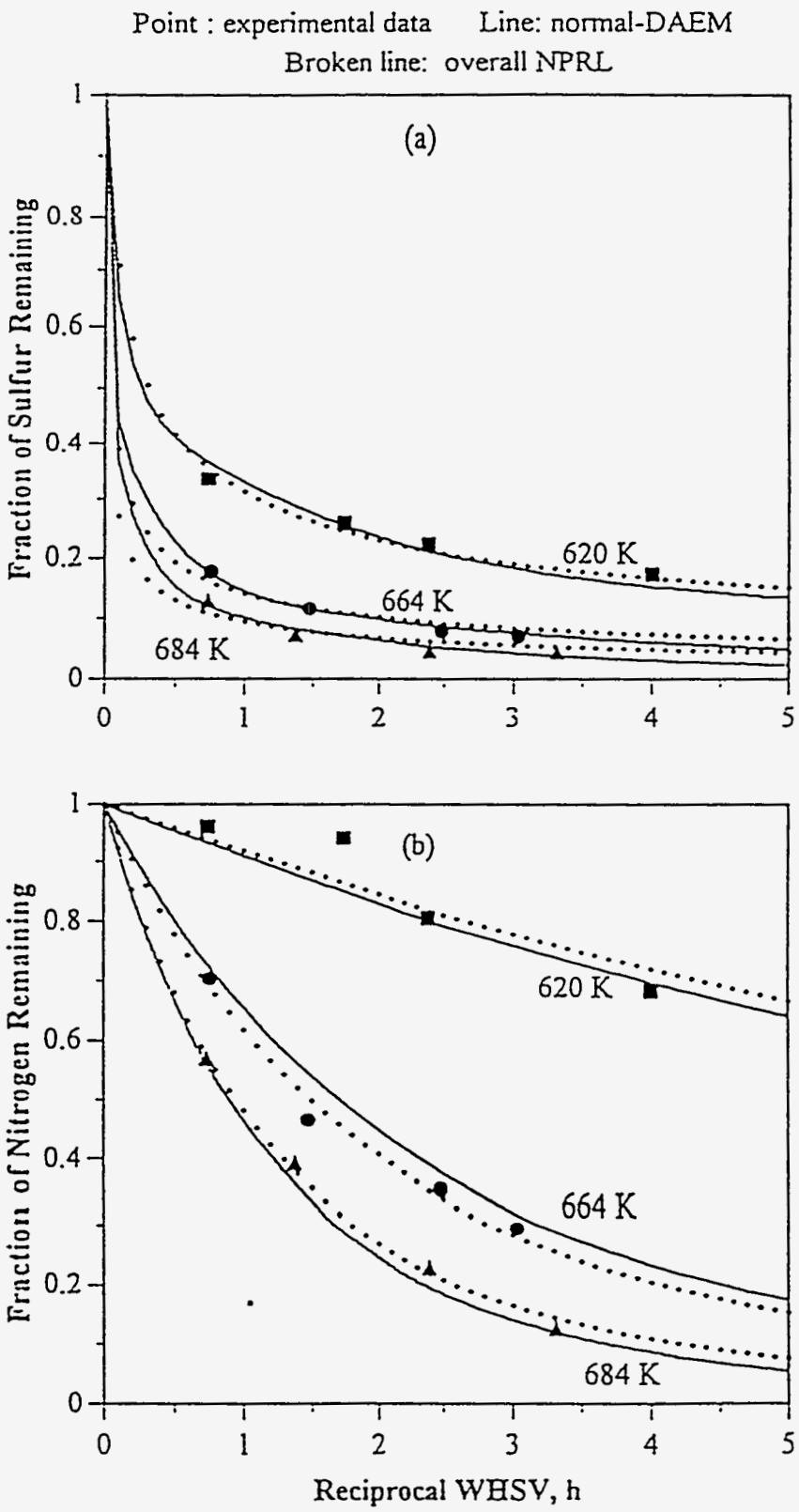
Point : experimental data Line: normal-DAEM
Broken line: overall NPRL
(a)
Fraction of Sulfur Remaining
620 K
664 K
684 K
(b)
Fraction of Nitrogen Remaining
620 K
664 K
684 K
Reciprocal WHSV, h

Figure 293

Comparison with experimental data from nth power rate law and normal DAEM for (a) residuum (b) CCR conversion over A-HDN catalyst at constant pressure (13.7 MPa)

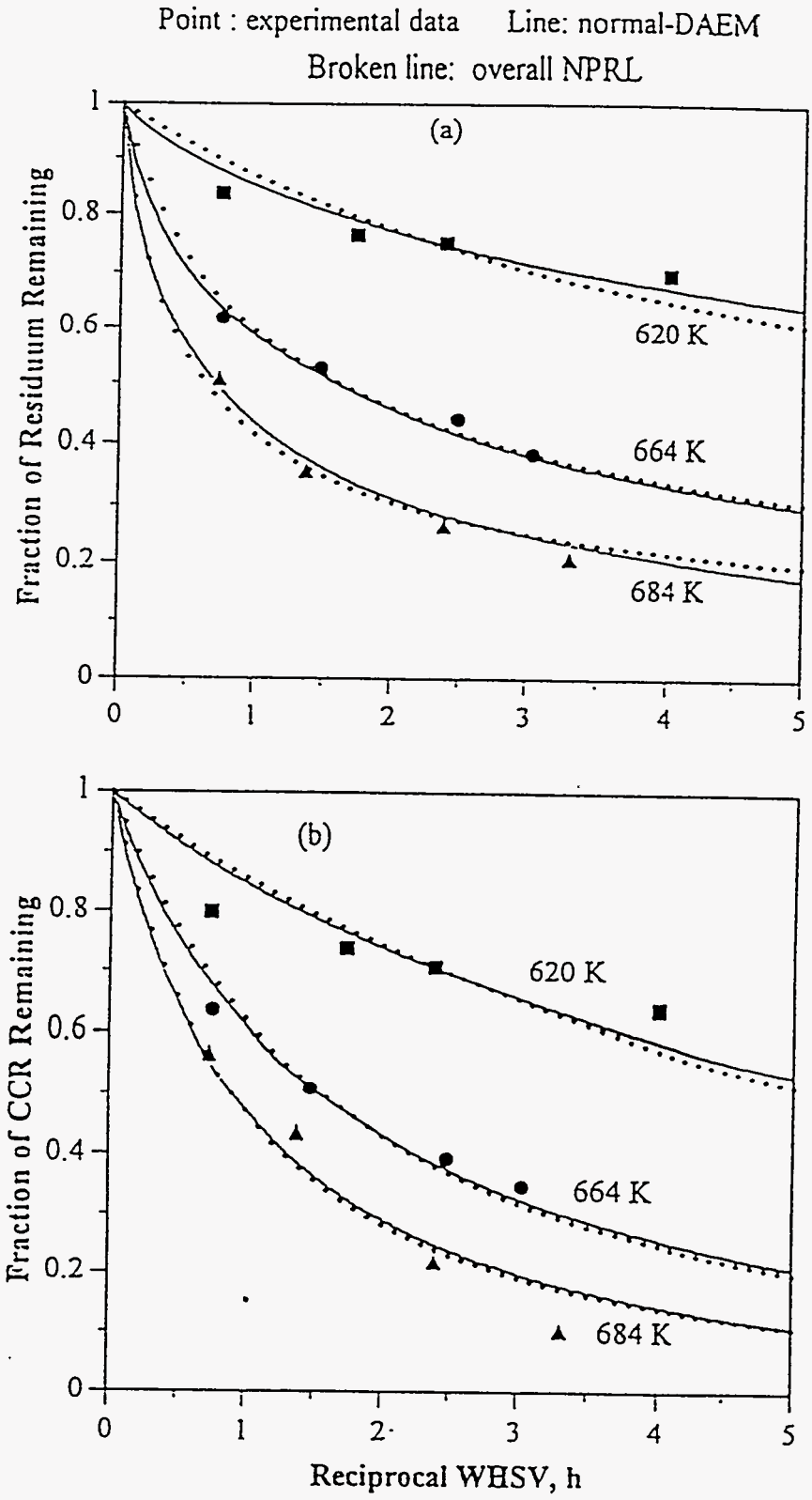
Point : experimental data Line: normal-DAEM
Broken line: overall NPRL
(a)
Fraction of Residuum Remaining
620 K
664 K
684 K
(b)
Fraction of CCR Remaining
620 K
664 K
684 K
Reciprocal WHSV, h

Figure 294

Comparison with experimental data from nth power rate law

and normal DAEM for (a) sulfur (b) nitrogen conversion over B-HDN catalyst

at constant pressure (13.7 MPa)

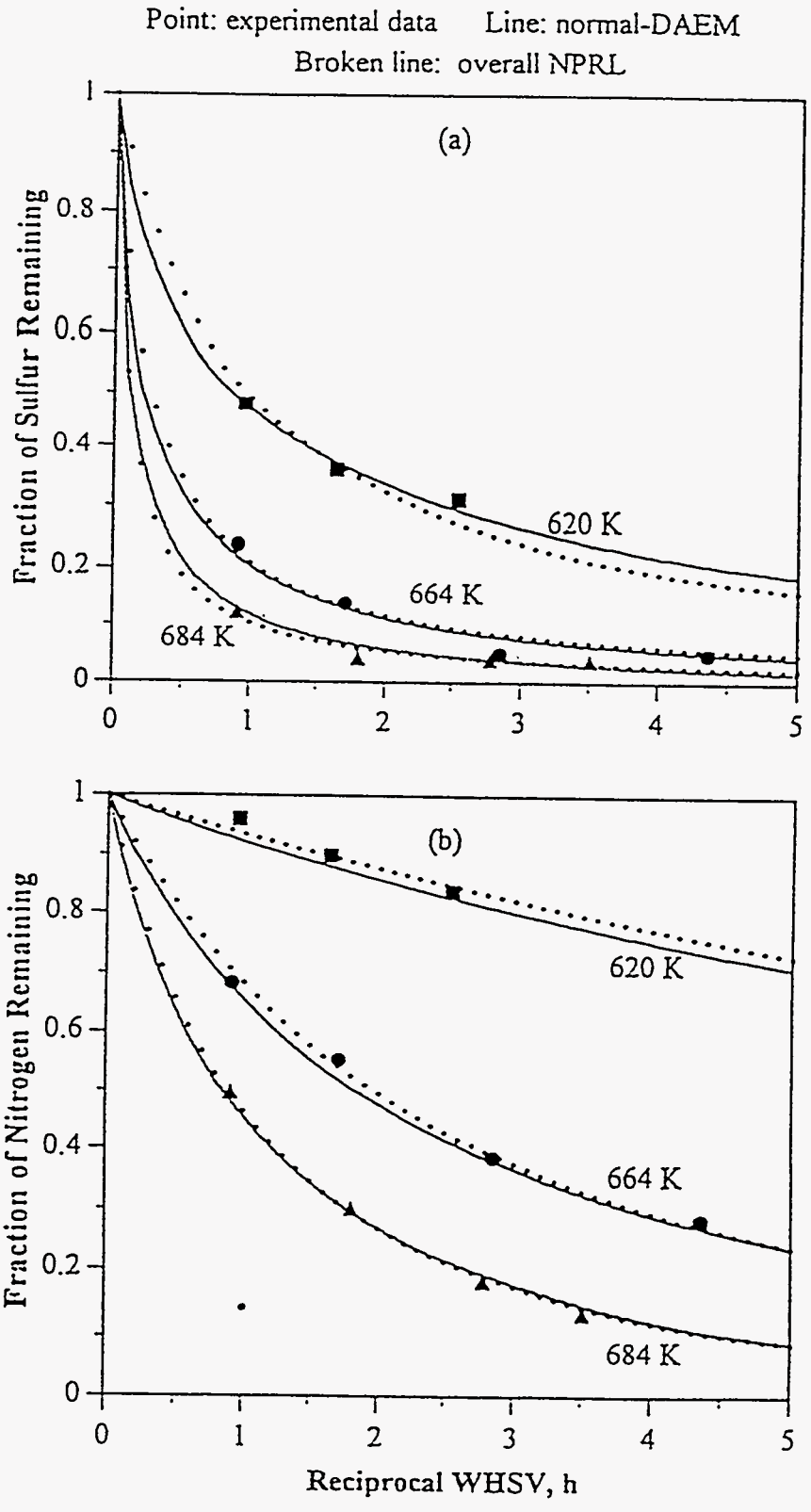
Point: experimental data Line: normal-DAEM
Broken line: overall NPRL
(a)
Fraction of Sulfur Remaining
620 K
664 K
684 K
(b)
Fraction of Nitrogen Remaining
620 K
664 K
684 K
Reciprocal WHSV, h

Figure 295

Comparison with experimental data from nth power rate law and normal DAEM for (a) residuum (b) CCR conversion over the B-HDN catalyst at constant pressure (13.7 MPa)

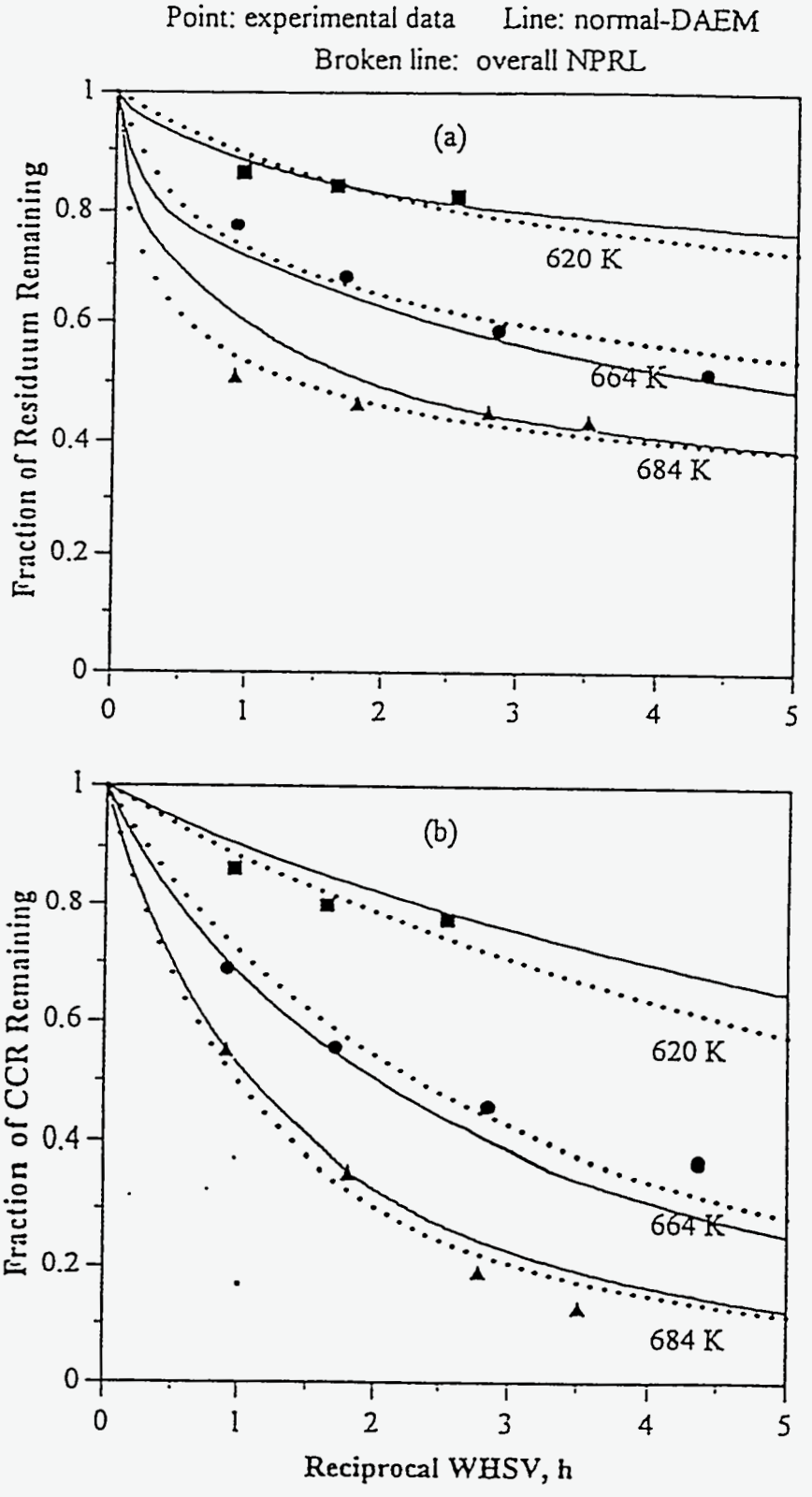
Point: experimental data Line: normal-DAEM
Broken line: overall NPRL
(a)
620 K
664 K
684 K
Fraction of Residuum Remaining
(b)
620 K
664 K
684 K
Fraction of CCR Remaining
Reciprocal WHSV, h

Figure 296

Comparison with experimental data from nth power rate law

and normal DAEM for (a) sulfur (b) nitrogen conversion over the C-HDN catalyst

at constant pressure (13.7 MPa)

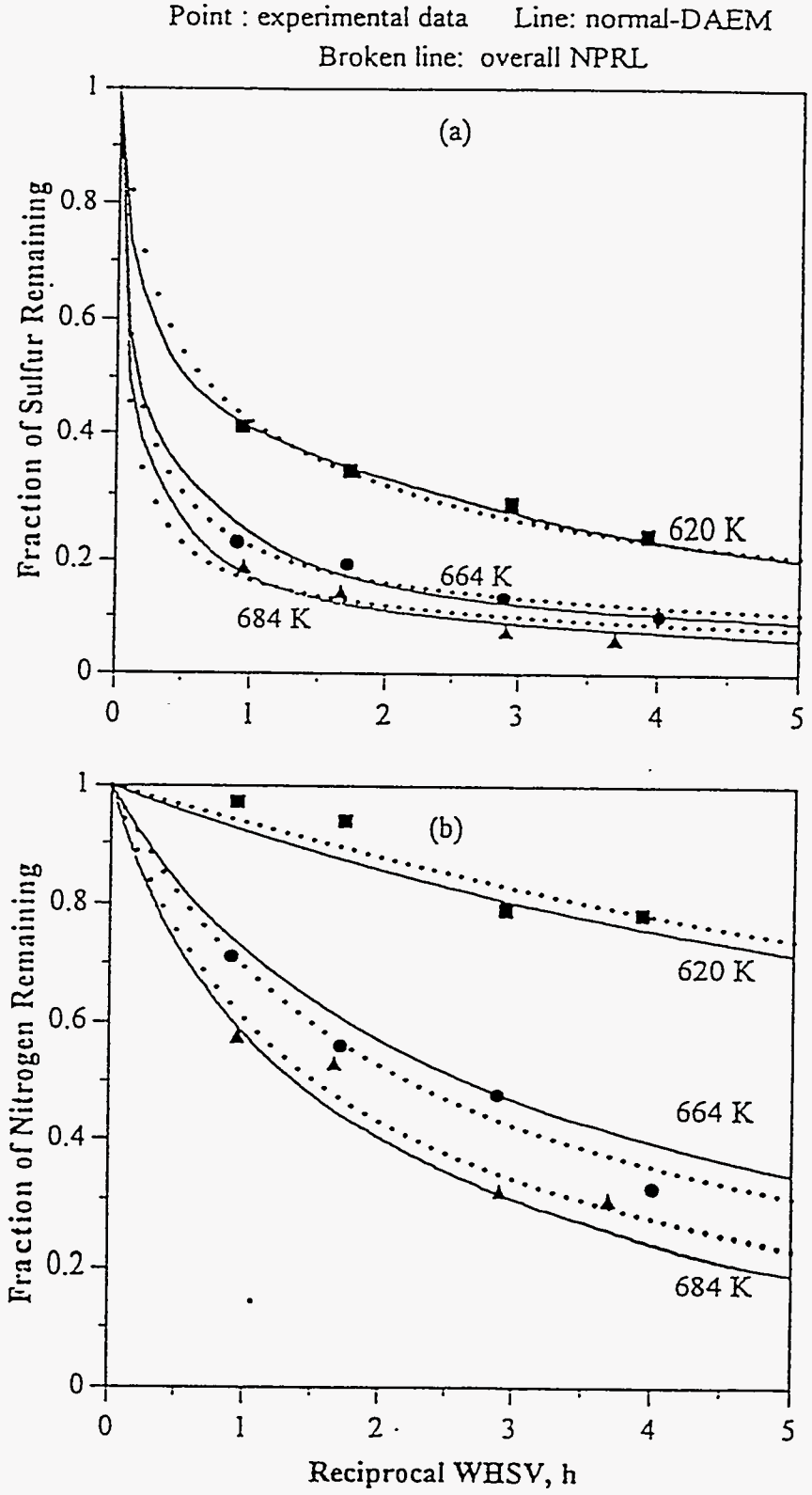
Point : experimental data Line: normal-DAEM
Broken line: overall NPRL
(a)
Fraction of Sulfur Remaining
620 K
664 K
684 K
(b)
Fraction of Nitrogen Remaining
620 K
664 K
684 K
Reciprocal WHSV, h

Figure 297

Comparison with experimental data from nth power rate law

and normal DAEM for (a) residuum (b) CCR conversion over the C-HDN catalyst

at constant pressure (13.7 MPa)

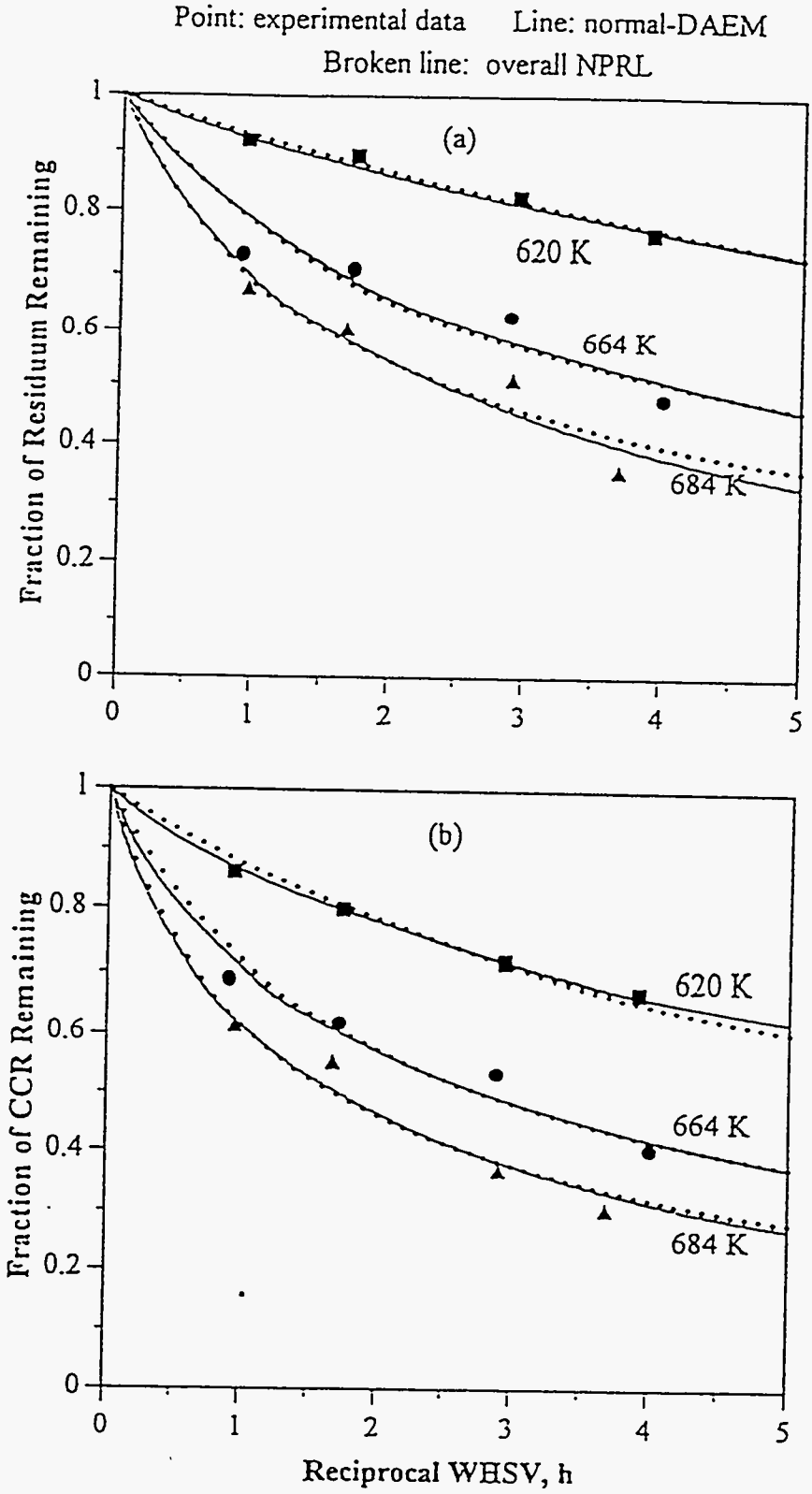
Point: experimental data
Line: normal-DAEM
Broken line: overall NPRL
(a)
620 K
664 K
684 K
Fraction of Residuum Remaining
(b)
620 K
664 K
684 K
Fraction of CCR Remaining
Reciprocal WHSV, h

Table 109

Comparison of Apparent Kinetic Parameters from the Overall nth Power Rate Law and Normal-Distributed Activation Model at Constant Pressure (13.7 MPa)

	Overall nth Power Law			Normal-DAEM		
Catalyst	n	k_o /h	E_o kcal/mol	k_o /h	E_o kcal/mol	σ_E cal/mol
A-HDN						
Sulfur	3.1	3.9E13	34.3	1.4E9	25.2	3035
Nitrogen	1.3	4.3E9	30.3	1.5E9	29.1	719
Residuum	2.9	6.9E7	33.8	3.7E11	36.4	2370
CCR	1.6	5.9E7	23.3	4.7E7	24.5	1293
B-HDN						
Sulfur	2.0	8.0E9	27.0	1.5E9	26.4	2007
Nitrogen	1.5	8.3E10	34.3	1.1E11	34.9	1193
Residuum	5.7	1.3E5	40.0	3.2E12	40.8	3560
CCR	1.6	8.5E6	23.9	4.1E8	27.7	1123
C-HDN						
Sulfur	3.1	7.9E10	27.6	8.9E7	22.5	2984
Nitrogen	1.9	3.2E9	30.2	1.6E9	29.8	1391
Residuum	2.6	6.2E4	24.5	2.3E7	24.9	1680
CCR	2.4	8.3E4	20.5	5.0E4	22.4	1866

sulfur and nitrogen over B-HDN catalyst are almost the same, whereas for the other lumped species, they are slightly different. This comparison suggests that for the hydrotreating of bitumens the nth power rate law could be used to obtain reaction order, whereas the normal distribution activation energies model could be used to obtain realistic activation energies.

Apparent kinetic parameters for both models are listed in Table 109. The pre-exponential factors cannot be compared directly because the units of k_o in two models are different. The mean activation energy trends for both models for each lumped species over the HDN catalysts are the same except for the activation energies of sulfur conversion over the A-HDN catalyst which is higher than that of nitrogen removal. The mean activation energies data are similar except for sulfur removal over the A- and C-HDN catalysts. The mean activation energies calculated from the overall nth power rate law model are close to those calculated from the normal distribution-DAEM.

Investigation of Process Variables

The primary objective of catalytic upgrading is to remove the heteroatoms from the bitumen and simultaneously to reduce molecular weight distribution of the bitumen.

The process variables investigated in this study were the liquid (weight) hourly space velocity, the reactor temperature, and the hydrogen partial pressure. The effects of process variables on heteroatom and metal removal; residuum, CCR, and asphaltenes conversion; viscosity reduction; and product distribution over three HDN catalysts were determined.

Effect of Weight Hourly Space Velocity

Removal of Species

The WHSV was varied at fixed temperatures and pressure to determine the reaction orders and the rate constants for lumped species by an overall nth power rate law. The overall reaction orders for sulfur and nitrogen removal and residuum and CCR conversion over three HDN catalysts are presented in Table 105.

The effect of WHSV on the fractional conversions of lumped species, such as sulfur, nitrogen, residuum, CCR, and asphaltenes, over HDN catalysts are plotted in

Figures 298-300. (The effect of WHSV on conversions of some lumped species can be also seen in Figures 280-285.) These figures indicate that the conversions increase as the reciprocal WHSV increased; however, the asphaltenes conversions exhibited a different trend at 620 K. The reciprocal WHSV represents residence time or contact time in the reactor. At the higher residence times, the liquid contact time was sufficient to permit the catalytic and thermal reactions to approach completion.

For sulfur removal, the conversion is strongly influenced by residence time, especially below 1 h. When the reciprocal WHSV was greater than 1 h, the conversion increased slowly with increasing residence time and then leveled off. The time at which the conversion leveled off depended upon the reactor temperature and the catalyst employed.

The conversion of nitrogen increased significantly as residence time increased for reactor temperatures of 664 and 684 K. However, this positive influence decreased at 620 K. At 620 K, the nitrogen conversion doubled when the reciprocal WHSV was 2 h.

The conversions of residuum and CCR exhibited similar trends; that is, the conversions increased with increasing residence time. Asphaltenes conversion exhibited the same trend as residuum and CCR conversion at 664 and 684 K. However, at 620 K, the asphaltenes conversion increased to a maximum (about reciprocal WHSV = 0.9 h) and then decreased as residence time increased. Comparing the conversion at three reactor temperatures, the asphaltenes conversion decreased only at a LHSV of 0.9 h^{-1}. Therefore, the trend at the lower temperature of 620 K over the same catalyst may be related to the space velocity as well as the temperatures.

Comparing the conversions , sulfur removal is much more facile than the others. The nitrogen removal is more difficult than others at lower temperature 620 K. However, the asphaltenes conversion is less than the others at higher temperature 664 and 684 K where asphaltene-like species may actually be created.

Nickel removal increased with increasing residence time for the three HDN catalysts shown in Tables 88-90, respectively. A comparison of the nickel and asphaltenes conversions over the HDN catalysts is presented in Table 110. This table indicates nickel removal, and asphaltenes conversion are related: The greater the asphaltenes conversion, the more nickel removal.

Figure 298

Fractional conversion of lumped species versus reciprocal WHSV

over the A-HDN catalyst at different temperatures and constant pressure

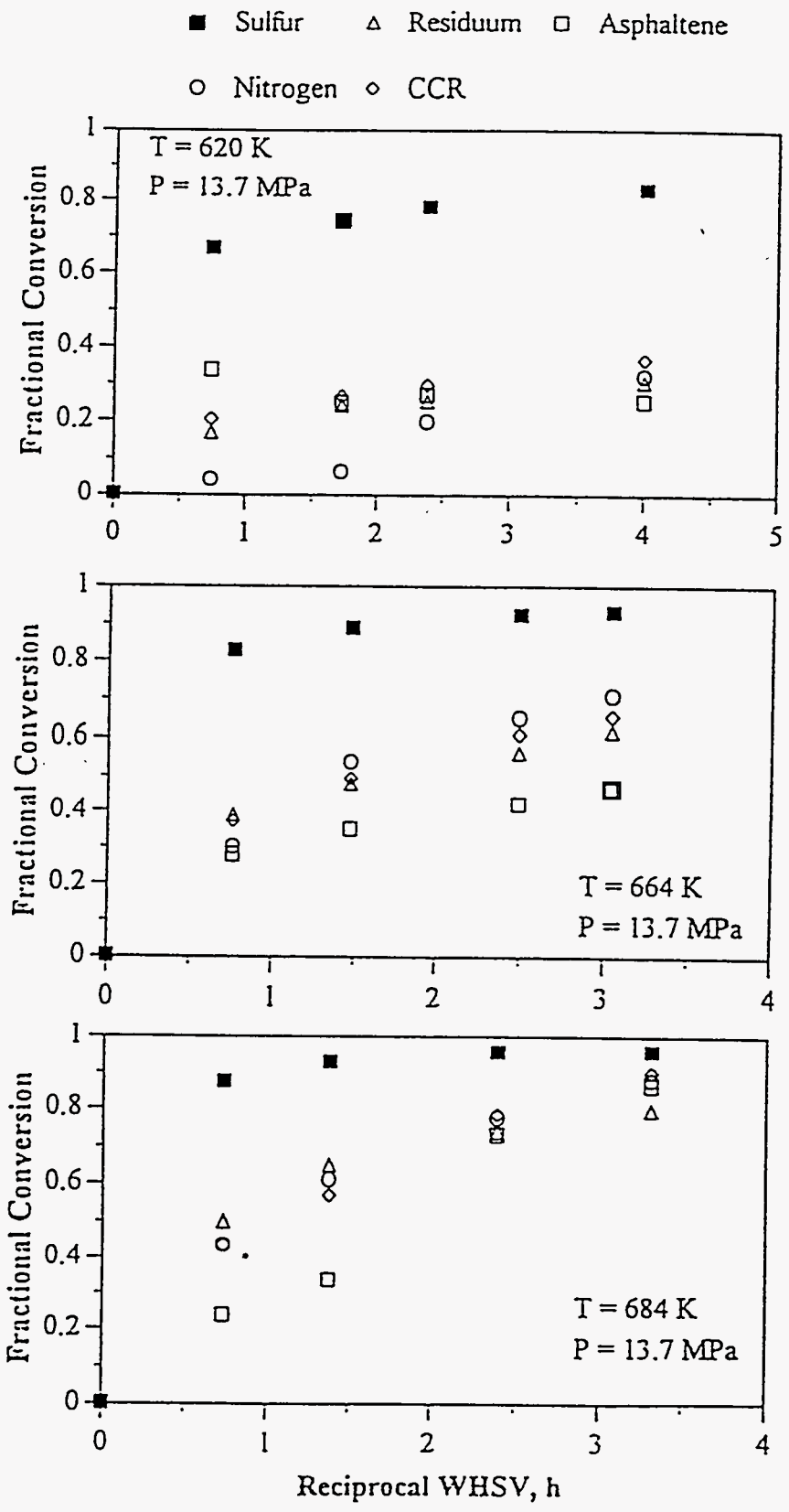
Sulfur
Residuum
Asphaltene
Nitrogen
CCR
T = 620 K
P = 13.7 MPa
T = 664 K
P = 13.7 MPa
T = 684 K
P = 13.7 MPa
Fractional Conversion
Reciprocal WHSV, h

Figure 299

Fractional conversion of lumped species versus reciprocal WHSV

over the B-HDN catalyst at different temperatures and constant pressure

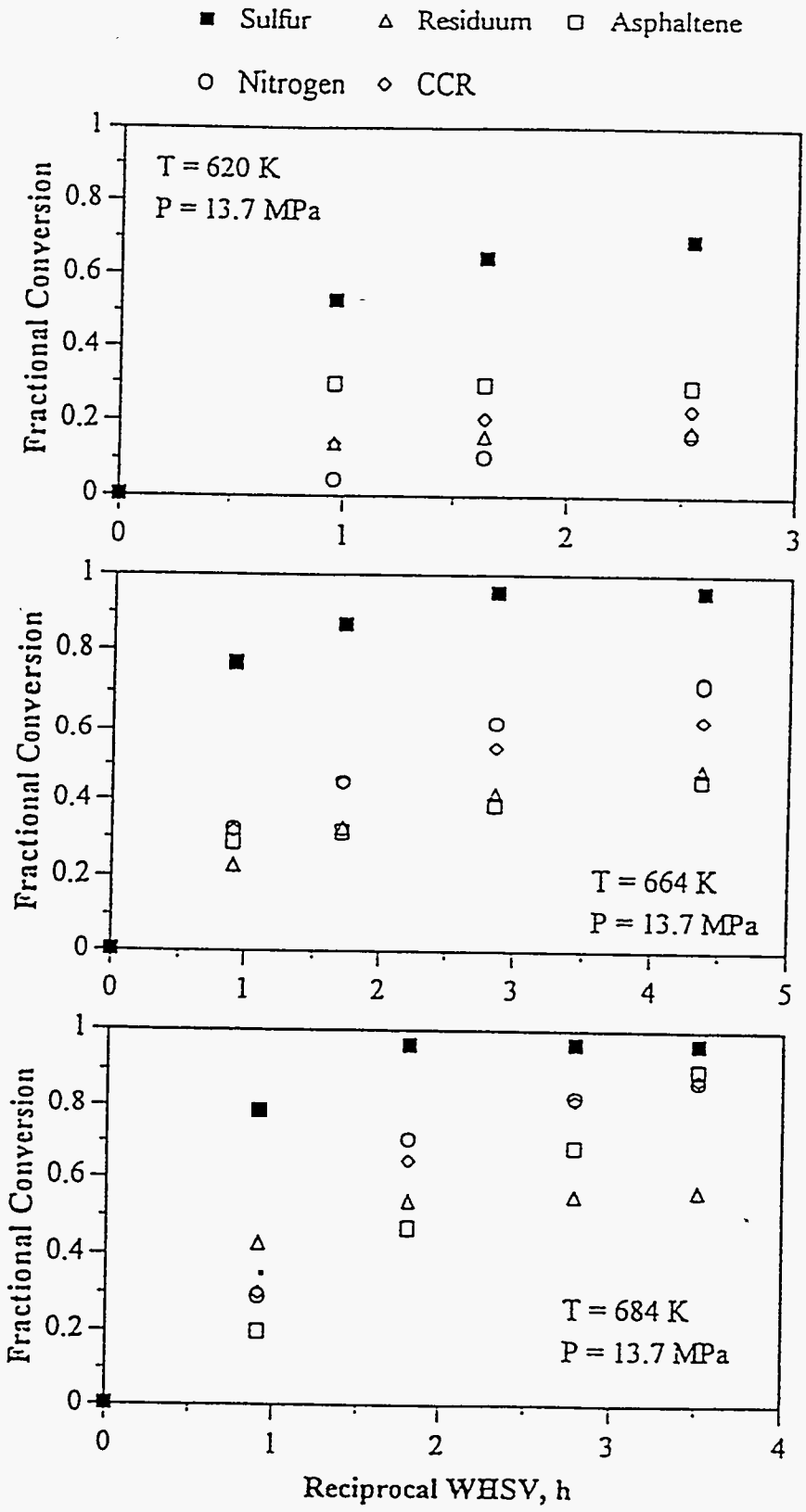
Sulfur
Residuum
Asphaltene
Nitrogen
CCR
T = 620 K
P = 13.7 MPa
T = 664 K
P = 13.7 MPa
T = 684 K
P = 13.7 MPa
Fractional Conversion
Reciprocal WHSV, h

Figure 300

Fractional conversion of lumped species versus reciprocal WHSV

over the C-HDN catalyst at different temperatures and constant pressure

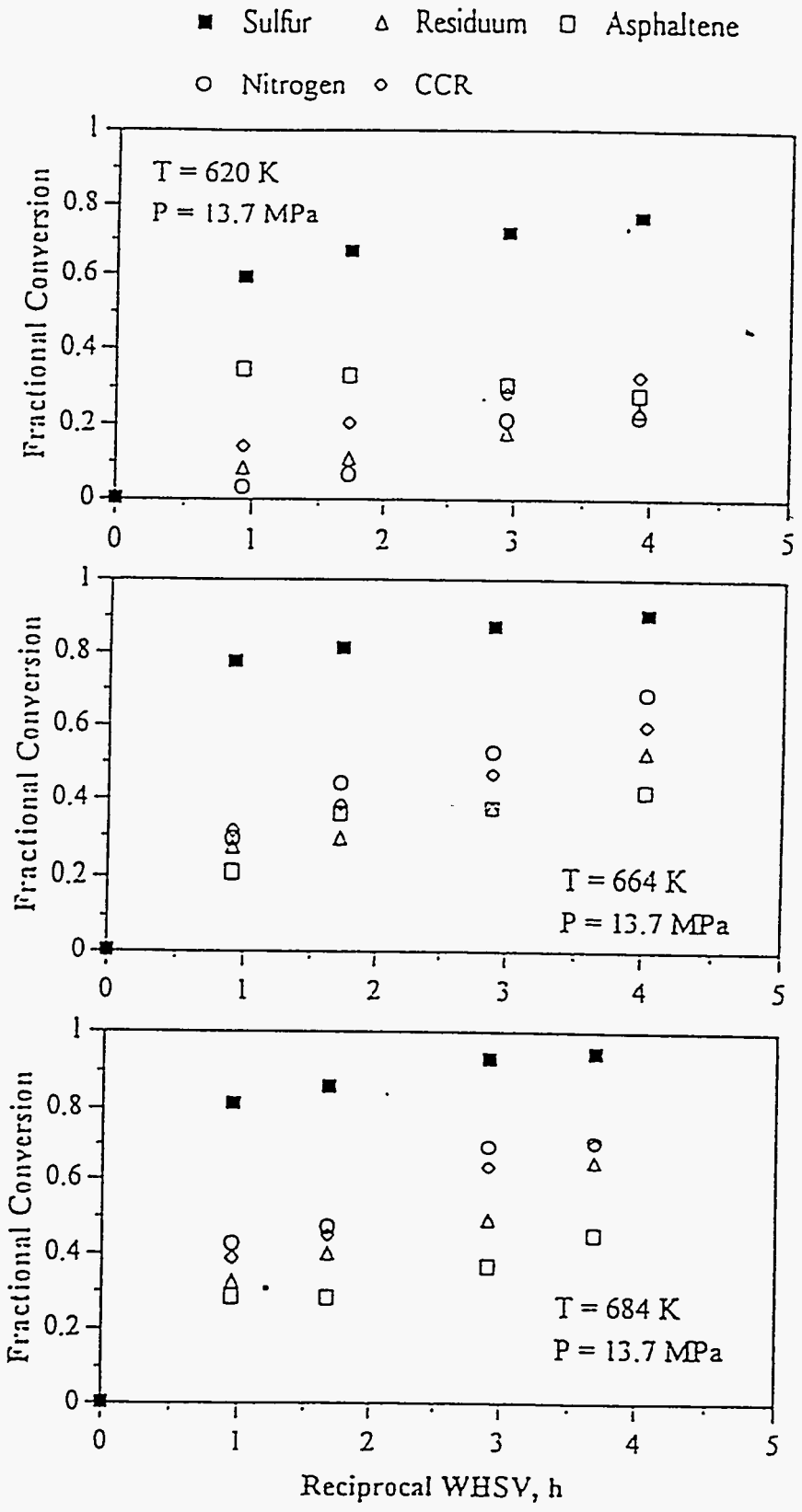
Sulfur
Residuum
Asphaltene
Nitrogen
CCR
T = 620 K
P = 13.7 MPa
T = 664 K
P = 13.7 MPa
T = 684 K
P = 13.7 MPa
Fractional Conversion
Reciprocal WHSV, h

Table 110

Comparison between Conversions of Nickel and Asphaltenes over the HDN Catalysts

Conditions			Catalyst					
			A-HDN		B-HDN		C-HDN	
T	P	LHSV	Nickel	Asphaltenes	Nickel	Asphaltenes	Nickel	Asphaltenes
K	MPa	h^{-1}	%	%	%	%	%	%
620	13.7	0.9	61.6	33.4	43.0	28.9	45.3	34.6
664	13.7	0.48	70.9	34.7	-	-	60.5	35.6
664	13.7	0.28	74.4	41.8	55.8	38.4	64.0	37.2
684	13.7	0.2	83.7	85.9	90.7	89.6	70.9	43.9

It has been observed that the conversions of sulfur, nitrogen, CCR, residuum, and nickel increased as the conversion of asphaltenes increased especially at higher temperature. The reason is that the asphaltene molecules consist of highly condensed polyaromatic units bearing long aliphatic and alicyclic substituents with heteroatoms (S, N, and O) as part of the aromatic system and trace metals as porphyrins(65). Physical methods indicate that high proportion of asphaltenes and resins even account for up to 50% (or higher) of the residuum(65) and moieties that give rise to CCR are distributed in the asphaltenes fraction.

Viscosity Reduction

The viscosity is a measure of its internal resistance to motion of a fluid caused by cohesive forces between molecules and molecular groupings and is the most important single fluid characteristic governing the motion of the fluid. For the fuel system designer, the viscosity is of primary interest as a prime factor to calculate the pressure drops in lines through its relationship to Reynolds number.

The influence of reciprocal WHSV on viscosity reduction of bitumen over the HDN catalysts is presented in Figure 301. As can be seen, the viscosities of hydrotreated bitumens decreased with increasing residence time at specific temperature and pressure.

Product Distribution

The yields and distributions of products produced from the Asphalt Ridge bitumen over the three HDN catalysts as a function of reciprocal WHSV at specific temperature and pressure are plotted in Figures 302-304.

With these three Figures, they exhibit the same trends as a function of residence time at the same operating conditions. The residuum content decreased as the residence time increased. The gas, naphtha, and distillate fractions monotonically increased with increasing residence time. The gas oil yields increased rapidly up to residence time of 1.5 h and then increased slowly at higher residence time at 620 and 664 K. However, the yields of gas oil reach a maximum point and then decrease as reciprocal WHSV increases at 684 K. The same result has been reported by other authors(243, 292, 342).

Figure 301

Effect of reciprocal WHSV on viscosity over the HDN catalysts

at different temperatures and constant pressure (13.7 MPa)

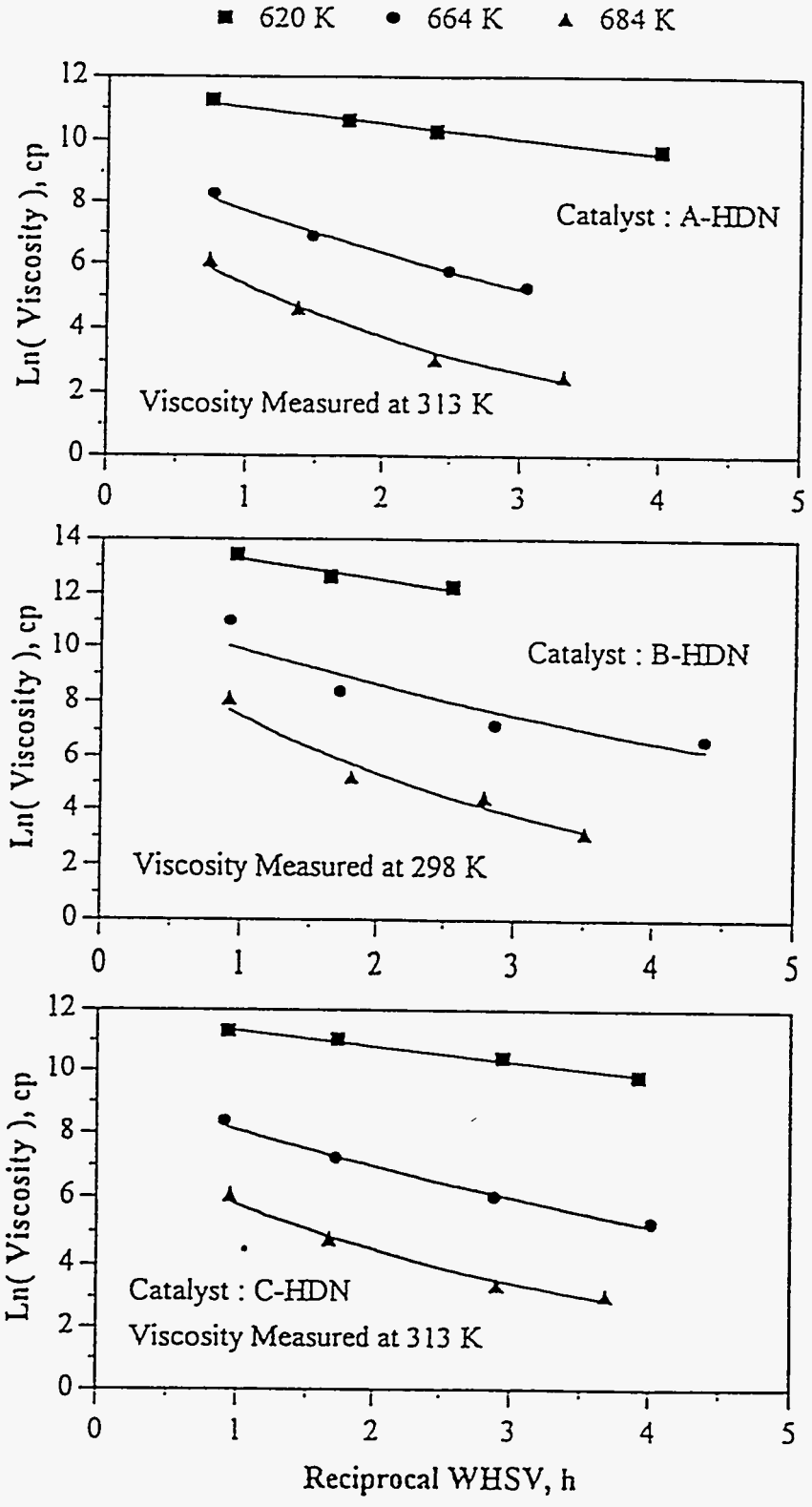
620 K
664 K
684 K
Ln(Viscosity), cp
Catalyst : A-HDN
Viscosity Measured at 313 K
Catalyst : B-HDN
Viscosity Measured at 298 K
Catalyst : C-HDN
Viscosity Measured at 313 K
Reciprocal WHSV, h

Figure 302

Yields of boiling fraction of bitumen conversion versus reciprocal WHSV over the A-HDN catalyst at different temperatures

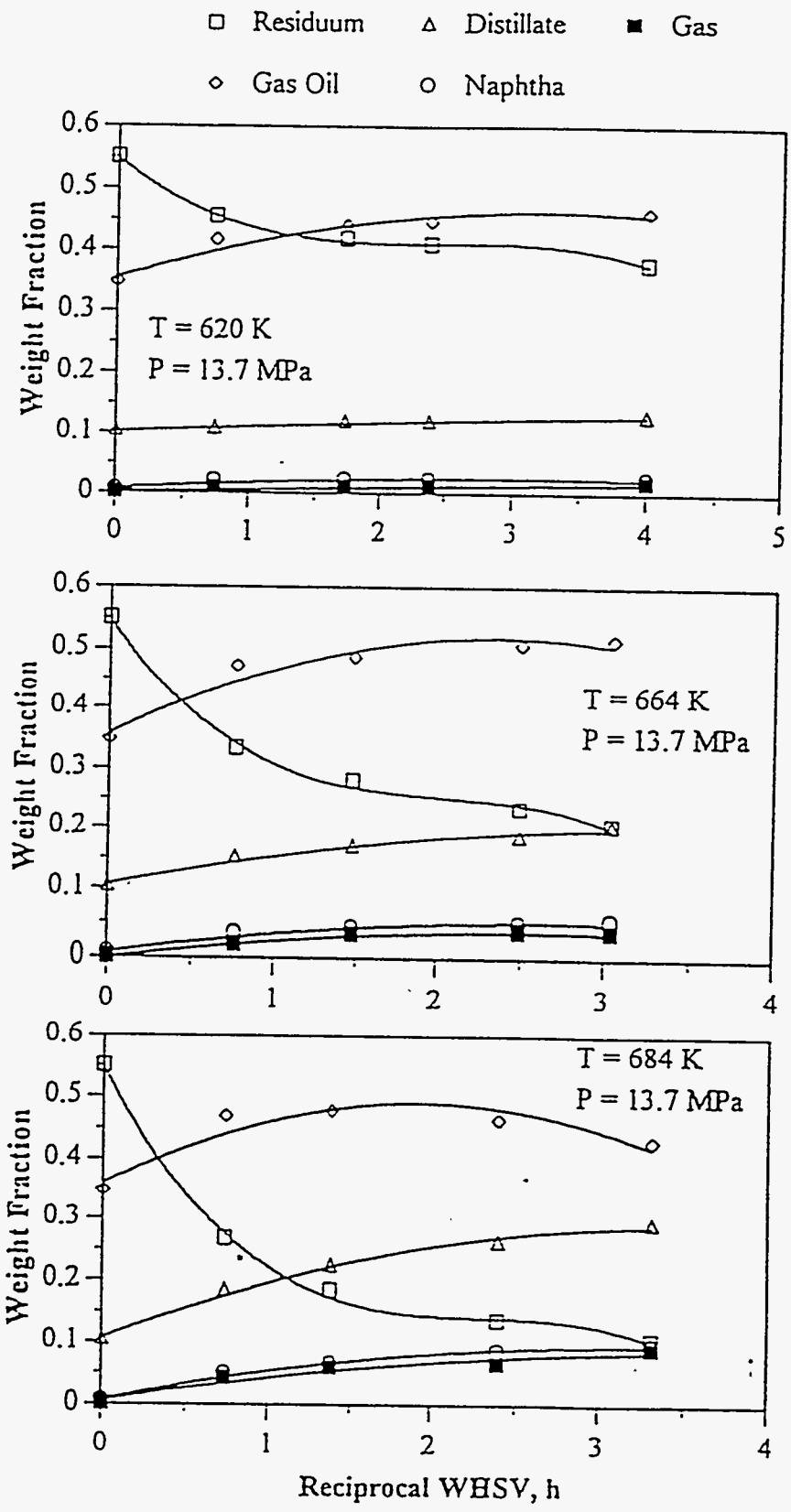
Residuum
Distillate
Gas
Gas Oil
Naphtha
Weight Fraction
T = 620 K
P = 13.7 MPa
T = 664 K
P = 13.7 MPa
T = 684 K
P = 13.7 MPa
Reciprocal WHSV, h

Figure 303

Yields of boiling fraction of bitumen conversion versus reciprocal WHSV

over the B-HDN catalyst at different temperatures

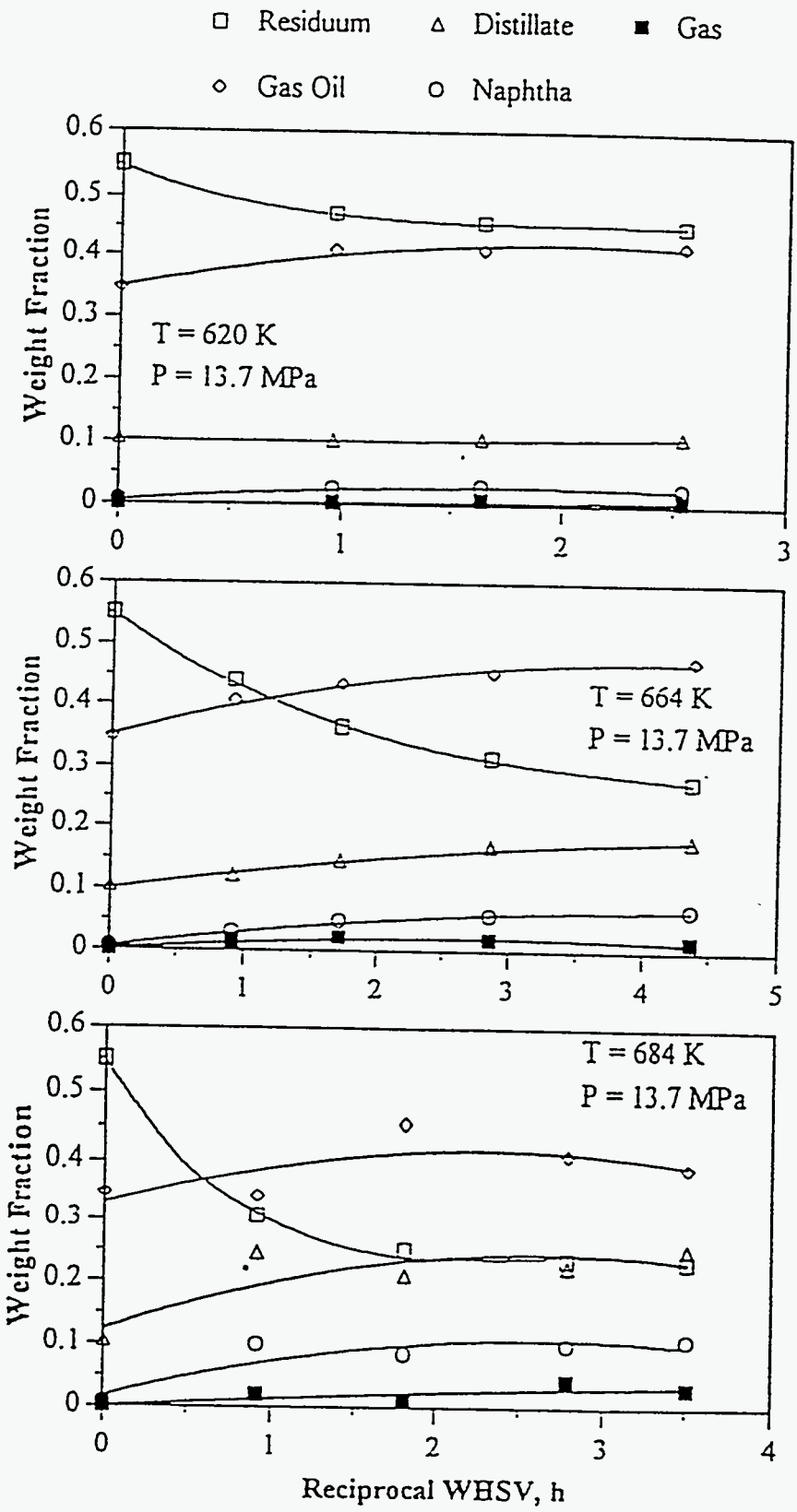
Residuum
Distillate
Gas
Gas Oil
Naphtha
Weight Fraction
T = 620 K
P = 13.7 MPa
T = 664 K
P = 13.7 MPa
T = 684 K
P = 13.7 MPa
Reciprocal WHSV, h

Figure 304

Yields of boiling fraction of bitumen conversion versus reciprocal WHSV over the C-HDN catalyst at different temperatures

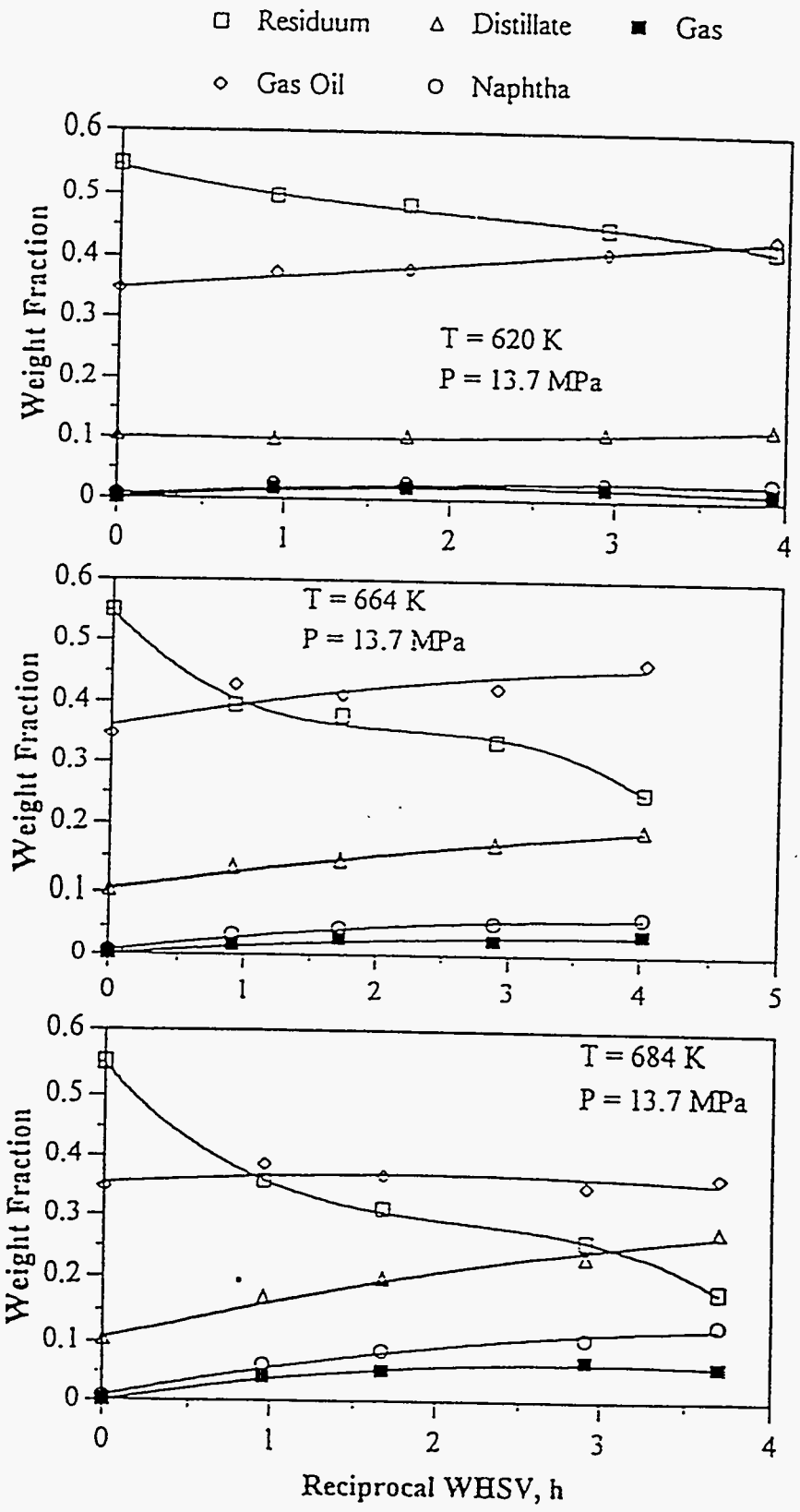
Residuum
Distillate
Gas
Gas Oil
Naphtha
Weight Fraction
T = 620 K
P = 13.7 MPa
T = 664 K
P = 13.7 MPa
T = 684 K
P = 13.7 MPa
Reciprocal WHSV, h

The initial rapid increase in the volatiles (including gas, naphtha, and distillate) yields, and the gas oil yield having a maximum is related to the conversion of native residuum. When the conversion of native residuum to volatiles and gas oil decreases, the yields of volatiles increase as the residence time increase, due to the conversion of the gas oil fraction at the longer residence time, indicating that the produced gas oil undergoes secondary cracking to lower boiling materials.

Effect of Temperature

Removal of Species

The temperature was varied at fixed LHSV and pressure to determine the mean activation energies for conversion from an overall nth power rate law model or from a distributed activation energy model. The mean activation energy of both models for sulfur and nitrogen removal and residuum and CCR conversion over the three HDN catalyst are listed in Table 109 and have similar activation energies for each species conversion except those for sulfur conversion over the A- and C-HDN catalysts.

The influence of temperature on the fractional conversion of sulfur, nitrogen, residuum, CCR, and asphaltenes over the HDN catalyst at constant pressure are illustrated in Figures 305-310. (The effect of temperature on conversions of some species can be also seen in Figures 280-285.) It is observed from the figures that the conversions increased with increasing temperature with the exception of the asphaltenes conversions which exhibit different trends at a LHSV of 0.9 h^{-1} for the three HDN catalysts and at a LHSV of 0.48 h^{-1} for C-HDN catalyst

The relative extents of conversion among the lumped species depended upon temperature and LHSV for each of the HDN catalysts. For example, the conversion of nitrogen over the A-HDN catalyst is the lowest at 620 K and LHSV of 0.9 h^{-1} compared with other species. As the LHSV decreased to 0.2 h^{-1}, the relative conversion of nitrogen was higher than those of residuum and asphaltene.

The temperature dependencies of each species as determined by linear regression of the fractional conversion against temperature data are listed in Table 111. These data indicate that the conversions of the lumped species increase with increasing temperature,

Figure 305

Fractional conversion of lumped species versus temperature

over the A-HDN catalyst at LHSV = 0.2 and 0.28 h^{-1} and constant pressure

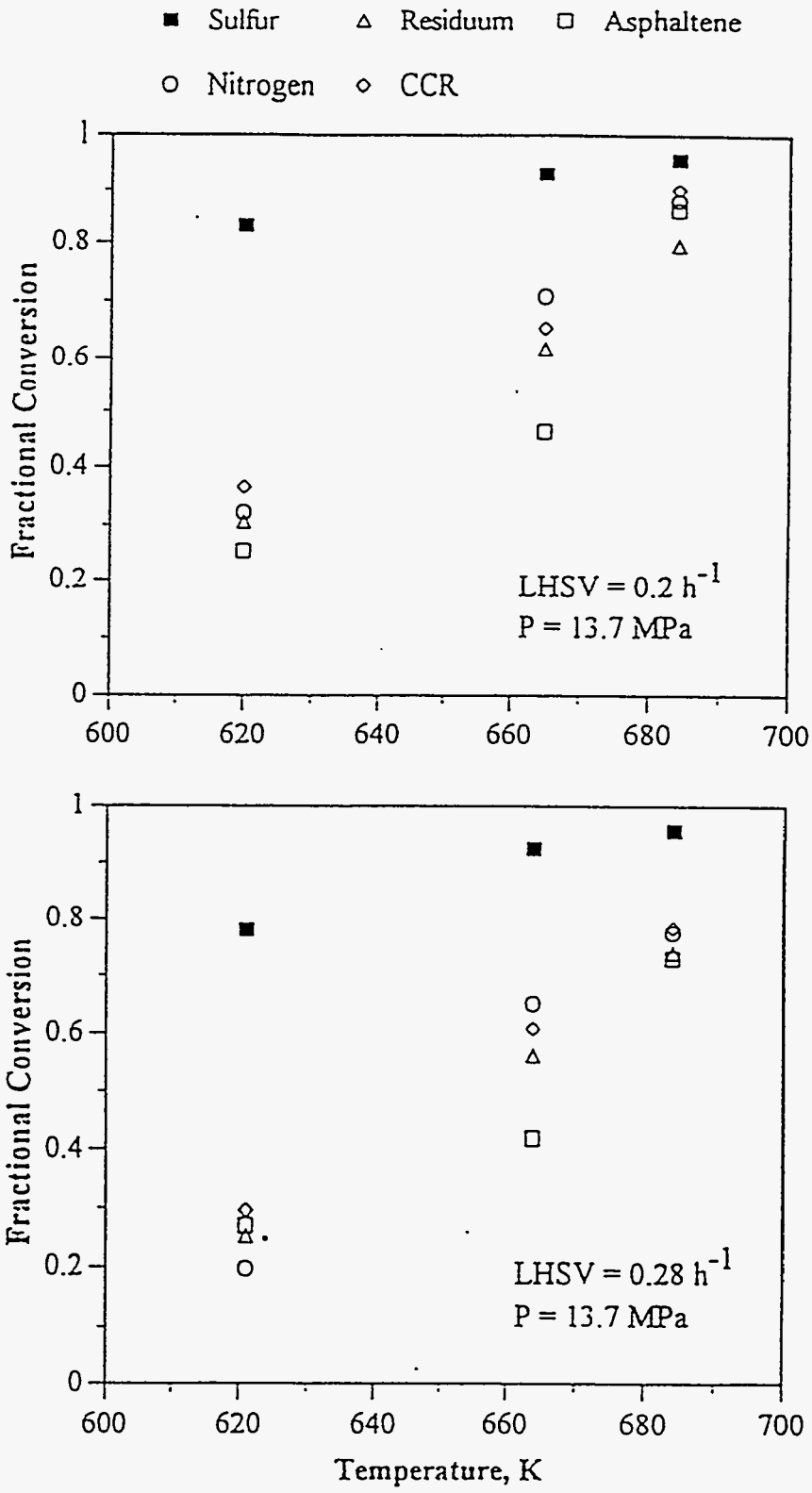
Sulfur
Residuum
Asphaltene
Nitrogen
CCR
Fractional Conversion
LHSV = 0.2 h-1
P = 13.7 MPa
LHSV = 0.28 h-1
P = 13.7 MPa
Temperature, K
0
0.2
0.4
0.6
0.8
1
600
620
640
660
680
700

Figure 306

Fractional conversion of lumped species versus temperature

over the A-HDN catalyst at LHSV = 0.48 and 0.9 h^{-1} and constant pressure

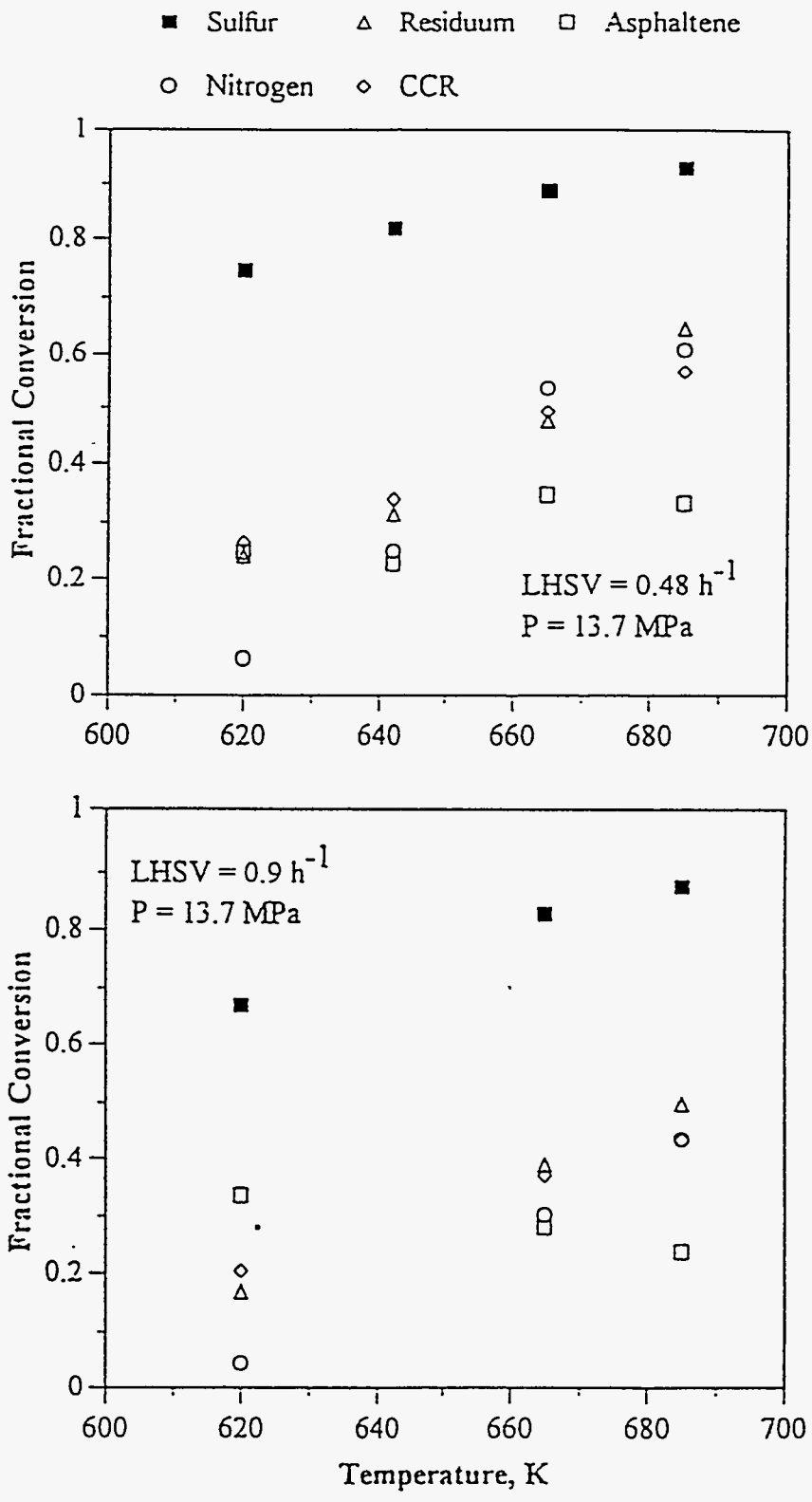
Sulfur
Residuum
Asphaltene
Nitrogen
CCR
Fractional Conversion
LHSV = 0.48 h-1
P = 13.7 MPa
LHSV = 0.9 h-1
P = 13.7 MPa
Temperature, K
0
0.2
0.4
0.6
0.8
1
600
620
640
660
680
700

Figure 307

Fractional conversion of lumped species versus temperature

over the B-HDN catalyst at LHSV = 0.2 and 0.28 h^{-1} and constant pressure

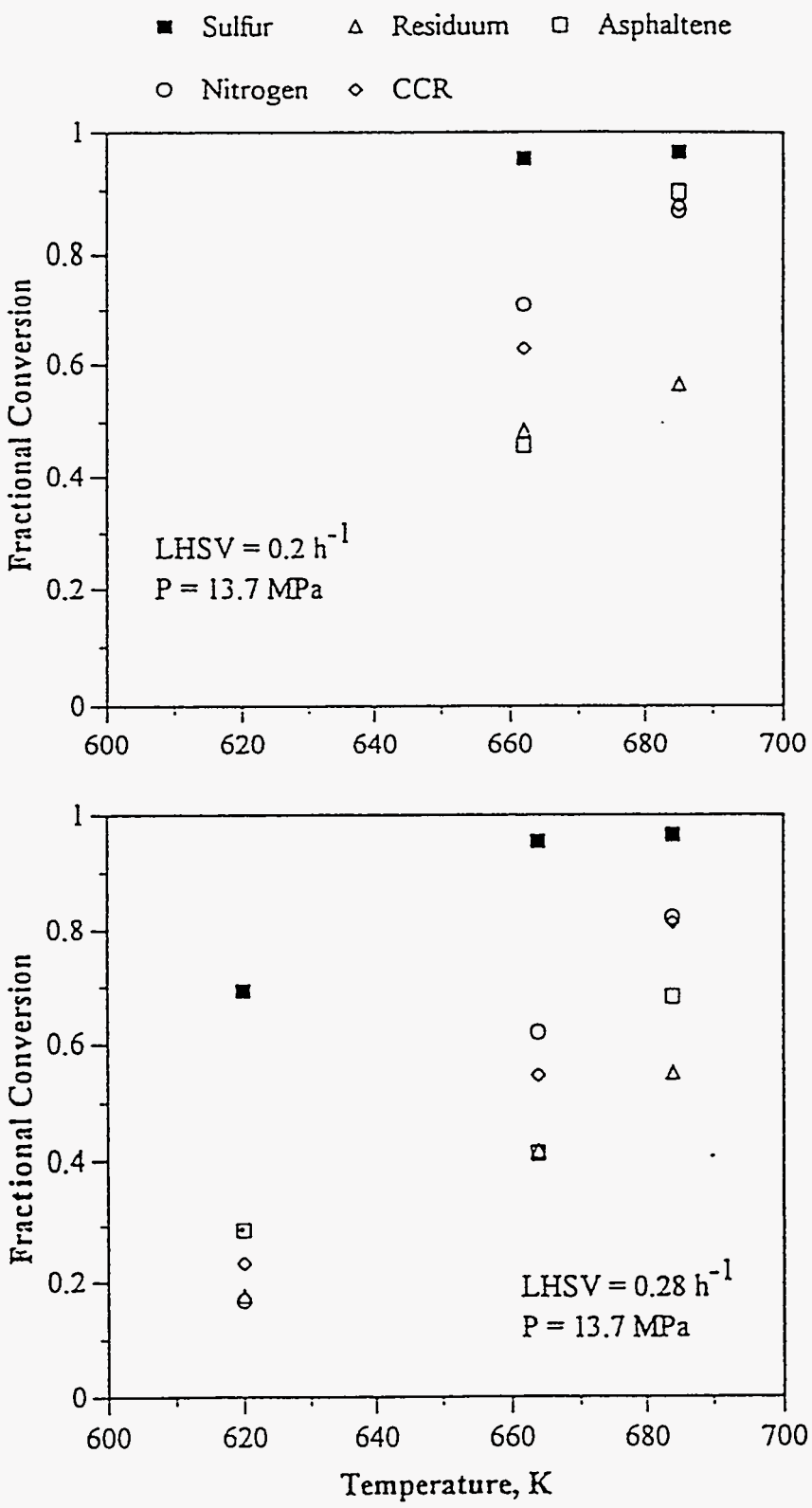
Sulfur
Residuum
Asphaltene
Nitrogen
CCR
Fractional Conversion
LHSV = 0.2 h-1
P = 13.7 MPa
LHSV = 0.28 h-1
P = 13.7 MPa
Temperature, K
0
0.2
0.4
0.6
0.8
1
600
620
640
660
680
700

Figure 308

Fractional conversion of lumped species versus temperature

over the B-HDN catalyst at LHSV = 0.48 and 0.9 h^{-1} and constant pressure

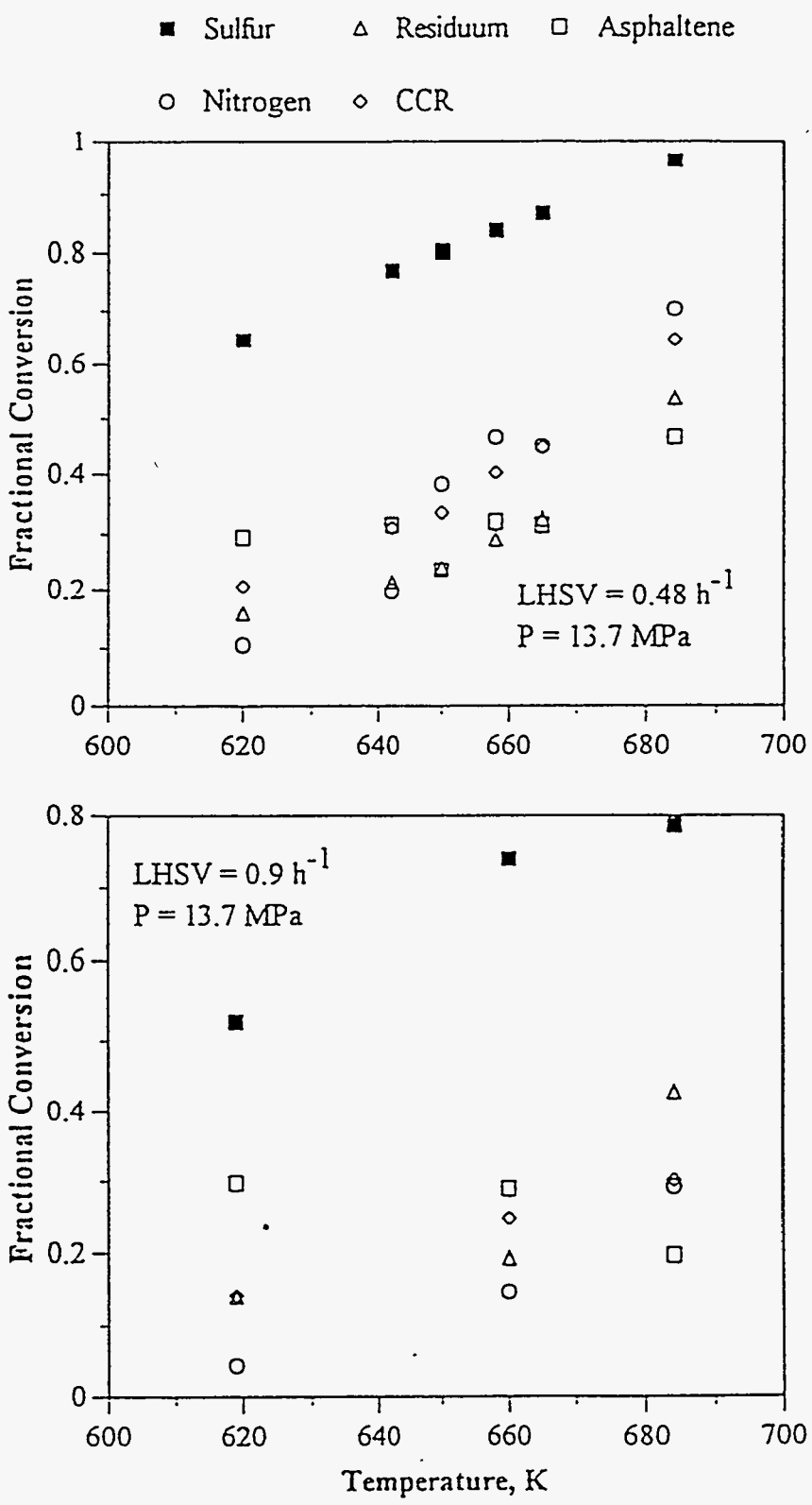
Sulfur
Residuum
Asphaltene
Nitrogen
CCR
Fractional Conversion
LHSV = 0.48 h-1
P = 13.7 MPa
LHSV = 0.9 h-1
P = 13.7 MPa
Temperature, K

Figure 309

Fractional conversion of lumped species versus temperature

over the C-HDN catalyst at LHSV = 0.2 and 0.28 h^{-1} and constant pressure

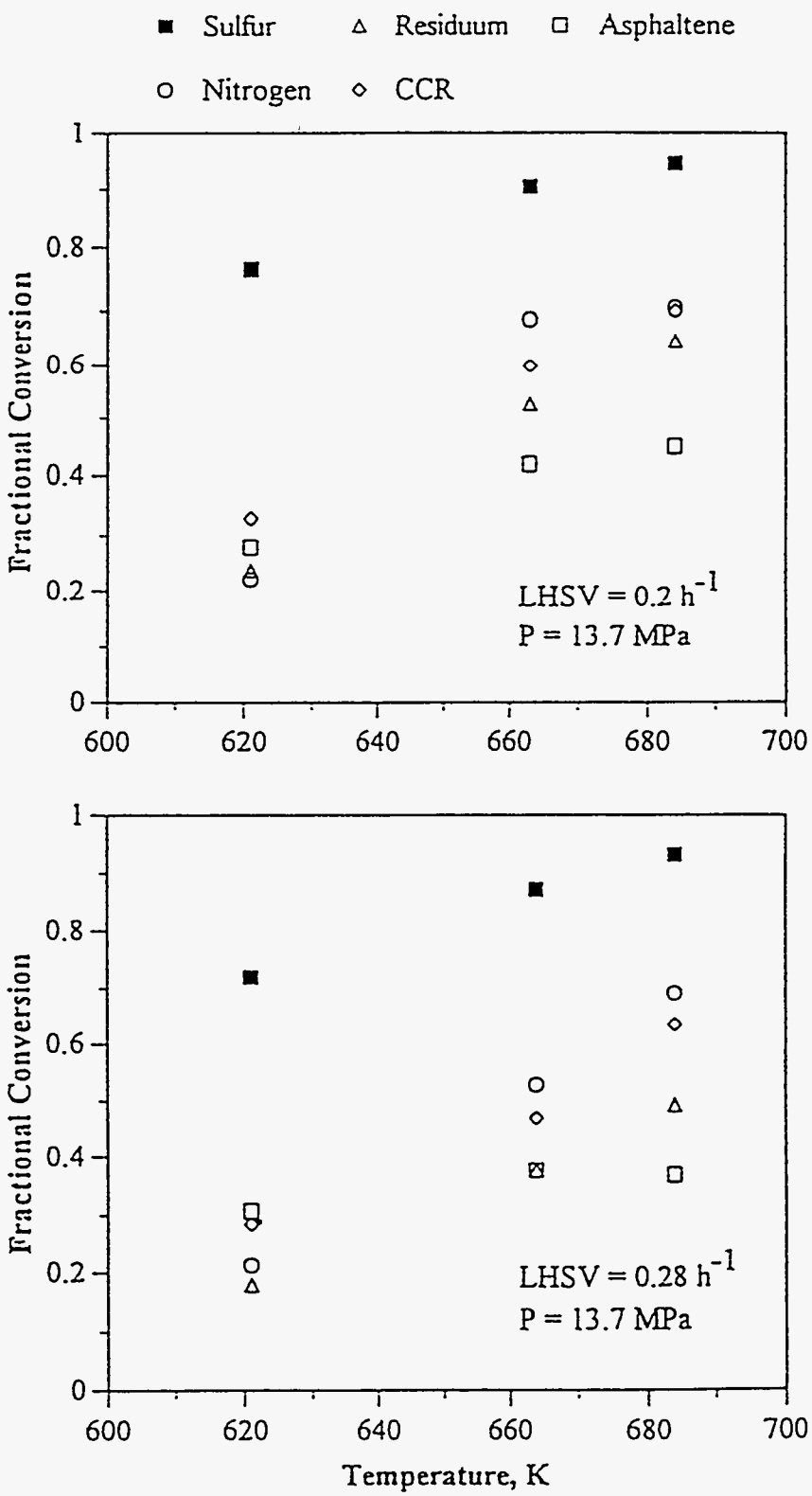
Sulfur
Residuum
Asphaltene
Nitrogen
CCR
Fractional Conversion
LHSV = 0.2 h-1
P = 13.7 MPa
LHSV = 0.28 h-1
P = 13.7 MPa
Temperature, K
0
0.2
0.4
0.6
0.8
1
600
620
640
660
680
700

Figure 310

Fractional conversion of lumped species versus temperature

over the C-HDN catalyst at LHSV = 0.48 and 0.9 h^{-1} and constant pressure

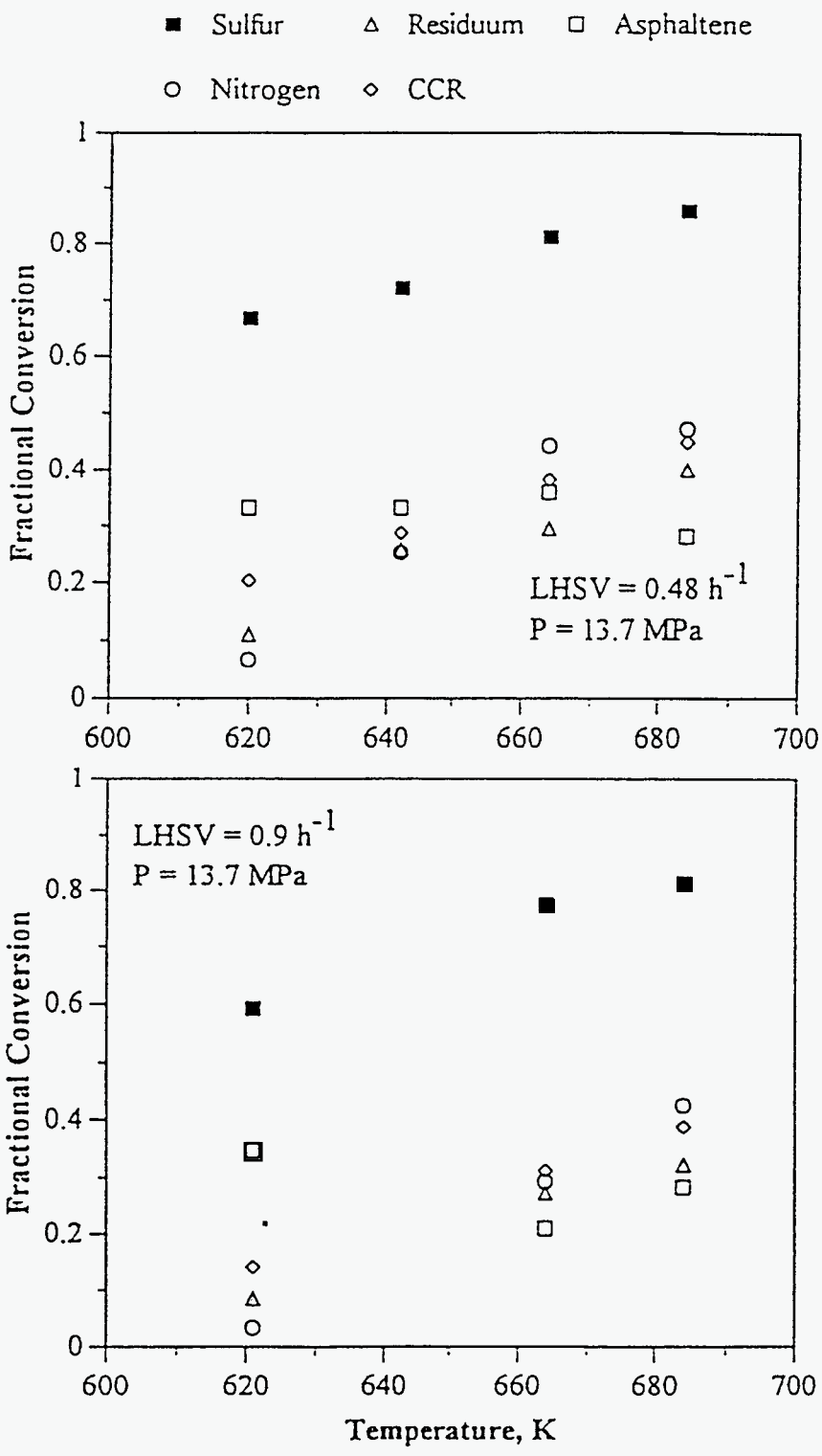
Sulfur
Residuum
Asphaltene
Nitrogen
CCR
Fractional Conversion
LHSV = 0.48 h-1
P = 13.7 MPa
LHSV = 0.9 h-1
P = 13.7 MPa
Temperature, K
0
0.2
0.4
0.6
0.8
1
600
620
640
660
680
700

Table 111

Temperature Dependence of Lumped Species over the HDN Catalysts at Constant Pressure (13.7 MPa)

Catalyst	$\Delta x/\Delta T$ x1000 LHSV, h^{-1}			
	0.2	0.28	0.48	0.9
A-HDN				
Sulfur	2.05	2.88	2.86	3.22
Nitrogen	8.68	9.38	8.89	5.98
Residuum	7.54	9.97	6.35	5.02
CCR	8.00	7.69	4.89	3.56
Asphaltene	8.63	6.70	1.77	-1.48
B-HDN				
Sulfur	5.07	4.53	4.87	4.13
Nitrogen	6.86	10.24	9.52	3.67
Residuum	3.49	5.81	5.69	4.10
CCR	10.77	8.77	6.72	2.46
Asphaltene	19.16	5.56	2.40	-1.38
C-HDN				
Sulfur	2.94	3.39	3.13	3.63
Nitrogen	8.15	7.53	6.62	6.22
Residuum	6.54	4.92	4.24	3.92
CCR	5.92	5.34	3.90	3.92
Asphaltene	2.80	1.06	-0.54	-1.37

x : Fractional Conversion
T: Temperature

except for the asphaltene conversions in which the temperature dependencies are positive or negative depending upon the space velocity.

The relationship between temperature dependence and reciprocal LHSV is plotted in Figure 311. The effects of temperature on sulfur conversion decreased for the A- and C-HDN catalysts and increased slightly for the B-HDN catalyst as the reciprocal LHSV increased. For nitrogen and residuum conversion, the temperature dependencies increased to a maximum (reciprocal LHSV of 3.5 h) and then decreased with increasing reciprocal LHSV for the A- and B-HDN catalysts; however, for the C-HDN catalyst, the temperature effect always increased as reciprocal LHSV increased. This may be related to the fact that the A-and B-HDN catalysts had larger pore volumes than the C-HDN catalyst. The temperature dependence of CCR and asphaltene increase with increasing reciprocal LHSV and the order of temperature effect is B-HDN >> A-HDN > C-HDN catalyst. This result implies that B-HDN catalyst is suitable for CCR and asphaltene conversion.

Nickel removal increased as the temperature increased for the B-HDN catalyst as indicated in Table 88.

Viscosity Reduction

The effect of temperature on viscosity reduction of the bitumen over the HDN catalysts at constant pressure is displayed in Figure 312. As can be seen, viscosity varies considerably with temperature, and the influence of temperature is more than that of reciprocal LHSV. From the performance of catalysts for viscosity reduction, the A-HDN and B-HDN catalysts exhibited similar influence and were superior to the C-HDN catalyst for viscosity reduction.

Lowering the temperature of the fuel products has the influence of increasing its viscosity. In fact, many fuel specifications specify maximum viscosity limits at low temperature to assure pumping and flow capabilities. The variation of viscosity with temperature was a straight line for each LHSV as presented in Figure 312. Therefore, viscosities can be extrapolated over reasonable ranges to a desired temperature; however, caution must be exercised not to extend the extrapolations through phase changes.

Figure 311

Relationship of temperature dependence

with reciprocal LHSV

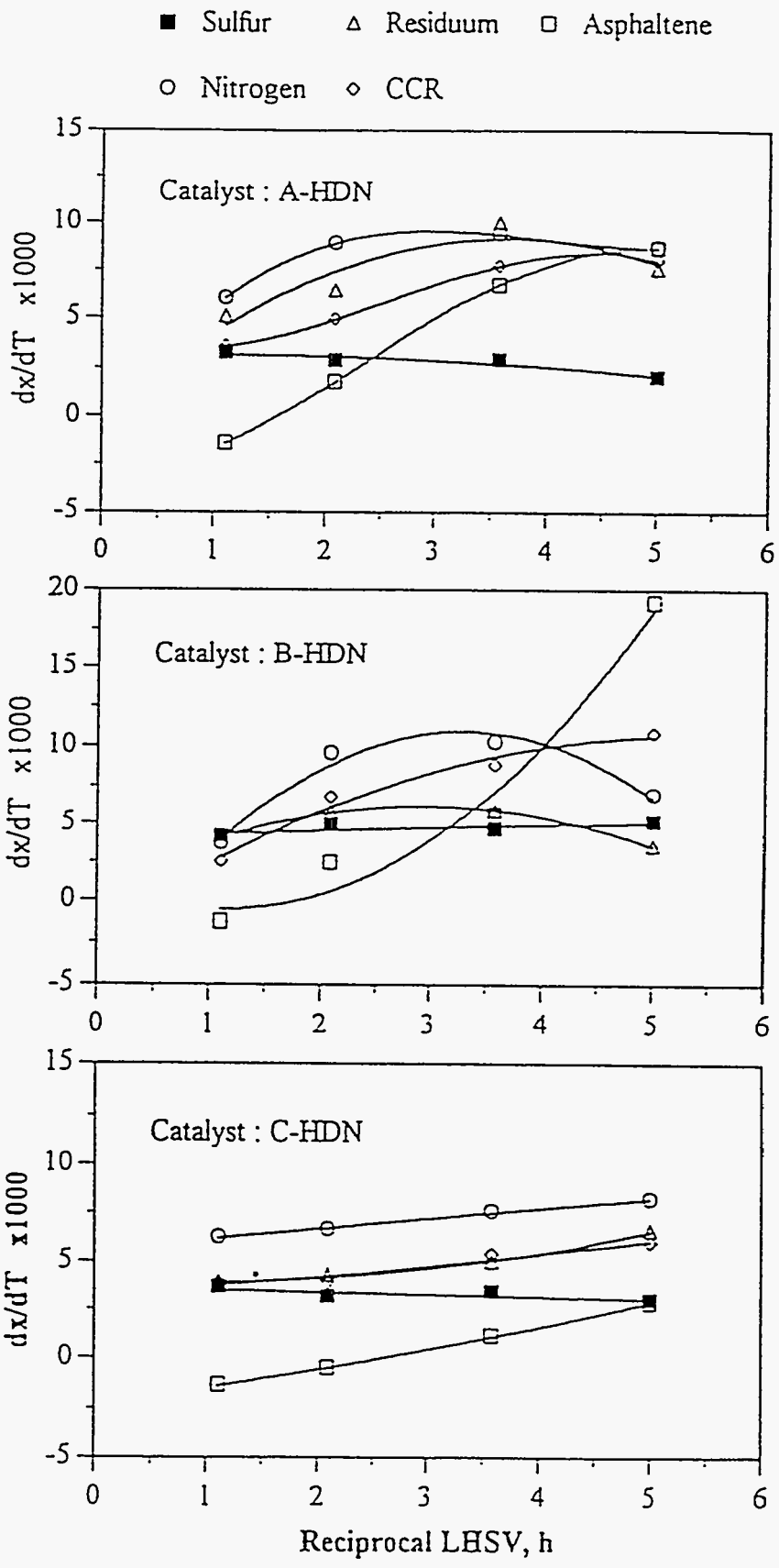
Sulfur
Residuum
Asphaltene
Nitrogen
CCR
Catalyst : A-HDN
Catalyst : B-HDN
Catalyst : C-HDN
dx/dT x1000
Reciprocal LHSV, h

Figure 312

Effect of temperature on viscosity over the HDN catalysts

at different space velocities and constant pressure (13.7 MPa)

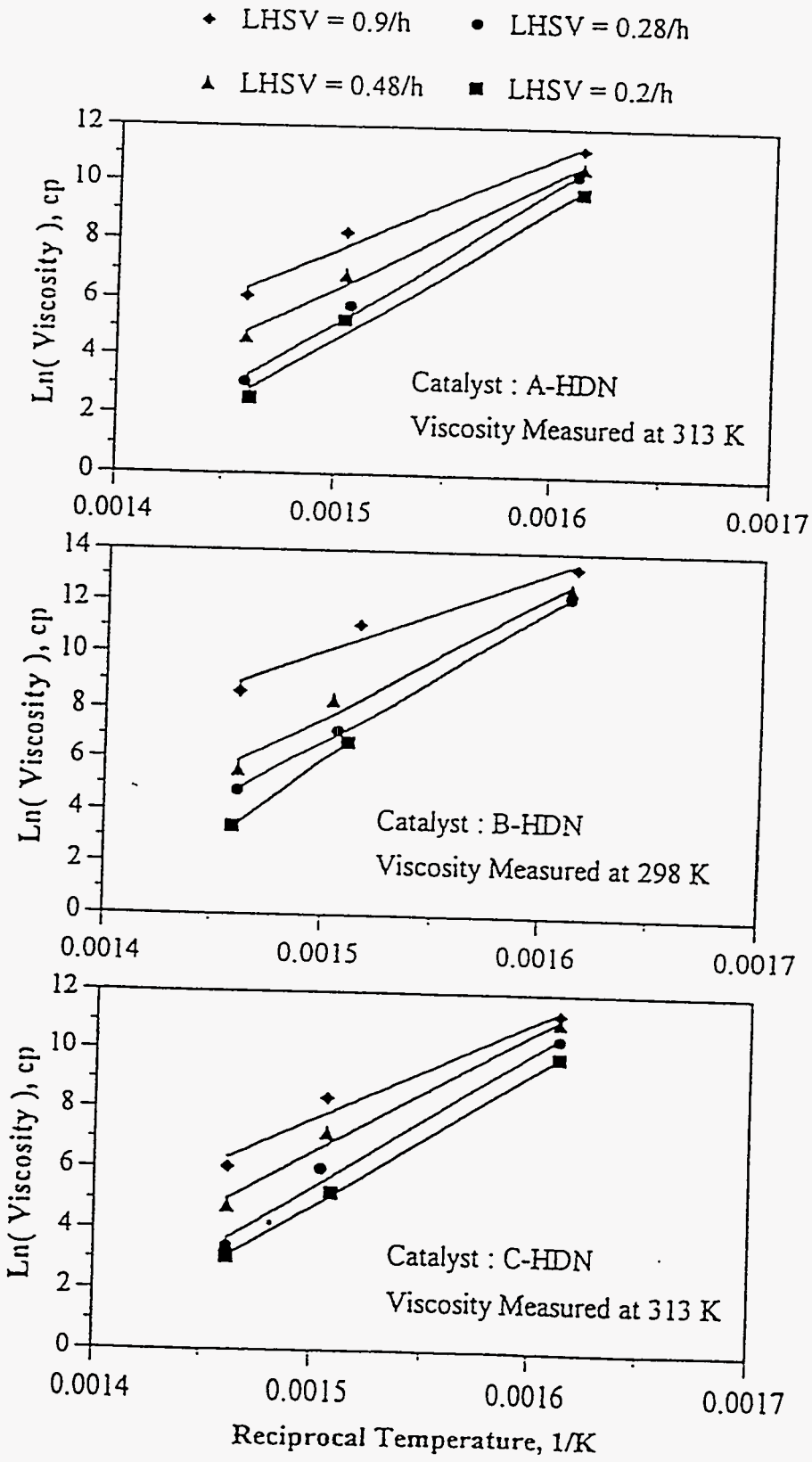
LHSV = 0.9/h
LHSV = 0.28/h
LHSV = 0.48/h
LHSV = 0.2/h
Ln(Viscosity), cp
Catalyst : A-HDN
Viscosity Measured at 313 K
Catalyst : B-HDN
Viscosity Measured at 298 K
Catalyst : C-HDN
Viscosity Measured at 313 K
Reciprocal Temperature, 1/K

The slopes of the straight lines in Figure 312 is equal to $\Delta G^{\bullet} / R$ based on the kinetic approach of Eyring and coworkers(343, 344) where $\Delta G^{\bullet}$ is the change in the molar Gibbs free energy of activation and R is gas constant. This approach is based on the theory of rate processes applied to relaxation processes which may be important in determining the nature of the flow. Equation 173 relates the viscosity to temperature in the form of an Arrehenius equation (detailed procedures of derivation in Reference 344), that is,

$$\mu = \frac{h\lambda_1}{\kappa\lambda^2\lambda_2\lambda_3}\exp(\frac{\Delta G^{\bullet}}{RT}) \qquad (173)$$

where μ is viscosity; h is Plank's constant; κ is a transmission coefficient used to correct for the fact that not all molecules arriving at the activated state pass over the barrier; λ is the distance traveled by the particle; λ_1, λ_2, and λ_3 are molecular distances in three-dimensional coordinates, respectively. Equation 173 is more simply expressed as

$$\mu = A\exp(\frac{\Delta G^{\bullet}}{RT}) \qquad (174)$$

The change in the molar Gibbs free energies of activation, $\Delta G^{\bullet}$, were determined by linear regression of the logarithmic plot of viscosity against reciprocal temperature. The $\Delta G^{\bullet}$ of hydrotreated bitumen over the three HDN catalysts under specific operating conditions are listed in Table 112. Compared to the free energy of activation of water of 3.68 kcal/mol(345), the $\Delta G^{\bullet}$ of hydrotreated bitumen are much higher. The free energies of activation of liquid products increase with increasing temperature and reciprocal LHSV and change slightly with pressure.

It has been shown that free energies of activation correlate well with the internal energy of vaporization, ΔE_{vap}, at the normal boiling point(344), that is,

$$\Delta E_{vap} = 2.45\Delta G^{\bullet} \qquad (175)$$

Table 112

Gibbs Free Energy of Activation and Internal Energy of Vaporization of the Hydrotreated Bitumen Derived Liquid Produced over the HDN Catalysts

T	P	LHSV			A-HDN		B-HDN		C-HDN	
			$\Delta G^{\ddagger}$	ΔE_{vap}	$\Delta G^{\ddagger}$	ΔE_{vap}	$\Delta G^{\ddagger}$	ΔE_{vap}	$\Delta G^{\ddagger}$	ΔE_{vap}
K	MPa	h^{-1}				kcal/mol				
First Pass										
Feed: Raw Bitumen			22.4	54.9						
Products :										
620	13.7	0.2			19.0	46.6			19.1	46.8
620	13.7	0.28			20.2	49.5	22.2	54.4	20.5	50.2
620	13.7	0.48			20.6	50.5	22.6	55.4	21.3	52.2
620	13.7	0.9			21.6	52.9	23.0	56.4	21.9	53.7
650	13.7	0.48					21.0	51.5		
658	13.7	0.48					18.5	45.3		
664	13.7	0.2			12.4	30.4	17.5	42.9	14.1	34.5
664	13.7	0.28			13.4	32.8	17.5	42.9	16.3	39.9
664	13.7	0.48			15.8	38.7	18.3	44.8	19.6	48.0
664	13.7	0.9			19.1	46.8	22.5	55.1	22.5	55.1
664	11.1	0.48			17.1	41.9	17.8	43.6	17.3	42.4
664	15.3	0.48			16.9	41.4	17.3	42.4	17.5	42.9
684	13.7	0.2			8.1	19.8	8.5	20.8	8.0	19.6
684	13.7	0.28			9.1	22.3	10.6	26.0	9.1	22.3
684	13.7	0.48			12.8	31.4	13.5	33.1	12.5	30.6
684	13.7	0.9			16.4	40.2	19.2	47.0	15.1	37.0
Second Pass										
Feed : Hydrotreated Bitumen (Prepared at Base Case Condition)					21.3	52.2				
Product :					19.5	47.8				
Feed : Hydrotreated Bitumen (Prepared at 684 K, 13.7 MPa, and LHSV of 0.2 h^{-1})					7.6	18.6				
Product :					7.5	18.4				

$\Delta H_{vap} = \Delta E_{vap} + RT_b$ [238]

The internal energies of vaporization, ΔE_{vap}, of hydrotreated bitumen are presented in Table 112. Kincaid et al.(344) also derived an equation relating the enthalpy of vaporization and ΔE_{vap} as follow:

$$\Delta H_{vap} = \Delta E_{vap} + RT_b \qquad (176)$$

the heats of vaporization of hydrotreated bitumen could be calculated from Equation 176 if the normal boiling point were known. The suitability of Equation 176 for application to complex mixtures could be demonstrated by comparing experimental data on heat of vaporization of hydrotreated bitumen to the calculated values.

Product Distribution

The yields and distributions of products produced from the bitumen over the three HDN catalysts as a function of temperature at a specific reciprocal LHSV and pressure are plotted in Figures 313-318.

They have the same trend, comparing these figures, as a function of temperature at the same operating conditions. The residuum content decreased increasing temperature. The gas, naphtha, and distillate fractions monotonically increased as the temperature increased. The gas oil yield reached a maximum and then decreased as temperature increased especially at lower reciprocal LHSV; however, the yield of gas oil at a LHSV of 0.48 h^{-1} over the B-HDN catalyst increased monotonically.

The temperatures at which the maximum gas oil yields were produced, T_{max}, depended upon the space velocity and the catalyst. For example, T_{max} at space velocities of 0.2 and 0.28 h^{-1} over the A-HDN catalyst were about 650 and 655 K, respectively, and over the A- and C-HDN catalysts at a LHSV of 0.2 h^{-1} were about 650 and 645 K, respectively.

The effect of temperature on the yield of gas oil was similar to that of residence time. The initial increase in the volatiles (including gas, naphtha, and distillate) and the gas oil results from the conversion of native residuum. When the conversion of native residuum to volatiles and gas oil decreases, the yields of volatiles kept increasing with

Figure 313

Yields of boiling fraction of bitumen conversion versus temperature

over the A-HDN catalyst at LHSV = 0.2 and 0.28 h^{-1} and constant pressure

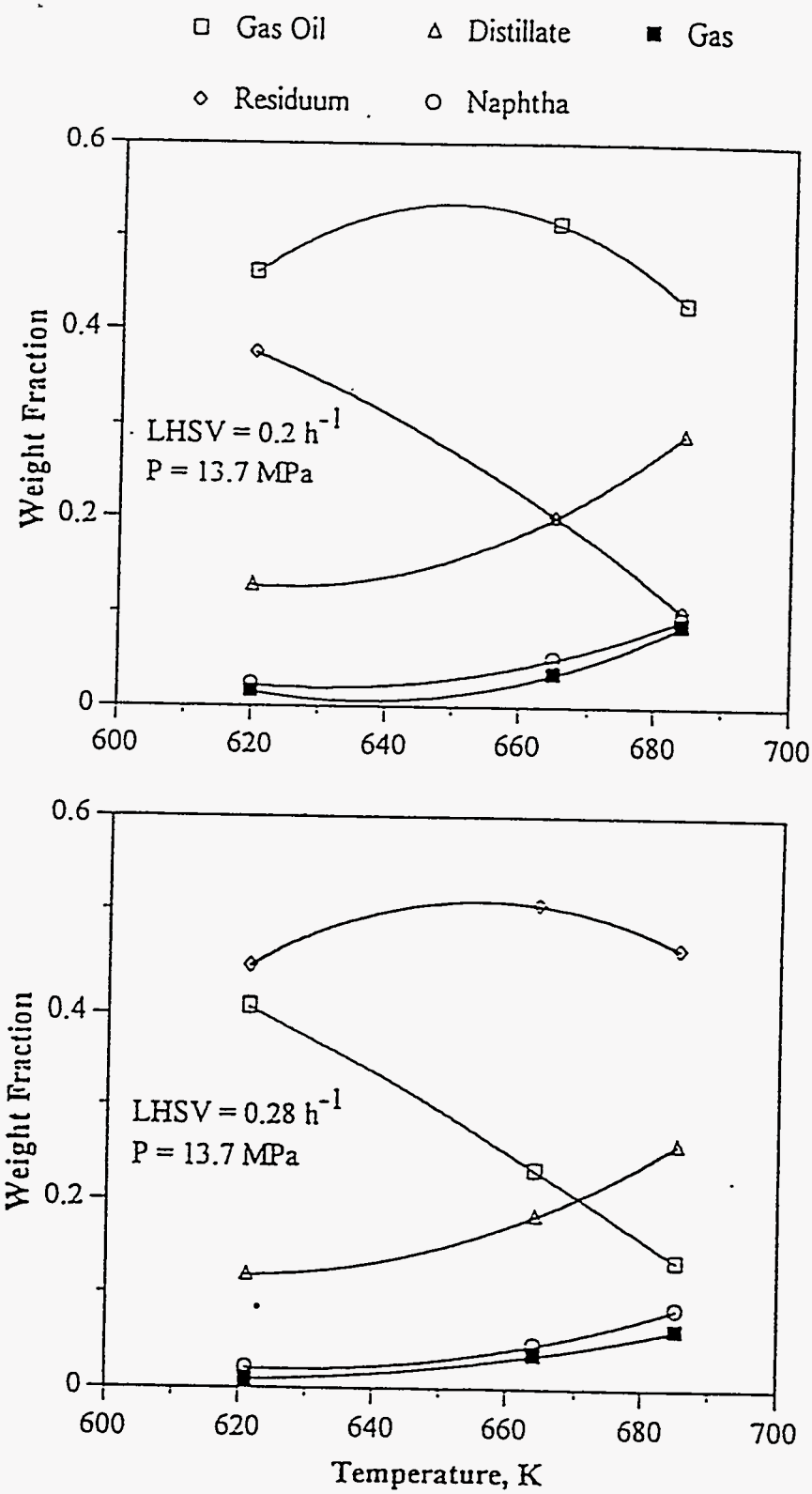
Gas Oil
Distillate
Gas
Residuum
Naphtha
Weight Fraction
LHSV = 0.2 h-1
P = 13.7 MPa
LHSV = 0.28 h-1
P = 13.7 MPa
Temperature, K
0
0.2
0.4
0.6
600
620
640
660
680
700

Figure 314

Yields of boiling fraction of bitumen conversion versus temperature over the A-HDN catalyst at LHSV = 0.48 and 0.9 h^{-1} and constant pressure

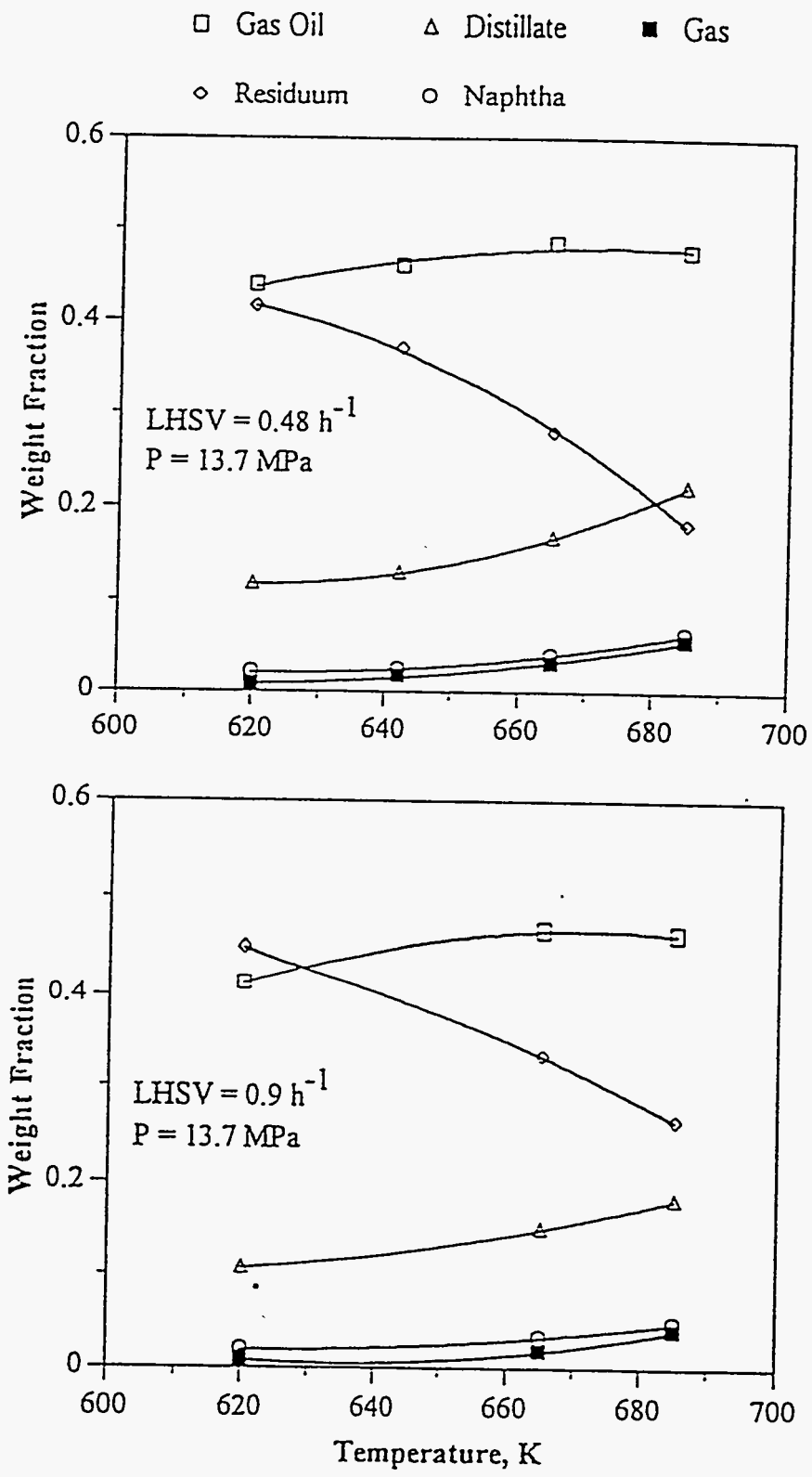
Gas Oil
Distillate
Gas
Residuum
Naphtha
0.6
0.4
0.2
0
Weight Fraction
LHSV = 0.48 h-1
P = 13.7 MPa
600
620
640
660
680
700
LHSV = 0.9 h-1
P = 13.7 MPa
Temperature, K

Figure 315

Yields of boiling fraction of bitumen conversion versus temperature

over the B-HDN catalyst at LHSV = 0.2 and 0.28 h^{-1} and constant pressure

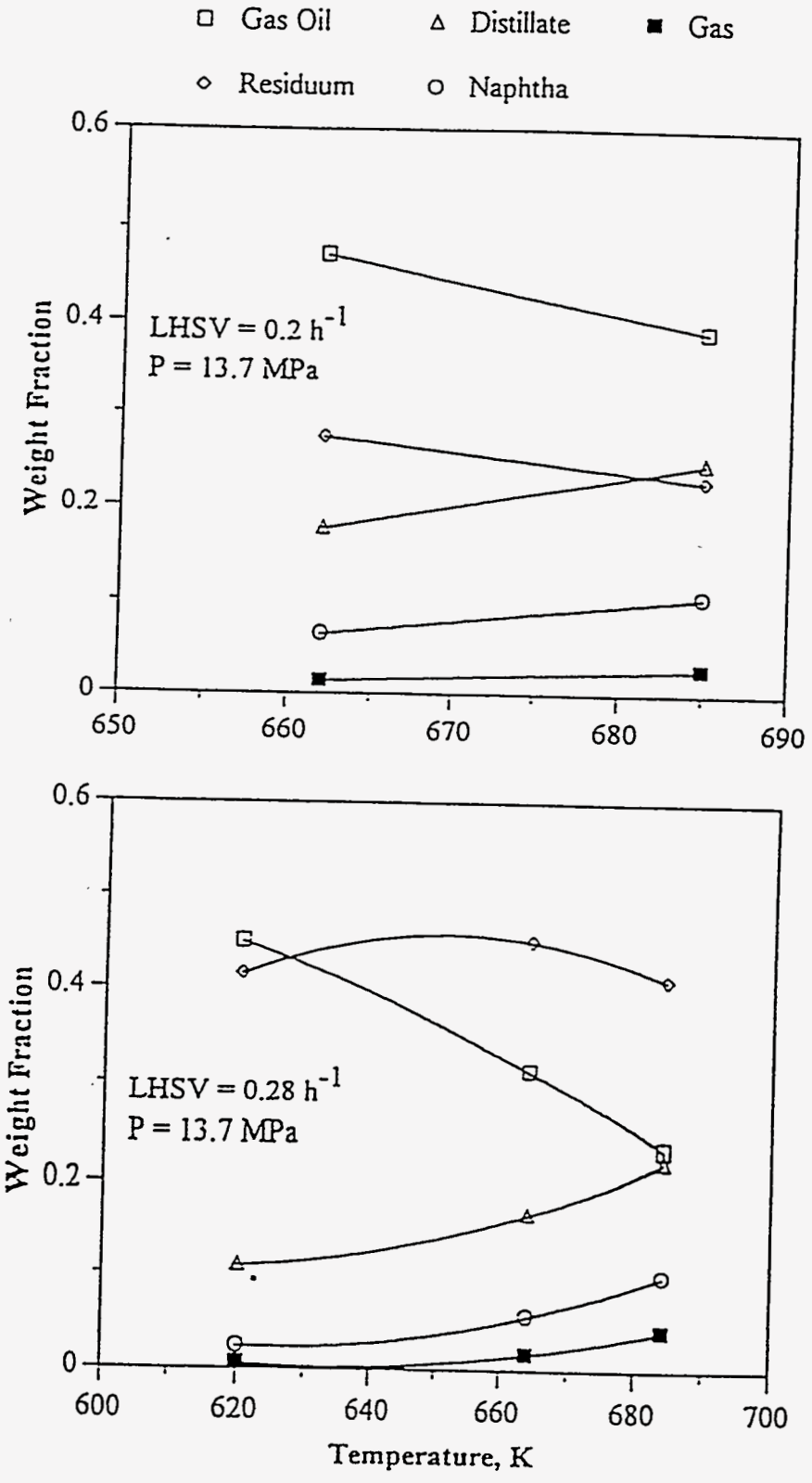
Gas Oil
Distillate
Gas
Residuum
Naphtha
0.6
0.4
0.2
0
Weight Fraction
LHSV = 0.2 h-1
P = 13.7 MPa
650
660
670
680
690
LHSV = 0.28 h-1
P = 13.7 MPa
600
620
640
660
680
700
Temperature, K

Figure 316

Yields of boiling fraction of bitumen conversion versus temperature

over the B-HDN catalyst at LHSV = 0.48 and 0.9 h^{-1} and constant pressure

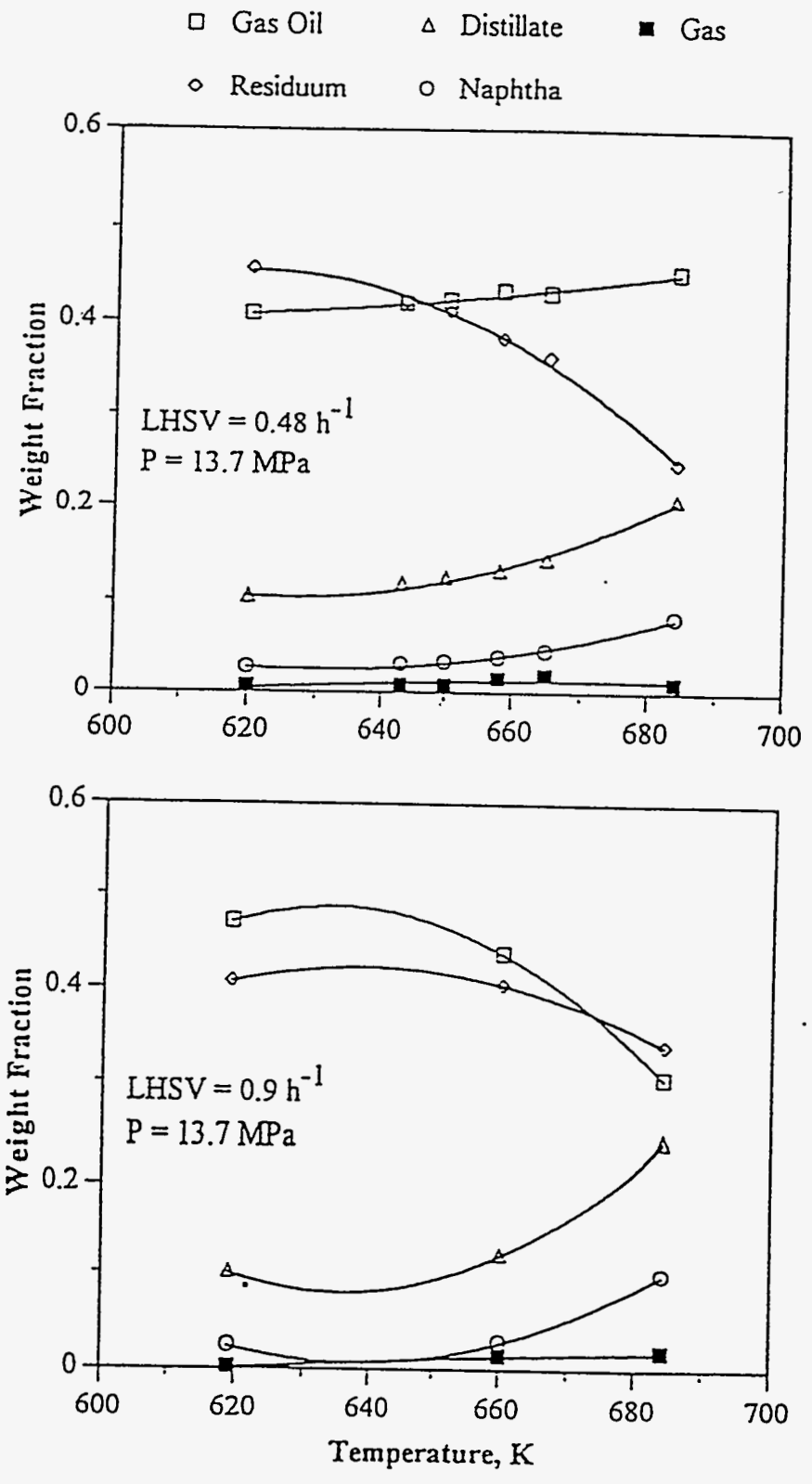
Gas Oil
Distillate
Gas
Residuum
Naphtha
0.6
0.4
0.2
0
Weight Fraction
LHSV = 0.48 h-1
P = 13.7 MPa
600
620
640
660
680
700
LHSV = 0.9 h-1
P = 13.7 MPa
Temperature, K

Figure 317

Yields of boiling fraction of bitumen conversion versus temperature over the C-HDN catalyst at LHSV = 0.2 and 0.28 h^{-1} and constant pressure

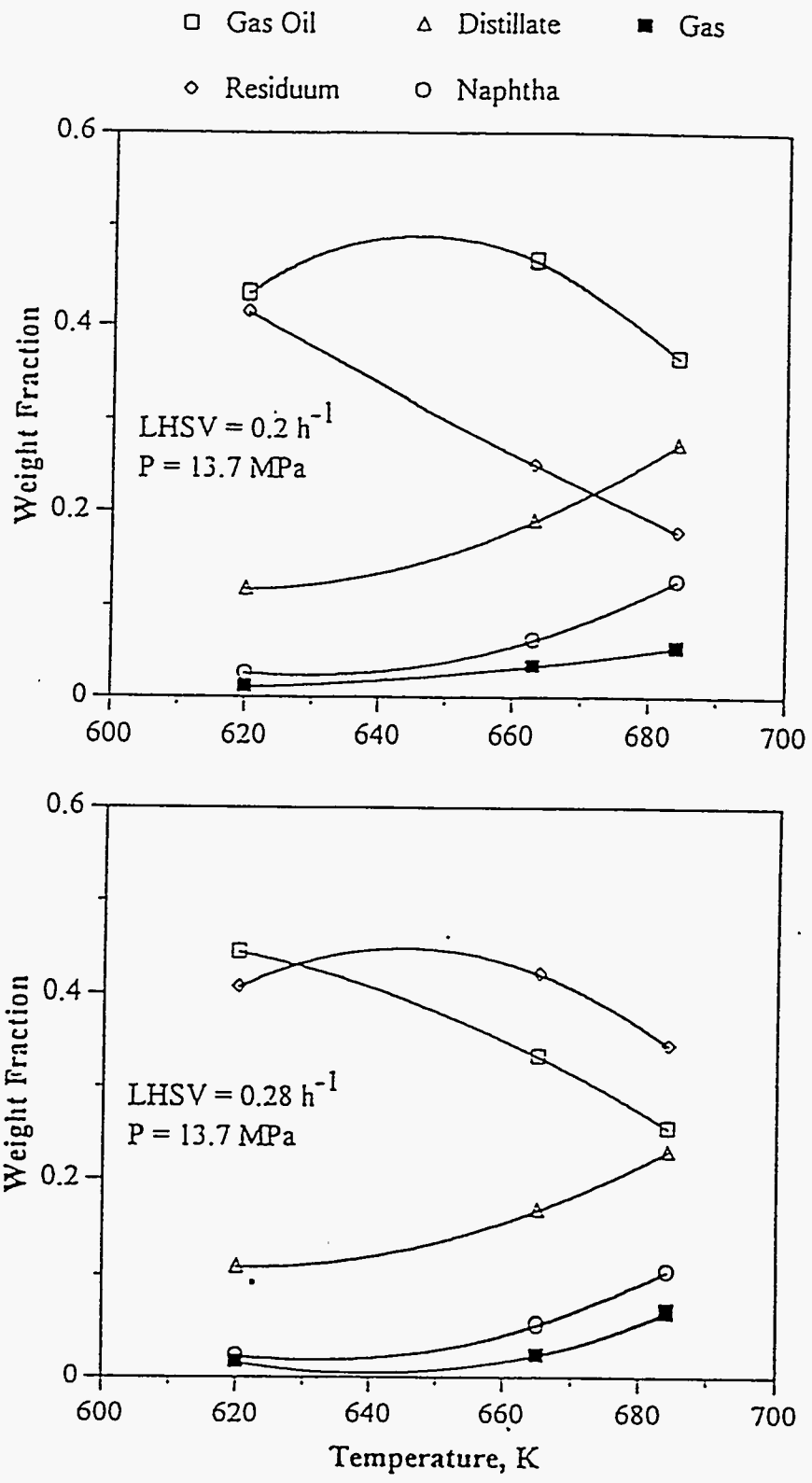
Gas Oil
Distillate
Gas
Residuum
Naphtha
Weight Fraction
LHSV = 0.2 h-1
P = 13.7 MPa
LHSV = 0.28 h-1
P = 13.7 MPa
Temperature, K
0
0.2
0.4
0.6
600
620
640
660
680
700

Figure 318

Yields of boiling fraction of bitumen conversion versus temperature

over the C-HDN catalyst at LHSV = 0.48 and 0.9 h^{-1} and constant pressure

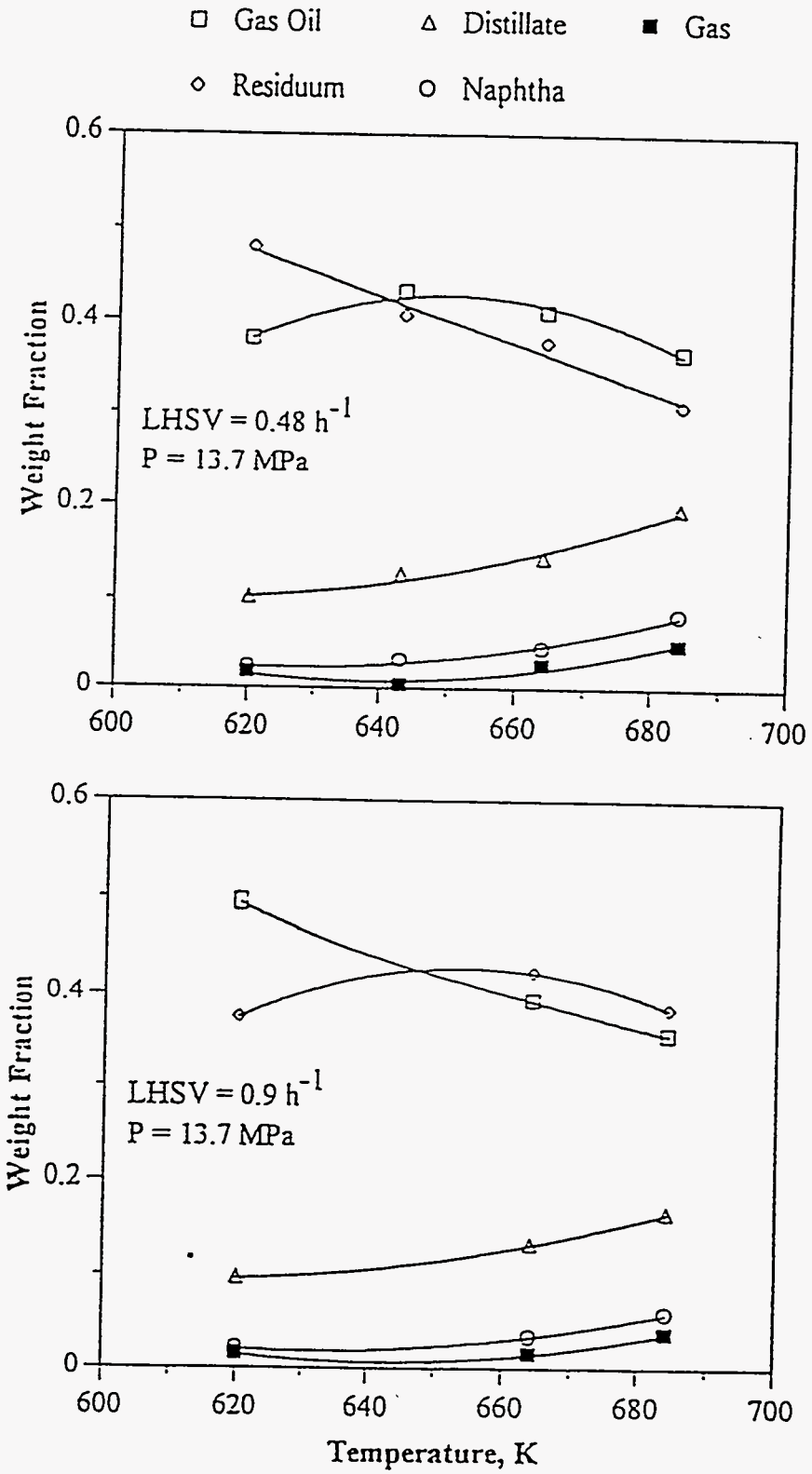
Gas Oil
Distillate
Gas
Residuum
Naphtha
Weight Fraction
LHSV = 0.48 h-1
P = 13.7 MPa
LHSV = 0.9 h-1
P = 13.7 MPa
Temperature, K

increased temperature; however, the yield of gas oil passed through a maximum and then decreased with increasing temperature. This indicated that the produced gas oil underwent secondary cracking to lower boiling materials at the higher temperature.

Effect of Pressure

Removal of Species

When the effects of WHSV and temperature were investigated, the reaction order (n) and apparent rate constant (k) were determined (shown in Table 103) at constant total system pressure. When the system operated at fixed space velocity and temperature, the reaction order of each species for each HDN catalyst did not change with pressure. The effect of pressure was studied at a specific reaction order by assuming that apparent rate constant was related to the partial pressure of hydrogen in the power rate law.

The reaction order (β) of hydrogen partial pressure was determined from the logarithmic plot of the apparent rate constant versus hydrogen partial pressure which yielded a straight line with a slope that is equal to β. The apparent rate constants and hydrogen partial pressure reaction orders at a temperature of 664 K and LHSV of 0.48 h^{-1} over the three HDN catalysts are presented in Table 113. The values of β are positive except for sulfur conversion over the B-HDN catalyst. Comparing the β for each species, the reaction order, β, of hydrogen partial pressure depends on the catalyst employed.

The hydrogen partial pressure reaction orders (β) for sulfur conversion over the A-, B-, and C-HDN catalysts were 0.57, -0.19, and 1.78, respectively. $\beta < 0$ for sulfur conversion suggested that the sulfur removal was inhibited as hydrogen partial pressure increased. This disagrees with the chemistry of hydroprocessing. The TOS should be considered in order to understand the reason for this phenomena. The TOS of data measured were 340, 244, and 507 h for pressure at 11, 13.7, and 15 MPa, respectively. The data obtained at 244 and 340 h of TOS indicated β is 0.04. The positive value but close to zero of β is easily affected by deactivation of catalyst via increasing TOS. For sulfur removal of Athabasca bitumen-derived coker gas oil, the β varied from 0.6 to 1.1(312). Longstaff(292) reported that the $\beta \approx 0$ for Whiterocks bitumen over HDN

Table 113

Apparent Rate Constant (k) and Reaction Order (β) of Hydrogen Partial Pressure Determined from nth Power Rate Law at T = 664 K and LHSV = 0.48 h^{-1}

	Pressure, MPa			
Catalyst	11	13.7	15	
		k		β
A-HDN				
Sulfur	22.69	33.35	26.17	0.57
Nitrogen	0.311	0.587	0.491	1.55
Residuum	2.94E-5	4.59E-5	8.12E-5	2.98
CCR	1.31E-2	2.09E-3	1.79E-3	1.06
B-HDN				
Sulfur	4.09	4.12	3.82	-0.19
Nitrogen	0.231	0.432	0.605	3.07
Residuum	1.58E-5	1.76E-5	1.85E-5	0.50
CCR	9.25E-2	1.01E-1	9.84E-2	0.22
C-HDN				
Sulfur	13.87	35.12	20.96	1.78
Nitrogen	0.222	0.441	0.235	0.66
Residuum	1.63E-5	1.97E-5	5.68E-5	3.45
CCR	2.17E-3	3.92E-3	2.66E-3	0.98

catalyst. The β = 0.7 for Whiterocks bitumen over HDM catalyst was reported by Kwak(342).

For nitrogen removal, the β's are 1.55, 3.07, and 0.66 for the A-, B-, and C-HDN catalysts, respectively. These data indicate that the HDN activity of the catalyst increased with increasing the hydrogen partial pressure. This result agrees with data relating to known mechanisms of HDN, which indicate that the hydrogenation of aromatic ring is important for nitrogen removal. Yui(312) reported that the range of β varied from 1.2 to 1.8 for nitrogen removal of Athabasca bitumen-derived coker gas oil. Previous studies(243, 292, 342) found that the reaction orders, β, of hydrogen partial pressure were 0.74 and 0.67 for Whiterocks bitumen and the bitumen-derived liquid oil over an HDN catalyst, respectively, and 1.5 for Whiterocks bitumen over an HDM catalyst, and 0.67 for the PR Spring bitumen over the B-HDN catalyst.

The hydrogen partial pressure reaction orders, β, for residuum and CCR conversions are positive. This indicates that the activities for residuum and CCR conversions increased as the hydrogen partial pressure increased. The A- and C-HDN catalysts appeared to exert a greater influence on residuum and CCR conversions than the B-HDN catalyst as indicated by the value of β. Kwak(342) reported that the reaction orders (β) of hydrogen partial pressure were 0.8 for residuum and CCR conversions over an HDM catalyst.

The effect of pressure on the conversions of asphaltenes and nickel is presented in Figure 319. This figure indicates that the activities of the catalyst for asphaltenes and nickel conversions increased with increasing the hydrogen partial pressure.

Viscosity Reduction

The influence of pressure on viscosity reduction during bitumen hydrotreating over the three HDN catalysts is presented in Figure 320. The viscosity decreased with increasing pressure for the B-HDN catalyst but increased as pressure increased for the A- and C-HDN catalysts. The slope of ln(μ) versus pressure are very small, about $\pm$ 0.004. The effect of pressure, therefore, on viscosity is not significant.

Figure 319

Effect of pressure on asphaltenes and nickel conversions

over the HDN catalysts at LHSV = 0.48 h^{-1} and T = 664 K

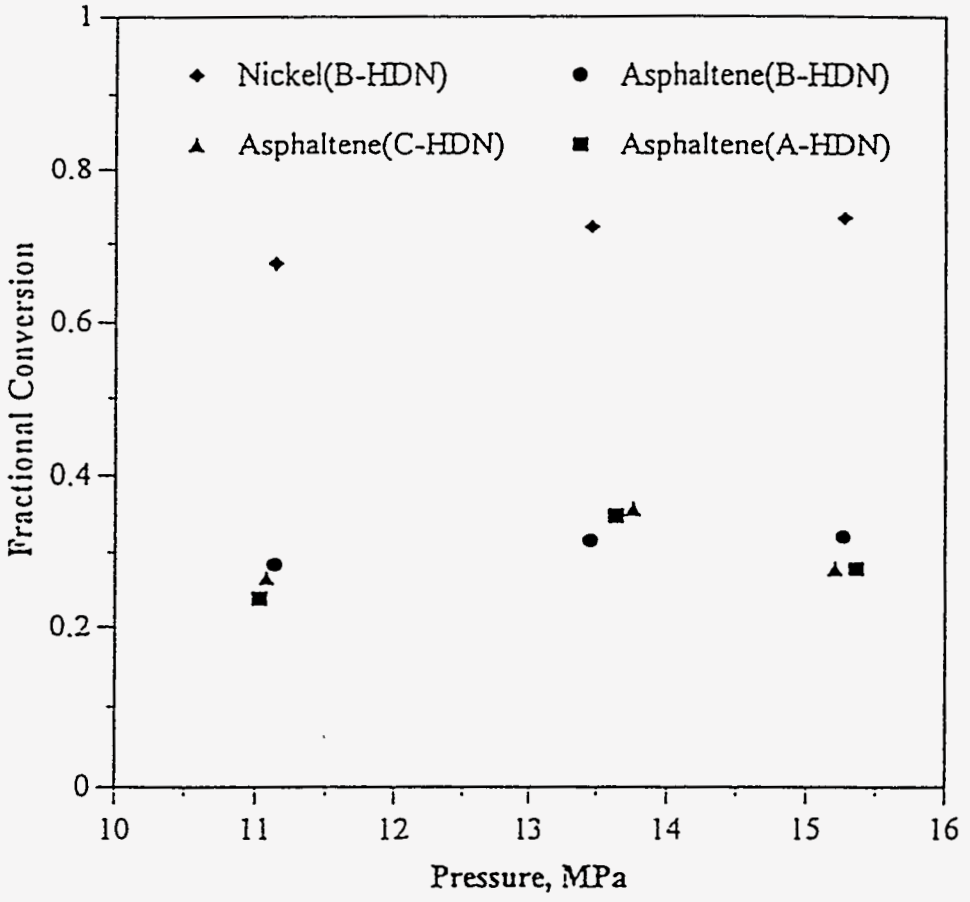
Nickel(B-HDN)
Asphaltene(B-HDN)
Asphaltene(C-HDN)
Asphaltene(A-HDN)
Fractional Conversion
Pressure, MPa
0
0.2
0.4
0.6
0.8
1
10
11
12
13
14
15
16

Figure 320

Effect of pressure on viscosity over the HDN catalysts

at LHSV = 0.48 h^{-1} and T = 664 K

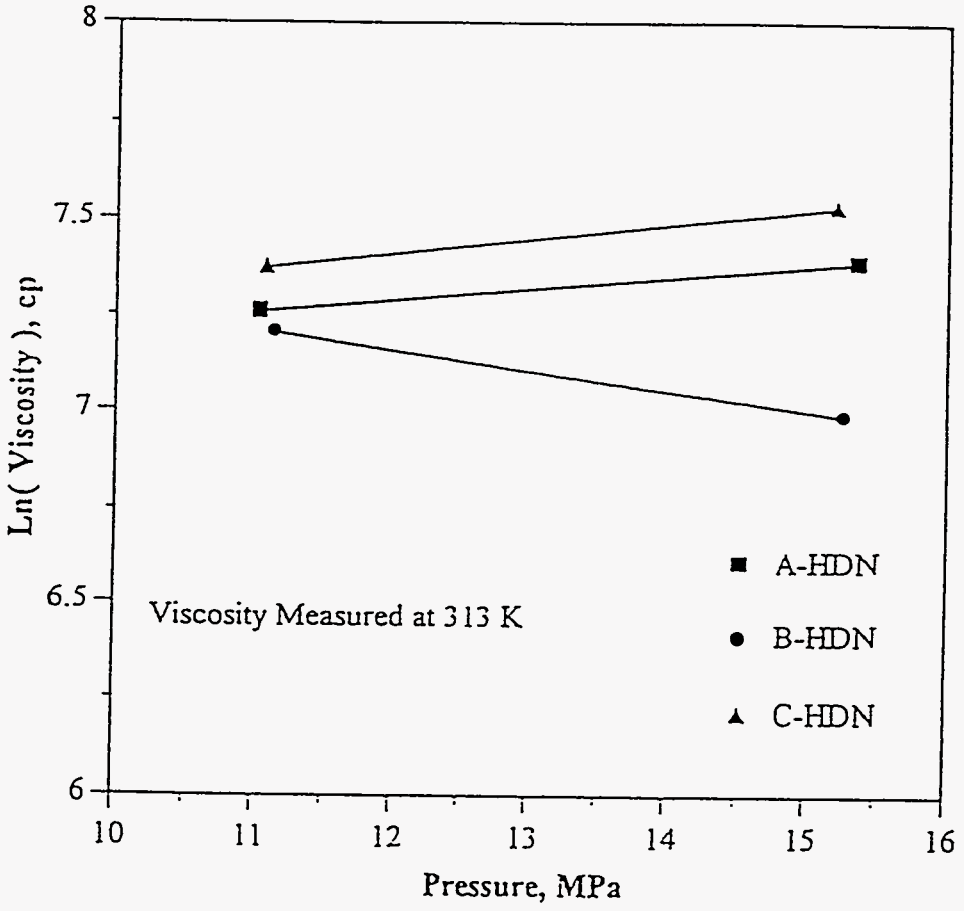
8
7.5
7
6.5
6
Ln(Viscosity), cp
10
11
12
13
14
15
16
Pressure, MPa
Viscosity Measured at 313 K
A-HDN
B-HDN
C-HDN

With the effect of process variables on viscosity reduction, the order is temperature dependence >> residence time dependence >> pressure dependence. For example, there were a 1000-fold reduction in viscosity from 620 to 684 K, a 50-fold reduction from LHSV of 0.9 to 0.2 h^{-1}, and only a 20% reduction from 11 to 15 MPa over the B-HDN catalyst.

Product Distribution

The yields and distributions of products produced from the bitumen over the three HDN catalysts as a function of pressure at a temperature of 664 K and a LHSV of 0.48 h^{-1} are displayed in Figure 321.

The residuum content decreased as the pressure increased. The concentration of gas oil and distillate increased with increasing pressure, with gas oil yield increasing at a relatively higher rate. The weight fraction of gas and naphtha did not change significantly with pressure. Thus, the residuum converted mostly to the gas oil fraction and to distillate fractions.

Evaluation of Catalyst Performance

An evaluation of the performance of the three HDN catalysts (their chemical composition and physical properties shown in Table 83) was accomplished as a function of process variables. The effect of catalysts on nitrigen, sulfur, and nickel removal; on residuum, CCR, and asphaltenes conversion; and on viscosity reduction were determined for the Asphalt Ridge bitumen.

Hydrodenitrogenation

Nitrogen in bitumen is present mostly in heterocyclic aromatic compounds. Nitrogen removal from these organonitrogen compounds, classed as basic and nonbasic, requires hydrogenation of the ring containing the nitrogen atom before hydrogenolysis of the carbon-nitrogen bond occurs. The relatively large energy of the carbon-nitrogen bonds is reduced through the hydrogenation of the heteroring. Thus, HDN is a process in which organonitrogen compounds are converted into hydrocarbon products and ammonia. Nitrogen reduction is required to minimize acid catalyst poisoning, especially

Figure 321

Yields of boiling fraction of bitumen conversion versus pressure

over the HDN catalysts at LHSV = 0.48 h^{-1} and T = 664 K

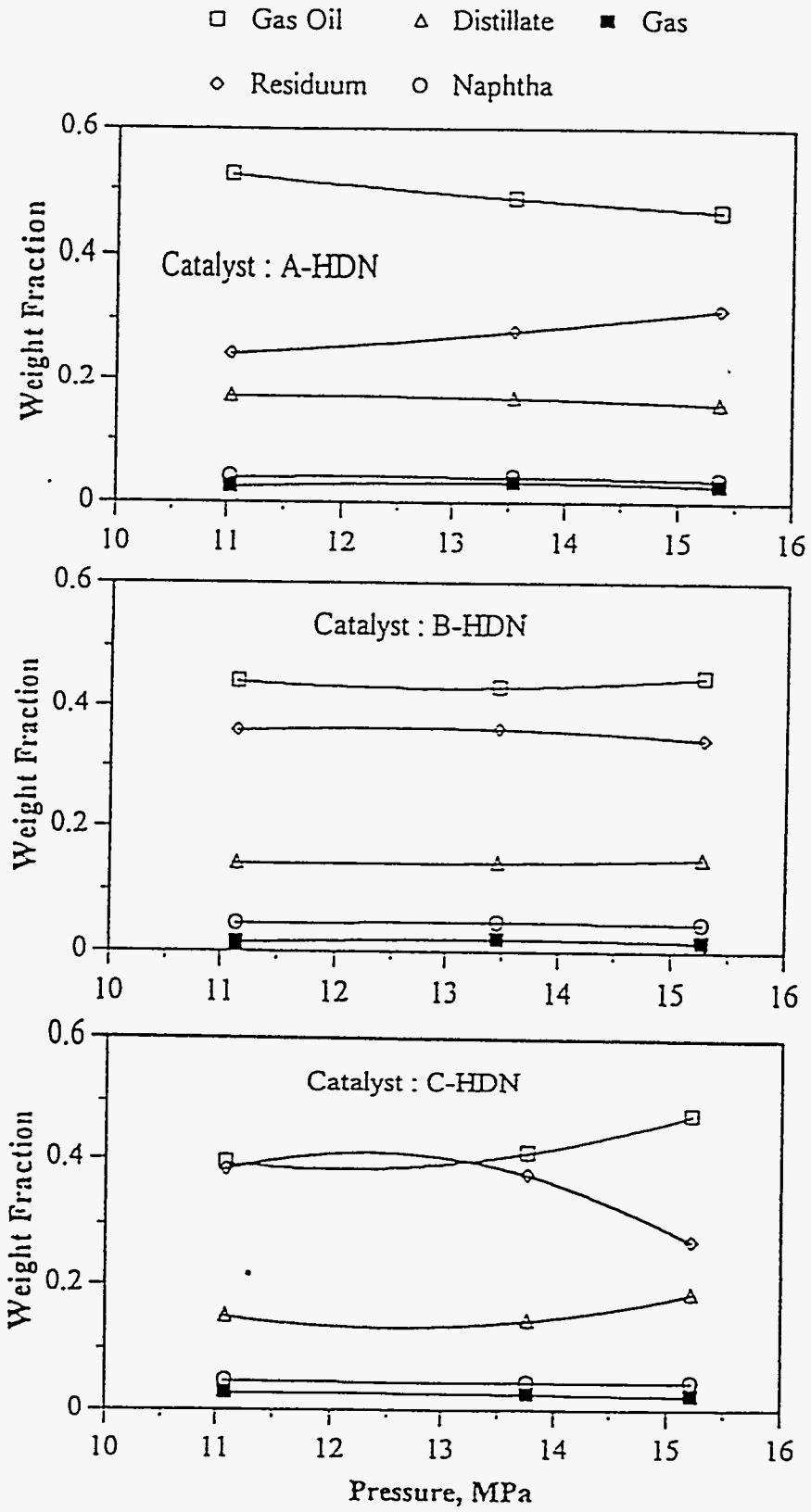
Gas Oil
Distillate
Gas
Residuum
Naphtha
Catalyst : A-HDN
Catalyst : B-HDN
Catalyst : C-HDN
Weight Fraction
Pressure, MPa
0.6
0.4
0.2
0
10
11
12
13
14
15
16

by basic nitrogen compounds, and in subsequent processing to meet product specifications or environmental regulations.

The effect of catalyst on nitrogen removal at different reciprocal WHSV and temperatures is displayed in Figure 322. At 620 K, the order of nitrogen conversion was A-HDN > B-HDN = C-HDN. As the temperature increased, the rank of nitrogen removal shifted to A-HDN > B-HDN > C-HDN at 664 K, and to A-HDN = B-HDN > C-HDN at 684 K. The HDN activity of the A-HDN catalyst was always higher than that of C-HDN catalyst. Comparing the properties of catalyst, A-HDN catalyst has higher surface area and pore volume, but lower metal loading than C-HDN catalyst. This higher surface area may have resulted in a higher dispersion of the active phase which would have contributed to higher HDN activity. The intermediate metal content as in the A-HDN catalyst was sufficient for the removal of nitrogen compounds in the Asphalt Ridge bitumen. For the B-HDN catalyst, its HDN activity was similar to that of the C-HDN catalyst at 620 K and close to the activity of the A-HDN catalyst at 684 K. When temperature increased, the rate of hydrogenolysis was favorable. Thus, the intermediate products that contain nitrogen penetrated pores of the B-HDN catalyst and the higher nitrogen conversion is obtained.

The HDN activities of the catalysts were ranked as A-HDN > B-HDN > C-HDN and depended strongly on the surface area of the catalyst in this investigation.

Hydrodesulfurization

HDS has long been one of the most important process in refining operations. The purposes are the removal of sulfur from naphtha reformer feedstocks and from heavier fractions to minimize the emissions of sulfur oxides. With increasingly stringent air quality regulations demanding removal of even the least reactive organosulfur compounds, deep HDS has been required.

The effect of catalyst on sulfur removal at different reciprocal WHSVs and temperatures is presented in Figure 323. At 620 K, the HDS activity of the A-HDN catalyst which has the higher surface area was higher than for the B- and C-HDN catalysts. For the B- and C-HDN catalysts, the sulfur conversion over C-HDN catalyst is greater than over the B-HDN catalyst especially in the higher space velocity regions

Figure 322

Effect of catalyst on nitrogen conversion

at different reciprocal WHSVs and temperatures

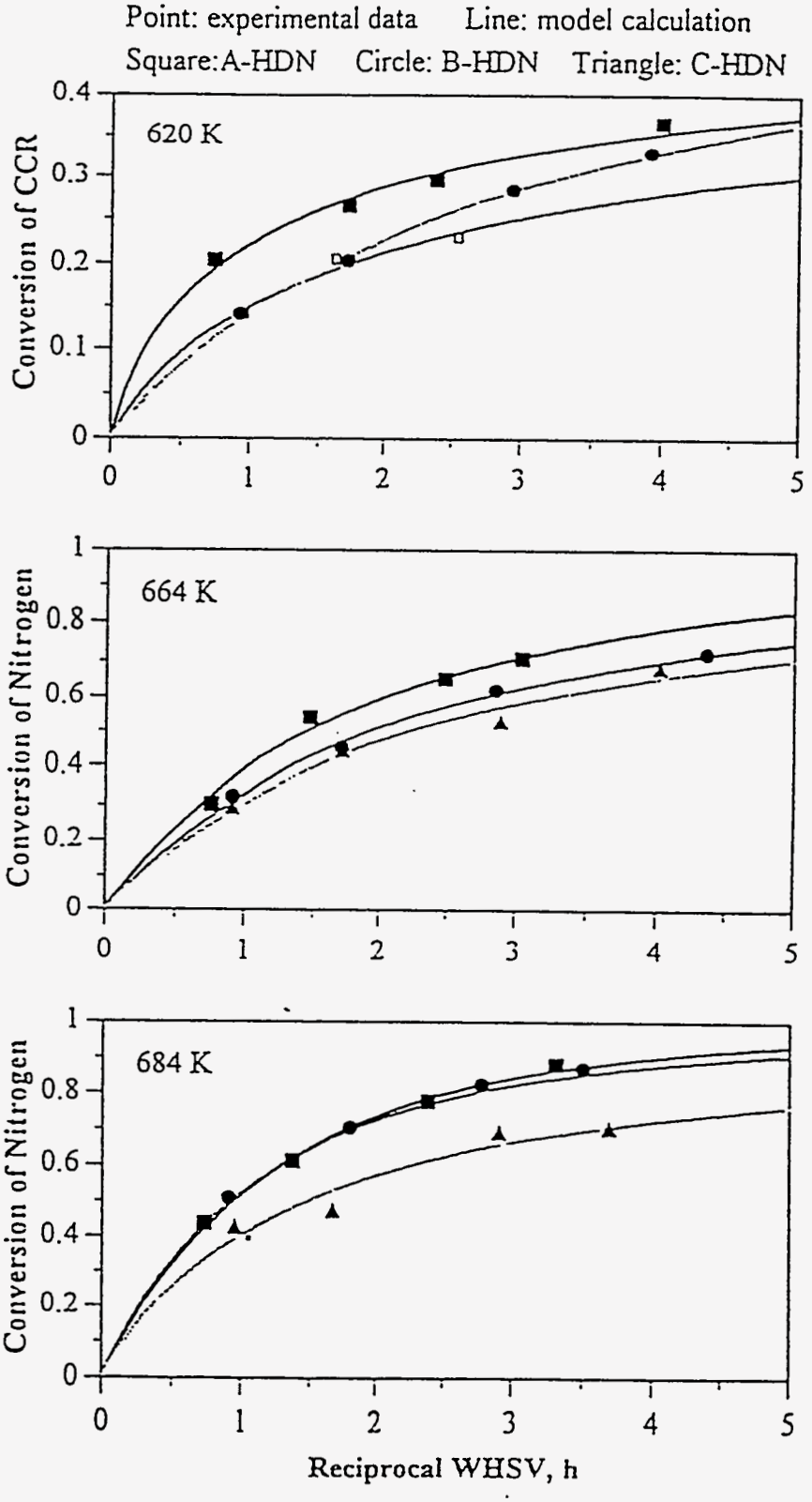
Point: experimental data Line: model calculation
Square:A-HDN Circle: B-HDN Triangle: C-HDN
620 K
664 K
684 K
Conversion of CCR
Conversion of Nitrogen
Conversion of Nitrogen
Reciprocal WHSV, h

Figure 323

Effect of catalyst on sulfur conversion

at different reciprocal WHSVs and temperatures

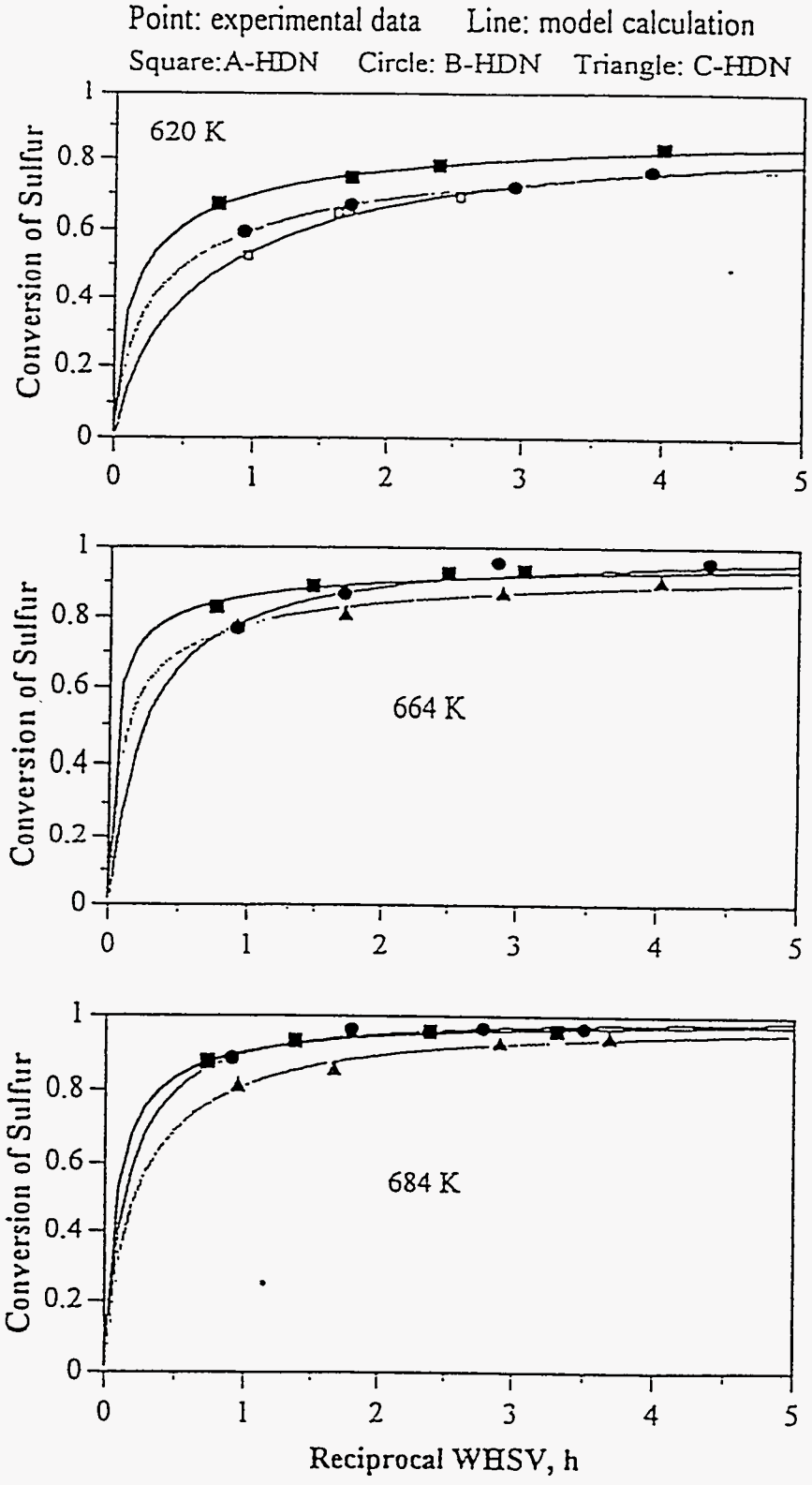
Point: experimental data Line: model calculation
Square:A-HDN Circle: B-HDN Triangle: C-HDN
620 K
664 K
684 K
Conversion of Sulfur
Reciprocal WHSV, h
0
0.2
0.4
0.6
0.8
1
0
1
2
3
4
5

because the C-HDN catalyst has a relatively higher surface area. As the space velocity decreased, the sulfur compounds have enough time to penetrate the pores of the catalyst. Thus, the sulfur conversion of the B-HDN catalyst having wider pore size distribution, and higher pore volume is larger than that of the C-HDN catalyst.

With increasing temperature, the HDS activity of the B-HDN catalyst increased and eventually exceeded that of the A-HDN catalyst. This infers that the effect of wider pore size distribution on sulfur removal is more significant at higher temperature.

As discussed, the HDS activity of catalyst depends strongly on the reaction conditions.

Metal Removal

The metal components, especially nickel, from metal-containing compounds in bitumen were removed via hydrotreating. These compounds could be classed as porphyrinic and nonporphyrinic structural types. Unlike hydrodenitrogenation, hydrodesulfurization, and hydrodeoxygenation with gaseous products (NH_3, H_2S, and H_2O), metal removal leads to solid products deposited on the catalyst surface. Thus, the catalyst was deactivated by the metal deposition.

The conversions of nickel over the three HDN catalysts are listed in Table 110. At 620 K, the order of nickel removal was A-HDN > C-HDN > B-HDN which suggests a dependence on the surface area. However, the rank of nickel conversion is B-HDN > A-HDN > C-HDN at 684 K because the B-HDN catalyst has a wider pore size distribution. This was also observed in sulfur removal.

The conversions of nickel and asphaltenes (Table 110) exhibit similar trends which infers that the nickel and vanadium were distributed in the resins and asphaltenes fractions(65).

Residuum Conversion

The residuum conversion is an important reaction in resid and bitumen hydroprocessing. The role of the catalyst in residuum conversion is uncertain. Some authors(346, 347) reported that catalyst does not affect residuum conversion and that residuum conversion is primarily thermal and involves a free radical mechanism to

convert residuum molecules to volatile products and gas oil. Other researchers(348, 349) reported that a combination of catalytic and thermal reactions occurs in residuum conversion. Thus, catalyst selection affects the relative ratio of catalytic to thermal reaction. Hydrogen must be present to prevent retrograde polymerization reactions, but the extent of conversion is independent of hydrogen partial pressure.

The effect of catalyst on residuum conversion at different residence time and temperatures is illustrated in Figure 324. The figure indicates that the A-HDN catalyst exhibits the highest activity for residuum conversion. This may indicate that the surface area is a dominant factor in residuum conversion.

The B- and C-HDN catalysts exhibit similar trends at 620 K and 684 K. That is, the B-HDN catalyst has relatively higher activity for residuum conversion in the lower residence time region (less than about 3 h) but has relatively lower activity in the region of residence time more than 3 h. It may be that the larger pore volume of the B-HDN catalyst is a key factor at residence times less than 3 h, and that the higher surface area of the C-HDN catalyst is dominant factor at residence times in excess 3 h. At 664 K, they exhibit similar activities for residuum conversion.

Conradson Carbon Residue Conversion

The carbon residue is an important property which measures the coking tendency of the feedstock. Thus, Conradson carbon residue conversion is an important reaction in residuum hydroprocessing. It has been reported that carbon residue is related to molecules that contain five or more aromatic rings(350). The conversion of CCR occurs by hydrogenation of a number of these rings, followed by hydrogenolysis of the hydrogenated rings.

The effect of catalyst on CCR conversion at different reciprocal WHSV and temperatures is presented in Figure 325. At 620 K, the order of CCR conversion is A-HDN > C-HDN > B-HDN. As temperature increased, the rank of CCR conversion shifted to A-HDN > B-HDN > C-HDN at 664 K and to A-HDN = B-HDN > C-HDN at 684 K. The activity for CCR conversion of the A-HDN catalyst is always higher than that of the C-HDN catalyst. Comparing the properties of catalyst, the A-HDN catalyst has higher surface area and pore volume but lower metal loading than C-HDN catalyst. This implies that high surface area may have led to greater dispersion of the active phase

Figure 324

Effect of catalyst on residuum conversion

at different reciprocal WHSVs and temperatures

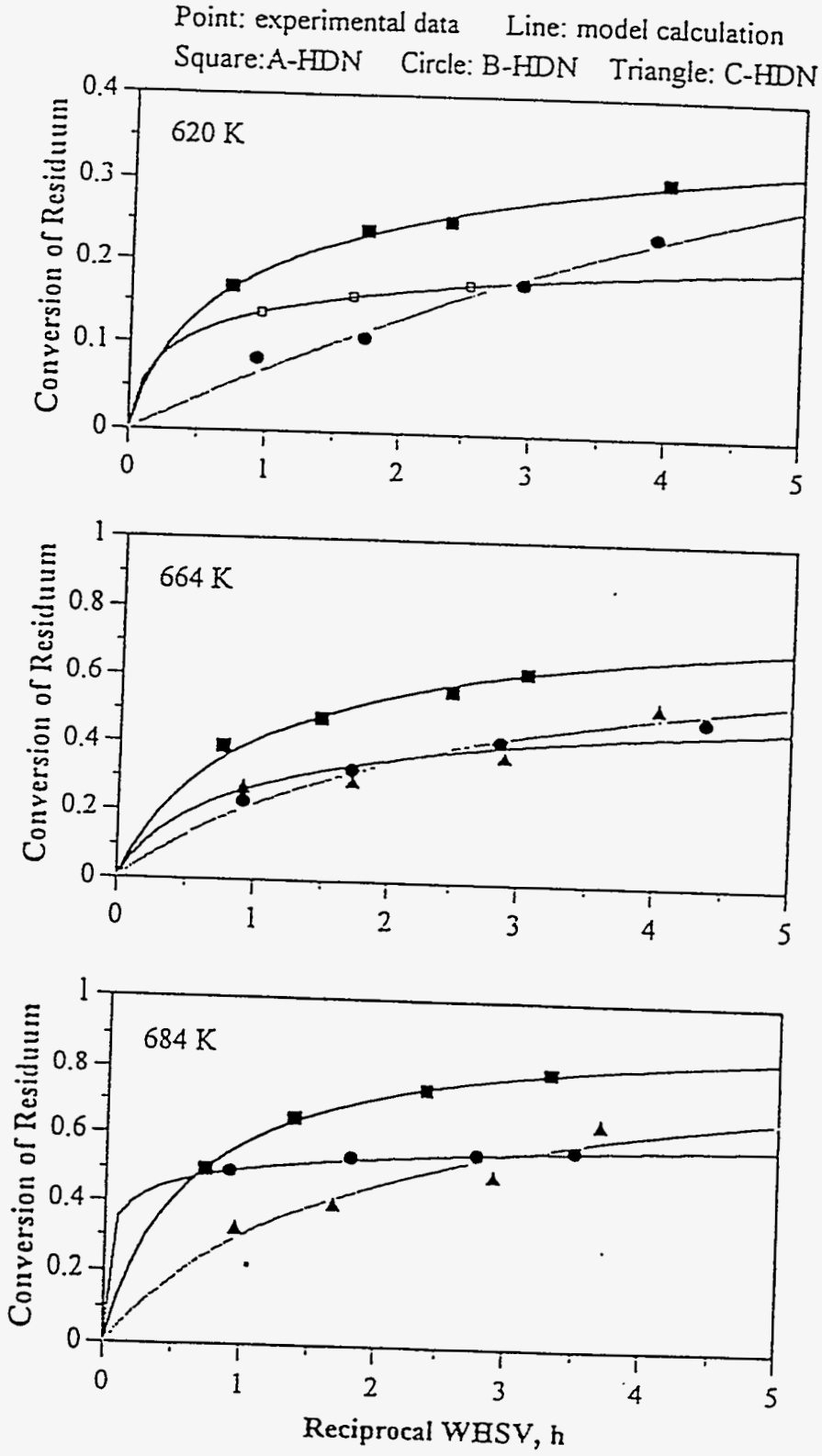
Point: experimental data Line: model calculation
Square:A-HDN Circle: B-HDN Triangle: C-HDN
620 K
664 K
684 K
Conversion of Residuum
Reciprocal WHSV, h

Figure 325

Effect of catalyst on CCR conversion

at different reciprocal WHSVs and temperatures

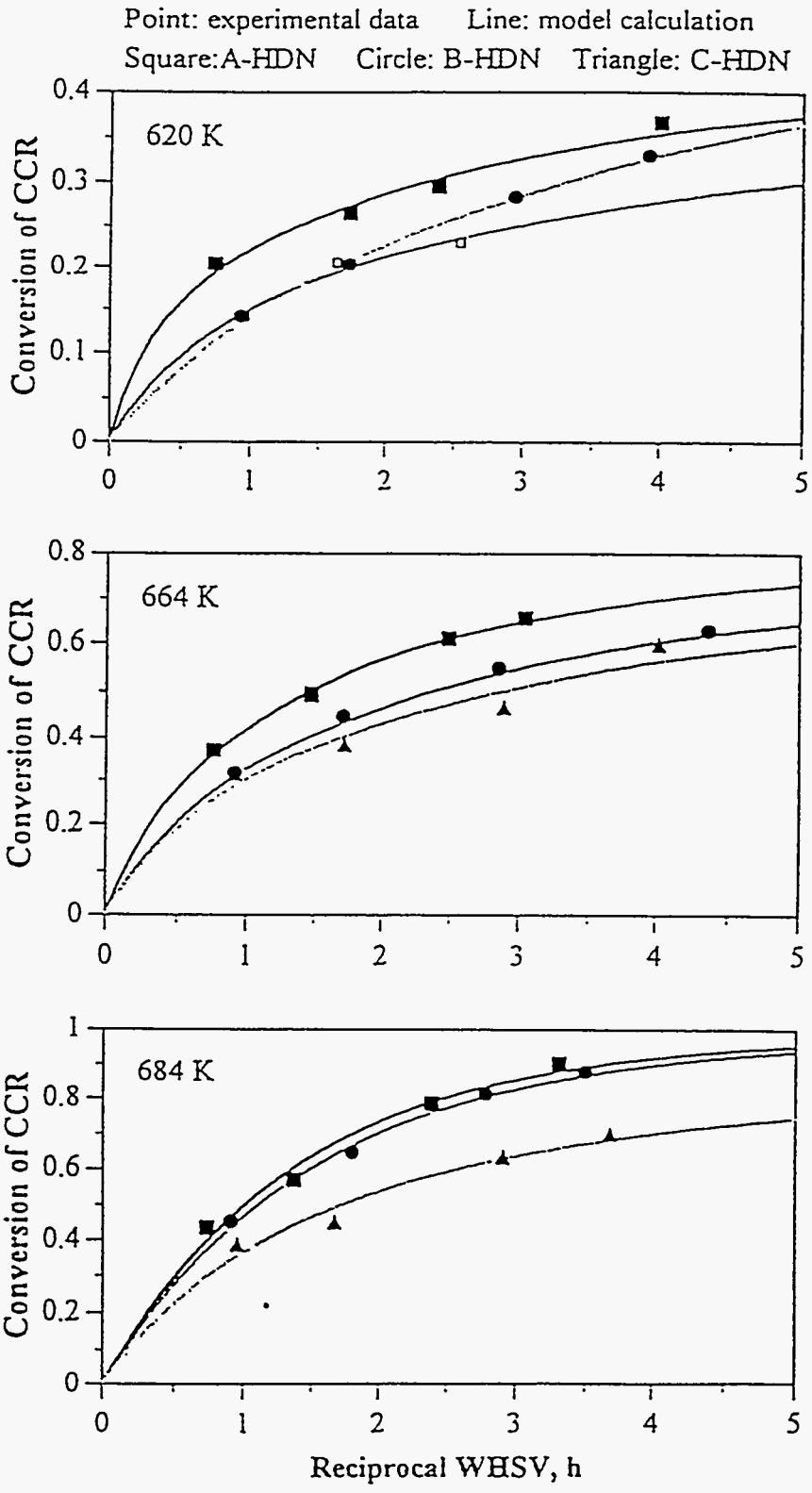
Point: experimental data Line: model calculation
Square:A-HDN Circle: B-HDN Triangle: C-HDN
620 K
664 K
684 K
Conversion of CCR
Reciprocal WHSV, h

which contributed to the high activity for CCR conversion, and the intermediate metal content of the A-HDN catalyst was sufficient to maintain activity.

The activity of the B-HDN catalyst for CCR conversion was lower than that of the C-HDN catalyst at 620 K, and close to the activity of the A-HDN catalyst at 684 K. The rate of hydrogenolysis is favorable with increasing temperature. Thus, the more intermediate products can penetrate the pores of the B-HDN catalyst and higher CCR conversion is obtained.

The activity of CCR conversion for the catalysts was ranked as A-HDN > B-HDN > C-HDN and depends strongly on the surface area and pore size distribution of the catalyst.

Asphaltenes Conversion

Asphaltenes are a problem for their tendency to flocculate and precipitate during both oil production and oil refining. In the first case, they cause a dramatic reduction in oil flow or even blockage of the formation during production. In the second case, they cause severe drawbacks during the processing of heavy ends such as the tendency to form coke, catalyst deactivation, and poisioning(351). Asphaltenes conversion involves a combination of catalytic and thermal reactions.

The influence of catalyst on asphaltenes conversion at different reciprocal WHSVs and temperatures is presented in Figure 326. At 620 K, the conversion of asphaltenes rapidly increased to a maximum (at a residence time of about 1 h) and then decreased with increasing residence time. This result contradicts current understanding of asphaltenes conversion. The real reason is unknown but may be related to hydrodynamics in the catalyst bed. The A-HDN catalyst with higher surface area, larger pore volume, and lower metal contents, exhibited relatively lower conversion for asphaltenes than the C-HDN catalyst at 620 K.

At 664 K, however, the conversion of asphaltenes increased with increasing residence time. The performance of the three HDN catalysts were similar. At 684 K, the asphaltenes conversion over the A- and B-HDN catalysts increased linearly with increasing residence time. However, the temperature effect was not favorable for asphaltenes conversion and was similar to that at 664 K, over the C-HDN catalyst. From

Figure 326

Effect of catalyst on asphaltene conversion

at different reciprocal WHSVs and temperatures

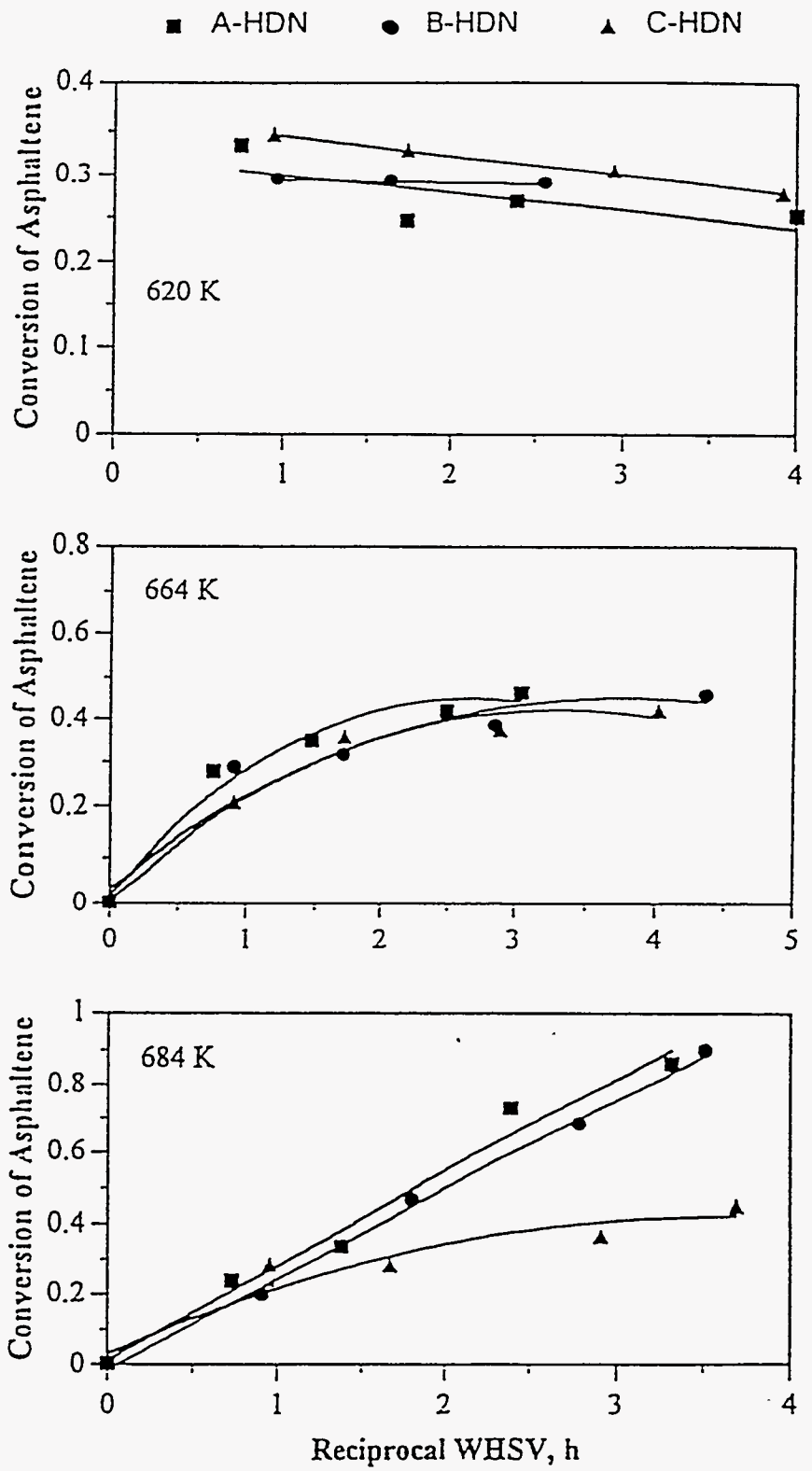
A-HDN
B-HDN
C-HDN
Conversion of Asphaltene
620 K
664 K
684 K
Reciprocal WHSV, h

the properties of catalysts, the catalyst surface area and the pore size distribution appeared to influence asphaltenes conversion.

For asphaltenes conversion, the A- and B-HDN catalyst were preferred.

Viscosity Reduction

The effect of catalyst on viscosity reduction at different reciprocal WHSVs and temperatures is plotted in Figure 327. The viscosities were measured at 313 K. As shown in the figure, the viscosity reduction with the A-HDN catalyst with high surface area was better than achieved with the B- and C-HDN catalysts. At 620 K, the viscosity reduction accomplished with the B-HDN catalyst was less than with the C-HDN catalyst which has relatively higher surface area.

Secondary Hydrotreating

Two experiments were conducted to evaluate second pass (secondary) hydrotreating over the A-HDN catalyst. The comparison between first and second pass hydrotreating is presented in Table 114. After second pass hydrotreating at 684 K and a LHSV of 0.2 h^{-1}, the liquid produced improved quality, including conversion,viscosity and molecular weight reduction, and higher H/C ratio of the final liquid products was improved The hydrogen consumptions in the second pass were significantly decreased relative to the first pass; however, this was difficult to quantify.

Conversion

For the first case (temperature = 642 K, LHSV = 0.48 h^{-1}), the fractional conversions of CCR and asphaltenes were very small, 3.7% and 1.7%, respectively; however, it was 16% for residuum. Thus, the fractional conversion of sulfur and nitrogen, 20% and 7.5%, respectively, appear to be related to residuum conversion during second pass hydrotreating.

For the second case (temperature = 684 K, LHSV = 0.48 h^{-1}), the fractional conversion of residuum is very small, 1.8%, indicating that the refractory fraction of residuum is 0.2 under these conditions. The fractional conversions of sulfur and nitrogen were 85.1%, 61.5%, respectively, and higher than those of CCR and asphaltenes, 52.6%

Figure 327

Effect of catalyst on viscosity (measured at 313 K)

at different reciprocal WHSVs and temperatures

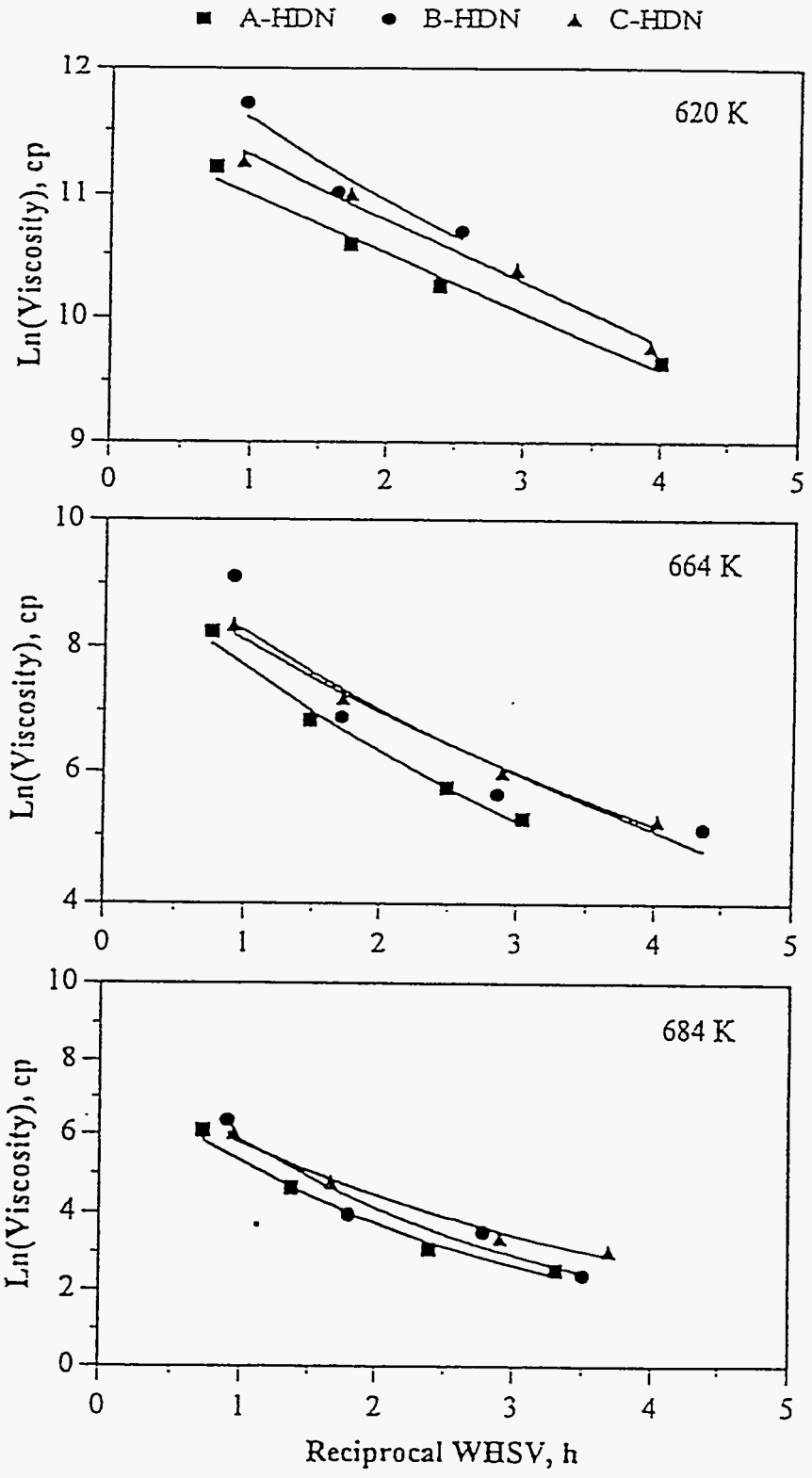
A-HDN
B-HDN
C-HDN
620 K
664 K
684 K
Ln(Viscosity), cp
Reciprocal WHSV, h

Table 114

Comparison with First and Second Pass Hydrotreating over the A-HDN Catalyst at Constant Pressure (13.7 MPa)

Operating Conditions	T, K	LHSV, h^{-1}		T, K	LHSV, h^{-1}	
	642	0.48		684	0.2	
Properties	First Pass	Second Pass		First Pass	Second Pass	
Conversion, %	Total	Total	Fractional	Total	Total	Fractional
Sulfur	82.5	86.0	20.0	96.3	99.5	85.1
Nitrogen	30.9	36.1	7.5	86.6	94.8	61.5
Residuum	30.5	41.6	16	79.4	79.8	1.8
CCR	39.0	41.3	3.7	89.5	95.0	52.6
Asphaltenes	31.5	32.7	1.7	85.6	92.2	45.5
Viscosity, mPa s (at 313 K)	8274	4564		13.6	6.18	
Yields and Distributions of Products						
C_1-C_4	1.7	0.8		8.7	5.3	
C_5-478 K	2.5	2.6		9.4	12.0	
478-616 K	12.9	14.9		29.0	35.7	
616-811 K	45.9	50.0		42.8	37.4	
> 811 K	37.0	31.7		10.2	9.5	
H/C Ratio	1.62	1.68		1.77	1.80	
H_2 Consumption, liter/liter	87	13		154	30	

Total Conversion = $1-(C_{i,j})_{product}/(C_{i,1})_{feed}$

Fractional Conversion = $1-(C_{i,2})_{product}/(C_{i,2})_{feed}$

i = Lumped Species, j = First (1) or Second (2) Pass

and 45.5%, respectively. Therefore, during second pass hydrotreating at severe conditions, i.e., higher temperature, the conversions of sulfur and nitrogen appear to be related CCR and asphaltenes conversions.

Comparing the total and fractional conversions in the second case, the refractory fraction of the residuum does not appear to contain the CCR and asphaltenes. The two classes of molecules in residuum could be classified CCR residuum and non-CCR residuum or asphaltenes residuum and nonasphaltenes residuum. This result agrees with Sanford's reports(282).

The CCR and asphaltene conversions are presumed to occur via thermal reaction pathways as indicated by these two experiments.

Product Distribution

For the first case, the yields of gas and residuum decrease, whereas of naphtha, distillate, and gas oil mildly increase. However, the yield of gas oil also decreases together with gas and residuum in the second case. The yields of naphtha and distillate increase significantly. As can be seen, the gas oil undergoes cracking to produce naphtha and distillate at lower space velocity and higher temperature.

SUMMARY AND CONCLUSIONS

The conversions of sulfur, nitrogen, residuum, CCR, and asphaltenes increased as reciprocal WHSV increased; however, the asphaltenes conversion at 620 K increased initially and then decreased with increasing residence time. Sulfur, nitrogen, residuum, and CCR conversion increased with increasing temperature, whereas the asphaltenes conversion decreased with temperature at LHSV of 0.9 h^{-1}. The effect of pressure on the conversion was positive. The reaction order, β, of hydrogen partial pressure depended on catalyst and the reactant species.

Viscosity of bitumen over HDN catalysts was reduced significantly with increasing temperature at fixed WHSV, and also reduced as reciprocal WHSV increased at fixed temperature, but was not affected by pressure. The relationship of viscosity and temperature was well described by the equation, $\mu = A \exp(\Delta G^{*}/RT)$, where ΔG^{*} is the Gibbs free energy of activation.

The yield and distribution of products produced from the bitumen over the HDN catalysts were a function of process variables. The gas oil fraction underwent secondary cracking to lower boiling materials at higher temperatures and longer residence times.

The catalyst with higher surface area, larger pore volume, and wider pore size distribution should be better for sulfur, nitrogen, and nickel removal; CCR, asphaltenes, and residuum conversion; and viscosity reduction in the hydrotreating of bitumens. For example, at a lower temperature of 620 K, the performance of the A-HDN catalyst with higher surface area (215 m^2/g) was most active for conversion of various classes of compounds. At a higher temperature of 684 K, the A- and B-HDN catalysts exhibited similar performance which was better than the C-HDN catalyst. The better performance of B-HDN catalyst, in comparison with C-HDN catalyst, results from its presumed wider pore size distribution and larger pore volume.

Under the severest condition, the total conversions of sulfur, CCR, nitrogen, asphaltenes, and residuum over A-HDN catalyst were 99.5%, 95.0%, 94.8%, 92.2%, and 79.8%, respectively, after secondary hydrotreating. It was found that the sulfur

and nitrogen removal resulted from CCR and asphaltenes conversion, not from residuum conversion which was not converted during second pass hydrotreating. This implies that the refractory fraction, 0.2, of residuum contained little CCR and asphaltenes and was more difficult to convert than asphaltenes.

The weight fractions of naphtha, distillate, and residuum in the total liquid product were considerably changed relative to bitumen. For example, the naphtha increased from 0.5% in the feedstock to 12% in the liquid product, the distillate fraction increased from 10.2% in the bitumen to 35.7% in the liquid product, and the residuum decreased from 54.5% in the feedstock to 9.5% in the liquid product after second pass hydrotreating. At the same time, the viscosity, measured at 313 K, was reduced by a factor in excess of four orders of magnitude.

Pore volume and surface area of the three HDN catalysts decreased following use in hydrotreating the Asphalt Ridge bitumen. A- and C-HDN catalysts lost about one third of their pore volume and surface area. A slight shift to smaller pore radii is observed for the extracted spent catalysts.

The kinetics of sulfur and nitrogen removal and CCR and residuum conversion, in bitumen hydrotreating were well represented by nth-order power rate law to obtain reaction orders and by a distributed activation energy model using a normal distribution function to obtain more realistic activation energies.

The apparent reaction orders for conversion were a function of temperature and catalyst and could be higher than two. The reaction orders obtained from an nth-order power rate law support experimentally the validity of the asymptotic lumped kinetic model in the high conversion regime especially for deep hydrodesulfurization.

The kinetic equations for sulfur and nitrogen removal and residuum and CCR conversion did not follow a single first-order reaction model in the hydrotreating of bitumen. The relative proportion of facile and refractory fraction of bitumen was a function of temperature, catalyst, and feedstock at constant pressure.

BITUMEN UPGRADING BY HYDROPYROLYSIS

Research Assistant Professor: John V. Fletcher
Graduate Student: Brett Jenkins

Introduction

Hydroprolysis (HP) is a novel heavy oil and bitumen upgrading process previously studied at the University of Utah for conversion of heavy, carbonaceous feedstocks into valuable liquid and gaseous products without major formation of coke and without the need for heterogeneous catalysts. The HP process has been applied to conversion of feedstocks exhibiting in excess of 10 percent Conradson Carbon Residue. Production of 80 percent liquids (plus gaseous products) has been reported (352). The important chemical reactions responsible for these results have been identified and verified (353). Preliminary economic assessment shows that HP conversion is no more costly than conventional refinery operations utilizing the addition of hydrogen (354). The University of Utah has been awarded a patent on HP technology (355).

Work on a hydropyrolysis process development unit (PDU) was suspended in December, 1987 (356). One of the primary reasons the hydropyrolysis PDU was not operated after 1987 is the complexity of the equipment compared to the experience and skill level of a typical graduate student. In most experiments, the PDU required at least two persons for operation.

When the Departments of Chemical Engineering and Fuels Engineering at the University of Utah merged in 1992, a series of laboratory consolidations and trades was initiated. This necessitated the movement of the PDU, which had an 8' x 20' footprint.

That move was completed in the spring of 1993.

In the same time frame, DOE requested that the hydropyrolysis studies be restarted in order to develop the data base of process variables necessary for comparing hydropyrolysis to other upgrading options. The upgrading by hydropyrolysis was funded for 1993-1994, the year covered by this report.

As part of the disassembly and moving process, each component of the PDU was critically evaluated. This included visual inspections and detailed discussions with previous operators (353, 354). This evaluation plus the operational complexity mentioned above led to the decision to redesign and rebuild the PDU rather than reassemble it in its pre-move configuration.

Heavy Oil and Bitumen Upgrading

Several options are available for heavy oil and bitumen upgrading. An upgrading sequence usually includes hydrotreating for the removal of nitrogen (and a small amount of sulfur) and a molecular weight reducing step. Hydropyrolysis and hydrocracking are the two most promising molecular weight reducing processes. The work performed at the University of Utah through 1987 showed hydropyrolysis to be a low-coke and high-yield technology that would be a feasible upgrading process for oil sand bitumens and bitumen-derived liquids. Thus the project had a two-fold mission. First, to evaluate the larger scale applicability of the hydropyrolysis process. Second, to critically review all possible production - upgrading combinations and identify the best possible technical and economic pathways.

The hydropyrolysis process typically operates at 450-550°C, 7-17 MPa pressure and residence times of 1-50 seconds. Research at the University has yielded data on the effect of process variables on process performance. Using this data and data on the hydropyrolysis of model compounds, a comprehensive kinetic model for the hydropyrolysis process scheme and process simulations were performed using commercial process simulators. These simulations

provided optimum operating conditions based on definite criteria. Process simulations were performed to optimize the entire flow sheets with different heat exchanger configurations (354).

Operationally it was difficult to streamline the hydropyrolysis process, particularly, the high-pressure atomizer that sprays the bitumen in the form of fine droplets into the reactor. Variations in reactor configurations were explored in the previous work. It was therefore necessary to evaluate the hydropyrolysis process in the context of other short residence time processes and examine alternative reactor and process configurations that would allow streamlining of a larger-scale hydropyrolysis operation.

1993-1994 Project Objectives

Within the context of a required move of the PDU and its history of operational complexity the goal of the project was to return the PDU to operational status with simplified and/or automated operating procedures. Using previous data and process simulation models PDU improvements were also planned.

The specific project objectives included:

1. Disassemble and move the hydropyrolysis PDU.
2. Reassemble the PDU.
3. Install Utilities and other process supports.
4. Systematically evaluate the condition and safety of each PDU component and the assembled PDU.
5. Verify the operating procedure and hardware integrity of each PDU component. Repair, replace, revise, as required.
6. Verify the operating procedure and performance of the PDU.
7. Assess the validity of the previously proposed process models, and compare model

predictions with PDU results for a replicate experiment based on previous studies with this PDU.

Accomplishments

The Old PDU

The PDU process flow diagram from 1987 (Figure 328) no longer represented the system when disassembled. Several "visiting scholars" had attempted to operate the system over the intervening years and left no documentation. High pressure pumps, valves, etc. were coated with heavy hydrocarbons. Much of the electrical system was not to present code. In summary, after disassembling the PDU and moving it to another laboratory almost every subsystem and component had to be cleaned, repaired, and/or replaced. Given this situation , it was decided to redesign the PDU and rebuild it based on the new design.

The New PDU

In consultation with C.H. Tsai (353), the hydropyrolysis PDU was redesigned as shown in Figure 329. A systematic evaluation of components allowed us to begin the process of assembling a new PDU that would be more accessible and simpler to operate. Hydrogen recycle, an important economic consideration, was not included in this phase in the interest of simplicity. The design and configuration do include recycle for future inclusion.

In addition to the problems related to the PDU and its condition, two other subsystems were identified for redesign, the hydrogen heater and the hydropyrolysis reactor.

The Hydrogen Heater

The old PDU used a fluidized sand bath heater. This was basically a box of hot sand with H_2 coils running through it. The old unit was in disrepair and deemed ineffective as well as dirty. A large thermal block with gas coils and an external heater was found and adapted for H_2 heating.

Figure 328

Hydropyrolysis process development unit process flow diagram

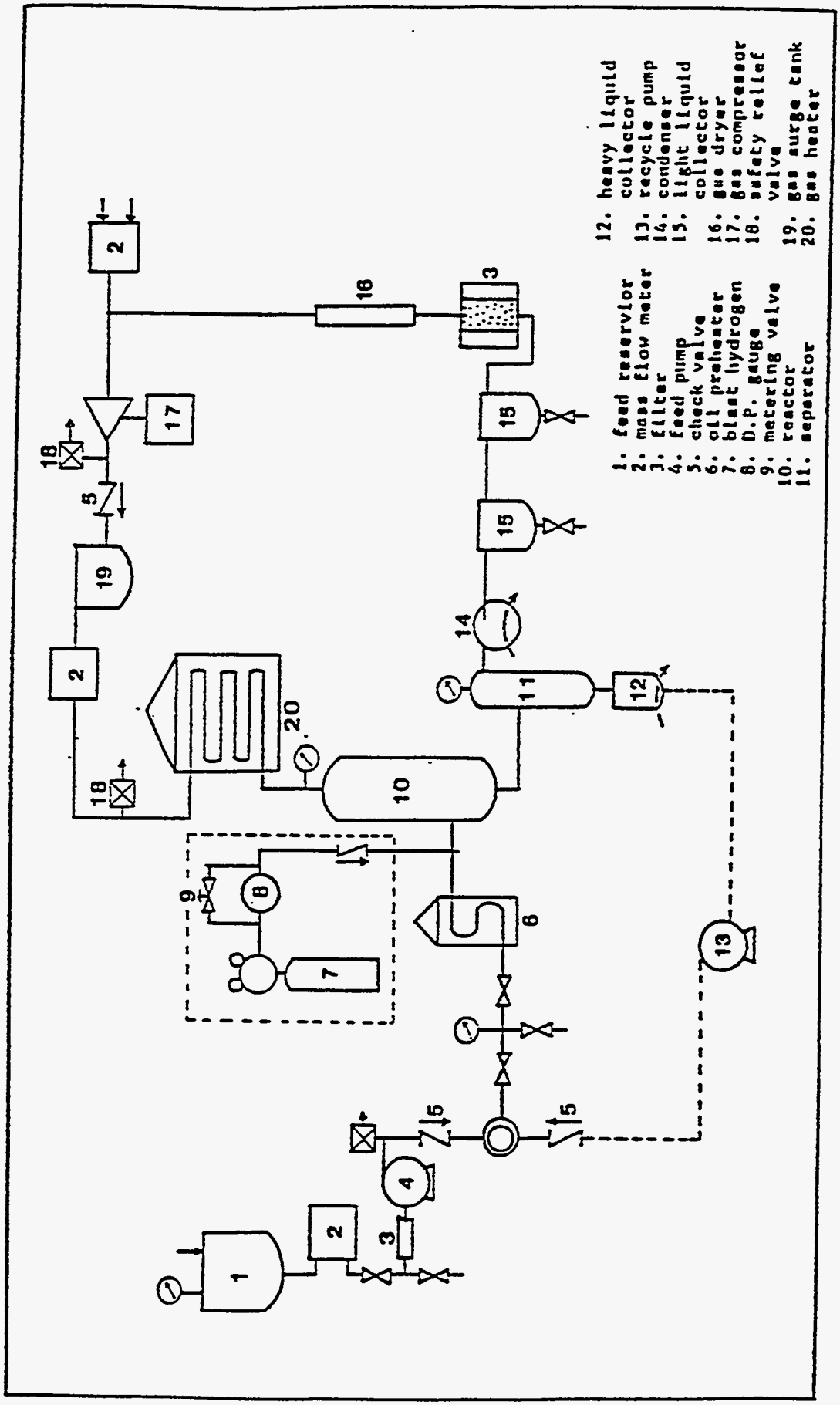
1. feed reservior
2. mass flow meter
3. filter
4. feed pump
5. check valve
6. oil preheater
7. blast hydrogen
8. D.P. gauge
9. metering valve
10. reactor
11. separator
12. heavy liquid collector
13. recycle pump
14. condenser
15. light liquid collector
16. gas dryer
17. gas compressor
18. safety relief valve
19. gas surge tank
20. gas heater

Figure 329

Revised Hydropyrolysis Process Flow Diagram

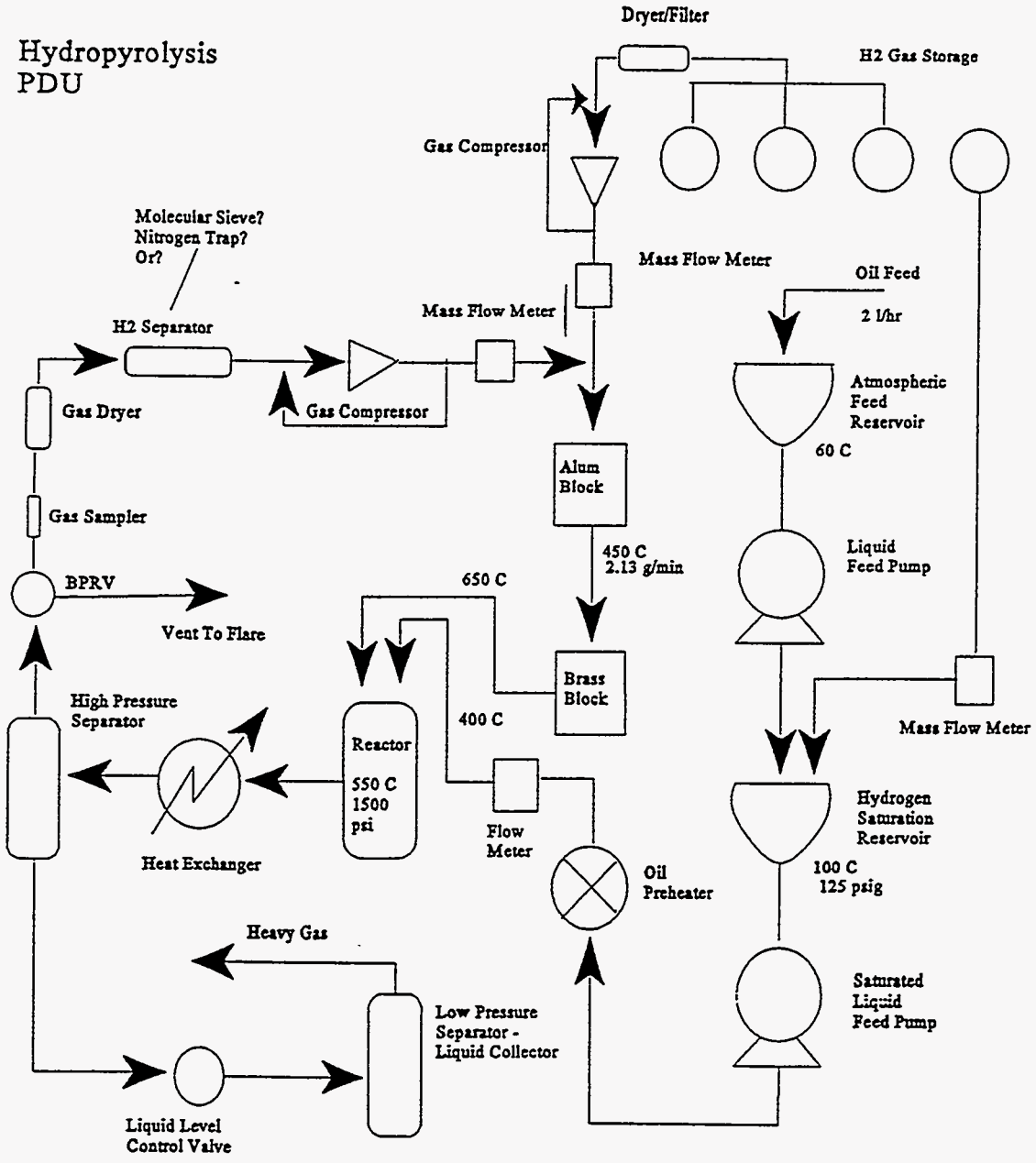
Hydropyrolysis
PDU
Dryer/Filter
H2 Gas Storage
Gas Compressor
Molecular Sieve?
Nitrogen Trap?
Or?
Mass Flow Meter
Oil Feed
2 l/hr
H2 Separator
Mass Flow Meter
Atmospheric
Feed
Reservoir
60 C
Gas Dryer
Gas Compressor
Alum
Block
Gas Sampler
450 C
2.13 g/min
Liquid
Feed Pump
BPRV
650 C
Vent To Flare
Brass
Block
High Pressure
Separator
400 C
Mass Flow Meter
Reactor
550 C
1500
psi
Hydrogen
Saturation
Reservoir
Flow
Meter
Heat Exchanger
Oil
Preheater
100 C
125 psig
Heavy Gas
Saturated
Liquid
Feed Pump
Low Pressure
Separator -
Liquid Collector
Liquid Level
Control Valve

A preheater was also installed.

The Hydropyrolysis Reactor

Previous PDU experiments have utilized two reactor designs with multiple lengths and diameters. In 1984 (DOE Report 1984-87) Bunger et.al. reported on shifting from a coiled-tube reactor to a vertical tube, downflow reactor in an effort to reduce residence times and improve yields. Inspection of these tubes showed coke deposits 2 to 8 inches from the nozzle. A need to redesign the reactor and the nozzle was reported by Bunger in 1987 (Tar Sand Report 1984-1987) when the PDU was mothballed.

Nozzle and Reactor Design

A short path reactor was chosen in order to keep residence times in the <1 second range. Co-current H_2 flow was also chosen with the gas flow directed along the reactor walls as a protecting envelope.

A commercial nozzle built by Lechler was obtained and tested using diesel oil and a standard test bench for truck nozzles. Visual observation of the nozzle showed it to produce an excellent pattern. Measurements of the pattern were used to design the recess and fan angle for the short path reactor. The average drop diameter is 50 microns and its linear velocity is expected to be 5000 to 6000 inches/sec. Using the time required to heat and vaporize a drop of oil and the linear velocity, the reactor length required for these two steps is 1.27 inches. The actual length of our new reactor is 3 inches.

Conclusion

1993-94 program year was actually extended into 1995 in order to allow students to complete their degrees. The redesign and rebuilding of the hydropyrolysis PDU was not completed even with the extension. The graduate student initially funded by the project was

forced to find employment before the project was completed. The PDU is approximately 60% complete. The reactor has been redesigned and built. The nozzle was been procured and tested. A coker gas oil has been characterized in preparation for use as a feed once the PDU is operational.

REFERENCES

1. Oblad, A.G., Bunger, J.W., Dahlstrom, D.A., Deo, M.D., Hanson, F.V., Miller, J.D., and Seader, J.D., 1992 Final Report, "The Extraction of Bitumen from Western Oil Sands", Contract No.: DE-FC21-89MC26268, (August 1992).

2. Oblad, A.G., Bunger, J.W., Dahlstrom, D.A., Deo, M.D., Hanson, F.V., Miller, J.D., and Seader, J.D., 1993 Final Report, "The Extraction of Bitumen from Western Oil Sands", Contract No.: DE-FC21-89MC26268, (December 1993).

3. Oblad, A.G., Bunger, J.W., Hanson, F.V., Miller, J.D., Ritzma, H.R., and Seader, J.D., "Tar Sand Research and Development at the University of Utah", *Ann. Rev. Energy*, **12**, 283-356, 1987.

4. Bowman, C.W., " Molecular and Interfacial Properties of Athabasca Tar Sands", *Proc. of the 7th World Petroleum Congress*, **3**, Elsevier, Amsterdam, pp.583-604, 1967.

5. Drelich, J., and Miller, J.D., " Surface and Interfacial Tension of the Whiterocks Bitumen and Its Relationship to Bitumen Release from Tar Sands during Hot Water Processing", *Fuel,* **73**, 1504-1510, 1994.

6. Drelich, J., "The Role of Wetting Phenomena in the Hot Water Process for Bitumen Recovery from Tar Sand", Ph.D. Dissertation, University of Utah, Salt Lake City, Utah, 1993.

7. Deshpande, D.A., Deo, M.D., and Hanson, F.V., "Correlations for Effective Bubble Rise Velocity in Three-Phase Ebullieted Beds", *Fuel Proces. Technol.*, **32**, 3-23, 1992.

8. Hupka, J., and Miller, J.D., "Electrophoretic Characterization and Processing of Asphalt Ridge and Sunnyside Tar Sands", *Int. J. Mineral Proces.*, **31**, 217-231, 1991.

9. Isaacs, E.E., and Smolek, K.F., "Interfacial Tension Behavior of Athabasca Bitumen/aqueous Surfactant Systems", *Can. J. Chem. Eng.*, **61**, 233-240, 1983.

10. Potoczny, Z.M., Vargha-Butler, E.I., Zubovits, T.K., and Neumann, A.W., "Surface Tension of Bitumen", *AOSTRA J. Res.*, **1**, 105-120, 1984.

11. Vargha-Butler, E.I., Zubovits, T.K., Budziak, C.J., Neumann, A.W., and Potoczny, Z.M., "Surface Tension of Bitumen from Contact Angle Measurements on Films of Bitumen", *Energy Fuels*, **2**, 653-656, 1988.

12. Neumann, A.W., Good, R.J., Hope, C.J., and Sejpal, M., "An Equation-of-State Approach

to Determine Surface Tensions of Low-Energy Solids from Contact Angles", *J. Colloid Interface Sci.*, **49**, 291-304, 1974.

13. Adamson, A.W., "Physical Chemistry of Surfaces", John Wiley & Sons, Inc., New York, 1990.

14. Kloubek, J., "Development of Methods for Surface Free Energy Determination Using Contact Angles of Liquids on Solids", *Adv. Colloid Interface Sci.*, **38**, 99-142, 1992.

15. Girifalco, L.A., and Good, R.J., "A Theory for the Estimation of Surface and Interfacial Energies. I. Derivation and Application to Interfacial Tensions", *J. Phys. Chem.*, **61**, 904-909, 1957.

16. Li, D., and Neumann, A.W., "A Reformulation of the Equation-of-State for Interfacial Tensions", *J. Colloid Interface Sci.*, **137**, 304-307, 1990.

17. Li, D., and Neumann, A.W., "Contact Angles on Hydrophobic Surfaces and Their Interpretation", *J. Colloid Interface Sci.*, **148**, 190-200, 1992.

18. Hupka, J., White, R.R., Yang, J.Y., Drelich, J., Miller, J.D., Hanson, F.V., and Oblad, A.G., "Residual Solvent Effect on the Viscosity of the Bitumen Extracted from the Whiterocks Oil Sand", *AOSTRA J. Res.*, 1994.

19. Bukka, K., Hanson, F.V., Miller, J.D., and Oblad, A.G., "Fractionation and Characterization of Whiterocks Tar Sand Bitumens", *Energy Fuels*, **6**, 160-165, 1992.

20. Hupka, J., Oblad, A.G., and Miller, J.D., "Diluent-Assisted Hot-Water Processing of Domestic Tar Sands", *AOSTRA J. Res.*, **3**, 95-102, 1987.

21. Shun, D., "The Pyrolysis of Bitumen-Impregnated Sandstone from the Circle Cliffs (Utah) Deposit in a Fluidized-Bed Reactor", Ph.D. Dissertation, University of Utah, Salt Lake City, Utah, 1990.

22. Bukka, K., Miller, J.D., and Oblad, A.G., "Fractionation and Characterization of Utah Tar Sand Bitumens: Influence of Chemical Composition on Bitumen Viscosity", *Energy Fuels*, **5**, 333-340, 1991.

23. Oblad, A.G., Seader, J.D., Miller, J.D., and Bunger, J.W., "Recovery of Bitumen from Oil-Impregnated Sandstone Deposits of Utah", AIChE Symp. Ser. No.155, Oil Shale and Tar Sands, **72**, 69-77, 1976.

24. Wu, S., "Polymer Interface and Adhesion", Marcel Dekker, Inc., New York, 1982.

25. Lee, L.H., "Scope and Limitations of the Equation of State Approach for Interfacial Tensions", *Langmuir*, **9**, 1898-1905, 1993.

26. Drelich, J., and Miller, J.D., "Examination of Neumann's Equation-of-State for Interfacial Tensions", *J. Colloid Interface Sci.*, **167**, 217-220, 1994.

27. Lelinski, D., "ASH Flotation of Dispersed Oil Droplets - a Model System for Bitumen Flotation from Tar Sands", M.S. Thesis, University of Utah, Salt Lake City, Utah, 1993.

28. Lelinski, D., Miller, J.D., and Hupka, J., "The Potential for Air-Sparged Hydrocyclone Flotation in the Removal of Oil from Oil-in-Water Emulsions", Paper No. 1-22-016, Proc. of the First World Congress on Emulsion, Oct. 19-22, Paris, France., 1993.

29. Becher, P., "Emulsions: Theory and Practice", Reinhold Publishing Co., New York, 1965.

30. Fischer, E.K., and Harkins, W.D., "Monomolecular Films. The Liquid-Liquid Interface and the Stability of Emulsions", *J. Phys. Chem.*, **36**, 98-110, 1932.

31. Dixon, W.J., and Massey, F.J., Jr., "Introduction to Statistical Analysis", 2nd ed., McGraw-Hill Book Co., Inc., New York, 1957.

32. Takahashi, T., Miyahara, T., and Nishizaki, Y., "Separation of Oily Water by Bubble Column", *J. Chem. Eng. Jpn*, **12**, 394-399, 1979.

33. Angelidou, C., Keshavarz, E., Richardson, M.J., and Jameson, G.J., "The Removal of Emulsified Oil Particles from Water by Flotation", *Ind. Eng. Chem., Process Des. Dev.*, **16**, 436-441, 1977.

34. van Ham, N.J.M., Bechie, L.A., and Svrcek, W.Y., "The Effect of Air Distribution on the Induced Air Flotation of Fine Oil in Water Emulsions", *Can. J. Chem. Eng.*, **61**, 541-547, 1983.

35. Leja, J., and Bowman, C.W., "Application of Thermodynamics to the Athabasca Tar Sands", *Can. J. Chem. Eng.*, **46**, 479-481, 1968.

36. Hupka, J., and Miller, J.D., "Moderate-Temperature Water-Based Bitumen Recovery from Tar Sand", *Fuel*, **70**, 1308-1312, 1991.

37. Drelich, J., Hupka, J., Miller, J.D., and Hanson, F.V., "Water Recycle in Moderate-Temperature Bitumen Recovery from Whiterocks Oil Sands", *AOSTRA J. Res.*, **8**, 139-147, 1992.

38. Shaw, R.C., Czarnecki, J., Schramm, L.L., and Axelson, D., "Bituminous Froths in the Hot

Water Flotation Process", in "Foams, Fundamentals and Applications in the Petroleum Industry," Schramm, L.L. (Ed.), American Chemical Society, New York, 1994.

39. Petersen, J.C., "The Potential Use of Tar Sand Bitumen as Paving Asphalt", *Fuel Sci. Technol. Int.*, **6**, 225-254, 1988.

40. Thomas, K.P., Harnsberger, P.M., and Guffey, F.D., "An Evaluation of Asphalt Ridge (Utah) Tar Sand Bitumen as a Feedstock for the Production of Asphalt and Turbine Fuels", *Fuel Sci. Technol. Int.*, **12**, 281-302, 1994.

41. Tsai, C.H., Deo, M.D., Hanson, F.V., and Oblad, A.G., "Characterization and Potential Utilization of Whiterocks (Utah) Tar Sand Bitumen", *Fuel Sci. Technol. Int.*, **9**, 1259-1286, 1991.

42. Heitzman, M.A., "Design and Construction of Asphalt Paving Materials with Crumb Rubber Modifier", Transportation Research Report, No. 1339, Washington, D.C., 1992.

43. Camp, F.W., "Tar Sands", *Kirk-Othmer Encyclopedia of Chemical Technology*, 3 ed., Interscience Publishers, New York, **22**, 601 (1982).

44. Clark, H.A., and Pasternack, D.S., "Hot Water Separation of Bitumen from Alberta Bituminous Sands", *Ind. Eng. Chem.*, **24**, 1410 (1932).

45. Hupka, J., Oblad, A.G., and Miller, J.D., "Diluent Assisted Hot Water Processing of Tar Sands", *AOSTRA J. Res.*, **3**, 95 (1987).

46. Funk, E.W., "Behavior of Tar Sand Bitumen with Paraffinic Solvents and Its Application to Separations for Athabasca Tar Sands", *Can. J. Chem. Eng.*, **57**, 333 (1979).

47. Parks, B.D. and Meadus, F.W., "A Combined Solvent Extraction and Agglomeration Technique for the Recovery of Bitumen from Tar Sands", *Proc. 27th Can. Chem. Eng. Conference on Oil Sands*, Ottawa, Ontario, 45 (1977).

48. Sparks, B.D. and Meadus, F.W., "A Combined Solvent Extraction and Agglomeration Technique for the Recovery of Bitumen from Tar Sands", *Energy Proc., Can.*, **72**, 55 (1979).

49. Sparks, B.D. and Meadus, F.W., "A Study of Some Factors Affecting Solvent Losses in the Solvent Extraction-Spherical Agglomeration of Oil Sands", *Fuel Process. Tecnol.*, **4**, 251 (1981).

50. Venkatesan, V.N., "Fluid Bed Thermal Recovery of Synthetic Crude from Bituminous Sands of Utah", Ph.D. Dissertation, University of Utah, Salt Lake City (1980).

51. Dorius, J.C., "The Pyrolysis of Bitumen-Impregnated Sandstone from the PR Spring (Utah) Deposit in a Fluidized Bed", Ph.D. Dissertation, University of Utah, Salt Lake City (1985).

52. Lynch, K.Z., Hood, R.I., Maraven, O.G., and Aquino, L.G., "Rose - A Flexible Process for Upgrading Heavy Crude and Atmospheric or Vacuum Residue", *Proc. Sixth Unitar/UNDP International Conference on Heavy Crude and Tar Sands*, Houston, Texas, Paper #27 (Feb. 11-14, 1995).

53. Sprague, S., Washimi, K., and Ishibashi, M., "Upgrading Cold Lake Bitumen Using the HSC-ROSE Process", Paper presented in the 1986 Tar Sands Symposium (1986).

54. Sanford, E.C., and Chung, K.H., "The Mechanism of Pitch Conversion During Coking, Hydrocracking and Catalytic Hydrocracking of Athabasca Bitumen", *AOSTRA J. Res.* **7**, 37 (1991).

55. Weiss, H. and Schmalfeld, "Coking of Residue Oil by LP-Process", *Erdol Kohle*, **42**, 235 (1989).

56. Nelson, L.R., MacKinnon, M., and Gulley, J.R., "Environmental Issues on Reclamation of Oil Sand Fine Tails", *Proc. Sixth Unitar/UNDP International Conference on Heavy Crude and Tar Sands*, 1995, Houston, Texas, Paper #163 (Feb. 11-14, 1995).

57. McHugh, M.A. and Krukonis, V.J., *Supercritical Fluid Extraction-Principles and Practice*, Butterworths, Boston, (1993).

58. Bukka, K., Hanson, F.V., Miller, J.D., and Oblad, A.G., "Fractionation and Characterization of Whiterocks Tar Sand Bitumen", *Energy & Fuels*, **6**, 160 (1992).

59. Subramanian, M., Deo, M.D., and Hanson, F.V., "Compositional Analysis of Bitumen and Bitumen-Derived Products", *J. Chromo. Sci.*, **34**, 20 (1996).

60. Kehlen, H., Ratzsch, M.T., and Bergmann, J., "Continuous Thermodynamics of Multicomponent System", *AICHE J.*, **31**, 1136 (1985).

61. Cotterman, R.L., "Phase Equilibria for Complex Fluid Mixtures at High Pressures. Development and Application of Continuous Thermodynamics", Ph.D. Dissertation, Chapter 2, 3. University of California, Berkeley (1985).

62. Peng, D.Y. and Robinson, D.B., "A New Two-Constant Equation of State", *Ind. Eng. Chem. Fundam.*, **15**, 59 (1976).

63. Hwang, J., "Supercritical Fluid Extraction of Complex Hydrocarbon Mixtures Using CO_2 and Propane", Ph.D. Dissertation, University of Utah, Salt Lake City (1992).

64. Subramanian, M., "Application of Supercritical Fluid Extraction to Upgrading Oil Sand Bitumens", M.S. Thesis, University of Utah, Salt Lake City (1994).

65. Speight, J.G., *The Chemistry and Technology of Petroleum*, 2 ed., Marcel Dekker, Inc., New York, New York (1991).

66. Bukka, K., Miller, J.D., and Oblad, A.G., "Fractionation and Characterization of Utah Tar Sands Bitumens: Influence of Chemical Composition on Bitumen Viscosity", *Energy & Fuels*, **5**, 333 (1991).

67. Starling, K.E., *Fluid Thermodynamic Properties for Light Petroleum Systems*, Gulf Publishing Co., Houston, Texas (1973).

68. Jamaluddin, A.K.M., Kalogerakis, N.E., and Chakma, A., "Predictions of CO_2 Solubility and CO_2 Saturated Liquid Density of Heavy Oil and Bitumens Using a Cubic Equation of State", *Fluid Phase Equilibria*, **64**, 22 (1991).

69. Martin, J.J., "Cubic Equation of State - Which?", *Ind. Eng. Chem. Fundam.*, **18**, 81 (1979).

70. Floyd, R.H., Personal Communication, The M.W. Kellogg Company, Houston, TX, March 1996.

71. Johnston, K.P., "New Directions in Supercritical Fluid Science and Technology", *Supercritical Fluid Science and Technology*, Johnston, K.P., and Penninger, J.M.L. eds., American Chemical Society, Washington, DC (1989).

72. Nellesteyn, F.J., "The Colloidal Structure of Bitumen", *The Science of Petroleum*, Oxford U. press, New York City, **4** , 2750 (1938).

73. Swanson, J., *J Chemical Physics*, **46**, 141 (1943).

74. Witherspoon, P.A. and Munir, Z.A., *Producers Monthly*, **24**, 20 (1960).

75. Dickie, J.P. and Yen, T.F., "Macrostructures of the Asphaltenic Fractions by Various Instrumental Methods", *Anal. Chemistry*, **39**, 1847, (1967).

76. Koots, J.A. and Speight, J.C., "Relation of Petroleum Resins to Asphaltenes", *Fuel*, **54**, 179 (1975).

77. Mansoori, G.A., Jiang, T.S., and Kawanaka, S., "Asphaltene Deposition and its Role in Petroleum Production and Processing", *Arab. J. Sci. And Eng.*, **13**, 17 (1988).

78. Mitchell, D.L. and Speight, J.G., "The Solubility of Asphaltenes in Hydrocarbon Solvents", *Fuel*, **52**, 149 (1973).

79. Speight, J.G., Long, R.B., and Trowbridge, T.D., "Factors Influencing the Separation of Asphaltenes from Heavy Petroleum Feedstocks", *Fuel*, **63**(5), 616 (1984).

80. Kokal, S.L. and Sayegh, S.G., "Gas Saturated Bitumen Density Prediction Using the Volume Translated Peng-Robinson Equation of State", Report 1988-14, Petroleum Recovery Institute, Calgary, Canada (1988).

81. Schumacher, M.M., "*Heavy Oil and Tar Sands Recovery and Upgrading*, Noyes Data Corporation, Park Ridge, New Jersey (1982).

82. Oblad, A.G., Bunger, J.W., Hanson, F.V., Miller, J.D., Ritzma, H.R., and Seader, J.D., "Tar Sand Research and Development at the University of Utah", *Ann. Rev. Energy*, **12**, 283, (1987).

83. Duerkson, C.H., "Gravity drainage processes for recovery and in-situ upgrading of heavy oil and bitumen", 16th Rocky Mountain Fuel Society Symposium, Salt Lake City, Utah, 1993.

84. Longstaff, D.C., "Hydrotreating the Whiterocks Oil Sand Bitumen and Bitumen Derived Liquid", Ph.D. Dissertation, University of Utah, Salt Lake City, Utah, 1992.

85. Ryu, H., "Kinetic Modeling Applied to Hydrocarbon Process Design and Engineering: I. Hydropyrolysis of Heavy Oils; II. Acetylene from Calcium Carbide", Ph.D. Dissertation, University of Utah, Salt Lake City, Utah, 1989.

86. Boduszinski, M.M., "Composition of Heavy Petroleums. 1. Molecular weight deficiency, and heteroatom concentration as a function of atmospheric equivalent boiling point up to 1400°F (760°C)", *Energy & Fuels*, **1**:2-11 (1987).

87. Boduszinski, M.M., "Composition of Heavy Petroleums. 2. Molecular Characterization", *Energy & Fuels*, **2**:597-613 (1988).

88. Altgelt, K.H., and Boduszinski, M.M., "Composition of Heavy Petroleums. 3. An improved boiling point-molecular weight relation", *Energy & Fuels*, **6**:68-72 (1992).

89. Boduszinski, M.M. and Altgelt, K.H., "Composition of heavy petroleums 4. Significance of the extended atmospheric equivalent boiling point (AEBP) scale", *Energy & Fuels*, **6**:72-76 (1992).

90. ASTM D2892-90, *Distillation of Crude Petroleum (15-Theoretical Plate Column)* (1990).

91. ASTM D2887-89, *Boiling Range Distribution of Petroleum Fractions by Gas Chromatography* (1989).

92. ASTM D5307-92, *Determination of Boiling Point Distribution of Crude Petroleum by Gas Chromatography* (1992).

93. Worman and Green, L.E., "Simulated Distillation of High Boiling Petroleum Fractions", *Anal. Chem.*, **37**, 1620 (1965).

94. Neer, L. and Deo, M.D., "Simulated Distillation of Oils with a Wide Carbon Number Distribution", *J. Chromo. Sci.*, **33**, 133 (1995).

95. "Selected values of properties of hydrocarbons and related compounds", TRC Thermodynamic Table, API Project No. 44, October 31, 1972.

96. AOSTRA, "Syncrude Analytical Methods for Oil Sand and Bitumen Processing", Syncrude Canada, Edmonton, Alberta, Canada, 1979.

97. TSC, "Production of Synthetic Fuel from Tar Sands", Rocky Mountain Oil and Gas Association, Inc., Tar Sands Committee, Technical Subcommittee, August 6 (1981).

98. Probstein, R.F. and Hicks, R.E., "Synthetic Fuels", pH Press, Cambridge, MA (1990).

99. Camp, F.W., "Tar Sands", in Kirk-Othmer, Encuclopedia of Chemical Technology, 2nd ed., Interscience Publishers, New York, **19**, 682 (1969).

100. Baughman, G.L., "Synthetic Fuels Data Handbook", 2nd ed., Cameron Engineers, Inc., Denver, Colorado (1978).

101. Camp, F.W., "Tar Sands of Alberta, Canada", Cameron Engineers, Denver, Colorado (1974).

102. Clark, K.A., "Hot Water Separation of Bitumen from Alberta Bituminous Sand", Research Council of Alberta, Report 1922, Edmonton, Alberta, Canada, 42 (1923).

103. Clark, K.A., "Hot Water Separation of Alberta Bituminous Sands", Can. Insti. Min. Metall. Trans., **47**, 257 (1944).

104. Hanson, F.V. and Oblad, A.G., "The Fluidized Bed Pyrolysis of Bitumen-Impregnated Sandstone from the Tar Sand Deposits of Utah", Fourth UNITAR/UNDP Proceedings, **5**, Paper No. 155, 421 (1988).

105. Cha, S., "Pyrolysis of Oil Sands from the Whiterocks Tar Sand Deposit in a Rotary Kiln",

Ph.D. Dissertation, University of Utah, Salt Lake City, Utah (1991).

106. Nagpal, S., "Pyrolysis of Oil Sand in a Large Diameter Fluidized Bed Reactor", M.S. Thesis, University of Utah, Salt Lake City, Utah (1995).

107. Gishler, P.E., "The Fluidization Technique Applied to Direct Distillation from Bituminous Sand", *Can. J. Res.*, F.27, 104 (1944).

108. Peterson, W.S. and Gishler, P.E., "A Small Fluidized Solids Pilot Plant for the Direct Distillation of Oil from Alberta Bituminous Sands", *Can. J. Res.*, **28**, 62 (1950).

109. Rammler, R.W., "The Production of Synthetic Crude Oil from Oil Sand by Application of the Lurgi-Ruhrgas Process", *Can. J. Chem. Eng.*, **48**, 552 (1970).

110. Donnelly, J.K., Moore, R.G., Bennion, D.W., and Trenkwalder, A.E., "A Fluidized Bed Retort for Oil Sands", *Can. J. Chem. Eng.*, **59**, 68 (1981).

111. Taciuk, W., "Process for Thermal Cracking a Heavy Hydrocarbon", U.S. Patent 4, 180, 455 (1977).

112. Taciuk, W., "Apparatus and Process for Recovery of Hydrocarbon from Inorganic Host Materials", U.S. Patent 4, 285, 773 (1979).

113. Hanson, F.V., Cha, S.M., Deo, M.D., and Oblad, A.G., "Pyrolysis of Oil Sand from the Whiterocks Deposit in a Rotary Kiln", *Fuel*, **71**, 1455 (1992).

114. Wang, J., "The Production of Hydrocarbon Liquids from a Bitumen-Impregnated Sandstone in a Fluidized Bed Pyrolysis Reactor", M.S. Thesis, University of Utah, Salt Lake City, Utah (1983).

115. Weeks, J.K., Jr., "Fluidized-Bed Processing of Utah Tar Sands", M.S. Thesis, Unversity of Utah, Salt Lake City, Utah (1977).

116. Jayakar, K.M., "Thermal Recovery of Oil from Tar Sands", Ph.D. Dissertation, University of Utah, Salt Lake City, Utah (1979).

117. Smart, L.M., "Thermal Processing of Utah Tar Sands", M.S. Thesis, Unversity of Utah, Salt Lake City, Utah (1984).

118. Coronella, J.C., Jr., "Optimizing a Thermal Fluidized-Bed Tar-Sands Extraction Process", Ph.D. Dissertation, University of Utah, Salt Lake City, Utah (1994).

119. Sung, S.H., "The Fluidized Bed Pyrolysis of Bitumen-Impregnated Sandstone in a Large

Diameter Reactor", M.S. Thesis, University of Utah, Salt Lake City, Utah (1988).

120. Shun, D., "The Pyrolysis of Bitumen-Impregnated Sandstone from the Circle Cliffs (Utah) Deposit in a Fluidized-Bed Reactor", Ph.D. Dissertation, University of Utah, Salt Lake City, Utah (1990).

121. Fletcher, J.V., "Pyrolysis of Oil Sands in a Fluidized Bed at Reduced Pressure", Ph.D. Dissertation, Fuels Engineering, University of Utah, Salt Lake City,. Utah (1992).

122. Hanson, F.V., Fletcher, J.V., and Zheng, H., "Performance of Auger-Type Dry Materials Feeders when Feeding Oil Sands", *Fuel Process. Tech.*, **41**, 289 (1995).

123. Dietz, W.A., "Response Factors for Gas Chromatographic Analysis", *J. Gas. Chromatogr.*, **5**, 68, February (1967).

124. Rosie, D.M. and Barry, E.F., "Quantitation of Thermal Conductivity Detectors", *J. Chromatogr. Sci.*, **11**, 237 (1973).

125. Tang, H., "Combustion of Carbonaceous Residues on Spent Oil Sands in a Fluidized Bed Reactor", MS Thesis, University of Utah, Salt Lake City, Utah (1995).

126. Allen, T., "Particle Size Measurement", 4th ed., Chapman and Hall, London (1990).

127. "Syncrude Analytical Methods for Oil Sand and Bitumen Processing", Syncrude Canada Ltd. (1979).

128. Geldart, D., "Gas Fluidization Technology", John Wiley & Sons, Chichester, Great Britain (1986).

129. Knowlton, T.M. and Hirsan, I., "L-Valves Characterized for Solids Flow", *Hydrocarbon Process.*, **3**, 149 (1978).

130. Frick, A.E. and Novak, F., "Control of Solid Heat Circulation Using an L-Valve", The Eleventh Australian Conference on Chemical Engineering, CHENECA **83**, 547 (1983).

131. Geldart, D. and Jones, P., "The Behaviour of L-Valves with Granular Powders", *Powder Technol.*, **67**, 163 (1991).

132. Yang, W.C. and Knowlton, T.M., "L-Valve Equations", *Powder Technol.*, **77**, 49 (1993).

133. Cheremisinoff, N.P. and Cheremisinoff, P.N., "Hydrodynamics of Gas-Solids Fluidization", Gulf Publishing Company, Houston, Texas (1984).

134. Howard, J.R., "Fluidized Bed Technology: Principles and Applications", Adam Hilger, Bristol (1989).

135. Kunii, D. and Levenspiel, O., "Fluidization Engineering", 2nd ed., Butterworth-Heinemann, Boston (1991).

136. Knowlton, T.M., "Solid Transfer in Fluidized Systems", *Gas Fluidization Technology* ed by Geldard, D., John Wiley & Sons, Chidester, Great Britain (1986).

137. Botterill, M.S.J., Teoman, Y., and Yuregir, K.R., "The Effect of Operating Temperature on the Velocity of Minimum Fluidization, Bed Voidage and General Behaviour", *Powder Technol.*, **31**, 101 (1982).

138. Saxena, S.C., Rao, N.S., and Zhou, S.J., "Fluidization Characteristics of Gas Fluidized Beds at Elevated Temperatures", *Energy*, **15**(11) 1001 (1990).

139. Kusakabe, K., Kuriyama, T., and Morooka, S., "Fluidization of Fine Particles at Reduced Pressure", *Powder Technol.*, **58**, 125 (1989).

140. Wriath, A.E. and Harris, R., "Fluidization of a Mineral Concentrate at Reduced Pressure", *Miner. Eng.*, **5**(9), 993 (1992).

141. Germain, B. and Claudel, B., "Fluidization of Mean Pressure less than 30 Torr", *Powder Technol.*, **13**, 115 (1976).

142. Ergun, S., "Fluid Flow through Packed Columns", *Chem. Eng. Prog.*, **48**(2), 89 (1952).

143. Fletcher, J.V., Deo, M.D., and Hanson, F.V., "Re-examination of Minimum Fluidization Velocity Correlation's Applied in Group B Sands and Coked Sands", *Powder Technol.*, **69**, 147 (1992).

144. Lippens, B.C. and Mulder, J., "Prediction of the Minimum Fluidization Velocity", *Powder Technol.*, **75**, 67 (1993).

145. Wen, C.Y. and Yu, Y.H., "A Generalized Method for Predicting the Minimum Fluidization Velocity", *AIChE J.*, **12**, 610 (1966).

146. Morgan, M.H., III, "Analytical Expressions for the Spout/Annulus Pressure Drop and Pressure Gradient in Spout Beds of Coarse Particles", in Fluidization V Proceedings of the Fifth Engineering Fluidization Conference on Fluidization, ed. by Comerer, Engineering Foundation, New York, 249 (1986).

147. Shi, Y., Yu, Y.S., and Fan, L.T., "Incipient Fluidization Condition for a Tapered Fluidized

Bed", *Ind. Eng. Chem. Fundam.*, **23**, 484 (1984).

148. Toyohara, H. and Kawamura, Y., "Fluidization of a Tapered Fluidized-Bed of a Binary Particle-Mixture", *Int. Chem. Eng.*, **32**(1), 164 (1992).

149. Saxena, S.C. and Vogel, G.S., "The Measurement of Incipient Fluidization Velocities in a Bed of Coarse Dolomite at Temperature and Pressure", *Trans. Inst. Chem. Eng.*, **55**, 184 (1977).

150. Wu, S.Y. and Baeyens, J., "Effect of Operating Temperature on Minimum Fluidization Velocity", *Powder Technol.*, **67**, 217 (1991).

151. Botterill, M.S.J. and Teoman, Y., "Fluid-Bed Behaviors at Elevated Temperature", Fluidization, Ed. By Grace, J.R. and J.M. Maten, Plenum Press, New York, 93 (1980).

152. Mii, T., Yoshida, K., and Kunii, D., "Temperature Effects on the Characteristics of Fluidized Bed", *J. Chem. Eng. Japan*, **6**(1), 100 (1973).

153. White, F.M., "Heat and Mass Transfer", Addison-Wesley, New York (1988).

154. Raso, R., D'Amore, M., Formisani, B., and Lignola, P.G., "The Influence of Temperature on the Properties of the Particulate Phase at Incipient Fluidization", *Powder Technol.*, **72**, 71 (1992).

155. Christensen, R.J., Lindberg, R.W., and Dorrence, S.M., "Viscous Characteristics of a Utah Tar Sand Bitumen", *Fuel*, **63**(9), 1312 (1984).

156. Bhadkamkar, A.S., "Optimizing the Operation of a Thermally Coupled Fluidized Bed Tar Sands Extraction Process", Ph.D. Dissertation, University of Utah, Salt Lake City, Utah (1995).

157. Oblad, A.G., Bunger, J.W., Dahlstrom, D.A., Deo, M.D., Hanson, F.V., Miller, J.D., and Seader, J.D., "The Extraction of Bitumen from Western Oil Sands", Final Report for the Period July 6, 1992 to September 29, 1993 to U.S. Department of Energy, Contract No.: DE-FC21-89MC26268 (1993).

158. Miller, J.D. and Mishra, M., "Hot Water Process Development for Utah Tar Sands", *Fuel Process. Tech.*, **6**, 27 (1982).

159. Miller, J.D. and Mishra, M., "Concentration of Utah Tar Sands by an Ambient Temperature Floatation Process", *Int. J. Min. Process.*, **9**(3), 269 (1982).

160. Mishra, M. and Miller, J.D., "Comparison of Water-Based Physical Separation Processes for U.S. Tar Sands", *Fuel Process. Tech.* **27**, No. 1, 3 (1991).

161. Fletcher, J.V., Deo, M.D., and Hanson, F.V., "Fluidized Bed Pyrolysis of Oil Sands at Less than Ambient Pressure", *Fuel* (1995).

162. Nagpal, S., Fletcher, J.V., and Hanson, F.V., "Pyrolysis of Uinta Basin Oil Sands in Fluidized Bed and Rotary Kiln Reactors", *Sixth UNITAR/UNDP Conference*, Papr #118 (1995).

163. Longstaff, D.C., Balaji, G., Kim, J., Kwak, S., Tsai, C.H., and Hanson, F.V., "Hydrotreating Uinta Basin Bitumen-Derived Heavy Oils", *Sixth UNITAR/UNDP Conference*, (1995).

164. Seader, J.D. and Jayakar, K.M., "Process and Apparatus to Produce Crude Oil from Tar Sands", U.S. Patent No. 4, 160.720 (1979).

165. Venkatesan, V.N., Hanson, F.V., and Oblad, A.G., "A Fluidized Bed Thermal Pyrolysis Process for the Recovery of a Bitumen-Derived Liquid from the Bitumen Impregnated Sandstone Deposits of Utah", *AIChE Symp. Ser.*, **78** (216), 42 (1982).

166. Hanson, F.V., Dorius, C.J., Utley, J.K., and Nguyen, T.V., "The Application of Compound Type Analyses to the Correlation of Product Distribution and Yields from Fluidized-Bed Pyrolysis of Oil Sands", *Fuel*, **71,** 1365 (1992).

167. Deo, M.D., Fletcher, J.V., Shun, D., Hanson, F.V., and Oblad, A.G., "Modelling the Pyrolysis of Tar Sands in Fluidized Bed Reactors", *Fuel*, **70**, 1271 (1991).

168. Clift, R., in *Gas Fluidization Technology*, D. Geldart, Ed., John Wiley, London (1986).

169. Cha, S.M., Hanson, F.V., Longstaff, D.C., and Oblad, A.G., "Pyrolysis of Bitumen-Impregnated Sandstones: A Comparison of Fluidized Bed and Rotary Kiln Reactors", *Fuel*, **70**, 1357-1361 (1991).

170. Kenkel, J., "Analytical Chemistry Refresher Manual", Lewis Publishers, Inc., Michigan (1992).

171. Bulmer, J.T. and Starr, J., Eds., "Syncrude Analytical Methods for Oil Sands and Bitumen Processing", Syncrude Canada Limited, Edmonton, Alberta Canada (1979).

172. Babu, S.P., Shah, B., and Talwalker, A., "Fluidization Correlations for Coal Gasification Materials - Minimum Fluidization Velocity and Bed Expansion Ratio", *AIChE Symp. Ser.*, **74**, 176-186 (1978).

173. Mathur, A., Saxena, S.C., and Zhang, Z.F., "Hydrodynamic Characteristics of Gas-Fluidized Beds Over a Broad Temperature Range", *Powder Tech.*, **47**, 247 (1986),

174. Grewal, N.S. and Gupta, A., "Total and Gas Convective Heat Transfer from a Vertical Tube to a Mixed Particle Gas-Solid Fluidized Bed", *Powder Technol.*, 57, 27-38 (1989).

175. Baeyens, J. and Geldart, D., Chapter 5 in *Gas Fluidization Technology*, D. Geldart Ed., Chichester: John Wiley & Sons, Inc. (1986).

176. Allred, V.D., "Kinetics of Oil Shale Pyrolysis", *Chem. Engr. Prog.*, **62**, No. 8, 55 (1966).

177. Phillips, C.R., Haidar, N.I., and Poon, Y.C., "Kinetic Models for the Thermal Cracking of Athabasca Bitumen: The Effect of the Sand Matrix", *Fuel*, **64**, 678 (1985).

178. Conesa, J.A., Marcilla, A., and Font, R., "Kinetic Model of the Pyrolysis of Polyethylene in a Fluidized Bed Reactor", *J. Anal. And App. Pyrolysis*, **30**, 101-120 (1994).

179. Peterson, W.S. and Gishler, P.E., "Oil from Alberta Bituminous Sands", *Petrol. Engr.*, **23**, C-66 (1951).

180. Carberry, J.J., *Chemical and Catalytic Reaction Engineering*, McGraw-Hill Book Company, Inc., New York (1976).

181. Meyer, R.F. and Duford, J.M., "Resources of Heavy Oil and Natural Bitumen Worldwide", in Proc. Fourth UNITAR/UNDP International Conference on Heavy Crude and Tar Sands, ed. by R.F. Meyer and E.J. Wiggins, August 7-12, 1988, Paper #147 (1988).

182. "Major Tar Sands and Heavy Oil Deposits of the United States", Interstate Oil Compact Commission, U. of Oklahoma Press, Norman, Oklahoma (1984).

183. Meyer, R.F. and Dietzman, W.D., "World Geography of Heavy Crude Oils", A paper presented at the First International Conference on the Future of Heavy Crude and Tar Sands (UNITAR), Edmonton, Alberta, Canada, June 4-12 (1979).

184. Marchant, L.C., "U.S. Tar Sands Projects, 1985", Third International Conference on Heavy Crude and Tar Sands, Long Beach, CA (1985).

185. Ritzma, H.R. and Campbell, J.A., "Oil-Impregnated Sandstone Deposits in Utah", Map 47 - Utah Geological and Mineral Survey (1979).

186. Crysdale, B.L. and Shenk, C.J., "Bitumen-Bearing Deposits of the United States", U.S.G.S. Bull. #1784, 45 (1988).

187. McLendon, T.R., U.S. "Department of Energy Tar Sand Program Overview", Proceedings of the Eastern Oil Shale Symposium (1990).

188. Stosur, G.J., "Heavy Oil and Tar Sands Recovery Technology in the Year 2000 and Beyond", U.S. Department of Energy, Fourth UNITAR/UNDP Conference on Heavy Crude and Tar Sands, 4 (1988).

189. Bezama, R.J., "An Energy-Efficient Method for Thermal Processing of Utah Tar Sands", Ph.D. Dissertation, University of Utah, Salt Lake City, Utah (1983).

190. Coronella, C.J., "Modelling a Coupled Fluidized-Bed Reactor for Extraction of Bitumen from Tar Sands", MS Thesis, University of Utah, Salt Lake City, Utah (1989),

191. Coronella, C.J. and Seader, J.D., "Combustion of Coked Sand in a Two-Stage Fluidized Bed System", *Fuel*, **71**, 143 (1992).

192. Stubinton, J.F., Barrett, D., and Lowry, G., "Bubble Size Measurements and Correlation in a Fluidized Bed at High Temperatures", *Chem. Eng. Res., Des.*, **62**, 173 (1984).

193. Darton, R.C., LaNauze, R.D., Davidson, J.F., and Harrison, D., "Bubble Growth Due to Coalescence in Fluidised Beds", *Trans. Instn. Chem. Engrs.*, **55**, 274 (1977).

194. Grace, J.R., "Generalized Models for Isothermal Fluidized-Bed Reactors", *Recent Advances in Engineering Analysis of Chemically Reacting Systems*, L.K. Doraiswami, ed., Wiley Eastern, New Delhi, p. 237 (1984).

195. Levenspiel, O., *Chemical Reaction Engineering*, John Wiley, New York (1969).

196. Phillips, C.R., Haidar, N.I., and Poon, Y.C., "Kinetic Models for the Thermal Cracking of Athabasca Bitumen", *Fuel*, **64**, 678 (1985).

197. Lin, L.C., Deo, M.D., Hanson, F.V., and Oblad, A.G., "Kinetics of Tar Sand Pyrolysis Using a Distribution of Activation Energy Model", *AIChE J.*, **36**(10), 1585 (1990).

198. Field, M.A., Fill, D.W., Morgan, B.B., and Hawksley, P.G.W., *Combustion of Pulverized Coal*, Cheney and Sons, Banbury, England (1967).

199. Hottel, H.C., Williams, G.C., Nerheim, N.M., and Schneider, G.R., "Kinetic Studies in Stirred Reactors: Combustion of Carbon Monoxide and Propane", *Tenth Symp. (International) on Combustion*, Combustion Institute, Pittsburgh, 111 (1965).

200. Coyle, T.D., "Silica", *Encyclopedia* of Chemical Technology, R.E. Kirk and D.F. Othmer, John Wiley, New York, eds., vol. 20, p. 757 (1982)
Darton, R.C., R.D. LaNauze, J.F. Davidson, and D. Harrison, "Bubble Growth Due to Coalescence in Fluidized Beds", *Trans. Inst. Chem. Engr.*, 55, 274 (1977).

201. API, *Technical Data Book - Petroleum Refining*, American Petroleum Institute, New York (1966).

202. Chi, S.W., *Heat Pipe Theory and Practice*, McGraw-Hill, New York (1976).

203. Dunn, P. and Reay, D.A., "Heat Pipes", Pergamon Press Ltd., Elmsford, New York (1982).

204. Saxena, S.C., "Heat Transfer Between Immersed Surfaces and Gas-Fluidized Beds", *Adv. Heat Transfer*, Academic Press, New York, **19**, 97 (1989).

205. Saxena, S.C. and Ganzha, V.L., "Heat Transfer to Immersed Surfaces in Gas-Fluidized Beds of Large Particles and Powder Classification", *Powder Technol.*, **39**, 199 (1984).

206. Wender, L. and Cooper, G.T., "Heat Transfer between Fluidized-Solids Beds and Boundary Surfaces-Correlation of Data", *AIChE J.*, **4**(1), 15 (1958).

207. Vreedenberg, H.A., J. Appl. Chem., 2, suppl. issue No. 1, S-26, (1952), cf. Wender and Cooper, (1958).

208. Mickley, H.S. and Fairbanks, D.F., "Mechanism of Heat Transfer to Fluidized Beds", *AIChE J.*, **1**, 374 (1955).

209. Molerus, O., "Arguments on Heat Transfer in Gas Fluidized Beds", *Chem. Eng. Sci.*, **48**(4), 761 (1993)
Oblad, A.G., Bunger, J.W., Hanson, F.V., Miller, J.D., Ritzma, H.R., and Seader, J.D., "Tar Sand Research and Development at the University of Utah", *Ann. Rev. Energy*, **12**, 283 (1987).

210. Thring, R.H., "Fluidized Bed Combustion for the Stirling Engine", *Int. J. Heat Mass Transfer*, **20**, 911 (1977).

211. Gelperin, N.I. and Einstein, V.G., "Heat Transfer in Fluidized Beds", *Fluidization*, J.F. Davidson and D. Harrison, eds., Academic Press, New York, 471 (1971).

212. Verma, R.S. and Saxena, S.C., "Heat Transfer from an Immersed Vertical Tube to a Gas Fluidized Bed", *Energy*, **8**(12), 909 (1983).

213. Bhadkamkar, A.S., "Optimizing the Operation of Thermally Coupled Fluidized-Bed Sands Extraction Process", Ph.D. Dissertation, University of Utah, Salt Lake City, Utah (1995).

214. Bunger, J.W., "Processing Utah Tar Sand Bitumen", Ph.D. Dissertation, University of Utah, Salt Lake City, Utah (1979).

215. Albright, L.F., Crynes, B.L., and Corcoran, W.H., "Pyrolysis: Theory and Industrial Practice", Academic Press, New York (1983).

216. Seader, J.D. and Jayakar, K.M., "Process and Apparatus to Produce Crude Oil from Tar Sands", U.S. Patent No. 4, 160, 720 (1979).

217. Hsu, J.C.L. and Seader, J.D., "Digital Control of a Coupled Fluidized-Bed Thermal Processing System for Tar Sands", *Fuel. Processing Technol.*, **21**, 1 (1989).

218. Bianco, A.D., Panariti, N., Anelli, M., Beltrame, P.L., and Carniti, P., "Thermal Cracking of Petroleum Residues", *Fuel*, **72**, 75 (1993).

219. Zou Renjun, *Fundamentals of Pyrolysis in Petrochemistry and Technology*, CITIC Publishing House, Beijing, China (1993).

220. Shabtai, J.S., Personal Communication, University of Utah, Salt Lake City, Utah (1994).

221. Altgelt, K.H., "Composition and Analysis of Heavy Petroleum Fractions", Marcel-Dekker (1994).

222. Khot, K.S., "Modelling a Coupled Fluidized-Bed Process for Extraction of Tar Sand Bitumen", M.S. Thesis, University of Utah, Salt Lake City, Utah (1995).

223. Rao, S.S., *Optimization: Theory and Applications*, Wiley Eastern Limited, New York (1979).

224. Joshi, S.D., "A Review of Horizontal Well Technology", *JPT*, 1302-1304 (Nov. 1991).

225. Jurgens, R. and Bitto, R., "Horizontal Drilling and Completions: A Review of Available Technology", *Pet. Engineer International*, 15-20 (Feb. 1991).

226. Gust, D., "Horizontal Drilling Evolving from Art to Science", *Oil and Gas J.*, 43-52 (July 1989).

227. Butler, R.M., "Thermal Recovery of Oil and Bitumen", Prentice Hall: Englewood Cliffs, New Jersey (1991).

228. "Steam and Additive Reservoir Simulator (STARS)-Gas, Solvent and Aqueous Additives, Version 95.00", Computer Modeling Group, Calgary, Alberta, Canada (Fall 1994).

229. Edmunds, N.R., Haston, J.A., Best, D.A., "Analysis and Implementation of the Steam Assisted Gravity Drainage Process at the AOSTRA UTF", Presented at the Fourth UNITAR/UNDP Conference on Heavy Crude and Tar Sands, Edmonton, Alberta, Canada, August 1988, paper 125.

230. Sarkar, A., "Thermal Enhances Oil Recovery Processes Using a Combination of Vertical and Horizontal Well", M.S. Thesis, University of Utah, Salt Lake City, (1993).

231. Closeman, P.J. and Smith, R.A., "Temperature Observations and Steam-Zone Rise in the Vicinity of a Steam-Heated Fracture", *Soc. Pet, Eng. J.*, 575-586 (August 1983).

232. Campbell, J.A. and Ritzma, H.R., "Geology and Petroleum Resources of the Major Oil-Impregnated Sandstone Deposits of Utah", Utah Geol. And Miner. Survey, Special Studies 50, p. 25 (1979).

233. Chung, K.-H. and Butler, R.M., "A Theoretical and Experimental Study of Steam-Assisted Gravity Drainage Process", in R.F. Meyers and E.J. Wiggins (Editors), The Fourth UNITAR/UNDP International Conf. On Heavy Crude and Tar Sands, Vol. 4: In-situ Recovery, AOSTRA, Edmonton, p. 191-210 (1988).

234. DeBiase, R. and Elliott, J.D., *Hydrocarbon Processing*, 99 (May 1982).

235. Allan, D.w., Metrailer, W.J., and King, R.C., *Chem. Eng. Progr.*, 49 (Dec. 1981).

236. Heck, R.H., Rankel, L.A., and DiGuiseppi, F.T., *Fuel Proc. Technol.*, **30**, 69 (1992).

237. Heck, R.H. and DiGuiseppi, F.T., *Prprnt. Am. Chem. Soc. Div. Pet. Chem.*, **38**, 417 (1993).

238. Speight, J.G., *Fuels Science and Technology Handbook*, Marcel Dekker, New York (1990).

239. Beaton, E.I. and Bertolacini, R.J., *Catal. Rev.-Sci. Eng.* **33**(3&4), 281 (1991).

240. Quann, R.J., Ware, R.A., Hung, C., and Wei, J., *Advances in Chemical Engineering*, **14**, 95 (1988).

241. McColgan, E.C. and Parsons, B.I., *Can. Mines. Br. Res. Rep.*, R-253 (1972).

242. Dewind, N., Plantenga, F.L., Heineman, J.J.L. and Homan Free, N.W., *Appl. Catal.*, **43**, 239 (1988).

243. Kim, J.W., "Catalytic and Thermal Effects in the Upgrading of Bitumen-Derived Heavy Oils", Ph.D. Dissertation, University of Utah, Salt Lake City, Utah (1995).

244. Ho, T.C., *Catal. Rev.-Sci. Eng.*, **30**, 117 (1988).

245. Longstaff, D.C., Deo, M.D., and Hanson, F.V., *Fuel*, **73**(9), 1523 (1994).

246. Strausz, O.P., *Prprnt. Am. Chem. Soc. Div. Pet. Chem.*, **38**, 417 (1989).

247. Trytten, L.C., Gray, M.G., and Sanford, E.C., *Ind. Eng. Chem. Res.*, **29**(5), 725 (1990).

248. Longstaff, D.C., Deo, M.D., and Hanson, F.V., *Fuel*, **73**, 1523 (1994).

249. Schuit, G.C.A. and Gates, B.C., *AIChE J.*, **19**(3), 417 (1973).

250. Homan-Free, H. and Lovink, H.J., *Erdoel Kohle*, **40**, 346 (1987).

251. Reynolds, J.G., *Liquid Fuels Technol.*, **3**, 73 (1985).

252. Tsai, C.H., Deo, M.D., Hanson, F.V., and Oblad, A.G., *Fuel Sci. Technol. Int.*, **9**, 1259, (1991).

253. Flinn, R.A., Larson, O.A., and Beuther, H., *Prprnt. Am. Chem.*, **7**, 165 (1962).

254. Mosby, J.F., Butte, R.D., Cox, J.A., and Nickolaides,k C., *Chem. Eng. Sci.*, **41**(2), 989 (1986).

255. Riley, K.L., *Prprnt. Am. Chem. Soc. Div. Pet. Chem.*, **23**, 1104, (1978).

256. Absi-Halabi, M., Stanislaus, A., and Trimm, D.L., *Appl. Catal.*, **72**, 193 (1991).

257. Longstaff, D.L., Balaji, G., Kim, J., Kwak, S., Tsai, C.H., and Hanson, F.V., Proceedings of the 6th UNITAR International Conference on Heavy Crude and Tar Sands, Houston, Texas, Vol. E, p. 427 (1995).

258. Miki, Y., Yamadaya, S., Oba, M., and Suggimoto, Y., *J. Catal.*, **83**, 371 (1983).

259. Sanford, E.C. and Chung, K.H., *AOSTRA J. Res.*, 7, 37 (1991).

260. Bianco, A.D., Panariti, N., Anelli, N., Beltrame, P.L., and Carniti, P., *Fuel*, **72**, 75 (1993).

261. Khorasheh, F., Rangwala, H., Gray, M.R., and Dalla Lana, I.G., *Energy & Fuels*, **3**, 716 (1989).

262. Miale, J.N., Chen, N.Y., and Weisz, P.B., *J. Catal.*, **61**, 390 (1966).

263. Weisz, P.B. and Miale, J.N., *J. Catal.*, **4**, 527 (1965).

264. Pines, H., *J. Catal.*, **78**, 1 (1982).

265. Longstaff, D.C., Personal communication (July 1996).

266. Gray, M.R., Khorasheh, F., Wanke, S.E., Achia, U., Krzywrcki, A, Sanford, E., O.K.Y. Sy and M. Ternan, *Energy & Fuels*, **6**, 478 (1992).

267. Gray, M.R., Ayasse, A.R., Chan, E.W., and Velijkovic, M., *Energy & Fuels,* **9**, 500 (1995).

268. Asaoka, S., Nakata, S., Shiroto, Y., and Takeuchi, C., *Ind. Eng. Chem. Proc. Des. Dev.* **22**, 242 (1983).

269. Houlla, M., Broderick, D.H., Sapre, A.V., Nag, N.K., de Beer, V.H.J., Gates, B.C., and Kwart, H., *J. Catal.*, **61**, 523 (1980).

270. Takeuchi, C., Asaoka, S., Nakata, S., and Shiroto, T., *ACS Prepr. Div. Petrol. Chem.*, **30**, 96 (1985),

271. Speight, J.G., Proceedings of the 1991 Eastern Oil Shale Symposium, Lexington, Kentucky, pp 17-33 (1991).

272. Komatsu, S., Hori, Y., and Shimizu, S., *Hydro. Proc.*, **64**(5), 42 (1985).

273. Nakata, S., Shimizu, S., Asaoka, S., Shiroto, Y., and Fukui, Y., *Prprnts. Am. Chem. Soc. Div. Pet. Chem.*, **32**, 477 (1987).

274. Dabkowski, M.J., Shin, S.S. and Albison, K.R., *AIChE Symp.Ser.*, **87**, 53 (1991).

275. Gollakota, S.V., Guin, J.A. and Curtis, C.W., *Ind. Eng. Chem. Proc. Des. Dev.*, **24**, 1148 (1985)..

276. Eccles, R.M., *Fuel Proc. Technol.*, **35**, 21 (1993).

277. Gray, M.R., *AOSTRA J. Res.*, **6**, 185 (1990).

278. Aboul-Gheit, A.K., *Am. Chem. Soc. Div. Pet. Chem.*, **32**, 278 (1987).

279. Hung, C.W. and Wei, J., *Ind. Eng. Chem. Proc. Des. Dev.* **19**, 250 (1980).

280. Agrawal, R. and Wei, J., *Ind. Eng. Chem. Proc. Des. Dev., 23, 505 (1984).*

281. Ware, R.A. and Wei, J., J. Catal., *93, 100 (1985).*

282. Sanford, E.C., Energy & Fuels, **9**, 549 (1995).

283. Lepage, J.F., Morel, F., Trassard, A.M., and Bousquet, J., *ACS Prprnts. Div. Pet. Chem.*, **32**(2), 470 (1987).

284. McColgan, E.C., Soutar, P.S., Denis, J.M., and Parson, B.I., *Can. Mines Br. Res. Rep.*, R-261 (1973).

285. Koseoglu, R.O. and Phillips, C.R., *Fuel*, **67**, 1201 (1988).

286. Henderson, J.H. and Weber, L.J., *Can. Pet. Tech.*, 206 (1965).

287. Howell, R.L., Hung, C.W., Gibson, K.R., and Chen, H., "Catalyst Selection Important for Residuum Hydroprocessing", *Oil Gas J.*, **83**(30), 121 (1985).

288. LePage, J.F., Morel, F., Trassard, A.M., and Bousquet, J., *ACS Prepr. Div. Petrol. Chem.*, **32**(2), 470 (1987).

289. Tsai, C.H., Longstaff, D.C., Deo, M.D., Hanson, F.V., and Oblad, A.G., "Characterization and Utilization of Hydrotreated Products from the Whiterocks (Utah) Tar Sand Bitumen-Derived Liquid", *Fuel*, **71**, 1473 (1992).

290. Tsai, C.H., Longstaff, D.C., Deo, M.D., Hanson, F.V., and Oblad, A.G., "Potential of Jet Fuels from Utah Tar Sand Bitumens and Bitumen-Derived Liquids", *Am. Chem. Soc. Div. Pet. Chem.*, **37**(2), 521 (1992).

291. Ho, T.C. and Aris, R., *AIChE J.*, **33**(6), 1050 (1987).

292. Longstaff, D.C., Ph.D. Dissertation, University of Utah, Salt Lake City, Utah (1992).

293. Ohtsuka, T., *Catal. Rev. Sci. Eng.*, **16**, 291 (1977).

294. Yeh, T., Ph.D. Dissertation, University of Utah, Salt Lake City, Utah (1997).

295. Boduszynski, M.M., *Energy and Fuels*, **2**, 592 (1988).

296. Eyring, H., *Ann. Rev. Phys. Chem.*, **28**, 1 (1977).

297. Schucker, R.C. and Keweshan, C.F., *Am. Chem. Soc. Div. Fuel. Chem. Prepr.*, **25**(3), 155 (1980).

298. Longstaff, D.C., private communication (1995).

299. Larson, O.A. and Beuther, H. *Preprnt. Am. Chem. Soc. Div. Pet. Chem.*, **11**, B95 (1966).

300. Lakshmanan, C.C. and White, N., *Energy & Fuels*, **8**, 1158 (1994).

301. Geneste, P., Amblad, P., Bonnet, M., and Graffin, P., *J. Catal.*, **61**, 115 (1980).

302. Houlla, M., Nag, N.K., Sapre, A.V., Broderick, D.H., and Gates, B.C., *AIChE J.*, **24**, 1015 (1978).

303. Dalay, F.P., *J. Catal.*, **42**, 467 (1976).

304. Dautzenberg, F.M. and DeDekeu, J.C., *ACS Prepr. Div. Petrol., Chem.*, **30**, 8 (1985).

305. Hung, C.W. and Wei, J., *Ind. Eng. Chem. Process Des. Dev.*, **19**, 257 (1980).

306. Agrawal, R. and Wei, J., Ind. Eng. Chem. Process Des. Dev., **23**, 505, 515 (1984).

307. Ware, R.A. and Wei, J., *J. Catal.*, **93**, 100, 120, 135 (1985).

308. Constable, F.H., *Proc. Roy. Soc. London Ser. A.*, **108**, 355 (1925).

309. Galway, A.K., *J. Catal.*, **84**, 270 (1983).

310. Schwab, G.-M., *J. Catal.*, **84**, 1 (1983).

311. Voltz, S.E., Nace, D.M., and Weekman, V.W. Jr., *Ind. Eng. Chem. Process Des. Develop.*, **10**(4), 538 (1971) and Weekman, V.J. Jr., *AIChE Monogr. Ser.*, **75**(11) (1979).

312. Yui, S.M., *AOSTRA J. Res.*, **5**, 211 (1989).

313. Yui, S.M. and Sanford, E.C., *Ind. Eng. Chem. Res.*, **28**, 1278 (1989).

314. Speight, J.G., "The Desulfurization of Heavy Oils and Residue", Marcel Dekker, New York (1981).

315. Gray, M.R., "Upgrading Petroleum Residues and Heavy Oil", Marcel Dekker, New York (1994).

316. McConville, L.B., *Min. Eng.*, **27**(1), 19-38 (1975).

317. Schuetze, B. and Hofman, H., *Hydro. Process.*, **63**(2), 75 (1984).

318. Murphy, J.R., Whittington, E.L., and Chang, C.P., *Hydro. Process.*, **58**(9), 119 (1979).

319. Topsoe, H., Clausen, B.S., and Massoth, F.E., "Hydrotreating Catalysis", Springer-Verlag

Berlin Heidelberg, New York, 15 (1996).

320. Wei, J., "In Catalyst Design: Progress and Perspectives", Heges, L.G. Ed., Wiely, New York (1988).

321. Nakata, S., Shimizu, S., Asaoka, S., Shiroto, Y., and Fukui, Y., *Prprnts. Am. Chem. Soc. Div. Pet. Chem.*, ACS, **32**, 477 (1987).

322. Wei, J., "In Catalyst Design: Progress and Perspectives", Hegedus, L., Ed., Wiley, New York, 245 (1988).

323. Syncrude Canada Ltd., Syncrude Analytical Methods for Oil Sand and Bitumen Processing-Method 5.4", 1st ed., *AOSTRA*, Edmonton, Alberta (1979).

324. Tsai, C.H., Massoth, F.E., Lee, S.Y., and Seader, J.D., *Fuel Proc. Tech.*, **29**, 153 (1991).

325. Topsoe, H., Clausen, B.S., and Massoth. F.E., "Hydrotreating Catalysis", Springer-Verlag Berlin Heidelberg, New York, 3 (1996).

326. DeDrago, G., Guitian, J., Krasuk, J., Larrauri, J., Marzin, R., Silva, F., Solari, B., *Prprnt. Am. Chem. Soc. Div. Pet. Chem.*, **35**, 584 (1990).

327. Ho, T.C., *AIChE J.*, **42**(1), 214 (1996).

328. Ho, T.C., *Chem. Eng. Science*, **46**(1), 281-289 (1991).

329. Ocone, R., and Astarita, G., *AIChE J.*, **39**(2), 288 (1993).

330. Ho, T.C. White, B.S., and Hu, R., *AIChE J.*, **36**(5), 685, (1990).

331. Aris, R., *AIChE J.*, **35**(4), 539, (1989).

332. Chou, M.Y, and Ho, T.C., *AIChE J.*, **35**(4), 533 (1989).

333. Astarita, G. and Ocone, R., *AIChE J.*, **34**(8), 1299 (1988).

334. Chou, M.Y. and Ho, T.C., *AIChE J.*, **34**(9), 1519 (1988).

335. Ozaki, H., Satomi, Y., Hisamitsu, *In Proc. World Pet. Cong. 6 PD*, **18**(4), 97 (1976).

336. Ho, T.C. and White, B.S., *AIChE J.*, **41**(6), 1513 (1995).

337. Braun, R.L. and Burnham, A.K., *Energy Fuels*, **1**, 153-161 (1987).

338. Liliedahl, T. and Sjostrom, K., *AIChE J.*, **40**(9), 1515 (1994).

339. Lakshmanan, C.C. and White, N., *Energy Fuels*, **5**, 110-117 (1991).

340. Miura, K., *Energy Fuels*, **9**, 302-307 (1995).

341. Abramowitz, M. and Stegun, I.A., Eds., *Handbook of Mathematical Functions*, Dover Publications, New York, 923-925 (1970).

342. Kwak, S.W., Ph.D. Dissertation, University of Utah (1994).

343. Eyring, H., *Journal of Chemical Physics*, 283 (1936).

344. Kincaid, J.F., Eyring, H., and Stearn, A.L., *Chem. Revs.*, **28**, 301-365 (1941).

345. Brodkey, R.S., *Transport Phenomena: A Unified Approach*, McGraw Hill, New York, 736 (1988).

346. DeJong, K.P., *Ind. Chem. Res.* **33**, 821 (1994).

347. Mosby, J.F., Buttke, R.D., Cox, J.A., and Nikolaides, C., *Chemical Engineering Science*, **41**(4), 989 (1986).

348. Sanford, E.C., *Ind. Eng. Chem. Res.*, **33**, 109 (1994).

349. Kennepohl, D. and Sanford, E., *Energy Fuels*, **10**, 229-234 (1996).

350. Furimsky, E. and Massoth, F.E., *Catalyst Today*, **17**(4), 537-660 (1993).

351. Ignasiak, T.M., Bimer, J., Samman, N., Montgomery, O.P., and Strausz, D.S., *Prepr.-Am. Chem. Soc. Div. Pet. Chem.*, **24**(4), 1001 (1979).

APPENDIX A

WHITEROCKS OIL SAND DEPOSIT BIBLIOGRAPHY

Ball Associates, Ltd., 1964, Surface and Shallow Oil-Impregnated Rocks and Shallow Oil Fields in the United States, U.S. Bureau of Mines, Monograph 12.

Ball, D., Marchant, L.C., and Goldburg, A., 1982, The IOCC Monograph Series: Tar Sands, Interstate Oil Compact Commission, Oklahoma City, Oklahoma.

Barb, C.F., 1942, Rubber from the Uinta Basin of Utah, Mines Magazine 32, #10, 521-524.

Barb, C.F., and J.O. Ball, 1944, Hydrocarbons of the Uinta Basin of Utah and Colordo, Quarterly, Colorado School of Mines 39, #1, 115 p.

Bukka, K., Miller, J.D., Hanson, F.V., and Oblad, A.G., 1991, Mineral Matter Distribution during the Hot Water Processing of Utah Tar Sand, AOSTRA J. Res. 7, 101-109.

Campbell, J.A., and H.R. Ritzma, 1976, Structural Geology and Petroleum Potential of the South Flank of the Uinta Mountain Uplift [abstract], Amer. Assoc. Petrol. Geol., Bull. 60, 1392-1393.

Cashion. W.B., Jr., 1964, Other Bituminous Substances, Utah Geol. Miner. Survey, Bull. 73, 63-70, Mineral and Water Resources of Utah.

Cha, S., 1991, Pyrolysis of the Whiterocks Tar Sand in a rotary Kiln Reactor, Ph.D. Dissertation, University of Utah, Salt Lake City, Utah.

Cha, S., Longstaff, D.C., Hanson, F.V., and Oblad A.G., 1991, Pyrolysis of Bitumen Impregnated Sandstones, A Comparison of Fluidized - Bed and Rotary Kiln Reactors, Proc. 1990 Eastern Oil Shale Symp., 136-145.

Cha, S., Longstaff, D.C., Hanson, F.V., and Oblad, A.G., 1991, Pyrolysis of Bitumen Impregnated Sandstones, A Comparison of Fluidized-Bed and Rotary-Kiln Reactors, FUEL 70, 1357-1361.

Covington, R.E., 1963, Bituminous Sandstone and Limestone Deposits of Utah, Utah Geol. Miner. Survey, Bull. 54, 225-247.

Covington, R.E., 1964, Bituminous Sands with Viscous Crude Oils, Brigham Young University, First Intermtn. Symp. Fossil Hydrocarbons, 364-374.

Covington, R.E., 1964, Bituminous Sandstone in the Uinta Basin, Intermtn. Assoc. of Petrol. Geol., 13th Annual Field Conference, 227-242.

Covington, R.E., 1964, Thermal Recovery May Bring Industry's Quiet Revolution, Oil & Gas J. 62, #47, 112-118.

Covington, R.E., 1965, Some Possible Applications of Thermal Recovery in Utah, J. Petrol. Tech. 17, #11, 1277-1284.

Deo, M.D., and Hanson, F.V., 1993, Asphaltene Precipitation: A Need for a Broader View, SPE 25193.

Deo, M.D., Hwang, J., and Hanson, F.V., 1993, The Effect of Cosolubilizing Lighter Components on the Asphaltene Content of Heavy Oils, Fuel Proc. Tech. 34, 217-228.

Deo, M.D., Hwang, J., and Hanson, F.V., 1992, Supercritical Fluid Extraction of a Crude Oil, Bitumen-Derived Liquid and Bitumen by Carbon Dioxide and Propane, FUEL 71, 1519-1526.

Dorius, J.C., 1985, The Pyrolysis of Bitumen Impregnated Sandstone from the PR Spring (Utah) Deposit in a Fluidized Bed, Ph.D. Dissertation, University of Utah, Salt Lake City, Utah.

Drelich, J., 1993, The Role of Wetting Phenomena in the Hot Water Process for Bitumen Recovery from Tar Sand, Ph.D. Dissertation, University of Utah, Salt Lake City, Utah.

Drelich, J., Hanson, F.V., Hupka, J, and Miller, J.D., 1993, Water Recycle in Moderate-Temperature Bitumen Recovery from Whiterocks Tar Sands, AOSTRA J. Res, in press.

Drelich, J., and Miller, J.D., 1993, Surface/Interfacial Tension of the Whiterocks Bitumen and its Relationship to Tar Sand Processing, Proc. 1992 Eastern Oil Shale Symp., 265-275.

Fletcher, J.V., Deo, M.D., and Hanson, F.V., 1993, Fluidized Bed Pyrolysis of Bitumen-Impregnated Sandstone at Sub-Atmospheric Conditions, Proc. 1992 Eastern Oil Shale Symp., 247-256.

Hanson, F.V., Dorius, J.C., Utley, J.K., and Van Nguyen, T., 1992, The Application of Compound-Type Analyses to the Correlation of Product Distributions and Yields from the Fluidized-Bed Pyrolysis of Oil Sands, FUEL 71, 1365-1372.

Hunt, J.M., F. Stewart, and P.A. Dickey, 1954, Origin of Hydrocarbons of Uinta Basin, Utah, Amer. Assoc. Petrol. Geol., Bull. 38, #8, 1671-1698.

Hupka, J., Drelich, J., Miller, J.D., White, R.R., Hanson, F.V., and Oblad, A.G., 1991, Impact of Water Recycle on Water-Based Processing of Whiterocks Tar Sand, Proc. 1990 Eastern Oil Shale Symp., 39-44.

Hupka, J., Drelich J., Miller, J.D., White, R.R., Hanson, F.V., and Oblad, A.G., 1991, Impact

of Water Recycle on Water-Based Processing of Whiterocks Tar Sand, FUEL 70, 1313-1316.

Hwang, J., 1993, Application of Supercritical Fluid Extraction to the Recovery and Upgrading of Oil Sands, Ph.D. Dissertation, University of Utah, Salt Lake City, Utah.

Keefer, T.N., and McQuivey, R.S., 1979, Water Availability for Development of Major Tar Sands Areas in Utah, U.S. Department of Energy, Final Report LETC-0013-1, 228 pp.

Kinney, D.M., 1951, Geology of Uinta River and Brush Creek-Diamond Mountain Areas, Duchesne and Uinta Counties, Utah, U.S. Geol. Survey, Bull. 1007, Map.

Kuuskra, V.V., and Hammershaimb, V.A., eds., 1984, The IOCC Monograph Series: Major Tar Sand and Heavy Oil Deposits of the United States, Interstate Oil Compact Comm., Oklahoma City, Oklahoma.

Kwak, S., Longstaff, D.C., Deo, M.D., and Hanson, F.V., 1993, Hydrotreating Process Kinetics for Bitumen and Bitumen-Derived Liquids, Proc. 1992 Eastern Oil Shale Symp., 208-215.

Longstaff, D.C., 1992, Hydrotreating the Whiterocks Oil Sand Bitumen and Bitumen-Derived Liquid, Ph.D. Dissertation, University of Utah, Salt Lake City, Utah.

Longstaff, D.C., Deo, M.D., Hanson, F.V., Oblad, A.G., and Tsai, C.H., 1992, Hydrotreating the Bitumen-Derived Hydrocarbon Liquid Produced in a Fluidized Bed Pyrolysis Reactor, FUEL 71, 1407-1419.

Longstaff, D.C., Deo, M.D., and Hanson, F.V., 1993, Hydrotreating the Bitumen from the Whiterocks Oil Sand Deposit, Proc. 1992 Eastern Oil Shale Symp., 199-207.

Oblad, A.G., Bunger, J.W., Hanson, F.V., Miller, J.D., Ritzma, H.R., and Seader, J.D., 1987, Tar Sand Research and Development at the University of Utah. Ann. Rev. Energy. 12, 283-356.

Peterson, P.R., 1985, The Whiterocks Tar Sand Deposit, Utah Geolog. Assoc., Publ. 12, 243-252.

Pruitt, R.G., Jr., 1961, The Mineral Resources of Uintah County, Utah Geol. Miner. Survey, Bull. 71, 101 pp.

Resnick, B.S., Dike, D.H., English, L.M. III, and Lewis, A.G., 1981, Evaluation of Tar Sand Mining, Volume 1 - An Assessment of Resources Amenable to Mine Production: U.S. DOE, Final Report, DOE/ET/30201-1.

Ritzma, H.R., 1968, Preliminary Location Map Oil - Impregnated Rock Deposits of Utah, Utah Geol. Miner. Survey, Map No. 25, 1 pg.

Ritzma, H.R., 1973, Oil-Impregnated Rock Deposits of Utah, Utah Geol. Miner. Survey, Map No. 33, 2pp.

Ritzma, H.R., 1979, Oil-Impregnated Rock Deposits of Utah, Utah Geol. Miner. Survey, Map No. 47, 2pp.

Sung, S.H., 1988, The Fluidized Bed Pyrolysis of Bitumen-Impregnated Sandstone in a Large Diameter Reactor, M.S. Thesis, University of Utah, Salt Lake City, Utah.

Tsai, C.H., Deo, M.D., Hanson, F.V., and Oblad, A.G., 1991, Characterization and Potential Utilization of Whiterocks (Utah) Tar Sand Bitumen, Fuel Sci. Tech. Int. 9, 1259-1286.

Tsai, C.H., Deo, M.D., Hanson, F.V., and Oblad, A.G., 1992, Characterization and Potential Utilization of Whiterocks Tar Sand Bitumen II. Pyrolysis Man Spectrometry and Nuclear Magnetic Resonance Analyses, Fuel Sci. Tech. Int. 10, 1437-1459.

Wang, J., 1983, The Production of Hydrocarbon Liquids from a Bitumen-Impregnated Sandstone in a Fluidized Bed Pyrolysis Reactor, M.S. Thesis, University of Utah, Salt Lake City, Utah.

Wang, J., Hanson, F.V., Obald, A.G., 1983, The Fluidized Bed Pyrolysis of the Bitumen-Impregnated Sandstone from the Whiterocks (Utah) Deposit, Prprnt. AICHE Symp. Adv. Tar Sand Tech., Denver, Colorado, August 1983.

APPENDIX B

ASPHALT RIDGE OIL SAND DEPOSIT BIBLIOGRAPHY

Abraham, H., 1969, Asphalts and Allied Substances, 6th Edition, 5 Volumes, D. Van Nostrand Co., Inc., Princeton, New Jersey.

Alford, H.E., and Derby, R.E., 1981, Utah Tar Sands to be Developed, Hydrocarbon Proc. 60, #6, 127-130.

Anonymous, 1974, Fairbrim & Arizona Fuels to Begin Oil Sands Recovery Tests on Sohio Property in Utah, Synthetic Fuels, September.

Anonymous, 1981, Sohio Slates Tar Sands Pilot Plant in Utah, Oil & Gas J., 79, #3, 42-43.

Ball, D., Marchant, L.C., and Goldburg, A., 1982, The IOCC Monograph Series: Tar Sands, Interstate Oil Compact Comm., Oklahoma City, Oklahoma.

Ball, M.W., 1951, Oil-Impregnated Strippable Deposits in Utah, May 22, 1950, U.S. BuMines, The Synthetic Liquid Fuel Potential of Utah, Appendix D, p. 1-18.

Ball Associates, Ltd., 1965, Surface and Shallow Oil-Impregnated Rocks and Shallow Oil Fields in the United States, U.S. Bureau of Mines, Monograph 12, 375 p.

Barb, C.F., 1942, Rubber from the Uinta Basin of Utah, Mines Magazine 32, #10, 521-524.

Barb, C.F., 1944, Hydrocarbons of the Uinta Basin of Utah and Colorado, Review of Geology and Field Work, Colorado School of Mines, Quarterly, Colorado School of Mines, 39, #1, 115.

Barb, C.F., and Ball, J.O., 1944, Hydrocarbons of the Uinta Basin of Utah and Colordo, Quarterly, Colorado School of Mines, 39, #1.

Barbour, R.V., Dorrence, S.M., Vollmer, H., and Harris, J.D., 1976, Pyroloysis of Utah Tar Sands--Products and Kinetics, Amer. Chem. Soc., Div. Fuel Chem. 21, (6), 278-289.

Bunger, J.W., 1974, Characterization of a Utah Tar Sand Bitumen, Amer. Chem. Soc., Div. Fuel Chem. 19 (2), 231-241, Shale Oil, Tar Sands and Related Fuel Sources, T. F. Yen [Ed], Adv. Chem. Ser. 151, c. 10, 121-136.

Bunger, J.W., 1974, Characterization of a Utah Tar Sand Bitumen, Amer. Chem. Soc., Div. Fuel Chem. 19 (2), 231-241, Shale Oil, Tar Sands and Related Fuel Sources, T. F. Yen [Ed], Adv. Chem. Ser. 151, c. 10, 121-136, 1976.

Bunger, J.W., Cogswell, D.E., and Oblad, A.G., 1978, Thermal Processing of a Utah Tar Sand Bitumen, Canadian Institute of Mining and Metallurgy, CIM Special 17- Proceedings of the Canada-Venezuela Oil Sands Symp.-77, 178-182.

Bunger, J.W., Cogswell, D.E., and Oblad, A.G., 1979, Catalytic Cracking of Asphalt Ridge Bitumen, Amer. Chem. Soc., Refining of Synthetic Crude Oils, Adv. Chem. Ser. 179, 67-84.

Campbell, J.A., and Ritzma, H.R., 1976, Structural Geology and Petroleum Potential of the South flank of the Uinta Mountain Uplift [Abstract], Amer. Assoc. Petrol. Geol., Bull. 60, 1902-1393.

Campbell, J.A., and Ritzma, H.R., 1979, Geology and Petroleum Resources of the Major Oil-Impregnated Sandstone Deposits of Utah, Utah Geol. and Miner. Survey, Special Studies 50, 25 pp.

Campbell, J.A., and Ritzma, H.R., 1979, Geology and Petroleum Resources of the Major Oil-Impregnated Sandstone Deposits of Utah, U.N. Inst. for Training and Research, First Internat. Conf. on the Future of Heavy Oil and Tar Sands, (UNITAR), June 4-12, 1979, Edmonton, Alberta, Canada.

Cashion, W.B., Jr., 1964, Other Bituminous Substances, Utah Geol. and Miner. Survey Bull. 73, Mineral and Water Resources of Utah, 63-70.

Covington, R.E., 1957, The Bituminous Sandstones of the Asphalt Ridge Area, Northeastern Utah, Intermtn. Assoc. Petrol. Geol., 8th Ann. Field Confer., 172-175.

Covington, R.E., 1963, Bituminous Sandstone and Limestone Deposits of Utah, Utah Geol. Miner. Survey, Bull. 54, 225-247.

Covington, R.E., 1964, Bituminous Sands With Viscous Crude Oils, Brigham Young University, First Intermtn. Symp. on Fossil Hydrocarbons, 364-374.

Covington, R.E., 1964, Bituminous Sandstone in the Uinta Basin, Intermtn. Assoc. Petrol. Geol. 13th Ann. Field Conf., 227-242.

Covington, R.E., 1964, Thermal Recovery May Bring Industry's Quiet Revolution, Oil & Gas J. 62, #47, 112-118.

Covington, R.E., 1965, Some Possible Applications of Thermal Recovery in Utah, J. Petrol. Tech. 17, #11, 1277-1284.

Covington, R.E., and McDonald, R.L., 1965, Stratigraphic and Structural Controls of Bituminous Sandstone Deposits in Utah [Abstract], Amer. Assoc. of Petrol. Geol., Bull. 49, #9, 1577.

Covington, R.E., and Young, K.J., 1985, Brief History and Recent Developments in Tar Sand Deposits of Uinta Basin, Utah Geol. Assoc. Publication 12, Geology and Energy Resources, Uinta Basin of Utah, 227-242.

Dyni, J.R., and Goodwin, J.C., 1972, American Assoc. of Petroleum Geologists Field Trip Roadlog- Vernal, Utah to Rio Blanco, Colorado, Rocky Mountain Assoc. of Geol., Intermtn. Geol. 9, #2-3, 115-134.

Eldridge, G.H., 1901, Asphalt and Bituminous Rock Deposits, U.S. Geol. Survey, Ann. Report 22, 361-364.

Erickson, R.L., Myers, A.T., and Horr, C.A., 1954, Association of Uranium and Other Metals with Crude Oil, Asphalt, and Petroliferous Rock, Amer. Assoc. Petrol. Geol., Bull. 38, #10, 2200-2218.

Hills, R.C., 1985, Description of an Asphalt-Like Mineral from Asphalt Wash, Utah, Colorado Sci. Soc., Proc. 2, part 1, 27-28.

Hunt, J.M., Stewart, F., and Dickey, P.A., 1954, Origin of Hydrocarbonsof Uinta Basin, Utah, Amer. Assoc. Petro. Geol., Bull. 38, #8, 1671-1698.

Hupka, J., and Miller, J.D., 1991, Temperature Water-Based Bitumen Recovery from Tar Sand, FUEL 70, 1308-1312.

Hupka, J., and Miller, J.D., 1991, Electrophoretic Characterization and Processing of Asphalt Ridge and Sunnyside Tar Sands, Internat., J. Miner. Proc. 31, 217-231.

Kayser, R.B., 1966, Bituminous Sandstone Deposits Asphalt Ridge, Utah Geol. Miner. Survey, Special Studies 19, 62 pp.

Keefer, T.N., and McQuivey, R.S., 1979, Water Availability for Development of Major Tar Sands Areas in Utah, U.S. DOE, Final Rept. LETC-0013-1, 228 p.

Kinney, D.M., 1955, Geology of Uinta River and Brush Creek-Diamond Mountain Areas, Duchesne and Uinta Counties, Utah, U.S. Geol. Survey, Bull. 1007.

Kuuskra, V.V., and Hammershaimb, V.A., eds., 1984, Major Tar Sand and Heavy Oil Deposits of the United States, Interstate Oil Compact Comm., Oklahoma City, Oklahoma.

Lowe, R.M., 1976, The Asphalt Ridge Tar Sand Deposits, AIChE Symp. Ser. 72, #155, 55-60.

Mauger, R.L., Kayser, R.B., and Gwynn, J.W., 1973, A Sulfur Isotopic Study of Uinta Basin Hydrocarbons, Utah Geol. Miner. Survey, Special Studies 41, 17 p.

Oblad, A.G., Seader, J.D., Miller, J.D., and Bunger, J.W., 1976, Recovery of Bitumen from Oil-Impregnated Sandstone Deposists of Utah, AIChE, Oil Shale and Tar Sand Symp., AIChE Symp. Sec. 155 (72), 69-78.

Oblad, A.G., Seader, J.D., Miller, J.D., Bunger, J.W., and Cogswell, D.E., 1977, Recovery of Oil from Utah's Tar Sands, NTIS Report PB-294-680.

Oblad, A.G., Bunger, J.W., Hanson, F.V., Miller, J.D., Ritzma, H.R., and Seader, J.D., 1987, Tar Sand Research and Development at the University of Utah, Ann. Rev. Energy. 12 283-356.

Pruitt, R.G., Jr., 1961, The Mineral Resources of Uinta County, Utah Geol. Miner. Survey, Bull. 71, 101 p.

Resnick, B.S., Dike, D.H., English, L.M., III, and Lewis, A. G., 1981, Evaluation of Tar Sand Mining, Volume 1 - An Assessment of Resources Amenable to Mine Production: U.S. DOE, Final Report DOE/ET/30201-1.

Ritzma, H.R., 1968, Preliminary Location Map Oil - Impregnated Rock Deposits of Utah, Utah Geol. Miner. Survey, Map No. 25, 1 pg.

Ritzma, H.R., 1973, Oil-Impregnated Rock Deposits of Utah, Utah Geol. Miner. Survey, Map No. 33, 2pp.

Ritzma, H.R., 1974, Asphalt Ridge, Structure, Stratigraphy, and Oil-Impregnated Sands, Utah Geol. Assoc., Publication 4, 60.

Ritzma, H.R., 1979, Oil-Impregnated Rock Deposits of Utah, Utah Geol. Miner. Survey, Map No. 47, 2pp.

Shea, G.B., and Higgins, R.V., 1952, Separation and Utilization Studies of Bitumens from Bituminous Sandstones of the Vernal and Sunnyside, Utah Deposits, U.S. BuMines ROI 4871.

Sinks, D.J., 1985, Geologic Influence on the In-Situ Process of Tar Sand at the North West Asphalt Ridge Deposit, Utah, U.S. DOE, Report No. AD-89-F-0-026-0.

Smith, R.J., 1980, Asphalt Ridge Tar Sands, Flotation Behavior and Process Design, M.S. Thesis, University of Utah, Salt Lake City, Utah.

Smith, R.J., and Miller, J.D., 1981, Flotation Behavior of Digested Asphalt Ridge Tar Sands, Mining Eng. 33, 1719-1724, Discussion of Article, 34, 1598.

Speiker, E.M., 1931, Bituminous Sandstone Near Vernal, Utah, U.S. Geol. Survey, Bull. 822-C, 77-100.

Stone, G.H., 1891, Note on the Asphaltum of Utah and Colorado, Am. J. Sci. 142, 148-159.

Tsai, C.H., Deo, M.D., Hanson, F.V., and Oblad, A.G., 1993, Characterization and Potential Utilization of the Asphalt Ridge Tar Sand Bitumen I. Gas Chromatography - Mass Spectrometry and Pyrolysis - Mass Spectrometry Analysis Fuel Sci. Tech. Int'l. 11, 475-506.

U.S. Bureau of Land Management, 1986, Proposed Leased Conversion for Sohio Within the Asphalt Ridge Special Tar Sand Area, U.S. Department of Interior.

Untermann, G.E., and Untermann, B.R., 1964, Geology of Uinta County, Utah Geol. Miner. Survey, Bull. 72, 112 pp.

Walton, P.T., 1944, Geology of the Cretaceous of the Uinta Basin, Utah, Geol. Soc. Amer., Bull. 55, 91-130.

Wenger, W.J., Hubbard, R.L., and Whisman, M.L., 1952, Separation and Utilization Studies of Bitumens from Bituminous Sandstones of the Vernal and Sunnyside, Utah Deposits, U.S. BuMines, ROI 4871, Part II, Analytical Data on Asphalt Properties and Cracked Products of the Separated Bitumens.

Wolfgramm, R.P., 1978, Asphalt Ridge Tar Sands Characterization, Honors Degree Thesis, University of Utah, Salt Lake City, Utah.

Wood, R.E., and Ritzma, H.R., 1972, Analyses of Oil Extracted from Oil-Impregnated Sandstone Deposits in Utah, Utah Geol. and Miner. Survey, Special Studies 39, 19 pp.

APPENDIX C

PR SPRING OIL SAND DEPOSIT BIBLIOGRAPHY

Abraham, H., 1960, Asphalts and Allied Substances, 6th Edition, 5 volumes, D. Van Nostrand Co., Inc., Princeton, New Jersey.

Ball, D., Marchant, L.C., and Goldburg, A., 1982, The IOCC Monograph Series: Tar Sands, Interstate Oil Compact Commission, Oklahoma City, Oklahoma.

Ball, M.W., 1951, Oil-Impregnated Strippable Deposits in Utah, May 22, 1950, U.S. BuMines, The Synthetic Liquid Fuel Potential of Utah, Appendix D, 1-18.

Barbour, R.V., Dorence, S.M., Vollmer, H., and Harris, J.D., 1976, Pyroloysis of Utah Tar Sands--Products and Kinetics, Amer. Chem. Soc., Div. of Fuel Chem. 21 (6), 278-289.

Bunger, J.W., Cogswell, D.E., and Oblad, A.G., 1978, Thermal Processing of a Utah Tar Sand Bitumen, Canadian Institute of Mining and Metallurgy, CIM Special volume 17- Proc. of the Canada-Venezuela Oil Sands Symp.-77, 178-182.

Byrd, W.D., II, 1967, Geology of the Bituminous Sandstone Deposits, Southeastern Uinta Basin, Uintah and Grand Counties, Utah, M.S. Thesis, University of Utah, Salt Lake City, Utah.

Byrd, W.D., II, 1970, P.R. Spring Oil-Impregnated Sandstone Deposit, Uintah and Grand Counties, Utah, Utah Geol. Miner. Survey, Special Studies 31, 34 pp.

Campbell, J.A., and Ritzma, H.R., 1979, Geology and Petroleum Resources of the Major Oil-Impregnated Sandstone Deposits of Utah, Utah Geol. and Miner. Survey, Special Studies 50, 25 pp.

Campbell, J.A., and Ritzma, H.R., 1979, Geology and Petroleum Resources of the Major Oil-Impregnated Sandstone Deposits of Utah, First Internat. Conf. on the Future of Heavy Oil and Tar Sands, (UNITAR), June 4-12, 1979, Edmonton, Alberta, Canada.

Cashion, W.B., Jr., 1964, Other Bituminous Substances, Utah Geol. Miner. Survey, Bull. 73, Mineral and Water Resources of Utah.

Cashion, W.B., Jr., 1967, Geology and Fuel Resources of the Green River Formation, Southeastern Uinta Basin, Utah and Colorado, U.S. Geol. Survey, Prof. Paper 548.

Clem, K.C., 1984, Economic Potential of the P.R. Spring Oil-impregnated Deposit, Uinta Basin, Utah, Utah Geol. Miner. Survey, Special Studies 65, 38 pp.

Covington, R.E., 1963, Bituminous Sandstone and Limestone Deposits of Utah, Utah Geol. Miner. Survey, Bull. 54, 225-247.

Covington, R.E., 1964, Bituminous Sands with Viscous Crude Oils, Brigham Young University, First Intermtn. Symp. on Fossil Hydrocarbons, 364-374.

Covington, R.E., 1965, Some Possible Applications of Thermal Recovery in Utah, J. Petr. Tech. 17, #11, 1277-1284.

Covington, R.E., and R.L. McDonald, 1965, Stratigraphic and Structural Controls of Bituminous Sandstone Deposits in Utah [abstract], Amer. Assoc. Petrol. Geol., Bull. 49, #9, 1577.

Cupps, C.Q., L.A. Johnson, and L.C. Marchant, 1976-a, Properties of Utah Tar Sands, South Seep Ridge Area, P.R. Spring Deposit, U.S. DOE, ROI DOE-LC-RI-75/6.

Dahm, J.N., 1980, Tar Sand Reserves - P.R. Spring Deposit, Uintah and Grand Counties, Utah, Utah Geol. Miner. Survey, Open File Report 27.

Dahm, J.N., 1980, Tar Sand Reserves - P.R. Spring Deposit, Uintah and Grand Counties, Utah, University of Utah, State College of Mines and Mineral Industries, Utah Engineering Experiment Station, Phase I, Final Rept., 1981.

Dana, G.F., and D.J. Sinks, 1984, Characteristics of the P.R. Spring Tar Sand Deposit, Uinta Basin, Utah, U.S.A., U.N. Institute for Training and Research, 2nd Internat. Conf., The Future of Heavy Crude and Tar Sands, 220-236.

Dorius, J.C., 1985, The Pyrolysis of Bitumen-Impregnated Sandstone from the P.R. Spring (Utah) Deposit in a Fluidized Bed, Ph.D. Dissertation, University of Utah, Salt Lake City, Utah.

Eldridge, G.H., 1901, Asphalt and Bituminous Rock Deposits, U.S. Geol. Survey, Ann. Report 22, 361-364.

Fouch, T.D., W.B. Cashion, R.T. Ryder, and J.A. Campbell, 1976, Field Guide to Lacustrine and Related Nonmarine Depositational Environments in Tertiary Rocks, Uinta Basin, Utah, Professional Contributions of the Colorado School of Mines, No. 8, 358-385.

Glassett, J.M., and J.A. Glassett, 1976, The Production of Oil from Intermtn. West Tar Sands Deposits, U.S. BuMines, Contract No. S024429.

Gwynn, J.W., 1971, Instrumental Analysis of Tar and Their Correlations in Oil-Impregnated Sandstone Beds, Uintah and Grand Counties, Utah, Utah Geol. and Miner. Survey, Special Studies 37,

Gwynn, J.W., 1971, Instrumental Analysis of Tar and Their Correlations in Oil-Impregnated Sandstone Beds, Department of Geol. and Geophysical Sciences, Ph.D. Dissertation University of Utah, Salt Lake City, Utah.

Hanson, F.V., Dorius, J.C., Utley, J.K., and Van Nguyen, T., 1992, The Application of Compound-Type Analyses to the Correlation of Product Distributions and Yields from the Fluidized-Bed Pyrolysis of Oil Sands, FUEL 71, 1365-1372.

Hunt, J.M., F. Stewart, and P.A. Dickey, 1954, Origin of Hydrocarbons of Uinta Basin, Utah, Amer. Assoc. Petrol. Geol., Bull. 38, #8, 1671-1698.

Johnson, L.A., L.C. Marchant, and C.Q. Cupps, 1975, Properties of Utah Tar Sands - Asphalt Wash Area, P.R. Spring Deposit, U.S. BuMines, ROI 8030.

Johnson, L.A., L.C. Marchant, and C.Q. Cupps, 1975, Properties of Utah Tar Sands - North Seep Ridge area, P.R. Spring Deposit, U.S. DOE, ROI ERDA LERC/RI-75/6.

Johnson, L.A., L.C. Marchant, and C.Q. Cups, 1975, Properties of Utah Tar Sands - South Seep Ridge area, P.R. Spring Deposit, U.S. BuMines, ROI 8003.

Keefer, T.N., and McQuivey, R.S., 1979, Water Availability for Development of Major Tar Sands Areas in Utah, U.S. DOE, Final Report LETC-0013-1.

Kuuskra, V.V., and Hammershaimb, V.A., Eds., 1984, The IOOC Monograph Series: Major Tar Sand and Heavy Oil Deposits of the United States, Interstate Oil Compact Comm., Oklahoma City, Oklahoma.

Laramie Energy Technology Center, 1983, Unpublished Lithologic Descriptions of Oil Shale Core Holes in the P.R. Spring Area, Uintah County, Utah, U.S. DOE.

Marchant, L.C., L.A. Johnson, and C.Q. Cupps, 1974, Properties of Utah Tar Sands - Threemile Canyon, P.R. Spring Deposit, U.S. BuMines, ROI 7923.

Oblad, A.G., Bunger, J.W., Hanson, F.V., Miller, J.D., Ritzma, H.R., and Seader, J.D. 1987, Tar Sand Research and Development at the University of Utah, Ann. Rev. Energy. 12, 283-356.

Peterson, P.R., 1975, Lithologic Logs and Correlation of Coreholes, P.R. Spring and Hill Creek Oil-Impregnated Sandstone Deposits, Uintah County, Utah, Utah Geol. Miner. Survey, ROI 100.

Peterson, P.R., and H.R. Ritzma, 1974, Informational Core Drilling in Utah's Oil-Impregnated Sandstone Deposits, Southeast Uinta Basin, Uintah County, Utah, Utah Geol. Miner. Survey, ROI 88.

Picard, M.D., 1971, Petrographic Criteria for Recognition of Lacustrine and Fluvial Sandstone, P.R. Spring Oil-Impregnated Sandstone Area, Southeast Uinta Basin, Utah, Utah Geol. Miner. Survey, Special Studies 36.

Picard, M.D., and L.R. High, Jr., 1970, Sedimentology of Oil-Impregnated Lacustrine and Fluvial Sandstone, P.R. Spring Area, Southeast Uinta Basin, Utah, Utah Geol. and Miner. Survey, Special Studies 33.

Pitman, J.K., Fouch, T.D., and Glodhaber, M.B., 1982, Depositational Setting and Diagenetic Evolution of some Tertiary Unconventional Reservoir Rocks, Uinta Basin, Utah, Amer. Assoc. Petrol. Geol., Bull. 66, #10.

Pruitt, R.G., Jr., 1961, The Mineral Resources of Uintah County, Utah Geol. Miner. Survey, Bull. 71.

Reed, W.E., 1977, Molecular Compositions of Weathered Petroleum and Comparison with its Possible Source, Geochima et Cosmochim. Acta, 41, #2, 237-247.

Resnick, B.S., D.H. Dike, L.M. English, III, and Alan G. Lewis, 1981, Evaluation of Tar Sand Mining, Volume 1 - An Assessment of Resources Amenable to Mine Production, U.S. DOE, Final Report DOE/ET/30201-1.

Ritzma, H.R., 1968, Preliminary Location Map Oil - Impregnated Rock Deposits of Utah, Utah Geol. Miner. Survey, Map No. 25, 1 pg.

Ritzma, H.R. 1973. Oil-Impregnated Rock Deposits of Utah, Utah Geol. Miner. Survey, Map No. 33, 2pp.

Ritzma, H.R., 1979, Oil Impregnated Rock Deposits of Utah, Utah Geol. Miner. Survey, Map No. 47, 2pp.

Ritzma, H.R., and Campbell, J.A., 1981, Geology and Petroleum Resources of the Major Oil-Impregnated Sandstone Deposits of Utah, United Nations Instit. for Training and Research (UNITAR), First International Conference on the Future of Heavy Crude Oils and Tar Sands, Edmonton, Alberta, Canada.

Sinks, D.J., 1985, Geologic Influence on the In-situ Process of Tar Sand at the North West Asphalt Ridge Deposit, Utah, U.S. DOE, No. AD-89-F-0-026-0.

Sinks, D.J., and G.F. Dana, 1984, Bituminous Sandstone Resource Evaluation of P.R. Spring Deposit, Uintah and Grand Counties, Utah [abstract], Amer. Assoc. Petrol. Geol., Bull. 68, #4, 528.

U.S. Bureau of Land Management, 1985, P.R. Spring Combined Hydrocarbon Lease Conversion, Final Environmental Impact Statement, U.S. Department of Interior.

Utah Geol. Miner. Survey, Internal Files, PR Spring Oil Sand Deposit.

Whittier, W.H., and R.C. Becker, 1945, Geologic Map and Sections of the Bituminous Sandstone Deposits in the P.R. Spring Area, Grand and Uintah Counties, Utah, U.S. Geol. Survey, Open File Report.

Wiley, D.R., 1967, Petrology of Bituminous Sandstones in the Green River Formation, Southeastern Uinta Basin, Utah, M.S. Thesis, University of Utah, Salt Lake City, Utah.

Wood, R.E., and H.R. Ritzma, 1972. Analyses of Oil Extracted from Oil-Impregnated Sandstone Deposits in Utah, Utah Geol. Miner. Survey, Special Studies 39, 19 p.

APPENDIX D

SUNNYSIDE OIL SAND DEPOSIT BIBLIOGRAPHY

Abraham, H., 1960, Asphalts and Allied Substances, 6th Edition, 5 Volumes, D. Van Nostrand Co., Inc., Princeton, New Jersey.

Ball Associates, Ltd., 1964, Surface and Shallow Oil-Impregnated Rocks and Shallow Oil Fields in the United States, U.S. BuMines, Monograph 12.

Ball, M.W., 1951, Oil-Impregnated Strippable Deposits in Utah, May 22, 1950, U.S. BuMines, The Synthetic Liquid Fuel Potential of Utah, Appendix D, 1-18.

Barb, C.F., 1942, Rubber from the Uinta Basin of Utah, The Mines Magazine, 32, #10, 521-524.

Barb, C.F., and Ball, J.O., 1944, Hydrocarbons of the Uinta Basin of Utah and Colorado, Quarterly, Colorado School of Mines, 39, #1, 115 p.

Bukka, K., Miller, J.D., and Oblad, A.G., 1991, Fractionation and Characterization of Utah Tar Sand Bitumens, Influence of Chemical Composition on Bitumen Viscosity, Energy & Fuels 5, 333-340.

Bunger, J.W., Cogswell, D.E., and Oblad, A.G., 1979, Catalytic Cracking of Asphalt Ridge Bitumen, Refining of Sythetic Crude Oils, Amer. Chemical Soc., Adv. in Chem. Ser. 179, 67-84.

Campbell, J.A., and Ritzma, H.R., 1979, Geology and Petroleum Resources of the Major Oil-Impregnated Sandstone Deposits of Utah, Utah Geol. and Miner. Survey, Special Studies 50, 25 pp.

Campbell, J.A., and Ritzma, H.R., 1979, Geology and Petroleum Resources of the Major Oil-Impregnated Sandstone Deposits of Utah, First Internat. Conf. on the Future of Heavy Oil and Tar Sands, (UNITAR), June 4-12, 1979, Edmonton, Alberta, Canada.

Cashion, W.B., Jr., 1964, Other Bituminous Substances, Utah Geol. Miner. Survey, Bull. 73, Mineral and Water Resources of Utah, 63-70.

Clark, F.R., 1928, Economic Geology of the Castlegate, Wellington, and Sunnyside Quadrangles, Carbon County, Utah, U.S. Geol. Survey, Bull. 793, 165 p.

Clem, K.C., 1985, Economic Potential of State-Owned Lands in the Sunnyside Special Tar Sand Area, Carbon County, Utah, Utah Geol. Miner. Survey, ROI 196, 29 p.

Covington, R.E., 1963, Bituminous Sandstone and Limestone Deposits of Utah, Utah Geol. Miner. Survey, Bull. 54, 225-247.

Covington, R.E., 1964, Bituminous Sands With Viscous Crude Oils, Brigham Young University, First Intermtn. Symp. on Fossil Hydrocarbons, 364-374.

Covington, R.E., 1964, Bituminous Sandstone in the Uinta Basin, Intermtn. Assoc. of Petrol. Geol., 13th Ann. Field Conf., 227-242.

Covington, R.E., 1964, Thermal Recovery May Bring Industry's Quiet Revolution, Oil & Gas J. 62, #47, 112-118.

Covington, R.E., 1965, Some Possible Applications of Thermal Recovery in Utah, J. Petrol. Tech. 17, #11, 1277-1284.

Covington, R.E., and McDonald, R.L., 1965, Stratigraphic and Structural Controls of Bituminous Sandstone Deposits in Utah [Abstract], Amer. Assoc. Petrol. Geol., Bull. 49, #9, 1577.

Covington, R.E., and Young, K.J., 1985, Brief History and Recent Developments in Tar Sand Deposits of Uinta Basin, Utah Geol. Assoc., Publication 12, Geology and Energy Resources, Uinta Basin of Utah, 227-242.

Cross, A.T., E.B. Maxfield, E. Cotter, and C.C. Cross, 1975, Field Guide and Road Log to the Western Book Cliffs, Castle Valley, and Parts of the Wasatch Plateau: Brigham Young University, Geology Studies, 22, pt. 2.

Fouch, T.D., W.B. Cashion, R.T. Ryder, and J.A. Campbell, 1976, Field Guide to Lacustrine and Related Nonmarine Depositational Environments in Tertiary Rocks, Uinta Basin, Utah, Professional Contributions of the Colorado School of Mines, #8, 358-385.

Glassett, J.M., and J.A. Glassett, 1976, The Production of Oil from Intermountain West Tar Sands Deposits, Final Rept., Contract No. S-0241129, U.S. BuMines, Department of Interior.

Gwynn, J.W., 1986, Overburden Map and Thickness Determinations Sunnyside Oil-Impregnated Sandstone Deposit, Carbon and Duchesne Counties, Utah: Utah Geol. Miner. Survey, ROI 210, <4> Leaves, Maps.

Holmes, C.N., Page, B.M., and P. Averitt, 1948, Geology of the Bituminous Sandstone Deposits near Sunnyside, Carbon County, Utah, U.S. Geol. Survey, Oil and Gas Investigations Prelim. Map 86.

Holmes, C.N., B.M. Page, and P. Averitt, 1956, Geology of the Bituminous Sandstone Deposits near Sunnyside, Carbon Co., Utah, Intermtn. Assoc. of Petrol. Geol. 7th Ann. Field Conf., U.S.

Geol. Sketch Map, 171-177.

Hunt, J.M., F. Stewart, and P.A. Dickey, 1954, Origin of Hydrocarbons of Uinta Basin, Utah, Amer. Assoc. Petrol. Geol., Bull. 38, #8, 1671-1698.

Jacob, A.F., 1969, Delta Facies of the Green River Formation (Eocene), Carbon and Duchesne Counties, Utah, University of Colorado, Ph.D. Dissertation, Boulder, Colorado.

Mauger, R.L., R.B. Kayser, and J.W. Gwynn, 1973, A Sulfur Isotopic Study of Uinta Basin Hydrocarbons, Utah Geol. Miner. Survey, Special Studies 41, 17 p.

Murany, E.E., 1964, Wasatch Formation of the Uinta Basin: Intermtn. Assoc. Petrol. Geol. 13th Ann. Field Conf., 145-155.

Oblad, A.G., Seader, J.D., Miller, J.D, and Bunger, J.W., 1976, Recovery of Bitumen from Oil-Impregnated Sandstone Deposists of Utah, Oil Shale and Tar Sand Symp., AIChE Symp. Ser., 155 (72), 69-78.

Picard, M.D., and E.Y. Banks, 1986, Petrography and Provenance of Sandstone Sunnyside Oil-Impregnated Deposit, Uinta Basin, Utah [abstract]: Amer. Assoc. Petrol. Geol., Bull. 70, #5, 632-633.

Pollastro, R.M., and C.J. Schenk, 1986, Characterizing and Evaluating Tar-Sand Reservoirs with Scanning Electron Microscope- -an Example from Sunnyside, Utah [abstract], Amer. Assoc. Petrol. Geol. 70, #5, 633-634.

Resnick, B.S., Dike, D.H., English, L.M. III, and Lewis, A.G., 1981, Evaluation of Tar Sand Mining, Volume 1 - An Assessment of Resources Amenable to Mine Production: U.S. DOE, Final Rept., DOE/ET/30201-1.

Ritzma, H.R., 1968, Preliminary Location Map Oil - Impregnated Rock Deposits of Utah, Utah Geol. Miner. Survey, Map No. 25, 1 pg.

Ritzma, H.R. 1973, Oil-Impregnated Rock Deposits of Utah, Utah Geol. Miner. Survey, Map No. 33, 2pp.

Ritzma, H.R. 1979, Oil-Impregnated Rock Deposits of Utah, Utah Geol. Miner. Survey, Map No. 47, 2pp.

Shea, G.B., and Higgins, R.V. 1952, Separation and Utilization Studies of Bitumens from Bituminous Sandstones of the Vernal and Sunnyside, Utah Deposits, U.S. BuMines, ROI 4871.

Thurber, J.L., and M.E. Welbourn, 1977. How Shell Attempted to Unlock Utah Tar Sand,

Petrol. Eng. 49, #12, 31-42.

Venkatesan, V.N., F.V. Hanson, and A.G. Oblad, 1979, The Thermal Recovery of a Synthetic Crude from the Bituminous Sands of the Sunnyside (Utah) Deposit, U.N. Instit. for Training and Research (UNITAR), First Internat. Conf. on the Future of Heavy Oil and Tar Sands.

Wenger, W.J., Hubbard, R.L., and Whisman, M.L., 1952, Separation and Utilization Studies of Bitumens from Bituminous Sandstones of the Vernal and Sunnyside, Utah Deposits, Part II, Analytical Data on Asphalt Properties and Cracked Products of the Separated Bitumens, U.S. BuMines, ROI 4871, 28 pp.

APPENDIX E

CIRCLE CLIFFS OIL SAND DEPOSIT BIBLIOGRAPHY

Bukka, K., Miller, J.D., Hanson, F.V., and Oblad, A.G., 1993, Characterization of Circle Cliffs Oil Sand of Utah, Energy & Fuels, (in Press).

Campbell, J.A., and Ritzma, H.R., 1979, Geology and Petroleum Resources of the Major Oil-Impregnated Sandstone Deposit of Utah, Utah Geol. Miner. Survey, Special Studies 50, 25 pp.

Campbell, J.A., and Ritzma, H.R., 1979, Geology and Petroleum Resources of the Major Oil Impregnated Sandstone Deposit of Utah, First Internat. Conf. on the Future of Heavy Oil and Tar Sands, (UNITAR), June 4-12, 1979, Edmonton, Alberta, Canada.

Davidson, E.S., 1967, Geology of the Circle Cliffs Area, Garfield and Kane Counties, Utah, U.S. Geol. Survey, Bull. 1229, 3 maps, 140 pp.

Erickson, R.L., Myers, A.T., and Horr, C.A., 1954, Association of Uranium and Other Metals with Crude Oil, Asphalt, and Petrolifeous Rock, Amer. Assoc. Petrol. Geol., Bull. 38, #10, 2200-2219.

Glassett, J.M. and Glassett, J.A., 1976, The Production of Oil from Intermtn. West Tar Sands Deposits, Final Report, Contract Number S0241129, U.S. BuMines, Department of the Interior, 91 pp.

Gregory, H.E., and Moore, R.C., 1931, The Kaiparowits Region, U.S. Geol. Survey, Prof. Paper 164.

Heylmun, E.B., 1964, Shallow Oil and Gas Possibilities in East and South Central Utah, Utah Geol. Miner. Survey, Special Studies 8, 39 pp.

Hooper, W.G., 1972, Geologic Report, Rio Vista Oil Ltd. Property, Circle Cliffs Uplift, Garfield Co., Utah.

Resnick, B.S., Dike, D.H., English, L.M. III, and Lewis, A.G., 1981, Evaluation of Tar Sand Mining, Volume 1 - An Assessment of Resources Amenable to Mine Production: U.S. DOE, Final Rept., DOE/ET/30201-1.

Ritzma, H.R., 1968, Preliminary Location Map Oil - Impregnated Rock Deposits of Utah, Utah Geol. Miner. Survey, Map No. 25, 1 p.

Ritzma, H.R. 1973. Oil-Impregnated Rock Deposits of Utah, Utah Geol. Miner. Survey, Map No. 33, 2 pp.

Ritzma, H.R. 1979. Oil-Impregnated Rock Deposits of Utah, Utah Geol. Miner. Survey, Map No. 47, 2 pp.

Ritzma, R.H., 1980, Oil Impregnated Sandstone Deposits, Circle Cliffs Uplift, Utah, Utah Geol. Assoc. - 1980 Henry Mountains Symp., 343-351.

Shun, D., Hanson, F.V., and Oblad, A.G., The Fluidized-Bed Pyrolysis of Bitumen-Impregnated Sandstone from the Circle Cliffs (Utah) Tar Sand Deposit. Bitumen Characterization and Preliminary Pyrolysis Studies, Prprnt. Tar Sand Symp., AIChE Nat. Mtg., Denver, Colorado.

Shun, D., 1990, The Pyrolysis of Bitumen-Impregnated Sandstone from the Circle Cliffs (Utah) Deposit in a Fludizied-Bed Reactor, Ph.D. Dissertation, University of Utah, Salt Lake City, Utah.

Steed, R. H., 1954, Geology of Circle Cliffs Anticline, Intermtn. Assoc. of Petrol. Geol., 5th Ann. Field Conf., Central and South-Central Utah, 102.

Sung, S.H., 1988, The Fludized Bed Pyrolysis of Bitumen-Impregnated Sandstone in a Large Diameter Reactor, M.S. Thesis, University of Utah, Salt Lake City, Utah.

Wood, R.E., & Ritzma, H.R., 1972, Analyses of Oil Extracted from Oil-Impregnated Sandstone Deposit in Utah, Utah Geol. Miner. Survey, Special Studies 39, 19 pp.

Draft Environmental Impact Statement on the Circle Cliffs Combined Hydrocarbon Lease Conversion, 1984, U.S. BLM, Department of Interior, November.

APPENDIX F

UNIVERSITY OF UTAH OIL SANDS BIBLIOGRAPHY

THESES AND DISSERTATIONS

Sepulveda, J.E., 1977, Hot Water Separation of Bitumen from Utah Tar Sands, M.S. Thesis, University of Utah, Salt Lake City, Utah.

Weeks, J.K. Jr., 1977, Fluidized-Bed Processing of Utah Tar Sands, M.S. Thesis, University of Utah, Salt Lake City, Utah.

Bunger, J.W., 1979, Processing Utah Tar Sand Bitumen, Ph.D. Dissertation, University of Utah, Salt Lake City, Utah.

Hanks, K.C., 1979, Chemistry of Oil Production from Tar Sand, M.S. Thesis, University of Utah, Salt Lake City, Utah.

Jayakar, K.M., 1979, The Thermal Recovery of Oil from Tar Sand, Ph.D. Dissertation, University of Utah, Salt Lake City, Utah.

Venkatesan, V.N., 1979, Fluidized-Bed Thermal Recovery of Synthetic Crude from Bituminous Sands of Utah, Ph.D. Dissertation, University of Utah, Salt Lake City, Utah.

Smith, R.J., 1980, Asphalt Ridge Tar Sands—Flotation Behavior and Process Design, M.S. Thesis, University of Utah, Salt Lake City, Utah.

Misra, M., 1981, Physical Separation of Bitumen from Utah Tar Sands, Ph.D. Dissertation, University of Utah, Salt Lake City, Utah.

Brechtel, C.E., 1981, Hydrotreating Utah Tar Sand Products, M.S. Thesis, University of Utah, Salt Lake City, Utah.

Umoh, R.A., 1981, Steam Cracking of Utah Tar Sand Bitumen in a Kellogg Millisecond Furnace, M.S. Thesis, University of Utah, Salt Lake City, Utah.

Aguilar, R., 1982, The Importance of Bitumen Viscosity Control in the Hot Water Processing of Utah Tar Sands, M.S. Thesis, University of Utah, Salt Lake City, Utah.

Bezama, R.J., 1983, An Energy Efficient Method for Thermal Processing of Utah Tar Sands, Ph.D. Dissertation, University of Utah, Salt Lake City, Utah.

Hsu, C.L.S., 1983, Digital Control of Thermal Processing System for Tar Sands, M.S. Thesis, University of Utah, Salt Lake City, Utah.

Wang, J., 1983, The Production of Hydrocarbon Liquids from a Bitumen-Impregnated Sandstone in a Fluidized Bed Pyrolysis Reactor, M.S. Thesis, University of Utah, Salt Lake City, Utah.

Smart, L.M., 1984, Thermal Processing of Tar Sands, M.S. Thesis, University of Utah, Salt Lake City, Utah.

Wang, C.J., 1984, The Solubility of Carbon Dioxide in Tar Sand Bitumens, M.S. Thesis, University of Utah, Salt Lake City, Utah.

Dorius, J.C., 1985, The Pyrolysis of Bitumen Impregnated Sandstone from the P.R. Spring (Utah) Deposit in a Fluidized Bed, Ph.D. Dissertation, University of Utah, Salt Lake City, Utah

Tsai, C.H., 1987, Reaction Kinetics and Mechanisms of Hydropyrolysis Processing of Tar Sand Bitumen and Related Materials, M.S. Thesis, University of Utah, Salt Lake City, Utah.

Lin, L.C., 1988, The Kinetics of the Pyrolysis of Tar Sand and of the Combustion of Coked Sands, Ph.D. Dissertation, University of Utah, Salt Lake City, Utah.

Sung, S.H., 1988, The Fluidized Bed Pyrolysis of Bitumen-Impregnated Sandstone in a Large Diameter Reactor, M.S. Thesis, University of Utah, Salt Lake City, Utah.

Coronella, C.J., 1989, Modelling a Coupled Fluidized-Bed Reactor for Extraction of Bitumen from Tar Sands, M.S. Thesis, University of Utah, Salt Lake City, Utah.

Ryu, H., 1989, Kinetic Modelling Applied to Hydrocarbon Process Design and Engineering, I Hydropyrolysis of Heavy Oils, II, Acetylene from Calcium Carbide, Ph.D. Dissertation, University of Utah, Salt Lake City, Utah.

Cogswell, D., 1990, Effect of H_2S on the Hydropyrolysis of Tetralin, M.S. Thesis, University of Utah, Salt Lake City, Utah.

Shun, D., 1990, Fluidized Bed Pyrolysis of the Bitumen-Impregnated Sandstone from the Circle Cliffs Deposit, Ph.D. Dissertation, University of Utah, Salt Lake City, Utah.

Cha, S.M., 1991, Pyrolysis of Oil Sands from the Whiterocks Tar Sand Deposit in a Rotary Kiln, Ph.D. Dissertation, University of Utah, Salt Lake City, Utah.

Deshpande, D.A., 1992, Application of Three Phase Ebullieted Bed Reactors to Petroleum Upgrading, Ph.D. Dissertation, University of Utah, Salt Lake City, Utah.

Fletcher, J.V., 1992, The Pyrolysis of Oil Sands in a Fludized Bed at Reduced Pressure, Ph.D. Dissertation, University of Utah, Salt Lake City, Utah.

Longstaff, D.C., 1992, Hydrotreating the Whiterocks Oil Sand Bitumen and Bitumen-Derived Liquid, Ph.D. Dissertation, University of Utah, Salt Lake City, Utah.

Coronella, C.J., 1993, Optimizing a Thermal Fluidizing-Bed Tar-Sands Extraction Process, Ph.D. Dissertation, University of Utah, Salt Lake City, Utah.

Deng, R., 1993, Evaluation of Utah Tar Sands Economics, M.S. Thesis, University of Utah, Salt Lake City, Utah.

Drelich, J., 1993, The Role of Wetting Phenomena in the Hot Water Process for Bitumen Recovery from Tar Sand, Ph.D. Dissertation, University of Utah, Salt Lake City, Utah.

Hwang, J., 1993, Application of Dynamic Supercritical Fluid Extraction to the Recovery and Upgrading of Complex Hydrocarbon Mixtures, Ph.D. Dissertation, University of Utah, Salt Lake City, Utah.

Lelinski, D., 1993, Ash Flotation of Dispersed Oil Droplets - A Model System for Bitumen Flotation from Tar Sand, M.S. Thesis, University of Utah, Salt Lake City, Utah.

Rose, P.E., 1993, Steam-Assisted Gravity Drainage of Oil Sand Reservoirs, Ph.D. Dissertation, University of Utah, Salt Lake City, Utah.

Kwak, S., 1994, Hydrotreating a Uinta Basin Bitumen over a Commercial HDM Catalyst, Ph.D. Dissertation, University of Utah, Salt Lake City, Utah.

Sarkan, A., 1994, Thermal Enhanced Oil Recovery Processes with Vertical and Horizontal Wells, M.S. Thesis, University of Utah, Salt Lake City, Utah.

Subramanian, M., 1994, Application of Supercritical Fluid Extraction to Upgrading Oil Sand Bitumens, M.S. Thesis, University of Utah, Salt Lake City, Utah.

Bhadkamar, A.S., 1995, Optimizing a Thermally Coupled Fluidized-Bed Tar Sands Extraction Process, Ph.D. Dissertation, University of Utah, Salt Lake City, Utah.

Chu, K.-S., 1995, Effect of Bitumen-Derived Coke on Deactivation of a Hydrodemetallation Catalyst, Ph.D. Dissertation, University of Utah, Salt Lake City, Utah.

Jiazhi Pu, 1995, Economic Evaluation of Bitumen Upgrading Alternatives, Ph.D. Dissertation, University of Utah, Salt Lake City, Utah.

Khot, K.R., 1995, Modeling a Coupled Fluidized-Bed Process for Extraction of Tar-Sand Bitumen, M.S. Thesis, University of Utah, Salt Lake City, Utah.

Kim, J., 1995, Catalytic and Thermal Effects in the Upgrading of Bitumen-Derived Heavy Oils, Ph.D., Dissertation, University of Utah, Salt Lake City, Utah.

Nagpal, S., 1995, Pyrolysis of Oil Sands in a Large Diameter Fluidized Bed Reactor, M.S. Thesis, University of Utah, Salt Lake City, Utah.

Subramanian, M., 1996, Supercritical Fluid Extraction of Oil Sands Bitumens from the Uinta Basin, Ph.D. Dissertation, University of Utah, Salt Lake City, Utah.

Tang, H., 1995, Combustion of Carbonaceous Residues on Spent Oil Sands in a Transport Reactor, Ph.D. Dissertation, University of Utah, Salt Lake City, Utah.

Tang, Q., 1995, Fluidization of Coked Sands and Pyrolysis of Oil Sands in a Fluidized Bed Reactor, MS Thesis, University of Utah, Salt Lake City, Utah.

Zheng, H., 1995, Performance and Calibration of Dry Materials Feeders When Feeding Oil Sands and Residence Time and Residence Time Distribution in a Rotary Kiln, ME Final Report/Thesis, University of Utah, Salt Lake City, Utah.

Balaji, G., 1996, Contribution of Thermal Effects in Hydrotreating Oil Sands Derived Heavy Oils over Commercial Ni-Mo/Al_2O_3 Catalysts, Ph.D. Dissertation, University of Utah, Salt Lake City, Utah.

FINAL REPORTS

Oblad, A.G., Bunger, J.W., Miller, J.D., and Seader, J.D., 1977, Recovery of Oil from Utah's Tar Sands. Final Rept. Grant ASR74-21867, NSF Fdn. RANN Program.

Oblad, A.G., Bunger, J.W., Hanson, F.V., Miller, J.D., and Seader, J.D., 1979, Recovery of Oil from Utah's Tar Sands. Final Report, 1977-79. U.S. (DOE) Contract No. ET77-S-03-1762. 140 pp.

Bunger, J.W., and Wells, H.M., 1980, Economic Evaluation of Tar Sand Resources Located in the State of Utah. Phase I. Final Report. UEES, Salt Lake City, Utah, 211 pp.

Oblad, A.G., Bunger, J.W., Hanson, F.V., Miller, J.D., and Seader, J.D., 1984, Recovery of Oil from Utah's Tar Sands. Final Report, U.S. DOE Contract No. DE-AS20-80LC10332, May.

Oblad, A.G., Bunger, J.W., Hanson, F.V., Miller, J.D., and Seader, J.D., 1984, Recovery and Hydropyrolysis of Oil from Utah's Tar Sands. Final Report, U.S. DOE Contract No.

DE-AS20-82LC10942, December.

Wells, H.M., Bunger, J.W., and Jensen, G.F., 1984, Economic Evaluation of Oil Shale and Tar Sands Located in the State of Utah. Final Report, 5 volumes, UEES, Salt Lake City, Utah.

Oblad, A.G., Bunger, J.W., Hanson, F.V., Miller, J.D., and Seader, J.D., 1985, Recovery and Upgrading of Oil from Utah Tar Sands. First Ann. Report, U.S. DOE Contract No. DE-FC20-84LC11057, September.

Oblad, A.G., Bunger, J.W., Hanson, F.V., Miller, J.D., and Seader, J.D., 1986, Recovery and Upgrading of Oil from Utah Tar Sands. Second Ann. Rept., U.S. DOE Contract No. DE-FC20-84LC11057, September.

Oblad, A.G., Bunger, J.W., Hanson, F.V., Miller, J.D., and Seader, J.D., 1987, Recovery and Upgrading of Oil from Utah Tar Sands. Final Tech. Rept., U.S. DOE Contract No. DE-FC20-84LC11057, January.

Oblad, A.G., and Hanson, F.V., 1988, Production of Bitumen-Derived Hydrocarbon Liquids from Utah's Tar Sands. Final Tech. Rept., U.S. DOE Contract No. DE-FC21-87MC11090, September.

Oblad, A.G., Bunger, J.W., Hanson, F.V., Miller, J.D., and Seader, J.D., 1989, The Extraction of Bitumen from Western Tar Sands, Final Tech. Rept., U.S. DOE Contract No. DE-FC21-88MC25046.

Oblad, A.G., Bunger, J.W., Deo, M.D., Hanson, F.V., Miller, J.D., and Seader, J.D., 1990, The Extraction of Bitumen from Western Tar Sands, Final Tech. Rept., U.S. DOE Contract No. DE-FC21-89MC26268.

Oblad, A.G., Bunger, J.W., Deo, M.D., Hanson, F.V., Miller, J.D., and Seader, J.D., 1991, The Extraction of Bitumen from Western Tar Sands, Final Tech. Rept., U.S. DOE Contract No. DE-FC21-89MC26268.

Oblad, A.G., Bunger, J.W., Deo, M.D., Hanson, F.V., Miller, J.D., and Seader, J.D., 1992, The Extraction of Bitumen from Western Tar Sands, Final Tech. Rept., U.S. DOE Contract No. DE-FC21-89MC26268.

Oblad, A.G., Bunger, J.W., Deo, M.D., Hanson, F.V., Miller, J.D., and Seader, J.D., 1993, The Extraction of Bitumen from Western Tar Sands, Final Tech. Rept., U.S. DOE Contract No. DE-FC21-89MC26268.

PATENTS

Miller, J.D., and Sepulveda, J.E., Oct. 17, 1978, Separation of Bitumen from Dry Tar Sands. U.S. Pat. 4,120,776.

Seader, J.D., and Jayakar, K.M., July 10, 1979, Process and Apparatus to Produce Synthetic Crude Oil from Tar Sands. U.S. Pat. 4,160,720.

Oblad, A.G., and Shabtai, J.S., Nov. 3, 1981, Hydropyrolysis of Tar Sand Bitumens and Heavy Petroleum Oils. U.S. Pat. 4,298,487.

Hanson, F.V., Miller, J.D., and Oblad, A.G., June 29, 1982, Process for Obtaining Products from Tar Sands. U.S. Pat. 4,337,143.

Hanson, F.V., Miller, J.D., and Oblad, A.G., Oct. 11, 1983, Process for Recovering Products from Tar Sand. U.S. Pat. 4,409,090.

Miller, J.D., and Hupka, J., Sept. 11, 1984, Bitumen Recovery from Tar Sands. U.S. Pat. 4,470,899.

Miller, J.D., and Misra, M., Dec. 4, 1984, Process for Separating High Viscosity Bitumen from Tar Sands. U.S. Pat. 4,486,294.

PUBLICATIONS

1976

Bunger, J.W., Mori, S., Oblad, A.G., 1976, Processing of Tar Sand Bitumens, Part I. Thermal Cracking of Utah and Athabasca Tar Sand Bitumens, Amer. Chem. Soc., Prprnts. Div. Fuel Chem., 21 (6),147.

Oblad, A.G., Seader, J.D., Miller, J.D., and Bunger, J.W., 1976, Recovery of Bitumen from Oil-Impregnated Sandstone Deposits of Utah. Oil Shale and Tar Sands Symp., AIChE Symp. Ser. 72, 155, 69.

Sepulveda, J.E., Miller, J.D., Oblad, A.G., 1976, Hot Water Extraction of Bitumen from Utah Tar Sands. I. Symp. on Oil Shale, Tar Sands and Related Materials—Production and Utilization of Synfuels, Amer. Chem. Soc., Prprnts. Div. Fuel Chem., 21 (6), 110.

1977

Bunger, J.W., 1977, Development of Utah Tar Sands—A Status Report, Mines Miner. Rept. #5, 1-10, Oct.

Bunger, J.W., 1977, Techniques of Analysis of Tar Sand Bitumens. Prprnts., Div. Pet. Chem., Amer. Chem. Soc. 22 (2), 716-26.

Bunger, J.W., Cogswell, D.E., and Oblad, A.G., 1977, Thermal Processing of a Utah Tar Sand Bitumen. Proc. Canada-Venezuela Oil Sand Symp.-77. Edmonton, Alberta, Canada; The Oil Sands of Canada-Venezuela-1977, ed. D.A. Redford, A.G. Winestock. 1978. CIM Special 17,178-82.1979

1978

Bunger, J.W., Cogswell, D.E., and Oblad, A.G., 1978, Influence of Chemical Factors on Primary Processing of Utah Tar Sand Bitumen. Prprnts., Div. Fuel Chem., ACS 23(4),98-109.

Sepulveda, J.E., and Miller, J.D., 1978, Separation of Bitumen from Utah Tar Sands by a Hot Water Digestion-Flotation Technique. Min. Eng. 30(9),1311 (also published in Trans SME/AIME, September 1978).

Sepulveda, J.E., Miller, J.D., and Oblad, A.G., 1978, Hot Water Extraction of Bitumen from Utah Tar Sands III. Mining Eng. 30,1311.

1979

Bunger, J.W., Cogswell, D.E., and Oblad, A.G., 1979, Catalytic Cracking of Asphalt Ridge Bitumen. Refining of Synthetic Crude Oils, ACS Adv. Chem., Ser. 179, 67.

Bunger, J.W., Cogswell, D.E., and Zilm, K.W., 1979, Characteristics of Tar Sand Bitumen Asphaltenes and the Effect of Asphaltenes on Conversion of Bitumen by Hydropyrolysis, Preprints, Division of Petroleum Chemistry, ACS, 24 (4), 1017-1027.

Bunger, J.W., 1979, Chemistry of Asphaltenes - Summary of Symposium, Preprints, Division of Petroleum Chemistry, ACS, 24 (4), 1028-1031.

Venkatesan, V.N., Hanson, F.V., and Oblad, A.G., 1979, The Thermal Recovery of Synthetic Crude from the Bituminous Sands of the Sunnyside (Utah) Deposit, Proc. First Int. Conf. on the Future of Heavy Crude and Tar Sands, (UNITAR), June 4-12, 1979 Edmonton, Alberta, Canada.

1980

Bunger, J.W. and Li, N.C., (eds.), 1980, Chemistry of Asphaltenes, Advances in Chemistry Series - 195, American Chemical Society, Washington, D.C.

Hanson, F.V., Miller, J.D., and Oblad, A.G., 1980, A Combined Hot Water-Thermal Pyrolysis Strategy for the Production of Bitumen-Derived Liquids. 15th Intersoc. Energy Conversion Conf.

Seattle, Washington, August.

1981

Bunger, J.W. and Cogswell, D.E., 1981, Characteristics of Tar Sand Bitumen Asphaltenes as Studied by Conversion of Bitumen by Hydropyrolysis. Chemistry of Asphaltenes, ACS Adv. Chem. Ser., Ed. J.W. Bunger and N.C. Li. No. 195, pp. 219-36. ACS, Washington, D.C.

Bunger, J.W., Cogswell, D.E., and Oblad, A.G., 1981, Hydropyrolysis—Potential for Primary Upgrading. Oil Shale, Tar Sands and Related Material, Ed. H. Stauffer, Amer. Chem. Soc., Symp. Ser., No. 163, 369-80.

Miller, J.D. and Misra, M., 1981, Hot Water Process Development for Utah Tar Sands. Pres. at the 90th Natl. AIChE Mtg. Houston, Texas Apr. 5-8.

Misra, M., Miller, J.D., 1981, Surface Chemistry Features in the Hot Water Processing of Utah Tar Sands. Pres. at the Symp. on Separation Sci. and Tech., Gatlinburg, Tennessee, May 5-8; Separation Sci. Tech. 16 (10), 1523-44.

Smith, R.J. and Miller, J.D., 1981, Flotation Behavior of Digested Asphalt Ridge Tar Sands, Mining Eng. 33 (12), 1724.

1982

Hupka, J., Miller, J.D., Aguilar, R., and Cortes, A., 1982, Modified Hot Water Processing of Domestic Tar Sands. AIME Ann. Meet., Dallas, Texas, Feb. 14-18, 1982, No. 82-85. Submitted for publication.

Miller, J.D. and Misra, M., 1982, Hot Water Process Development for Utah Tar Sands, Fuel Proc. Tech. 6, 27-59.

Miller, J.D. and Misra, M., 1982, Concentration of Utah Tar Sands by an Ambient Flotation Process, Internat. J. Miner. Proc. 9, 269-87.

Venkatesan, V.N., Hanson, F.V., and Oblad, A.G., 1982, A Fluidized Bed-Thermal Process for the Recovery of a Bitumen-Derived Liquid from the Bitumen-Impregnated Sandstone Deposits of Utah, AIChE, Symp. Ser. 216, 78, 42-55.

1983

Hupka, J., Miller, J.D., and Cortes, A., 1983, The Importance of Bitumen Viscosity in the Hot Water Processing of Domestic Tar Sands, SME/AIME, Mining

Wang, J., Hanson, F.V., and Oblad, A.G., 1983, The Fluidized Bed Pyrolysis of the Bitumen-Impregnated Sandstone from the Whiterocks (Utah) Deposit, Prprnt. AIChE Symp. Adv. Tar Sand Tech. Denver, Colorado, August.
Eng. 35(12),1635-41.

1984

Bunger, J.W., 1984, Upgrading Utah Tar Sand Bitumen to Syncrude. Proc. WRI-DOE Tar Sand Symp., Vail, Colorado, June 26-29.

Dorius, J.C., Hanson, F.V., and Oblad, A.G., 1984, The Pyrolysis of the Bitumen-Impregnated Sandstone from the P.R. Spring (Utah) Deposit in a Fluidized-Bed, Proc. WRI-DOE Tar Sand Symp., Paper 5-1, Vail, Colorado, June 26-29.

Hatfield, K.E. and Oblad, A.G., 1984, Pilot Plant Program for Upgrading of Heavy Oils by Hydropyrolysis. Proc. of the Second Internat. Conf. Heavy Crude and Tar Sand, (UNITAR), Caracas, Venezuela, Feb. 7-17, UNITAR, 1175-79.

Hupka, J., Miller, J.D., and Oblad, A.G., 1984, Hot Water Processing of U.S. Tar Sands—Water Recycle and Tailing Disposal, Stud. Environ. Sci. 23, 253-267.

Smart, L. and Seader, J.D., 1984, Thermal Recovery of Bitumen. Proc. WRI-DOE Tar Sand Symp., Vail, Colorado, June 26-29.

1985

Bunger, J.W. and Oblad, A.G., 1985, Upgrading of Bitumen by Hydropyrolysis—a Process for Low Coke and High Syncrude Yields. Proc. Third Internat. Conf. on Heavy Crude and Tar Sands, (UNITAR/UNDP), Los Angeles, California, 1717-26, Jul. 22-31.

Bunger, J.W., 1985, Reactions of Hydrogen During Hydropyrolysis Processing of Heavy Crudes, Amer. Chem. Soc., Div. Pet. Chem. 30 (4),658-63.

Bunger, J.W., 1985, Inhibition of Coke Formation in Hydropyrolysis of Residual Oils, Amer. Chem. Soc., Prprnts. Div. Pet. Chem. 30 (3),549-554.

1986

Bunger, J.W., Tsai, C.H., and Russell, C.P., 1986, Competing Reactions During Hydropyrolysis Upgrading of Tar Sand Bitumen and Residual Materials. Proc. WRI/DOE Tar Sand Symp., Westhoff, J.D., and Marchant, L.C. Eds. Jackson, Wyoming, July 7-10, 1986.

Lin, L.C., Hanson, F.V., and Oblad, A.G., 1986, A Preliminary Mathematical Model of the

Pyrolysis of Bitumen-Impregnated Sandstone in a Fluidized Bed, Proc. WRI/DOE Tar Sand Symp., ed. Westhoff, J.D., and Marchant, L.C. Eds. Jackson, Wyoming, July 7-10, 1986.

Seader, J.D., Bezama, R.J., and Charavarty, T., 1986, Design and Economic Evaluation of an Energy-Integrated Thermal Process for Recovery of Oil from Tar Sands, Proc. WRI/DOE Tar Sand Symp., Westhoff, J.D., and Marchant, L.C. Eds., Jackson, Wyoming, July 7-10, 1986.

1987

Hupka, J., Miller, J.D., and Oblad, A.G., 1987, Diluent-Assisted Hot Water Processing of Tar Sands, AOSTRA J. Res. 3, 95-102.

Lin, L.C., Hanson, F.V., Oblad, A.G., and Westhoff, J.D., 1987, The Pyrolysis of Bitumen-Impregnated Sandstone in Short-Contact Time Reactors. I. Cyclone Reactor, Fuel Proc. Tech. 16, 173-190.

Oblad, A.G., Bunger, J.W., Hanson, F.V., Miller, J.D., Ritzma, H.R., and Seader, J.D., 1987, Tar Sand Research and Development at the University of Utah, Ann. Rev. Energy. 12, 283-356.

1988

Bunger, J.W., Tsai, C.H., Ryu, H., and Devineni, P., 1988, Developments in Upgrading of Bitumen by Hydropyrolysis, Proceedings, 4th International Conference on Heavy Crude and Tar Sands, UNITAR/UNDP, Edmonton, Canada.

Hanson, F.V. and Oblad A.G., 1988, The Fluidized Bed Pyrolysis of Bitumen-Impregnated Sandstone from the Tar Sand Deposits of Utah. Proc. UNITAR/UNDP Internat. Conf. on Heavy Crude and Tar Sands, Vol. 5. Extraction, Upgrading, Transportation, Paper No. 155, 421-438, Edmonton, Alberta, Canada.

Hanson, F.V., Shun, D., and Oblad, A.G., 1988, The Fluidized Bed Pyrolysis of Bitumen-Impregnated Sandstone from the Circle Cliffs (Utah) Tar Sand Deposit, Preprint 36h, Advances in Synthetic Fuels Tech. Symposium, National AIChE Mtg.

1989

Hsu, J.C.L., and Seader, J.D., 1989, Digital Control of a Coupled Fluidized-Bed Thermal Processing System for Tar Sands, Fuel Proc. Tech., 21, 1-17.

Lin, L.C., Hanson, F.V., and Oblad, A.G., 1989, Mathematical Model of the Pyrolysis of Bitumen-Impregnated Sandstone Particles. I. Diffusion Dominant Transport Regime, Fuel Proc. Tech. 22, 41-63.

Yang, Y.J., Bukka, K., and Miller, J.D. 1989. Selection and Evaluation of Diluents in the Modified Hot Water Process, Energy Proc. Canada, 82 (1), 14-21.

1990

Lin, L.C., Deo, M.D., Hanson, F.V., and Oblad, A.G., 1990, Kinetics of Tar Sands Pyrolysis Using a Distribution of Activation Energy Model. AIChE J. 36, 1585-1588.

1991

Bukka, K., Miller, J.D., Hanson, F.V., and Oblad, A.G., 1991, Mineral Matter Distribution During the Hot Water Processing of Utah Tar Sand, AOSTRA J. Res. 7, 101-109.

Bukka, K., Miller, J.D., and Oblad, A.G., 1991, Fractionation and Characterization of Utah Tar Sand Bitumens, Influence of Chemical Composition on Bitumen Viscosity. Energy & Fuels 5, 333-340.

Cha, S., Hanson, F.V., Longstaff, D.C., and Oblad, A.G., 1991, Pyrolysis of Bitumen Impregnated Sandstones, A Comparison of Fluidized-Bed and Rotary-Kiln Reactors, FUEL 70, 1357-1361.

Cha, S., Longstaff, D.C., Hanson, F.V., and Oblad, A.G., 1991, Pyrolysis of Bitumen Impregnated Sandstones, A Comparison of Fluidized - Bed and Rotary Kiln Reactors, Proc. 1990 Eastern Oil Shale Symp., 136-145.

Deo, M.D., Fletcher, J.V., Shun, D.W., Hanson, F.V., and Oblad, A.G., 1991, Modeling of the Pyrolysis of Tar Sand in Fluidized Bed Reactors. Proc. 1990 Eastern Oil Shale Symp., 105-119.

Deo, M.D., Fletcher, J.V., Shun, D., Hanson, F.V., and Oblad, A.G., 1991, Modeling the Pyrolysis of Tar Sands in Fluidized Bed Reactors, FUEL, 70, 1271-1276.

Deo, M.D., Hwang, J., and Hanson, F.V., 1991, Solubility of Carbon Dioxide in Tar Sand Bitumen, Experimental Determination and Modeling, Ind. Eng. Chem. Res. 30 (3), 532-536.

Hupka, J., Lelinski, D., and Miller, J.D., 1991, Air Bubble Filming During Bitumen Flotation from Digested Tar Sand Slurry, Proc. 22nd Ann. Meeting of the File Particle Society, 83-84.

Hupka, J., Drelich, J., Miller, J.D., White, R.R., Hanson, F.V., and Oblad, A.G., 1991, Impact of Water Recycle on Water-Based Processing of Whiterocks Tar Sands, Proc. 1990 Eastern Oil Shale Symp., 39-44.

Hupka, J., Drelich, J., Miller, J.D., White, R.R., Hanson, F.V., and Oblad, A.G., 1991, Impact

of Water Recycle on Water-Based Processing of Whiterocks Tar Sand, FUEL 70, 1313-1316.

Hupka, J., and Miller, J.D., 1991, Temperature Water-Based Bitumen Recovery from Tar Sand, FUEL 70, 1308-1312.

Hupka, J., and Miller, J.D., 1991, Electrophoretic Characterization and Processing of Asphalt Ridge and Sunnyside Tar Sands, Internat., J. Miner. Proc. 31, 217-231.

Hupka, J. and Miller, J.D., 1991, Moderate-Temperature Water-Based Bitumen Recovery from Tar Sands, Proc. 1990 Eastern Oil Shale Symp., 130-135.

Lin, L.C., Deo, M.D., Hanson, F.V., and Oblad, A.G., 1991, Nonisothermal Analysis of the Kinetics of the Combustion of Coked Sand, Ind. Eng. Chem. Res. 30, 1795-1801.

Misra, M., and Miller, J.D., 1991, Comparison of Water-Based Physical Separation Processes for U.S. Tar Sands, Fuel Proc. Tech. 27, 3-20.

Seader, J.D. and Coronella, C.J., 1991, An Advanced Energy-Efficient Coupled Fluidized-Bed System for Recovering Bitumen From Tar Sands, Proc. 1990 Eastern Oil Shale Symp., 120-129.

Tsai, C.H., Deo, M.D., Hanson, F.V., and Oblad, A.G., 1990, Characterization and Potential Utilization of Whiterocks (Utah) Tar Sand Bitumen, Fuel Sci. Tech. Int., 9, 1259-1286.

1992

Bukka K., Hanson, F.V., Miller, J.D., and Oblad, A.G., 1992, Fractionation and Characterization of Whiterocks Tar Sands Bitumen, Energy & Fuels 6, 160.

Coronella, C.J., and Seader, J.D., 1992, Combustion of Coked Sand in a Two-Stage Fluidized-Bed System, FUEL 71, 143-150.

Deo, M.D., Hwang, J., and Hanson, F.V., 1992, Supercritical Fluid Extraction of a Crude Oil, Bitumen-Derived Liquid and Bitumen by Carbon Dioxide and Propane, FUEL 71, 1519-1526.

Deshpande, D.A., Deo, M.D., Hanson, F.V., and Oblad, A.G., 1992, A Model for the Prediction of Bubble Size at a Single Orifice in Two-Phase Gas-Liquid Systems, Chem. Eng. Sci. 47, 1669-1676.

Drelich, J., Bryll, G., Kapczynski, J., Hupka, J., Miller, J.D., and Hanson, F.V., 1992, The Effect of Electric Field Pulsation Frequency on Breaking Water-in-Oil-Emulsions, Fuel Proc. Tech. 31, 105-113.

Drelich, J., Hanson, F.V., Hupka, J, and Miller, J.D., 1992, Water Recycle in Moderate-Temperature Bitumen Recovery from Whiterocks Tar Sands, AOSTRA J. Res, 8, 139-147.

Drelich, J., and Miller, J.D., 1992, The Effect of Surface Heterogeneity on Pseudo-Line Tension

and the Flotation Limit of Fine Particles, Colloids and Surfaces 69, 35-43.

Drelich, J., and Miller, J.D., 1992, The Line/Pseudo-Line Tension in Three-Phase Systems, Particulate Sci. Tech. 10, 1-20.

Fletcher, J.V., Deo, M.D., and Hanson, F.V., 1992, Reexamination of Minimum Fluidization Velocity Correlations Applied to Group B Sands and Coked Sands, Powder Technol. 69 (2), 147-155.

Hanson, F.V., Dorius, J.C., Utley, J.K., and Van Nguyen, T., 1992, The Application of Compound-Type Analyses to the Correlation of Product Distributions and Yields from the Fluidized-Bed Pyrolysis of Oil Sands, Proc. 1991 Eastern Oil Shale Symp., 34-46.

Hanson, F.V., Cha, S., Deo, M.D., and Oblad, A.G., 1992, Pyrolysis of Oil Sand from the Whiterocks Deposit in a Rotary Kiln, FUEL 71, 1455-1463.

Hanson, F.V., Dorius, J.C., Utley, J.K., and Van Nguyen, T., 1992, The Application of Compound-Type Analyses to the Correlation of Product Distributions and Yields from the Fluidized-Bed Pyrolysis of Oil Sands, FUEL 71, 1365-1372.

Hanson, F.V., Cha, S.M., and Oblad, A.G., 1992, Pyrolysis of Oil Sand from the Whiterocks Tar Sand Deposit in a Rotary Kiln, Proc. 1991 Eastern Oil Shale Symp., 116-128.

Hupka, J., Budzich, M., and Miller, J.D., 1992, Preliminary Examination of Oil Bonding at Sand Surfaces and its Influence on Hot Water Separation, Proc. 1991 Eastern Oil Shale Symp., 202-207.

Hwang, J., Deo, M.D., Hanson, F.V., and Oblad, A.G., 1992, Supercritical Fluid Extraction of a Crude Oil, Bitumen-Derived Liquid and Bitumen by Carbon Dioxide and Propane, Proc. 1991 Eastern Oil Shale Symp., 209-221.

Longstaff, D.C., Deo, M.D., Hanson, F.V., Oblad, A.G., and Tsai, C.H., 1992, Hydrotreating the Bitumen-Derived Hydrocarbon Liquid Produced in a Fluidized Bed Pyrolysis Reactor, FUEL 71, 1407-1419.

Tsai, C.H., Deo, M.D., Hanson, F.V., and Oblad, A.G., 1992, Characterization and Potential Utilization of Whiterocks (Utah) Tar Sand Bitumen II. Pyrolysis Mass Spectrometry and Nuclear Magnetic Resonanace Analyses, Fuel Sci. Technol. Int. 10, 1437-1459.

Tsai, C.H., Longstaff, D.C., Deo, M.D., Hanson, F.V., and Oblad, A.G., 1992, Characterization and Utilization of Hydrotreated Products from the Whiterocks (Utah) Tar Sand Bitumen-Derived Liquid, FUEL 71, 1473-1482.

Tsai, C.H., Deo, M.D., Hanson, F.V., and Oblad, A.G., 1992, Characterization and Utilization of Hydrotreated Products Produced from Whiterocks (Utah) Tar Sand Bitumen-Derived Liquid,

Proc. 1991 Eastern Oil Shale Symp., 79-90.

1993

Coronella, C.J., Lee, S.Y., and Seader, J.D., 1993, Minimum Slugging Velocity in Fluidized Beds Containing Vertical Rods, Proc. 1992 Eastern Oil Shale Symp., 238-246.

Coronella, C.J., Lee, S.Y. and Seader, J.D., 1993, Minimum Slugging Velocity in Fluidized Beds Containing Vertical Rods, Proc. 1992 Eastern Oil Shale Symp., 238-246.

Deo, M.D., Hwang, J., and Hanson, F.V., 1993, The Effect of Cosolubilizing Lighter Components on the Asphaltene Content of Heavy Oils, Fuel Proc. Technol. 34, 217-228.

Deo, M.D. and Hanson, F.V., 1993, Asphaltene Precipitation: A Need for a Broader View, SPE 25193.

Deo, M.D., and Hanson, F.V., 1993, Asphaltene Rejection from Bitumens via Supercritical Fluid Extraction, Proc. 1992 Eastern Oil Shale Symp., 159-168.

Deshpande, D.A., Deo, M.D., and Hanson, F.V., 1993, Similitude Studies in Three-Phase Ebullieted Bed Reactors, Proc. 1992 Eastern Oil Shale Symp., 216-226.

Drelich, J., Miller, J.D., and Hupka, J., 1993, The Effect of Drop Size on Contact Angle over a Wide Range of Drop Volumes, Colloid Interface Sci., 155, 379-385.

Drelich, J., and Miller, J.D., 1993, Surface/Interfacial Tension of the Whiterocks Bitumen and its Relationship to Tar Sand Processing, Proc. 1992 Eastern Oil Shale Symp., 265-275.

Drelich, J., and Miller, J.D., 1993, Modification of the Cassie Equation, Langmuir 9, 619-621.

Fletcher, J.V., Deo, M.D., and Hanson, F.V., 1993, Fluidization of a Multi-Sized Group B Sand at Reduced Pressure, Powder Technol. 76 (2), 141-148.

Fletcher, J.V., Deo, M.D., and Hanson, F.V., 1993, Fluidized Bed Pyrolysis of Bitumen-Impregnated Sandstone at Sub-Atmospheric Conditions, Proc. 1992 Eastern Oil Shale Symp., 247-256.

Hupka, J., and Miller, J.D., 1993, Tar Sand Pretreatment with Diluent, Prprnt. No. 92-122 of the 121st SME/AIME Ann. Mtg. in Phoenix, Arizona, Feb. 24-27, 1992, Minerals and Metallurgical Processing, in print.

Kwak, S., Longstaff, D.C., Deo, M.D., and Hanson, F.V., 1993, Hydrotreating Process Kinetics for Bitumen and Bitumen-Derived Liquids, Proc. 1992 Eastern Oil Shale Symp., 208-215.

Lee, S.Y., Coronella, C.J., Bhadkamkar, A.S., and Seader, J.D., 1993, Modeling and

Temperature Regulation of a Thermally Coupled Reactor System via Internal Model Control Strategy, Ind. Eng. Chem. Res., 32, 3029-3036.

Lee, S.Y., Coronella, C.J., Seader, J.D., and Pitt, C.H., 1993, Erosion-Corrosion of 316 Stainless Steel Rods Immersed in a Bubbling Fluidized Bed, Chem Eng. Science 48, 1437-1445.

Lelinski, D., Miller, J.D., and Hupka, J., 1993, The Potential for Air-Sprayed Hydrocyclone Flotation in the Removal of Oil from Oil-in-Water Emulsions, Proc. First World Congress on Emulsions, 1-22-016/01 to 1-22-016/06.

Longstaff, D.C., Deo, M.D., and Hanson, F.V., 1993, Hydrotreating the Bitumen from the Whiterocks Oil Sand Deposit, Proc. 1992 Eastern Oil Shale Symp., 199-207.

Rose, P.E., Bukka, K., Deo, M.D., Hanson, F.V., and Oblad, A.G., 1993, Characterization of Uinta Basin Oil Sand Bitumens, Proc. 1992 Eastern Oil Shale Symp., 277-282.

Sarkan, A. and Deo, M.D., 1993, Comparison of Thermal EOR Processes Using Combinations of Vertical and Horizontal Wells, Proc. Int. Thermal Operations Symp., Bakersfield, Ca., 175.

Tsai, C.H., Deo, M.D., Hanson, F.V., and Oblad, A.G., 1993, Characterization and Potential Utilization of the Asphalt Ridge Tar Sand Bitumen I. Gas Chromatography Mass Spectrometry Analyses, Fuel Sci. Technol. Int'l. 11 (3-4), 475-506.

1994

Bukka, K., Miller, J.D., Hanson, F.V., Misra, M., and Oblad, A.G., 1994, The Influence of Carboxylic Acid on Bitumen Viscosity, FUEL, 73 (9), 257-268.

Bukka, K., Miller, J.D., Hanson, F.V., and Oblad, A.G., 1994, Characterization of Circle Cliffs Tar Sands of Utah, Fuel Proc. Technol. 38 (2), 111-125.

Chu, K.-S., Hanson, F.V., and Massoth, F.E., 1994, Effect of Bitumen-Derived Coke on Deactivation of an HDM Catalyst, Fuel Proc. Technol. 40, 79-95.

Coronella, C.J., Lee, S.Y., and Seader, J.D., 1994, Minimum Slugging Velocity in Fluidized Beds Containing Vertical Rods, FUEL, 73, 1537-1543.

Deo, M.D. and Hanson, F.V., 1994, Asphaltene Rejection via Supercritical Fluid Extraction, FUEL 73 (9), 1493-1498.

Drelich, J., Bukka, K., Miller, J.D., and Hanson, F.V., 1994, Surface Tension of Toluene-Extracted Bitumens from Utah Oil Sands as Determined by Wilhemy Plate and Contact Angle Technique, Energy & Fuels 8, 700-704.

Drelich, J., Lelinski, D., Hupka, J., and Miller, J.D., 1994, The Role of Gas Bubbles in Bitumen

Recovery from Tar Sands in Hot-Water Processing, Proc. 1993 Eastern Oil Shale Symp., 100-109.

Drelich, J., Bukka, K., Miller, J.D., and Hanson, F.V., 1994, Surface Tension of Toluene-Extracted Bitumens from Utah Oil Sands as Determined by Wilhelmy Plate and Contact Angle Techniques, Energy & Fuels, 8, 700-704.

Drelich, J., and Miller, J.D., 1994, Examination of Neumann's Equation-of-State for Interfacial Tensions, Journal of Colloid and Interface Science, 167, 217-220.

Drelich, J., and Miller, J.D., 1994, Surface and Interfacial Tension of the Whiterocks Bitumen and its Relations to Bitumen Release from Tar Sands during Hot Water Processing, Fuel, 73, 1504-1510.

Kwak, S., Longstaff, D.C., Deo, M.D., and Hanson, F.V., 1994, Hydrotreatment Process Kinetics for Bitumen and Bitumen-Derived Liquids, FUEL 73 (9), 1531-1530.

Kwak, S., Longstaff, D.C., and Hanson, F.V., 1994, Catalytic Upgrading of a Uinta Basin Bitumen Over a Commercial HDM Catalyst, Proc. 1993 Eastern Oil Shale Symp., 168-176.

Longstaff, D.C., Deo, m.D., and Hanson, F.V., 1994, Hydrotreatment of Bitumen from the Whiterocks Oil Sand Deposit, FUEL 73 (9), 1523-1530.

Longstaff, D.C., Hanson, F.V., and Kwak, S., 1994, Uinta Basin Bitumen Hydrotreating: A Comparison of HDN and HDM Catalyst Performance, Proc. 1993 Eastern Oil Shale Symp., 177-185.

Subramanian, M., Deo, m.D., Fletcher, J.V., and Hanson, F.V., 1994, Supercritical Fluid Extraction of Oil Sand Bitumen, Proc. 1993 Eastern Oil Shale Symp., 241-252.

Tang, H.Q., Fletcher, J.V., and Hanson, F.V., 1994, Combustion of Carbonaceous Residues on Spent Oil Sands in a Laboratory Scale Dense Phase Transport Reactor, Proc. 1993 Eastern Oil Shale Symp., 153-160.

Zheng, H., Tang, Q., Fletcher, J.V., and Hanson, F.V., 1994, Performance and Calibration of Dry Materials Feeders When Feeding Oil Sands, Proc. 1993 Eastern Oil Shale Symp., 144-150.

1995

Drelich, J., Lelinski, D., Hupka, J., and Miller, J.D., 1995, The Role of Gas Bubbles in Bitumen Release during Oil Sand Digestion, Fuel, 74, 1150-1155.

Drelich, J., Lelinski, D., and Miller, J.D., 1995, Microscopic Observations of Bitumen Spreading at Gas Bubble Surfaces, Proc. 1st UBC-McGill Bi-Annual International Symp. on Fundamentals of Mineral Processing, 291-304.

Fletcher, J.V., Deo, M.D., and Hanson, F.V., 1995, Fluidized Bed Pyrolysis of a Uinta Basin Oil Sand, FUEL 74 (3), 311-316.

Hanson, F.V., Fletcher, J.V., and Zheng, H., 1995, Performance of Auger-Type Dry Material Feeders When Feeding Oil Sands, Fuel Proc. Tech., 41, 289-304.

Hwang, J., Park, S.J., Deo, M.D., and Hanson, F.V., 1995, Phase Behavior of CO_2/Crude Oil Mixtures in Supercritical System: Experimental Data and Modeling, E&EC Research 34, 1280-1286.

Longstaff, D.C., Balaji, G., Kim, J., Kwak, S., Tsai, C.H., and Hanson, F.V., 1995, Hydrotreating Uinta Basin Bitumen-Derived Heavy Oils, Paper #115, Proc. 6th UNITAR Intnl. Conf. Hvy. Crude Tar Sands, Edmonton, Alberta.

Nagpal, S., Fletcher, J.V., and Hanson, F.V., 1995, Pyrolysis of Uinta Basin Oil Sands in Fluidized Bed and Rotary Kiln Reactors, Paper #118, Proc. 6th UNITAR Intnl. Conf. Hvy. Crude Tar Sands, Edmonton, Alberta.

Rose, P.E. and Deo, M.D., 1995, Steam-Assisted Gravity Drainage in Oil Sand Reservoirs Using a Combination of Vertical and Horizontal Wells, FUEL, Vol. 74, No. 8, 1180.

Subramanian, M., Deo, M.D., and Hanson, F.V., 1995, Supercritical Fluid Extraction of Uinta Basin Bitumens, Paper #116, Proc. 6th UNITAR Intnl. Conf. Hvy. Crude Tar Sands, Edmonton, Alberta.

1996

Drelich, J., Lelinski, D., and Miller, J.D., 1996, Bitumenh Spreading and Formation of Thin Bitumen Films at a Water Surface, Colloids and Surfaces A: Physicochemical and Engineering Aspects, in press.

Subramanian, M., Deo, M.D., and Hanson, F.V., 1996, Compositional Analysis of Bitumen and Bitumen-Derived Products, J. Chromat. Sci. 34 (1), 20-26.